Journal of Applied Mechanics

(Contributions of the ASME Applied Mechanics Division)

Airload Determination for Orthotropic Plane Stress and Plane Strain . . . . . H. A. Lang 1
The Spherically Bending of Thin Circular Rods . . . . . H. D. Conway 7
Asymmetrical Bending of a Cylindrically Aeolotropic Tapered Disk . . . . . E. S. Barlig and H. D. Conway 11
Stability of Orthogonally Stiffened Plates . . . . . N. J. Huffington, Jr. 15
Large Deflections of Elliptical Plates . . . . . N. A. Weil and N. M. Newmark 21
Plastic Buckling of Plates . . . . . P. P. Bijlaard 27
Buckling Curves and Its Application on Beam-Columns . . . . . L. W. Hu and N. H. Trustr 35
Combined Stress Tests in Plasticity . . . . . Aris Phillips and Lloyd Ketchele 43
The Load-Carrying Capacity of Circular Plates at Large Deflection . . . . . R. T. Shaat and E. M. Haythornthwaite 49
Plastic Deformations in a Deeply Notched Bar . . . . . L. Gun, E. H. Lee, and A. J. Wang 56
Axially Symmetric Bending of Nearly Cylindrical Shells . . . . . R. A. Clark and E. Reissner 59
Analysis of Short Thin Axisymmetrical Shells Under Axisymmetrical Edge Loading . . . . . G. Herrmann, C. Lhakon, and J. S. Bern 68
Displacements in an Elastic-Plastic Cylindrical Shell . . . . . P. G. Hodge, Jr. 73
Stress Concentration Caused by Multiple Punches and Cracks . . . . . Michael Sadowsky 80
The Stress Distribution in a Strip Loaded in Tension by Means of a Central Pin . . . . . P. S. Theocaris 85
Solutions of the Equations of Elasticity for Porous Materials . . . . . M. A. Biot 91
Natural Frequencies of Continuous Plates . . . . . A. S. Veletsos and N. M. Newmark 97
Bending Vibrations of Variable Section Beams . . . . . E. T. Cranch and Alfred A. Adler 103
Matrix Solution for Vibration of Non-Uniform Disks . . . . . P. F. Ehrich 109
Impact in Dynamic Photoelasticity . . . . . M. M. Frocht and P. D. Pitman 116
The Effect of the Earth's Rotation on Laminar Flow in Pipes . . . . . G. S. Benton 125
Flow of Gas Through Porous Media . . . . . J. S. Aronofsky and J. D. Porter 128
Discussions on previously published papers by W. N. Findley and J. J. Pyrnnsky; David Shanley; M. M. Frocht and Herman Guernsey, Jr.; G. A. Zitzias; M. C. Junger; R. T. Shield, C. Ip, and J. S. Prentis; R. J. Sapp and D. E. Carver; H. Ōkubo and S. Sato; H. Becker; W. S. Brand; E. A. Davis; I. Cornet and C. C. Grant; J. Dumont and R. S. Hartenberg; F. M. Lewis; N. J. Huff, H. G. Hopkins and W. Heiple; R. A. McClintock; C. T. Wang, R. J. Vaccaro, and D. F. De Santo; B. W. Shaffer and R. N. Hinton, Jr.; B. T. Plymale and R. Gendstein; and M. Mordchelson, S. W. Yuan, and H. Reismer 133
Book Reviews 161

MARCH, 1956

VOL. 23, No. 1

Transactions of The American Society of Mechanical Engineers

Journal of Applied Mechanics

Papers Contributed to the Transactions by the ASME Applied Mechanics Division

EXECUTIVE COMMITTEE OF THE APPLIED MECHANICS DIVISION

R. D. Mindlin, *Chairman* M. Hetényi, *Secretary*

James M. Lemelle, *Technical Editor*

Published Quarterly by

The American Society of Mechanical Engineers

Publication Office, 20th and Northampton Streets, Easton, Pa.
Editorial Department at the Headquarters of the Society, 29 West Thirty-Ninth Street, New York 18, N. Y.

OFFICERS OF THE SOCIETY

J. W. Barker, *President*

James A. Hone, *Treasurer* C. E. Davies, *Secretary*

F. J. Kerr, *Assistant Treasurer*

PUBLICATIONS COMMITTEE

Otto de Lorenzi, *Chairman*

George A. Stetson, *Editor*
K. W. Clementson, *Asy. Editor*

By-Law: The Society shall not be responsible for statements or opinions advanced in papers or . . . printed in its publications (B13, Par. 4)

Published quarterly by The American Society of Mechanical Engineers. Publication office at 20th and Northampton Streets, Easton, Pa. The editorial department is located at the headquarters of the Society, 29 West Thirty-Ninth Street, New York 18, N. Y. Cable address, "Dynamic," New York. Price ($1.50 a copy; $5.00 a year; to members $2.50 a year; single copy price to members, $1.00. Add 25c for postage to all countries outside the United States, Canada, and Pan-American Union. Changes of address must be received at Society headquarters seven weeks before they are to be effective on the mailing list. Please send old as well as new address. . . . By-Law: The Society shall not be responsible for statements or opinions advanced in papers or. . . . printed in its publications (B13, Par. 4). . . . Entered as second-class matter March 14, 1955, at the Post Office at Easton, Pa., under the act of August 24, 1912. . . .
© Copyright, 1956, by The American Society of Mechanical Engineers. Reprints from this publication may be made on condition that full credit be given the JOURNAL OF APPLIED MECHANICS and the author, and that date of publication be stated.

The Affine Transformation for Orthotropic Plane-Stress and Plane-Strain Problems

By H. A. LANG,[1] SANTA MONICA, CALIF.

It is demonstrated that a single affine transformation of the type $x = ax'$, $y = by'$ immediately extends the solution of any isotropic plane-stress or plane-strain problem to the solution of an orthotropic plane problem where the orthotropic material is characterized by three independent constants. Since orthotropy, defined as elastic symmetry with respect to two orthogonal axes, implies four independent elastic constants, the affine transformation introduces a restriction upon the orthotropic shear modulus. The orthotropic shear modulus differs from that used by previous investigators. This difference alters the equation which the orthotropic stress function must satisfy and, therefore, directly affects the solution to every plane-stress or plane-strain problem. Some arguments are advanced to favor the shear modulus, as here defined, whenever orthotropy must be restricted to three elastic constants. The two solutions of the orthotropic half plane subjected to a normal concentrated load are contrasted to illustrate the effect of the two definitions of orthotropic shear modulus.

Introduction

WHILE increased emphasis has been given in recent years to the solution of elasticity problems in orthotropic materials, attention has been directed principally to the solution of individual problems or the extension of methods of classical isotropic elasticity. The objective of this paper is to point out that an affine transformation of the form $x = ax'$, $y = by'$ can be applied to the solution of every isotropic plane-stress or plane-strain problem to obtain the solution of an equivalent orthotropic plane-stress or plane-strain problem. This necessitates defining orthotropy as elastic symmetry with respect to two orthogonal axes in the body. The affine transformation is referred to these axes.

Elastic symmetry requires only a plane body specified by four elastic constants. One of these independent elastic constants is the shear modulus. The affine transformation can, at most, represent a body having three independent elastic constants. The definition of the shear modulus resulting from this restriction differs from that used by other investigators. The effect of this difference is illustrated by solving the problem of the half plane under normal concentrated load.

Since many plastics, laminates, and multicellular structures exhibit strong directional elastic effects, the restriction of the shear modulus is undesirable. The equations of this paper represent a point of departure for a companion paper in which the restriction is removed.

The Plane Orthotropic Body

The general orthotropic plane-stress or plane-strain problem is formulated as follows: To determine stresses (σ_x, σ_y, τ_{xy}), strains (e_x, e_y, γ_{xy}), and displacements (u, v) in a region R of an orthotropic material having body force (X, Y). The boundary C of the region R has prescribed on it, in whole or in part, surface displacements ($\bar{u}$, $\bar{v}$) and/or surface stresses ($\bar{X}$, $\bar{Y}$). The orthotropic material is characterized by four independent elastic constants (E_x, E_y, ν_x, G).

For plane strain, orthotropy is defined as elastic symmetry with respect to the two orthogonal planes XZ and YZ of Fig. 1(a). This is equivalent to the existence of principal axes of orthotropy XY in every cross section as shown in Fig. 1(b). For plane stress, the same definition applies but the prismatic bar is conceptually reduced in the Z-direction to a thin plate.

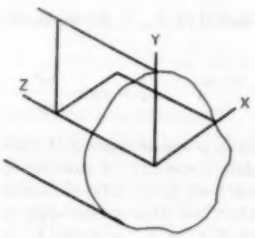

Fig. 1(a)

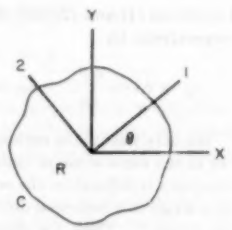

Fig. 1(b)

The corresponding stress-strain relations in matrix notation are as follows

$$\begin{bmatrix} \sigma_x \\ \sigma_y \\ \sigma_z \\ \tau_{xy} \\ \tau_{yz} \\ \tau_{zx} \end{bmatrix} = \begin{bmatrix} c_{11} & c_{12} & c_{13} & 0 & 0 & 0 \\ c_{12} & c_{22} & c_{23} & 0 & 0 & 0 \\ c_{13} & c_{23} & c_{33} & 0 & 0 & 0 \\ 0 & 0 & 0 & c_{44} & 0 & 0 \\ 0 & 0 & 0 & 0 & c_{55} & 0 \\ 0 & 0 & 0 & 0 & 0 & c_{66} \end{bmatrix} \begin{bmatrix} e_x \\ e_y \\ e_z \\ \gamma_{xy} \\ \gamma_{yz} \\ \gamma_{zx} \end{bmatrix}$$

This form shows that the plane XY is also a plane of elastic symmetry. The symmetry reduces the aelotropic strain-energy function (referred to the X, Y, Z-axes) from a quadratic function in the strains containing 21 elastic constants to an expression containing only 9 elastic constants (1).[2]

We take the point of view that, given such an orthotropic body, tests have been made to determine the values of the nine elastic constants. In general, none of these constants is zero. Of the nine elastic constants, c_{55}, c_{66} may be ignored because of the further assumption now made that $\tau_{xz} = \tau_{yz} = 0$ everywhere.

The plane-strain requirement $e_z = 0$ implies the stress-strain relations

---

[1] Associate Engineer, The Rand Corporation.

Contributed by the West Coast Committee of the Applied Mechanics Division and presented at the West Coast Conference of the Applied Mechanics Division, Monterey, Calif., September 12–13, 1955, of The American Society of Mechanical Engineers.

Discussion of this paper should be addressed to the Secretary, ASME, 29 West 39th Street, New York, N. Y., and will be accepted until April 10, 1956, for publication at a later date. Discussion received after the closing date will be returned.

Note: Statements and opinions advanced in papers are to be understood as individual expressions of their authors and not those of the Society. Manuscript received by ASME Applied Mechanics Division, May 6, 1955. This paper was not preprinted.

[2] Numbers in parentheses refer to the Bibliography at the end of the paper.

$$\begin{bmatrix}\sigma_x\\ \sigma_y\\ \tau_{xy}\end{bmatrix}=\begin{bmatrix}c_{11} & c_{12} & 0\\ c_{12} & c_{22} & 0\\ 0 & 0 & c_{44}\end{bmatrix}\begin{bmatrix}e_x\\ e_y\\ \gamma_{xy}\end{bmatrix}$$

since c_{23} can be disregarded and c_{13}, c_{23} are needed only to determine $\sigma_z = c_{13}e_x + c_{23}e_y$. The inverse matrix is

$$\begin{bmatrix}e_x\\ e_y\\ \gamma_{xy}\end{bmatrix}=\begin{bmatrix}\frac{1}{E_x} & \frac{-\nu_x}{E_y} & 0\\ \frac{-\nu_y}{E_x} & \frac{1}{E_y} & 0\\ 0 & 0 & \frac{1}{G}\end{bmatrix}\begin{bmatrix}\sigma_x\\ \sigma_y\\ \tau_{xy}\end{bmatrix} \quad \ldots\ldots\ldots [1]$$

where

$$\left.\begin{aligned} E_x &= \frac{c_{11}c_{22}-c_{12}^2}{c_{22}} \qquad E_y = \frac{c_{11}c_{22}-c_{12}^2}{c_{11}}\\ \nu_x &= c_{12}/c_{11} \qquad \nu_y = c_{12}/c_{22}\\ G &= c_{44}\end{aligned}\right\} \quad \ldots\ldots [2]$$

The last equations show that $E_y\nu_y = E_x\nu_x$ as required by the reciprocal identity $c_{12} = c_{21}$. Thus Poisson's ratio ν_y is not an independent elastic constant. For plane stress $\sigma_z = 0$ and

$$e_z = \frac{-c_{13}e_x - c_{23}e_y}{c_{33}}$$

Equations [1] and [2] may still be used if c_{11}, c_{12}, c_{22} are replaced, respectively, by

$$\overline{c_{11}} = c_{11} - \frac{c_{13}^2}{c_{33}}, \qquad \overline{c_{12}} = c_{12} - \frac{c_{13}c_{23}}{c_{33}}, \qquad \overline{c_{22}} = c_{22} - \frac{c_{23}^2}{c_{33}}$$

We note that plane orthotropic stress is approximate in character in the same sense as isotropic plane stress (2). A modulus of elasticity is defined for the orthotropic body as the ratio of a stress to a strain in a principal direction when "no other stresses exist in the plane." Thus, for plane strain, if $\sigma_y = \tau_{xy} = 0$ and $\sigma_x = E_x e_x$, a stress

$$\sigma_z = \frac{(c_{22}c_{13} - c_{12}c_{23})}{c_{22}}e_x$$

exists in the z-direction. This definition contrasts with that used by Love (2) who defines a modulus of elasticity by requiring that "no other stresses exist."

The Transformation

The affine transformation is defined by the equations

$$\left.\begin{aligned}
&(a) \quad x = \lambda x' \qquad y = y'/\lambda\\
&(b) \quad u = u'/\lambda \qquad v = v'\lambda\\
&(c) \quad e_x = e_x'/\lambda^2 \qquad e_y = e_y'\lambda^2 \qquad \gamma_{xy} = \gamma_{xy}'\\
&(d) \quad \sigma_x = \sigma_x'\lambda^2 \qquad \sigma_y = \sigma_y'/\lambda^2 \qquad \tau_{xy} = \tau_{xy}'\\
&(e) \quad X = \lambda X' \qquad Y = Y'/\lambda\\
&(f) \quad \bar{X}ds = \lambda\bar{X}'ds'\\
&\qquad \bar{Y}ds = \frac{\bar{Y}'ds'}{\lambda}
\end{aligned}\right\} \quad \ldots\ldots [3]$$

where (a) to (f) refer, respectively, to co-ordinates, displacements, strains, stresses, body forces, and boundary stresses. The primed quantities refer to an isotropic plane body of boundary curve C' enclosing the region R'.

The parameter λ and the isotropic modulus E are given by

$$E_x = \lambda^4 E \qquad E_y = E/\lambda^4 \qquad \nu_x = \nu/\lambda^4 \qquad \nu_y = \lambda^4\nu \quad \ldots [4]$$

Since in an isotropic body

$$G' = \frac{E}{2(1+\nu)}$$

the transformation implies

$$G = \frac{\tau_{xy}}{\gamma_{xy}} = \frac{\tau'_{xy}}{\gamma'_{xy}} = G' = \frac{E}{2(1+\nu)}$$

In an alternative form, this is

$$\frac{1}{G'} = \frac{\lambda^4}{E_x} + \frac{1}{\lambda^4 E_y} + \frac{2\nu_x}{E_y} \quad \ldots\ldots [5]$$

The first column of Table 1 contains the principal equations of the orthotropic plane body. Applying the transformation of Equations [3a] to [3f] it can be verified that the strain-displacement, equilibrium, and compatibility equations of the orthotropic body become the primed, isotropic equations listed in the second column. The boundary stresses transform if

$$\lambda \cos\alpha ds = \cos\alpha' ds' \quad \ldots\ldots [6]$$

Observing that α is the angle between the outward normal to the boundary curve C and the X-axis, there are the equations

$$\left.\begin{aligned} \sin\alpha &= -\frac{dx}{ds} \qquad \sin\alpha' = -\frac{dx'}{ds'}\\ \cos\alpha &= \frac{dy}{ds} \qquad \cos\alpha' = \frac{dy'}{ds'}\end{aligned}\right\} \quad \ldots\ldots [7]$$

Equation [4] is seen to be equivalent to

$$\lambda\, dy = dy'$$

which follows from Equation [3a]. From $dx = \lambda\, dx'$, an alternative equation connecting the lengths of arc is

$$\sin\alpha ds = \lambda \sin\alpha' ds' \quad \ldots\ldots [8]$$

Another useful relation, obtained by dividing Equation [8] by Equation [7] is

$$\lambda^2 \tan\alpha' = -\frac{dx'}{dy'} = -\frac{dx}{dy} = \tan\alpha \quad \ldots\ldots [9]$$

The stress-strain relations can be written

$$\lambda^2 e_x = \frac{\sigma_x}{\lambda^2}\frac{1}{E} - \frac{\nu}{E}(\sigma_y\lambda^2)$$

$$e_y/\lambda^2 = (\lambda^2\sigma_y)\frac{1}{E} - \frac{\nu}{E}\frac{\sigma_x}{\lambda^2}$$

and reduce to the isotropic stress-strain equations by virtue of Equations [3c] and [3d]. This transformation, by imbedding the parameter λ, formally reduces the region R bounded by the curve C of the orthotropic plane body to a region R' bounded by the curve C' in which the equations of elasticity of an isotropic body with elastic constants E, ν are applicable. Conversely, any solution of an isotropic problem can be converted into a solution of an orthotropic problem subject to the restriction that the orthotropic shear modulus G is defined by Equation [5].

The expressions for strain energy and work also transform from the orthotropic body to the isotropic body. Thus

$$u = \frac{1}{2}\left[\frac{\sigma_x^2}{E_x} + \frac{\sigma_y^2}{E_y} - \frac{2\nu_x\sigma_x\sigma_y}{E_y}\right] + \frac{\tau_{xy}^2}{2G}$$

TABLE 1 ORTHOTROPIC AND ISOTROPIC EQUATIONS

	Orthotropic Equations	Isotropic Equations
(1) Strain-displacement equations	$e_x = \frac{\partial u}{\partial x}$	$e_x' = \frac{\partial u'}{\partial x'}$
	$e_y = \frac{\partial v}{\partial y}$	$e_y' = \frac{\partial v'}{\partial y'}$
	$\gamma_{xy} = \frac{\partial u}{\partial y} + \frac{\partial y}{\partial x}$	$\gamma_{xy}' = \frac{\partial u'}{\partial y'} + \frac{\partial v'}{\partial x'}$
(2) Stress-strain relations	$e_x = \frac{\sigma_x}{E_x} - \nu_x \frac{\sigma_y}{E_y}$	$e_x' = \frac{\sigma_x'}{E} - \nu \frac{\sigma_x'}{E}$
	$e_y = \frac{\sigma_y}{E_y} - \nu_y \frac{\sigma_x}{E_x}$	$e_y' = \frac{\sigma_y'}{E} - \nu \frac{\sigma_x'}{E}$
(3) Equilibrium equations	$\frac{\partial \sigma_x}{\partial x} + \frac{\partial \tau_{xy}}{\partial x} + X = 0$	$\frac{\partial \sigma_x'}{\partial x'} + \frac{\partial \tau_{xy}'}{\partial y'} + X' = 0$
	$\frac{\partial \sigma_y}{\partial y} + \frac{\partial \tau_{xy}}{\partial x} + Y = 0$	$\frac{\partial \sigma_y'}{\partial y'} + \frac{\partial \tau_{xy}'}{\partial x'} + Y' = 0$
(4) Compatibility equation	$\frac{\partial^2 e_x}{\partial y^2} + \frac{\partial^2 e_y}{\partial x^2} = \frac{\partial^2 \gamma_{xy}}{\partial x\, \partial y}$	$\frac{\partial^2 e_x'}{\partial y'^2} + \frac{\partial^2 e_x'}{\partial x'^2} = \frac{\partial^2 \gamma_{xy}'}{\partial x' \partial y'}$
(5) Boundary displacements	$u = \bar{u}$ on C	$u' = \bar{u}'$ on C'
	$v = \bar{v}$	$v' = \bar{v}'$
(6) Boundary stresses	$\bar{X} = \sigma_x \cos \alpha + \tau_{xy} \sin \alpha$ on C	$\bar{X}' = \sigma_x' \cos \alpha' + \tau_{xy}' \sin \alpha'$ on C'
	$\bar{Y} = \sigma_y \sin \alpha + \tau_{xy} \cos \alpha$	$\bar{Y}' = \sigma_y' \sin \alpha + \tau_{xy}' \cos \alpha'$

reduces to

$$u = \frac{1}{2E} [\sigma_x'^2 + \sigma_y'^2 - 2\nu\sigma_x'\sigma_y'] + \frac{\tau_{xy}'^2}{2G'}$$

since $G = G'$.

If the displacements are single-valued for each circuit of a multiply connected region in an isotropic body, the displacements of the orthotropic body continue to be single-valued. Consequently, the transformation can be applied to multiply connected orthotropic bodies.

We note further that if F_x', F_y', M' are force and moment resultants on an arc $A'B'$ of an isotropic body, the corresponding quantities on an arc AB of an orthotropic body are

$$F_x = \lambda F_x'$$
$$F_y = F_y'/\lambda$$
$$M = M'$$

These follow directly applying the transformation to the isotropic equations given by Timoshenko (3). From J. H. Michell's investigations and the foregoing results (4), we can conclude that if the stress distribution in the multiply connected isotropic body is independent of the elastic constants, the stress distribution of the multiply connected orthotropic body depends only on the ratio of elastic moduli expressed by λ.

The fact that the stresses $(\sigma_x, \sigma_y, \tau_{xy})$ in the orthotropic body are derived from a stress function ϕ in R' by the same form of equations which determine the stresses $(\sigma_x', \sigma_y', \tau_{xy}')$ from $\phi = \phi'$ in R' can be used to obtain general curvilinear orthotropic expressions corresponding to those developed by E. Goursat, N. I. Muschelisvili, G. Kolosoff, and others (5) for isotropic bodies.

DISCUSSION OF TRANSFORMATION

The orthotropic constants (E, λ, ν) are evidently equivalent to the elastic constants (E_x, E_y, ν_x). The parameter λ which determines the amount by which E_x and E_y differ is a measure of the degree of orthotropy. When $\lambda = 1$, the orthotropic equations reduce to the isotropic equations.

The affine transformation $x = \lambda x'$, $y = y'/\lambda$ preserves infinitesimal areas and straight lines. In particular, points on the principal orthotropic axes X, Y are transformed, respectively, into points on the axes X', Y'. Angles and arc lengths are not preserved.

The more general affine transformation $x = ax'$, $y = by'$ leads to the conclusion that the transformation of the strains, stresses, moduli, and Poisson's ratios always involves the ratio a/b. Consequently, there is no loss of generality in taking $a = \lambda$ and $b = 1/\lambda$.

If we take $\gamma_{xy} = c\gamma_{xy}'$ and $\tau_{xy} = cd\,\tau_{xy}'$, the isotropic shear modulus

$$G' = \frac{\tau_{xy}'}{\gamma_{xy}'}$$

would be related to the orthotropic shear modulus

$$G = \frac{\tau_{xy}}{\gamma_{xy}}$$

by the equation $G = dG'$. We might hope in this way to remove the restriction on G. The quantity c is equivalent to increasing the surface loads and there is again no loss of generality in taking $c = 1$. The quantity d leads to the equations

$$E_x = \lambda^4 Ed, \qquad E_y = \frac{Ed}{\lambda^4}, \qquad \text{so } Ed = \sqrt{E_x E_y}$$

Since

$$E = 2G'(1 + \nu), \qquad G = dG' = \frac{\sqrt{E_x E_y}}{2(1 + \nu)}$$

and there is still a restriction on G. It can be concluded that the affine transformation of type $x = ax'$, $y = by'$ is, at most, capable of representing a three constant orthotropic body. The shear modulus is always restricted by Equation [5] which is equivalent to

$$G = \frac{\sqrt{E_x E_y}}{2(1 + \nu)}$$

where

$$\nu = \sqrt{\nu_x \nu_y} = \frac{\nu_x \sqrt{E_x}}{E_y}$$

The affine transformation of Equations [3a] and [3b] preserve the displacements $u = \alpha xy$ and $v = \alpha xx$ which occur in the torsion problem. If the parameter λ is defined by $(G_1/G_2)^{1/4}$ and the isotropic shear modulus is $G = \sqrt{G_1 G_2}$ where G_1 and G_2 are the shear moduli in the orthotropic body (referred to the principal axes of orthotropy), the equations of orthotropic torsion immediately become the equations appropriate to isotropic torsion. We can obtain all the equations given by Sokolnikoff (6) who uses, instead of Equations [3a], the equivalent transformation $x = \lambda^2 x'$ $y = y'$. The only nonvanishing stresses τ_{xz} and τ_{yz} must be referred to the principal axes of orthotropy.

The Two Definitions of Shear Modulus, G. In an orthotropic body, the moduli and Poisson's ratios vary with direction. For the arbitrary axes 1, 2 in Fig. 1(*b*), shear modulus G_{12} is

$$\frac{1}{G_{12}} = \sin^2 2\theta \left[\frac{1}{E_x} + \frac{2\nu_x}{E_y} + \frac{1}{E_y}\right] + \frac{\cos^2 2\theta}{G}$$

The general equations for transforming the elastic constants in aelotropic bodies are given by Love (7).

When $\theta = 45$ deg, we have

$$\frac{1}{G_{12}} = \left(\frac{1}{E_x} + \frac{2\nu_x}{E_y} + \frac{1}{E_y}\right) \qquad [10]$$

This is the definition of shear modulus suggested by Wolf (8). Thus Wolf chooses for the shear modulus G connected with the orthotropic axes X, Y, the value G_{12} properly related to axes intersecting the orthotropic axes. This choice of shear modulus leads to the requirement that the stress function ϕ must satisfy the equation

$$\left(\frac{\partial^2}{\partial x^2} + \frac{1}{\lambda^2}\frac{\partial^2}{\partial y^2}\right)\left(\frac{\partial^2}{\partial x^2} + \frac{\partial^2}{\partial y^2}\right)\phi = 0 \text{ (in } R) \qquad [11]$$

Consider the isotropic stress function $\phi(x', y')$ which is biharmonic in R' and apply the affine transformation. The result is that $\phi(x, y)$ satisfies, instead of Equation [11]

$$\left(\frac{\lambda^2 \partial^2}{\partial x^2} + \frac{1}{\lambda^2}\frac{\partial^2}{\partial y^2}\right)^2 \phi = 0 \text{ (in } R)$$

where

$$(\sigma_x, \sigma_y, \tau_{xy}) = \left(\frac{\partial^2}{\partial y^2}, \frac{\partial^2}{\partial x^2}, \frac{-\partial^2}{\partial x\, \partial y}\right)\phi$$

This leads to the question of determining which choice of G and which choice of ϕ is to be preferred for orthotropic plane bodies having only three independent elastic constants. For a material for which the c_{ij} have been determined, the two values of G can be computed and compared with the measured value of c_{44}. The preferred G would be that which minimized $|\, G - c_{44}\,|$. We can also argue as follows:

Write $1 + \beta$ for λ in every orthotropic equation and expand to the first order in β; the equations obtained can be regarded as defining an orthotropic stress state infinitesimally near the corresponding isotropic stress state. All stresses and strains vary to first order in β with the exception of τ_{xy} and γ_{xy}. Since the shear stress and strain remain unchanged to first order in β, it would be natural to define their ratio G exactly as in the isotropic case.

When the shear modulus is restricted by Equation [5] its value is

$$G = \frac{\sqrt{c_{11}\, c_{22}} - c_{12}}{2}$$

for plane strain. For plane stress, it has the different value

$$G = \frac{\sqrt{\overline{c_{11}}\, \overline{c_{22}}} - \overline{c_{12}}}{2}$$

This is unlike the case of isotropy, where (for constant body force) the shear modulus is unaltered by the process of replacing E and ν in a plane-stress problem by $E/1 - \nu^2$ and $\nu/1 - \nu$ to obtain the strains and displacements in the comparable plane-strain problem.

In both cases, the shear modulus of Equation [5] is greater than the shear modulus G_{12} of Equation [10] which attains its minimum value at $\theta = \pm 45$ deg.

The Half Plane Subjected to a Normal Concentrated Load

Applying the transformation to the stresses $\sigma_{x'}$, $\sigma_{y'}$, $\tau_{xy'}$ of the isotropic solution shown in Fig. 2(*a*), the orthotropic "three constant" stresses are (Fig. 2*b*)

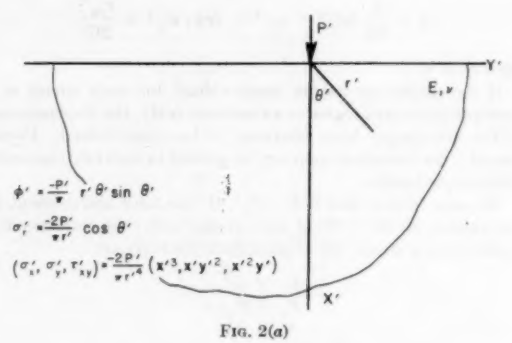

Fig. 2(*a*)

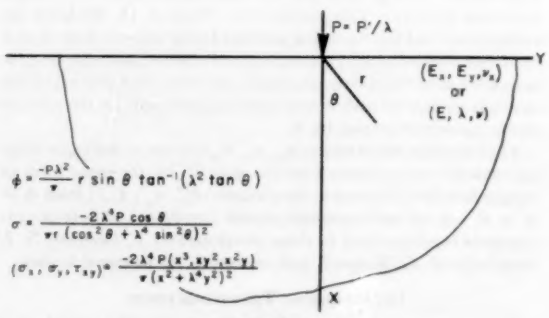

Fig. 2(*b*)

$$(\sigma_x, \sigma_y, \tau_{xy}) = \frac{-2\lambda^4 P}{\pi} \frac{(x^3, xy^2, x^2y)}{(x^2 + \lambda^4 y^2)^2} \text{ where } P = \frac{P'}{\lambda} \quad [12]$$

The polar stresses cannot be transformed directly but the stress function

$$\phi' = \phi = \frac{-\lambda^2 Pr}{\pi} \sin\theta \tan^{-1}(\lambda^2 \tan\theta) = \frac{-Py\lambda^2}{\pi} \tan^{-1}\frac{\lambda^2 y}{x}$$

The polar stresses in the orthotropic body can be found from the stress function (exactly as in the isotropic case). For example

$$\sigma_r = \frac{1}{r}\frac{\partial\phi}{\partial r} + \frac{1}{r^2}\frac{\partial^2\phi}{\partial\theta^2} = \frac{-2\lambda^4 P\cos\theta}{\pi r(\cos^2\theta + \lambda^4\sin^2\theta)^2}$$

By direct transformation, the displacements (u, v) are

$$E_x u = \frac{-P\lambda^4}{\pi}\log\frac{(x^2 + \lambda^4 y^2)}{c^2} - \frac{(1+\nu)Py^2\lambda^8}{\pi(x^2 + \lambda^4 y^2)}$$

$$E_y v = \frac{-(1-\nu)}{\pi\lambda^2} P\tan^{-1}\left(\lambda^2\frac{y}{x}\right) + \frac{(1+\nu)P\,xy}{\pi(x^2 + \lambda^4 y^2)}$$

The strains are

$$\gamma_{xy} = \frac{-4(1+\nu)Px^2y}{\pi E_y(x^2 + \lambda^4 y^2)^2}$$

$$E_x e_x = \frac{-2P\lambda^4 x}{\pi(x^2 + \lambda^4 y^2)^2}(x^2 - \nu_y y^2)$$

$$E_y e_y = \frac{-2P\lambda^4 x}{\pi(x^2 + \lambda^4 y^2)^2}(y^2 - \nu_x x^2)$$

Using the identities

$$(1-\nu^2)\sigma_x = E_x e_x + E_y\nu_y e_y$$
$$(1-\nu^2)\sigma_y = E_y e_y + E_x\nu_x e_x$$
$$\tau_{xy} = G\gamma_{xy}$$

The stresses are

$$\tau_{xy} = \frac{-4G(1+\nu)Px^2y}{\pi E_y(x^2 + \lambda^4 y^2)^2}$$

$$\sigma_x = \frac{-2Px^3}{\pi(x^2 + \lambda^4 y^2)^2}\sqrt{\frac{E_x}{E_y}}, \quad \sigma_y = \frac{-2Pxy^2}{\pi(x^2 + \lambda^4 y^2)^2}\sqrt{\frac{E_x}{E_y}}$$

It is easily verified that these stresses satisfy the equilibrium equations and are identical with the stresses obtained from Equation [12]. In the expression for $E_x u$, the constant c^2 determines a point where $u = 0$ and has no effect on the strains or displacements.

Comparison With an Alternative Solution

The same problem has recently been solved by Conway (9) using Wolf's equations [10] and [11]. Considering only the polar stress σ_r, and expressing his result in the present notation

$$\sigma_r = \frac{-P(1+\lambda^4)}{\pi r}\frac{\cos\theta}{\lambda^8\sin^2\theta + \cos^2\theta}$$

the polar stress σ_r found here is

$$\sigma = \frac{-2\lambda^4 P}{\pi r}\frac{\cos\theta}{(\cos^2\theta + \lambda^4\sin^2\theta)^2}$$

Both solutions reduce to the known isotropic solution when $\lambda = 1$. The solutions are distinctly different. This justifies the earlier comment that the form of $G = f(E_x, E_y, \nu_x)$ has a critical effect on the solution of every plane orthotropic body characterized by three independent elastic constants.

Whenever $\lambda < 1.0$, the strain-energy density of the solution of this paper is less than the strain-energy density of Conway's solution. When $\lambda > 1.0$, the converse holds and Conway's solution involves the lower amount of strain energy. Therefore, when $\lambda \neq 1$, we cannot infer in general which solution leads to minimum work and energy.

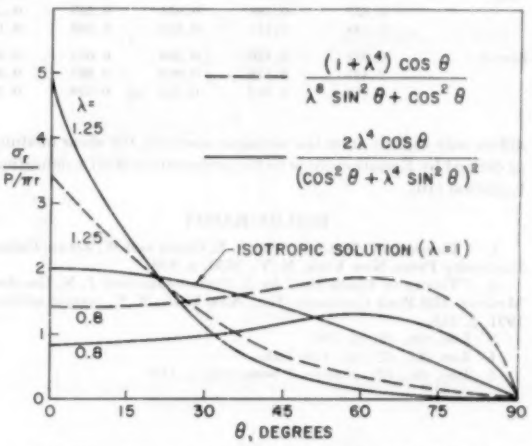

Fig. 3 Comparison of Two Solutions for the Half-Plane Problem for $\lambda = 1.25, 1.0, 0.8$
(Conway's solution – – –, present solution ——)

The solutions are compared in Fig. 3 for values of $\lambda = 0.8$, 1.0, and 1.25. When $\lambda > 1.0$, the radial stress of both solutions is greater on the axis but decays more rapidly than in the isotropic solution. When $\lambda < 1.0$, the maximum radial stress occurs at

$$\cos^2\theta = \frac{\lambda^8}{1 - \lambda^8}$$

for Conway's solution and at

$$\cos^2\theta = \frac{\lambda^4}{3(1 - \lambda^4)}$$

for the solution of this paper.

Comparison of Computed and Experimental Shear Moduli

The values of the nine elastic constants for four species of wood have been compiled by F. S. Hearmon (10). These values are reproduced in Table 2. Since any pair of axes can be identified with the axes of orthotropy X, Y, each species of wood yields three sets of plane elastic constants.

In Table 2 the measured value of the shear modulus is compared with the restriction of this paper, Equation [5], and with the definition of Wolf, Equation [10]. The shear modulus which is nearest the measured value is underlined. Of the twelve sets of elastic constants shown, the shear modulus of this paper differs least from the experimental value in four cases. The shear modulus as defined by Wolf differs least from the experimental value in seven cases. The two moduli are nearly identical in the remaining case.

It is interesting to observe that when the shear modulus of this paper is nearest the experimental value, the corresponding values of λ (underlined in Table 2) lie near unity. This conclusion supports the previous argument that when the orthotropic material

TABLE 2 ELASTIC CONSTANTS OF WOOD (REFERENCE 10)

	$E_r \times 10^{-6}$, psi	$E_\theta \times 10^{-6}$, psi	$\nu_{r\theta}$	$\nu_{\theta r}$	$E \times 10^{-6}$, psi	ν	λ	$\lambda^2 = E_r/E_\theta$	$G \times 10^{-6}$, psi (exp)	$G \times 10^{-6}$, psi (this paper)	$G \times 10^{-6}$ psi (Wolf)
Beech	0.165	1.997	0.522	0.043	0.574	0.150	0.731	0.083	0.149	0.250	0.199
	1.997	0.325	0.073	0.450	0.805	0.182	1.250	6.149	0.226	0.341	0.319
	0.325	0.165	0.370	0.727	0.231	0.519	1.088	1.962	0.064	0.076	0.215
Oak	0.140	0.829	0.505	0.085	0.339	0.207	0.800	0.168	0.110	0.140	0.140
	0.829	0.310	0.127	0.339	0.507	0.208	1.130	2.674	0.177	0.210	0.277
	0.310	0.139	0.291	0.650	0.207	0.434	1.105	2.223	0.053	0.072	0.161
Pine	0.131	2.377	0.403	0.022	0.557	0.095	0.696	0.055	0.122	0.254	0.129
	2.377	0.188	0.031	0.393	0.669	0.111	1.372	12.617	0.131	0.301	0.185
	0.188	0.131	0.415	0.599	0.157	0.499	1.047	1.442	0.109	0.526	0.151
Spruce	0.092	2.420	0.568	0.021	0.471	0.110	0.664	0.038	0.124	0.212	0.092
	2.421	0.118	0.018	0.367	0.534	0.081	1.460	20.534	0.091	0.247	0.116
	0.118	0.092	0.334	0.428	0.104	0.378	1.032	1.284	0.124	0.038	0.083

differs only slightly from the isotropic material, the shear modulus as defined by Equation [5] is to be preferred to Wolf's definition, Equation [10].

BIBLIOGRAPHY

1 "Theoretical Elasticity," by A. E. Green and W. Zerna, Oxford University Press, New York, N. Y., 1954, p. 159.

2 "Theory of Elasticity," by S. Timoshenko and J. N. Goodier, McGraw-Hill Book Company, Inc., New York, N. Y., second edition, 1951, p. 241.

3 Loc. cit., (2), p. 190.

4 Loc. cit., (2), pp. 118–120.

5 Loc. cit., (2), chapter 7 beginning p. 179.

6 "Mathematical Theory of Elasticity," by I. S. Sokolnikoff, McGraw-Hill Book Company, Inc., New York, N. Y., 1946, pp. 212–217.

7 "The Mathematical Theory of Elasticity," by A. E. Love, University Press, Cambridge, England, fourth edition, 1934, pp. 106–107.

8 "Ausbreitung der Kraft in der Halbebene bei Anisotropen Material," by K. Wolf, *Zeitschrift für angewandte Mathematik und Mechanik*, vol. 15, 1935, p. 249.

9 "Some Problems of Orthotropic Plane Stress," by H. C. Conway, JOURNAL OF APPLIED MECHANICS, Trans. ASME, vol. 75, 1953, p. 72.

10 "The Elastic Constants of Anisotropic Materials," by R. F. S. Hearmon, *Reviews of Modern Physics*, vol. 18, July, 1946, p. 429.

The Nonlinear Bending of Thin Circular Rods

By H. D. CONWAY,[1] ITHACA, N. Y.

Two examples of the nonlinear bending of thin circular rods are discussed using the Bernoulli-Euler equation, which states that the change of curvature of a rod is proportional to the bending moment producing it. Numerical results are presented.

Introduction

THE subject of the nonlinear bending of thin rods is one of great historic interest and has received renewed attention of late, solutions of various specific problems having been given by Barten (1),[2] Bisshopp and Drucker (2), Hymans (3), and the author (4). Most of the investigations have been confined to rods bent by concentrated forces or couples because of the relative simplicity of such problems. However, problems of uniformly distributed loading recently have been treated by Rohde (5) and by Truesdell (6).

The present work deals with the bending, by concentrated forces, of initially circular rods. Two cases of loading are considered.

Vertical Loading

Fig. 1 shows a rod, free at one end and clamped at the other, under the action of a vertical load P. It is assumed that the unstrained form of the rod is a circular arc of radius R, subtending an angle β at its ends. Under the action of P, the free end descends an amount $(h_0 - h)$ and moves laterally by an amount $(b - b_0)$. It is required to compute $(h_0 - h)$ and $(b - b_0)$ according to the elastica theory, assuming that the square of the derivative in the curvature formula cannot be neglected. Thus the problem is a nonlinear one.

Taking the origin at the clamped end and assuming that, in the loaded state, a tangent to the column makes an angle ϕ with the vertical, the Bernoulli-Euler equation of bending may be expressed as

$$D\frac{d\phi}{ds} - \frac{D}{R} = P(b - y) \quad [1]$$

where D is the flexural rigidity of the cross section of the rod. Differentiating with respect to s and writing $P/D = a^2$ for convenience, it follows that

$$\frac{d^2\phi}{ds^2} = -a^2 \sin\phi \quad [2]$$

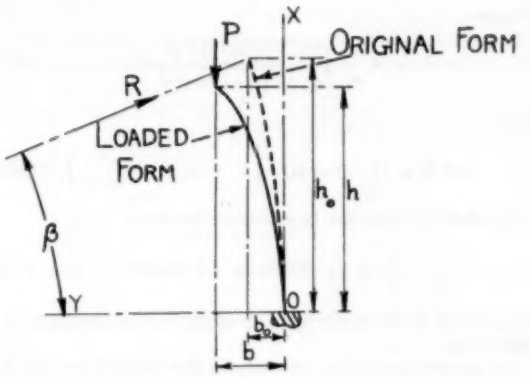

FIG. 1 ROD, FREE AT ONE END AND CLAMPED AT THE OTHER, UNDER VERTICAL LOAD P

Hence, after integrating

$$\frac{1}{2}\left(\frac{d\phi}{ds}\right)^2 = a^2\cos\phi + C(\text{const}) \quad [3]$$

At

$$y = b,\ \phi = \phi_0,\ \frac{d\phi}{ds} = \frac{1}{R} \text{ and } C = \frac{1}{2R^2} - a^2\cos\phi_0$$

Hence

$$\frac{1}{2}\left(\frac{d\phi}{ds}\right)^2 = a^2(\cos\phi - \cos\phi_0) + \frac{1}{2R^2} \quad [4]$$

At

$$y = 0,\ \phi = 0,\ \frac{d\phi}{ds} = \frac{1}{R} + a^2 b$$

and

$$\frac{1}{2}\left(\frac{1}{R} + a^2 b\right)^2 = a^2(1 - \cos\phi_0) + \frac{1}{2R^2} \quad [5]$$

After simplification, this may be written in the form

$$\frac{b^2}{R^2} + \frac{2}{a^2R^2}\frac{b}{R} - \frac{2}{a^2R^2}(1 - \cos\phi_0) = 0 \quad [6]$$

thus giving a quadratic equation connecting the unknowns b and ϕ_0. Introducing an auxiliary angle α according to the equation

$$\cos\alpha = \cos\phi_0 - \frac{1}{2a^2R^2} \quad [7]$$

Equation [4] becomes

$$\frac{d\phi}{ds} = \frac{d\phi}{dx}\frac{dx}{ds} = \frac{d\phi}{dx}\cos\phi = \sqrt{2}\,a\sqrt{\cos\phi - \cos\alpha} \quad [8]$$

---

[1] Professor of Mechanics, Cornell University.

[2] Numbers in parentheses refer to the Bibliography at the end of the paper.

Contributed by the Applied Mechanics Division and presented at the Diamond Jubilee Annual Meeting, Chicago, Ill., November 13–18, 1955, of THE AMERICAN SOCIETY OF MECHANICAL ENGINEERS.

Discussion of this paper should be addressed to the Secretary, ASME, 29 West 39th Street, New York, N. Y., and will be accepted until April 10, 1956, for publication at a later date. Discussion received after the closing date will be returned.

NOTE: Statements and opinions advanced in papers are to be understood as individual expressions of their authors and not those of the Society. Manuscript received by ASME Applied Mechanics Division, February 21, 1955. Paper No. 55—A-24.

Thus

$$h = \frac{1}{\sqrt{2}a}\int_0^{\phi_0} \frac{\cos\phi d\phi}{\sqrt{\cos\phi - \cos\alpha}} \quad \ldots\ldots [9]$$

This integral may be written in a standard form by the introduction of an angle θ, defined by

$$(1 - \cos\phi) = 2k^2\sin^2\theta = (1 - \cos\alpha)\sin^2\theta \quad \ldots [10]$$

whence

$$h = \frac{1}{a}\int_0^{\theta_1} \frac{1 - 2k^2\sin^2\theta}{\sqrt{1 - k^2\sin^2\theta}}\, d\theta \quad \ldots\ldots [11]$$

where

$$\sin^2\theta_1 = (1 - \cos\phi_0)\Big/\left(1 - \cos\phi_0 + \frac{1}{2a^2R^2}\right) \quad \ldots [12]$$

Equation [11] may now be written in the form

$$\frac{h}{R} = \frac{1}{aR}\left[2E(\theta_1, k) - F(\theta_1, k)\right] \quad \ldots\ldots [13]$$

where F and E are elliptic integrals of the first and second kind, respectively.

The remaining equation necessary for the complete solution of the problem is obtained from the assumption that the length of the axis of the rod remains unchanged. It follows from Equation [8] that

$$R\beta = \frac{1}{\sqrt{2}a}\int_0^{\phi_0} \frac{d\phi}{\sqrt{\cos\phi - \cos\alpha}}$$

hence

$$aR\beta = \int_0^{\theta_1} \frac{d\theta}{\sqrt{1 - k^2\sin^2\theta}} = F(\theta_1, k) \quad \ldots\ldots [14]$$

where F is an elliptic integral of the first kind.

The solution of the problem is now formally complete, but some explanation of the method for obtaining numerical results from Equations [6], [13], and [14] is necessary.

A suitable method for obtaining numerical results is as follows: For a specific rod, the value of the nondimensional quantity $a^2R^2 = PR^2/D$ will be known. Assuming a value of ϕ_0, the final value of the slope at the top of the rod, the values of θ_1 and k are determined from Equations [12] and [10], respectively. Using tables of elliptic integrals, Equation [14] gives the corresponding value of the angle β originally subtended by the rod, and Equations [6] and [13] give the nondimensional ratios b/R and h/R, respectively.

The deflection ratios $(b - b_0)/R$ and $(h_0 - h)/R$ are then determined. Repeating the calculations for various values of ϕ_0 (and hence β), the deflection ratios for the specific value of β required are found by interpolation.

By way of illustration, Figs. 2 and 3 show plots of $(b - b_0)/R$ and $(h_0 - h)/R$ versus β for $a^2R^2 = PR^2/D = 1$. Also shown are the results obtained from the assumption that the geometry of the rod is essentially unchanged by the loading. According to the linear theory, the nondimensional deflection ratios are

$$\left.\begin{aligned} \frac{b - b_0}{R} &= a^2R^2\left(\cos\beta - \frac{\beta}{2}\sin 2\beta - \frac{3}{4}\cos 2\beta - \frac{1}{4}\right) \\ \frac{h_0 - h}{R} &= a^2R^2\left(\beta - \frac{3}{4}\sin 2\beta + \frac{\beta}{2}\cos 2\beta\right) \end{aligned}\right\} \quad \ldots [15]$$

Horizontal Loading

For the rod loaded as shown in Fig. 4, the Bernoulli-Euler equation gives

$$D\frac{d\phi}{ds} - \frac{D}{R} = P(h - x) \quad \ldots\ldots [16]$$

whence

$$\frac{d^2\phi}{ds^2} = -a^2\cos\phi; \quad a^2 = P/D \quad \ldots\ldots [17]$$

Integrating then gives

$$\frac{1}{2}\left(\frac{d\phi}{ds}\right)^2 = -a^2\sin\phi + C(\text{const}) \quad \ldots\ldots [18]$$

At

$$x = h, \ \phi = \phi_0, \ \frac{d\phi}{ds} = \frac{1}{R}$$

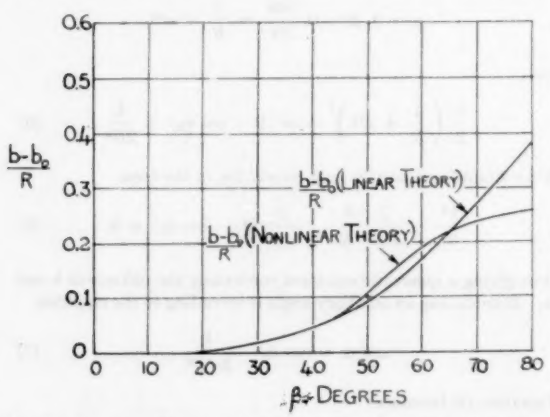

FIG. 2 GRAPH OF HORIZONTAL DEFLECTION RATIO VERSUS INITIAL ANGLE SUBTENDED FOR CIRCULAR ROD SUBJECTED TO VERTICAL LOAD

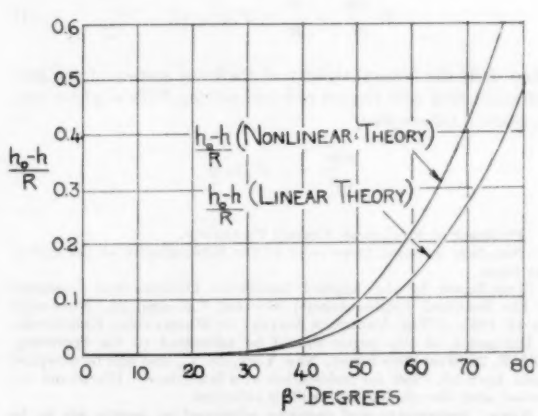

FIG. 3 GRAPH OF VERTICAL DEFLECTION RATIO VERSUS INITIAL ANGLE SUBTENDED FOR CIRCULAR ROD SUBJECTED TO VERTICAL LOAD

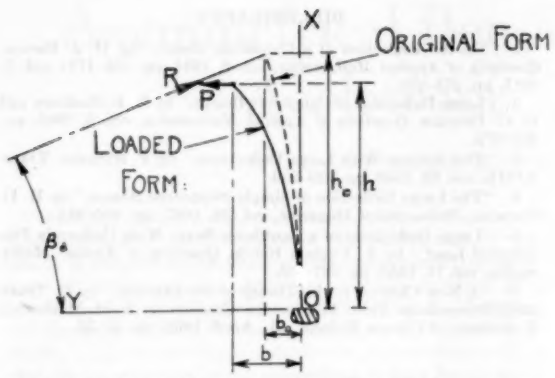

FIG. 4 ROD, FREE AT ONE END AND CLAMPED AT THE OTHER, UNDER HORIZONTAL LOAD P

and

$$C = \frac{1}{2R^2} + a^2 \sin \phi_0 \quad \ldots\ldots [19]$$

hence

$$\frac{1}{2}\left(\frac{d\phi}{ds}\right)^2 = a^2(\sin \phi_0 - \sin \phi) + \frac{1}{2R^2} \quad \ldots\ldots [20]$$

At

$$x = 0,\ \phi = 0,\ \frac{d\phi}{ds} = \frac{1}{R} + a^2 h$$

and

$$\frac{1}{2}\left(\frac{1}{R} + a^2 h\right)^2 = a^2 \sin \phi_0 + \frac{1}{2R^2} \quad \ldots\ldots [21]$$

After simplification, this becomes

$$\frac{h^2}{R^2} + \frac{2}{a^2R^2}\frac{h}{R} - \frac{2}{a^2R^2}\sin \phi_0 = 0 \quad \ldots\ldots [22]$$

Introducing an angle α such that

$$\sin \alpha = \sin \phi_0 + \frac{1}{2a^2R^2} \quad \ldots\ldots [23]$$

Equation [20] gives

$$b = \frac{1}{\sqrt{2}a}\int_0^{\phi_0} \frac{\sin \phi}{\sqrt{\sin \alpha - \sin \phi}}\, d\phi \quad \ldots\ldots [24]$$

To write this integral in standard form, introduce the angle θ such that

$$1 + \sin \phi = 2k^2 \sin^2 \theta = (1 + \sin \alpha)\sin^2 \theta \quad \ldots\ldots [25]$$

whence

$$b = \frac{1}{a}\int_{\theta_2}^{\theta_1} \frac{2k^2 \sin^2 \theta - 1}{\sqrt{1 - k^2 \sin^2 \theta}}\, d\theta \quad \ldots\ldots [26]$$

where

$$\sin^2 \theta_1 = (1 + \sin \phi_0)\Big/\left(1 + \sin \phi_0 + \frac{1}{2a^2R^2}\right),$$

$$\sin^2 \theta_2 = 1\Big/\left(1 + \sin \phi_0 + \frac{1}{2a^2R^2}\right)$$

Equation [26] may be written in the form

$$\frac{b}{R} = \frac{1}{aR}\left[F(\theta_1, k) - 2E(\theta_1, k) - F(\theta_2, k) + 2E(\theta_2, k)\right] \quad \ldots\ldots [27]$$

The remaining equation necessary for the complete solution follows from the inextensibility of the rod. From Equation [20]

$$R\beta = \frac{1}{\sqrt{2}a}\int_0^{\phi_0} \frac{d\phi}{\sqrt{\sin \alpha - \sin \phi}}$$

whence

$$aR\beta = \int_{\theta_2}^{\theta_1} \frac{d\theta}{\sqrt{1 - k^2 \sin^2 \theta}} = F(\theta_1, k) - F(\theta_2, k) \quad \ldots\ldots [28]$$

Numerical results may be obtained from Equations [22], [27],

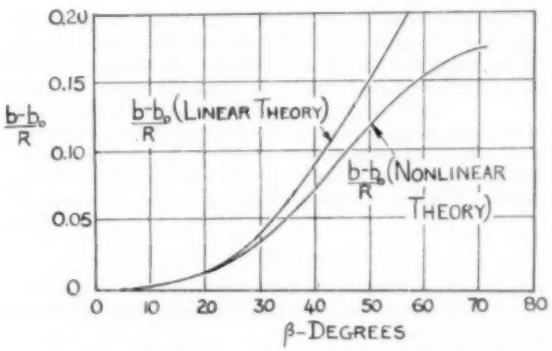

FIG. 5 GRAPH OF HORIZONTAL DEFLECTION RATIO VERSUS INITIAL ANGLE SUBTENDED FOR CIRCULAR ROD SUBJECTED TO HORIZONTAL LOAD

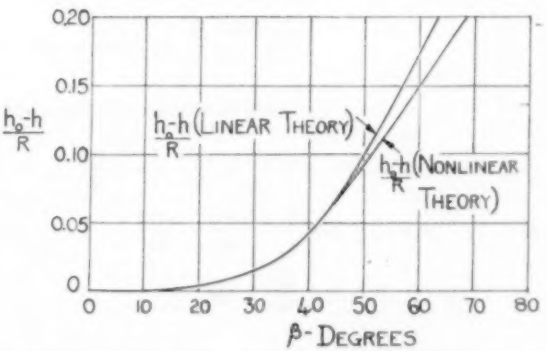

FIG. 6 GRAPH OF VERTICAL DEFLECTION RATIO VERSUS INITIAL ANGLE SUSTENDED FOR CIRCULAR ROD SUBJECTED TO HORIZONTAL LOAD

and [28] as previously explained. Figs. 5 and 6 show plots of $(b - b_0)/R$ and $(h_0 - h)/R$ versus β for $a^2R^2 = 1$, where they are compared with corresponding plots obtained from the linear theory according to which

$$\left.\begin{aligned}\frac{b - b_0}{R} &= a^2R^2\left(\beta \sin^2 \beta + \frac{3}{4}\sin 2\beta + \frac{\beta}{2} - 2\sin\beta\right)\\ \frac{h_0 - h}{R} &= a^2R^2\left(\cos\beta - \frac{3}{4}\cos 2\beta - \frac{\beta}{2}\sin 2\beta - \frac{1}{4}\right)\end{aligned}\right\} \quad [29]$$

BIBLIOGRAPHY

1 "On the Deflection of a Cantilever Beam," by H. J. Barten, *Quarterly of Applied Mathematics*, vol. 2, 1944, pp. 168–171; vol. 3, 1945, pp. 275–276.

2 "Large Deflection of Cantilever Beams," by K. E. Bisshopp and D. C. Drucker, *Quarterly of Applied Mathematics*, vol. 3, 1945, pp. 272–275.

3 "Flat Springs With Large Deflections," by F. Hymans, Trans. ASME, vol. 68, 1946, pp. 223–230.

4 "The Large Deflection of Simply Supported Beams," by H. D. Conway, *Philosophical Magazine*, vol. 38, 1947, pp. 905–911.

5 "Large Deflections of a Cantilever Beam With Uniformly Distributed Load," by F. Virginia Rohde, *Quarterly of Applied Mathematics*, vol. 11, 1953, pp. 337–338.

6 "A New Chapter in the Theory of the Elastica," by C. Truesdell, Proceedings First Midwestern Conference, Solid Mechanics, University of Illinois, Urbana, Ill., April, 1953, pp. 52–55.

Asymmetrical Bending of a Cylindrically Aeolotropic Tapered Disk

By E. S. BACLIG[1] and H. D. CONWAY,[2] ITHACA, N. Y.

Variations of thickness, anisotropy, and asymmetry of loading usually tend to increase the mathematical difficulty of obtaining solutions to the small-deflection problems of plate bending. However, for the bending of a cylindrically aeolotropic disk twisted about its diameter and having a certain thickness variation, it is possible to obtain a relatively simple solution in closed form. This solution is presented here, numerical results being given for oak and for isotropic material.

Nomenclature

The following nomenclature is used in the paper:

r, θ, z = cylindrical co-ordinates

$\epsilon_r, \epsilon_\theta, \gamma_{r\theta}$ = radial, tangential, and shear strains

$\sigma_r, \sigma_\theta, \sigma_z$ = radial, tangential, and longitudinal normal stresses

$S_{ij} (i, j = 1, 2, \ldots 6)$ = elastic constants

$M_r, M_\theta, M_{r\theta}$ = bending and twisting moments per unit length

Q_r, Q_θ = shearing forces per unit length

q = load per unit area of disk surface

w = deflection of middle surface of disk

r_o, r_i = outer and inner radii of disk

x = dimensionless ratio r/r_o

k = ratio r_i/r_o

h = disk thickness taken as $h = h_o(r/r_o)^{-n/3}$. At outer radius, $h = h_o$

D = flexural rigidity $D = \dfrac{S_{22}h^3}{12(S_{11}S_{22} - S_{12}^2)}$

M = external twisting moment applied to disk

$b = \dfrac{2(S_{11}S_{22} - S_{12}^2) - S_{12}S_{66}}{S_{22}S_{66}} = 1$ for isotropy

$c = S_{11}/S_{22} = 1$ for isotropy

$\mu = -S_{12}/S_{22}$ = Poisson's ratio ν for isotropy[3]

$\alpha = \dfrac{2b + 1}{c} = 3$ for isotropy

$\beta = \mu/c$ = Poisson's ratio ν for isotropy

$\gamma = 1/c = 1$ for isotropy

Introduction

A material is said to be cylindrically aeolotropic if its elastic constants, referred to the cylindrical co-ordinate system, are independent of the radial co-ordinate r and remain invariant by (a) rotation about the z-axis, (b) translation along the z-axis, and (c) reversal of the z-axis. The stress-strain equations for such a material are of the form

$$\epsilon_\theta = S_{11}\sigma_\theta + S_{12}\sigma_r$$

$$\epsilon_r = S_{12}\sigma_\theta + S_{22}\sigma_r$$

$$\gamma_{r\theta} = S_{44}\tau_{r\theta}$$

The foregoing definition has been given by Carrier[4] who has developed a small-deflection theory for the bending of cylindrically aeolotropic plates of constant thickness and has given specific solutions. Using this theory, Sen Gupta[5] has discussed the case of a circular plate carrying an eccentric normal load.

The theory will be generalized here by allowing the thickness of the plate to vary, and a closed-form solution will be given for a circular disk with a rigid central core twisted about a diameter. The isotropic version of the problem has been discussed by Gradwell.[6]

Basic Equations

Making the usual assumptions of small-deflection plate theory, Carrier[4] has shown that the bending moments are given by

$$\left.\begin{aligned} M_r &= -D\left[c\,\frac{\partial^2 w}{\partial r^2} + \mu\left(\frac{1}{r}\,\frac{\partial w}{\partial r} + \frac{1}{r^2}\,\frac{\partial^2 w}{\partial \theta^2}\right)\right] \\ M_\theta &= -D\left[\frac{1}{r}\,\frac{\partial w}{\partial r} + \frac{1}{r^2}\,\frac{\partial^2 w}{\partial \theta^2} + \mu\,\frac{\partial^2 w}{\partial r^2}\right] \\ M_{r\theta} &= D(b - \mu)\,\frac{\partial}{\partial r}\left(\frac{1}{r}\,\frac{\partial w}{\partial \theta}\right) \end{aligned}\right\} \quad \ldots [1]$$

The equations of equilibrium are

$$\left.\begin{aligned} \frac{\partial M_r}{\partial r} - \frac{1}{r}\,\frac{\partial M_{r\theta}}{\partial \theta} + \frac{1}{r}\,(M_r - M_\theta) - Q_r &= 0 \\ \frac{1}{r}\,\frac{\partial M_\theta}{\partial \theta} - \frac{\partial M_{r\theta}}{\partial r} - \frac{2}{r}\,M_{r\theta} - Q_\theta &= 0 \\ \frac{\partial}{\partial r}\,(rQ_r) + \frac{\partial Q_\theta}{\partial \theta} + qr &= 0 \end{aligned}\right\} \quad \ldots [2]$$

from which, by eliminating the shearing forces, we obtain

---

[1] Captain, Philippines Military Academy, Baguio City, Philippines; formerly, Graduate Student, Department of Mechanics, Cornell University, Ithaca, N. Y.

[2] Professor of Mechanics, Cornell University, Ithaca, N. Y.

[3] In the Nomenclature of Carrier's paper,[4] this ratio is incorrectly defined as $-S_{12}/S_{11}$ due to a typographical error. The exponent 2 also is missing in S_{12} in the expression for D.

Contributed by the Applied Mechanics Division and presented at the Diamond Jubilee Annual Meeting, Chicago, Ill., November 13–18, 1955, of The American Society of Mechanical Engineers.

Discussion of this paper should be addressed to the Secretary, ASME, 29 West 39th Street, New York, N. Y., and will be accepted until April 10, 1956, for publication at a later date. Discussion received after the closing date will be returned.

Note: Statements and opinions advanced in papers are to be understood as individual expressions of their authors and not those of the Society. Manuscript received by ASME Applied Mechanics Division, November 17, 1954. Paper No. 55—A-20.

[4] "The Bending of the Cylindrically Aeolotropic Plate," by G. F. Carrier, Trans. ASME, vol. 66, 1944, p. 129.

[5] "Bending of a Cylindrically Aeolotropic Circular Plate With Eccentric Load," by A. M. Sen Gupta, Journal of Applied Mechanics, Trans. ASME, vol. 74, 1952, p. 9.

[6] "Asymmetrical Bending of Tapered Discs," by C. F. Gradwell, *Aircraft Engineering*, vol. 22, 1950, p. 209.

$$\frac{\partial}{\partial r}(2M_r - M_\theta) - 2\frac{\partial^2 M_{r\theta}}{\partial r \partial \theta} + r\frac{\partial^2 M_r}{\partial r^2} + \frac{1}{r}\frac{\partial^2 M_\theta}{\partial \theta^2} - \frac{2}{r}\frac{\partial M_{r\theta}}{\partial \theta} = -qr \quad [3]$$

Substituting Equations [1] in [3] and assuming that D is now a function of r, we obtain, after some reduction

$$D\left[c\frac{\partial^4 w}{\partial r^4} + \frac{2c}{r}\frac{\partial^3 w}{\partial r^3} - \frac{1}{r^2}\frac{\partial^2 w}{\partial r^2} + \frac{1}{r^3}\frac{\partial w}{\partial r} + \frac{2b}{r^2}\frac{\partial^4 w}{\partial r^2 \partial \theta^2} - \frac{2b}{r^3}\frac{\partial^3 w}{\partial r \partial \theta^2} + \frac{2(b+1)}{r^4}\frac{\partial^2 w}{\partial \theta^2} + \frac{1}{r^4}\frac{\partial^4 w}{\partial \theta^4}\right] + \frac{dD}{dr}\left[2c\frac{\partial^3 w}{\partial r^3} + \frac{2c+\mu}{r}\frac{\partial^2 w}{\partial r^2} - \frac{1}{r^2}\frac{\partial w}{\partial r} + \frac{2b}{r^2}\frac{\partial^3 w}{\partial r \partial \theta^2} - \frac{2b+1}{r^3}\frac{\partial^2 w}{\partial \theta^2}\right] + \frac{d^2 D}{dr^2}\left[c\frac{\partial^2 w}{\partial r^2} + \frac{\mu}{r}\frac{\partial w}{\partial r} + \frac{\mu}{r^2}\frac{\partial^2 w}{\partial \theta^2}\right] = q \quad [4]$$

This is the differential equation to be solved.

Analysis

To solve the problem of a disk twisted about a diameter by a couple applied to a rigid core at the center, we assume a deflection of the form

$$w = R(r)\cos\theta$$

where θ is measured from a diameter at right angles to that about which the plate is twisted. It will be seen later that this equation can be made to satisfy the boundary conditions of our problem and, as $q = 0$, Equation [4] reduces to

$$R^{iv} + 2\left[\frac{1}{r} + \frac{D'}{D}\right]R''' + \left[-\frac{2b+1}{cr^2} + \frac{2c+\mu}{cr}\frac{D'}{D} + \frac{D''}{D}\right]R'' + \left[\frac{2b+1}{cr^3} - \frac{2b+1}{cr^2}\frac{D'}{D} + \frac{\mu}{cr}\frac{D''}{D}\right]R' + \left[-\frac{2b+1}{cr^4} + \frac{2b+1}{cr^3}\frac{D'}{D} - \frac{\mu}{cr^2}\frac{D''}{D}\right]R = 0$$

This equation may be made homogeneous by assuming that the disk thickness h varies as an arbitrary power of the radius r. Then, if D_o is the flexural rigidity at the outer radius

$$D = D_o\left(\frac{r}{r_o}\right)^{-n}, \quad \frac{D'}{D} = -\frac{n}{r}, \quad \frac{D''}{D} = \frac{n(n+1)}{r^2}$$

With this assumption, the differential equation simplifies to

$$r^4R^{iv} + 2(1-n)r^3R''' - [n(1-n) + (\alpha+\beta n)]r^2R'' + r[(n+1)(\alpha+\beta n)]R' - [(n+1)(\alpha+\beta n)]R = 0$$

which, by the transformation $z = \ln r$, becomes the homogeneous equation

$$\frac{d^4R}{dz^4} - 2(n+2)\frac{d^3R}{dz^3} + [(n^2+5n+5) - (\alpha+\beta n)]\frac{d^2R}{dz^2} + (n+2)[(\alpha+\beta n) - (n+1)]\frac{dR}{dz} - (n+1)(\alpha+\beta n)R = 0 \quad [5]$$

For solutions of the form $R = e^{\lambda z}$, its characteristic equation factors to

$$[\lambda - 1][\lambda - (n+1)][\lambda^2 - (n+2)\lambda - (\alpha+\beta n)] = 0$$

which has roots

$$\lambda = 1, \quad (n+1);$$

$$\lambda_3, \lambda_4 = \frac{(n+2) \pm \sqrt{(n+2)^2 + 4(\alpha+\beta n)}}{2}$$

In practice, the materials used have elastic constants which give positive values of α and β; moreover, the usual taper gives a decrease in thickness toward the rim of the disk; that is, n is positive. Hence the roots of the characteristic equation are real and distinct. The deflection is then of the form

$$w = [A_1 r + A_2 r^{(n+1)} + A_3 r^{\lambda_3} + A_4 r^{\lambda_4}]\cos\theta \quad [6]$$

The constants of integration will now be determined from the boundary conditions. Considering first the equilibrium of a circular portion of the disk at radius r as shown in Fig. 1, we have

$$M = \int_0^{2\pi}(M_{r\theta}\sin\theta + M_r\cos\theta - rQ_r\cos\theta)r\,d\theta$$

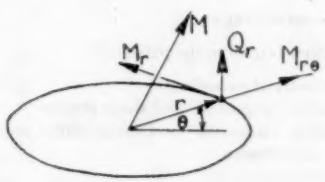

Fig. 1

Using Equations [1] and [2] to express the integrand in terms of w, we have after integration and Equation [6]

$$\frac{M}{\pi cD} = -n[(\alpha+1) + n(\beta+1)]A_2 r^n + (\lambda_3 - 1)[\lambda_3^2 - (n+2)\lambda_3 - (\alpha+\beta n)]A_3 r^{\lambda_3 - 1} + (\lambda_4 - 1)[\lambda_4^2 - (n+2)\lambda_4 - (\alpha+\beta n)]A_4 r^{\lambda_4 - 1}$$

Since λ_3 and λ_4 are the roots of $\lambda^2 - (n+2)\lambda - (\alpha+\beta n) = 0$, the foregoing equation simplifies to

$$\frac{M}{\pi cD} = -n[(\alpha+1) + n(\beta+1)]A_2 r^n$$

or, because $Dr^n = D_o r_o^n$, we have finally A_2 in terms of the external twisting moment M as

$$A_2 = -\frac{M}{\pi cnD_o r_o^n[(\alpha+1) + n(\beta+1)]} \quad [7]$$

Before proceeding to evaluate the remaining constants it will be found convenient to introduce the dimensionless radius x defined as $x = r/r_o$. Equation [6] then becomes

$$w = [a_1 x + a_2 x^{(n+1)} + a_3 x^{\lambda_3} + a_4 x^{\lambda_4}]\cos\theta \quad [8]$$

and a_2 from Equation [7] is

$$a_2 = -\frac{Mr_o}{\pi cnD_o[(\alpha+1) + n(\beta+1)]} \quad [9]$$

To establish the boundary conditions on w, consider the effects of a small rotation ϕ of the disk about the diameter for which $\theta = 90$ deg. This rotation produces the rotation ψ at r as shown in Fig. 2.

The effect of edge supports will now be considered

Case 1 Outer Edge Clamped. With the outer edge clamped, the shape of the mid-surface along a radius of the disk will be as shown in Fig. 3. From Fig. 3 the boundary conditions on w for this case are

$$x = k, \begin{cases} w = 0 \\ \dfrac{\partial w}{\partial r} = \dfrac{1}{r_o}\dfrac{\partial w}{\partial x} = 0 \end{cases} \quad \text{or} \quad R(x) = dR/dx = 0$$

$$x = 1, \begin{cases} w = -r_o\phi\cos\theta \\ \dfrac{\partial w}{\partial r} = \dfrac{1}{r_o}\dfrac{\partial w}{\partial x} = -\phi\cos\theta \end{cases} \quad \text{or} \quad R(x) = dR/dx = -r_o\phi$$

The foregoing boundary conditions then give the following system of equations for the evaluation of a_1, a_2, a_3, and a_4

$$a_1 + a_2k^n + a_3k^{\lambda_3-1} + a_4k^{\lambda_4-1} = 0$$

$$a_1 + (n+1)a_2k^n + \lambda_3a_3k^{\lambda_3-1} + \lambda_4a_4k^{\lambda_4-1} = 0$$

$$a_1 + a_2 + a_3 + a_4 = -r_o\phi$$

$$a_1 + (n+1)a_2 + \lambda_3a_3 + \lambda_4a_4 = -r_o\phi$$

Setting Δ equal to the determinant of the coefficients of the equations, we have, after considerable reduction

$$\Delta = k^n[-2n(\lambda_3 - \lambda_4) + (\lambda_3 - 1)^2(k^{\lambda_3-1} + k^{1-\lambda_3}) - (\lambda_4 - 1)^2(k^{\lambda_3-1} + k^{1-\lambda_3})]$$

and obtain as the solution for the constants of integration

$$a_1 = \frac{k^nr_o\phi}{\Delta}[n(\lambda_3 - \lambda_4) - (\lambda_3 - 1)^2k^{\lambda_3-1} + (\lambda_4 - 1)^2k^{\lambda_3-1}]$$

$$a_2 = \frac{k^nr_o\phi}{\Delta}[(\lambda_3 - 1)(\lambda_4 - 1)(k^{1-\lambda_4} - k^{1-\lambda_3})]$$

$$a_3 = \frac{k^nr_o\phi}{\Delta}[n(\lambda_4 - 1)(k^{1-\lambda_3} - 1)]$$

$$a_4 = -\frac{k^nr_o\phi}{\Delta}[n(\lambda_3 - 1)(k^{1-\lambda_4} - 1)]$$

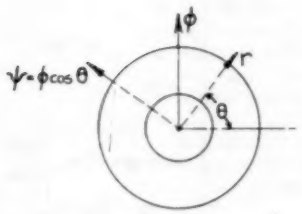

FIG. 2

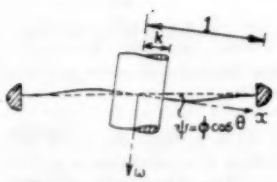

FIG. 3

Thus from Equation [9]

$$\frac{k^nr_o\phi}{\Delta} = \frac{Mr_o}{\pi cD_on[(\alpha+1) + n(\beta+1)]^2[k^{1-\lambda_4} - k^{1-\lambda_3}]}$$

and from Equation [1]

$$M_r = -\frac{D}{r^2}ex^{(n+2)}[n(n+\beta+1)a_2x^{-1} + (\lambda_3 - 1)(\lambda_3 + \beta)a_3x^{-\lambda_3} + (\lambda_4 - 1)(\lambda_4 + \beta)a_4x^{-\lambda_4}]\cos\theta$$

$$M_\theta = -\frac{D}{r^2}(b+\mu)x^{(n+2)}[(1+\mu\{n+1\})a_2x^{-1} + (\lambda_3 - 1)(\mu\lambda_3 + 1)a_3x^{-\lambda_3} + (\lambda_4 - 1)(\mu\lambda_4 + 1)a_4x^{-\lambda_4}]\cos\theta$$

$$M_{r\theta} = -\frac{D}{r^2}(b+\mu)x^{(n+2)}[na_2x^{-1} + (\lambda_3 - 1)a_3x^{-\lambda_3} + (\lambda_4 - 1)a_4x^{-\lambda_4}]\sin\theta$$

By substituting the values of the constants already obtained, we have

$$M_r = \frac{M\cos\theta}{\pi r_o[(\alpha+1) + n(\beta+1)]}\left\{(n+\beta+1)x^{-1} + (\lambda_3+\beta)\left[\frac{k^{1-\lambda_3} - 1}{k^{1-\lambda_4} - k^{1-\lambda_3}}\right]x^{-\lambda_3} - (\lambda_4+\beta)\left[\frac{k^{1-\lambda_4} - 1}{k^{1-\lambda_4} - k^{1-\lambda_3}}\right]x^{-\lambda_4}\right\} \quad [10]$$

$$M_\theta = \frac{M\cos\theta}{\pi r_o[(\alpha+1) + n(\beta+1)]}\left\{[\gamma + \beta(n+1)]x^{-1} + (\beta\lambda_3 + \gamma)\left[\frac{k^{1-\lambda_3} - 1}{k^{1-\lambda_4} - k^{1-\lambda_3}}\right]x^{-\lambda_3} - (\beta\lambda_4 + \gamma)\left[\frac{k^{1-\lambda_4} - 1}{k^{1-\lambda_4} - k^{1-\lambda_3}}\right]x^{-\lambda_4}\right\} \quad [11]$$

$$M_{r\theta} = \frac{M\sin\theta}{\pi r_o[(\alpha+1) + n(\beta+1)]}\left(\frac{\alpha-\gamma}{2} - \beta\right)\left\{x^{-1} + \left[\frac{k^{1-\lambda_3} - 1}{k^{1-\lambda_4} - k^{1-\lambda_3}}\right]x^{-\lambda_3} - \left[\frac{k^{1-\lambda_4} - 1}{k^{1-\lambda_4} - k^{1-\lambda_3}}\right]x^{-\lambda_4}\right\} \quad [12]$$

where $\alpha = \dfrac{2b+1}{c}$, $\beta = \mu/c$, and $\gamma = 1/c$

Case 2 Outer Edge Simply Supported. With the outer edge simply supported, the deflection of the middle surface along a radius r of the disk caused by the rotation ϕ is as shown in Fig. 4. It will be seen that the boundary conditions are

$$x = k, \begin{cases} w = 0 \\ \dfrac{\partial w}{\partial r} = \dfrac{1}{r_o}\dfrac{\partial w}{\partial x} = 0 \end{cases} \quad \text{or} \quad R(x) = \frac{dR}{dx} = 0$$

$$x = 1, \begin{cases} w = -r_o\phi\cos\theta \\ M_r = 0 \end{cases}$$

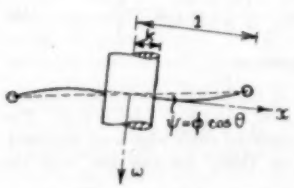

FIG. 4

The foregoing conditions result in the following system of equations in the four constants of integration a_1, a_2, a_3, and a_4

$$a_1 + k^na_2 + k^{\lambda_3-1}a_3 + k^{\lambda_4-1}a_4 = 0$$

$$a_1 + (n+1)k^na_2 + \lambda_3k^{\lambda_3-1}a_3 + \lambda_4k^{\lambda_4-1}a_4 = 0$$

$$a_1 + a_3 + a_3 + a_4 = -r_o\phi$$
$$n(n + \beta + 1)a_2 + (\lambda_3 - 1)(\lambda_3 + \beta)a_3 + (\lambda_4 - 1)(\lambda_4 + \beta)a_4 = 0$$

from which, after reduction and simplification, the determinant equal to the coefficients of the equations gives

$$\Delta = k^n[-2n(n + \beta + 1)(\lambda_3 - \lambda_4) - (\lambda_4 - 1)^2(\lambda_4 + \beta)k^{\lambda_3 - 1} + (\lambda_3 - 1)^2(\lambda_3 + \beta)k^{\lambda_4 - 1} + (\lambda_3 - 1)^2(n + \beta + \lambda_4)k^{1-\lambda_4} - (\lambda_4 - 1)^2(n + \beta + \lambda_3)k^{1-\lambda_3}]$$

The constants of integration are then

$$a_1 = \frac{k^n r_o\phi}{\Delta}[-(\lambda_3 - 1)^2(\lambda_3 + \beta)k^{\lambda_4 - 1} + (\lambda_4 - 1)(\lambda_4 + \beta)k^{\lambda_3 - 1} + n(n + \beta + 1)(\lambda_3 - \lambda_4)]$$

$$a_2 = -\frac{k^n r_o\phi}{\Delta}(\lambda_3 - 1)(\lambda_4 - 1)[(\lambda_4 + \beta)k^{1-\lambda_3} - (\lambda_3 + \beta)^{1-\lambda_4}]$$

$$a_3 = \frac{k^n r_o\phi}{\Delta} n(\lambda_4 - 1)[(n + \beta + 1)k^{1-\lambda_3} - (\lambda_4 + \beta)]$$

$$a_4 = -\frac{k^n r_o\phi}{\Delta} n(\lambda_3 - 1)[(n + \beta + 1)k^{1-\lambda_4} - (\lambda_3 + \beta)]$$

Thus from Equation [9]

$$\frac{k^n r_o\phi}{\Delta} = \frac{Mr_o}{\pi c D_o n[(\alpha + 1) + n(\beta + 1)]^2 [(\lambda_4 + \beta)k^{1-\lambda_4} - (\lambda_3 + \beta)k^{1-\lambda_3}]}$$

The bending moments are

$$M_r = \frac{M\cos\theta}{\pi r_o[(\alpha + 1) + n(\beta + 1)]}\left\{(n + \beta + 1)x^{-1} + (\lambda_3 + \beta)\frac{(n + \beta + 1)k^{1-\lambda_3} - (\lambda_4 + \beta)}{(\lambda_4 + \beta)k^{1-\lambda_4} - (\lambda_3 + \beta)k^{1-\lambda_3}}x^{-\lambda_3} - (\lambda_4 + \beta)\frac{(n + \beta + 1)k^{1-\lambda_4} - (\lambda_3 + \beta)}{(\lambda_4 + \beta)k^{1-\lambda_4} - (\lambda_3 + \beta)k^{1-\lambda_3}}x^{-\lambda_4}\right\} \quad [13]$$

$$M_\theta = \frac{M\cos\theta}{\pi r_o[(\alpha + 1) + n(\beta + 1)]}\left\{[\gamma + \beta(n + 1)]x^{-1} + (\beta\lambda_3 + \gamma)\frac{(n + \beta + 1)k^{1-\lambda_3} - (\lambda_4 + \beta)}{(\lambda_4 + \beta)k^{1-\lambda_4} - (\lambda_3 + \beta)k^{1-\lambda_3}}x^{-\lambda_3} - (\beta\lambda_4 + \gamma)\frac{(n + \beta + 1)k^{1-\lambda_4} - (\lambda_3 + \beta)}{(\lambda_4 + \beta)k^{1-\lambda_4} - (\lambda_3 + \beta)k^{1-\lambda_3}}x^{-\lambda_4}\right\} \quad [14]$$

$$M_{r\theta} = \frac{M\sin\theta}{\pi r_o[(\alpha + 1] + n(\beta + 1)]}\left(\frac{\alpha - \gamma}{2} - \beta\right)\left\{x^{-1} + \frac{(n + \beta + 1)k^{1-\lambda_3} - (\lambda_4 + \beta)}{(\lambda_4 + \beta)k^{1-\lambda_4} - (\lambda_3 + \beta)k^{1-\lambda_3}}x^{-\lambda_3} - \frac{(n + \beta + 1)k^{1-\lambda_4} - (\lambda_3 + \beta)}{(\lambda_4 + \beta)k^{1-\lambda_4} - (\lambda_3 + \beta)k^{1-\lambda_3}}x^{-\lambda_4}\right\} \quad [15]$$

Examples

To obtain numerical values of the bending moments, analyses were made for the case where $n = 1$ and $k = r_i/r_o = 0.25$. The cases of built-in and simply supported outer edge were analyzed. The elastic constants given by Hörig[7] for oak are, with the present notation, $S_{11} = 0.01015$, $S_{12} = -0.003$, $S_{22} = 0.00457$, and $S_{66} = 0.025$ mm²/kg. From these it is found that $\alpha = 1.64$, $\beta = 0.30$, and $\gamma = 0.45$ and hence the characteristic equation has the roots $\lambda_3 = 3.55$ and $\lambda_4 = -0.55$.

The results of the analyses are presented in Figs. 5, 6, and 7, where the bending and twisting moments are compared with those for isotropic material.

[7] "Anwendung der Elastizitätstheorie Anisotroper Körper auf Messungen an Holz," by H. Hörig, *Ingenieur Archiv*, vol. 6, 1935, p. 8.

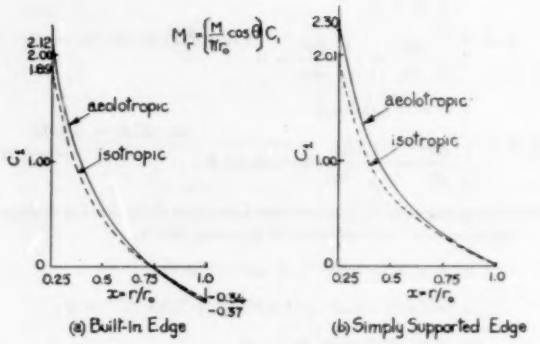

Fig. 5 Effect of Aeolotropy on Bending Moment M_r of a Tapered Disk

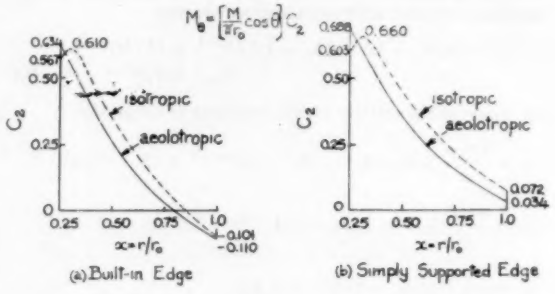

Fig. 6 Effect of Aeolotropy on Bending Moment M_θ of a Tapered Disk

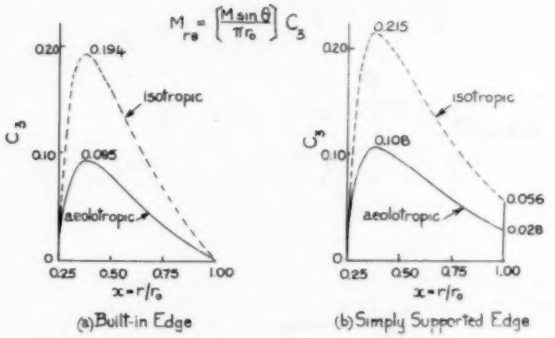

Fig. 7 Effect of Aeolotropy on Twisting Moment $M_{r\theta}$ of a Tapered Disk

Theoretical Determination of Rigidity Properties of Orthogonally Stiffened Plates[1]

By N. J. HUFFINGTON, JR.,[2] BLACKSBURG, VA.

The analysis of bending and buckling of orthogonally stiffened plates may be simplified by conceptually replacing the plate-stiffener combination by an "equivalent" homogeneous orthotropic plate of constant thickness. This procedure requires the determination of the four elastic rigidity constants which occur in the theory of thin orthotropic plates. Methods are presented whereby these quantities may be determined analytically in terms of the elastic constants and geometrical configuration of the component parts of the structure.

Nomenclature

The following nomenclature is used in the paper:

$D = \dfrac{Eh^3}{12(1-\nu^2)}$, flexural rigidity of isotropic plate

D_x, D_y, D_{xy}, D_1 = rigidity constants of orthotropic plate

E = Young's modulus of isotropic material

G = shear modulus of isotropic material

I = moment of inertia of beam

$V_y = -D\left[\dfrac{\partial^3 w}{\partial y^3} + (2-\nu)\dfrac{\partial^3 w}{\partial x^2 \partial y}\right]$, Kirchhoff shear reaction at boundary y = const

a = width of plate in x-direction

b = width of plate in y-direction

c = half-width of plate segment, y-direction

e = half-width of stiffener

f = height of stiffener

h = thickness of plate

p = applied pressure

s = $2(c + e)$, width of repeating section

w = displacement function, z-direction

w_b = displacement of beams

ν = Poisson's ratio of isotropic material

Introduction

The investigation of the bending displacements and stresses of orthogonally stiffened plates from the viewpoint of the theory of thin orthotropic plates of constant thickness has been discussed by several writers (1, 2, 3, 4, 5).[3] There are two phases to the analysis of stiffened plates by this method. First, effective elastic rigidity constants D_x, D_y, D_{xy}, and D_1 must be determined for use in the differential equation (6)

$$D_x \frac{\partial^4 w}{\partial x^4} + 2(D_1 + 2D_{xy}) \frac{\partial^4 w}{\partial x^2 \partial y^2} + D_y \frac{\partial^4 w}{\partial y^4} = p(x, y) \quad \ldots\ldots [1]$$

The second phase of the analysis involves finding a solution of Equation [1] satisfying the existing boundary conditions. This latter problem has been dealt with in the literature for many particular sets of boundary conditions and will not be considered further here.

The flexural and twisting rigidity constants D_x, D_y, D_{xy}, and D_1 are conceived as applying to a homogeneous orthotropic plate of constant thickness which is equivalent to the actual plate-stiffener combination. The term equivalent requires careful definition since the orthotropic plate obviously cannot be equivalent to the stiffened plate in every respect. For example, one might require that either the deflections or one of the strain components of the actual and equivalent orthotropic plates be the same at some point within the plate boundaries when the plates have the same loading and boundary conditions. Or one might require that the mean difference in deflections (or of strain components) of the actual and equivalent plates be zero. Still another possibility is to base equivalence upon equality of strain energies. If the application of these various criteria for equivalence were to result in significantly different sets of orthotropic constants, then clearly the concept of analyzing the stiffened plate with the aid of orthotropic plate theory would be useless. However, both experimental results (5, 7) and conclusions from the present investigation indicate that orthotropic plate theory is applicable to stiffened plates provided that the ratios of stiffener spacing to plate-boundary dimensions are small enough (s/a, $s/b \ll 1$) to insure approximate homogeneity of stiffness.

In admitting the applicability of orthotropic plate theory to the problem of the orthogonally stiffened plate, one tacitly accepts the principle that the flexural and twisting rigidity factors do not depend on the boundary conditions of the plate or on the distribution of the transverse load. This principle, coupled with an equivalence criterion, provides a basis for the determination of the effective rigidity factors. For, if the deflections of both actual and equivalent orthotropic plates can be found for some applied loading and a particular set of boundary conditions, the application of the equivalence criterion will provide an equation in which the only unknown quantities are the desired rigidity factors. Clearly, it is advantageous to choose cases of boundary conditions and applied loads, each of which will involve but one of the rigidity constants.

To reduce the complexity of presentation, the methods of determination of D_x, D_y, D_{xy}, and D_1 will be explained initially for the restricted case of equally spaced stiffeners of rectangular cross

---

[1] From a dissertation submitted in partial fulfillment of the requirements for the degree of Doctor of Engineering, The Johns Hopkins University, Baltimore, Md., May, 1954.

[2] Associate Professor of Applied Mechanics, Virginia Polytechnic Institute. Assoc. Mem. ASME.

Contributed by the Applied Mechanics Division and presented at the Diamond Jubilee Annual Meeting, Chicago, Ill., November 13–18, 1955, of The American Society of Mechanical Engineers.

Discussion of this paper should be addressed to the Secretary, ASME, 29 West 39th Street, New York, N. Y., and will be accepted until April 10, 1956, for publication at a later date. Discussion received after the closing date will be returned.

Note: Statements and opinions advanced in papers are to be understood as individual expressions of their authors and not those of the Society. Manuscript received by ASME Applied Mechanics Division, December 17, 1954. Paper No. 55—A-12.

[3] Numbers in parentheses refer to the Bibliography at the end of the paper.

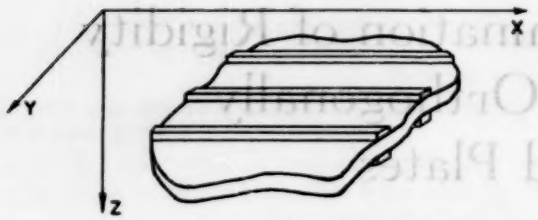

FIG. 1 PORTION OF STIFFENED PLATE

section, disposed symmetrically with respect to the middle plane of the plate, Fig. 1. As a further simplification, it is assumed that the plate and stiffeners are fabricated of the same isotropic material and that a perfect bond exists between stiffeners and plate. The strain-energy criterion will be used in the determination of all constants except D_1, for which special consideration is indicated.

DETERMINATION OF D_x

One of the symmetry directions of the equivalent orthotropic plate will coincide with the direction of the stiffeners on the actual plate. Taking the x-co-ordinate direction to be parallel to the stiffeners, the orthotropic flexural rigidity associated with bending in the direction of the stiffeners will be denoted by D_x. Consider

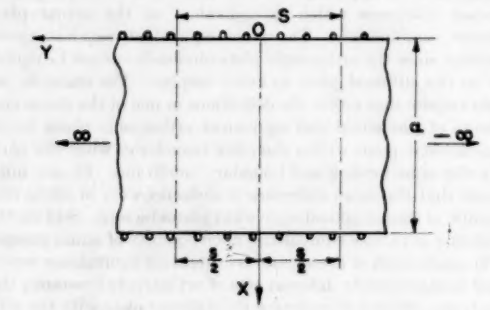

(a)

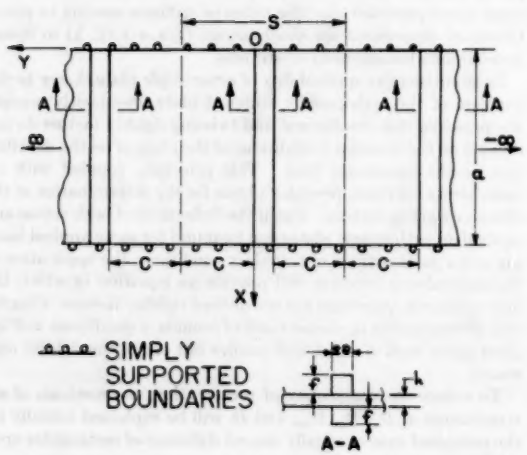

(b)

FIG. 2 GEOMETRY OF INFINITELY LONG STRIPS

an infinitely long strip of the equivalent orthotropic plate, having simply supported boundaries at $x = 0$ and $x = a$, Fig. 2(a), which is loaded by a uniform pressure p_0. The strip will be deformed to the cylindrical surface

$$w = \frac{p_0}{24D_x}(x^4 - 2ax^3 + a^3x) \quad [2]$$

in which the only elastic parameter is the desired flexural rigidity.

In the analysis of the actual stiffened plate, Fig. 2(b), this composite structure will be considered as made up of a series of plates of width $2c$, separated by beams of rectangular cross section having width $2e$ and depth $2f + h$. The deflections of this structure are periodic in y, recurring for each repeating section of width s. Owing to symmetry, in the determination of displacements, it is only necessary to consider one half of a plate (width $= c$) and one stiffener.

The plate deflections must satisfy the Lagrange differential equation

$$D\nabla^4 w = p_0 \quad [3]$$

while the beam deflections satisfy the equation

$$EI\frac{d^4w_b}{dx^4} = 2ep_0 + 2V_y|_{y=0} \quad [4]$$

The boundary conditions for the plate segment are

$$\left.\begin{aligned} w &= w_b \\ \frac{\partial w}{\partial y} &= 0 \end{aligned}\right\} \text{ at } y = 0 \qquad \left.\begin{aligned} \frac{\partial w}{\partial y} &= 0 \\ V_y &= 0 \end{aligned}\right\} \text{ at } y = c \quad [5][4]$$

One may satisfy the boundary conditions at the simply supported edges by assuming a solution of the Lévy type (8); the resulting displacement functions are

$$w = \sum_{m=1,3,5}^{\infty}\left(A_m\cosh\frac{m\pi y}{a} + B_m\sinh\frac{m\pi y}{a} + C_m\frac{m\pi y}{a}\cosh\frac{m\pi y}{a} + D_m\frac{m\pi y}{a}\sinh\frac{m\pi y}{a} + \frac{4p_0a^4}{m^5\pi^5D}\right)\sin\frac{m\pi x}{a} \text{ for } 0 \le y \le c \quad [6]$$

$$w_b = \sum_{m=1,3,5}^{\infty}\left(A_m + \frac{4p_0a^4}{m^5\pi^5D}\right)\sin\frac{m\pi x}{a} \quad [7]$$

where

$$A_m = \frac{\frac{4p_0a^3}{m^4\pi^4}\left(2e - \frac{EI}{D}\right)}{EI\frac{m\pi}{a} + 4Dk_m\sinh\alpha_m} \qquad \alpha_m = \frac{m\pi c}{a}$$

$$B_m = -C_m = -k_mA_m\sinh\alpha_m \qquad k_m = \frac{1}{\cosh\alpha_m + \alpha_m\operatorname{csch}\alpha_m}$$

$$D_m = -k_mA_m\cosh\alpha_m$$

The strain energies of bending and twisting stored in one repeating section of the actual and equivalent orthotropic plates may now be determined. Finally, by taking equivalence of strain energies as the equivalence criterion, one obtains

[4] The deformation of the stiffener produced by the moment M_y is neglected. This approximation should be satisfactory for most plate-stiffener configurations.

$$D_x = \frac{\pi^4 sD}{960 \sum_{m=1,3,5}^{\infty} Q_m} \quad \ldots\ldots\ldots\ldots\ldots\ldots [8]$$

where

$$Q_m = \frac{1}{m^4}\left[\left(\frac{2c - \frac{EI}{D}}{\frac{EI}{D} m\pi + 4ak_m \sinh \alpha_m}\right)^2 \times \left\{\frac{EI}{D} + 4ck_m^3\left(1 + \frac{\sinh \alpha_m \cosh \alpha_m}{\alpha_m}\right)\right\}^2 + \frac{2}{m\pi}\left(\frac{2c - \frac{EI}{D}}{\frac{EI}{D} m\pi + 4ak_m \sinh \alpha_m}\right) \times \left\{\frac{2ck_m}{\alpha_m}[(1-\nu)(1+\alpha_m - \cosh \alpha_m) + (1+\nu)\sinh \alpha_m] + \frac{EI}{D}\right\} + \frac{1}{m^2\pi^2}\left(2c + \frac{EI}{D}\right)\right]$$

This expression defines D_x in terms of the elastic constants of the actual stiffened plate and the geometry of a repeating section of it. The Relation [8] also exhibits the dependence of D_x on the span a between the simply supported boundaries. Numerical investigation shows that as a is increased from zero, D_x rapidly approaches an asymptotic value. This result is consistent with the previous stipulation that the boundary dimensions be large in comparison to the stiffener spacing in order that orthotropic plate theory be applicable.

The limiting value of D_x as the span is increased indefinitely (i.e., as the plate becomes infinitely large in both x and y-directions) is of particular interest. A study of the Function [8] as $a \to \infty$ reveals that D_x approaches the limiting value

$$D_x = \frac{2cD + EI}{s} \quad \ldots\ldots\ldots\ldots\ldots [9]$$

The quantity I is the moment of inertia of two stiffeners and the intervening plate segment; consequently

$$I = I_s + \frac{2cD}{E}$$

where I_s is the moment of inertia of the two stiffeners with respect to the middle plane of the plate and the latter term is appropriate because the plate segment is laterally restrained. Then

$$D_x = D + \frac{EI_s}{s} \quad \ldots\ldots\ldots\ldots\ldots [10]$$

This result is consistent with the result one obtains by treating the stiffened plate as a wide beam. Owing to its simplicity, it is recommended that Relation [10] be used to determine D_x unless one wishes to investigate problems in which the ratio a/s is not large enough to justify use of the asymptotic value of D_x.

Determination of D_y

The case of flexure used in the determination of D_y is identical with that employed in the determination of D_x except that the stiffeners are reoriented to lie parallel to the simply supported boundaries, Fig. 3. Consequently, the deflection surface and strain-energy function for the equivalent orthotropic plate may be derived from those of the previous case by interchange of x and y.

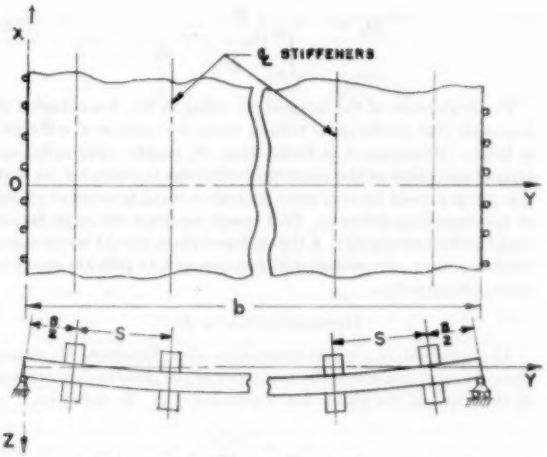

Fig. 3 Geometry of Longitudinally Stiffened Strip

The actual stiffened plate also will deform to a cylindrical surface; i.e., w will be a function of y alone. Then, the moment-curvature relationship for the stiffened plate is

$$M_y = -D(y)\frac{d^2w}{dy^2} = \frac{p_0}{2}(by - y^2) \quad \ldots\ldots\ldots [11]$$

where $D(y)$, the variable flexural rigidity of the stiffened plate, requires special interpretation. For a rigorous determination of the moment-curvature relationship in the region of an abrupt transition in $D(y)$, the plane-strain problem of the bending of the plate-stiffener section would have to be solved. Lacking this solution, it is necessary to choose $D(y)$, being guided by the following considerations:

1 $D(y)$ is physically a continuous function of y.

2 A lower bound to D_y may be found by taking $D(y) = D$. This corresponds to neglect of the stiffeners when estimating the transverse rigidity, a course which has been followed by practically all investigators in the past.

3 An upper bound to D_y may be obtained by taking

$$D(y) = \frac{E[h(y)]^3}{12(1-\nu^2)}$$

where $h(y)$ is the total thickness of the plate-stiffener combination (subject to the limitation of item 4).

4 When the ratio of stiffener height to stiffener width is greater than unity, a reduced height, of the order of the stiffener width, should be employed. This may be deduced by reference to the principle of Saint Venant.

5 The transition regions at the edges of the stiffeners where the material is not fully effective become percentagewise less significant as the stiffener width is increased. The presence of fillets is very effective in smoothing out discontinuities in stiffness which occur at stiffeners; for a specific plate specimen having large fillets and shallow stiffeners it was found satisfactory to take the full width of stiffener as being effective.

The strain energy of bending stored in a strip of the stiffened plate having unit width in the x-direction may be obtained readily using Relation [11]. Equating this strain energy to that for a corresponding unit strip of the equivalent orthotropic plate, one obtains for the transverse flexural rigidity

$$D_y = \frac{b^5}{30\int_0^b \frac{(by - y^2)^2}{D(y)}\,dy} \quad \ldots\ldots [12]$$

The evaluation of the integral occurring in the denominator of Equation [12] can be quite tedious when the number of stiffeners is large. However, it is found that D_y rapidly approaches an asymptotic value as the number of stiffeners is increased, so that this integral need be evaluated for only a small number of cycles of the repeating pattern. This result confirms the expectation that the flexural rigidity of the stiffened plate should be constant whenever there are enough stiffeners present to provide approximate homogeneity.

Determination of D_{xy}

The constant D_{xy} which appears in plate Equation [1] enters through consideration of the resistance of the plate to deformation in the plane of the plate, i.e., to strains γ_{xy}. By definition

$$D_{xy} = \frac{G_{xy}h_e^3}{12} \quad \ldots\ldots [13]$$

where G_{xy} is one of the three shear moduli of the orthotropic material and h_e is the thickness of the equivalent orthotropic plate. The other two shear moduli, G_{yz} and G_{xz}, do not enter into the analysis of transverse displacements of thin orthotropic plates, since shear deformations involving strains γ_{yz} and γ_{xz} have been neglected in the derivation of Equation [1].

The effective orthotropic shear modulus G_{xy} may be determined by comparison of the torsional rigidities of the actual and equivalent orthotropic plates. Consider the Saint Venant torsion problem for a bar of orthotropic material having a narrow rectangular cross section, Fig. 4.

Letting the x-axis be the axis of twist, the problem resolves itself into the solution of the differential equation

$$\frac{1}{G_{xy}}\frac{\partial^2\varphi}{\partial z^2} + \frac{1}{G_{xz}}\frac{\partial^2\varphi}{\partial y^2} = -2\theta \quad \ldots\ldots [14]$$

for the stress function φ, subject to the boundary condition $\varphi = 0$. θ is the angle of twist per unit length in the x-direction.

From the solution of this problem one obtains the following relation between the twisting moment M_t and the quantity θ

$$M_t = K_e G_{xy}\theta \quad \ldots\ldots [15]$$

where

$$K_e = \frac{256bh_e^3}{\pi^4}\sum_{l=1,3,5}^{\infty}\sum_{m=1,3,5}^{\infty}\frac{1}{l^2m^2\left[\frac{l^2}{\left(\frac{b}{h_e}\right)^2\frac{G_{xz}}{G_{xy}}} + m^2\right]} \quad \ldots\ldots [16]$$

An investigation (9) of the function K_e reveals that this quantity becomes insensitive to the value of G_{xz} when the ratio b/h_e becomes large, i.e., when the rectangular bar becomes a plate, and that for this case G_{xz} may be assumed equal to G_{xy} with negligible error. Then Relation [16] reduces to that for the form factor of a rectangular bar of isotropic material.

By application of the strain-energy criterion one obtains

$$G_{xy} = \frac{K_a}{K_e}G \quad \ldots\ldots [17]$$

where K_a is a form factor depending on the geometry of the cross section of the actual stiffened plate. The determination of K_a requires the solution of the Saint Venant torsion problem for the plate-stiffener cross section. For irregular cross sections, an exact solution of the elasticity problem is not likely to be found. However, satisfactory approximate values of K_a may be obtained by use of the Prandtl membrane analogy or of relaxation methods. Useful empirical methods for estimation of the torsional rigidity of composite cross sections have been presented by Trayer and March (10) and by Griffith and Taylor (11).

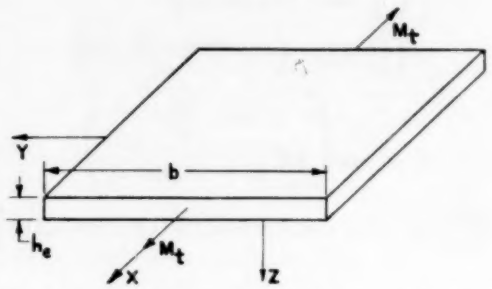

Fig. 4 Orthotropic Plate Subjected to Twisting Moment

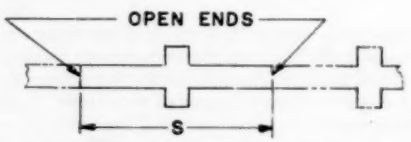

Fig. 5 Repeating Cross Section of Stiffened Plate

The membrane deflection surface for the plate-stiffener cross section will be substantially periodic (recurring for each repeating section) except at the ends of the plate cross section, where the membrane deflection must be zero. This end effect may be neglected provided that there are enough repeating sections to satisfy the homogeneity condition. Then it is only necessary to determine a factor K_a' for one repeating section, Fig. 5, since $K_a \approx nK_a'$, where n is the number of repeating sections.

The factor K_a' must be determined on the basis of open ends for the membrane deflection surface at the boundaries so indicated in Fig. 5; in terms of the torsion problem, the stress function must satisfy the condition $\partial\varphi/\partial y = 0$ at these boundaries. A similar situation exists for the equivalent orthotropic plate; again neglecting the end effect, one may employ the value of K_e for $b/h = \infty$. Then

$$K_e' = \frac{K_e}{n} = \frac{1}{3}sh_e^3 \quad \ldots\ldots [18]$$

Finally, making use of Equations [13], [17], and [18] one obtains for the twisting rigidity

$$D_{xy} = \frac{K_a'G}{4s} \quad \ldots\ldots [19]$$

Note that D_{xy} does not depend on h_e, so that it is unnecessary to define the thickness of the equivalent orthotropic plate.

Determination of D_1

Although, for consistency, it might be preferable to determine D_1 by means of the strain-energy criterion, experience (9) with

this approach has shown that practical difficulties arise from the insensitivity of the strain-energy function to variations in D_1. It has been found expedient to employ a criterion which involves the Poisson cross-contraction effect more intimately, namely, the equality of bending moments for the direction normal to the plane of maximum curvature. For the bending of the infinitely long orthotropic strip considered in the determination of D_x, the significant moment is

$$M_y = -\frac{p_0 D_1 x(x-a)}{2D_x} \quad [20]$$

The corresponding moment for the stiffened plate varies with y; it is appropriate to introduce a mean value of this quantity defined by

$$\bar{M}_y = \frac{\int_0^c M_y dy + eM_y(0)}{c+e} \quad [21]$$

The mean moment $\bar{M}_y$ may be determined by substituting Relation [6] into

$$M_y = -D\left(\frac{\partial^2 w}{\partial y^2} + \nu \frac{\partial^2 w}{\partial x^2}\right) \quad [22]$$

and the result into Equation [21]. Equating the value of $\bar{M}_y$ to M_y for the equivalent orthotropic plate (each being evaluated at $x = a/2$), one obtains

$$D_1 = D_x \left[\nu - \frac{32\left(2e - \frac{EI}{D}\right)}{\pi^3(c+e)} \sum_{m=1,3,5}^{\infty} \frac{(-1)^{\frac{m-1}{2}}}{m^3\left(\frac{EI}{D}\frac{m\pi}{a} + 4k_m \sinh \alpha_m\right)} \right.$$

$$\left. \left\{(1-\nu)(1-k_m \cosh \alpha_m)\sinh \alpha_m - (1+\nu)k_m \sinh \alpha_m + k_m(1-\cosh \alpha_m) + \frac{e\alpha_m}{c}(1-\nu-2k_m \cosh \alpha_m)\right\}\right] \quad [23]$$

This expression, like Relation [8], contains the span dimension a. By investigation of the Function [23] as $a \to \infty$ and introduction of the previously obtained asymptotic value of D_x, it is found that D_1 takes on the limiting value

$$D_1 = \nu D \quad [24]$$

The two Poisson's ratios for the equivalent orthotropic plate may be obtained by use of the relations

$$\nu_{xy} = \frac{D_1}{D_y} \qquad \nu_{yx} = \frac{D_1}{D_x} \quad [25]$$

Generalizations of the Method

When the stiffeners are not symmetrically disposed with respect to the middle plane of the plate, as, for example, when the stiffeners are located on only one side of the plate, the unknown locations of the neutral surfaces of the bending stresses inject added complexity into the determination of the orthotropic rigidity factors. Certain assumptions must be made regarding the stress distribution in order to fix the locations of these neutral surfaces.

In the determination of D_x, for closely spaced stiffeners one may assume the existence of a neutral plane for the stresses σ_x, which is parallel to the middle plane of the plate and located at a distance z_p from it. The latter distance may be determined from the condition that the resultant force acting on a repeating cross section must be zero. Then

$$D_x = D + \frac{Ehz_p^2}{(1-\nu^2)} + \frac{EI_s'}{s} \quad [26]$$

where I_s' is the moment of inertia of the stiffener(s) with respect to the assumed neutral axis. When the stiffener spacing is great enough that the assumption of a plane neutral surface is unsatisfactory, the approximate location of the neutral surface may be established by means of a minimum-energy approach similar to that used by Smith, Heebink, and Norris (12).

The flexural rigidity D_y may be determined by use of Relation [12] even in the asymmetric case, the selection of the proper function $D(y)$ providing the only difficulty. If the variable depth $h(y)$ does not change abruptly, the neutral surface may be assumed to be located at one half of the effective thickness $h(y)$. When the thickness varies discontinuously, a judicious selection of continuous functions to represent the neutral surface and the effective thickness must be made.

The determination of D_{xy} will proceed in the same manner as in the symmetric case, K_s' being the form factor for one cycle of the asymmetric cross section. The method of determination of D_1 is basically the same, but the existence of different neutral surfaces for the stresses σ_x and σ_y produces a quasi-orthotropy in the actual stiffened plate, which requires a modification of Relation [23].

The alterations in the analysis required when the stiffener cross sections are other than rectangular are fairly obvious (e.g., I_s becomes the moment of inertia of the actual stiffener cross section about the neutral axis of the plate-stiffener combination). It should be noted that, for conventional stiffener shapes, only the flange attached to the plate is effective in stiffening the plate in the y-direction and thus deserves to be included in the formulation of $D(y)$.

Correlation With Test Data

Although the relations for the rigidity constants were derived on a rational basis, the necessary approximations in the analysis make a comparison with experimental evidence desirable. Such evidence is afforded by the results of an investigation (13) using test fixtures which were scaled-up versions of those described in (5, 14). In these fixtures rectangular plates were subjected to pure bending in one principal direction (with zero bending moment in the other principal direction) and square-plate specimens were loaded in pure twist by the application of properly oriented forces at the corners. The edges of these plates were unsupported. Deflection measurements on the resulting anticlastic surfaces were made with a micrometer equipped with a pilot indicator. Specimens fabricated from $^1/_4$-in. hot-rolled steel plate were grooved on one side and later on both sides. Nominal groove dimensions were $^1/_2$ in. wide $\times$ $^1/_{16}$ in. deep $\times$ $^1/_{16}$ in. fillet radius and the groove pitch was approximately $^3/_4$ in. The bending

specimens were 6 in. wide × 18 in. long while the twisting specimens were 12 in. on a side. Consequently, there was a sufficient number of grooves on each specimen to satisfy the condition of approximate homogeneity.

The boundary conditions and load distributions for the test specimens were quite different from those assumed in the analysis. Therefore these cases provide a good opportunity to apply the theory of this paper to predict the deflections of the test specimens. However, to simplify the presentation of results, experimental load-deflection data were used to calculate effective rigidity constants for the test specimens. In Table 1 these values are compared with those predicted theoretically. The theoretical

TABLE 1 ORTHOTROPIC RIGIDITY CONSTANTS OF TEST SPECIMENS

		D_x (lb-in.)	D_y (lb-in.)	D_{xy} (lb-in.)	D_1 (lb-in.)
Plate grooved on one side only	Theoretical	32600	27550	9600[a] 10200[b]	6250
	Experimental	33300	26300	8920	7370
Plate grooved on both sides	Theoretical	21100	11150	5800[a] 6300[b]	2030
	Experimental	23250	11660	6480	5090

[a] K_s' determined by extrapolation of Trayer and March data.
[b] K_s' determined by soap-film method.

values of D_x and D_1 shown in the table were obtained by use of the asymptotic Relations [10] and [24]; the values obtained by use of the actual plate spans were in each case slightly less.

Conclusions

Methods have been presented by which the effective rigidity constants of orthogonally stiffened plates may be determined on a theoretical basis in terms of the elastic constants of the material and the plate-stiffener geometry. These constants may then be employed in conjunction with the bending theory of thin orthotropic plates to predict the mean deflections and stresses of the stiffened plate. The methods of this paper should be satisfactory for the determination of the longitudinal bending stresses. It should be noted that the transverse bending stresses, given by $\sigma_y = 6M_y/h^2$, must be modified by an appropriate stress-concentration factor (15) for the regions where the stiffeners are located.

It should be stressed that this is essentially a plate theory. Not only is its application subject to the limitations of the theory of thin homogeneous plates of constant thickness but also the ratio of stiffener rigidity to plate rigidity must not become so large that the beam action is predominant. For the latter case, the method of analysis whereby the stiffened plate is treated as a series of beams, the flexural rigidity of each being augmented by an "effective breadth" of plate, should be more appropriate.

When compared with the rather meager experimental data presently available, the theoretically determined orthotropic constants show a satisfactory agreement. The somewhat low theoretical values of D_x may be attributed to neglect f deformation of the stiffeners caused by the moment M_y. Since the test-specimen stiffeners were unusually wide and shallow, the discrepancy normally will be less than the observed. The difference between the theoretical and experimental values of the constant D_1 do not necessarily discredit the analytical method since the possible error in the experimental determination of this constant is much greater than for the other three rigidity factors.

Acknowledgments

The author wishes to express his gratitude to Prof. W. H. Hoppmann, 2nd, for his guidance and criticism of this investigation.

Bibliography

1 "Die Grundlagen einer rationellen Berechnung der kreuzweise bewehrten Eisenbetonplatten," by M. T. Huber, Zeitschrift des Österreiches Ingenieur und Architekten-Vereines, No. 30, 1914, pp. 557–564.

"Théorie rationelle des hourdis en bèton armé, considérés comme des plaques minces, d'une simple anisotropie orthogonale," by M. T. Huber, *Comptes Rendus*, vol. 170, 1920, pp. 511–513.

"Sur la flexion d'un hourdis nervuré," by M. T. Huber, *Comptes Rendus*, vol. 180, 1925, pp. 1243–1245.

"Biegungsprobleme eines durch Querrippen versteiften orthotropen Plattenstreifens," by M. T. Huber, Proceedings of the 2nd International Congress for Applied Mechanics, Zurich, Switzerland, 1926, pp. 397–402.

2 "Beitrag zur Frage des Ausbeulens von versteiften Platten bei Schubbeanspruchung," by E. Seydel, *Luftfahrtforschung*, vol. 8, 1930, pp. 71–81.

3 "Application of Orthotropic Plate Theory to Ship Bottom Structure," by H. A. Schade, Proceedings of the 5th International Congress for Applied Mechanics, Cambridge, Mass., John Wiley & Sons, Inc., New York, N. Y., 1938, pp. 140–144.

"Bending Theory of Ship Bottom Structure," by H. A. Schade, Trans. SNAME, vol. 46, 1938, pp. 176–205.

"The Orthogonally Stiffened Plate Under Uniform Lateral Load," by H. A. Schade, Trans. ASME, vol. 62, 1940, p. A-143.

4 "Critical Buckling Strength of Stiffened Flat Plywood Plates in Compression and Shear—Closely Spaced Stiffeners," by C. B. Norris, W. J. Kommers, and P. F. McKinnon, U. S. Forest Products Laboratory Report No. 1800, Madison, Wis., February, 1948.

5 "Bending of Orthogonally Stiffened Plates," by W. H. Hoppmann, 2nd, Journal of Applied Mechanics, Trans. ASME, vol. 77, 1955, pp. 267–271.

6 "Theory of Plates and Shells," by S. Timoshenko, McGraw-Hill Book Company, Inc., New York, N.Y., 1940, pp. 1–3, 50, 88, 188–194.

7 "Orthogonally Stiffened Steel Plates," by F. F. Petersen, E. S. Johnson, and E. N. Jacobs, Final Report, Navy Contract N6-onr-25513 (NR-035-258), Mechanical Engineering Laboratory, Stanford University, Standard, Calif., 1949.

8 "Sur l'équilibre élastique d'une plaque rectangulaire," by M. Lévy, *Comptes Rendus*, vol. 129, 1899, pp. 535–539.

9 "Theoretical Determination of Rigidity Properties of Orthogonally Stiffened Plates," by N. J. Huffington, Jr., Dissertation, The Johns Hopkins University, Baltimore, Md., 1954.

10 "The Torsion of Members Having Sections Common in Aircraft Construction," by G. W. Trayer and H. W. March, NACA Report No. 334, 1930.

11 "The Use of Soap Films in Solving Torsion Problems" and "The Determination of the Torsional Stiffness and Strength of Cylindrical Bars of Any Sections," by A. A. Griffith and G. I. Taylor, Technical Report of the Advisory Committee for Aeronautics (British) for 1917–1918, vol. 3, Strength of Construction, Nos. 333 and 334.

12 "The Effective Stiffness of a Stiffener Attached to a Flat Plywood Plate," by C. B. Smith, T. B. Heebink, and C. B. Norris, U. S. Forest Products Laboratory Report No. 1557, September, 1946.

13 "Experimental Study of a Theory of Bending of Orthogonally Stiffened Plates," by W. H. Hoppmann, 2nd, N. J. Huffington, Jr., and L. Magness, U. S. Army Contract DA-36-034-ORD 1297 (RD), Report No. 1, The Johns Hopkins University, Baltimore, Md., to be published in 1955.

14 "Determination of Elastic Constants of Orthotropic Materials With Special Reference to Laminates," by R. K. Witt, W. H. Hoppmann, 2nd, and R. S. Buxbaum, American Society for Testing Materials Bulletin No. 194, December, 1953, pp. 53–57.

15 "Design Data and Methods—Applied Mechanics," ASME, New York, N. Y., 1953, pp. 57–58.

Large Deflections of Elliptical Plates

By N. A. WEIL[1] and N. M. NEWMARK[2]

A solution is obtained by means of the Ritz method for the "large-deflection" problem of a clamped elliptical plate of constant thickness, subjected to a uniformly distributed load. Two shapes of elliptical plate are treated, in addition to the limiting cases of the circular plate and infinite strip, for which the exact solutions are known. Center deflections as well as total stresses at the center and edge decrease as one proceeds from the infinite strip through the elliptical shapes to the circular plate, holding the width of the plates constant. The relation between edge-stress at the semiminor axis (maximum stress in the plate) and center deflection is found to be practically independent of the proportions of the elliptical plate. Hence the governing stress may be determined from a single curve for a given load on an elliptical plate of arbitrary dimensions, if the center deflection is known.

Nomenclature

The following nomenclature is used in the paper:

ϵ = strain
N = force per unit width
M = moment per unit width
σ', σ'' = membrane and bending stresses, respectively
u, v = displacements in x and y-direction, respectively
w = vertical deflection
q = uniformly distributed normal load
h = constant plate thickness
a, b = length of semiminor and semimajor axes of the elliptical plate, respectively
E = modulus of elasticity
ν = Poisson's ratio
$D = \dfrac{Eh^3}{12(1-\nu^2)}$ = flexural rigidity of plate
$\nabla^2 = \left(\dfrac{\partial^2}{\partial x^2} + \dfrac{\partial^2}{\partial y^2}\right)^2$ = square of Laplacian operator
V_1 = total bending energy absorbed by plate
V_2 = total membrane energy retained by plate in stretching of middle surface
a_{00}, a_{20}, a_{02} = arbitrary parameters for deflection function
b_{00}, b_{20}, b_{02}, b_{22}; c_{00}, c_{20}, c_{02}, c_{22} = arbitrary parameters for displacement functions in x and y-direction, respectively

$\bar{u} = u/h^2$; $\bar{v} = v/h^2$; $\bar{w} = w/h$; $\bar{q} = 2q/Dh$; $qa^4/Eh^4 = \bar{q}a^4/21.84$; $\bar{\sigma} = \sigma a^2/Eh^2$

The subscript x or y indicates a quantity acting in the respective direction. The subscript xy denotes shearing forces, stresses, strains, or twisting moments. The subscript o refers to quantities at the center of the plate.

Introduction

Solutions for plates with large deflections are known only for the simplest cases. The uniformly loaded clamped circular plate was solved by Way (1),[3] using an iteration and successive interpolation process. Approximate solutions exist for the clamped circular plate, subjected to uniformly distributed loads (2, 3, 4, 5) or moments uniformly distributed around the edge (6), the simply supported circular plate (7), the uniformly loaded square plate (8), and for rectangular plates subjected to uniformly distributed lateral loads (9), or a combination of lateral loads and end thrusts (10, 11).

The present work was undertaken to extend the large-deflection solutions to elliptic plates. The small-deflection (or elementary) solution of this problem can be derived by using either rectilinear co-ordinates (12) or curvilinear co-ordinates (13).

Elliptical plates of uniform thickness are considered, which have a clamped boundary and are subjected to uniformly distributed lateral loads. The treatment of the problem is extended to the limiting cases of the circular plate and infinite strip, for which exact solutions are available in the literature. The method of attack follows the well-established energy-method principle, in which rectilinear co-ordinates are used for the solution of the problem.

Solution of the Small-Deflection Problem by the Energy Method

The small-deflection solution takes into account only that part of the energy imparted to the plate which is due to bending. This is given by

$$V_1 = \frac{D}{2}\int_A\int\left\{\nabla^2 w - 2(1-\nu)\left[\frac{\partial^2 w}{\partial x^2}\,\frac{\partial^2 w}{\partial y^2} - \left(\frac{\partial^2 w}{\partial x\,\partial y}\right)^2\right] - \frac{2}{D}\,qw\right\} dx\,dy \quad [1]$$

Equation [1] includes only terms depending on the action of bending and twisting moments and lateral loads; the effect of shearing forces on the complementary energy of the plate is ignored.

If w vanishes along the closed boundary curve of area A of the plate (which is the case for any clamped plate), it can be shown that the middle term of Equation [1] likewise vanishes, reducing the bending energy of a clamped elliptical plate to

$$V_1 = 2D\int_0^b\int_0^{a\sqrt{1-y^2/b^2}} (\nabla^2 - q_1)w\,dx\,dy \quad [2]$$

where

$$q_1 = 2q/D$$

[1] Development Engineer, The M. W. Kellogg Company, New York, N. Y.

[2] Research Professor, Structural Engineering, University of Illinois, Urbana, Ill. Mem. ASME.

Contributed by the Applied Mechanics Division and presented at the Diamond Jubilee Annual Meeting, Chicago, Ill., November 13–18, 1955, of The American Society of Mechanical Engineers.

Discussion of this paper should be addressed to the Secretary, ASME, 29 West 39th Street, New York, N. Y., and will be accepted until April 10, 1956, for publication at a later date. Discussion received after the closing date will be returned.

Note: Statements and opinions advanced in papers are to be understood as individual expressions of their authors and not those of the Society. Manuscript received by ASME Applied Mechanics Division, March 21, 1955. Paper No. 55—A-2.

[3] Numbers in parentheses refer to the Bibliography at the end of the paper.

For a clamped plate, the boundary conditions can be expressed as

$$w = 0; \quad \frac{\partial w}{\partial x} = 0; \quad \frac{\partial w}{\partial y} = 0 \quad \text{at the boundary.}$$

These boundary conditions will be satisfied by

$$w = \left(1 - \frac{x^2}{a^2} - \frac{y^2}{b^2}\right)^2 (a_{00} + a_{20}x^2 + a_{02}y^2) \ldots\ldots [3]$$

which also satisfies the condition that the shape of the deflected plate be symmetrical about both its major and minor axes.

If Equation [3] is substituted into Equation [2] and the integration is carried out, one arrives at an expression of the total energy in the plate as a function of the three assumed constants. The true values of these parameters will be those which render the total energy a minimum. Three simultaneous equations are obtained by this process, which can be solved for the three unknowns a_{00}, a_{20}, and a_{02} to yield

$$a_{00} = \frac{0.08333}{\dfrac{4}{a^4} + \dfrac{2.667}{a^2 b^2} + \dfrac{4}{b^4}}\, q_1; \quad a_{20} = a_{02} = 0 \ldots\ldots [4]$$

Substituting Equations [4] into [3] and recalling that $q_1 = 2q/D$, the deflection function can be given as

$$w = \frac{q}{8D\left[\dfrac{3}{a^4} + \dfrac{2}{a^2 b^2} + \dfrac{3}{b^4}\right]} \left(1 - \frac{x^2}{a^2} - \frac{y^2}{b^2}\right)^2 \ldots [5]$$

This result is identical with that obtained by solving the differential equation for the small-deflection solution of this problem (12).

Solution of Large-Deflection Problem by Energy Method

The major difference between the small and large-deflection theories for plates is found in the expressions for the strain-displacement relations. These relations, representing second-degree approximations, take the following form for the case of large deflections (14)

$$\left.\begin{aligned} \epsilon_x &= \frac{\partial u}{\partial x} + \frac{1}{2}\left(\frac{\partial w}{\partial x}\right)^2 \\ \epsilon_y &= \frac{\partial v}{\partial y} + \frac{1}{2}\left(\frac{\partial w}{\partial y}\right)^2 \\ \epsilon_{xy} &= \frac{\partial u}{\partial y} + \frac{\partial v}{\partial x} + \frac{\partial w}{\partial x}\frac{\partial w}{\partial y} \end{aligned}\right\} \ldots\ldots [6]$$

Using Equations [6], the strain-energy absorbed by the plate due to the extension of its middle surface can be given as (15)

$$V_2 = \frac{Eh}{2(1-\nu^2)} \int_A \int \left\{ \left(\frac{\partial u}{\partial x}\right)^2 + \frac{\partial u}{\partial x}\left(\frac{\partial w}{\partial x}\right)^2 + \left(\frac{\partial v}{\partial y}\right)^2 + \frac{\partial v}{\partial y}\left(\frac{\partial w}{\partial y}\right)^2 + \frac{1}{4}\left[\left(\frac{\partial w}{\partial x}\right)^2 + \left(\frac{\partial w}{\partial y}\right)^2\right]^2 + 2\nu\left[\frac{\partial u}{\partial x}\frac{\partial v}{\partial y} + \frac{1}{2}\frac{\partial u}{\partial x}\left(\frac{\partial w}{\partial y}\right)^2 + \frac{1}{2}\frac{\partial v}{\partial y}\left(\frac{\partial w}{\partial x}\right)^2\right] + \frac{1-\nu}{2}\left[\left(\frac{\partial u}{\partial y} + \frac{\partial v}{\partial x}\right)^2 + 2\left(\frac{\partial u}{\partial y} + \frac{\partial v}{\partial x}\right)\frac{\partial w}{\partial x}\frac{\partial w}{\partial y}\right]\right\} dx\, dy \ldots\ldots [7]$$

Equation [7] represents the amount of energy which is ignored in the small-deflection solution. The total energy absorbed by the plate during deflection will be given by the sum of Equations [2] and [7]. Introducing the new variables

$$\bar{w} = \frac{w}{h}; \quad \bar{u} = \frac{u}{h^2}; \quad \bar{v} = \frac{v}{h^2}; \quad \bar{q} = \frac{2q}{Dh}$$

the expression for total energy simplifies to

$$V = \frac{24\,D}{h^2} \int_0^b \int_0^{a\sqrt{1-y^2/b^2}} \left\{ \frac{1}{12}(\nabla^2 - \bar{q})\bar{w} + \left(\frac{\partial \bar{u}}{\partial x}\right)^2 + \frac{\partial \bar{u}}{\partial x}\left(\frac{\partial \bar{w}}{\partial x}\right)^2 + \left(\frac{\partial \bar{v}}{\partial y}\right)^2 + \frac{\partial \bar{v}}{\partial y}\left(\frac{\partial \bar{w}}{\partial y}\right)^2 + \frac{1}{4}\left[\left(\frac{\partial \bar{w}}{\partial x}\right)^2 + \left(\frac{\partial \bar{w}}{\partial y}\right)^2\right]^2 + \nu\left[2\frac{\partial \bar{u}}{\partial x}\frac{\partial \bar{v}}{\partial y} + \frac{\partial \bar{u}}{\partial x}\left(\frac{\partial \bar{w}}{\partial y}\right)^2 + \frac{\partial \bar{v}}{\partial y}\left(\frac{\partial \bar{w}}{\partial x}\right)^2\right] + \frac{1-\nu}{2}\left[\left(\frac{\partial \bar{u}}{\partial y} + \frac{\partial \bar{v}}{\partial x}\right)^2 + 2\left(\frac{\partial \bar{u}}{\partial y} + \frac{\partial \bar{v}}{\partial x}\right)\frac{\partial \bar{w}}{\partial x}\frac{\partial \bar{w}}{\partial y}\right]\right\} dx\, dy \ldots\ldots [8]$$

In addition to functions of $\bar{w}$, Equation [8] involves expressions depending on $\bar{u}$ and $\bar{v}$. To solve the problem one must assume suitable functions for the displacements as well as for the deflection. The boundary conditions for the clamped elliptical plate can be given as

$$\bar{u} = \bar{v} = \bar{w} = \frac{\partial \bar{w}}{\partial x} = \frac{\partial \bar{w}}{\partial y} = 0 \text{ at the boundary.}$$

The boundary and symmetry conditions will be satisfied by adopting the following infinite series for deflection and displacements

$$\left.\begin{aligned} \bar{w} &= \left[1 - \frac{x^2}{a^2} - \frac{y^2}{b^2}\right]^2 \sum_{m,n=0}^{\infty} a_{2m,2n}\, x^{2m}\, y^{2n} \\ \bar{u} &= \left[1 - \frac{x^2}{a^2} - \frac{y^2}{b^2}\right] x \sum_{m,n=0}^{\infty} b_{2m,2n}\, x^{2m}\, y^{2n} \\ \bar{v} &= \left[1 - \frac{x^2}{a^2} - \frac{y^2}{b^2}\right] y \sum_{m,n=0}^{\infty} c_{2m,2n}\, x^{2m}\, y^{2n} \end{aligned}\right\} \ldots\ldots [9]$$

Naturally, it is impossible to determine the triple infinity of coefficients involved in the solution of Equations [9]. However, a good approximation can be obtained by retaining only a few initial terms of the infinite series. This renders the deflection and displacement functions to become

$$\left.\begin{aligned} \bar{w} &= \left[1 - \frac{x^2}{a^2} - \frac{y^2}{b^2}\right]^2 (a_{00} + a_{20}x^2 + a_{02}y^2) \\ \bar{u} &= \left[1 - \frac{x^2}{a^2} - \frac{y^2}{b^2}\right] x\,(b_{00} + b_{20}x^2 + b_{02}y^2 + b_{22}x^2y^2) \\ \bar{v} &= \left[1 - \frac{x^2}{a^2} - \frac{y^2}{b^2}\right] y\,(c_{00} + c_{20}x^2 + c_{02}y^2 + c_{22}x^2y^2) \end{aligned}\right\} \ldots [10]$$

These expressions may now be substituted into Equation [8]. If the integration is then carried out over the prescribed limits, the resulting energy expression will again be a function of the

assumed constants, whose numerical value[4] can be determined from the condition that the incremental energy due to a variation in any of the assumed parameters be zero. Thus we have

$$\left.\begin{aligned} &\frac{\partial V}{\partial a_{00}} = \frac{\partial V}{\partial a_{20}} = \frac{\partial V}{\partial a_{02}} = 0 \\ &\frac{\partial V}{\partial b_{00}} = \frac{\partial V}{\partial b_{20}} = \frac{\partial V}{\partial b_{02}} = \frac{\partial V}{\partial b_{22}} = 0 \\ &\frac{\partial V}{\partial c_{00}} = \frac{\partial V}{\partial c_{20}} = \frac{\partial V}{\partial c_{02}} = \frac{\partial V}{\partial c_{22}} = 0 \end{aligned}\right\} \quad \ldots\ldots\ldots [11]$$

The three equations resulting from the first line of Equations [11] will be cubic in the a_{mn} and linear in the other parameters. The eight equations resulting from the second and third lines of Equations [11] will contain only linear terms in the b_{mn} and c_{mn} along with quadratic terms in the a_{mn}.

In the numerical solution, these latter eight equations were first solved for the eight b_{mn} and c_{mn} parameters which were then

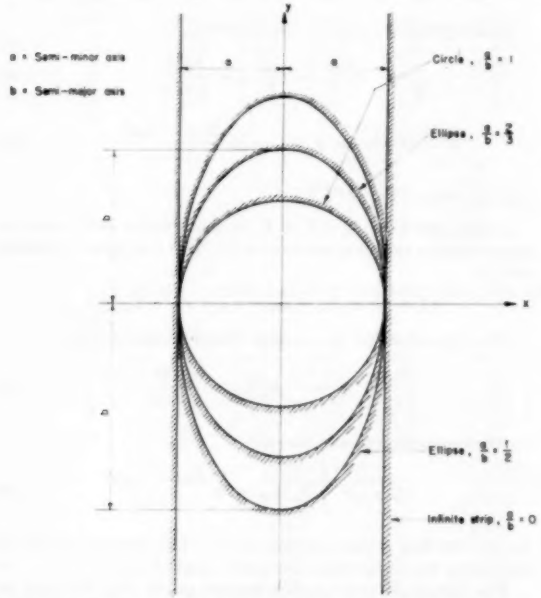

FIG. 1 REPRESENTATIVE SHAPES OF PLATES SOLVED NUMERICALLY

substituted into the first set of equations. The resulting three simultaneous cubic equations were solved by the Newton-Raphson method (16) to yield the a_{mn} in terms of $\bar{q}$.

Numerical solutions were obtained for elliptical plates represented by the following ratios of minor to major axes:

$a/b = 1$ (circular plate of radius a)	Case (I)
$a/b = 2/3$	Case (II)
$a/b = 1/2$	Case (III)
$a/b = 0$ (infinite strip of width $2a$)	Case (IV)

The respective shapes of the four cases investigated are shown in Fig. 1. The results of these calculations are presented for Cases (I) to (IV) in Tables 1 to 4.

Substitution of the numerical values of the assumed parameters into Equations [10] completely determines the deflection and displacement functions. The dimensionless center deflection

$$\bar{w}_0 = \bar{w}|_{x=y=0} = a_{00} \quad \ldots\ldots\ldots\ldots\ldots [12]$$

is shown as a function of the dimensionless load in Fig. 2. For a given load, the deflections increase as one proceeds from the circular plate through the elliptical shapes to the infinite strip, holding the width of the plates ($=2a$) constant, as shown in Fig. 1. The elementary (small-deflection) solution, also shown in Fig. 2, represents the initial tangents to these curves.

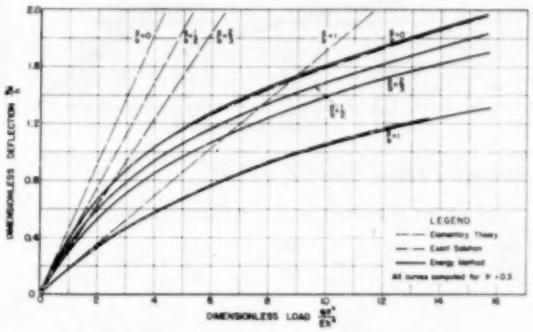

FIG. 2 CENTER DEFLECTION AS FUNCTION OF LOAD

The deviation between the elementary and large-deflection solutions increases progressively with the magnitude of loading. In general, the error involved in the elementary solution becomes significant when the center deflection of the plate exceeds 40 per cent of the plate thickness.

Exact solutions for two of the cases treated in this paper, namely, the circle (I) and the infinite strip (17), are also presented in Fig. 2 by dash-dot curves. Deflections obtained by the energy-method solution are close to the exact values, the deviation not exceeding 1 per cent.

The dimensionless membrane stresses are obtained from the following identities

$$\left.\begin{aligned} \bar{\sigma}_x' &= \frac{a^2}{1-\nu^2}\left[\frac{\partial \bar{u}}{\partial x} + \nu\frac{\partial \bar{v}}{\partial y} + \frac{1}{2}\left(\frac{\partial \bar{w}}{\partial x}\right)^2 + \frac{\nu}{2}\left(\frac{\partial \bar{w}}{\partial y}\right)^2\right] \\ \bar{\sigma}_y' &= \frac{a^2}{1-\nu^2}\left[\nu\frac{\partial \bar{u}}{\partial x} + \frac{\partial \bar{v}}{\partial y} + \frac{\nu}{2}\left(\frac{\partial \bar{w}}{\partial x}\right)^2 + \frac{1}{2}\left(\frac{\partial \bar{w}}{\partial y}\right)^2\right] \\ \bar{\sigma}_{xy}' &= \frac{a^2}{2(1+\nu)}\left(\frac{\partial \bar{u}}{\partial y} + \frac{\partial \bar{v}}{\partial x} + \frac{\partial \bar{w}}{\partial x}\frac{\partial \bar{w}}{\partial y}\right) \end{aligned}\right\} \quad \ldots [13]$$

The bending stresses at the bottom and top surfaces of the plate can be expressed as

$$\left.\begin{aligned} \bar{\sigma}_x'' &= \mp\frac{a^2}{2(1-\nu^2)}\left(\frac{\partial^2 \bar{w}}{\partial x^2} + \nu\frac{\partial^2 \bar{w}}{\partial y^2}\right) \\ \bar{\sigma}_y'' &= \mp\frac{a^2}{2(1-\nu^2)}\left(\nu\frac{\partial^2 \bar{w}}{\partial x^2} + \frac{\partial^2 \bar{w}}{\partial y^2}\right) \\ \bar{\sigma}_{xy}'' &= \pm\frac{a^2}{2(1+\nu)}\frac{\partial^2 \bar{w}}{\partial x\,\partial y} \end{aligned}\right\} \quad \ldots\ldots [14]$$

Extreme values of these stresses arise at the center of the plate and at the end of the semiminor axis. At these points the stress equations reduce to the following simple forms:

[4] $\nu = 0.3$ was assumed in all of the calculations.

TABLE 1 DISPLACEMENT PARAMETERS AND STRESS VALUES FOR CIRCULAR PLATE; $a/b = 1$

Dimensionless load qa^4/Eh^4	a_{00}	$a_{20}a^2$	$b_{00}a^2$	$b_{20}a^4$	$b_{22}a^4$	$b_{11}a^4$
1	0.169	0.002	0.015	—0.024	—0.034	0.035
2	0.323	0.013	0.056	—0.089	—0.125	0.121
3	0.457	0.035	0.116	—0.179	—0.249	0.226
6	0.761	0.144	0.356	—0.514	—0.683	0.472
10	1.035	0.319	0.727	—0.984	—1.249	0.545
15	1.279	0.529	1.207	—1.546	—1.876	0.347

Dimensionless bending stress		Dimensionless membrane stress		Dimensionless total stress	
At center	At edge	At center	At edge	At center	At edge
0.481	0.752	0.021	0.020	0.502	0.772
0.906	1.478	0.080	0.072	0.986	1.550
1.257	2.163	0.164	0.139	1.421	2.302
1.969	3.976	0.508	0.348	2.477	4.324
2.503	5.952	1.039	0.564	3.542	6.517
2.898	7.949	1.724	0.745	4.622	8.694

Generalized Ellipse, Cases (II) and (III)

(*a*) Center of plate ($x = 0$, $y = 0$)

$$\frac{\partial \bar{u}}{\partial x} = b_{00}; \quad \frac{\partial \bar{v}}{\partial y} = c_{00}; \quad \frac{\partial^2 \bar{w}}{\partial x^2} = -\frac{4a_{00}}{a^2} + 2a_{20};$$

$$\frac{\partial^2 \bar{w}}{\partial y^2} = -\frac{4a_{00}}{b^2} + 2a_{02}$$

$$\frac{\partial \bar{u}}{\partial y} = \frac{\partial \bar{v}}{\partial x} = \frac{\partial \bar{w}}{\partial x} = \frac{\partial \bar{w}}{\partial y} = \frac{\partial^2 \bar{w}}{\partial x\, \partial y} = 0$$

Hence the membrane stresses, Equations [13], become

$$\left.\begin{aligned} \bar{\sigma}_x'|_{0,0} &= \frac{b_{00}a^2 + \nu\, c_{00}a^2}{1-\nu^2} \\ \bar{\sigma}_y'|_{0,0} &= \frac{\nu\, b_{00}a^2 + c_{00}a^2}{1-\nu^2} \\ \bar{\sigma}_{xy}'|_{0,0} &= 0 \end{aligned}\right\} \quad \ldots\ldots\ldots\ldots [15]$$

The dimensionless bending stresses at the center, Equations [14], can be expressed as

$$\left.\begin{aligned} \bar{\sigma}_x''|_{0,0} &= \pm \frac{2\left(1 + \nu\frac{a^2}{b^2}\right)a_{00} - a_{20}a^2 - \nu a_{02}a^2}{1-\nu^2} \\ \bar{\sigma}_y''|_{0,0} &= \pm \frac{2\left(\frac{a^2}{b^2} + \nu\right)a_{00} - \nu a_{20}a^2 - a_{02}a^2}{1-\nu^2} \\ \bar{\sigma}_{xy}''|_{0,0} &= 0 \end{aligned}\right\} \quad \ldots [16]$$

where upper signs refer to the bottom surface.

(*b*) End of semiminor axis (at edge), ($x = a$, $y = 0$)

$$\frac{\partial \bar{u}}{\partial x} = -2(b_{00} + b_{20}a^2); \quad \frac{\partial^2 \bar{v}}{\partial x^2} = \frac{8}{a^2}(a_{00} + a_{20}a^2)$$

$$\frac{\partial \bar{u}}{\partial y} = \frac{\partial \bar{v}}{\partial x} = \frac{\partial \bar{v}}{\partial y} = \frac{\partial \bar{w}}{\partial x} = \frac{\partial \bar{w}}{\partial y} = \frac{\partial^2 \bar{w}}{\partial y^2} = \frac{\partial^2 \bar{w}}{\partial x\, \partial y} = 0$$

These expressions will render the dimensionless membrane stresses at the edge to be

$$\left.\begin{aligned} \bar{\sigma}_x'|_{a,0} &= -\frac{2(b_{00}a^2 + b_{20}a^4)}{1-\nu^2} \\ \bar{\sigma}_y'|_{a,0} &= \nu\bar{\sigma}_x'|_{a,0} \\ \bar{\sigma}_{xy}'|_{a,0} &= 0 \end{aligned}\right\} \quad \ldots\ldots\ldots [17]$$

Similarly, the bending stresses at the edge simplify to

$$\left.\begin{aligned} \bar{\sigma}_x''|_{a,0} &= \mp \frac{4(a_{00} + a_{20}a^2)}{1-\nu^2} \\ \bar{\sigma}_y''|_{a,0} &= \nu\bar{\sigma}_x''|_{a,0} \\ \bar{\sigma}_{xy}''|_{a,0} &= 0 \end{aligned}\right\} \quad \ldots [18]$$

Certain simplifications are feasible for the extreme cases (circle, infinite strip) in the derivations outlined in the foregoing. These can be detailed as follows:

Circular Plate, Case (I)

The semimajor and semiminor axes are equal in this case ($a = b$) and a radial symmetry exists. The parameters assumed in Equations [10] must therefore obey the following conditions

$$a_{20} = a_{02}; \quad b_{00} = c_{00}; \quad b_{20} = c_{02}; \quad b_{02} = c_{20}; \quad b_{22} = c_{22}$$

Thus Equations [15] and [16] reduce to

$$\bar{\sigma}_x'|_{0,0} = \bar{\sigma}_y'|_{0,0} = \frac{b_{00}a^2}{1-\nu} \quad \ldots\ldots\ldots [19]$$

$$\bar{\sigma}_x''|_{0,0} = \bar{\sigma}_y''|_{0,0} = \pm\frac{2a_{00} - a_{20}a^2}{1-\nu} \quad \ldots\ldots\ldots [20]$$

Infinite Strip, Case (IV)

In this case $b = \infty$, $a/b = 0$, so that neither deflections nor displacements can be a function of y. This condition is satisfied only if

$$a_{02} = b_{02} = b_{22} = c_{00} = c_{20} = c_{02} = c_{22} = 0$$

The expressions for the stresses, therefore, simplify to

$$\bar{\sigma}_x'|_{0,0} = \frac{1}{\nu}\bar{\sigma}_y'|_{0,0} = \frac{b_{00}a^2}{1-\nu^2} \quad \ldots\ldots\ldots [21]$$

for the membrane stresses, and to

$$\bar{\sigma}_x''|_{0,0} = \frac{1}{\nu}\bar{\sigma}_y''|_{0,0} = \pm\frac{2a_{00} - a_{20}a^2}{1-\nu^2} \quad \ldots\ldots\ldots [22]$$

for the bending stresses at the center. The shearing stresses at the center line of the plate are again equal to zero.

The membrane and bending stresses at the edge for both the circular plate and the infinite strip retain their expressions unaltered as given in Equations [17] and [18], respectively.

The stresses at the center and the edge of the plates are listed in Tables 1 to 4. Only stresses acting in the x-direction were tabulated, since they are numerically equal to, or greater than, the stresses acting in the y-direction.

Stresses as a function of the distributed load are shown in Fig. 3 for stresses at the center and in Fig. 4 for stresses at the edge of the plate. These figures are quite similar in appearance to Fig. 2. The small-deflection theory reaches its limit of validity of application when the total stress at the center attains a value of about 1.25, or when the dimensionless stress at the edge becomes equal to roughly 2.0.

The energy-method solution is again compared with the exact solution for the total stresses at the edge, Fig. 4. For the circular plate the agreement is good, the difference being of the order of 1.5 per cent. Somewhat worse results are obtained for the infinite strip, the deviation being about 5.5 per cent, although this error lies on the safe side.

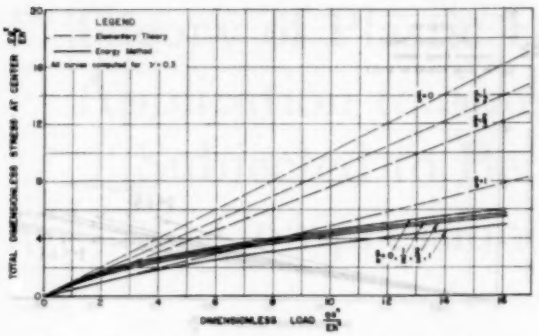

FIG. 3 TOTAL STRESS AT CENTER AS FUNCTION OF LOAD

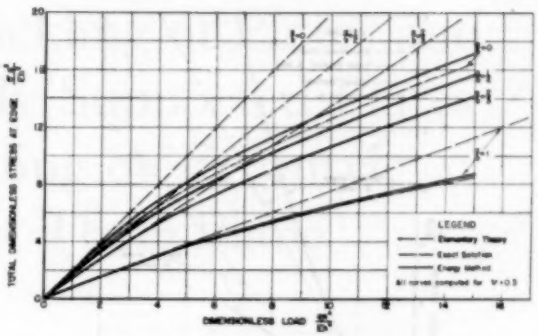

FIG. 4 TOTAL STRESS AT EDGE AS FUNCTION OF LOAD

TABLE 2 DISPLACEMENT PARAMETERS AND STRESS VALUES FOR ELLIPTICAL PLATE; $a/b = 2/3$

Dimensionless load qa^4/Eh^4	a_{00}	$a_{02}a^2$	$a_{04}a^3$	$b_{02}a^2$	$b_{12}a^4$	$b_{04}a^4$	$b_{12}a^6$	$c_{02}a^2$	$c_{04}a^4$	$c_{24}a^4$	$c_{12}a^6$
1	0.290	0.007	0.006	0.038	—0.084	—0.033	0.038	0.022	—0.063	—0.017	0.026
2	0.523	0.039	0.031	0.130	—0.277	—0.107	0.111	0.074	—0.203	—0.058	0.075
3	0.704	0.092	0.073	0.245	—0.509	—0.193	0.175	0.140	—0.362	—0.106	0.119
6	1.074	0.296	0.228	0.636	—1.230	—0.443	0.243	0.366	—0.815	—0.254	0.166
10	1.388	0.577	0.430	1.169	—2.125	—0.727	0.123	0.676	—1.312	—0.438	0.099
15	1.663	0.895	0.649	1.813	—3.132	—1.021	—0.201	1.048	—1.819	—0.643	—0.086

Dimensionless bending stress		Dimensionless membrane stress		Dimensionless total stress	
At center	At edge	At center	At edge	At center	At edge
0.739	1.305	0.049	0.100	0.788	1.405
1.250	2.471	0.167	0.323	1.417	2.795
1.629	3.498	0.316	0.579	1.945	4.077
2.275	6.021	0.820	1.305	3.095	7.326
2.683	8.638	1.508	2.100	4.191	10.738
2.945	11.243	2.338	2.898	5.283	14.141

TABLE 3 DISPLACEMENT PARAMETERS AND STRESS VALUES FOR ELLIPTICAL PLATE; $a/b = 1/2$

Dimensionless load qa^4/Eh^4	a_{00}	$a_{02}a^2$	$a_{04}a^3$	$b_{02}a^2$	$b_{12}a^4$	$b_{04}a^4$	$b_{12}a^6$	$c_{02}a^2$	$c_{04}a^4$	$c_{24}a^4$	$c_{12}a^6$
1	0.344	0.011	0.009	0.052	—0.119	—0.022	0.026	0.019	—0.059	—0.008	0.013
2	0.600	0.058	0.043	0.169	—0.369	—0.066	0.061	0.063	—0.173	—0.025	0.030
3	0.789	0.123	0.092	0.309	—0.650	—0.110	0.071	0.117	—0.289	—0.044	0.035
6	1.163	0.365	0.196	0.762	—1.476	—0.224	—0.026	0.296	—0.575	—0.098	—0.008
10	1.490	0.683	0.334	1.362	—2.463	—0.338	—0.307	0.533	—0.854	—0.162	—0.126
15	1.790	1.033	0.472	2.078	—3.556	—0.449	—0.748	0.811	—1.118	—0.233	—0.302

Dimensionless bending stress		Dimensionless membrane stress		Dimensionless total stress	
At center	At edge	At center	At edge	At center	At edge
0.798	1.559	2.964	0.145	0.862	1.705
1.343	2.884	0.207	0.438	1.550	3.322
1.699	4.011	0.379	0.749	2.077	4.760
2.282	6.719	0.935	1.570	3.217	8.289
2.660	9.550	1.673	2.420	4.333	11.970
2.939	12.409	2.551	3.247	5.490	15.656

The findings of the exact theory are not shown for the stresses at the center of the plates. The deviations between the energy-method and the exact solution, however, are smaller in this case than for the stresses at the edge of the plates, as seen for the circular plate in Fig. 5.

The second set of graphs show stresses in terms of deflections. Fig. 5 depicts the variation of membrane and bending stresses in a circular plate individually, and draws them into comparison with the exact solution derived by Way (1), and the elementary theory. The satisfactory correlation between the energy-method and the exact solution is again demonstrated. Fig. 5 also reveals that, due to the cumulative nature of deviations, considerably greater differences should be expected to occur between the large-deflection and elementary theory for total stresses at the edge than for those at the center, where deviations in the component stresses are of opposite signs.

This deduction is substantiated by Figs. 6 and 7. Fig. 7 shows, moreover, that the edge stress versus center-deflection relation is its dimensionless form remains independent of the shape of the plate for the large-deflection solution as well as for the elementary theory. This is an important finding, if one recalls that the

TABLE 4 DISPLACEMENT PARAMETERS AND STRESSES FOR INFINITE STRIP; $a/b = 0$

Dimensionless load qa^4/Eh^4	a_{00}	$a_{02}a^2$	$b_{02}a^2$	$b_{12}a^4$
1	0.393	0.016	0.069	—0.152
2	0.669	0.074	0.216	—0.456
3	0.872	0.156	0.387	—0.787
6	1.267	0.421	0.926	—1.748
10	1.606	0.744	1.533	—2.904
15	1.927	1.084	2.432	—4.195

Dimensionless bending stress		Dimensionless membrane stress		Dimensionless total stress	
At center	At edge	At center	At edge	At center	At edge
0.847	1.797	0.076	0.182	0.923	1.979
1.389	3.268	0.238	0.526	1.626	3.794
1.745	4.516	0.425	0.879	2.171	5.395
2.272	7.423	1.017	1.808	3.340	9.230
2.712	10.332	1.795	2.791	4.507	13.123
3.042	13.235	2.672	3.874	5.715	17.110

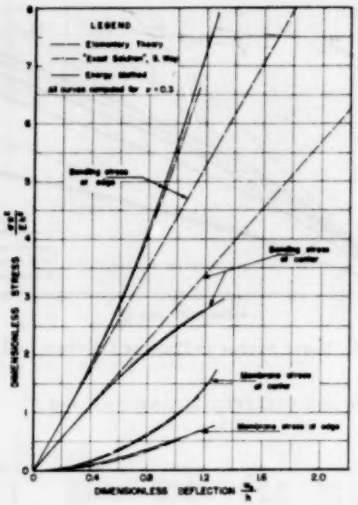

FIG. 5 BENDING AND MEMBRANE STRESSES IN TERMS OF CENTER DEFLECTION FOR A CIRCULAR PLATE

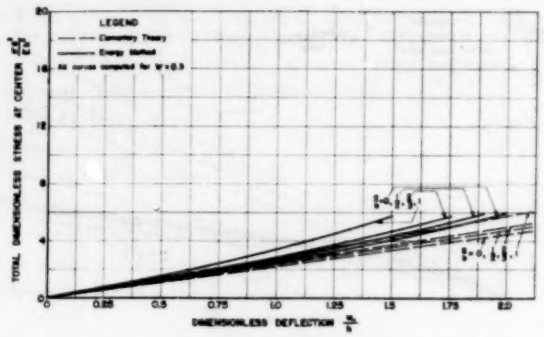

FIG. 6 INTERRELATION OF TOTAL STRESS AT CENTER AND CENTER DEFLECTION

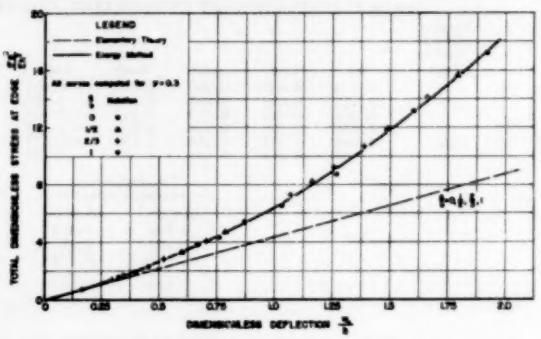

FIG. 7 INTERRELATION OF TOTAL STRESS AT EDGE AND CENTER DEFLECTION

stress at the edge represents the maximum stress over the plate, and would thus govern design considerations. If, therefore, the dimensionless center deflection can be ascertained, e.g., from Fig. 2 by interpolation, for a given load on an elliptical plate of arbitrary dimensions, the governing stress can be determined immediately from the single curve portrayed in Fig. 7.

ACKNOWLEDGMENTS

This investigation formed part of a program resulting from a co-operative agreement between the Engineering Experiment Station of the University of Illinois and the Copper and Brass Research Association. The authors gratefully acknowledge the help of Mrs. A. C. Weil for carrying out the numerical work and checking the derivations incorporated in the solution.

BIBLIOGRAPHY

1 "Bending of Circular Plates With Large Deflections," by S. Way, Trans. ASME, vol. 56, 1934, pp. 627–636.

2 "Elastische Platten," by A. Nádai, Julius Springer, Berlin, Germany, 1925, p. 228.

3 "Über den Spannungszustand in kreisrunden Platten mit verschwinderden Biegungssteifigkeit," by H. Hencky, *Zeitschrift für Mathematik und Physik*, vol. 63, 1915, pp. 311–317.

4 "Large Deflection of a Circular Clamped Plate Under Uniform Pressure," by W. Z. Chien, *Chinese Journal of Physics*, vol. 7, 1947, pp. 102–113.

5 "Asymptotic Behavior of a Clamped Circular Plate Under Uniform Normal Pressure at Very Large Deflection," by W. Z. Chien, Sci. Rep. Nat. Tsing Hua University, series A, vol. 5, 1948, pp. 71–94.

6 "Bending of Plates With a Small Initial Curvature," by S. Timoshenko, *Memoirs of the Institute of Ways of Communication*, St. Petersburg, Russia, vol. 89, 1915, p. 23.

7 "Large Deflection of Circular Plates," by M. Stippes and A. H. Hausrath, JOURNAL OF APPLIED MECHANICS, Trans. ASME, vol. 74, 1952, pp. 287–292.

8 "Drang und Zwang," by A. Föppl and L. Föppl, R. Oldenburg, Berlin, Germany, vol. 1, 1924, p. 226.

9 "Uniformly Loaded, Clamped, Rectangular Plates With Large Deflection," by S. Way, Proceedings of the Fifth International Congress for Applied Mechanics, Cambridge, Mass., 1938, pp. 123–128.

10 "Bending of Rectangular Plates With Large Deflections," by S. Levy, NACA Technical Note No. 846, May, 1941.

11 "Rechnerische und experimentelle Ermittlung der Durchbiegungen und Spannungen von quadratischen Platten bei freier Auflagerung an den Rändern, gleichmässig verteilter Last und grossen Ausbiegungen," by R. Kaiser, *Zeitschrift für angewandte Mathematik und Mechanik*, bd. 16, heft 2, April, 1936, pp. 73–98.

12 "Theory of Plates and Shells," by S. Timoshenko, McGraw-Hill Book Company, Inc., New York, N. Y., 1940, pp. 290–293.

13 "The Bending of Thin Elliptic Plates," by C. L. Perry, Proceedings of the Symposium on Applied Mathematics, vol. 3, 1950, pp. 131–139.

14 Reference (12), p. 304.

15 Reference (12), p. 345.

16 "Numerical Mathematical Analysis," by J. B. Scarborough, The Johns Hopkins Press, second edition, 1950.

17 Reference (12), pp. 1–17.

Theory of Plastic Buckling of Plates and Application to Simply Supported Plates Subjected to Bending or Eccentric Compression in Their Plane

By P. P. BIJLAARD,[1] ITHACA, N. Y.

After some general considerations on the plastic buckling of plates, the plastic buckling stresses are calculated for long plates, subject to longitudinal bending or eccentric compression in their plane, and simply supported at their unloaded edges. The solutions are based on the author's theory of plastic plate buckling and are obtained by reducing the governing partial differential equation to ordinary finite-difference equations. Second-order finite differences are used, with a spacing equal to one ninth of the plate width. A simple design formula is presented for the plastic reduction factor with which the elastic buckling stress has to be multiplied for obtaining the plastic buckling stress.

Introduction

Up to now the plastic reduction factors η, with which one has to multiply the elastic buckling stress to obtain the plastic buckling stress, have been calculated for practically all important cases of homogeneous stress distribution and for several boundary conditions.

It is the purpose of the present paper and subsequent ones to derive similar data for cases of nonhomogeneous stress distribution. This paper deals with long simply supported plates subjected to bending or eccentric compression in their plane. In subsequent papers other cases, such as simply supported flanges subjected to the same loading and simply supported plates, subject to combined bending or eccentric compression and shear, will be dealt with.

Before dealing with the present case of nonhomogeneous stress distribution a short outline will be given of the principles on which the author's theory is based and it will be shown that these principles are confirmed by recent tests. Then a comprehensive account is presented of the publications where the necessary data for cases of homogeneous stress distribution can be found. Finally, the new formulas for buckling of simply supported plates subjected to bending or eccentric compression in their plane will be derived.

Basic Principles of Theory

The theory assumes that the shear (distortion) energy governs the plastic deformation and that the plastic part of the deformations occurs quasi-isotropically, that is, in a similar way as the elastic deformation, but with a variable plastic modulus and with a Poisson's ratio equal to 0.5. Both these hypotheses are in good accordance with experimental work. Actually, the plastic deformations occur by sliding along numerous crystallographic planes and the assumption of quasi-isotropic deformation is tantamount to assuming that in all planes the plastic shear strains are proportional to the shear stresses in these planes.

With incipient buckling of plates and shells a state of stress with infinitely small stress components is superimposed on the original state of stress before buckling. In general the ratios of the superimposed stress components will differ from those of the original ones. In such a case additional assumptions are necessary. Two extreme ones are (*a*) deformation theory (Hencky body), (*b*) simple flow theory (Prandtl-Reuss body). In deformation theory it is assumed that the final strains are the same as if the stress components had increased from zero to their final values with constant ratios equal to these ratios in the final state of stress. Therefore the final deviatoric strain components are proportional to the final deviatoric stress components. In flow theory it is assumed that at any instant the increments of the deviatoric plastic-strain components are proportional to the total deviatoric stress components at that instant. For the special case of plastic plate buckling, where, at incipient buckling, only infinitely small strains are superimposed, this leads to the same results as deformation theory, if the plastic deformations before buckling are neglected (1).[2] Hence the plastic reduction factors from flow theory follow immediately from those from deformation theory by assuming $E_s = E$, where E_s and E are the secant and elastic moduli, respectively; on the other hand, the tangent modulus E_t remains unchanged. This means that flow theory leads to higher plastic buckling stresses than deformation theory.

From Kollbrunner's buckling tests on angles (2) the author concluded (1) that for aluminum, flow theory leads to too high buckling stresses. To remain on the safe side he therefore based his resulting formulas on deformation theory. From later tests by Kollbrunner (3), Stussi (4), and the NACA (5) it could be concluded (6) that the buckling stresses based on deformation theory are in excellent agreement with those from experiments, while the predictions from flow theory are much too high. This was confirmed by later tests (7, 8, 9).

It may be understood why in the special case of plastic plate buckling the assumptions of deformation theory are practically in complete agreement with the actual behavior. This was explained briefly,[3] but will be considered here in some more detail.

---

[1] Professor of Structural Engineering, Cornell University.

Contributed by the Applied Mechanics Division and presented at the Diamond Jubilee Annual Meeting, Chicago, Ill., November 13–18, 1955, of The American Society of Mechanical Engineers.

Discussion of this paper should be addressed to the Secretary, ASME, 29 West 39th Street, New York, N. Y., and will be accepted until April 10, 1956, for publication at a later date. Discussion received after the closing date will be returned.

Note: Statements and opinions advanced in papers are to be understood as individual expressions of their authors and not those of the Society. Manuscript received by ASME Applied Mechanics Division, November 19, 1954. Paper No. 55—A-8.

[2] Numbers in parentheses refer to the Bibliography at the end of the paper.

[3] Reference (6), pp. 532–533.

The differences between the predictions from deformation and flow theory are most pronounced in the case of torsional buckling of a simply supported long flange or of a cruciform section. According to deformation theory the plastic reduction factor is here slightly lower than E_s/E, in exact agreement with buckling tests.[4] In contrast, flow theory predicts a reduction factor one, in marked contradiction of what follows from tests.

At incipient torsional buckling of a long flange or cruciform section pure shear stresses are superimposed on the original pure compressive stresses, somewhat (but not quite) in a similar way as in a tube that is first subjected to compression and subsequently twisted, leaving the compressive stresses constant. In the latter case, the stress in a plane normal to the original compression is first represented by point A in Fig. 1 and, after superposition of infinitely small shear stresses, by point A'. Similarly, the stresses in other planes, as indicated just before applying the torque by points B, C, and D, after superposition of the torque are represented by the points B', C', and D', respectively. Hence in the planes indicated by points on the Mohr circle near the solid arrows the absolute values of the shear stresses increase, while they decrease in the planes represented by points near the dashed arrows.

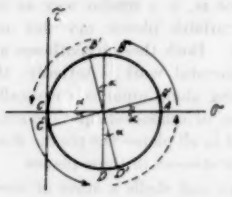

FIG. 1 MOHR CIRCLE FOR STRESSES IN TUBE, SUBJECTED TO COMPRESSION AND SUBSEQUENTLY INFINITESIMALLY TWISTED

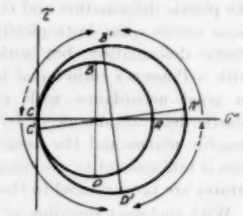

FIG. 2 MOHR CIRCLES FOR STRESSES IN CRUCIFORM SECTION, BEFORE AND AFTER TORSIONAL BUCKLING

In this case flow theory would predict no plastic deformation at all. This is unlikely, since in the planes indicated by points near the solid arrows the absolute value of the shear stresses increases and therefore plastic deformations can be assumed to occur in these planes. On the other hand, according to deformation theory, the final plastic deformations are the same as if the torque were applied simultaneously with the compression, so that in all planes the shear stresses would increase monotonically up to their final value. For the planes where the shear stresses increase during the actual sequence of loading (solid arrows) this assumption is likely to be right, but for the planes where the shear stresses decrease (dashed arrows) one would have to assume that the plastic shear strains decrease during application of the torque. This is not likely, since decrease of the shear stresses will only diminish the elastic shear strains, but not the plastic ones. Therefore the actual deformation for this case is likely to be between the predictions of flow and deformation theory. This is confirmed by tests with aluminum alloy 14S-T4 at Pennsylvania State College (11). For 14S-T6 the plastic shear strains were even higher than those predicted by deformation theory. Although for the case of infinitely small superimposed shear stresses earlier tests seemed to favor flow theory, recent tests (12) show that the initial plastic shear modulus for the superimposed shear stresses, which according to flow theory would be equal to the elastic one, in certain cases is smaller than that by approximately a factor of 2.

At incipient buckling of a long simply supported flange or cruciform section, however, a somewhat different case arises. In analogy to Shanley's principle for columns (13) and in connection with unavoidable initial eccentricities, simultaneously with the twisting of the flange the compressive stresses will increase here. Hence the stress in a normal section, before twisting indicated by point A in Fig. 2, after a small twist will be represented by point A' (σ as well as τ increases here). Similarly, the stresses in the planes originally indicated by B, C, and D will then be given by points B', C', and D'. Fig. 2 shows that in all planes indicated by points near the solid arrows the shear stresses increase. They decrease only in planes designated by points near the small dashed arrows, where the shear stresses are small and therefore contribute very little to the entire plastic deformation. Hence during the entire process practically in all planes the shear stresses increase.

It is logical to assume that for materials like aluminum, where a given uniaxial stress causes a definite plastic strain, also a given combination of shear stresses in various planes will cause a definite combination of plastic shear strains, if the resolved shear stresses, that is, the components of the shear stresses in the slip planes of the crystallites in the slip directions, increase continuously. In that case the plastic shear strains, and therefore the resulting plastic deformation, will be the same as if during the entire loading the ratios between the stress components remained constant, that is, the same as predicted by deformation theory. This obviously happens with plastic buckling of plates and explains the excellent agreement between the theoretical predictions, based on deformation theory, and the experimental results. The same explanation was given by the author in more condensed form.[3] A practically analogous explanation was simultaneously given by Batdorf (14).

The foregoing principles are very well illustrated by a recent experiment made by Feigen (15). The present Fig. 3 is a simplified copy of his fig. 38. A tube of aluminum alloy 24S-T3 was first loaded in tension up to an axial strain of 8000 microinches per in. Then a torque, causing shear stresses of $\tau = 265$ psi, was applied instantaneously to the specimen. Leaving the torque constant, the axial load was then increased further and readings of the plastic shear strains were taken up to an axial strain of 11,500 microinches per in. Fig. 3 shows the experimental results and the predictions from deformation and flow theory. The instantaneous application of the shear stresses obviously causes a decrease of the shear stresses in a large number of planes (dashed arrows in Fig. 1), so that the additional plastic strains will be smaller than indicated by deformation theory, since the latter assumes that in the planes where the shear stresses decrease the plastic shear strains would decrease, while actually only the elastic ones decrease. However, with further increase of the axial stress a stage is reached where practically in all planes the shear stresses are higher than in any earlier stage, so that a situa-

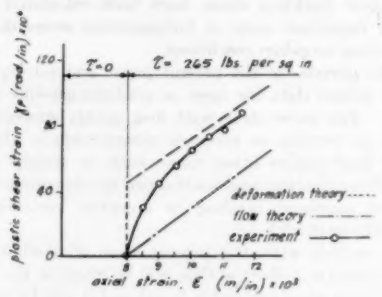

FIG. 3 EXPERIMENT BY FEIGEN

[4] Reference (10), fig. 3.

tion occurs as was illustrated in Fig. 2. Therefore with further increase of the axial strain (and stress) the plastic shear strains will approach the predictions of deformation theory, as is very well confirmed by Fig. 3.

Available Data

Formulas for the plastic reduction factors for several cases, derived in the author's earlier publications, have been assembled in table 5 of reference (6). Additional data were derived in reference (16), where the pertinent formulas are given in equations [73 to 76] and [27].

The coefficients A, B, D, and F in these formulas, with the exception of Case 6 of (6) and equation [75] of (16), are given by equation [22] or [23] of (17) and by equation [21] or [21a] of (6). These coefficients (as stated on page 535 of reference 6) were derived for cases where the axes of the excess state of stress, superimposed with incipient buckling, are placed in the directions of the principal stresses of the original state of stress, before buckling. As follows from the derivation in (1) or (18) of the formula for a square plate under pure shear (Case 6 of reference 6) and of equation [75] in reference (16) for a long plate under pure shear, where the axes of the superimposed state of stress are not in the directions of the principal axes of the original state of stress, for both these cases A, B, and F are given by equations [57] of (1) or equations [36] of (18). The same expressions for A, B, and F may also be found in a more recent paper.[5]

Formulas for T-sections have been derived in (20). The plastic reduction factors for sandwich plates have been determined in (16) and (19) and those of alclad plates in (27).

For the special case of structural steel the author's theory was completely worked out in (21) for all kinds of boundary conditions and for bridge members with customary cross sections, taking account of the restraint exerted on each other by the component plates. A table is given there of the width-to-thickness ratios of the plates required to make the local buckling stress equal to the buckling stress of the member as a whole.

[5] Top of second column on page 345 of reference (19).

In order to facilitate the application of the theory to other materials such as aluminum, magnesium, and titanium alloys, carpet plots have been made by the Bell Aircraft Corporation, from which the coefficients A, B, D, and F and also the plastic reduction factors η for important cases can be read immediately as a function of E_s/E and E_t/E, where E_s and E_t are the secant and tangent moduli, respectively (22). Some of these plots probably will be published. A copy of such a plot for a long plate in compression, simply supported at the unloaded edges, is given in Fig. 4.

Simply Supported Plate Subjected to Longitudinal Bending or Eccentric Compression in Its Plane

1 *Derivation of Finite-Difference Buckling Equations.* The difficulty that arises if cases of nonhomogeneous stress distribution are considered is that in the plastic range the reduction coefficients A, B, D, and F, as given by equations [22] and [23] of (17) and by equations [21] and [21a] of (6), vary with the co-ordinates x and y, since they depend on the state of stress before buckling. This would lead to a much more complicated differential equation than equation [23] of (6) (given below as Equation [1]). However, in the present case (Fig 5), where the state of stress before buckling varies in the Y-direction only, this difficulty can be coped with by dividing the plate into imaginary longitudinal strips, running in the X-direction. If it is then assumed that within these strips the plastic reduction coefficients

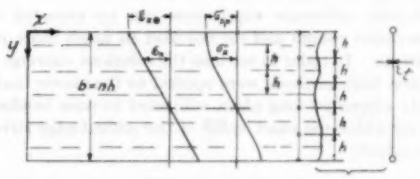

Fig. 5 Web Subjected to Eccentric Compression in Its Plane

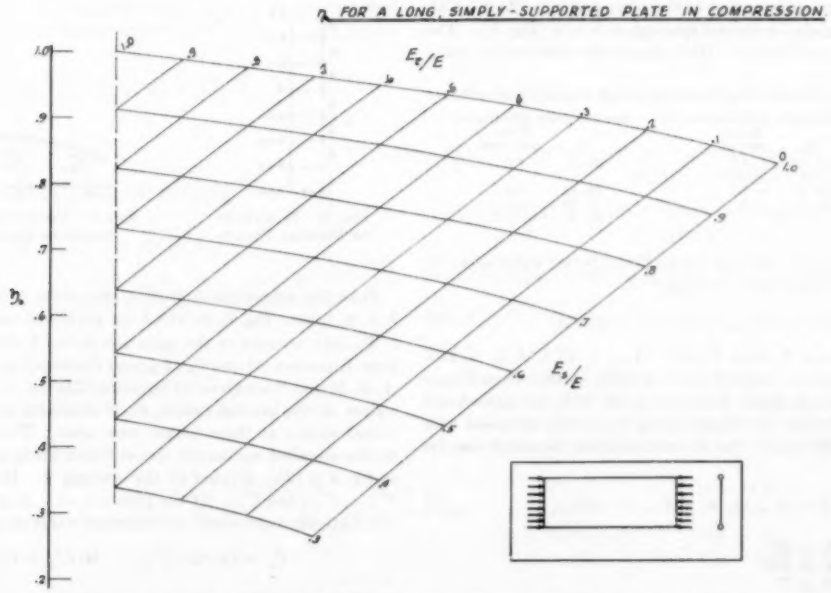

Fig. 4 Plastic Reduction Factor η_c for a Long, Simply Supported Plate in Compression

A, B, and D and F are constant, for each of these individual strips equation [23] of (6)

$$EI\left[A\frac{\partial^4 w}{\partial x^4} + 2(B+2F)\frac{\partial^4 w}{\partial x^2 \partial y^2} + D\frac{\partial^4 w}{\partial y^4}\right] + t\sigma_x\frac{\partial^2 w}{\partial x^2} = 0 \quad \ldots\ldots [1]$$

applies, where w is the buckling deflection and t and σ_x are the plate thickness and the appropriate value of σ_x for that strip. Further, E is the elastic modulus and $I = t^3/12$. With

$$w = Y \sin \pi x/a = Y \sin \lambda x \quad \ldots\ldots [2]$$

where Y is a function of y only and a is the half-wave length in the X-direction, this differential equation transforms to

$$DY^{IV} - 2(B+2F)\lambda^2 Y'' + (A\lambda^4 - \rho\lambda^2\varphi^2)Y = 0 \quad \ldots [3]$$

Here (Fig. 5)

$$\rho = \sigma_x/\sigma_{xp} \text{ and } \varphi^2 = t\sigma_{xp}/EI \quad \ldots\ldots [4]$$

where σ_{xp} is the edge stress at $y = 0$. Further, in Equation [3] a prime denotes a differentiation with respect to y.

Equation [3] was written as a set of finite-difference equations, that lead to a determinant from which φ^2, and thus the edge buckling stress σ_{xp}, can be calculated, as will be shown. This may be carried out in different ways; namely, by writing the derivatives in Equation [3] as first or as second-order differences.[6] Second-order difference expressions can be expected to give more accurate results and do not lead to much more involved calculations. In order to see how the solutions converge in both cases, first both methods were applied to the elastic buckling of a simply supported long plate, subjected to pure bending in its plane, for which the exact value of the critical edge stress σ_{xe} is known, namely[7]

$$\sigma_{xe} = k_e\frac{\pi^2 N}{b^2 t} \quad \ldots\ldots [5]$$

where N is the flexural rigidity of the plate and $k_e = 23.9$. Calculations were made for several spacings $h = b/n$ (Fig. 5). The results are given in Table 1. With the results obtained by using

TABLE 1 RESULTS OF CALCULATIONS FOR VARIOUS SPACINGS

	First-order differences		Second-order differences	
n	k_e	Error, per cent	k_e	Error, per cent
3	21.05	−12	24.3	+2
4	<20	−>20		
5	21.4	−10	23.43	−2
7	22.6	−5	23.78	−0.5
9			23.87	−0.1

first-order differences, one can try to find a better value of k_e by using the h^2-extrapolation formulas[8]

$$k = A_{(n1)(n2)} = \alpha_1 A_{(n1)} + \alpha_2 A_{(n2)} \quad \ldots\ldots [6]$$

With $n_1 = 5$, $n_2 = 7$, from Table 1, $A_{(n1)} = 21.4$, $A_{(n2)} = 22.6$ and from (23) $\alpha_1 = -1.0417$, $\alpha_2 = 2.0417$, so that from Equation [6] the extrapolated value of k_e is 23.9, in accordance with the exact value. Similarly, using the results obtained with second-order differences, the h^4-extrapolation formula[9] can be used. This is

$$k = A_{(n1)(n2)} = \gamma_1 A_{(n1)} + \gamma_2 A_{(n2)} \quad \ldots\ldots [7]$$

[6] Reference (23), p. 69.
[7] Reference (24), p. 355.
[8] Reference (23), p. 77.
[9] Ibid., p. 79.

Using again $n_1 = 5$, $n_2 = 7$, from Table 1, $A_{(n1)} = 23.43$, $A_{(n2)} = 23.78$. From (23), $\gamma_1 = -0.3519$, $\gamma_2 = 1.3519$, so that Equation [7] yields $k_e = 23.9$.

Although these extrapolation formulas were not intended to be used in cases of nonhomogeneous stress distribution, it appears that in both the foregoing cases they lead to accurate results, so that in the elastic range it would be preferable to use the more simple first differences. However, it may not be expected that these formulas will work in the case of plastic buckling, because here, besides the errors in the finite differences, additional errors occur as a result of the assumption of constant values A, B, D, and F within the strips. Thus it cannot be expected that the errors are proportional to h^2 or h^4 when using first or second differences, respectively, as is assumed in the derivation of the extrapolation formulas. Hence one can only rely on the directly calculated results, which, from Table 1, are much more accurate if calculated with second-order finite differences. Therefore these were used in all further calculations.

Using pivotal points with a spacing h, Fig. 5, at a pivotal point k (Fig. 6)[10]

$$\left.\begin{aligned} Y'' &= [1/(12h^2)]\,(-Y_{k-2} + 16Y_{k-1} \\ &\qquad - 30Y_k + 16Y_{k+1} - Y_{k+2}) \\ Y^{IV} &= [1/(6h^4)]\,(-Y_{k-2} + 12Y_{k-2} \\ &\qquad - 39Y_{k-1} + 56Y_k - 39Y_{k+1} + 12Y_{k+2} - Y_{k+3}) \end{aligned}\right\} \quad \ldots [8]$$

Inserting this into Equation [3], one obtains the following finite-difference equation for point k

$$-D_k Y_{k-2} + C_{1k}Y_{k-1} + C_{2k}Y_{k-1} + (C_{3k} - 6\lambda^2 h^4 \rho_k \varphi^2)Y_k + C_{2k}Y_{k+1} + C_{1k}Y_{k+2} - D_k Y_{k+3} = 0 \quad \ldots\ldots [9]$$

where

$$\left.\begin{aligned} C_{1k} &= 12\,D_k + (B+2F)_k\,\lambda^2 h^2 \\ C_{2k} &= -39\,D_k - 16(B+2F)_k\lambda^2 h^2 \\ C_{3k} &= 56\,D_k + 30(B+2F)_k\lambda^2 h^2 + 6A_k\lambda^4 h^4 \end{aligned}\right\} \quad \ldots [10]$$

FIG. 6 NOTATION OF PIVOTAL POINTS

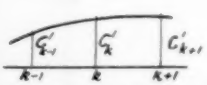

FIG. 7 NOTATION OF COEFFICIENTS IN EQUATION [11]

Here the subscripts k, $k+1$, etc., refer to the pivotal points k, $k+1$, etc., Fig. 6, to which the pertinent values belong.

To take account of the variation in the Y-direction of $\rho_k = \rho$ from Equation [4] and C_{1k}, C_{2k}, and C_{3k} from Equation [10], where A, B, D, and F are given by equation [21a] of (6), instead of these values at the pivotal points, their statically equivalent concentrated values at these points were used. These are equivalent to the so-called equivalent concentrated loads used by Newmark in fig. 5 of (25), divided by the spacing h. Hence, with values C'_{k-1}, C'_k, and C'_{k+1} at the points $k-1$, k, and $k+1$ (Fig. 7) the statically equivalent concentrated value at point k is

$$C_k = (1/12)\,(C'_{k-1} + 10\,C'_k + C'_{k+1}) \quad \ldots\ldots [11]$$

[10] Reference (23), p. 69.

This formula is adequate for smoothly varying values of ρ, C_{1k}, C_{2k}, and C_{3k}, as will obtain for materials having smooth stress-strain curves, like aluminum. However, with a stress-strain diagram like that for structural steel, which for the present purpose may be approximated by the straight lines in Fig. 8, at the yield point the distribution of ρ shows a break and that of C_{1k}, C_{2k}, and C_{3k} shows a jump, as illustrated in Figs. 9 and 10, respectively. In the elastic range ρ varies linearly and C_{1k}, C_{2k}, and C_{3k} are constant. Denoting again the actual values at the pivotal points by additional primes, it is a simple problem of statics to obtain the statically equivalent concentrated values to be inserted into Equation [9]. From Fig. 9

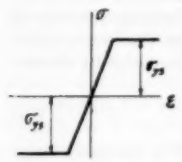

FIG. 8 SIMPLIFIED STRESS-STRAIN DIAGRAM OF MILD STEEL

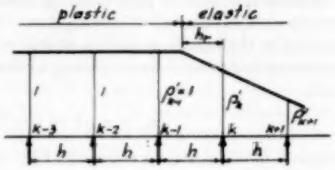

FIG. 9 NOTATION OF VALUES IN EQUATION [12]

$$\left.\begin{aligned}
\rho_{k-2} &= 1 \\
\rho_{k-1} &= 1 - (1/6)\,(1 - \rho_k')\,(h_r/h)^2 \\
\rho_k &= (1/6)\,(2\rho_k' + \rho'_{k+1}) + \frac{1}{2} \\
&\quad - \frac{1}{2}\,(1 - \rho_k')\,(h_r/h)\,[1 - (1/3)\,(h_r/h)] \\
\rho_{k+1} &= \rho'_{k+1}
\end{aligned}\right\} \quad \ldots [12]$$

In Fig. 10 it may be assumed that in the plastic range the values C vary linearly between the pivotal points. This leads from Fig. 10 to the following statically equivalent concentrated values C_{1k}, C_{2k}, or C_{3k} represented by the symbol C_k, to be inserted into Equation [9]

$$\left.\begin{aligned}
C_{k-2} &= (1/6)\,(C'_{k-1} + 4C'_{k-2} + C'_{k-3}) \\
C_{k-1} &= \frac{1}{2}\,(h_r/h)^2\,C'_{el} \\
&\quad + \frac{1}{2}\,(h_l/h)\,[1 - (2/3)\,(h_l/h)]C'_k \\
&\quad + \left\{\frac{1}{2}\,(h_l/h)\,[1 - (1/3)\,(h_l/h)]\right. \\
&\qquad \left. + (1/3)\right\} C'_{k-1} + (1/6)C'_{k-2} \\
C_k &= \left\{\frac{1}{2} + (h_r/h)\left[1 - \frac{1}{2}\,(h_r/h)\right]\right\} C'_{el} \\
&\quad + (1/3)\,(h_l/h)^2 C'_k + (1/6)\,(h_l/h)^2 C'_{k-1} \\
C_{k+1} &= C'_{el}
\end{aligned}\right\} \quad \ldots [13]$$

Here C'_{el} represents the constant values of C'_{1k}, C'_{2k}, or C'_{3k} in the elastic range and C'_k is the magnitude of the same parameters in the plastic range at the boundary with the elastic range, Fig. 10.

In order to judge into how many spacings the plate width b should be divided in order to obtain accurate results in the plastic range, calculations were made with $n = b/h = 3$, 5, 7, and 9. To save space only the determinant for $n = 5$ will be given here.

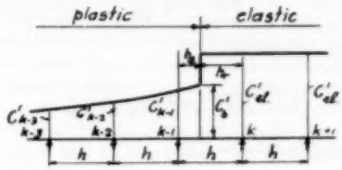

FIG. 10 NOTATION OF VALUES IN EQUATION [13]

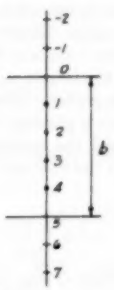

FIG. 11 PIVOTAL POINTS TO WHICH EQUATIONS [14] REFER

In that case, from Equation [9], and assuming imaginary points outside the plate, the difference equations for the points 1, 2, 3, and 4 become, respectively, Fig. 11

$$\left.\begin{aligned}
&-D_1Y_{-2} + C_{11}Y_{-1} + C_{21}Y_0 + (C_{21} - 6\lambda^2h^4\rho_1\varphi^2)Y_1 \\
&\qquad + C_{21}Y_2 + C_{11}Y_3 - D_1Y_4 = 0 \\
&-D_2Y_{-1} + C_{12}Y_0 + C_{22}Y_1 + (C_{22} - 6\lambda^2h^4\rho_2\varphi^2)Y_2 \\
&\qquad + C_{22}Y_3 + C_{12}Y_4 - D_2Y_5 = 0 \\
&-D_3Y_0 + C_{13}Y_1 + C_{23}Y_2 + (C_{23} - 6\lambda^2h^4\rho_3\varphi^2)Y_3 \\
&\qquad + C_{23}Y_4 + C_{13}Y_5 - D_3Y_6 = 0 \\
&-D_4Y_1 + C_{14}Y_2 + C_{24}Y_3 + (C_{24} - 6\lambda^2h^4\rho_4\varphi^2)Y_4 \\
&\qquad + C_{24}Y_5 + C_{14}Y_6 - D_4Y_7 = 0
\end{aligned}\right\} \quad \ldots [14]$$

From the simple supports at the edges $y = 0$ and $y = b$, Fig. 5

$$Y_{-2} = -Y_2; \quad Y_{-1} = -Y_1; \quad Y_0 = 0; \quad Y_5 = 0; \quad Y_6 = -Y_4; \quad Y_7 = -Y_3 \quad \ldots [15]$$

Inserting this into Equations [14] one obtains four homogeneous linear equations in terms of the deflections Y_1, Y_2, Y_3, and Y_4, that can yield deflections differing from zero only if the determinant of the system is equal to zero. This yields

$$\begin{vmatrix}
C_{21} - C_{11} - 6\lambda^2h^4\rho_1\varphi^2 & D_1 + C_{21} & C_{11} & -D_1 \\
D_2 + C_{22} & C_{22} - 6\lambda^2h^4\rho_2\varphi^2 & C_{22} & C_{12} \\
C_{13} & C_{23} & C_{33} - 6\lambda^2h^4\rho_3\varphi^2 & D_3 + C_{23} \\
-D_4 & C_{14} & D_4 + C_{24} & C_{34} - C_{14} - 6\lambda^2h^4\rho_4\varphi^2
\end{vmatrix} = 0 \quad \ldots [16]$$

In the special case of pure bending $\rho_2 = -\rho_3$, $\rho_4 = -\rho_1$, and the plastic reduction coefficients D, C_1, C_2, and C_3 for the points 3 and 4 are equal to those for the points 2 and 1, respectively. For example, $C_{24} = C_{21}$.

For an assumed ratio a/b, from which $\lambda = \pi/a$ can be expressed in terms of b, $\varphi^2 b^2$ is the only unknown in the determinant and can be calculated. Expressing σ_{xp}, analogously to σ_{xe} in Equation [5], as

$$\sigma_{xp} = k_p \frac{\pi^2 N}{b^2 t} \quad \ldots\ldots [17]$$

from Equations [4] and [17]

$$t\sigma_{xp} = EI\varphi^2 = k_p \frac{\pi^2 EI}{(1-\nu^2)b^2}$$

or, with Poisson's ratio $\nu = 0.3$

$$k_p = \varphi^2 b^2/10.856 \quad \ldots\ldots [18]$$

k_p is determined by the smallest root $\varphi^2 b^2$ of the determinant. However, $\lambda = \pi/a$ has to be chosen such as to make the buckling-stress coefficient k_p a minimum. To this end the calculation was carried out for three different values of λ, in such a way that for the smallest as well as for the largest value of λ the resulting k_p was larger than that for the medium λ-value. Plotting k_p versus λ the equation of the parabola passing through the points so obtained can be established and the minimum ordinate of this parabola can be considered as the minimun k_p-value.

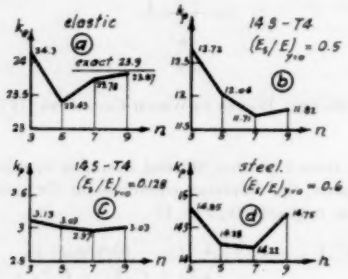

FIG. 12 CONVERGENCE OF BUCKLING STRESS COEFFICIENTS k COMPUTED BY USING 3, 5, 7, AND 9 SPACINGS

2 *Numerical Results.* Figs. 12 (a to d) show the resulting values of the buckling-stress coefficients k for four cases, as functions of the number of spacings $n = b/h$. Here k_e refers to Equation [5] for elastic buckling and k_p refers to Equation [17] for plastic buckling. In all four cases the plate is subjected to pure bending in its plane, for which the exact value k_e in the elastic range is $k_e = 23.9$ (24). Fig. 12(a) presents the k_e-values for elastic buckling, which are also given at the right side of Table 1. From $n = 5$ on, the results approximate the exact value of 23.9 from below. Fig. 12(b) refers to pure bending in the plastic range for a plate of aluminum alloy 14S-T4 and for a ratio $E_s/E = 0.5$ at the edges. This means that with edge stresses σ_{xp} the edge strains are

$$\epsilon_{xe} = \sigma_{xp}/E_s = \sigma_{xp}/(0.5E) = 2\sigma_{xp}/E$$

Fig. 12(c) refers to the same material, but here $E_s/E = 0.128$ at the edges. Fig. 12(d) refers to a steel plate, with a stress-strain diagram as shown in Fig. 8 and with $E_s/E = 0.6$ at the edges. In Figs. 12(b to d) the lowest values k_p are obtained for $n = 7$ and from then on k_p begins to increase again. This difference in behavior with that in the elastic case, Fig. 12(a), is apparently caused by the additional errors occurring in these plastic cases, from assuming the plastic reduction coefficients A, B, D, and F to be constants within strips of width h, as pointed out previously. The upward trend begins here at $n = 7$ instead of $n = 5$ for the elastic case. In connection with the small error for the elastic case for $n = 9$ (0.1 per cent) it was concluded that for the plastic case the results for $n = 9$ can be considered as conservative and sufficiently accurate.

Besides the cases of pure bending mentioned, also cases of eccentric compression were investigated. To indicate the type of loading in the elastic as well as plastic ranges, the strains ϵ_x are expressed in terms of the strains ϵ_{xe} at the upper edge by the formula

$$\epsilon_x = \epsilon_{xe}[1 - (\alpha y/b)] \quad \ldots\ldots [19]$$

where y is measured as shown in Fig. 5. The accessory stress distribution is that belonging to the strains ϵ_x at any point and follows from the pertinent stress-strain diagram, Fig. 5. In Equation [19] $\alpha = 2$ designates pure bending, $\alpha = 0$ indicates pure compression and, for example, for $\alpha = 3/2$ the strains at the lower edge are $-1/2$ times those at the upper edge. Table 2 gives the results obtained with $n = b/h = 9$.

TABLE 2 RESULTS OF CALCULATIONS FOR VARIOUS CASES

Case no.	1	2	3	4	5	6
Material	Elastic	14S-T4	14S-T4	Steel	Steel	Steel
α	2	2	2	2	3/2	1
$(E_s/E)_{y=0}$	1	0.50	0.128	0.60	0.50	0.50
k_e or k_p	23.87	11.82	3.03	14.75	6.73	3.68
a/b	2/3	0.55	0.49	0.63	0.84	0.87
η	1	0.495	0.127	0.617	0.502	0.471
η from Eq. [22]	1	0.50	0.128	0.60	0.483	0.465

The buckling stress coefficients k_e and k_p refer to Equations [5] and [17] for the buckling stresses at the upper edge ($y = 0$). The optimum half-wave lengths a, given in Table 2 by the ratios a/b, belong to the minimum buckling stresses. The plastic reduction factors η are found by dividing k_p by the elastic buckling stress coefficients k_e for a stress distribution that is determined by the same strain distribution as the plastic case and given by Equation [19]. Hence for the comparable elastic case

$$\sigma_x = \sigma_{xe}[1 - (\alpha y/b)] \quad \ldots\ldots [20]$$

where σ_{xe} is the edge stress at $y = 0$. For $\alpha = 2$, $k_e = 23.9$. For $\alpha = 3/2$ and 1, k_e is 13.40 and 7.81, respectively.

It appears from Table 2 that for pure bending ($\alpha = 2$) the plastic reduction factor η is about equal to E_s/E, independent of the form of the stress-strain diagram of the plate material (compare Cases 2 and 4) and also independent of the zones of plastic deformation or of the ratios E_s/E at the edges (compare Cases 2 and 3). The case of pure bending was investigated independently by Mr. G. Johnston at the Bell Aircraft Corporation, for an aluminum alloy 14S-T3, using the energy method. He found η to be only slightly less than E_s/E at the edges.

For Case 6, with $\alpha = 1$, that is, with zero edge strains at the lower edge, η is somewhat smaller than E_s/E at the upper edge. For $\alpha = 0$, that is, for pure compression, Case 2 of table 5 (6), η is equal to

$$\eta_0 = 0.455(\sqrt{AD} + B + 2F) \quad \ldots\ldots [21]$$

η_0 may be about 20 per cent smaller than E_s/E, Fig. 4.

3 *Design Formula.* The plastic reduction factor η may be expressed sufficiently accurately by the following simple formula

$$\eta = \sigma_{xp}/\sigma_{xe} = k_p/k_e = 0.5\alpha(E_s/E)_u + (1 - 0.5\alpha)(\eta_0)_u \quad \ldots [22]$$

where k_e refers to the stress distribution determined by Equation [20]. $(E_s/E)_u$ refers to the upper edge of the plate where the compressive stresses are highest. Further, $(\eta_0)_u$ is given by

Equation [21] and can be read directly from Fig. 4 as a function of E_s/E and E_t/E at the upper edge. For $\alpha = 2$, Equation [22] yields $\eta = (E_s/E)_u$ and for $\alpha = 0$ (pure compression) $\eta = \eta_0$, the exact value for pure compression. At the bottom of Table 2 also η from Equation [22] is listed. It appears to be in good agreement with the exact values of η in the preceding line and is slightly conservative.

4 *Simple Way of Understanding Equation [22].* The fact that in cases of pure bending and in cases of eccentric compression where α is not much smaller than 2, the reduction factor η is approximately equal to E_s/E at the upper edge, may be understood directly from Figs. 13(a and b). Let the elastic buckling-stress distribution be given by the dashed straight line in Fig. 13(b), so that the edge stress is σ_{xx}. The accessory stress-strain diagram for this elastic case is given by the dashed straight line with a slope $\tan^{-1} E$ in Fig. 13(a) in such a way that, at any horizontal line, the stresses are equal to those in Fig. 13(b). Hence the stress $\sigma_x = E\epsilon_x$ at any point A in Fig. 13(b) is determined by ϵ_x in Fig. 13(a).

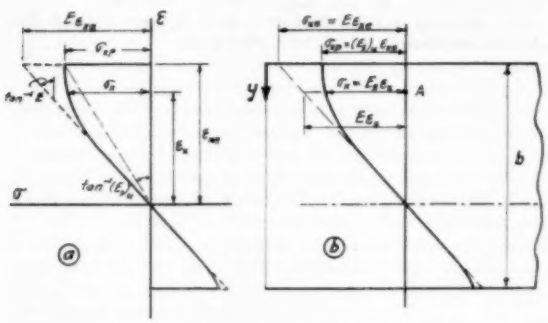

FIG. 13 STRESS-STRAIN DIAGRAM AND STRESS DISTRIBUTION IN A PLATE SUBJECTED TO ECCENTRIC COMPRESSION IN ITS PLANE

Assume now a material, with the same elastic modulus E, but with a stress-strain diagram where, for the same strains ϵ_x in Fig. 13(a), the stresses are given by the solid curve in Fig. 13(a). Then, again for the same (edge-) strains as in the elastic case, the stress distribution in the plate would be given by the solid curve in Fig. 13(b) which is identical to that in Fig. 13(a). At an arbitrary point A, the stress is now $\sigma_x = E_s\epsilon_x$, where E_s is the secant modulus belonging to the stress σ_x at point A. Since in the plastic case σ_x is now E_s/E times that in the elastic case, for a given deflection also the deflecting forces $-t\sigma_x(\partial^2 w/\partial x^2)\,dxdy$, exerted on any plate element $tdxdy$, are E_s/E times those in the elastic case. On the other hand, in the plastic case the resistant forces exerted on the same element, from Equations [9] and [10], are mainly proportional to the coefficients $(B + 2F)$ and D, which in the plastic range are about E_s/E times their value in the elastic range, the latter being $1/(1 - \nu^2)$. The coefficients A are considerably smaller than E_s/E, but this will only diminish the bending rigidity of the X-strips (running in the X-direction, Fig. 5) close to the edges $y = 0$ and $y = b$, which has only a slight influence on the buckling rigidity of the entire plate.

It is assumed that in the elastic case, with edge stresses σ_{xx}, Fig. 13(b), the plate is just at the point of buckling, so that the deflecting and resistant forces on any element are just in equilibrium. Hence, in the plastic case considered, where both deflecting and resistant forces are E_s/E times those in the elastic case, these forces will still be in equilibrium, so that also under the plastic-stress distribution of Fig. 13(b) the plate is just at the point of buckling. This means that for plastic buckling the edge strains ϵ_{xx} are equal to those for elastic buckling with the same value α in Equations [19] and [20]. Also, from Fig. 13, at incipient buckling the upper edge stress is $\sigma_{xp} = (E_s/E)_u\sigma_{xx}$, where σ_{xx} is the elastic buckling stress for an equal parameter α, in accordance with what follows from Table 2.

INVESTIGATION AND DESIGN OF A PLATE

To investigate whether a plate is stable under an assumed stress distribution, as, for example, sketched in Fig. 5, one takes the elastic buckling stress for the same α-value, as determined by Equations [19] and [20], and multiplies it with the plastic reduction factor from Equation [22]. If this buckling stress is higher than the assumed edge stress σ_{xp} at the upper edge (where the compressive stress is highest) the plate is stable.

Also, the required thickness of a plate for resisting an assumed stress distribution can be calculated. In the same way as the foregoing one determines the buckling-stress coefficient k_s for the elastic case with the same parameter α. Then one obtains the plastic buckling stress coefficient $k_p = \eta k_s$. For a given width b the plate thickness has to be chosen such as to resist the assumed edge stress σ_{xp}, so that from Equation [17], with $\nu = 0.3$

$$\sigma_{xp} = k_p \frac{\pi^2 E t^2}{12(1 - \nu^2)b^2 t} = 0.905\eta k_s E\left(\frac{t}{b}\right)^2$$

Hence the plate thickness required for an edge buckling stress σ_{xp} is

$$t = 1.05\left(\frac{\sigma_{xp}}{\eta k_s E}\right)^{1/2} b \qquad [23]$$

ACKNOWLEDGMENT

This investigation was carried out at Cornell University under sponsorship and with the financial assistance of the Office of Ordnance Research of the U. S. Army. Most of the numerical calculations were done by Mr. Mario Johanning, graduate student until 1953. The author wishes to express his appreciation for the valuable co-operation of all concerned.

BIBLIOGRAPHY

1 "A Theory of Plastic Stability and Its Application to Thin Plates of Structural Steel," by P. P. Bijlaard, Proceedings of the Royal Netherlands Academy of Sciences, Amsterdam, Holland, vol. 41, September, 1938, pp. 731–743.

2 "Das Ausbeulen des auf Druck beanspruchten freistehenden Winkels," by C. F. Kollbrunner, Mitt. a.d. Institut für Baustatik a. d. E. T. H., Zurich, Switzerland, No. 4, 1935.

3 "Das Ausbeulen der auf einseitigen, gleichmässig verteilten Druck beanspruchten Platten im elastischen und plastischen Bereich," by C. F. Kollbrunner, Mitt. a.d. Institut für Baustatik a.d. E. T. H., Zurich, Switzerland, No. 17, 1946.

4 "Theorie and Versuche über das plastische Ausbeulen von Rechteckplatten under gleichmässig verteilten Langsdruck," by P. P. Bijlaard, C. F. Kollbrunner, and F. Stussi, International Association for Bridge and Structural Engineering, Third Congress, Liège, Belgium, September, 1948, Preliminary Publication, 1948, pp. 119–128.

5 "Prediction and Reduction to Minimum Properties of Plate Compressive Curves," by E. H. Schuette and J. C. McDonald, *Journal of the Aeronautical Sciences*, vol. 15, January, 1948, pp. 23–27.

6 "Theory and Tests on the Plastic Stability of Plates and Shells," by P. P. Bijlaard, *Journal of the Aeronautical Sciences*, vol. 16, September, 1949, pp. 529–541.

7 "Plastic Buckling of Simply Supported Compressed Plates," by R. A. Pride and G. J. Heimerl, NACA TN 1817, April, 1949.

8 "Plastic Buckling of a Simply Supported Plate in Compression," by R. A. Pride, *Journal of the Aeronautical Sciences*, vol. 19, January, 1952, pp. 69–70.

9 "Inelastic Buckling of Flat Plates," by R. Teodosiadis, H. L. Langhaar, and J. O. Smith, First Midwestern Conference on

Solid Mechanics, Engineering Experiment Station, University of Illinois, Urbana, Ill., April, 1953.

10 "Compressive Strength of Flanges," by E. Z. Stowell, NACA TN 2020, January, 1950.

11 "On Theories of Plasticity and the Plastic Stability of Cruciform Sections," by P. P. Bijlaard and H. A. B. Wiseman, *Journal of the Aeronautical Sciences*, vol. 20, November, 1953, pp. 787–788.

12 "An Experimental Study in Plasticity," by P. M. Naghdi and J. C. Rowley, Conference on Mechanics of Elasticity and Plasticity, Office of Ordnance Research, U. S. Army, February 11–12, 1954, p. 12.

13 "Inelastic Column Theory," by F. R. Shanley, *Journal of the Aeronautical Sciences*, vol. 14, May, 1947, pp. 261–268.

14 "Theories of Plastic Buckling," by S. B. Batdorf, *Journal of the Aeronautical Sciences*, vol. 16, July, 1949, pp. 405–408.

15 "Experimental Investigation of Inelastic Behavior Under Combined Tension and Torsion," by M. Feigen, thesis, University of California, Los Angeles, Calif., July, 1953.

16 "Analysis of the Elastic and Plastic Stability of Sandwich Plates by the Method of Split Rigidities—II," by P. P. Bijlaard, *Journal of the Aeronautical Sciences*, vol. 18, December, 1951, pp. 790–796, 829.

17 "A Theory of Plastic Buckling With Its Application to Geophysics," by P. P. Bijlaard, Proceedings of the Royal Netherlands Academy of Sciences, Amsterdam, Holland, vol. 41, May, 1938, pp. 468–480.

18 "Some Contributions to the Theory of Elastic and Plastic Stability," by P. P. Bijlaard, Publ. International Association for Bridge and Structural Engineering, Zurich, Switzerland, vol. 8, 1947, pp. 17–80.

19 "Analysis of the Elastic and Plastic Stability of Sandwich Plates by the Method of Split-Rigidities—I," by P. P. Bijlaard, *Journal of the Aeronautical Sciences*, vol. 18, May, 1951, pp. 339–349.

20 "Interaction of Column and Local Buckling in Compression Members," by P. P. Bijlaard and G. P. Fisher, NACA TN 2640, March, 1952.

21 "Theory of the Plastic Stability of Thin Plates," by P. P. Bijlaard, Publ. International Association for Bridge and Structural Engineering, Zurich, Switzerland, vol. 6, 1940–1941, pp. 45–69.

22 "Plasticity Parameters and Coefficients for Plates and Shells," by A. Krivetsky, Bell Aircraft Corporation Report No. 02-984-019, June, 1954.

23 "Numerical Methods in Engineering," by M. G. Salvadori and M. L. Baron, Prentice-Hall, Inc., New York, N. Y., 1952.

24 "Theory of Elastic Stability," by S. Timoshenko, McGraw-Hill Book Company, Inc., New York, N. Y., 1936.

25 "Numerical Procedure for Computing Deflections, Moments and Buckling Loads," by N. M. Newmark, Trans. ASCE, vol. 108, 1943, pp. 1161–1188.

26 "Present Situation in Switzerland With Regard to Experiments on Buckling With Indication of the Buckling Values k," by C. F. Kollbrunner, Fifteenth International Congress of the Steel Information Centres, Brussels, Belgium, October 5–9, 1953.

27 "Stability of Alclad Plates," by P. P. Bijlaard, *Journal of the Aeronautical Sciences*, vol. 17, no. 4, 1950, p. 252.

Bending Creep and Its Application to Beam-Columns

By L. W. HU[1] and N. H. TRINER[2]

A procedure for evaluating the creep deflection of members subjected to bending moment is suggested. The application of the suggested procedure to beam-columns is given. For checking the validity of the proposed method, an investigation on the creep behavior of beam-columns of magnesium alloy FS1-F at 260 F was conducted. The comparison of the experimental results with the theoretical predictions was found satisfactory.

Introduction

IN THE past two decades, creep in bending has been of great interest to the investigators in the field of mechanics of creep and many analytical procedures for predicting bending creep have been suggested by assuming various creep stress-strain-time relations for simple tension. MacCullough in 1933 reported the first analysis of creep in bending and demonstrated the linearity of creep strain with distance from the neutral axis (1).[3] More analytical and experimental work has been reported since then by Tapsell and Johnson (2), Marin and Zwissler (3), Davis (4), Popov (5), Marin and Hu (6), Pao and Marin (7), and Findley and Poczatek (8). However, some of these investigations considered only the secondary creep with a constant creep rate and some conceived and used the doubtful assumption that no stress redistribution occurred during bending creep.

It is the purpose of this paper to develop a procedure for predicting creep behavior of members subjected to constant or varying bending moments. Both primary and secondary creep will be considered. No restriction will be imposed on the stress redistribution during bending creep. The procedure developed will be applied to beam-columns in which the direct-stress component is much smaller than the bending-stress component. The creep of beam-columns was first investigated by Marin in 1947 (9). To check the validity of the theory developed, an experimental investigation on the creep behavior of beam-columns at elevated temperatures was conducted. The test results are compared with the theoretical predictions based on creep behavior of material tested under simple tension.

Theoretical Analysis

Consider a member, as shown in Fig. 1, subjected to a bending couple acting in an axial plane through one of the principal axes of the cross section. For any instant during loading, the following equations of equilibrium can be written

$$\int_{-h_2}^{h_1} \sigma b dz = 0 \quad \ldots\ldots [1]$$

$$\int_{-h_2}^{h_1} \sigma b z dz = M \quad \ldots\ldots [2]$$

The curvature of the deflection curve is defined as

$$\frac{1}{\rho} = \frac{\dfrac{\partial^2 y}{\partial x^2}}{\left[1 + \left(\dfrac{\partial y}{\partial x}\right)^2\right]^{3/2}} \quad \ldots\ldots [3]$$

in which the deflection y is a function of distance x and time t or $y = y(x, t)$. The changes in dimensions of the cross sections are assumed to be negligible.

During creep it is assumed that plane cross sections of the member remain plane. The validity of this assumption has been demonstrated by MacCullough (1) and Tapsell and Johnson (2). Therefore the linearity of strain with fiber distance from the neutral axis can be expressed by the equation

$$\epsilon = z/\rho \quad \ldots\ldots [4]$$

The creep stress-strain-time relations of isotropic materials can be assumed to be the same for both tension and compression cases. In this analysis, the following empirical creep stress-strain-time relation (10) is selected for simple tension and compression

$$\epsilon = \frac{\sigma}{E} + K\sigma^a(1 - e^{-\phi t}) + B\sigma^n t \quad \ldots\ldots [5]$$

The creep deflection of the member subjected to a bending couple can be determined by combining the creep stress-strain-time relation of Equation [5] with Equations [1] to [4] as follows:

For a member with a rectangular cross section of width b and depth h, it can be shown by Equation [1] that $h_1 = h_2$. Equation [2] then reduces to

$$M = b\int_0^{h_1} \sigma dz^2 = b[\sigma z^2 - \int z^2 d\sigma]_{0,0}^{\sigma_1, h_1} \quad \ldots\ldots [6]$$

where σ_1 is the stress value at the outer fiber of the member at the particular instant under consideration.

Substituting the value of z from Equation [4] into [6]

$$\frac{M}{b\rho^2} = [\sigma\epsilon^2 - \int \epsilon^2 d\sigma]_{0,0}^{\sigma_1, \epsilon_1} \quad \ldots\ldots [7]$$

where ϵ_1 is the strain value at the outer fiber of the member at the particular instant under consideration.

Placing the value of ϵ from Equation [5] into Equation [7] and integrating

$$\frac{M}{2b\rho^2} = \frac{1}{3}\sigma_1\Sigma_1^2 + \frac{\alpha}{2\alpha+1}\sigma_1\Sigma_2^2 + \frac{n}{2n+1}\sigma_1\Sigma_4^2 + \frac{\alpha+1}{\alpha+2}\sigma_1\Sigma_1\Sigma_2 + \frac{n+1}{n+2}\sigma_1\Sigma_1\Sigma_3 + \frac{\alpha+n}{\alpha+n+1}\sigma_1\Sigma_2\Sigma_3 \ldots [8]$$

---

[1] Assistant Professor of Engineering Research, The Pennsylvania State University, University Park, Pa.

[2] Senior Analytical Engineer, Pratt and Whitney Aircraft Division, United Aircraft Corporation, East Hartford, Conn.

[3] Numbers in parentheses refer to the Bibliography at the end of the paper.

Contributed by the Applied Mechanics Division and presented at the Diamond Jubilee Annual Meeting, Chicago, Ill., November 13–18, 1955, of The American Society of Mechanical Engineers.

Discussion of this paper should be addressed to the Secretary, ASME, 29 West 39th Street, New York, N. Y., and will be accepted until April 10, 1956, for publication at a later date. Discussion received after the closing date will be returned.

Note: Statements and opinions advanced in papers are to be understood as individual expressions of their authors and not those of the Society. Manuscript received by ASME Applied Mechanics Division, February 2, 1955. Paper No. 55—A-21.

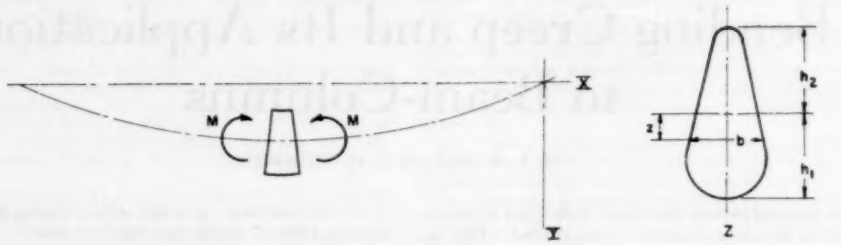

FIG. 1 BEAM DIAGRAM

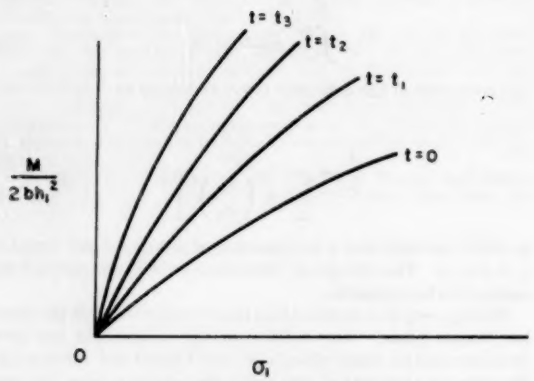

FIG. 2(a) ISOCHRONOUS MOMENT-STRESS CURVES

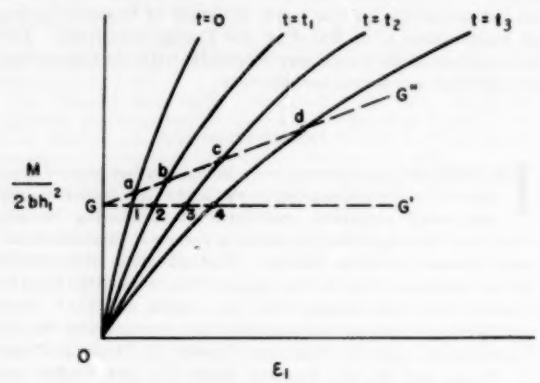

FIG. 2(b) ISOCHRONOUS MOMENT-STRAIN CURVES

where

$$\Sigma_1 = \frac{\sigma_1}{E}$$

$$\Sigma_2 = K\sigma^{\alpha}(1 - e^{-qt})$$

$$\Sigma_3 = B\sigma_1^{n}t$$

For the outer fiber, the strain $\epsilon = \epsilon_1$ and the radius of curvature ρ can be evaluated by combining Equations [4] and [5]

$$\frac{1}{\rho} = \frac{\epsilon_1}{h_1} = \frac{1}{h_1}[\Sigma_1 + \Sigma_2 + \Sigma_3]$$

Substituting the foregoing value of ρ into Equation [8]

$$\frac{M}{2bh_1^2} = \frac{\sigma_1}{[\Sigma_1 + \Sigma_2 + \Sigma_3]^2}\left\{\frac{1}{3}\Sigma_1^2 + \frac{\alpha}{2\alpha+1}\Sigma_2^2 + \frac{n}{2n+1}\Sigma_3^2 + \frac{\alpha+1}{\alpha+2}\Sigma_1\Sigma_2 + \frac{n+1}{n+2}\Sigma_3\Sigma_1 + \frac{\alpha+n}{\alpha+n+1}\Sigma_2\Sigma_3\right\} \ldots [9]$$

Equation [9] defines completely the stress σ_1 at the outer fiber at a time t for a member subjected to a bending couple M.

By assigning different values of stress at the outer fiber σ_1 and the time t in Equation [9], a family of isochronous moment-stress curves can be obtained, as shown in Fig. 2(*a*), provided the material constants B, E, K, α, q, and n are known. These isochronous moment-stress curves can be redrawn as isochronous moment-strain curves, as shown in Fig. 2(*b*), by using the creep stress-strain-time relation given by Equation [5]. From these curves, the stress or strain at a time t for the outer fiber of a member subjected to a constant or variable bending moment M can be determined completely.

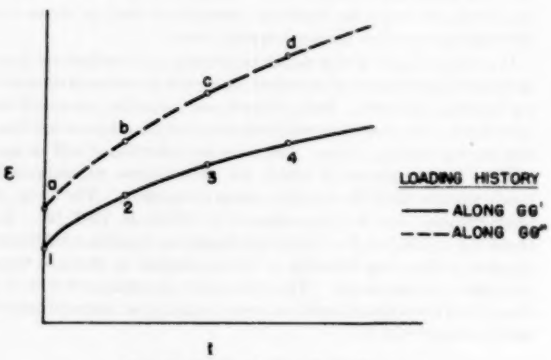

FIG. 3 CREEP STRAIN TIME CURVES

For a member subjected to a bending couple M of constant value, the stress σ_0 and strain ϵ_0 at the outer fiber during creep can be determined easily. A line such as GG' to represent a constant value of $M/2bh_1^2$ is then drawn in Fig. 2(*b*). The points of intersection of this line with the isochronous moment-strain curves will determine the variation of the creep strain with time for the member considered. The resulting creep strain-time relation for the outer fiber of a member subjected to bending moment M can now be plotted, as shown in Fig. 3, and the deflection of the member can be determined by means of geometrical considerations, namely

$$y = \frac{l^2}{8\rho} = \frac{l^2}{8}\left(\frac{\epsilon_0}{h_1}\right)$$

in which y is the deflection at the center of a span l.

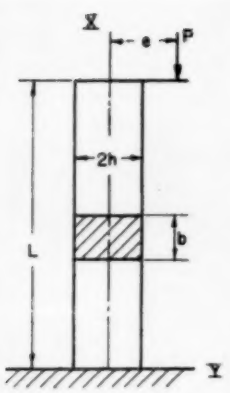

FIG. 4(a) BEAM-COLUMN

FIG. 4(b) DEFLECTION CURVE

APPLICATION TO BEAM-COLUMNS

Consider a member with a fixed end subjected to a sustained load P having a constant eccentricity e as shown in Fig. 4(*a*). The ratio of the direct-stress component σ_a to the bending-stress component σ_b at the cross section with a deflection y can be shown to be

$$\frac{\sigma_a}{\sigma_b} = \frac{P/2bh}{3M/2bh^2} = \frac{h}{3(e + \delta - y)}$$

If the eccentricity e is large, then the direct-stress component σ_a is much smaller than the bending-stress component σ_b and the creep in the member can be obtained by the following analysis:

Fig. 4(*b*) shows the deflection curve at time t for a beam-column subjected to an eccentric load P. Such a curve may be expressed in series form as follows

$$y = \delta\left[\left(\frac{x}{L}\right)^2 + a_4\left(\frac{x}{L}\right)^4 + a_6\left(\frac{x}{L}\right)^6 + a_8\left(\frac{x}{L}\right)^8 + \ldots\right] \quad [10]$$

provided that $a_4 + a_6 + a_8 + \ldots = 0$, where the free-end deflection δ and the coefficients a are functions of time. Equation [10] satisfies the two boundary conditions

$$\frac{\partial y}{\partial x} = 0 \quad \text{at } X = 0$$

and

$$y = \delta(t) \quad \text{at } X = L$$

By substituting the value of y from Equation [10] into Equation [3], the curvature at the fixed end, $x = 0$, is obtained

$$\frac{1}{\rho} = \frac{2\delta}{L^2} \quad [11]$$

Designating the strain at the outer fiber of the fixed end as ϵ_0, by Equations [4] and [11]

$$\frac{1}{\rho} = \frac{\epsilon_0}{h_1} = \frac{2\delta}{L^2} \quad \text{or} \quad \delta = \frac{L^2}{2h_1}\epsilon_0 \quad [12]$$

The bending moment M at the fixed end changes from an initial value $M = Pe$ to a value

$$M = P(e + \delta) = P\left(e + \frac{L^2}{2h_1}\epsilon_0\right) \quad [13]$$

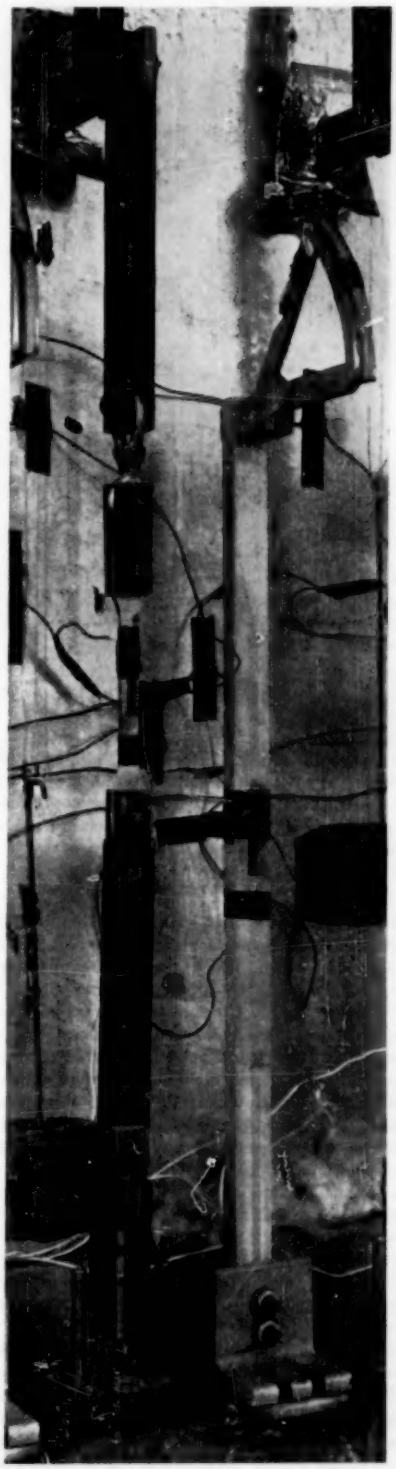

FIG. 5 TENSION-CREEP SPECIMEN AND BEAM-COLUMN

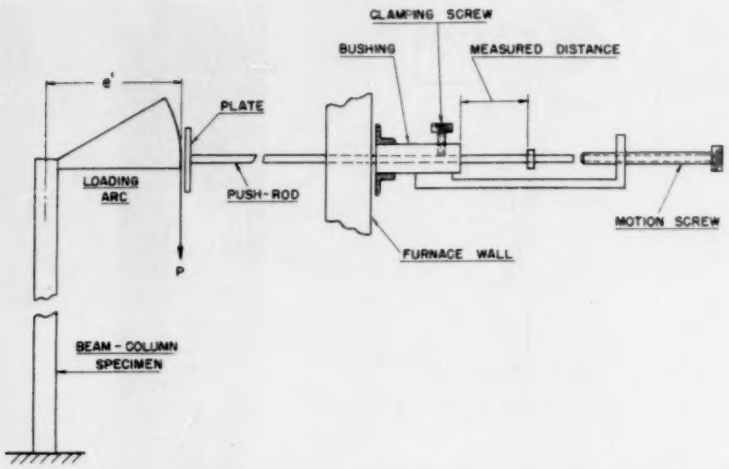

FIG. 6 DEFLECTION-MEASUREMENT APPARATUS

In other words, the relation between the bending couple M and the strain ϵ_0 of the outer fiber at the fixed end is established by Equation [13]. This equation may be plotted as the line GG'' in the isochronous moment-strain diagram in Fig. 2(b). The points of intersection of the line GG'' with the isochronous moment-strain curves will represent the variation of the strain ϵ_0 of the outer fiber at the fixed end with time t for load P and eccentricity e. Creep strain-time relation for the outer fiber at the fixed end, as shown in Fig. 3, can be obtained using Fig. 2(b) as indicated. Points a, b, c, and d in Fig. 3 correspond to points a, b, c, and d in Fig. 2(b). The relation between outer fiber strain at the fixed end and the deflection at the free end (as given by Equation [12]) can be used to obtain the desired creep deflection-time relation for the beam-column considered.

EXPERIMENTAL WORK

To check the validity of the analytical solution for creep of beam-columns as developed in the previous sections, a series of tests was conducted in which the limiting assumptions and boundary conditions of the analytical development were observed. The test program included two types of tests, i.e., tensile creep tests and creep tests of beam-columns. Both kinds of tests were conducted at a temperature of 260 F. The duration of each test was approximately 1000 hr. The material tested was a magnesium alloy designated as FS1-F and having a chemical composition as follows: Aluminum, 3.00 per cent; zinc, 1.10 per cent; manganese, 0.38 per cent; and magnesium, 95.52 per cent.

Tension specimens were cut from bars of 0.2 in. × 1 in. cross sections. With a total length of 7 1/2 in., the tension specimen had a reduced section of 0.2 × 1/2 in. and 3 1/2 in. in length. Beam-column specimens were taken from bars of 3/8 in. × 1 1/8 in. cross sections and had a total length of 27 1/2 in. To relieve the residual stresses produced during manufacturing and machining, the specimens were annealed in a Globar furnace for 48 hr at 350 F and air-cooled.

The creep deformations of the tensile creep specimens were measured with bonded electrical resistance strain gages, SR-4 Type AB-1. Temperature effects on the gages were eliminated by enclosing the dummy gages in the furnace. Loading on the tension-creep specimens was imposed by means of dead weights suspended on simple levers. As shown in Fig. 5, loading levers were mounted on double-row ball bearings at the fulcrum and at the loading points to minimize friction. Universal joints were located in the loading apparatus above and below the specimen and other points to insure axiality of loading.

The creep deflection at the free end of the beam-columns was measured by the horizontal movement of a rod which extended outside the furnace as shown in Fig. 6. The loading arc attached to the free end of the specimen made contact with the gage plate of the measuring rod. The contact between the gage plate and the loading arc was established by an electric indicator circuit. Measurement of the relative movement of two marked points as shown in Fig. 6 was made to 0.001 in. by vernier caliper. Since the overall deflection was found to be large, the method of measurement was considered satisfactory. Beam-column specimens were clamped securely at the lower end and were free at the upper end. The free end was attached with a sector or a circular arc over which dead weights were suspended as shown in Fig. 6. In this manner, the eccentricity could be maintained at a constant value of 6 in. throughout the tests as assumed in the analysis. Care was exercised in installing the beam-column specimens to avoid any twisting. Loads on the beam-column specimens were selected so that the fiber stresses in specimens were comparable to those used in tension-creep tests.

As shown in Fig. 7, the testing machine, enclosed in a high-temperature furnace, consisted of five tension-creep units and five beam-column creep units. Heat was provided by ten Finstrip heaters in circuit with mercury relay switches which were activated by the action of a thermoswitch. The heating chamber was directly below the test chamber and uniform circulation of hot air was obtained with a 400-rpm blower unit operating continuously along the bank of the heaters. Temperature measurement was made with bimetal-type Weston dial thermometers while a more precise check was accomplished by using copper-constantan thermocouples. Variation in temperature was observed to be not more than 2 F.

DISCUSSION

The results of the tension-creep tests of a magnesium alloy FS1-F at a temperature of 260 F are shown in Fig. 8. From these results the material constants in the creep stress-strain-time relation defined by Equation [5] were determined. Following the procedure described in the theoretical analysis, a family of isochronous moment-stress curves for the outer fibers of a rectangular cross

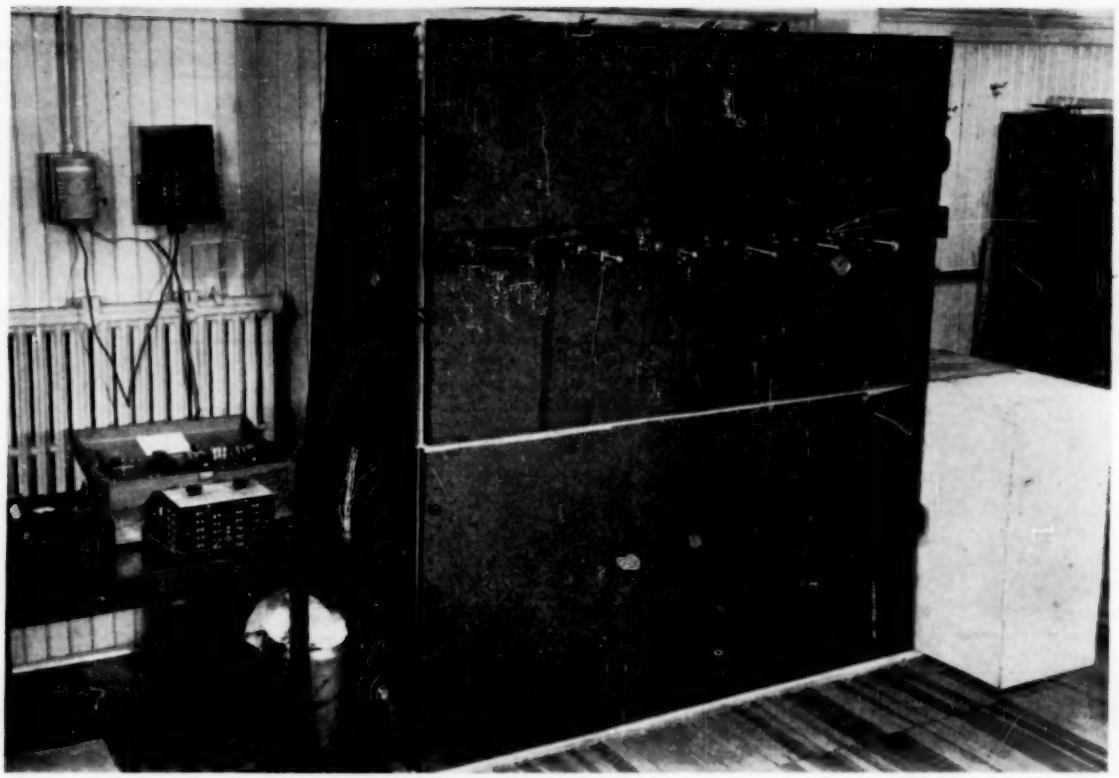

FIG. 7 OVER-ALL VIEW OF TESTING APPARATUS

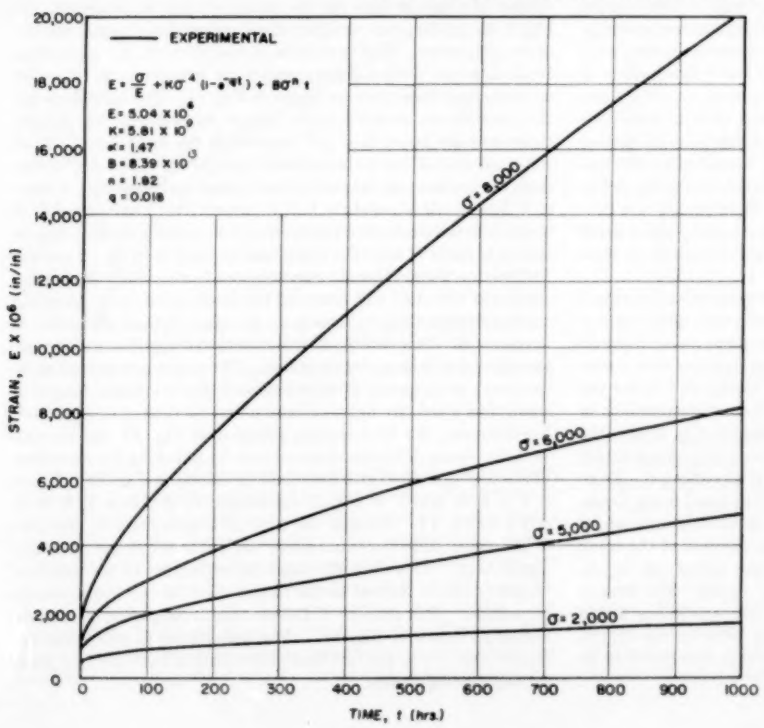

FIG. 8 CREEP STRESS-STRAIN-TIME RELATIONS FOR MAGNESIUM ALLOY FS1-F IN SIMPLE TENSION AT 260 F

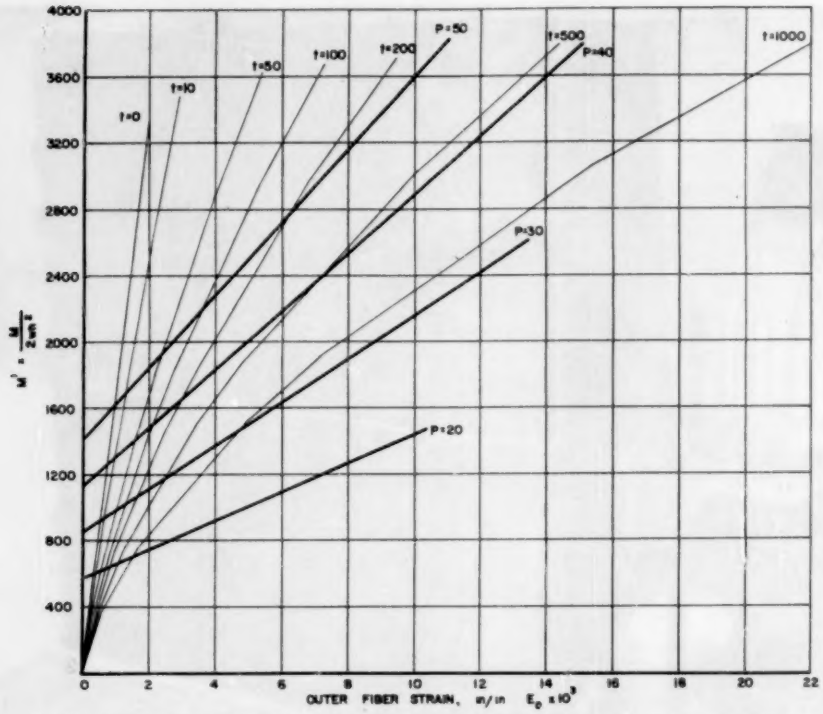

FIG. 9 ISOCHRONOUS MOMENT-STRAIN AND CONSTANT-LOAD MOMENT-STRAIN CURVES, 260 F

section was obtained from Equation [9] by using the material constants determined from the tension-creep tests. These curves were then transformed to a family of isochronous moment-strain curves as shown in Fig. 9, using the creep stress-strain-time relation of Equation [5] to evaluate values of outer fiber strain ϵ_0 corresponding to the selected time t and stresses σ_0. Such isochronous moment-strain curves then can be used to solve the creep deformation of FS1-F members of rectangular cross section subjected to bending at 260 F. In other words, after the isochronous moment-strain curves are constructed, the creep deformation of a member of width b and depth $2h$ subjected to a constant or varying moment M can be solved very easily and a great deal of time can be saved by using the described analysis to treat bending-creep problems.

In order to predict the creep behavior of beam-columns tested, the variation of bending moment M with the outer fiber strain ϵ_0 at the fixed end is plotted over the isochronous moment-strain curves. As shown in Fig. 9, the heavy lines indicate such variations of bending moment M as defined by Equation [13] for the various specimens tested. The strain values corresponding to the points of intersection of the two sets of lines in Fig. 11 give the outer fiber strain ϵ_0 at the fixed end at time t for the particular beam-column specimen subjected to a load P as indicated. From the values of outer fiber strain ϵ_0 at the fixed end and using Equation [12], the deflection δ of the specimen at the free end can be evaluated. In this manner the theoretical prediction of the creep deflection-time relations of the beam-columns tested can be obtained, as shown in Fig. 10 by the dotted curves. The experimental creep deflection-time relations for the specimens tested are also shown in Fig. 10. The comparison between the experimental results with the theoretical prediction is considered to be satisfactory.

Another significant feature of the proposed analysis is the prediction of a failure time for the beam-columns investigated. In Fig. 9 the isochronous moment-strain curves have a continuously decreasing slope. The variations of the M' with the outer fiber strain ϵ_0 at the fixed end are found to be straight lines. Now let us reproduce these lines as shown in Fig. 11. The light lines are the isochronous moment-strain curves labeled with the proper times and the heavy line AA' represents the variation of M' at the fixed end of the beam-column considered. Line AA' intersects the isochronous moment-strain curves corresponding to time t_0, t_1, t_2, $t_3 - \Delta t$ at points 0, 1, 2, 3, respectively; and line AA' is tangent to the isochronous moment-strain curve corresponding to time t_3 at point B after the creep time exceeds $t_3 - \Delta t$. Since the isochronous moment-strain curves have a continuously decreasing slope, the line AA' will intersect the isochronous moment-strain curve corresponding to time $t_3 - \Delta t$ again beyond the point of tangency B. This intersection has no actual significance because the elapsed time Δt is irrecoverable. The time t_3 corresponding to the point of tangency B thus indicates the maximum length of creep time which the beam-column under consideration can stand. Furthermore, the information obtained in Fig. 11 can be converted to creep deflection-time relation by following the procedure previously described and the result is shown in Fig. 12. Points 0, 1, 2, 3, B, and 3′ in Fig. 12 correspond to points 0, 1, 2, 3, B, and 3′ in Fig. 11. Because the time Δt is irrecoverable, the part of the creep deflection-time curve beyond point B has no actual significance. Therefore the time corresponding to the point of tangency can be defined as the failure time for the beam-column considered. This concept of failure time is supported by the test results as shown in Fig. 10. The importance of predicting the failure time lies in the fact that such a critical time can be a guide for engineering design.

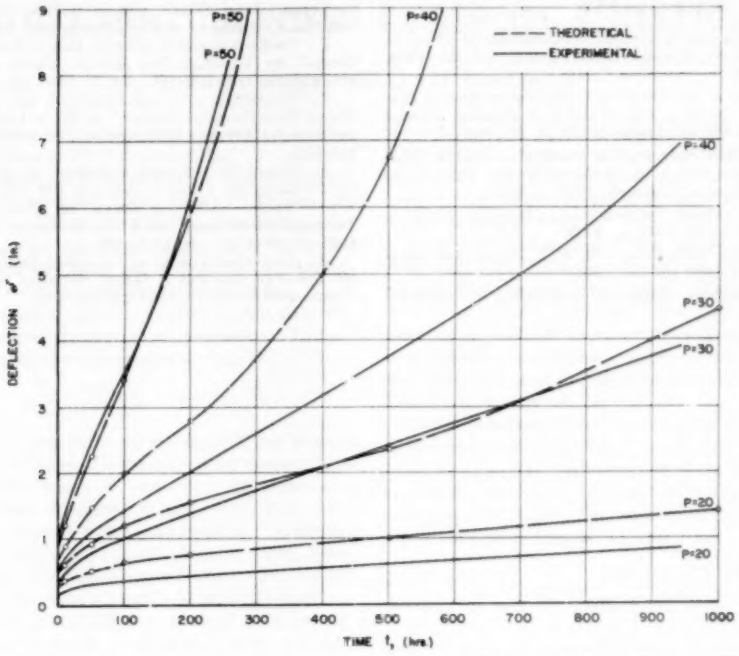

FIG. 10 THEORETICAL AND EXPERIMENTAL DEFLECTION-TIME CURVES FOR BEAM-COLUMNS, 260 F

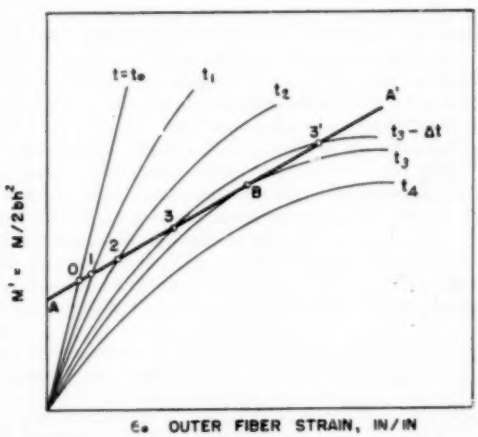

FIG. 11 ISOCHRONOUS MOMENT-STRAIN CURVES AND LOADING VARIATION LINE

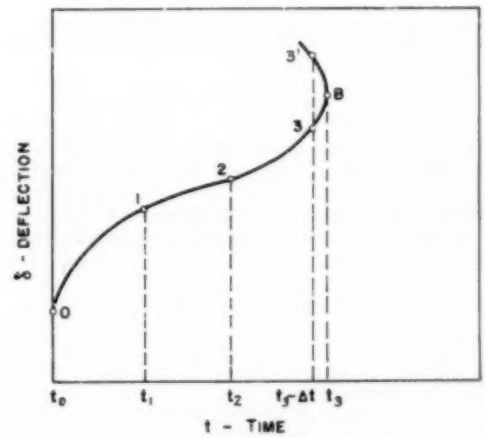

FIG. 12 CREEP DEFLECTION-TIME RELATION

CONCLUSION

An analytical procedure was developed to evaluate the creep deflection of a member subjected to pure bending of constant or varying magnitude based upon an assumed creep stress-strain-time relation for simple tension. For other creep stress-strain-time relations used for various materials, the same procedure can be used. The application of the theory to beam-columns subjected to axial load with large eccentricity was shown. An experimental investigation on the creep behavior of magnesium-alloy beam-columns at 260 F was conducted in order to check the validity of the proposed method. In general, the agreement between the experimental results and the theoretical prediction was found satisfactory. The analysis predicts failure times for beam-columns subjected to sustained loads. This concept of failure time is supported by the test results.

ACKNOWLEDGMENT

The authors wish to express their appreciation to Prof. Joseph Marin, Head, Department of Engineering Mechanics, The Pennsylvania State University, for his valuable advice. This investigation was made possible through the sponsorship of the National Science Foundation.

BIBLIOGRAPHY

1 "An Experimental and Analytical Investigation of Creep in Bending," by G. H. MacCullough, Trans. ASME, vol. 55, 1933, Paper APM—55-9, p. 55.

2 "An Investigation of the Nature of Creep Under Stresses Produced by Pure Flexure," by H. J. Tapsell and A. E. Johnson, *Journal of the Institute of Metals*, vol. 57, August, 1935, pp. 387–407.

3 "Creep of Aluminum Subjected to Bending at Normal Temperatures," by J. Marin and L. E. Zwissler, Proceedings of the American Society for Testing Materials, 1940, p. 937.

4 "Creep of Metals at High Temperatures in Bending," by E. A. Davis, Trans. ASME, vol. 60, 1938, p. A-29.

5 "Bending in Beams With Creep," by E. P. Popov, *Journal of Applied Physics*, vol. 20, 1949, pp. 251–256.

6 "Deflection of Members Subjected to Bending Accompanied by Creep," by J. Marin and L. W. Hu, Proceedings of the First National Congress of Applied Mechanics, 1952, pp. 613–618.

7 "Deflection and Stresses in Beams Subjected to Bending and Creep," by Yoh-Han Pao and J. Marin, JOURNAL OF APPLIED MECHANICS, Trans. ASME, vol. 74, 1952, pp. 478–484.

8 "Prediction of Creep-Deflection and Stress Distribution in Beams From Creep in Tension," by W. N. Findley and J. J. Poczatek, JOURNAL OF APPLIED MECHANICS, Trans. ASME, vol. 77, 1955, pp. 165–171.

9 "Creep Deflections in Columns," by J. Marin, *Journal of Applied Physics*, vol. 18, no. 1, 1947, pp. 103–107.

10 "Factors Affecting Choice of Working Stresses for High-Temperature Service," by P. G. McVetty, Trans. ASME, vol. 55, 1933, Paper APM—55-13, p. 99.

"An Analytical Theory of the Creep Deformation of Materials," by Yoh-Han Pao and J. Marin, JOURNAL OF APPLIED MECHANICS, Trans. ASME, vol. 75, 1953, pp. 245–252.

Combined Stress Tests in Plasticity[1]

By ARIS PHILLIPS[2] and LLOYD KAECHELE[3]

A substantial number of combined stress tests on thin-walled tubes of aluminum 2S-O are reported. In most of the tests the tubes have been subjected to combined tension and torsion with variable stress ratios. In the last six tests each tube has first been subjected to uniaxial tension until sufficiently deep in the plastic region and then this state of uniaxial stress has been rotated while the magnitude of the principal stresses remained constant.

The purpose of the tests was to get information as to the validity of the incremental theories of plasticity. The results of these tests favor the incremental theories.

Introduction

THE purpose of the tests which are described in this paper is to determine the validity of some basic assumptions made in the incremental theory of plasticity. In these tests thin-walled circular tubes of aluminum alloy 2S-O have been subjected to combined stresses in the plastic region. In the test series A, B, and C the tubes have been subjected to combined axial tension and torsion with variable stress ratios. In the test series D, each tube has first been subjected to uniaxial tension until sufficiently deep in the plastic region and then this state of uniaxial stress has been rotated while the magnitude of the principal stresses remained constant. The test series D has been made by subjecting the tube to combined axial tension, torsion, and internal pressure.

The material tested was pure aluminum designated as 2S-O. It was supplied in the annealed condition in tubular form with an internal diameter of 0.75 in. and a wall thickness of 1/4 in. The specimens had an over-all length of 11 in., with an intermediate length of 6 3/4 in. of reduced wall thickness equal to 0.030 ± 0.001 in. The internal diameter of the machined specimen was 0.78 in. The wall thickness of the tubular specimen was measured using the apparatus described in reference (1).[4] The ratio of the wall thickness to diameter was selected so as to delay buckling as much as possible and at the same time to insure an essentially uniform stress distribution throughout the wall of the specimen.

The load was applied by means of the testing machine described in reference (1), to which, for the test series D, a specially built pump unit has been added for applying the internal pressure.

For the test series A and B the strains were measured by means of a specially constructed mechanical-type strain gage, described in reference (1). This gage measures both the axial strains and angles of twist. The accuracy of the twistmeter part of the gage is $\sim \pm 6 \times 10^{-3}$ deg per in. of gage length. Similarly, the accuracy of the measurements of the axial strains is $\sim \pm 2 \times 10^{-6}$ in. per in. of gage length.

Because the mechanical-type strain gage does not provide for measuring lateral strains, we used for the test series C and D regular SR-4 electric strain gages, type A-7, placed in axial, lateral, and 45-deg directions. For each direction three gages have been placed 120 deg apart to compensate for any accidental lack of axiality; these three gages have been connected in series so that each reading of the strain indicator gives the average of the strains recorded by the three gages.

The formulas used for determining the stresses from the applied loads are the following: Let T, p, M represent the axial force, internal pressure, and torque applied in the tube, respectively. Let also t and d represent the initial wall thickness and initial internal diameter of the tube. The axial stress σ_x, due to the load T and the internal pressure p, is

$$\sigma_x = \frac{T}{\pi t(d + t)} + \frac{pd^2}{4t(d + t)} \quad [1]$$

The circumferential stress σ_y due to the internal pressure p is

$$\sigma_y = \frac{pd^2}{2t(d + t)} \quad [2]$$

Finally, the shearing stress τ_{xy} due to the torque M is

$$\tau_{xy} = \frac{2M}{\pi td(d + t)} \quad [3]$$

These are the values of the stresses at the outer surface of the tube, where the strains are measured. At the outer surface the radial stress is zero.

According to Drucker (2) the stress-plastic strain relations of the incremental theory of plasticity for loading, under very general conditions, are

$$d\epsilon_{ij}^{\,p} = G \frac{\partial f}{\partial \sigma_{ij}} df \quad [4]$$

where

$$df = \frac{\partial f}{\partial \sigma_{kl}} d\sigma_{kl} \geq 0 \quad [5]$$

In Equations [4] and [5] the functions f and G are functions of the stress components, the strain components, and the history of loading.

The simplest incremental theory of plasticity will be found by assuming that the function f is equal to the octahedral shearing stress τ_0

$$f = \tau_0 = \frac{1}{3}\sqrt{(\sigma_1 - \sigma_2)^2 + (\sigma_2 - \sigma_3)^2 + (\sigma_3 - \sigma_1)^2}$$

$$= \frac{1}{3}\sqrt{[(\sigma_x - \sigma_y)^2 + (\sigma_y - \sigma_z)^2 + (\sigma_z - \sigma_x)^2 + 3(\tau_{xy}^2 + \tau_{yz}^2 + \tau_{zx}^2 + \tau_{xy}^2 + \tau_{yz}^2 + \tau_{zx}^2)]} \quad [6]$$

[1] This paper is a result of investigations sponsored by the Office of Naval Research.

[2] Associate Professor of Civil Engineering, Yale University, New Haven, Conn. Mem. ASME.

[3] Graduate Student, Division of Engineering Mechanics, Stanford University, Stanford, Calif.

[4] Numbers in parentheses refer to the Bibliography at the end of the paper.

Contributed by the Applied Mechanics Division and presented at the Diamond Jubilee Annual Meeting, Chicago, Ill., November 13–18, 1955, of The American Society of Mechanical Engineers.

Discussion of this paper should be addressed to the Secretary, ASME, 29 West 39th Street, New York, N. Y., and will be accepted until April 10, 1956, for publication at a later date. Discussion received after the closing date will be returned.

Note: Statements and opinions advanced in papers are to be understood as individual expressions of their authors and not those of the Society. Manuscript received by the Applied Mechanics Division, January 31, 1955. Paper No. 55—A-15.

while the function G is a function of τ_0 alone. In such a case we find, for example

$$\frac{\vartheta\tau_0}{\vartheta\sigma_x} = \frac{2}{9\tau_0}\left[\sigma_x - \frac{1}{2}(\sigma_y + \sigma_z)\right]$$

$$\frac{\vartheta\tau_0}{\vartheta\tau_{xy}} = \frac{\tau_{xy}}{3\tau_0}$$

Hence Equation [4] becomes

$$\left.\begin{aligned}
d\epsilon_x'' &= \frac{2}{9}\frac{G(\tau_0)}{\tau_0}\left[\sigma_x - \frac{1}{2}(\sigma_y + \sigma_z)\right]d\tau_0 \\
d\epsilon_y'' &= \frac{2}{9}\frac{G(\tau_0)}{\tau_0}\left[\sigma_y - \frac{1}{2}(\sigma_x + \sigma_z)\right]d\tau_0 \\
d\epsilon_z'' &= \frac{2}{9}\frac{G(\tau_0)}{\tau_0}\left[\sigma_z - \frac{1}{2}(\sigma_x + \sigma_y)\right]d\tau_0 \\
d\gamma_{xy}'' &= \frac{2}{3}\frac{G(\tau_0)}{\tau_0}\tau_{xy}d\tau_0 \\
d\gamma_{yz}'' &= \frac{2}{3}\frac{G(\tau_0)}{\tau_0}\tau_{yz}d\tau_0 \\
d\gamma_{zx}'' &= \frac{2}{3}\frac{G(\tau_0)}{\tau_0}\tau_{zx}d\tau_0
\end{aligned}\right\} \quad \ldots [7]$$

The tests reported here will give information as to the validity of Equations [5] and [7].

In concluding this introduction, we mention the results of a metallurgical study of the material of the tubes used. Microscopic study of the material showed that the grains were equiaxed, with an average size of from 0.004 to 0.008 in. Random orientation was indicated by random light-reflection angles for different grains in the polished specimens.

The Flow Rule

From Equation [4] we see that $d\epsilon_{ij}''$ is proportional to $\vartheta f/(\vartheta\sigma_{ij})$. This proportionality expresses the flow rule. From the test series A, B, and C we can find whether this proportionality is correct for a given function f. In the case of the function $f = \tau_0$, the proportionality mentioned is expressed by

$$\frac{d\epsilon_x''}{\sigma_x - \frac{\sigma_y + \sigma_z}{2}} = \frac{d\epsilon_y''}{\sigma_y - \frac{\sigma_x + \sigma_z}{2}} = \frac{d\epsilon_z''}{\sigma_z - \frac{\sigma_x + \sigma_y}{2}} = \frac{d\gamma_{xy}''}{3\tau_{xy}} = \frac{d\gamma_{yz}''}{3\tau_{yz}} = \frac{d\gamma_{zx}''}{3\tau_{zx}} \quad \ldots [8]$$

In tension-torsion tests we have

$$\sigma_y = \sigma_z = 0, \quad \tau_{zx} = \tau_{yz} = 0$$

Hence Relations [8] become

$$\frac{d\epsilon_x''}{\sigma_x} = \frac{d\epsilon_y''}{-\frac{1}{2}\sigma_x} = \frac{d\epsilon_z''}{-\frac{1}{2}\sigma_x} = \frac{d\gamma_{xy}''}{3\tau_{xy}} \quad \ldots [9]$$

The octahedral shearing stress on a tension-torsion test is given by

$$\tau_0 = \frac{\sqrt{2}}{3}\sqrt{\sigma_x^2 + 3\tau_{xy}^2}$$

Hence

$$\left(\frac{3}{\sqrt{2}}\tau_0\right)^2 = \sigma_x^2 + 3\tau_{xy}^2$$

Therefore $\tau_0 =$ const. curves are circles in the σ_x, $\sqrt{3}\,\tau_{xy}$ plane with centers at the origin. For these curves, we have

$$2\sigma_x d\sigma_x + 2(\sqrt{3}\tau_{xy})d(\sqrt{3}\tau_{xy}) = 0$$

Hence the slope at any point on these curves is

$$\frac{d(\sqrt{3}\,\tau_{xy})}{d\sigma_x} = -\frac{\sigma_x}{\sqrt{3}\,\tau_{xy}}$$

The normal to these curves is given by the negative reciprocal, or $\sqrt{3}\,\tau_{xy}/\sigma_x$. From Equations [9] we find, however

$$\frac{\sqrt{3}\,\tau_{xy}}{\sigma_x} = \frac{d\gamma_{xy}''}{\sqrt{3}\,d\epsilon_x''} \quad \ldots [10]$$

Hence, if we superimpose a $(\sqrt{3}\,\epsilon_x'', \gamma_{xy}'')$ plane on the $(\sigma_x, \sqrt{3}\,\tau_{xy})$ plane, the vectors $(d\gamma_{xy}'', \sqrt{3}\,d\epsilon_x'')$ with the points of application $(\sigma_x, \sqrt{3}\,\tau_{xy})$ will be directed radially outward from the origin. This is a criterion for the validity of the proportionality expressed by Equations [9].[5] The distance of the point of application from the origin is equal to the corresponding value τ_0 multiplied by $3/\sqrt{2}$.

In the test series A, B, and C we used finite increments $d\tau_0$, due to increments $d\sigma_x$ and $d\tau_{xy}$. Therefore, instead of Equation [10], we have

$$\frac{\sqrt{3}\left(\tau_{xy} + \frac{d\tau_{xy}}{2}\right)}{\sigma_x + \frac{d\sigma_x}{2}} \cong \frac{d\gamma_{xy}''}{\sqrt{3}\,d\epsilon_x''} \quad \ldots [11]$$

Hence the vectors $(d\gamma_{xy}'', \sqrt{3}\,d\epsilon_x'')$ have now the points of application

$$\left(\sigma_x + \frac{d\sigma_x}{2}, \sqrt{3}\,\tau_{xy} + \frac{\sqrt{3}}{2}\,d\tau_{xy}\right)$$

In Fig. 1 we see the results of test series A concerning the validity of Criterion [11]. These tests consist of loading the specimen first in tension and then in torsion while keeping the tensile stress constant. In tests A-2, A-5, and A-10 we have a still more complicated loading pattern. All these tests show that Criterion [11] is valid with fair to good accuracy. Most increment vectors are parallel or nearly parallel to the radial lines. In only a few loading steps do the directions of the increment vectors disagree substantially with Criterion [11]; such steps are the first two torsion steps of test A-10 and the first step of test A-9. It should be noted that these steps are those with minimum τ_0 among all steps in the test series A. For values of $\tau_0 > 7000\sqrt{2}/3 = 3360$ psi, no substantial disagreements appear. (This value of τ_0 corresponds to the value $\sigma = 7000$ psi.)

A tentative explanation of these disagreements can be given easily by taking into account the value of the least readings of the strain-measuring instrument. The least reading for the axial strain is 20μ in/in., while for γ it is equal to 40μ in/in. Consider now the first torsion step in test A-9. Assuming an error of $+40\mu$ in/in. for $d\gamma''$ and of -20μ in/in. for $d\epsilon''$, we find

$$\frac{d\gamma''}{\sqrt{3}\,d\epsilon''} = \frac{79}{1.73 \times 85} = 0.54$$

The corresponding direction of the increment vector is given by

[5] A similar presentation of the results of combined stress tests has been given by Hohenemser and Prager (8).

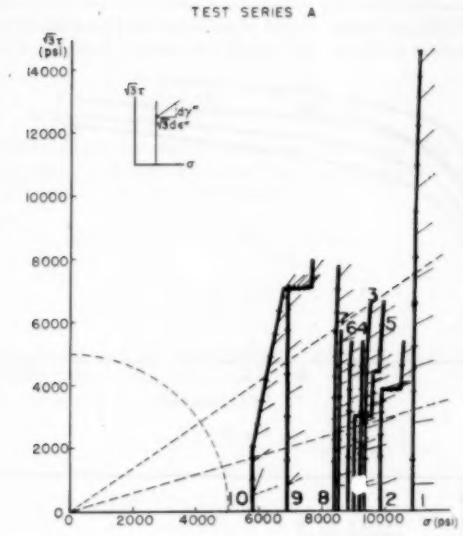

FIG. 1

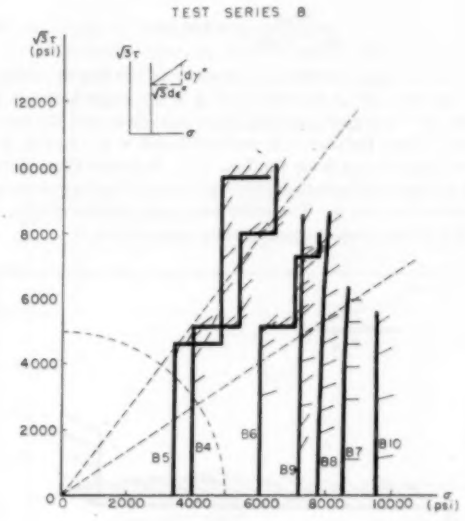

FIG. 2

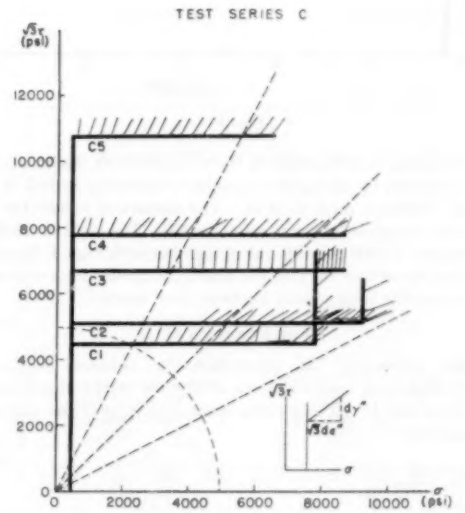

FIG. 3

the broken line. It is seen that the disagreement is much less now than it was before. In the case of the first torsion step in test A-10 we have

$$\frac{d\gamma^p}{\sqrt{3}\,d\epsilon^p} = \frac{27}{1.73 \times 34} = 0.40$$

The corresponding direction of the increment vector is given by the broken line. It is seen again that the disagreement is much less now than it was before.

In Fig. 2 we see the series B test results concerning the validity of Criterion [11]. These tests are of the same nature as those of the series A. If we consider loading steps with $\tau_0 > 8000\sqrt{2}/3 = 3840$ psi only, then with the exception of test B-7 the directions of the increment vectors agree substantially with Criterion [11]. For lower values of τ_0, the agreement is not as good. In particular, in several tests in this series, the plastic shear strain was found to be negative as measured for the first one or two increments of torque load. These negative values were found to be due to the strain-measuring equipment. The equipment was modified slightly after series A was completed in an attempt to reduce the weight, and tests using both the modified equipment and SR-4 gages showed that there was a slight lag in the twist-measuring portion of the modified equipment. The measurements were in agreement after the first one or two increments of torque load were applied.

In test series C, the specimens have been loaded first in torsion and then in tension. In Fig. 3 we see the results concerning the validity of Criterion [11]. With the exception of test C-3 and considering loading steps with $\tau_0 > 7000\sqrt{2}/3 = 3360$ psi only, the directions of the increment vectors agree substantially with the Criterion [11].

Tests C-3 and B-7 show similar behavior. In Test C-3 the specimen has been loaded first in torsion and then in tension; the tube deforms as if practically no tension has been applied. In Test B-7 the specimen has been loaded first in tension and then in torsion; the tube deforms as if practically no torsion has been applied.

Judging from these three series of tests, we conclude that these tests favor the Flow Rule [11]. We see also that Tests A and B agree with Condition [11] much better than do Tests C. It seems, therefore, that the form of the yield surface depends on the path of loading. Additional tests will be necessary, however, in order to verify this result and allow us to formulate this dependency.

Another way of deciding about the validity of the Flow Rule [11] is the following: From Equations [9] we find

$$\frac{d\gamma_{xy}{}^p}{d\epsilon_x{}^p - d\epsilon_y{}^p} = \frac{2\tau_{xy}}{\sigma_x} \quad \ldots\ldots\ldots\ldots\ldots\ldots [12]$$

We have, however

$$\frac{2\tau_{xy}}{\sigma_x} = \tan 2\theta \quad \ldots\ldots\ldots\ldots\ldots\ldots [13]$$

$$\frac{d\gamma_{xy}^{p}}{d\epsilon_x^{p} - d\epsilon_y^{p}} = \tan 2\phi \quad \ldots\ldots\ldots\ldots\ldots [14]$$

where θ is the angle between the direction of the largest principal stress and the axis of the tube and ϕ is the angle between the direction of the largest principal strain increment and the axis of the tube. From Relation [12] we find that $\theta = \phi$. In Fig. 4 we give the angles θ and ϕ for the Test C-1. It is seen that relation $\theta = \phi$ is fairly well satisfied, although in some loading steps ϕ is quite different from θ. The other tests gave similar results, except for C-3, where ϕ was consistently greater than θ.

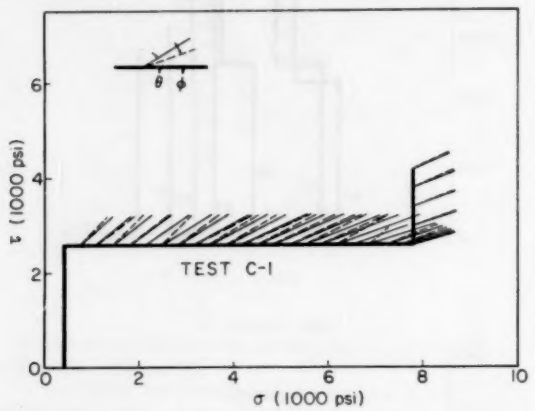

FIG. 4

In obtaining plastic strains in these experiments, elastic strains were computed by taking the modulus of elasticity as 10.5×10^6 psi and Poisson's ratio as 0.33. The numerical values for the measured strains are given in reference (3). The yield strength of the material is 5000 psi; this value, together with Figs. 1, 2, and 3, gives an idea of how far into the plastic range the tests were carried before the incremental loadings were started.

THE FUNCTION G

While previously the proportionality between $d\epsilon_{ij}^{p}$ and $\partial f/\partial\sigma_{ij}$ has been considered, we shall now study the function G in Equation [4]. Using stress-strain Relations [7] we calculate the quantity[6]

$$d\Gamma_0^{p} = \frac{2}{\sqrt{3}} \sqrt{d\epsilon_x^{p2} + d\epsilon_y^{p2} + d\epsilon_z^{p2} + \frac{1}{2}\left(d\gamma_{xy}^{p2} + d\gamma_{yz}^{p2} + d\gamma_{zx}^{p2}\right)}$$

and find

$$d\Gamma_0^{p} = \frac{2}{3} G(\tau_0) d\tau_0 \quad \ldots\ldots\ldots\ldots\ldots [15]$$

which after integration becomes

$$\Gamma_0^{p} = \frac{2}{3} \int G(\tau_0) d\tau_0 = \phi(\tau_0) \quad \ldots\ldots\ldots\ldots [16]$$

[6] In order to calculate the quantity $d\Gamma_0^{p}$ we use the measurements for $d\epsilon_x^{p}$, $d\epsilon_y^{p}$, and $d\gamma_{xy}^{p}$, the condition of incompressibility

$$d\epsilon_x^{p} + d\epsilon_y^{p} + d\epsilon_z^{p} = 0$$

and the conditions

$$d\gamma_{yz}^{p} = d\gamma_{zx}^{p} = 0$$

Because $d\epsilon_y^{p}$ has been measured in the series C only, it follows that $d\Gamma_0^{p}$ could be determined only in this series of tests.

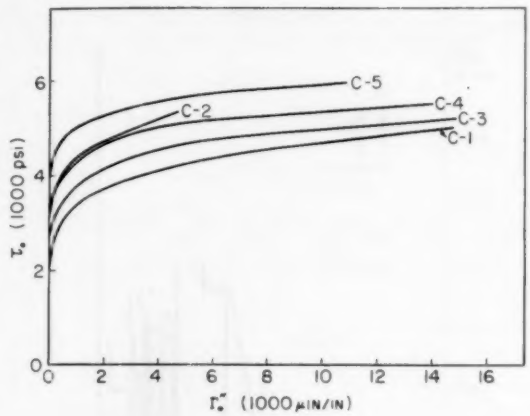

FIG. 5

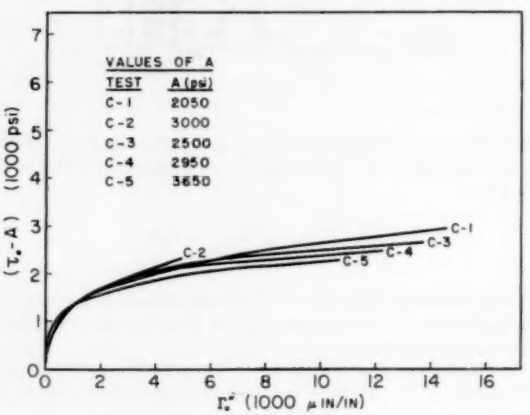

FIG. 6

Our problem will be to find if the relationship between Γ_0^{p} and τ_0 is the same for all combined stress tests as predicted by the stress-strain Relations [7] and [16].

In Fig. 5 we give the $\tau_0 - \Gamma_0^{p}$ curves for tests C-1 to C-5. We see that these curves do not coincide. Thus, for this material, a single relationship $\Gamma_0^{p} = \phi(\tau_0)$ for all combined stress tests does not seem to exist. From Fig. 6, however, it follows that with fair approximation we may write

$$\Gamma_0^{p} = \phi(\tau_0 - A) \quad \ldots\ldots\ldots\ldots [17]$$

where ϕ is the same function of $\tau_0 - A$ for all five Tests C, while A is a constant which varies from test to test.

Relationship [17] can be found analytically by assuming that in Equations [7] the function G is a function of $(\tau_0 - A)$. Then Equation [15] becomes

$$d\Gamma_0^{p} = \frac{2}{3} G(\tau_0 - A) d\tau_0 = \frac{2}{3} G(\tau_0 - A) d(\tau_0 - A)$$

from which we find

$$\Gamma_0^{p} = \frac{2}{3} \int G(\tau_0 - A) d(\tau_0 - A) = \phi(\tau_0 - A) \ldots [18]$$

From this and the preceding section of this paper we conclude

that the stress-strain Relations [4] for pure aluminum 28-O in the case of combined torsion and tension can be written in the form

$$d\epsilon_{ij}'' = G(\tau_0 - A)\frac{\partial \tau_0}{\partial \sigma_{ij}}\,d\tau_0 \quad \ldots\ldots\ldots\ldots [19]$$

It should be added that if the function f in Equation [4], which was assumed to be equal to τ_0 in Equation [6], is assumed to be equal to $\tau_0 - A$, Equation [4] will give

$$d\epsilon_{ij}'' = G(\tau_0 - A)\frac{\partial(\tau_0 - A)}{\partial \sigma_{ij}}\,d(\tau_0 - A)$$

$$= G(\tau_0 - A)\frac{\partial \tau_0}{\partial \sigma_{ij}}\,d\tau_0$$

which is identical with Equation [19]. Therefore the function f can be considered as equal to $\tau_0 - A$ or τ_0.

In engineering notation

$$d\epsilon_x'' = \frac{2}{9}\frac{G(\tau_0 - A)}{\tau_0}\left[\sigma_x - \frac{1}{2}(\sigma_y + \sigma_z)\right]d\tau_0$$

$$d\epsilon_y'' = \frac{2}{9}\frac{G(\tau_0 - A)}{\tau_0}\left[\sigma_y - \frac{1}{2}(\sigma_x + \sigma_z)\right]d\tau_0$$

$$d\epsilon_z'' = \frac{2}{9}\frac{G(\tau_0 - A)}{\tau_0}\left[\sigma_z - \frac{1}{2}(\sigma_y + \sigma_x)\right]d\tau_0$$

$$d\gamma_{xy}'' = \frac{2}{3}\frac{G(\tau_0 - A)}{\tau_0}\tau_{xy}d\tau_0$$

$$d\gamma_{yz}'' = \frac{2}{3}\frac{G(\tau_0 - A)}{\tau_0}\tau_{yz}d\tau_0$$

$$d\gamma_{zx}'' = \frac{2}{3}\frac{G(\tau_0 - A)}{\tau_0}\tau_{zx}d\tau_0$$

The dependency of the constant A upon the path of loading could not be determined because of the small number of experiments performed in the series C. To determine the dependency, it will be necessary to perform additional experiments in which $d\epsilon_x''$, $d\epsilon_y''$, and $d\gamma_{xy}''$ will be measured.

The Rotation Experiments

Rotation experiments such as described here have been proposed by Drucker (5), who advocated them as a means of deciding whether the incremental or the total strain theories are correct. The results of the tests described in this part[7] indicate that the incremental theories are the correct ones.

The rotation experiments have an additional meaning. If it is assumed that $d\epsilon_{ij}''$ is proportional to df as shown in Equation [4], then from the test series D we can determine whether the function f depends on all six stress components or on the three principal stresses only. Indeed, in this series we keep σ_1, σ_2, and σ_3 constant while we rotate the directions of the principal stresses. If f depends on the three principal stresses only, then df is zero during this rotation and therefore $d\epsilon_{ij}''$ also will be zero. On the other hand, if f depends on all six stress components, then df will not be zero during the rotation mentioned and therefore neither will $d\epsilon_{ij}''$ be zero.

In Figs. 7, 8, and 9 we give the results of the test series D. The specimen has been loaded to an axial tensil stress $\sigma_1 = 8000$ psi, and then the stress system $\sigma_1 = 8000$ psi, $\sigma_2 = 0$, $\sigma_3 = 0$, has been rotated by varying the axial force, torque, and internal pressure. The increments of these loads were applied in a sequence which prevented τ_0 from exceeding the maximum value it had before rotation was begun, i.e.

$$\frac{\sqrt{2}}{3}\sqrt{8000^2} = 3700 \text{ psi}$$

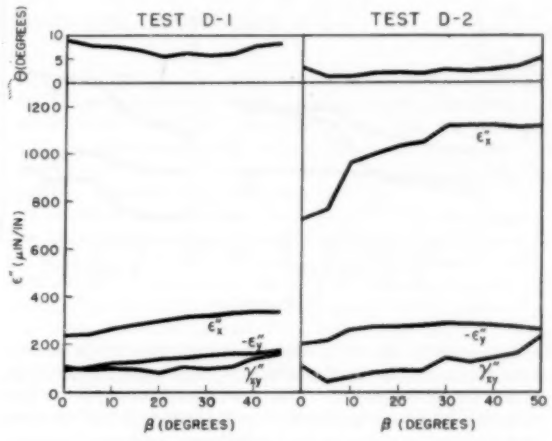

Fig. 7

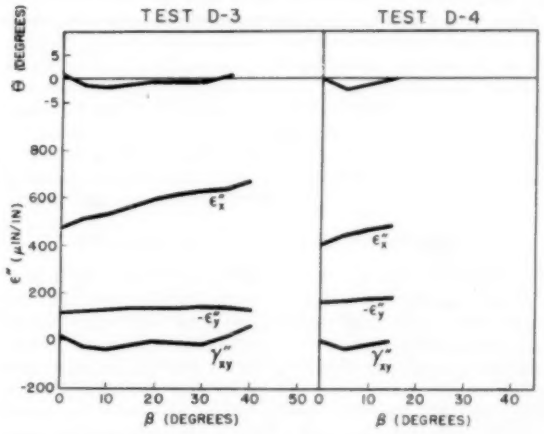

Fig. 8

The angle β represents the angle between the axis of the tube and the direction of the stress σ_1. We see that this angle increases in 5-deg steps up to final values ranging from 15 to 50 deg.

In Tests D-1, D-3, and D-4, the plastic-strain components remain essentially constant throughout the rotation. Hence, for these tests, $d\epsilon_x''$, $d\epsilon_y''$, and $d\gamma_{xy}''$ are zero or nearly zero and therefore the same is the case with df. We conclude, therefore, that for these three specimens f is a function of the principal stresses only. In the other three tests, anisotropic behavior is indicated, since one or more of the plastic-strain components shows marked increase as the stress direction is rotated.

The angle θ, shown in Figs. 7, 8, and 9, is the angle between the direction of the maximum total plastic-strain component ϵ_1'' and the axis of the tube. According to the incremental theories of plasticity, we must have θ = const. during the rotation process. This constant should be zero, since rotation begins from a state

[7] To the knowledge of the authors, these rotation tests are the first ever conducted. The interesting experiments by Marin and his group (9) and (10) are not true rotation tests because they kept only τ_0 constant and not all three principal stresses.

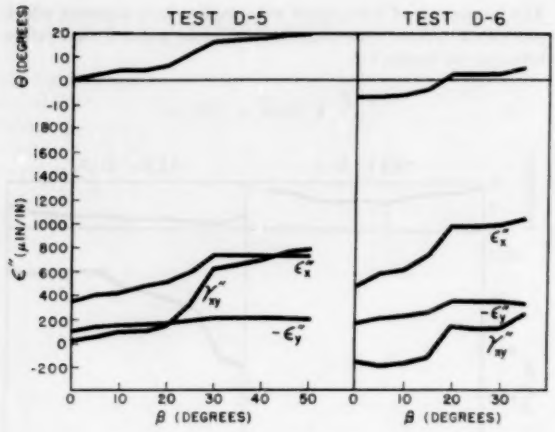

FIG. 9

of pure tension. In several tests the initial value of θ is different from zero owing to the appearance of some plastic shear strain during the tensile loading. This anomalous shear strain has been noted by other investigators (6, 7) and, as suggested by Morrison and Shepherd, may be due to an insufficient number of crystals in the cross section to produce polycrystalline behavior.

Total-strain theories, on the other hand, predict that $\theta = \beta$. These tests show that θ remains practically constant, and therefore the incremental theories are correct, while the total-strain theories are not.

BIBLIOGRAPHY

1 "Combined Tension-Torsion Tests for Aluminum Alloy 2S-O," by Aris Phillips, JOURNAL OF APPLIED MECHANICS, Trans. ASME, vol. 74, 1952, pp. 496–500.

2 "The Significance of the Criterion for Additional Plastic Deformation of Metals," by D. C. Drucker, *Journal of Colloid Science*, vol. 4, 1949, pp. 299–311.

3 "Combined Stress Tests in Plasticity," Aris Phillips and Lloyd Kaechele, Technical Report No. 19, Contract N6-ONR-251 (11), Stanford University, Calif., 1954.

4 "Plastic Flow of a Magnesium Alloy Under Biaxial Stresses," by D. M. Cunningham, E. G. Thomsen, and J. E. Dorn, Proceedings ASTM, vol. 47, 1947, pp. 546–553.

5 "Stress-Strain Relations for Strain-Hardening Materials: Discussion and Proposed Experiments," by D. C. Drucker, Proceedings of Symposia in Applied Mathematics, vol. 1, 1949, pp. 181–187.

6 "An Experimental Investigation of Plastic Stress-Strain Relations," by J. L. M. Morrison and W. M. Shepherd, Proceedings of The Institution of Mechanical Engineers, vol. 163, 1950, pp. 1–17.

7 "Experimental Studies of Polyaxial Stress-Strain Laws of Plasticity," by B. Budiansky, N. F. Dow, R. W. Peters, and R. P Shepherd, Proceedings of the First U. S. National Congress of Applied. Mechanics, 1951, pp. 503–512.

8 "Beitrag zur Mechanik des bildsamen Verhaltens von Flussstahl," by K. Hohenemser and W. Prager, *Zeitschrift für Angewandte Mathematik und Mechanik*, vol. 12, 1932, pp. 1–14.

9 "Plastic Stress-Strain Relations for Biaxial Tension and Variable Stress Ratios" by J. Marin and L. W. Hu, Proceedings ASTM, vol. 52, 1952, pp. 1098–1123.

10 "Plastic Stress-Strain Relations for Aluminum Alloy 14S-T6 Subjected to Combined Tension and Torsion," by J. Marin and H. A. B. Wiseman, *Journal of Metals*, Trans. AIME, September 1953, pp. 1181–1190.

The Load-Carrying Capacity of Circular Plates at Large Deflection[1]

By E. T. ONAT[2] and R. M. HAYTHORNTHWAITE,[3] PROVIDENCE, R. I.

This paper presents an approximate analysis for the load carrying capacities of initially flat circular plates under various loading and edge conditions and subjected to slowly increasing load. As a plate deforms, the carrying capacity is increased as a result of favorable changes in geometry. In this study, the load capacity after finite deflection is estimated by assuming a velocity field based on the boundary conditions and on the incipient velocity field of the flat plate, the analysis being made for a rigid plastic, nonstrain-hardening material that yields according to the maximum shear-stress criterion. In several cases the results obtained compare favorably with test data for mild-steel plates; however, for very thin plates, better agreement is obtained by means of a purely membrane-type analysis, which also is presented.

Introduction

THE analysis presented in this paper was prompted by the results of recent static loading tests on circular mild-steel plates in the plastic range (1, 2, 3, 4).[4] In each of these tests, the rate of increase in deflection did not approach the indefinitely high value expected from the theory of limit analysis (5). Instead, the load continued to increase without excessive deflection to well above the expected collapse load. The explanation of this will be sought through a study of the load-deflection relationship in the plastic range. The approach adopted may in itself prove useful as the basis of a more comprehensive technique for the limit analysis of plates.

The methods of limit analysis (5, 6) enable good estimates to be made of the useful carrying capacity of certain structural steel frameworks in which instability does not develop and in which unserviceability resulting from excessive deflection occurs before any member fails because of fracture. Tests have shown these to include, for example, some single span and multispan beams (7, 8, 9) and some portal frames (10) fabricated from low-carbon structural steel. In the theory, elasticity of the material usually is neglected and the load-carrying capacity is estimated as the load at which a model composed of an ideal rigid-plastic material would begin to deform. It can be shown that, if the material is perfectly plastic (i.e., nonstrain hardening) and if the accompanying change in geometry is disregarded, plastic flow continues under constant load (6). Thus, under monotonically increasing load, the rigid-plastic model collapses as soon as the yield-point load is reached, and this reflects quite accurately the observed behavior of structures of the types referred to.

The simplest limit analysis theory neglects both strain hardening and changes in geometry and this always must be borne in mind when attempting to broaden its field of application. When either of these factors is introduced in the theoretical model, it is found that, in general, plastic flow can continue only under either increasing or decreasing load (11). If the modified model is appropriate, the yield load may then be of less value as a measure of the carrying capacity of the actual structure. In practice, the rate of increase of deflection with load will usually be the significant factor. When this rate greatly exceeds the rate of deflection in the elastic range the structure will rapidly become unserviceable and the practical limit of carrying capacity will have been reached. This stage can be identified by investigating the load-deflection relationship beyond the yield load.

The foregoing considerations lead us to suppose that the observed post-yield behavior of circular plates probably is conditioned by change of geometry and by strain hardening. In this paper the role of the change of geometry will be investigated and the resulting theoretical load-deflection curves will be compared with the results of tests. Only rotationally symmetric, monotonically increasing loading will be considered. The case of reversing loads is discussed elsewhere (12).

Approximate Solutions at Finite Deflection

At finite deflection the plate becomes a shell of revolution. If an ideal rigid-plastic material is assumed, the deformed plate will be indistinguishable from a shell whose initial shape is the same as the current shape of the plate. Thus the deforming plate presents a series of classical rigid-plastic limit-analysis problems, with the additional complication that the shape is not known in advance, but is specified by the velocity fields associated with the exact solutions at previous levels of deformation. A technique for obtaining upper and lower bounds to the limit load of a shell of revolution has been described by Onat and Prager (13). Exact solutions, i.e., coincidence of upper and lower bounds, are difficult to find except in special cases and without them exact solutions to the problem of the deforming plate cannot be sought.

In developing an approximate treatment, we start by considering the exact solutions for flat plates due to Hopkins and Prager (14). If Tresca's yield condition is used, the equations of equilibrium may be integrated directly and the complete solution obtained, including the incipient velocity field and the stress distribution at the yield point. For example, a simply supported circular plate carrying a load concentrated at the center, Fig. 1, will begin to deform plastically when the load reaches the value[5] $2\pi M_0$, where M_0 is the bending moment per unit length inducing full plasticity of a cross section in the absence of other forces. The velocity field that initiates the plastic distortion is

[1] The results presented in this paper were obtained in the course of research sponsored by the Office of Ordnance Research under Contract No. DA-19-020-ORD-3172, Project No. TB2-0001 (1086).

[2] Formerly, Research Associate, Division of Applied Mathematics, Brown University; at present, Yenisehir, Ankara, Turkey.

[3] Assistant Professor, Division of Engineering, Brown University.

[4] Numbers in parentheses refer to the Bibliography at the end of the paper.

Contributed by the Applied Mechanics Division and presented at the Diamond Jubilee Annual Meeting, Chicago, Ill., November 13–18, 1955, of The American Society of Mechanical Engineers.

Discussion of this paper should be addressed to the Secretary, ASME, 29 West 39th Street, New York, N. Y., and will be accepted until April 10, 1956, for publication at a later date. Discussion received after the closing date will be returned.

Note: Statements and opinions advanced in papers are to be understood as individual expressions of their authors and not those of the Society. Manuscript received by ASME Applied Mechanics Division, January 20, 1955. Paper No. 55—A-14.

[5] The effect of shear is neglected.

$$v = 0;\ w = -c\left(1 - \frac{\xi}{R}\right)$$

where c is an undetermined positive constant and R is the radius of the plate. This equation suggests that the initially flat plate will become a conical shell.

Recent tests of plates loaded through a central punch have shown that, for mild-steel plates, the actual shape is very nearly conical and it remains so even when the permanent deflection is several times the thickness (3, 4). Other tests using various loading and edge conditions have shown that in each case the deformed shape also can be approximated by continuing the incipient velocity field obtained at zero deflection (3).

The facts just mentioned point to a method of attack that may be used to obtain approximate solutions. If a velocity field can be found that describes the position of the mid-surface of the plate at every stage with reasonable accuracy, then the applied loads associated with it might be used as estimates of the carrying capacity of the plate. Before this can be done, reasonable assumptions must be made concerning the radial component of the velocity. Here the force or velocity-boundary conditions at the support are a valuable guide.

Once both components of the velocity field have been chosen, the rate of dissipation of energy can be computed and the magnitude of the applied load follows at once by virtual work. In this approach, no use is made of the equilibrium equations, so the forces need not be computed. Instead, the rate of energy dissipation is found directly from the strain rates and the corresponding stresses.

Fig. 2 shows an element of a shell with the stress resultants transmitted across the boundary meridians and parallels; M_φ and M_θ are the meridional and circumferential bending moments,

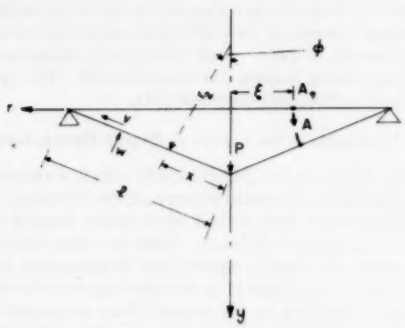

FIG. 1 SIMPLY SUPPORTED CIRCULAR PLATE WITH LOAD CONCENTRATION AT CENTER

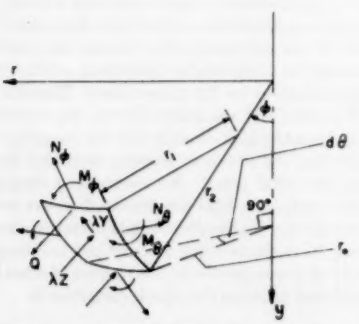

FIG. 2 ELEMENT OF SHELL SHOWING STRESS RESULTANTS

N_φ and N_θ the corresponding membrane forces, and Q the shear force, each measured per unit length of shell cross section. The load per unit area of the middle surface of the shell has the components λY in the direction of the meridian and λZ in the direction of the normal. Y and Z are supposed to be known and λ is the unknown load parameter. The arrows indicate the conventions for positive forces and couples. The principal rates of strain in the middle surface are

$$\epsilon_\varphi = \frac{1}{r_1}(v' - w);\ \epsilon_\theta = \frac{1}{r_2}(v\cot\varphi - w) \quad \ldots\ldots [1]$$

and the principal rates of curvature are

$$\kappa_\varphi = +\frac{1}{r_1}\left[\frac{1}{r_1}(v + w')\right]';\ \kappa_\theta = +\frac{\cot\varphi}{r_1 r_2}(v + w) \quad \ldots [2]$$

where the prime denotes differentiation with respect to φ. Terms v and w are velocity components parallel and normal to the plate, respectively. To obtain the velocity field of the plastic flow, the particles originally on the normal to the undeformed middle surface are assumed to remain on a normal to the middle surface as the latter is deforming. The rates of strain ϵ_θ, ϵ_φ for every point in the plate are

$$\epsilon_\theta = \epsilon_\theta + \kappa_\theta z;\ \epsilon_\varphi = \epsilon_\varphi + \kappa_\varphi z$$

where z is the height of the element above the mid-plane of the plate.

The components Y and Z of the exterior load are given to within a common factor λ that defines the unknown critical-load intensity. Since no energy is recoverable from a rigid-plastic shell, the total rate of energy dissipation must equal the rate at which the applied unit loads (multiplied by λ) do work. This condition is satisfied if λ is determined from

$$\lambda\left|\int (vY + wZ) r_0 r_1 d\varphi\right| = \int D\, r_0 r_1 d\varphi \quad \ldots\ldots [3]$$

where D is the rate of dissipation of energy per unit area and the integration is extended over the entire meridian. In the following, Equation [3] will be used to give an estimate of the load intensity λ. Once the approximate mode of deformation is decided upon with the help of the incipient-velocity field and the boundary conditions, then r_0 and r_1 and hence v and w may be computed as functions of φ and a timelike parameter, such as the maximum deflection δ. Equation [3] gives the load-intensity parameter λ in terms of δ, thus establishing a load-deflection relationship for the post yield-point loads.

This approach will now be applied to two cases for which test data are available. For the purpose of analysis, the ideal material is assumed to yield according to the maximum shear-stress criterion and subsequently to obey the corresponding flow rule. The rate of energy dissipation per unit volume during plastic flow is $\sigma_0|e|_{\max}$ where σ_0 is the yield stress in simple tension and $|e|_{\max}$ is the greatest principal strain rate. The use of the maximum shear-stress criterion results in particularly straightforward algebra, but any other criterion could be employed without introducing any basic difficulty providing the corresponding incipient-velocity field was known.

EXAMPLE 1 THE SIMPLY SUPPORTED CIRCULAR PLATE

Consider a circular plate of uniform thickness h, simply supported at the outer radius $r = R$ as shown in Fig. 1, and carrying a lateral load of intensity p applied to a central circular zone of radius $r = a$. As mentioned already, the incipient-velocity distribution at the limit load will tend to deform the plate into a right circular cone with apex at the center. This is known to be correct only at zero deflection when there are no membrane forces. The conical shape might reasonably be taken as a first approxima-

tion during small but finite deflections. The membrane forces are no longer zero and must be considered when computing the loads required to produce the deformation; also these forces satisfy boundary conditions with which any assumed velocity field should be made to fit, in so far as is possible.

The assumption of a conical shape for the deformed plate serves to fix one component of the velocity distribution in terms of the other, for example, that normal to the plate at any instant. To make a reasonable choice for the component in the plane of the plate we note that, if the plate is freely supported at the outer edge, radial membrane force at the edge will be zero; hence the corresponding strain component is probably small. Thus a reasonable assumption would seem to be to set the strain component in the plane of the plate zero at the outer edge. For simplicity, the component will be taken as zero throughout the plate, but the more general case could be treated on similar lines. The material point initially at A_0, Fig. 1, will move to A. The circumferential strain on the mid-surface is $\cos\varphi - 1 \approx -\varphi^2/2$ when φ is small; hence the circumferential strain rate (with respect to φ) is

$$\epsilon_\theta \approx -\varphi \approx -\frac{\delta}{R}$$

Also $x/r_2 = \tan\varphi \approx \varphi$; so $1/r_2 \approx \varphi/x$ and the circumferential curvature rate (with respect to φ) is

$$\kappa_\theta \approx \frac{1}{x} = \frac{1}{r}$$

The rate of energy dissipation per unit volume is $\sigma_0|e|_{max}$ where $|e|_{max}$ is the numerically largest principal strain rate; hence the rate of energy dissipation per unit area of the plate is

$$d = \sigma_0 \int_{-h/2}^{h/2} |e|_{max}\, dz$$

The only strain is in the circumferential direction so $|e|_{max} = |\epsilon_\theta + \kappa_\theta z|$ and by integration the area of the $|e|_{max}$ diagram, Fig. 3 is found to be

$$\frac{d}{\sigma_0} = \left\{ \begin{array}{ll} |\kappa_\theta|\frac{h^2}{2} + \frac{\epsilon_\theta^2}{|\kappa_\theta|} = \frac{h^2}{4r} + \frac{\delta^2 r}{R^2} \text{ when } r \le \frac{Rh}{2\delta} & (a) \\ |\epsilon_\theta| h = \frac{\delta h}{R} \qquad \text{when } r \ge \frac{Rh}{2\delta} & (b) \end{array} \right\} \quad \ldots [4]$$

For small deflections ($\delta/h < 1/2$), Equation [4a] applies throughout the plate. The total rate of energy dissipation is then

$$D = \int_0^R (2\pi r d)dr = 2\pi M_0 R\left(1 + \frac{4}{3}\frac{\delta^2}{h^2}\right)$$

where

$$M_0 = \frac{1}{4}\sigma_0 h^2$$

The rate of work by the applied pressure p is

$$E = 2\pi p \int_0^a r(R - r)dr = PR\left(1 - \frac{2}{3}\frac{a}{R}\right)$$

where $P = \pi a^2 p$ is the total load.

Using Equation [3] and writing

$$P_L = 2\pi M_0/(1 - 2a/3R)$$

for the yield load of the undeformed plate ($\delta = 0$)

$$\frac{P}{P_L} = \left\{ \begin{array}{ll} 1 + \frac{4}{3}\frac{\delta^2}{h^2} & \text{when } \delta/h \le 1/2 \\ 2\frac{\delta}{h} + \frac{1}{6}\frac{h}{\delta} & \text{when } \delta/h \ge 1/2 \end{array} \right\} \quad \ldots [5]$$

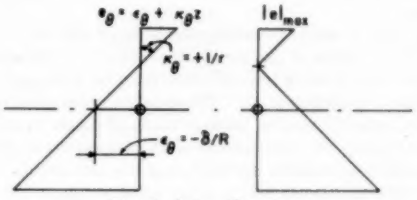

FIG. 3 $|e|_{max}$ DIAGRAM

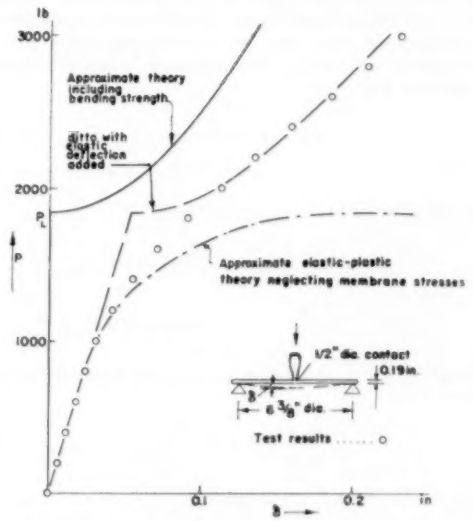

FIG. 4 SIMPLY SUPPORTED MILD-STEEL PLATE SUBJECTED TO A CENTRAL LOAD

Comparison With Tests. In Fig. 4 a load-deflection curve computed by means of Equations [5] is compared with observations of the central deflection of a simply supported mild-steel plate loaded through a centrally placed punch (4). In addition, a load-deflection curve is shown based on an approximate theory neglecting membrane stresses but allowing for the elasticity of the material (1). A third curve has been obtained by adding to the deflection found by means of Equations [5] an elastic deflection component proportional to the initial deflection rate.

The last-mentioned curve serves to show that the slope of the experimental points at high loads is very nearly the sum of the initial elastic slope and that obtained from the use of Equations [5]. It must be emphasized that this superposition has been made to illustrate the good agreement with the tests thus made possible. Lateral displacement of the curve based on a rigid-plastic model has no known theoretical justification; however, when sufficient confirmatory tests are available, it might prove useful in engineering practice as a method for obtaining conservative estimates of plate deflection.

In the early stages of plasticity the approximate elastic-plastic theory is probably more satisfactory for practical applications because it will overestimate deflection, providing shear is unimportant. Nevertheless the present theory gives a much better picture of the mechanics of post-yield behavior.

Example 2 The Clamped Circular Plate

Consider a plate similar to that of example 1, but clamped to a stiff ring at its outer radius $r = R$, as shown in Fig. 5. This ring is supposed to prevent all radial and rotational movements of the outer edge.

In this case it would be unreasonable to set the rate of strain zero in the direction of the plate mid-surface. If the edges are prevented from moving inward, there must be some such strain if the plate is to deflect at all. The simplest assumption is to set the radial velocity zero, so that all material points in the plate move vertically. A continuation of the incipient-velocity field then furnishes a complete description of the movement.

The incipient-velocity field is made up of two parts (14). In a central zone bounded by $r = \rho$ the plate deforms to a conical shape, as for the simply supported plate of example 1. Outside this zone the shape is logarithmic. Finite rotation occurs just inside the clamped edge, implying the formation of a kink or plastic hinge at that radius. Defining a function $C(\delta)$ of the central deflection δ by

$$C(\delta) = \frac{\delta}{1 + \ln \frac{R}{\rho}} \quad \ldots\ldots\ldots\ldots\ldots [6]$$

the rate of deflection with respect to C is (14)

$$\dot{y} = \left\{ \begin{array}{ll} 1 + \ln \dfrac{R}{\rho} - \dfrac{r}{\rho} & \text{when } 0 \leq r \leq \rho \\ \ln \dfrac{R}{r} & \text{when } \rho \leq r \leq R \end{array} \right\} \quad \ldots [7]$$

When $a/R \leq e^{-1/2} = 0.606$, ρ is found from the transcendental equation

$$1 - \frac{2}{3}\frac{a}{\rho}\left(1 + \ln \frac{R}{\rho}\right) = 0 \quad \ldots\ldots\ldots [8]$$

and when $a/R \geq 0.606$, it is found from

$$1 - \frac{a^2}{\rho^2}\left(1 + 2 \ln \frac{R}{a}\right) + \frac{2}{3}\left(1 + \ln \frac{R}{\rho}\right) = 0 \ldots [9]$$

We shall assume that the Expressions [7], known to be correct for zero deflection, are a reasonable approximation when the deflection is nonzero.

Exact determination of the rates of extension and curvature of the middle surface at finite deformations is rather involved in this case. The mathematical work is simplified considerably by making the following approximations, familiar from the elastic theory for shells

$$-1/r_1 \approx d^2y/dr^2; \quad \varphi \approx -dy/dr; \quad r_2 \approx -r/(dy/dr)$$

We then obtain from Equations [1] and [2], for $0 \leq r \leq \rho$

$$\epsilon_\varphi = dv/dr = +C/\rho^2; \quad \epsilon_\theta = \frac{1}{r_2}(v \cot \varphi - w) = 0$$

$$\kappa_\varphi = d^2w/dr^2 = 0; \quad \kappa_\theta = (dw/dr)/r_2 \sin \varphi = 1/\rho r$$

and for $r \leq \rho \leq R$

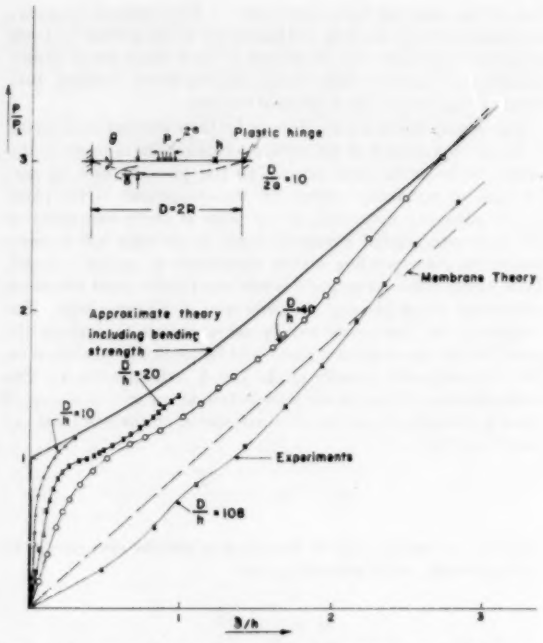

Fig. 5 Clamped Mild-Steel Plates Subjected to a Central Load

$$\epsilon_\varphi = (dv/dr)r_2 \cos \varphi/r_1 - w/r_1 = C/r^2; \quad \epsilon_\theta = 0$$

$$\kappa_\varphi = [d(v/r_1)/dr + d^2w/dr^2]r_2 \cos \varphi/r_1 = -1/r^2; \quad \kappa_\theta = +1/r^2$$

where the rates of strain and curvature are taken with respect to C. Fig. 6 shows the strain-rate diagrams for the foregoing. By integration of the $|e|_{max}$ diagram we obtain, for $0 \leq r \leq \rho$, Fig. 6(*a*)

$$\frac{d}{\sigma_0} = \left\{ \begin{array}{ll} \dfrac{Ch}{2\rho^2} + \dfrac{C^2r}{2\rho^3} + \dfrac{h^2}{4\rho r} & \text{when } \dfrac{C}{\rho} \leq \dfrac{h}{2r} \\ \dfrac{Ch}{\rho^2} + \dfrac{h^2}{8\rho r} & \text{when } \dfrac{C}{\rho} \geq \dfrac{h}{2r} \end{array} \right.$$

and for $\rho \leq r \leq R$, Fig. 6(*b*)

$$\frac{d}{\sigma_0} = \left\{ \begin{array}{ll} \dfrac{Ch}{2r^2} + \dfrac{C^2}{2r^2} + \dfrac{h^2}{4r^2} & \text{when } C \leq \dfrac{h}{2} \\ \dfrac{Ch}{r^2} + \dfrac{h^2}{8r^2} & \text{when } C \geq \dfrac{h}{2} \end{array} \right.$$

The rates of energy dissipation in the parts of the plate defined by $0 \leq r \leq \rho$ and $\rho \leq r < R$ (excluding $r = R$), are then obtained by integration. Toward the edge, $dy/dr = C/R$ just inside the plate and zero at the edge itself. The resulting plastic hinge requires the development of the fully plastic moment M_0 (if the effects of shear forces are neglected). The rate of energy dissipation at the plastic hinge is $2\pi R M_0(1/R) = 2\pi M_0$. The total rate of energy dissipation is then

$$D = 2\pi M_0 + \int_0^R (2\pi r d)dr = 2\pi M_0 A$$

where

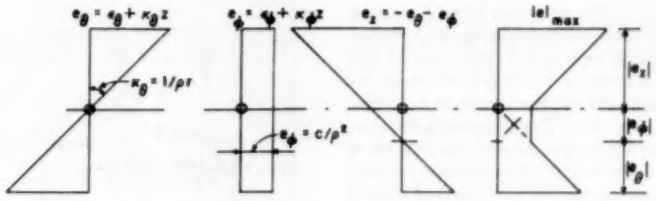

FIG. 6(a) STRAIN-RATE DIAGRAM

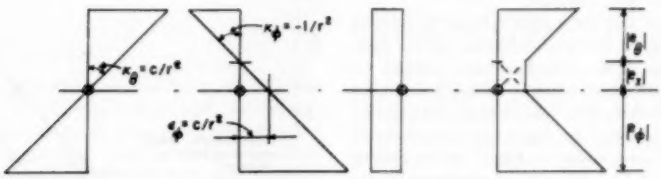

FIG. 6(b) STRAIN-RATE DIAGRAM

$$A = \begin{cases} 2 + \ln\frac{R}{\rho} + \frac{C}{h}\left(1 + 2\ln\frac{R}{\rho}\right) + \frac{C^2}{h^2}\left(\frac{2}{3} + 2\ln\frac{R}{\rho}\right) & \text{when } C \le h/2 \\ \frac{3}{2} + \frac{1}{2}\ln\frac{R}{\rho} + \frac{C}{h}\left(2 + 4\ln\frac{R}{\rho}\right) + \frac{h}{12C} & \text{when } C \ge h/2 \end{cases} \quad \ldots\ldots\ldots\ldots\ldots\ldots [10]$$

The rate at which work is done by the pressure loading p is

$$E = \int_0^a (2\pi r\dot{y}p)dr = BP$$

where $P = \pi a^2 p$ is the total load and

$$B = \begin{cases} 1 + \ln\frac{R}{\rho} - \frac{2a}{3\rho} & \text{when } \rho \ge a \\ \frac{1}{2} + \ln\frac{R}{a} - \frac{\rho^2}{6a^2} & \text{when } \rho \le a \end{cases} \quad \ldots\ldots [11]$$

Employing again Equation [3]

$$P = 2\pi M_0 A/B$$

where A and B are given by Equations [10] and [11]. The yield load of the undeformed plate is

$$P_L = 2\pi M_0 A_0/B$$

where

$$A_0 = 2 + \ln\frac{R}{\rho}$$

Hence, on substitution for C, Equation [6] in [10]

$$\frac{P}{P_L} = \frac{A}{A_0} = \begin{cases} 1 + \alpha_1\left(\frac{\delta}{h}\right) + \alpha_2\left(\frac{\delta}{h}\right)^2 \\ \quad \text{when } \frac{\delta}{h} \le \frac{1}{2} + \frac{1}{2}\ln\frac{R}{\rho} \\ \beta_1 + \beta_2\left(\frac{\delta}{h}\right) + \beta_3\left(\frac{h}{\delta}\right) \\ \quad \text{when } \frac{\delta}{h} \ge \frac{1}{2} + \frac{1}{2}\ln\frac{R}{\rho} \end{cases}$$

where

$$\alpha_1 = \frac{\left(1 + 2\ln\frac{R}{\rho}\right)}{\left(2 + \ln\frac{R}{\rho}\right)\left(1 + \ln\frac{R}{\rho}\right)};$$

$$\alpha_2 = \frac{2\left(1 + 3\ln\frac{R}{\rho}\right)}{3\left(2 + \ln\frac{R}{\rho}\right)\left(1 + \ln\frac{r}{\rho}\right)^2}$$

and

$$\beta_1 = \frac{\left(3 + \ln\frac{R}{\rho}\right)}{2\left(2 + \ln\frac{R}{\rho}\right)};\ \beta_2 = \frac{2\left(1 + 2\ln\frac{R}{\rho}\right)}{\left(2 + \ln\frac{R}{\rho}\right)\left(1 + \ln\frac{R}{\rho}\right)}$$

$$\beta_3 = \frac{1 + \ln\frac{R}{\rho}}{12\left(2 + \ln\frac{R}{\rho}\right)} \quad \ldots\ldots\ldots [12]$$

The value of ρ/R is found from Equation [8] or [9] depending on whether a/R is greater or less than $e^{-1/2}$.

Theory predicts a finite slope for the load-deflection curve immediately after yield. This result is exact in that at zero deflection the velocity field is known to be correct within the framework of the thin-plate theory.

Comparison With Tests. Data are available that enable a comparison to be made between the foregoing theory and the results of static tests of mild-steel plates (3). Fig. 5 shows observed central deflection versus applied load for a series of plates having various ratios of diameter to thickness. Each plate was clamped to a very stiff outer ring and was loaded through a centrally placed punch. Supposing the effects of nonuniformity of pressure beneath the punch to be purely local, the test conditions conform closely to those assumed in the theory. The solid

line shows the load-deflection curve computed from Equations [12]. For the plates of intermediate thickness, the general character of the post-yield behavior is represented quite well by the theory when due allowance is made for the neglect of elastic deflection. For the thickest plate, the increase in rate of deflection at the yield load is less than expected. This may result from the approximations of the simple plastic-plate theory, e.g., that plane sections remain plane, which are unlikely to be accurate for very thick plates, or the approximations used for the slope and radii of curvature of the mid-surface. For the thinnest plate, the pre-yield and post-yield deflection rates were similar so no marked change in slope was to be expected at the yield load.

Fig. 7 shows load-deflection data for a plate subject to uniform pressure. The solid line shows the load-deflection curve computed from Equations [12]. This case has been studied by means of membrane theory, in which bending action is neglected (15, 16, 17, 18). The load-deflection relationship obtained in (17) for rigid ideally plastic material obeying the maximum shear-stress criterion of yield has been added to Fig. 7 as the broken line. This is seen to represent the observations quite well over a wide range of deflection, although the theory cannot, of course, give an accurate guide to the rate of deflection in the neighborhood of the yield-point load.

Comparison of Figs. 5 and 7 suggests that membrane theory might also be of use for very thin plates loaded over only part of the surface. The membrane theory for this slightly more general case is developed in the following section.

Theory of Plastic Membranes

Consider a clamped circular plate on which a uniform pressure of intensity p acts over a central area bounded by $r = a$. Assuming that the slope at the meridian curve remains small, the equations of equilibrium become, for $r < a$

$$\left.\begin{aligned} rN_\varphi \frac{d^2y}{dr^2} + N_\theta \frac{dy}{dr} + pr &= 0 \\ 2N_\varphi \frac{dy}{dr} + pr &= 0 \end{aligned}\right\} \quad \ldots\ldots [13]$$

and for $a < r < R$

$$\left.\begin{aligned} rN_\varphi \frac{d^2y}{dr^2} + N_\theta \frac{dy}{dr} &= 0 \\ 2rN_\varphi \frac{dy}{dr} + pa^2 &= 0 \end{aligned}\right\} \quad \ldots\ldots [14]$$

When the maximum shear-stress criterion of yield is used for the plastically deforming portions of the shell, the stress point with the co-ordinates N_φ and N_θ will be situated on the yield hexagon shown in Fig. 8. It is easily seen that, when the stress state is represented by one of the sides of the yield hexagon, the unknown stress resultants may be eliminated from the equations of equilibrium to obtain an equation that contains only d^2y/dr^2, dy/dr, and p. This differential equation must be satisfied by the meridian curve of the deflected plate.

At the center of the plate $N_\theta = N_\varphi = N_0$ by symmetry. Therefore, for the neighboring plate elements, the stress state must be represented by either the regime AB or AF, i.e., $N_\varphi = N_0$, $N_0 \geq N_\theta \geq 0$ or $N_\theta = N_0$, $N_0 \geq N_\varphi \geq 0$. If the first condition is introduced in the equations of equilibrium, Equations [13], for $0 < r \leq a$

$$y = -\frac{pr^2}{4N_0} + \delta \quad \ldots\ldots [15]$$

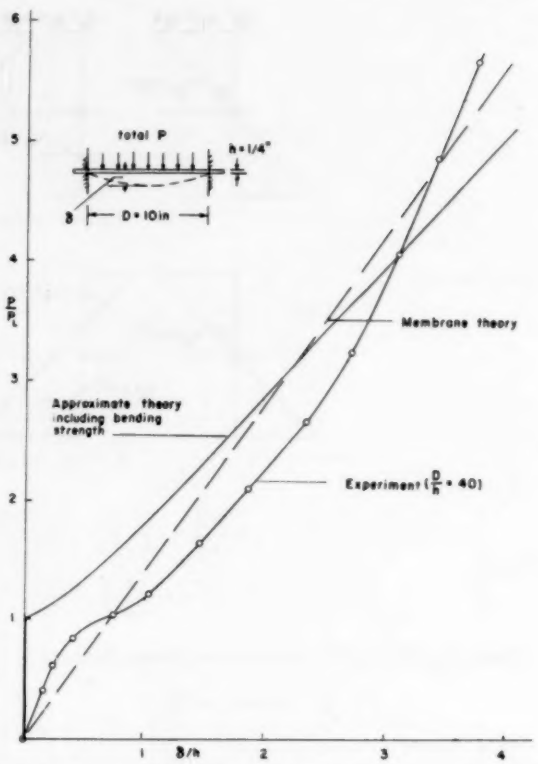

Fig. 7 Clamped Mild-Steel Plate Subjected to Uniform Pressure

where δ is the deflection at the center. Using these results in the first of Equations [13], $N_\theta = N_0$. Similarly, for $r > a$, $N_\varphi = N_\theta = N_0$ and

$$y = -\frac{pa^2}{2N_0} \ln \frac{r}{R} \quad \ldots\ldots [16]$$

where the boundary condition $y = 0$ at $r = R$ is satisfied automatically. The curves defined by Equations [15] and [16] will match at $r = a$ if

$$-\frac{pa^2}{2N_0} \ln \frac{a}{R} = -\frac{pa^2}{4N_0} + \delta$$

Writing the total load as $P = \pi a^2 p$, the load-deflection relationship becomes

$$P = 2\pi N_0 \frac{\delta}{\frac{1}{2} + \ln \frac{R}{a}} \quad \ldots\ldots [17]$$

This may be plotted nondimensionally after dividing through by the yield-point load P_L defined in the section, Approximate Solutions at Finite Deflection. The relationship is shown in Fig. 5 as the broken line. This line is in quite good agreement with the data for the thinnest plate, thus illustrating that a membrane-type theory also may be of use in certain cases of nonuniform loading.

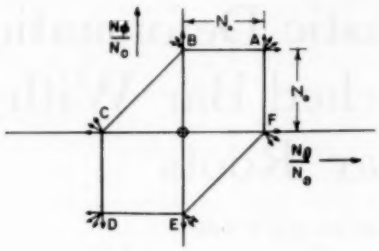

FIG. 8 YIELD HEXAGON

CONCLUSION

To place the results in perspective in relation to limit design (5, 6), it should be noted that the approximate stiff-plate theory developed here does not necessarily give an upper bound to the load-carrying capacity at a specified central deflection because, in general, the assumed shape of the plate is not exactly correct. We have found upper bounds to a slightly different problem. This point is well illustrated by the case shown in Fig. 7, for which at large deflection the carrying capacity of the membrane exceeds that computed for the stiff plate, presumably because the membrane assumes a more favorable shape. A theorem may exist to the effect that, under certain restrictions, the structure will assume the most favorable shape; but this has not yet been established. In the meantime the best procedure is to judge the utility of the results obtained in specific cases by direct comparison with tests.

The comparisons made with the results of tests on mild-steel plates suggest that, for mild steel, there is a substantial range of thicknesses in which the present stiff-plate theory represents the immediate post-yield behavior with fair accuracy, when due allowance is made for the neglect of elasticity. For both very thick and very thin plates, however, the results are less satisfactory. This is not unexpected. For very thick plates the assumptions of the simple bending theory of plates will not be met even approximately, while for very thin plates the relatively high rate of elastic deflection tends to mask the change in deflection rate at yield predicted by the rigid-plastic model. Settlement of the precise range of utility of the rigid-plastic theory must await further tests; however, on the evidence available, it seems likely that for clamped plates the thin-plate limit is reached when the elastic slope is about twice the ultimate post-yield slope β_2, Equation [12]. When the elastic slope is smaller than this, a membrane theory is probably better.

The point of greatest general interest emerging from the analysis is that it seems likely the continued strengthening of plates immediately above the yield-point load can be largely explained by taking into account the changes in geometry and without postulating strain-hardening or other change in the properties of the material as yield proceeds.

BIBLIOGRAPHY

1 "The Deflection of Plates in the Elastic-Plastic Range," by R. M. Haythornthwaite, Proceedings of the Second U. S. National Congress of Applied Mechanics, ASME, New York, N. Y., 1955, pp. 521–526.

2 "An Experiment on Circular Plates in the Plastic Range," by R. M. Cooper and G. A. Shifrin, Proceedings of the Second U. S. National Congress of Applied Mechanics, ASME, New York, N. Y., 1955, pp. 527–534.

3 "Report of Static Tests of Circular Mild Steel Plates," by J. Foulkes and E. T. Onat, 1955, Brown University Technical Report OOR 3172/3.

4 "Report of Static Tests of Circular Mild Steel Plates Under Reversed Loading," by R. M. Haythornthwaite, to appear as a Technical Note of the Division of Engineering, Brown University, Providence, R. I.

5 "Limit Design of Beams and Frames," by H. J. Greenberg and W. Prager, Proceedings of the American Society of Civil Engineers, vol. 77, Separate no. 59, 1951.

6 "Extended Limit Design Theorems for Continuous Media," by D. C. Drucker, W. Prager, and H. J. Greenberg, *Quarterly of Applied Mathematics*, vol. 9, 1952, pp. 381–389.

7 "Versuche mit eingespannten und einfachen Balken von I-Form aus St. 37," by H. Maier-Leibnitz, *Bautechnik*, vol. 7, 1929, p. 313.

8 "Beitrag zum Traglastverfahren," by F. Stüssi and C. F. Kollbrunner, *Bautechnik*, vol. 13, 1935, p. 264.

9 "Investigation Into the Behaviour of Welded Rigid Frame Structures," by J. F. Baker and J. W. Roderick, Trans. of the Institute of Welding, London, England, vol. 1, 1938, pp. 206–226, and vol. 3, 1940, pp. 83–92.

10 "Tests on Full-Scale Portal Frames," by J. F. Baker and J. W. Roderick, Proceedings of the Institution of Civil Engineers, vol. 1, part 1, 1952, p. 71.

11 "On the State of Stress in a Plastic-Rigid Body at the Yield Point," by R. Hill, *Philosophical Magazine*, vol. 42, series 7, 1951, pp. 868–875.

12 "The Load Carrying Capacity of Initially Flat Circular Steel Plates Under Reversed Loading," by R. M. Haythornthwaite and E. T. Onat, *J. Aero. Sci.*, vol. 22, 1955, pp. 857–859.

13 "Limit Analysis of Shells of Revolution," by E. T. Onat and W. Prager, Dutch Academy of Sciences: Proceedings B, vol. 57 (5), 1954, pp. 534–548.

14 "The Load Carrying Capacities of Circular Plates," by H. G. Hopkins and W. Prager, *Journal of Mechanics and Physics of Solids*, vol. 2, 1953, pp. 1–13.

15 "Plastic Deformation of a Circular Diaphragm Under Pressure," by A. Gleyzal, JOURNAL OF APPLIED MECHANICS, Trans. ASME, vol. 70, 1948, pp. 288–296.

16 "A Theory of the Plastic Bulging of a Metal Diaphragm by Lateral Pressure," by R. Hill, *Philosophical Magazine*, vol. 41, series 7, 1950, pp. 1133–1142.

17 "On the Theory of the Bulge Test," by E. W. Ross and W. Prager, *Quarterly of Applied Mathematics*, vol. 12, 1954, pp. 86–91.

18 "Investigation of the Work of a Circular Membrane Deformed Well Beyond the Elastic Limit," by A. S. Grigor'ev, Akad. Nauk USSR, *Inzenernyi Sbornik*, vol. 9, 1951, pp. 99–112 (Russian).

The Pattern of Plastic Deformation in a Deeply Notched Bar With Semicircular Roots[1]

By L. GARR,[2] E. H. LEE,[3] and A. J. WANG[4]

The plastic deformation in a notched bar with deep semicircular roots pulled in plane strain is determined theoretically. The finite deformation is analyzed according to plastic-rigid theory. The motion is unsteady, and the velocity field at any instant is given in terms of the current geometry of the deformed free surface. A graphical step-by-step method is used to determine the deformation of a square grid scribed on the undeformed cross section. The deformed pattern details the regions of large plastic strain, and may be useful in considering the initiation of fracture cracks.

Introduction

We consider the plastic flow in a deeply notched bar with semicircular roots pulled in tension as shown in Fig. 1. The theoretical analysis of this problem for a perfectly

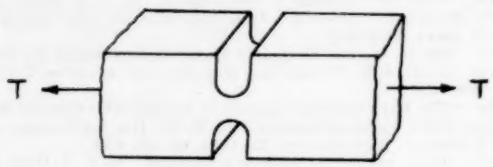

Fig. 1

plastic material in plane strain is given by Wang.[5] This solution provides the velocity vector at an arbitrary point at any time. To get the pattern of deformation at any time, an integration with respect to time is required. It is pointed out[5] that an analytic integration would be very complicated. A relatively easy integration is to find the deformation of the free boundary only. This was carried out in a step-by-step manner as shown in Fig. 9 of the paper cited.[5] In order to provide a more complete means of checking the solution experimentally, and also to obtain an idea of the strain distribution from which to study the initiation of fracture, it is of interest to obtain the deformation of a square grid scribed on a cross section of the undeformed bar. This is described in the present paper.

It is shown[5] that the deformed free boundary in the plastic region can again be represented by a circular arc to a high degree of approximation. Therefore, at any time, the slip-line field in which the plastic flow takes place is composed of two families of logarithmic spirals, Fig. 2. They are called the family of α-lines and the family of β-lines. Each point in the plastic region is represented by the co-ordinates (α, β). The complication in integrating the velocities arises due to the involved dependence of α and β on time for a particular material point. This is so because the geometry of the curvilinear co-ordinate net changes due to the

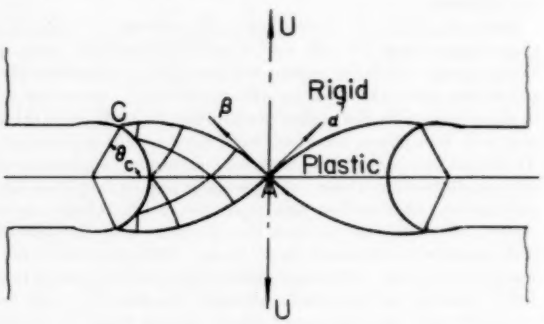

Fig. 2

variation in the angle $2\theta_c$ subtended by the current circular plastic boundary and due to the variation in the radius of this circle. To determine the velocity magnitudes, we take the velocity U with which the two heads are moving to be unity. Choosing a small time increment Δt, we obtain the subsequent positions of all intersection points of the initially square grid. In this manner we obtain the deformed grid at any time in a step-by-step manner.

Graphical Construction

We consider a deeply notched bar of the form shown in Fig. 1 with semiwidth at the root initially equal to $3.81a_0$, where a_0 is the initial radius of the semicircular notch. This geometry determines θ_c in Fig. 2 to be initially equal to $\pi/2$. Fig. 3 shows to scale a quarter of the notched bar, in the region of the root, cut off by the two center lines.

In order to study the strain distribution, the deformation of a square grid scribed on the undeformed cross section of the notch is computed. The grid dimension is taken to be $1/_{20}$ of the initial notch width as shown in Fig. 3. As mentioned previously and

---

[1] This work was carried out under Contract DA-19-020-ORD-2598, under the supervision of Watertown Arsenal Laboratory, and permission to publish is gratefully acknowledged.

[2] Formerly, Research Assistant, Division of Applied Mathematics, Brown University, Providence, R. I.

[3] Professor of Applied Mathematics, Brown University, Providence, R. I. Mem. ASME.

[4] Formerly, Assistant Professor of Mechanics, Illinois Institute of Technology, Chicago, Ill.

[5] "Plastic Flow in a Deeply Notched Bar With Semi-Circular Root," by A. J. Wang, *Quarterly of Applied Mathematics*, vol. 11, 1954, pp. 427–438.

Contributed by the Applied Mechanics Division and presented at the Diamond Jubilee Annual Meeting, Chicago, Ill., November 13–18, 1955, of The American Society of Mechanical Engineers.

Discussion of this paper should be addressed to the Secretary, ASME, 29 West 39th Street, New York, N. Y., and will be accepted until April 10, 1956, for publication at a later date. Discussion received after the closing date will be returned.

Note: Statements and opinions advanced in papers are to be understood as individual expressions of their authors and not those of the Society. Manuscript received by ASME Applied Mechanics Division, January 20, 1955. Paper No. 55—A-23.

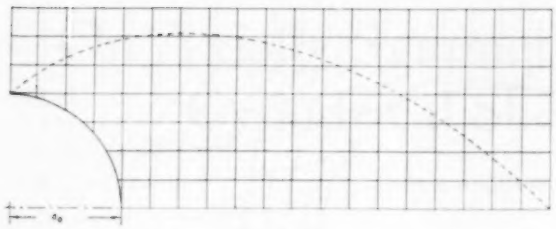

FIG. 3

detailed by Wang,[5] the instantaneous velocity of each mesh point of the grid can be obtained directly in terms of the (α, β) co-ordinates of the point, which, in turn, can be related simply to the polar co-ordinates of the point in question referred to the system containing the current circular boundary as a line of constant radius. Thus, in an increment of time Δt, the displaced positions of the mesh points can be obtained on the assumption that the velocity remains constant throughout the time interval. This is approximately true for a point which remains within the plastic region, and a detail refinement will be described below which improves this approximation by averaging the velocities at the beginning and end of the interval. If during the time interval Δt the point falls outside the plastic region, a discontinuity in velocity occurs during the time interval which must be taken into account as detailed later. The development of the deformation is easy to determine graphically since at any instant the current position of the free surface, according to simple algebraic expression for functions evaluated by Wang, determines the characteristic co-ordinates (α, β) of any physical point and its velocity components, as well as the current position of the plastic-rigid boundary. The detailed procedure with the particular mean-value approximation adopted, will be presented in the form of a detailed description of the first step. The increment of time Δt is taken as that in which the unit velocity travels $^1/_{10}$ of the current radius of the circular free surface. With the free-surface motion already determined,[5] this was found satisfactory for a finite-difference approximation. It gives approximately equal shrinking of the neck at each step throughout the deformation. The detailed procedure for the first step is given in the following.

The initial square grid is shown in Fig. 3. Having taken $U = 1$, $\Delta t_0 = a_0/10$ we can locate an approximation to the new position of each grid point by measuring off the vector $v_0 \Delta t_0$ where v_0 is the initial velocity at each point given directly by Equation [26] and Fig. 6 of the reference cited.[5] In a similar manner we can find the new circular free boundary and the new plastic-rigid boundary approximately. The points that move outside the new plastic-rigid boundary will be dealt with separately. Now, for those points remaining in the plastic region, we can again find new positions by measuring off $v_1 \Delta t_1$ where v_1 is the current velocity of the point in the displaced position again using the previous relations.[5] The increment of time Δt_1 is $^1/_{10}$ of the current radius of the circular free boundary a_1. For each point, the arithmetic mean of these two positions is taken to be the final position after the first step, and the increment of time for this step is $^1/_{20}(a_0 + a_1)$.

We have approximated the integral

$$\int_0^{1/2(\Delta t_0 + \Delta t_1)} v(t)dt \text{ by } \frac{1}{2}\,[v(0)\Delta t_0 + v(\Delta t_0)\Delta t_1]$$

It appears more tedious than the usual second approximation

$$\frac{1}{4}\,(\Delta t_0 + \Delta t_1)[v(0) + v(\Delta t_0)]$$

Comparing these two approximations by means of the Euler-Maclaurin finite-difference formula,[6] the present approximation is shown to be a better one, although the difference is in the third-order terms, i.e., $0(\Delta t_0^3)$. The extra effort therefore is perhaps not fully justified.

By connecting the displaced positions of the grid points, we get the pattern of deformation at $t = 0.110a_0$ as shown in Fig. 4. Both the free boundary and the plastic-rigid boundary are redrawn according to the averaged time increment.

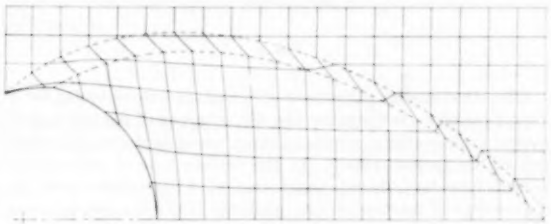

FIG. 4

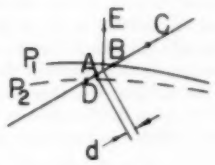

FIG. 5

For the points whose first increment of motion takes them outside the plastic region, we must modify their motion to take into consideration the speed of the plastic-rigid boundary. For example, in Fig. 5, P_1 is the original plastic-rigid boundary and P_2 its displaced position after a time increment $(\Delta t_0 + \Delta t_1)/2$. The first increment of motion would take the point A to C (after time increment Δt_0) and it is in the rigid region. Assuming velocities are constant in this time increment

$$d = \frac{\overline{AB}}{\overline{BD} + \overline{AC}\left(\dfrac{\Delta t_0 + \Delta t_1}{2\Delta t_0}\right)}$$

will be the approximate distance traveled by A before it meets the moving plastic-rigid boundary. For the rest of the time, the point moves in the rigid region vertically upward with unit velocity and arrives at E.

By repeating the construction described in the foregoing, the patterns of deformation are obtained for $t = 0.110a_0$, $0.240a_0$, $0.389a_0$, and $0.559a_0$ as shown in Figs. 4, 6, 7, and 8, respectively. The construction could be continued until only line contact occurs across the notch, but since in practice plastic flow is usually arrested at an earlier stage by the initiation of fracture, it is considered not worth while to complete the construction.

DISCUSSION

The form of the deformation field can be best assessed from Fig. 8. Large strains have occurred in the transition region between the initial and final positions of the plastic-rigid boundary and also adjacent to the notch root. In the plastic region near the center comparatively little deformation has taken place.

[6] "Modern Analysis," by E. T. Whitaker and G. N. Watson, Cambridge University Press, Cambridge, Mass., fourth edition, 1927, p. 128.

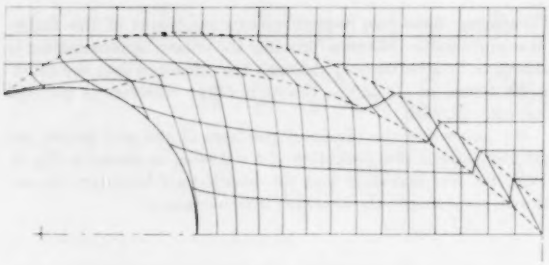

FIG. 6

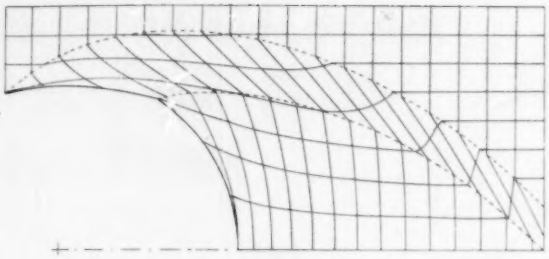

FIG. 7

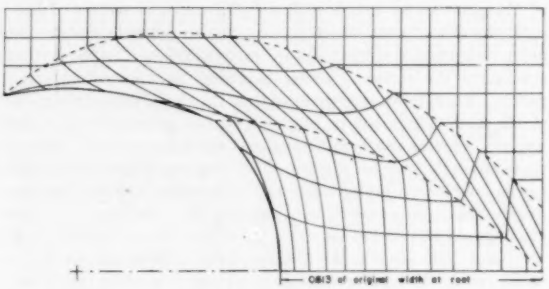

FIG. 8

Somewhat similar patterns of deformation were obtained for a deep V-notch.[7] In the latter case the influence of the notch apex caused a more abrupt strain gradient, which is shown smoothed out in the present result. In the present case of an initially smooth boundary, there is no opening up of the surface involving a flow type of fracture as was exhibited in the V-notch solution presented.[7]

It is hoped that these computed patterns will be of value in assessing the initiation of fracture in a notched-bar test. It should be borne in mind that, in addition to the strain field illustrated, the stress distribution will have an influence on the initiation of fracture. Near the center of the specimen the material is under triaxial tension, and the ductility will therefore be expected to be low. At the root of the notch the free surface limits the stress to biaxial tension, under which condition the ductility would be expected to be comparatively greater. These aspects must be considered in comparing the results of the present analysis with experimental observations of fracture.

[7] "Plastic Flow in a V-Notched Bar Pulled in Tension," by E. H. Lee, JOURNAL OF APPLIED MECHANICS, Trans. ASME, vol. 74, 1952, pp. 331–336.

On Axially Symmetric Bending of Nearly Cylindrical Shells of Revolution

By R. A. CLARK[1] and E. REISSNER[2]

The words "nearly cylindrical" are used in this paper to describe a thin elastic shell of revolution which is such that (*a*) the maximum variation of the radial dimension is small compared to the average radial dimension, and (*b*) the rate of change of the radial dimension with respect to the axial dimension is small compared to unity. For any particular type of loading a nearly cylindrical shell may or may not exhibit a behavior similar to that of a shell which is exactly cylindrical. The purpose of this paper is to demonstrate this fact and to present a method for obtaining approximate solutions for the stresses and deflections in either event. The method involves a perturbation procedure based on the assumption that all desired quantities can be represented as expansions in powers of two small parameters. The procedure leads to a set of linear differential equations with constant coefficients, which may be solved successively.

1 Introduction

A GENERAL perturbation procedure for certain shell problems is illustrated by applying it to the problem of a thin pipe with shallow circumferential corrugations subject to a constant axial force. Conditions under which a corrugated pipe does or does not behave like a straight pipe are established. In particular, it is found that the behavior of a corrugated pipe may differ quite radically from that of a straight pipe as regards both stresses and deflections, even though the corrugated pipe satisfies the requirement of being a nearly cylindrical shell.

Four different types of corrugations are treated here and comparisons are made with certain corresponding results given previously by Donnell (1)[3] and Hetényi (2). In one instance, a numerical comparison of force-deflection values shows a difference of 30 per cent between an earlier result and that found in the present work.

Finally, we also include some remarks concerning the relationship of the perturbation procedure adopted here and an approach, based on expansions in powers of one small parameter, which has been considered by Federhofer (3, 4).

2 Basic Equations

Using cylindrical co-ordinates r, θ, z, the middle surface of a shell of revolution may be represented by parametric equations of the form

$$r = a\left[1 + \frac{b}{a} f(\xi)\right], \quad z = c\xi \qquad [1]$$

The dimensions a, b, and c are shown in Fig. 1. The explicit nature of the function of $f(\xi)$ depends on the particular shape of the

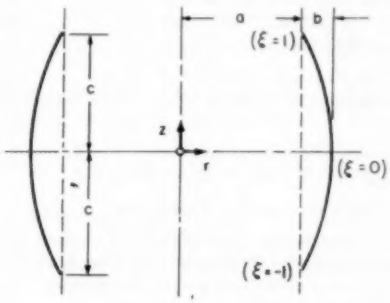

Fig. 1

meridian curves. In the present work the representation [1] is assumed to be such that $f(\xi)$, $f'(\xi)$, and $f''(\xi)$ are of the order of magnitude unity. Since the slope of a meridian curve is given by

$$\frac{dr}{dz} = \frac{b}{c} f'(\xi) \qquad [2]$$

it follows from Equation [1] and the assumed nature of $f(\xi)$ that a shell is nearly cylindrical in the sense of the present paper as long as the dimensions satisfy the order-of-magnitude relations

$$\frac{b}{a} \ll 1, \quad \frac{b}{c} \ll 1 \qquad [3]$$

The solution of problems of the linear theory of rotationally symmetric deformations of thin shells of revolution depends, basically, on the solution of two simultaneous second-order differential equations. These equations are taken here in the form in which they are given in reference (5), namely

$$\beta'' + \frac{(rD/\alpha)'}{(rD/\alpha)}\beta' - \left[\left(\frac{r'}{r}\right)^2 - \nu\frac{(r'D/\alpha)'}{(rD/\alpha)}\right]\beta + \frac{z'(rH)}{(rD/\alpha)} = \frac{r'(rV)}{(rD/\alpha)} \qquad [4]$$

$$(rH)'' + \frac{(r/\alpha C)'}{(r/\alpha C)}(rH)' - \left[\left(\frac{r'}{r}\right)^2 + \nu\frac{(r'/\alpha C)'}{(r/\alpha C)}\right](rH) - \frac{z'\beta}{(r/\alpha C)} = \left[\frac{r'z'}{r^2} + \nu\frac{(z'/\alpha C)'}{(r/\alpha C)}\right](rV) + \nu\frac{z'}{r}(rV)' - \left[\frac{(r/\alpha C)'}{(r/\alpha C)} + \nu\frac{r'}{r}\right](r\alpha p_H) - (r\alpha p_H)' \qquad [5]$$

---

[1] Assistant Professor of Mathematics, Case Institute of Technology, Cleveland, Ohio.

[2] Professor of Mathematics, Massachusetts Institute of Technology, Cambridge, Mass.

[3] Numbers in parentheses refer to the Bibliography at the end of the paper.

Contributed by the Applied Mechanics Division and presented at the Diamond Jubilee Annual Meeting, Chicago, Ill., November 13–18, 1955, of The American Society of Mechanical Engineers.

Discussion of this paper should be addressed to the Secretary, ASME, 29 West 39th Street, New York, N. Y., and will be accepted until April 10, 1956, for publication at a later date. Discussion received after the closing date will be returned.

Note: Statements and opinions advanced in papers are to be understood as individual expressions of their authors and not those of the Society. Manuscript received by ASME Applied Mechanics Division, September 16, 1954. Paper No. 55—A-18.

Primes denote differentiation with respect to ξ, the quantities H and V are stress resultants in radial and axial directions, respectively, p_H is the component of surface-load intensity in the radial direction, and β is the angle of rotation, due to deformation, of the tangent to a meridian. Furthermore

$$\alpha^2 = (r')^2 + (z')^2,\ C = Eh,\ D = Eh^3/12(1-\nu^2) \quad [6]$$

where E is Young's modulus, ν Poisson's ratio, and h the wall thickness of the shell. The quantity rV is given by

$$rV = -\int r\alpha p_V\, d\xi \quad [7]$$

where p_V is the component of surface load intensity in the axial direction.

Stress resultants and couples and displacements, defined in accordance with Figs. 2 and 3, are given in terms of β and (rH), as follows

$$\left.\begin{aligned} rN_\xi &= (r'/\alpha)(rH) + (z'/\alpha)(rV) \\ rQ &= -(z'/\alpha)(rH) + (r'/\alpha)(rV) \\ \alpha N_\theta &= (rH)' + r\alpha p_H \end{aligned}\right\} \quad [8]$$

$$\left.\begin{aligned} \alpha M_\xi &= D[\beta' + \nu(r'/r)\beta] \\ \alpha M_\theta &= D[\nu\beta' + (r'/r)\beta] \end{aligned}\right\} \quad [9]$$

$$\left.\begin{aligned} u &= (r/C)(N_\theta - \nu N_\xi) \\ w &= \int [-r'\beta + (z'/C)(N_\xi - \nu N_\theta)]d\xi \end{aligned}\right\} \quad [10]$$

3 The Perturbation Procedure

In what follows we restrict attention to shells of constant wall thickness h and symmetrize the differential Equations [4] and [5] in so far as the dependent variables β and rH are concerned, by introducing new variables η and ψ, given by

$$\eta = \frac{Eh^2}{\sqrt{12(1-\nu^2)}}\,\beta, \quad \psi = rH \quad [11]$$

We further define three parameters κ, λ, and μ as follows

$$\kappa = \left(\frac{b}{c}\right)^2, \quad \lambda = \frac{b}{a}, \quad \mu = \sqrt{12(1-\nu^2)}\,\frac{c^2}{ah} \quad [12]$$

With Equations [11] and [12], and with Equations [1] and [6], the differential Equations [4] and [5] assume the following form

$$\eta'' + \left[\frac{\lambda f'}{1+\lambda f} - \frac{\kappa f' f''}{1+\kappa(f')^2}\right]\eta' - \left[\left(\frac{\lambda f'}{1+\lambda f}\right)^2 - \frac{\nu\lambda f''}{(1+\lambda f)\,[1+\kappa(f')^2]}\right]\eta + \mu\,\frac{\sqrt{1+\kappa(f')^2}}{1+\lambda f}\,\psi = \kappa\mu f'\,\frac{\sqrt{1+\kappa(f')^2}}{1+\lambda f}\left(\frac{c}{b}\,rV\right) \quad [13]$$

$$\psi'' + \left[\frac{\lambda f'}{1+\lambda f} - \frac{\kappa f' f''}{1+\kappa(f')^2}\right]\psi' - \left[\left(\frac{\lambda f'}{1+\lambda f}\right)^2 + \frac{\nu\lambda f''}{(1+\lambda f)[1+\kappa(f')^2]}\right]\psi - \mu\,\frac{\sqrt{1+\kappa(f')^2}}{1+\lambda f}\,\eta = \left[\frac{\lambda^2 f'}{(1+\lambda f)^2} - \frac{\nu\kappa\lambda f' f''}{(1+\lambda f)[1+\kappa(f')^2]}\right]\left(\frac{c}{b}\,rV\right) + \frac{\nu\lambda}{1+\lambda f}\left(\frac{c}{b}\,rV\right)' - \left[\frac{(1+\nu)\lambda f'}{1+\lambda f} - \frac{\kappa f' f''}{1+\kappa(f')^2}\right](r\alpha p_H) - (r\alpha p_H)' \quad [14]$$

Some simplification of the system [13] and [14] is possible on the basis of the observation that terms with μ as a factor always dominate corresponding terms with λ as a factor. This is a consequence of the assumed thinness of the shell (that the thickness h is small compared to the principal radii of curvature of the middle surface), which may be deduced as follows: The curvature of a meridian is given by

$$\frac{1}{R_\xi} = \frac{d^2r}{dz^2}\left[1 + \left(\frac{dr}{dz}\right)^2\right]^{-3/2} = \frac{bf''}{c^2}\,[1+\kappa(f')^2]^{-3/2}$$

while, according to Equations [12]

$$\frac{\lambda}{\mu} = \frac{1}{\sqrt{12(1-\nu^2)}}\,\frac{hb}{c^2}$$

Thus $\lambda/\mu = O(h/R_\xi)$, implying that $\lambda \ll \mu$ if $h \ll R_\xi$, which in turn is one of the basic assumptions of the theory.

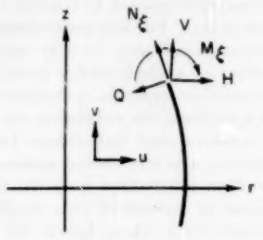

Fig. 2

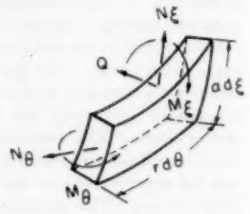

Fig. 3

In order to proceed further it is necessary at this point either to choose a specific function $f(\xi)$ or to look for further simplification of the differential equations for suitable classes of shells. The latter approach is adopted here. According to Relations [3] and the definitions, Equations [12] of the parameters κ and λ, a nearly cylindrical shell belongs to that class of shells for which

$$\kappa \ll 1, \quad \lambda \ll 1 \quad [15]$$

If Relations [15] hold, we may solve Equations [13] and [14] by a perturbation or successive approximation procedure.

The perturbation procedure presented here may be used for any type of loading. However, for the purpose of illustration, we shall consider the problem of a shell subject only to a constant axial force F. For this loading condition we have

$$rV = F/2\pi, \quad p_H = p_V = 0 \quad [16]$$

Introducing the change of variables

$$\eta = \frac{c}{b}\,\frac{F}{2\pi}\,X, \quad \psi = \frac{c}{b}\,\frac{F}{2\pi}\,Y \quad [17]$$

the following differential equations for X and Y are obtained

$$X'' + \left[\frac{\lambda f'}{1+\lambda f} - \frac{\kappa f' f''}{1+\kappa(f')^2}\right]X' - \left[\left(\frac{\lambda f'}{1+\lambda f}\right)^2 - \frac{\nu\lambda f''}{(1+\lambda f)[1+\kappa(f')^2]}\right]X + \mu\,\frac{\sqrt{1+\kappa(f')^2}}{1+\lambda f}\,Y = \kappa\mu f'\,\frac{\sqrt{1+\kappa(f')^2}}{1+\lambda f} \quad [18a]$$

$$Y'' + \left[\frac{\lambda f'}{1+\lambda f} - \frac{\kappa f' f''}{1+\kappa(f')^2}\right]Y' - \left[\left(\frac{\lambda f'}{1+\lambda f}\right)^2 + \frac{\nu\lambda f''}{(1+\lambda f)[1+\kappa(f')^2]}\right]Y - \mu\,\frac{\sqrt{1+\kappa(f')^2}}{1+\lambda f}\,X = \frac{\lambda^2 f'}{(1+\lambda f)^2} - \frac{\nu\kappa\lambda f' f''}{(1+\lambda f)[1+\kappa(f')^2]} \quad [18b]$$

The essence of our procedure is to develop X and Y in powers of the two small parameters κ and λ. To this end we write

$$X = X_{00} + \kappa X_{10} + \lambda X_{01} + \ldots\ldots = \Sigma \kappa^r \lambda^s X_{rs} \ldots [19a]$$

$$Y = Y_{00} + \kappa Y_{10} + \lambda Y_{01} + \ldots\ldots = \Sigma \kappa^r \lambda^s Y_{rs} \ldots [19b]$$

Substituting from Equations [17] and [19] into [18] we obtain the following successive pairs of differential equations

$$X_{00}'' + \mu Y_{00} = 0 \ldots\ldots [20]$$

$$Y_{00}'' - \mu X_{00} = 0 \ldots\ldots [21]$$

$$X_{10}'' + \mu Y_{10} = \mu f' + f' f'' X_{00}' - \frac{1}{2}\mu (f')^2 Y_{00} \ldots\ldots [22]$$

$$Y_{10}'' - \mu X_{10} = f' f'' Y_{00}' + \frac{1}{2}\mu (f')^2 X_{00} \ldots\ldots [23]$$

$$X_{01}'' + \mu Y_{01} = -f' X_{00}' - \nu f'' X_{00} - \mu f Y_{00} \ldots\ldots [24]$$

$$Y_{01}'' - \mu X_{01} = -f' Y_{00}' + \nu f'' Y_{00} + \mu f X_{00} \ldots\ldots [25]$$

A more compact treatment is possible by introducing a complex function Z, defined by

$$Z = X + iY \ldots\ldots [26]$$

Equations [18a] and [18b] can then be combined into a single equation, which may be written

$$\left[\frac{(1+\lambda f) Z'}{\sqrt{1+\kappa (f')^2}}\right]' - \left[i\mu + \frac{(\lambda f')^2}{(1+\lambda f)\sqrt{1+\kappa (f')^2}}\right] Z + \frac{\nu \lambda f''}{[1+\kappa (f')^2]^{3/2}} \bar{Z} = \kappa \mu f' - \frac{i\kappa \lambda \nu f' f''}{[1+\kappa (f')^2]^{3/2}} + \frac{i\lambda^2 f'}{(1+\lambda f)\sqrt{1+\kappa (f')^2}} \ldots\ldots [27]$$

where $\bar{Z}$ represents the complex conjugate of Z.

Expanding the coefficients of Equation [27] in powers of κ and λ and introducing

$$Z = \Sigma \kappa^r \lambda^s Z_{rs} = \Sigma \kappa^r \lambda^s (X_{rs} + i Y_{rs}) \ldots\ldots [28]$$

then yields the following system of differential equations

$$Z_{00}'' - i\mu Z_{00} = 0 \ldots\ldots [29]$$

$$Z_{10}'' - i\mu Z_{10} = \mu f' + \frac{1}{2}[(f')^2 Z_{00}']' \ldots\ldots [30]$$

$$Z_{01}'' - i\mu Z_{01} = -[f Z_{00}']' - \nu f'' \bar{Z}_{00} \ldots\ldots [31]$$

$$Z_{20}'' - i\mu Z_{20} = \frac{1}{2}[(f')^2 Z_{10}']' - \frac{3}{8}[(f')^4 Z_{00}']' \ldots\ldots [32]$$

$$Z_{11}'' - i\mu Z_{11} = \frac{1}{2}[(f')^2 Z_{01}']' - [f Z_{10}']' + \frac{1}{2}[f (f')^2 Z_{00}']' + \nu \left[-i f' f'' - f'' \bar{Z}_{10} + \frac{3}{2}(f')^2 f'' \bar{Z}_{00}\right] \ldots\ldots [33]$$

$$Z_{02}'' - i\mu Z_{02} = -[f Z_{01}']' - \nu f'' \bar{Z}_{01} + (f')^2 Z_{00} + i f' \ldots\ldots [34]$$

Equations [11], [17], and [19] are now introduced in Equations [8] to [10] in order to obtain appropriate expressions for stresses and displacements. As this is done it is convenient to express all stresses as multiples of the axial stress in a corresponding straight cylindrical shell, given by

$$\sigma_S = \frac{F}{2\pi a h} \ldots\ldots [35]$$

The resulting relations may then be written as

$$\sigma_{\xi D} = \frac{N_\xi}{h} = \sigma_S \left\{1 + f' Y_{00} + \kappa \left[f' Y_{10} - \frac{1}{2}(f')^2 (1 + f' Y_{00})\right] + \lambda [f' Y_{01} - f(1 + f' Y_{00})] + \ldots\right\} \ldots\ldots [36]$$

$$\sigma_{\theta D} = \frac{N_\theta}{h} = \frac{a}{b}\sigma_S \left\{Y_{00}' + \kappa \left[Y_{10}' - \frac{1}{2}(f')^2 Y_{00}'\right] + \lambda Y_{01}' + \ldots\right\} \ldots\ldots [37]$$

$$\sigma_{\xi B} = \frac{6 M_\xi}{h^2} = \frac{a}{b}\sigma_S \sqrt{\frac{3}{1-\nu^2}} \left\{X_{00}' + \kappa \left[X_{10}' - \frac{1}{2}(f')^2 X_{00}'\right] + \lambda [X_{01}' + \nu f' X_{00}] + \ldots\right\} \ldots\ldots [38]$$

$$\frac{u}{a} = \frac{a}{b}\frac{\sigma_S}{E} \left\{Y_{00}' + \kappa \left[Y_{10}' - \frac{1}{2}(f')^2 Y_{00}'\right] + \lambda [Y_{01}' + f Y_{00}' - \nu (1 + f' Y_{00})] + \ldots\right\} \ldots\ldots [39]$$

Instead of the axial component of displacement $w(\xi)$ it is convenient to consider the measures

$$\epsilon = \frac{w(4) - w(0)}{4c} \qquad \epsilon_S = \frac{\sigma_S}{E} \ldots\ldots [40]$$

and the ratio

$$\frac{\epsilon}{\epsilon_S} = \frac{1}{4}\int_0^4 \left\{1 + f' Y_{00} + \kappa \left[f' Y_{10} - \frac{1}{2}(f')^2 (1 + f' Y_{00})\right] + \lambda [f' Y_{01} - f(1 + f' Y_{00})] + \ldots\right\} d\xi - \frac{\nu}{4}\frac{a}{b}\int_0^4 \left\{Y_{00}' + \kappa \left[Y_{10}' - \frac{1}{2}(f')^2 Y_{00}'\right] + \lambda Y_{01}' + \ldots\right\} d\xi - \frac{\sqrt{12(1-\nu^2)}\, a}{4h}\int_0^4 f' \{X_{00} + \kappa X_{10} + \lambda X_{01} + \ldots\} d\xi \ldots [41]$$

A perturbation procedure based on expansions in powers of a single small parameter has been suggested by K. Federhofer (3). In Federhofer's work the small parameter is not specified for the general case but, apparently, is to be chosen according to the dimensions involved in any particular application. In the approach adopted here, if it is known that some definite relation holds between κ and λ, the expansions in powers of the two parameters are reduced effectively to expansions in powers of one parameter. Otherwise, it is felt that the two-parameter procedure allows greater freedom in varying the dimensional values in any solution found or in determining the influence of the different dimension ratios.

4 Fourier Series Solution for Corrugated Pipe

We now consider a shell with periodic corrugations. Assuming that the corrugations are symmetrical about their crests or troughs, the function $f(\xi)$ in Equations [1] can be represented by a Fourier series of the form

$$f(\xi) = \frac{a_0}{2} + \sum_{n=1}^{\infty} a_n \cos \frac{n\pi\xi}{2} \ldots\ldots [42]$$

One wave length, or period, of the corrugations goes from $\xi = -2$ to $\xi = 2$, so that the dimensional wave length is $4c$, Fig. 4.

We disregard end effects, which means that stresses are also periodic, of period 4 in ξ. The symmetry of the shell meridians then implies the following conditions

$$\xi = 0, \pm 2, \pm 4, \ldots : \beta = 0, \quad H = 0 \ldots\ldots [43]$$

According to Equations [11], [17], [26], and [28], Conditions [43] are equivalent to the following system of conditions for the solutions of the differential Equations [29] to [34]

$$\xi = 0, \pm 2, \pm 4, \ldots : Z_{r_0} = 0 \ldots\ldots [44]$$

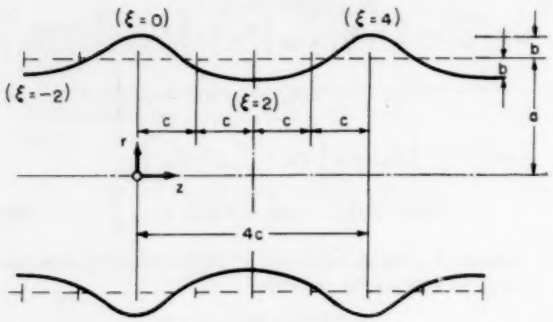

FIG. 4

Since differential Equation [29] is homogeneous, it follows that solutions of [29] and [31] satisfying boundary Conditions [44] are given by

$$Z_{00} \equiv 0, \qquad Z_{01} \equiv 0 \ldots\ldots [45]$$

Introducing Equations [45] and [42], the first significant differential Equation [30] now takes the form

$$Z_{10}'' - i\mu Z_{10} = -\frac{\pi}{2}\,\mu \sum_{n=1}^{\infty} n a_n \sin\frac{n\pi\xi}{2} \ldots\ldots [46]$$

A solution of Equation [46] which satisfies boundary Conditions [44] has the form

$$Z_{10} = X_{10} + iY_{10} = \sum_{n=1}^{\infty} (A_n + iB_n) \sin\frac{n\pi\xi}{2} \ldots\ldots [47]$$

After determination of the constants A_n and B_n we have

$$X_{10} = \left(\frac{\pi}{2}\right)^3 \mu \sum \frac{n^3 a_n}{\mu^2 + (n\pi/2)^4} \sin\frac{n\pi\xi}{2} \ldots\ldots [48]$$

$$Y_{10} = -\frac{\pi}{2}\,\mu^2 \sum \frac{n a_n}{\mu^2 + (n\pi/2)^4} \sin\frac{n\pi\xi}{2} \ldots\ldots [49]$$

We see that the right sides of differential Equations [32] to [34] are now known but we shall not determine Z_{20}, Z_{11}, or Z_{02} for the general case.

5 First-Approximation Theory

For many practical applications adequate results are given by a first approximation to the solution of the present problem. For this reason we now list separately the expressions for stresses and effective axial strain ϵ which corresponds to retaining only the first nonvanishing term of the expansions indicated in Equations [36] to [41]. Taking Equations [45] and the definitions [12] of the parameters into account we have as a first approximation

$$\sigma_{\xi D} = \sigma_S, \quad \sigma_{\theta D} = \sigma_S \frac{\kappa}{\lambda} Y_{10}' \ldots\ldots [50]$$

$$\sigma_{\xi B} = \sigma_S \frac{\kappa}{\lambda}\sqrt{\frac{3}{1-\nu^2}}\, X_{10}', \quad \sigma_{\theta B} = \nu\sigma_{\xi B} \ldots\ldots [51]$$

$$\frac{\epsilon}{\epsilon_S} = 1 - \mu\left(\frac{\kappa}{\lambda}\right)^2 \frac{1}{4}\int_0^4 f' X_{10}\, d\xi \ldots\ldots [52]$$

The first-approximation theory expressed by Equations [50] to [52] corresponds to approximating the original differential Equations [4] and [5], and Formulas [8] to [10] by

$$\left.\begin{aligned} \beta_{10}'' + \frac{c^2}{D} H_{10} &= \frac{bc}{aD}\frac{F}{2\pi} f' \\ H_{10}'' - Eh\left(\frac{c}{a}\right)^2 \beta_{10} &= 0 \end{aligned}\right\} \ldots\ldots [53]$$

$$\left.\begin{aligned} N_\xi = \frac{F}{2\pi a}, \quad Q = -H_{10} + \frac{b}{c}\frac{F}{2\pi a} f', \quad N_\theta = \frac{a}{c} H_{10}' \\ cM_\xi = D\beta_{10}', \quad cM_\theta = \nu D\beta_{10}' \end{aligned}\right\} \ldots [54]$$

$$u = \frac{a}{Eh}(N_\theta - \nu N_\xi),$$

$$w = \int\left[-bf'\beta_{10} + \frac{c}{Eh}(N_\xi - \nu N_\theta)\right] d\xi \ldots [55]$$

6 Explicit Solutions for Special Types of Corrugated Pipes

(a) *Sinusoidal Corrugations*

$$f(\xi) = \cos\frac{\pi\xi}{2}$$

First-Approximation Theory. For this type of corrugation we have immediately, from Equations [48] and [49]

$$X_{10} = \frac{\mu(\pi/2)^3}{\mu^2 + (\pi/2)^4} \sin\frac{\pi\xi}{2}, \quad Y_{10} = -\frac{\mu^2(\pi/2)}{\mu^2 + (\pi/2)^4} \sin\frac{\pi\xi}{2} \ldots [56]$$

These expressions substituted in Equations [50] to [52] give a first approximation for the stresses and effective axial strain. We see that the hoop stress $\sigma_{\theta D}$ and the bending stress $\sigma_{\xi B}$ will be proportional to $\cos(\pi\xi/2)$ and hence assume their maximum values at points such as $\xi = 0$ and $\xi = 2$. According to Equations [50] and [51]

$$\frac{\sigma_{\theta D,\,\max}}{\sigma_S} = \frac{\kappa}{\lambda}\frac{\mu^2(\pi/2)^2}{\mu^2 + (\pi/2)^4} \ldots\ldots [57]$$

$$\frac{\sigma_{\xi B,\,\max}}{\sigma_S} = \frac{\kappa}{\lambda}\sqrt{\frac{3}{1-\nu^2}}\frac{\mu(\pi/2)^4}{\mu^2 + (\pi/2)^4} \ldots\ldots [58]$$

Since $\sigma_{\theta B} = \nu\sigma_{\xi B}$, $\sigma_{\theta B,\,\max}$ occurs for $\xi = 0, \pm 2, \ldots$ as well as $\sigma_{\theta D,\,\max}$ so that

$$\sigma_{\theta,\,\max} = \sigma_{\theta D,\,\max} + \nu\sigma_{\xi B,\,\max} \ldots\ldots [59]$$

From Equation [52]

$$\frac{\epsilon}{\epsilon_S} = 1 + \frac{1}{2}\left(\frac{\kappa}{\lambda}\right)^2 \frac{\mu^2(\pi/2)^4}{\mu^2 + (\pi/2)^4} \ldots\ldots [60]$$

The second term in Equation [60] represents the axial strain due to bending. If we denote this term by ϵ_B/ϵ_S we may write Equation [60] in the form

$$\frac{\epsilon}{\epsilon_S} = 1 + \frac{\epsilon_B}{\epsilon_S} \ldots\ldots [61]$$

Curves giving the quantities $(\lambda/\kappa)(\sigma_{\theta D,\,\max}/\sigma_S)$, $(\lambda/\kappa)(\sigma_{\xi B,\max}/\sigma_S)$

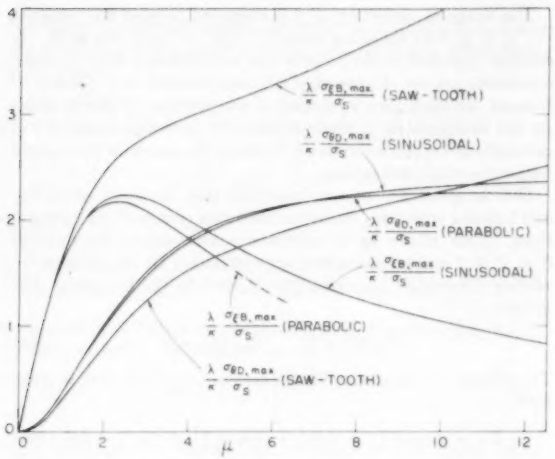

FIG. 5 VALUES OF AXIAL BENDING STRESSES $\sigma_{\xi B}$ AND CIRCUMFERENTIAL DIRECT STRESSES $\sigma_{\theta D}$ IN UNITS OF CORRESPONDING AXIAL STRESS σ_S FOR STRAIGHT PIPE AS FUNCTION OF PARAMETERS $\mu = [12(1-\nu^2)]^{1/2}c^2/a\hbar$, $\lambda = b/a$, $\kappa = (b/c)^2$

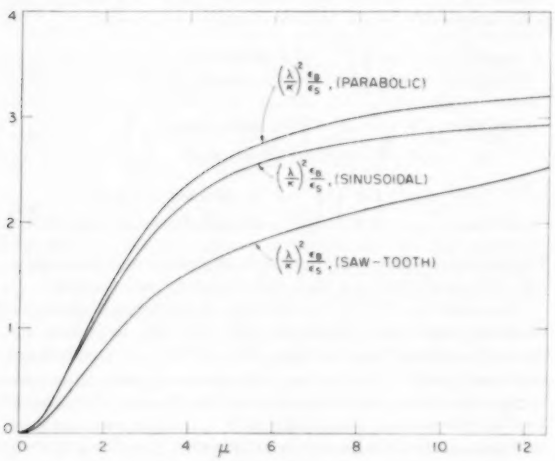

FIG. 6 EFFECTIVE AXIAL STRAINS ϵ_B IN UNITS OF CORRESPONDING AXIAL STRAINS ϵ_S FOR STRAIGHT PIPE AS FUNCTION OF $\mu = [12(1-\nu^2)]^{1/2}c^2/a\hbar$, $\lambda = b/a$, $\kappa = (b/c)^2$

and $(\lambda/\kappa)^2(\epsilon_B/\epsilon_S)$ as functions of μ may be found in Figs. 5 and 6.

Several observations can be made on the basis of the approximate solution given by Equations [57], [58], and [60]. First of all, when $\mu \ll 1$ the bending stress $\sigma_{\xi B}$ dominates the hoop stress $\sigma_{\theta D}$. Whether both of these stresses are dominated by $\sigma_{\xi D} = \sigma_S$ depends on the size of $(\kappa/\lambda)\mu$. According to definitions [12] we have

$$\frac{\kappa}{\lambda}\mu = \frac{b^2}{c^2}\frac{a}{b}\sqrt{12(1-\nu^2)}\frac{c^2}{a\hbar} = \sqrt{12(1-\nu^2)}\frac{b}{\hbar} \quad [62]$$

It follows that $\sigma_{\xi D}$ is the dominating stress only if $b \ll \hbar$. Since we also have $\epsilon_B/\epsilon_S = O(b^2/\hbar^2)$, we may conclude that when $\mu \ll 1$ a tube with sinusoidal corrugations behaves like a straight tube only if the maximum variation of the radial dimension from its mean value is small compared to the tube thickness, i.e., only if $b \ll \hbar$. Conversely, if $b > \hbar$ the maximum stress or the axial deflection in a corrugated tube will be larger, perhaps many times larger, than that produced in a straight tube by the same force. Results obtained when $\mu \to 0$, in the sense that the mean radius of the shell $a \to \infty$, corresponds to the solution for a corrugated plate. Taking Equation [62] into account we see that $\sigma_{\xi B}$ and ϵ_B have nonzero limits.

If μ is not small compared to unity it is readily apparent from Equations [57], [58], and [60] that a corrugated tube behaves like a straight tube only when $\kappa/\lambda \ll 1$, and that the behavior of the corrugated tube deviates more and more from that of a straight tube as κ/λ increases. If both $\mu \gg 1$ and $\kappa/\lambda \gg 1$, the dominating stress becomes $\sigma_{\theta D}$. In order to determine the significance of the ratio κ/λ for a corrugated tube we note that, according to Equation [12]

$$\frac{\kappa}{\lambda} = \frac{b^2/c^2}{b/a} = \frac{b/c}{c/a} \quad [63]$$

Since we are concerned only with problems for which $b/c \ll 1$, it follows from Equation [63] that $\kappa/\lambda = O(1)$ or $\kappa/\lambda \gg 1$ only if $c/a \ll 1$, or only if the dimensional wave length of the corrugations is small compared to the mean shell radius a.

When $\mu \to \infty$, the limiting solution obtained corresponds to what is known in shell theory as the "membrane" solution for the present problem. The bending stress $\sigma_{\xi B}$ then vanishes.

Higher-order approximation. Some indication of the accuracy of our first approximation to the solution can be found by calculating additional terms in Expansion [28]. These additional terms represent corrections to the first approximation so that their magnitude gives some idea of the size of the error in the first approximation. If κ and λ are of the same order of magnitude the contribution of each of the terms of [28] which is of second degree in κ and λ will be the same, in general. For the special case now being considered Z_{00} and Z_{-1} vanish identically and $Z_{10} = X_{10} + iY_{10}$ is given by Equation [56]. Differential Equations [32] to [34] now take the form

$$Z_{20}'' - i\mu Z_{20} = -\frac{1}{8}\left(\frac{\pi}{2}\right)^4 (A + iB)\left(\sin\frac{\pi\xi}{2} - 3\sin\frac{3\pi\xi}{2}\right) \quad [64]$$

$$Z_{11}'' - i\mu Z_{11} = \left(\frac{\pi}{2}\right)^2\left\{\left(1+\frac{\nu}{2}\right)A + \left[\left(1-\frac{\nu}{2}\right)B - \frac{\nu\pi}{4}\right]i\right\}\sin\pi\xi \quad [65]$$

$$Z_{02}'' - i\mu Z_{02} = -i\frac{\pi}{2}\sin\frac{\pi\xi}{2} \quad [66]$$

where

$$A = \frac{\mu(\pi/2)^2}{\mu^2 + (\pi/2)^4}, \quad B = -\frac{\mu^2(\pi/2)}{\mu^2 + (\pi/2)^4} \quad [67]$$

By the method of undetermined coefficients it follows that solutions of Equations [64] to [66] satisfying boundary Conditions [44] have the form

$$Z_{20} = (a_1 + ib_1)\sin\frac{\pi\xi}{2} + (a_2 + ib_2)\sin\frac{3\pi\xi}{2} \quad [68]$$

$$Z_{11} = (a_3 + ib_3)\sin\pi\xi \quad [69]$$

$$Z_{02} = (a_4 + ib_4)\sin\frac{\pi\xi}{2} \quad [70]$$

where

$$a_1 = -\frac{\mu}{8}\left(\frac{\pi}{2}\right)^5 \frac{\mu^2 - (\pi/2)^4}{[\mu^2 + (\pi/2)^4]^2}$$

$$b_1 = -\frac{1}{4}\frac{\mu^2(\pi/2)^7}{[\mu^2 + (\pi/2)^4]^2} \quad \ldots\ldots [71]$$

$$a_2 = \frac{3}{8}\mu\left(\frac{\pi}{2}\right)^5 \frac{\mu^2 - 9(\pi/2)^4}{[\mu^2 + (\pi/2)^4][\mu^2 + (3\pi/2)^4]}$$

$$b_2 = \frac{15}{4}\frac{\mu^2(\pi^2/2)^7}{[\mu^2 + (\pi/2)^4][\mu^2 + (3\pi/2)^4]} \quad \ldots\ldots [72]$$

$$a_3 = \mu\left(\frac{\pi}{2}\right)^3 \frac{\mu^2 - (4 + 3\nu/2)(\pi/2)^4}{[\mu^2 + (\pi/2)^4][\mu^2 + \pi^4]}$$

$$b_3 = \left(\frac{\pi}{2}\right)^5 \frac{(5 + \nu/2)\mu^2 + 2\nu(\pi/2)^4}{[\mu^2 + (\pi/2)^4][\mu^2 + \pi^4]} \quad \ldots\ldots [73]$$

$$a_4 = \frac{\mu(\pi/2)}{\mu^2 + (\pi/2)^4}, \quad b_4 = \frac{(\pi/2)^2}{\mu^2 + (\pi/2)^4} \quad \ldots\ldots [74]$$

Solutions [68] to [70] may be used to determine corrections to the first approximation. We shall give explicit results only for the effective axial strain. The portion of the axial strain due to bending is given by the last integral in Equation [41], which may now be written

$$\frac{\epsilon_B}{\epsilon_S} = -\sqrt{12(1-\nu^2)}\,\frac{a}{h}\,\frac{1}{4}\int_0^4 f'\{\kappa X_{10} + \kappa^2 X_{20} + \kappa\lambda X_{11} + \lambda^2 X_{02} + \ldots\}\,d\xi \quad \ldots\ldots [75]$$

Since $X_{rs} = Re\{Z_{rs}\}$ we have, using Equations [68] to [70]

$$\frac{\epsilon_B}{\epsilon_S} = \sqrt{12(1-\nu^2)}\,\frac{a}{h}\,\frac{\pi}{4}\{\kappa A + \kappa^2 a_1 + \lambda^2 a_4 + \ldots\} \ldots [75a]$$

Using Equations [67], [71], and [74], as well as Definitions [12], Equation [75a] may be written

$$\frac{\epsilon_B}{\epsilon_S} = \frac{1}{2}\left(\frac{\kappa}{\lambda}\right)^2 \frac{\mu^2(\pi/2)^4}{\mu^2 + (\pi/2)^4}\left\{1 - \kappa\,\frac{\pi^2}{32}\,\frac{\mu^2 - (\pi/2)^4}{\mu^2 + (\pi/2)^4}\right\} + \frac{\kappa}{2}\,\frac{\mu^2(\pi/2)^2}{\mu^2 + (\pi/2)^4} \quad \ldots\ldots [76]$$

The last term in Equation [76] corresponds to the λ^2 term in the expansion for Z or X. This term is, at most, of the order of magnitude of κ so that our previous conclusions about the behavior of the shell based on Equation [60] still follow.

Let us denote the portion of the effective axial strain due to direct extension by ϵ_D, so that $\epsilon = \epsilon_D + \epsilon_B$. As a first approximation we have already taken $\epsilon_D = \epsilon_S$. A second approximation is obtained from the first integral of Equation [41] and is given by

$$\frac{\epsilon_D}{\epsilon_S} = 1 + \kappa\,\frac{1}{4}\int_0^4 \left[f' Y_{10} - \frac{1}{2}\,(f')^2\right] d\xi \quad \ldots\ldots [77]$$

Introducing Y_{10} from Equation [56], [77] becomes

$$\frac{\epsilon_D}{\epsilon_S} = 1 + \frac{\kappa}{4}\left(\frac{\pi}{2}\right)^2 \frac{\mu^2 - (\pi/2)^4}{\mu^2 + (\pi/2)^4} \quad \ldots\ldots [78]$$

It is interesting to note that the second term in Equation [78], which comes from the linear κ term in the general expansion, is of the same order of magnitude when $\mu \gg 1$ as the last term in Equation [76], which comes from the λ^2 term.

(*b*) *Parabolic Corrugations*

$$f(\xi) = 1 - \xi^2, \qquad |\xi| \leq 1$$

The range of definition of f is extended beyond the interval $-1 \leq \xi \leq 1$ by requiring that $f(\xi + 2) = -f(\xi)$ for all ξ. A possible approach to the present case is to obtain a Fourier series representation for the function $f(\xi)$ and proceed as in Section 4. Instead, we shall give a solution of the problem in closed form. As the mathematics is fairly elementary, although some of the calculations are quite involved, we shall list many of the results without explicit derivations.

Due to symmetry we may conclude that the hoop stress $\sigma_{\theta D}$ and bending stress $\sigma_{\xi B}$ vanish at inflection points of the corrugations. This allows us to restrict our attention to the interval $0 \leq \xi \leq 1$ and obtain a first approximation to the solution by solving differential Equation [30] subject to the boundary conditions

$$Z_{10}(0) = 0, \qquad Z_{10}'(1) = 0 \quad \ldots\ldots [79]$$

The solution of Equation [30], subject to Equations [79], is given by

$$Z_{10} = c_1 \cosh(1 + i)m\xi + c_2 \sinh(1 + i)m\xi - 2i\xi \ldots [80]$$

where

$$m = \left(\frac{\mu}{2}\right)^{1/2}, \quad c_1 = 0, \qquad c_2 = \frac{2i}{(1 + i)m \cosh(1 + i)m} \ldots [81]$$

Separating Z_{10} into real and imaginary parts and substituting in Equations [50] to [52] leads eventually to the results

$$\frac{\sigma_{\theta D}(0)}{\sigma_S} = -\frac{\kappa}{\lambda}\left[2 - \frac{4\cosh m \cos m}{\cosh 2m + \cos 2m}\right] \quad \ldots\ldots [82]$$

$$\frac{\sigma_{\xi B}(0)}{\sigma_S} = \frac{\kappa}{\lambda}\sqrt{\frac{3}{1-\nu^2}}\left[\frac{4\sinh m \sin m}{\cosh 2m + \cos 2m}\right] \quad \ldots\ldots [83]$$

$$\frac{\epsilon}{\epsilon_S} = 1 + \left(\frac{\kappa}{\lambda}\right)^2\left[4 - \frac{2}{m}\,\frac{\sinh 2m + \sin 2m}{\cosh 2m + \cos 2m}\right] \ldots [84]$$

The expressions [82] to [84] are to be compared with those given [57], [58], and [60] for a shell with sinusoidal corrugations.

One would expect from the similarity of the present case to the sinusoidal case, that Equations [82] and [83] determine the maximum values of $\sigma_{\theta D}$ and $\sigma_{\xi B}$. This, however, is so only if μ is sufficiently small. As $m = \sqrt{\mu/2}$ increases $\sigma_{\xi B}(0)/\sigma_S$ alternates in sign with $\sin m$ which indicates that the position of maximum bending stress is not always at $\xi = 0$. Actually, one can show that $\sigma_{\xi B,\,\max}$ occurs at $\xi = 0$ only as long as $m \leq \pi/2$ or $\mu \leq \pi^2/2$. Also, $\sigma_{\theta D,\,\max}$ occurs at $\xi = 0$ only if $m \leq \pi$ or $\mu \leq 2\pi^2$.

It is interesting to note that the same type of phenomenon is encountered in studies of the bending of curved tubes or toroidal shells (6, 7). In these previous studies it was found that as μ increased positions of maximum stress would shift from points such as $\xi = 0$ to two positions located symmetrically to either side of $\xi = 0$ and that as μ increased further the positions of maximum stress continued to move further away from $\xi = 0$.

Curves showing the quantities $(\lambda/\kappa)(\sigma_{\theta D,\,\max}/\sigma_S)$, $(\lambda/\kappa)(\sigma_{\xi B,\,\max}/\sigma_S)$, and $(\lambda/\kappa)^2(\epsilon_B/\epsilon_S)$ as functions of $\mu = 2m^2$ are given in Figs. 5 and 6. As is evident from these curves the behavior of a shell with parabolic corrugations is quite similar to that of a shell with sinusoidal corrugations, at least for sufficiently small μ. Consequently, the remarks previously made concerning the conditions for which the shell behaves like a straight tube also apply to the present case.

With $f(\xi) = 1 - \xi^2$ and Z_{10} from Equation [80], the right sides of Equations [32], [33], and [34] may be determined and these differential equations solved to obtain higher-order approximations. The calculations begin to become impractical, but a solu-

tion has been obtained by the authors for the quantity Z_{20}. Using this solution a second approximation to ϵ_B/ϵ_S can be determined. The result is

$$\frac{\epsilon_B}{\epsilon_S} = \left(\frac{\kappa}{\lambda}\right)^2 \left\{4 - \frac{2}{m} M + \kappa\left[-4 + \frac{6}{m} M - \frac{15}{2m^2} L + \frac{4}{3} LM + \frac{1}{2m^2}(M^2 - L^2)\right]\right\} \quad [85]$$

where

$$L = \frac{\sinh 2m - \sin 2m}{\cosh 2m + \cos 2m}, \quad M = \frac{\sinh 2m + \sin 2m}{\cosh 2m + \cos 2m} \quad [86]$$

Substituting the imaginary part of Z_{10} from Equation [80] in [77] yields a second approximation to ϵ_D, namely

$$\frac{\epsilon_D}{\epsilon_S} = 1 + \kappa\left[\frac{2}{3} - \frac{L}{m^2}\right] \quad [87]$$

(c) Circular-Arc Corrugations. If the meridian curve for a corrugated pipe consists of circular arcs the shape function $f(\xi)$, appearing in Equations [1], becomes

$$f(\xi) = (\kappa - 1 + \sqrt{(1+\kappa)^2 - 4\kappa\xi^2})/2\kappa, \quad |\xi| \leqslant 1 \quad [88]$$

Again, the range of definition of f is extended by means of the relation $f(\xi + 2) = -f(\xi)$.

In all the previous work we have assumed that f was independent of the various parameters κ, λ, μ. The fact that f is now a function of κ as well as ξ does not introduce any theoretical difficulty but does require some modification of procedure. Since $\kappa \ll 1$ we may expand Equation [88] in powers of κ and obtain

$$f(\xi) = 1 - \xi^2 + \kappa(\xi^2 - \xi^4) - \kappa^2(\xi^2 - 3\xi^4 + 2\xi^6) + \ldots, \quad |\xi| \leqslant 1 \quad [89]$$

Since the leading term in Equation [89] is the same as the function taken for parabolic corrugations, it follows that the first approximation to the solution will be ide tical to that obtained for case (*b*). However, if higher approximations are calculated, the results for the two cases will differ slightly.

In order to obtain such higher approximations, one must first return to Equation [27] and introduce an expansion in powers of κ for the function f, as well as expansions for the various coefficients and for Z. This will yield a new set of differential equations for the functions Z_{mn}. The first three equations will be the same as Equations [29] to [31], but equations corresponding to Equations [32], [33], . . ., will be different. All this was done for the present case and a solution for Z_{20} was obtained. The second approximation then calculated for ϵ_B/ϵ_S was found to be

$$\left(\frac{\epsilon_B}{\epsilon_S}\right)_{\substack{\text{circular}\\ \text{case}}} = \left(\frac{\epsilon_B}{\epsilon_S}\right)_{\substack{\text{parabolic}\\ \text{case}}} + \left(\frac{\kappa}{\lambda}\right)^2 \kappa\left[8 - \frac{20}{m} M + \frac{24}{m^2} L\right] \quad [90]$$

It should perhaps be mentioned that semicircular corrugations cannot be treated by the present method as they would correspond to taking $\kappa = 1$ in Formula [88]. Since $f'(\xi)$ then becomes infinite at $\xi = \pm 1$, our basic assumption that $f'(\xi) = O(1)$ no longer holds. However, Donnell (1) has considered the problem for pipes with semicircular corrugations as a special case and has obtained results for the effective axial strain that are particularly appropriate when μ is not very large. The case when μ is large has been treated in (7) by methods of asymptotic integration.

(d) Saw-Tooth Corrugations

$$f(\xi) = 1 - |\xi|, \quad -2 \leqslant \xi \leqslant 2$$

This case has been considered previously by Donnell (1), who obtained a formula for the effective axial strain using energy methods. His results are equivalent to those which we would find using Fourier series.

We note that since $f'(\xi)$ is constant for the present case, differential Equations [13] and [14] reduce to equations with constant coefficients if we set $\lambda = 0$. Thus, if we neglect terms in λ, we may find an explicit solution for arbitrary values of κ.[4] This may be accomplished most easily by incorporating κ in the definition of μ. In other words, if we take the results for our first approximation and replace μ by the combination $\mu\sqrt{1+\kappa}$, we will obtain results valid for arbitrary κ instead of for $\kappa \ll 1$.

In particular, if we again require $f(\xi + 2) = -f(\xi)$ for all ξ, coefficients in the Fourier Expansion [42] become

$$a_{2n} = 0, \quad a_{2n+1} = \frac{8}{\pi^2}\frac{1}{(2n+1)^2}, \quad n = 0, 1, 2, \ldots \quad [91]$$

Coefficients [91] introduced in Series [48] and [49] determine a first approximation to functions X and Y, which are proportional to η and ψ or β and rH. If we write $\mu\sqrt{1+\kappa}$ in place of μ in Equations [48] and [49], we will have solutions for X and Y which are valid even if $\kappa \gg 1$. If we then calculate the effective axial strain the results will be identical to Donnell's except that Donnell's solution does not involve Poisson's ratio ν, which appears in our Definition [12] of μ.

In order to have results for the present example which can be compared with those obtained for cases (*a*) and (*b*), the solution of Equation [30] may be expressed in closed form and a first approximation for the effective axial strain likewise determined. One may restrict attention to the range $0 \leq \xi \leq 2$. With $\mu = 2m^2$, the solution of Equation [30], subject to boundary Conditions [44], is found to be

$$Z_{10} = -i + i\cosh(1+i)m\xi + k\sinh(1+i)m\xi \quad [92]$$

where

$$k = -i\tanh(1+i)m = \frac{\sin 2m - i\sinh 2m}{\cosh 2m + \cos 2m} \quad [93]$$

As in case (*a*) the maximum values of $\sigma_{\theta D}$ and $\sigma_{\xi B}$ occur at $\xi = 0$ and $\xi = 2$, and are found to be

$$\frac{\sigma_{\theta D,\,\max}}{\sigma_S} = \frac{\kappa}{\lambda} m \frac{\sinh 2m - \sin 2m}{\cosh 2m + \cos 2m} \quad [94]$$

$$\frac{\sigma_{\xi B,\,\max}}{\sigma_S} = \frac{\kappa}{\lambda}\sqrt{\frac{3}{1-\nu^2}}\, m \frac{\sinh 2m + \sin 2m}{\cosh 2m + \cos 2m} \quad [95]$$

$$\frac{\epsilon}{\epsilon_S} = 1 + \left(\frac{\kappa}{\lambda}\right)^2 m \frac{\sinh 2m - \sin 2m}{\cosh 2m + \cos 2m} \quad [96]$$

The results expressed in Equations [94] to [96] are to be compared with Relations [57], [58], and [60] and with Equations [82] to [84]. Curves showing the quantities $(\lambda/\kappa)(\sigma_{\theta D,\,\max}/\sigma_s)$, $(\lambda/\kappa)(\sigma_{\xi B,\,\max}/\sigma_S)$, and $(\lambda/\kappa)^2\,\epsilon_B/\epsilon_S$ as functions of $\mu = 2m^2$ are given in Figs. 5 and 6. It is seen that the behavior of the shell for small μ is quite similar to cases (*a*) and (*b*). In fact, except for the bending stress, the over-all behavior is of the same nature for

[4] Since we are dealing with a portion of a conical shell in the range $0 \leq \xi \leq 2$, it is known that differential Equations [13] and [14] can be solved explicitly in terms of Bessel functions for arbitrary values of κ and λ.

the range over which the curves extend. However, as $\mu \to \infty$ the values of all the quantities given by Equations [94] to [96] increase indefinitely, whereas for cases (a) and (b) all quantities either approach zero or finite values. The reason for this qualitative difference is the fact that there is no membrane solution for the present case.

Next, we may calculate Z_{20} as has been done in the previous cases. The result is

$$Z_{20} = \frac{m \sinh (1 + i)m\xi}{2(1 + i) \cosh^2 (1 + i)m} + \frac{\xi}{4} Z_{10}' \quad \ldots\ldots [97]$$

where Z_{10} is given by Equation [92]. Using Equations [92] and [97] in Equation [75] we obtain

$$\frac{\epsilon_B}{\epsilon_S} = \left(\frac{\kappa}{\lambda}\right)^2 \left\{ mL + \kappa \left[-\frac{m}{4} L + \frac{m^2}{4} (M^2 - L^2) \right] \right\} \quad \ldots\ldots [98]$$

where L and M are given in Equation [86]. Formula [98] corresponds to Equations [85] and [90].

From Equations [77] and [92], a second approximation to ϵ_D is found to be

$$\frac{\epsilon_D}{\epsilon_S} = 1 + \kappa \left[\frac{1}{2} - \frac{M}{2m} \right] \quad \ldots\ldots [99]$$

As has been mentioned, it is no more difficult to obtain a solution for arbitrary values of κ than to obtain a first approximation. Neglecting λ entirely, differential Equation [27] may be written, with $f = 1 - \xi$ and $f' = -1$

$$Z'' - i\mu \sqrt{1 + \kappa}\, Z = -\kappa\mu \sqrt{1 + \kappa} \quad \ldots\ldots [100]$$

The solution of Equation [100] satisfying the proper boundary conditions is

$$Z = \kappa \{ -i + i \cosh (1 + i)m_1 + k_1 \sinh (1 + i)m_1\xi \} \quad \ldots [101]$$

where

$$m_1 = \sqrt{(\mu/2) \sqrt{1 + \kappa}}$$

From Equations [10] and [40] we obtain

$$\frac{\epsilon_B}{\epsilon_S} = \sqrt{12(1 - \nu^2)}\, \frac{a}{h}\, \kappa\, \frac{L_1}{2m_1} = \left(\frac{\kappa}{\lambda}\right)^2 \frac{m_1 L_1}{\sqrt{1 + \kappa}} \quad \ldots [102]$$

where L_1 is the same as L, given by Equation [86], with m replaced by m_1. For ϵ_D we have

$$\frac{\epsilon_D}{\epsilon_S} = (1 + \kappa)^{-1/2} \int_0^1 (1 - Y) d\xi = \sqrt{1 + \kappa} - \frac{\kappa}{\sqrt{1 + \kappa}} \frac{M_1}{2m_1} \quad \ldots\ldots [103]$$

where M_1 follows from M of Equation [86] by changing m to m_1. Combining Equations [102] and [103]

$$\frac{\epsilon}{\epsilon_S} = \sqrt{1 + \kappa} + \frac{\kappa}{2m_1} \left[-\frac{M_1}{\sqrt{1 + \kappa}} + \sqrt{12(1 - \nu^2)}\, \frac{a}{h}\, L_1 \right] \quad \ldots\ldots [104]$$

Equation [104] neglects the effect of terms in λ entirely but is valid for arbitrary values of κ and μ.

7 A Numerical Example

Some years ago Donnell (1) carried out certain experimental tests on a corrugated pipe with dimensions

$$a = 5.330 \text{ in.}, \quad b = 0.235 \text{ in.}, \quad c = 0.670 \text{ in.}, \quad h = 0.065 \text{ in.} \quad \ldots\ldots [105]$$

He states that the corrugations were between saw tooth and sinusoidal in shape and that for a direct axial load an "effective" modulus of elasticity $E' = 1{,}510{,}000$ psi was observed. Thus experimentally

$$\frac{\epsilon}{\epsilon_S} = \frac{E}{E'} = \frac{30{,}000{,}000}{1{,}510{,}000} = 19.87 \quad \ldots\ldots [106]$$

For a shell with dimensions [105] one has, according to Equations [12], with $\nu = 0.3$

$$\kappa = 0.1230, \quad \lambda = 0.0441, \quad \mu = 4.2817, \quad m = 1.4632 \quad \ldots\ldots [107]$$

TABLE 1 RESULTS OF CALCULATIONS

	ϵ_B/ϵ_S		ϵ_D/ϵ_S		$\frac{\epsilon}{\epsilon_S} = \frac{\epsilon_B}{\epsilon_S} + \frac{\epsilon_D}{\epsilon_S}$			
Type of corrugations	First approx.	Second approx.	First approx.	Second approx.	First approx.	Second approx.	Other authors	
(a) Sinusoidal	17.79	17.45	1.00	1.04	18.79	18.49	25.0	(Donnell)
(b) Parabolic arcs	19.06	18.80	1.00	1.04	20.06	19.84	25.0	(Donnell)
(c) Circular arcs	19.06	19.55	1.00	1.04	20.06	20.59	26.95	(Hetényi)
(d) Saw tooth	12.37	12.03	1.00	1.01	13.37	13.04	13.3	(Donnell)

Using these values both a first and a second approximation to ϵ/ϵ_S have been calculated for the special cases discussed previously. The results are listed in Table 1. The second approximation corresponds to retaining terms in the general expansion, Equation [28], up to that in κ^2 but neglecting terms in $\kappa\lambda$ and λ^2, since λ is fairly small compared to κ. Thus the second approximation to ϵ_B/ϵ_S for the sinusoidal case was calculated from Equation [76] neglecting the last term in Equation [76]. (For the values given in Equation [107] the last term in Equation [76] is 0.114, amounting to less than 1 per cent of ϵ_B/ϵ_S.)

The first approximations to ϵ/ϵ_S were obtained from Equations [60], [84], and [96]. The second approximations to ϵ_B/ϵ_S were calculated using Equations [76], [85], [90], and [98], while the second approximations to ϵ_D/ϵ_S were found by using Equations [78], [87], and [99].

It is noted that the greatest deviation between the values for the first and second approximations to ϵ/ϵ_S amounts to only 2.5 per cent and occurs for cases (c) and (d). If for case (d) we use Formulas [102] and [103], which neglect only the effect of terms in λ, we find $\epsilon_B/\epsilon_S = 12.044$ and $\epsilon_D/\epsilon_S = 1.016$ or $\epsilon/\epsilon_S = 13.060$, which differs from the value of the second approximation given in Table 1 by less than 0.1 per cent. Although we have no means of giving a precise estimate of the error in the values of the second approximation to ϵ/ϵ_S, it would seem that the values in Table 1 are probably very close to the exact values in all cases.

We already have noted how Donnell calculated the value of ϵ/ϵ_S for case (d) using Fourier series. The values attributed to him in Table 1 for cases (a) and (b) were obtained from a formula which was said to be interpolated from the saw-tooth case and the case of semicircular corrugations. Hetényi (2) considered the case of a corrugated pipe with a meridian curve made up of circular arcs as an application of the theory of beams on elastic foundations. We have listed in Table 1 the value given in (2) for ϵ/ϵ_S, using Dimensions [105]. The numerical comparison illustrates the fact that the particular Dimensions [105] do not

satisfy very closely certain basic smallness assumptions made in (2).

ACKNOWLEDGMENT

The work of this paper was supported by the Office of Naval Research under a contract with the Massachusetts Institute of Technology and by the Office of Ordnance Research under a contract with Case Institute of Technology.

BIBLIOGRAPHY

1 "The Flexibility of Corrugated Pipes Under Longitudinal Forces and Bending," by L. H. Donnell, Trans. ASME, vol. 54, paper APM—54-7, 1932.

2 "Beams on Elastic Foundation," by M. I. Hetényi, University of Michigan Press, Ann Arbor, Mich., 1946.

3 "Spannungen in schwach ausgebauchten zylindrischen Behältern," by K. Federhofer, *Osterreichische Bauzeitschrift*, vol. 61, 1951, pp. 149–153.

4 "Contribucion al Calculo de Digues en Cupula," by K. Federhofer, *Tecnica, Tucuman*, vol. 1, 1952, pp. 227–233.

5 "On the Theory of Thin Elastic Shells," by E. Reissner, Reissner Anniversary Volume, J. W. Edwards, Ann Arbor, Mich., 1949, pp. 231–247.

6 "Bending of Curved Tubes," by R. A. Clark and E. Reissner, Academic Press, New York, N. Y., *Advances in Applied Mechanics*, vol. 2, 1951, pp. 93–122.

7 "On the Theory of Thin Elastic Toroidal Shells," by R. A. Clark, *Journal of Mathematics and Physics*, vol. 29, 1950, pp. 146–177

8 "Symmetrical Deformation of a Nearly Cylindrical Shell" (in Russian) by E. F. Burmistrov, *Prik. Math. Mekh.*, Vol. 13, 1949, pp. 401–412 (In this work which came to our attention after the present paper had been preprinted there may be found a *one*-parameter expansion procedure, effectively in terms of our parameter λ, and subject to the limitation $\epsilon \ll \lambda$.)

Analysis of Short Thin Axisymmetrical Shells Under Axisymmetrical Edge Loading[1]

By G. HORVAY,[2] C. LINKOUS,[3] AND J. S. BORN[4]

On the basis of recent work by Hildebrand, formulas are established for the effects of axisymmetrical edge moments and edge shears on short shells of variable wall thickness and variable meridional curvature. While the formulas are inferior in accuracy to those developed for bolted flange assemblies by Waters, Rossheim, Wesstrom, and Williams, in simplicity of use and speed of calculations, they are on a par with the well-known Geckeler formulas, without being subject to many of the limitations of the latter. The formulas are particularly suited for the analysis of the tapered hub portion of a flanged shell. Other uses are also obvious. Particular applications to redundant shell (torus-type) problems will be given in a separate paper.

Nomenclature

The following nomenclature is used in the paper; positive sign convention is defined in accordance with Figs. 1, 2, 3.

Co-Ordinates and Geometrical Parameters

x, θ, z = co-ordinates in meridional, azimuthal, and inward normal directions
φ = latitude angle
r = horizontal radius of shell middle surface
h = wall thickness
b = width of strip, Equation [4a]
k = stiffness of hoop ring in the z-direction (pounds of force per meridional inch length and horizontal inch width to cause 1-in. normal displacement of supported beam), Equation [4b]
D = bending rigidity of beam per unit width, Equation [2]
D = bending rigidity of shell, Equation [5]
l = attenuation length, Equation [5a]
l_A = axial component of l, Equation [7d]
f, ϵ = shell flexibility and expansivity, Equations [7b], [7c]
$2L$ = meridional length of shell
n = dimensionless distance from reference cross section, Equation [8]
$2L\dagger = 2Nl$ = virtual shell length, Equation [20a]
$2L_A\dagger$ = virtual shell height, Equation [20b]
c = x-location of virtual center, Equation [18]
x_m = x-co-ordinate referred to meridional center (when such distinction contributes to clarity), Fig. 2
$f\dagger, \epsilon\dagger$ = ring flexibility and expansivity, Equations [28a], [28b]
ρ, η, ϑ = ratios defined in Equation [6b]
$[]$ = $\rho^{1/4}\eta^{-3/4}\vartheta^{-3/4}$ in Equations [9], [13]
Subscripts 0, u, l = pertaining to reference cross section, upper edge, lower edge of shell
Subscripts s, a = symmetric, antisymmetric, Equation [21]

Forces, Moments, Deformations[5]

$p(x)$ = pressure load in the outward normal ($-z$) direction, psi
H = horizontal shear force, lb/in.
Q = normal shear force, lb/in.
M, M_θ = meridional moment, hoop moment, lb in/in.
N_x, N_θ = meridional force, hoop force, lb/in.
w, δ = displacements in z (inward) and r (outward) directions
χ = increase in latitude angle (angle of rotation)
∇ = axial (upward) displacement
E, ν = elastic constants
Superscript * = defined in Equations [9], [13]

Functions, Auxiliary Symbols

$g_1, \ldots, g_4$ = functions defined in Equations [30]
$j_1, \ldots, j_4$ = functions defined in Equations [30]
G_k, J_k = function values defined in Equations [33]
a, b, c, d = expressions defined in Equations [23]
A, B, C, D = integration constants, Equations [11]

1 Introduction

The "Geckeler approximation" serves the purpose of evaluating, in a particularly simple manner, the effects of edge moments and edge shears on a thin-walled shell. One replaces a non-too-flat shell by a conical shell of uniform wall thickness and indefinite length, which touches the given shell at a suitable lateral circle (usually the edge where the loads are applied), then analyzes the conical shell by means of modified cylindrical-shell formulas. These formulas are listed in many places, e.g., in a recent paper (1).[6] More accurate and, at the same time, more tedious calculational schemes are also available. Prominent among these is that contained in the booklet by the Taylor Forge and Pipe Works (2); another approach to the subject is due to Fergusson, Kudar

[1] The Knolls Atomic Power Laboratory is operated by the General Electric Company for the Atomic Energy Commission. The work reported here was carried out under Contract No. W-31-109 Eng.-52.

[2] Engineer, SIR Reactor Section, Knolls Atomic Power Laboratory, General Electric Company, Schenectady, N. Y. Mem. ASME.

[3] Technical Engineer, Fractional Horsepower Motors Engineering Department, General Electric Company, Fort Wayne, Ind.; formerly, Member, Advanced Engineering Program, General Electric Company.

[4] Engineering Assistant, SIR Reactor Section, Knolls Atomic Power Laboratory, General Electric Company, Schenectady, N. Y.

Contributed by the Applied Mechanics Division and presented at the Diamond Jubilee Annual Meeting, Chicago, Ill., November 13–18, 1955, of The American Society of Mechanical Engineers.

Discussion of this paper should be addressed to the Secretary, ASME, 29 West 39th Street, New York, N. Y., and will be accepted until April 10, 1956, for publication at a later date. Discussion received after the closing date will be returned.

Note: Statements and opinions advanced in papers are to be understood as individual expressions of their authors and not those of the Society. Manuscript received by ASME Applied Mechanics Division, March 31, 1955. Paper No. 55—A-3.

[5] Hildebrand uses symbols—$M\xi$, $-M\theta$, $-Q$, u, w, β, $\int \alpha d\xi$, where we write M, $M\theta$, Q, δ, ∇, χ, x.

[6] Numbers in parentheses refer to the Bibliography at the end of the paper.

and Harvey (3); a third method (developed at the University of Illinois) utilizes difference equations and numerical calculations (4); the tie-in with the design of pressure-vessel heads is summarized in a PVRC Report (5), based on work by Watts-Burrows (6), Rhys, Boardman, and many others. The question arises whether one may develop simple explicit formulas by extending the Geckeler method, through suitable modifications, to embrace shells of short length and of slowly varying meridional curvature and wall thickness. The answer is in the affirmative. The results are obtained by utilization of some formulas developed by Hildebrand (7).

2 The Tapered Curved Beam on Elastic Foundation

In Fig. 1(*a*) we illustrate a beam of width $b(x)$, thickness $h(x)$, inclination $\varphi(x)$, supported by perpendicular springs of stiffness $k(x)$, to which normal load $p(x)$ is applied. From the relations, see Fig. 1(*b*)

$$dw/dx = \chi, \qquad D d\chi/dx = M, \qquad d(Mb)/dx = Qb \ldots [1a]$$

$$d(Qb)/dx = -bkw - bp \ldots [1b]$$

$$D = Eh^3/12 \ldots [2]$$

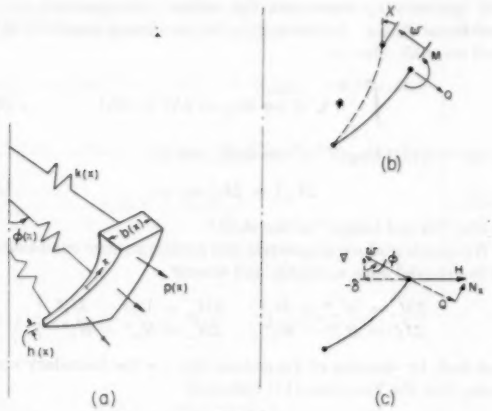

Fig. 1

there follows the familiar equation of the moderately curved tapered beam on elastic foundation

$$\frac{d^2}{dx^2}\left(bD\frac{d^2w}{dx^2}\right) + bkw = -bp \ldots [3]$$

3 The Shell

As is well known (8), the shell in Fig. 2 may be regarded as an assemblage of beams on elastic foundation of widths

$$b = r d\theta \ldots [4a]$$

supported by "hoop rings" of stiffness

$$k = Eh \sin^2 \varphi / r^2 \ldots [4b]$$

Relation [4*b*] expresses the equivalence of the spring force bkw and the normal component $N_\theta d\theta \sin^2 \varphi$ of the radial resultant $N_\theta d\theta \sin \varphi$ of the hoop forces N_θ acting on element bdx. For non-cylindrical shells this relation represents an approximation, as it neglects, for $\varphi \neq \pi/2$, a Poisson ratio effect. Writing now

$$D = Eh^3/12(1 - \nu^2) \ldots [5]$$

for the flexural rigidity of the strip, Equation [3] may be rewritten in the form

$$\frac{\rho}{\eta\vartheta^2}\frac{d^2}{dx^2}\left(\rho\eta^3\frac{d^2w}{dx^2}\right) + \frac{4}{l^4}w = -\frac{4}{l^4}\frac{r^2p}{Eh\sin^2\varphi} \ldots [6a]$$

where $\rho = r/r_0, \quad \eta = h/h_0, \quad \vartheta = \sin\varphi/\sin\varphi_0 \ldots [6b]$

and $l = [3(1 - \nu^2)]^{-1/4}(r_0h_0/\sin\varphi_0)^{1/2} \ldots [7a]$

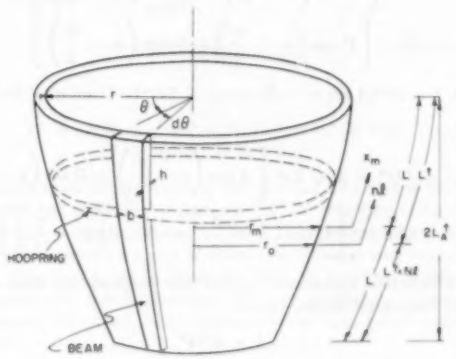

Fig. 2

It is to be noted that the quantity l, as well as the parameters

$$f = l/D_0 \qquad [D_0 = Eh_0^3/12(1 - \nu^2)] \ldots [7b]$$

$$\epsilon = fl_A^2/2 \ldots [7c]$$

$$l_A = l \sin\varphi_0 \ldots [7d]$$

to be used later, are formed in terms of the parameters of the reference cross section (as indicated by the subscripts zero), and therefore do not vary along the shell, but are constant.

Hildebrand (7), extending Reissner's analysis (9), has shown (using a different notation) that, when ρ, η, ϑ, p are slowly varying quantities, and φ is not too close to 0 or π, the introduction of the dimensionless distance parameter

$$n = \frac{1}{l}\int_0^x \sqrt{\vartheta/\rho\eta}\, dx \ldots [8]$$

greatly simplifies the analysis. For, on writing

$$\left.\begin{aligned} w &= []w^*, \ [] \equiv \rho^{1/4}\eta^{-3/4}\vartheta^{-3/4} \\ \chi &= (\vartheta/\rho\eta)^{1/2}[]\chi^* \\ M &= \eta^3(\vartheta/\rho\eta)[]M^* \\ Q &= \eta^3(\vartheta/\rho\eta)^{3/2}[]Q^* \\ p &= \eta^3(\vartheta/\rho\eta)^2[]p^* \end{aligned}\right\} \ldots [9]$$

one may reduce Equation [6*a*] to the equation with constant coefficients

$$\frac{d^4w^*}{dn^4} + 4w^* = -4\frac{r_0^2p^*}{Eh_0\sin^2\varphi_0} \left(= -fl^3p^*\right) \ldots [10]$$

This approximation corresponds to the use of a one-term asymptotic expansion.

Restricting ourselves to the case where there is no distributed load, i.e., $p^* = 0$, the general solution of Equation [10], involving four integration constants A, B, C, D, is

$$\delta^*/l_A = -w^*/l = e^n[A\cos n + B\sin n] + e^{-n}[C\cos n + D\sin n] \ldots [11a]$$

and by the "differentiation formulas"

$$d/dx = \sqrt{\vartheta/\rho\eta}\, d/l\, dn \ldots [12a]$$

$$l\chi^* = dw^*/dn, \quad fM^* = d\chi^*/dn, \quad lQ^* = dM^*/dn \ldots [12b]$$

($\sqrt{\vartheta/\rho\eta}$ is treated in the differentiations like a constant) we obtain the further expressions

$$\chi^* = \sqrt{2}\, e^n\left[A \sin\left(n - \frac{\pi}{4}\right) - B \cos\left(n - \frac{\pi}{4}\right)\right] + \sqrt{2}\, e^{-n}\left[C \cos\left(n - \frac{\pi}{4}\right) + D \sin\left(n - \frac{\pi}{4}\right)\right] \ldots [11b]$$

$$fM^* = 2e^n[A \sin n - B \cos n] + 2e^{-n}[-C \sin n + D \cos n] \ldots [11c]$$

$$fl_A H^* = flQ^* = 2\sqrt{2}\, e^n\left[A \cos\left(n - \frac{\pi}{4}\right) + B \sin\left(n - \frac{\pi}{4}\right)\right] + 2\sqrt{2}\, e^{-n}\left[C \sin\left(n - \frac{\pi}{4}\right) - D \cos\left(n - \frac{\pi}{4}\right)\right] \ldots [11d]$$

We include in Equations [11], for later purposes, the expressions of the horizontal displacement

$$\delta = \vartheta[]\delta^* \ldots [13a]$$

and horizontal shear, see Fig. 1(c)

$$H = \vartheta^{-1}\eta^2(\vartheta/\rho\eta)^{1/2}[]H^* \ldots [13b]$$

which are related to w and Q by

$$\delta = -w \sin \varphi, \quad H = Q/\sin \varphi \ldots [14a, b]$$

The variables δ and H are preferable to w and Q in shell analysis because δ has no axial-displacement component mixed into it, and the forces H, when summed around a latitude circle, are self-equilibrating, in contrast to the forces Q which have an axial resultant.

4 Boundary Conditions

The determination of the constants A, B, C, D of Equations [11] in terms of the prescribed boundary moments and shears

$$\left.\begin{array}{l}\text{At upper end of shell: } M^* = M_u^*, \quad H^* = H_u^* \\ \text{At lower end of shell: } M^* = M_l^*, \quad H^* = H_l^*\end{array}\right\} \ldots [15]$$

is particularly simple (the four simultaneous equations break up into two systems of two equations each) when the reference cross section is so chosen that on the n-scale the upper and lower ends of the shell are equal distances away.[7] We shall refer to this cross section as the "virtual center" of the shell in contrast with the "meridional center" which we define as the cross section which is equal meridional distance from the two ends.

Once we know δ, M, and H, the remaining shell variables ∇, M_θ, N_x, and N_θ are determined from the relations

$$\left.\begin{array}{ll}\nabla = -\delta \cot \varphi, & M_\theta = \nu M \\ N_x = H \cos \varphi, & N_\theta = Eh\delta/r\end{array}\right\} \ldots [16]$$

The location of the virtual center is most simply determined by iteration. Calling the "meridional length" of the shell $2L$, the integration [8] leads, when referred to the meridional center, to the expressions

$$\left.\begin{array}{l}\dfrac{1}{l}\displaystyle\int_{-L}^{0} \sqrt{\vartheta/\rho\eta}\, dx_m = \text{say, } N_l \\ \dfrac{1}{l}\displaystyle\int_{0}^{L} \sqrt{\vartheta/\rho\eta}\, dx_m = \text{say, } N_u\end{array}\right\} \ldots [17]$$

As improved center we now shift to the x_m location

$$c = (N_u - N_l)l/2 \ldots [18]$$

and, if necessary, repeat the process. As example, for a conical shell of uniform wall thickness and radius $r = r_m + x_m \cos \varphi$, we obtain

$$c = \frac{r_m}{\cos \varphi}\left[\sqrt{1 + L \cos \varphi/r_m} + \sqrt{1 - L \cos \varphi/r_m} - 2\right] \simeq \frac{-L^2}{4r_m/\cos \varphi} \ldots [19a]$$

and by iteration, still measuring c from $x_m = 0$

$$c \simeq \frac{-L^2}{-c + 4r_m/\cos \varphi} \ldots [19b]$$

The quantity r_m represents the radius corresponding to the meridional center. In contrast to the meridional length $2L$ of the shell we shall refer to

$$\int_{-L}^{+L} \sqrt{\vartheta/\rho\eta}\, dx_m \equiv 2Nl \equiv 2L\dagger \ldots [20a]$$

as the "virtual length" of the shell, and to

$$2L_A\dagger = 2L\dagger \sin \varphi_0 \ldots [20b]$$

as the "virtual height" of the shell.[8]

We now introduce symmetric and antisymmetric combinations of the starred edge moments and shears[9]

$$\left.\begin{array}{ll}2M_s = M_u^* + M_l^*, & 2M_a = M_u^* - M_l^* \\ 2H_s = H_u^* - H_l^*, & 2H_a = H_u^* + H_l^*\end{array}\right\} \ldots [21]$$

and find, by solution of Equations [15] for the boundary conditions, that the Formulas [11] reduce to

$$\left.\begin{array}{l}\delta^*(n)/fl_A = \dfrac{a}{2}g_3(n) + \dfrac{b}{2}g_4(n) + \dfrac{c}{2}g_1(n) + \dfrac{d}{2}g_2(n) \\ \chi^*(n)/f = -ag_4(n) + \dfrac{b}{2}g_1(n) - cg_2(n) - \dfrac{d}{2}g_3(n) \\ M^*(n) = ag_1(n) + bg_2(n) - cg_3(n) - dg_4(n) \\ l_A H^*(n) = 2ag_2(n) + bg_3(n) - 2cg_4(n) + dg_1(n)\end{array}\right\} \ldots [22]$$

where

$$\left.\begin{array}{l}a = [-2M_a g_4(N) + l_A H_a g_3(N)]/j_1(2N) \\ b = [2M_s g_1(N) + 2l_A H_s g_4(N)]/j_2(2N) \\ c = [-2M_a g_2(N) + l_A H_a g_1(N)]/j_1(2N) \\ d = [-2M_s g_3(N) + 2l_A H_s g_2(N)]/j_3(2N)\end{array}\right\} \ldots [23a]$$

In some problems boundary displacements and rotations are specified rather than boundary moments and shears (see Fig. 3b). Writing

[7] The prescribed boundary conditions specify M, etc., rather than M^*, but by Equations [9] one readily determines the boundary values of the starred quantities, and thus one may formulate the problem in terms of the latter.

[8] Note that the dimensions $L\dagger$, $L_A\dagger$, indicated in Fig. 2, are symbolical lengths, defined by Equations [20a], [20b] on a distorted scale.

[9] We need not attach stars to M_s, etc., because these combinations are defined only with respect to the starred quantities M_u^*, etc.

$$\left.\begin{aligned} 2\delta_s &= \delta_u^* + \delta_l^*, & 2\delta_a &= \delta_u^* - \delta_l^* \\ 2\chi_s &= \chi_u^* - \chi_l^*, & 2\chi_a &= \chi_u^* + \chi_l^* \end{aligned}\right\} \quad \ldots [24]$$

we arrive at the very same Equation [22], where a, b, c, d are now defined by

$$\left.\begin{aligned} a &= [4\delta_a g_2(N) + 2l_A\chi_a g_1(N)]/fl_A j_1(2N) \\ b &= [4\delta_a g_3(N) + 4l_A\chi_a g_2(N)]/fl_A j_2(2N) \\ c &= [-4\delta_a g_4(N) - 2l_A\chi_a g_3(N)]/fl_A j_3(2N) \\ d &= [4\delta_a g_1(N) - 4l_A\chi_a g_4(N)]/fl_A j_4(2N) \end{aligned}\right\} \quad [23b]$$

Of particular importance are the boundary values of displacement and rotation in terms of edge moments and forces, and vice versa. Reverting from $M_s, \ldots, \chi_a$ to $M_u^*, \ldots, \chi_l^*$, we obtain

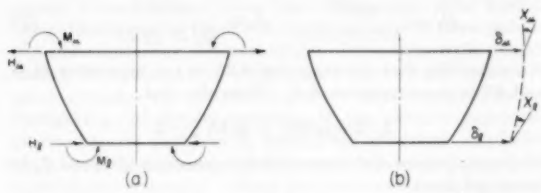

FIG. 3

$$\left.\begin{aligned} \delta_u^*/fl_A &= 2G_2M_l^* - \frac{1}{2}J_2M_u^* + G_1l_AH_l^* + \frac{1}{2}J_1l_AH_u^* \\ \chi_u^*/f &= -2G_2M_l^* + J_2M_u^* - 2G_2l_AH_l^* - \frac{1}{2}J_2l_AH_u^* \\ \delta_l^*/fl_A &= -\frac{1}{2}J_2M_l^* + 2G_2M_u^* - \frac{1}{2}J_1l_AH_l^* - G_1l_AH_u^* \\ \chi_l^*/f &= -J_2M_l^* + 2G_2M_u^* - \frac{1}{2}J_2l_AH_l^* - 2G_2l_AH_u^* \end{aligned}\right\} \quad [25a]$$

and

$$\left.\begin{aligned} \epsilon M_u^*/l_A &= -4G_2\delta_l^* + J_2\delta_u^* + 2G_1l_A\chi_l^* + J_1l_A\chi_u^* \\ \epsilon H_u^* &= -4G_2\delta_l^* + 2J_2\delta_u^* + 4G_2l_A\chi_l^* + J_2l_A\chi_u^* \\ \epsilon M_l^*/l_A &= J_2\delta_l^* - 4G_2\delta_u^* - J_1l_A\chi_l^* - 2G_1l_A\chi_u^* \\ \epsilon H_l^* &= -2J_2\delta_l^* + 4G_2\delta_u^* + J_2l_A\chi_l^* + 4G_2l_A\chi_u^* \end{aligned}\right\} \quad [25b]$$

As specific examples we cite the short shell subject (a) to symmetrical edge shear (tensile load)

$$H_u^* = -H_l^* = \frac{1}{2} \quad \ldots [26a]$$

and (b) to antisymmetric edge shear (bending load)

$$H_u^* = H_l^* = -\frac{1}{2} \quad \ldots [27a]$$

From Formulas [25] and [22] we find that in the first case

$$\left.\begin{aligned} \delta^*(\pm N) &= \epsilon\left(\frac{1}{2}J_1 - G_1\right) = \epsilon\dagger\left(1 + \frac{8}{15}N^4 + \ldots\right) \\ \delta^*(0) &= \epsilon\frac{g_4(N)g_4(0) + g_2(N)g_2(0)}{j_2(2N)} = \epsilon\dagger\left(1 - \frac{3}{10}N^4 + \ldots\right) \end{aligned}\right\} \quad [26b]$$

and in the second case

$$\left.\begin{aligned} \chi^*(\pm N) &= \frac{1}{2}fl_A\left(\frac{1}{2}J_2 + 2G_2\right) = f\dagger L_A\dagger\left(1 + \frac{4}{35}N^4 + \ldots\right) \\ \chi^*(0) &= \frac{1}{2}fl_A\frac{g_3(N)g_4(0) + g_1(N)g_2(0)}{j_1(2N)} = f\dagger L_A\dagger\left(1 - \frac{11}{210}N^4 + \ldots\right) \end{aligned}\right\} \quad [27b]$$

where

$$\left.\begin{aligned} \epsilon\dagger &\equiv \epsilon/4N = l^4\sin^2\varphi_0/8D_bL\dagger = r_a^2/2L\dagger h_bE \\ f\dagger &\equiv 3f/8N^3 = 3\epsilon\dagger/L_A\dagger^2 \end{aligned}\right\} \quad [28a, b]$$

The latter parameters reduce to the familiar formulas of ring expansivity and flexibility, equations [22] of reference (10), when $\varphi = \pi/2$, h = const. Formulas [26b], [27b] reveal that $N \sim 1/2$ forms the approximate demarcation line between ring and short shell. One is also led to Formulas [28a, b] by determining, by Equation [10], the displacement δ^* and rotation χ^* (constant throughout the short shell) caused by the distributed pressure loading

$$p^* = \sin\varphi_0/2L\dagger \quad \ldots [29a]$$

and distributed moment loading

$$p^* = -3n\sin\varphi_0/2NL\dagger \quad \ldots [29b]$$

respectively.

5 Redundant Shell Structures

Equations [22] to [25] give explicit expressions for the displacement, rotation, moment, and force distributions in a short shell under given self-equilibrating axisymmetric edge conditions.[10] The formulas reduce the problem of a redundant shell structure—such as two concentric conical shells joined by plates on top and bottom, as illustrated in Fig. 4 (a torus of quadrilateral cross section)—to one solving simultaneous linear equations for the unknown reactions. The steps involved are quite similar to framework analysis. The important role played by axial elongation of the shells, however, should be noted. Two interesting applications are discussed in reference (11). Another important application of the present results pertains, as mentioned already, to a flanged shell with a tapered hub.

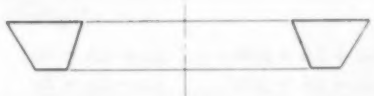

FIG. 4

It is well to point out again the limitations of the present approach. The angle φ should be greater than $\pi/4$ and less than $3\pi/4$ (and completely dependable results can be expected only in the range $\pi/3$ to $2\pi/3$); h, r, and p should vary but slowly with x, and h/r should be small; the shells and the applied loads alike are supposed to be axisymmetric.

When the shell length is greater than $3l$, the analysis of a redundant shell structure becomes simpler than the analysis of a corresponding framework, because the effects of self-equilibrating loads applied at one shell end are not transmitted to the other end. ($N \sim 3/2$ is the approximate demarcation line between

[10] The case of an edge subject to loads with a resultant force in the axial direction can be treated as the sum of two problems—the first is elementary (it is due to N_x loading), and the second is that due to H loading.

short shell and long shell.) In such a case we analyze each end of the shell separately for edge effects, using the values of l, f, ϵ appropriate to that end. Instead of dealing with four parameters, M_o, M_l, H_o, H_l, we now need to deal with only the loads M_0, H_0 applied at the reference cross section (these were denoted by $\mathfrak{M}$ and $\mathfrak{K}$ in reference 1). Equations [10] of reference (1) apply at once; one must only replace unstarred quantities by starred quantities, in accordance with the present Equations [11], and define n by the present Equation [8].

Appendix

The Functions g_k, j_k

We define

$$\left.\begin{aligned} g_1(n) &= \cosh n \sin n - \sinh n \cos n \\ g_2(n) &= \sinh n \sin n \\ g_3(n) &= \cosh n \sin n + \sinh n \cos n \\ g_4(n) &= \cosh n \cos n \end{aligned}\right\} \quad \ldots\ldots [30a]$$

$$\left.\begin{aligned} j_1(n) &= \sinh n - \sin n \\ j_2(n) &= \cosh n - \cos n \\ j_3(n) &= \sinh n + \sin n \\ j_4(n) &= \cosh n + \cos n \end{aligned}\right\} \quad \ldots\ldots\ldots [30b]$$

These functions are related by the formulas

$$g_1' = 2g_2, \quad g_2' = g_3, \quad g_3' = 2g_4, \quad g_4' = -g_1 \ldots [31a]$$

$$j_1' = j_3, \quad j_2' = j_4, \quad j_3' = j_1, \quad j_4' = j_2 \ldots [31b]$$

and the identities (the argument of a function in Equations [32] is n, unless otherwise indicated)

$$\left.\begin{aligned} g_3g_4 + g_1g_2 &= \tfrac{1}{2} j_3(2n) & g_3g_4 - g_1g_2 &= \tfrac{1}{2} g_3(2n) \\ g_2g_3 + g_4g_1 &= \tfrac{1}{2} g_1(2n) & g_2g_3 - g_4g_1 &= \tfrac{1}{2} j_1(2n) \\ g_3^2 + g_1^2 &= j_3(2n) & g_3^2 - g_1^2 &= g_2(2n) \\ g_4^2 + g_2^2 &= \tfrac{1}{2} j_4(2n) & g_4^2 - g_2^2 &= \tfrac{1}{2} + \tfrac{1}{2} g_4(2n) \\ j_3j_4 + j_1j_2 &= j_3(2n) & j_3j_4 - j_1j_2 &= 2g_3 \\ j_2j_3 + j_4j_1 &= j_1(2n) & j_2j_3 - j_4j_1 &= 2g_1 \\ j_3^2 + j_1^2 &= j_2(2n) & j_3^2 - j_1^2 &= 4g_2 \\ j_4^2 + j_2^2 &= 2 + j_4(2n) & j_4^2 - j_2^2 &= 4g_4 \\ &= 4 + 2j_1j_3 \end{aligned}\right\} \ldots [32]$$

The functions g_k are tabulated in the out-of-print book of Hohenemser-Prager (12) and are plotted in the book of Collatz (13).

The leading terms of the power-series expansions of g_1, j_1, and $(j_4 - 2)^{-1}$ are as follows

$$\left.\begin{aligned} g_1(n) &= \frac{2n^3}{3} - \frac{n^7}{315} + \frac{n^{11}}{623{,}700} \cdots \\ j_1(n) &= \frac{n^3}{3} + \frac{n^7}{2520} + \frac{n^{11}}{19{,}958{,}400} \cdots \\ \frac{1}{j_4(n) - 2} &= \frac{12}{n^4} - \frac{1}{140} + \frac{17n^4}{4{,}656{,}960} \cdots \end{aligned}\right\} \ldots [33]$$

The expansions of $g_2, \ldots, j_4$ may be determined by Equations [31]. In Equations [25a], [25b] we made use of the expressions

$$G_k \equiv \frac{g_k(2N)}{2j_1(2N)j_3(2N)}, \quad J_k \equiv \frac{j_k(4N)}{2j_1(2N)j_3(2N)} \ldots\ldots [34]$$

Note carefully that the argument is $2N$ in the numerator of G_k and $4N$ in the numerator of J_k. Note also that

$$2j_1(2N)j_3(2N) = j_4(4N) - 2$$

The leading terms of the power-series expressions of G_k and J_k are listed as follows

$$\left.\begin{aligned} 4NG_1 &= 1 - 0.228571N^4 + 0.032162N^8 \ldots \\ 16N^2G_2/3 &= 1 - 0.330159N^4 + 0.049284N^8 \ldots \\ 16N^2G_3/3 &= 1 - 0.685714N^4 + 0.112494N^8 \ldots \\ NJ_1 &= 1 + 0.152381N^4 - 0.016653N^8 \ldots \\ 4N^2J_2/3 &= 1 + 0.558730N^4 - 0.052304N^8 \ldots \\ 8N^3J_3/3 &= 1 + 1.980952N^4 - 0.124543N^8 \ldots \end{aligned}\right\} \ldots [35]$$

BIBLIOGRAPHY

1 "Membrane and Bending Analysis of Axisymmetrically Loaded Axisymmetrical Shells," by G. Horvay and I. M. Clausen, Journal of Applied Mechanics, Trans. ASME, vol. 77, 1955, p. 25.

2 "Development of General Formulas for Bolted Flanges," by E. O. Waters, D. B. Rossheim, D. B. Wesstrom, F. S. G. Williams, printed through the courtesy of Taylor Forge & Pipe Works, Chicago, Ill., 1949.

3 "The Strength Distribution in the Head of a Thin-Walled Pressure Vessel," by H. B. Fergusson, J. Kudar, R. B. Harvey, *Quarterly Journal of Mechanics and Applied Mathematics*, vol. 6, 1953, p. 1.

4 "A Numerical Procedure for the Analysis of Pressure Vessel Heads," by T. Au, L. E. Goodman, N. M. Newmark, University of Illinois Technical Report to ONR, 1951.

5 "Report on the Design of Pressure Vessel Heads," by Design Division of the PVRC, *Welding Journal*, Research Supplement, 1953.

6 "The Basic Elastic Theory of Vessel Heads Under Internal Pressure," by G. W. Watts and W. R. Burrows, Journal of Applied Mechanics, Trans. ASME, vol. 71, 1949, pp. 55–73.

7 "On Asymptotic Integration in Shell Theory," by F. B. Hildebrand, Proceedings of Symposia in Applied Mathematics, McGraw-Hill Book Company, Inc., New York, N. Y., vol. 3, 1950.

8 "Beams on Elastic Foundation," by M. Hetényi, University of Michigan Press, Ann Arbor, Mich., 1946.

9 "On the Theory of Thin Elastic Shells," by E. Reissner, Reissner Anniversary Volume, J. W. Edwards, Ann Arbor, Mich., 1949, p. 231.

10 "Stresses and Deformations of Flanged Shells," by G. Horvay and I. M. Clausen, Jr., Journal of Applied Mechanics, Trans. ASME, vol. 76, 1954, pp. 109–116.

11 "Torus-Type Shell Structures," by G. Horvay, R. L. Mathews, and J. Zickel, to be published.

12 "Dynamik der Stabwerke," by K. Hohenemser and W. Prager, Berlin, Germany, 1933.

13 "Eigenwertaufgaben," by L. Collatz, Akad. Verlagsgesellschaft, Leipzig, 1949.

Displacements in an Elastic-Plastic Cylindrical Shell[1]

By P. G. HODGE, JR.,[2] BROOKLYN, N. Y.

A reinforced cylindrical shell which is loaded with a uniform excess external radial pressure can support a load considerably greater than the elastic limit. While several recent investigations have been concerned with finding the collapse load of the shell, no attention has been paid to the corresponding deformations. Although rigid-plastic theory is sufficient to determine the collapse load, the more complex elastic-plastic theory must be used in investigating the displacements. In the present paper the elastic-plastic problem is stated for an ideal sandwich shell, and the stresses and deformations are computed for a particular example. Since the computations are found to be quite laborious, an approximate technique, applicable to all shells, is developed. The paper closes with some comments on the relation between the theoretical results and the behavior to be expected in real shells.

Introduction

SEVERAL recently published papers (1, 2, 3)[3] have been concerned with the analysis of rigid-plastic cylindrical shells. While such an analysis is considerably simpler than that of elastic-plastic shells, it provides no information at all concerning the displacements to be expected in a shell made of a more realistic material. It is conceivable that under certain conditions these deformations would become excessively large even though the collapse load had not been reached. A simple example of this phenomenon in the case of beams was analyzed in (4).

The present paper is concerned with the elastic-plastic analysis of a thin-walled circular cylindrical shell supported at either end by a rigid reinforcing ring, Fig. 1. The shell is loaded by an excess external radial pressure p and is free from end load. The resulting analysis obviously will be applicable to a typical bay of a long shell with several equally spaced reinforcing rings.

The cross section of the shell will be taken as an idealized sandwich of three layers. The two outer faces are indefinitely thin and can carry finite membrane stresses, but no bending moments. The center layer has finite thickness, carries no bending or membrane stresses, but can transmit any desired shear. Each layer is assumed to be incompressible (Poisson's ratio equals one

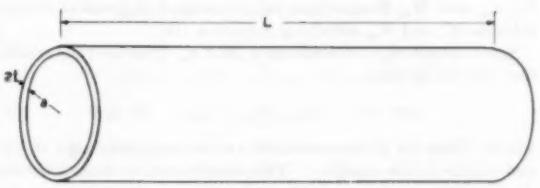

Fig. 1 Cylindrical Shell

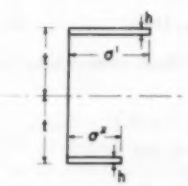

Fig. 2 Cross Section of Shell Wall

half). Since the two outer faces may carry different membrane stresses, the shell as a whole carries both membrane and bending stresses.

If the excess external pressure is slowly increased from zero, a typical section of the shell would, in general, pass through three stages; fully elastic, elastic-plastic, and fully plastic. For the ideal sandwich shell, however, under the particular loading here considered, it will be shown that both faces of the shell become plastic simultaneously; so that there is no elastic-plastic stage. Thus each element will either be elastic and governed by Hooke's law, or will be plastic. In the latter case it will be assumed to satisfy Tresca's (maximum shearing stress) yield condition without work hardening and the plastic potential stress-strain law.

The basic equations which define the problem will be collected in the next section and expressed in terms of dimensionless variables. A particular example will then be worked out in detail, carrying the analysis to 98 per cent of the yield load. In the following section an approximate method will be developed and a general expression for the maximum displacement of any shell obtained. Finally, certain conclusions concerning the relation of the solution of the idealized problem here considered to various real problems will be drawn.

Basic Equations

It will be assumed that the relative order of magnitude of various quantities is the same in this elastic-plastic problem as in the classical elastic problem. In the spirit of thin-shell theory, then, the state of stress in the shell is fully described by axial and circumferential tension and moment resultants and by a radial shear resultant. In the absence of end load the axial force will vanish

$$N_x = 0 \qquad [1a]$$

and the remaining resultants must satisfy two equilibrium relations which may be written (5)

$$d^2 M_x/dx^2 + N_\varphi/a + p = 0 \qquad [1b]$$

$$Q_x = d M_x/dx \qquad [1c]$$

In an elastic portion of the shell, these equations must be supplemented by two stress-strain relations furnished by Hooke's

---

[1] The results presented in this paper were obtained in the course of research conducted under Contract Nonr-267(00) with the Office of Naval Research.

[2] Associate Professor of Applied Mechanics, Department of Aeronautical Engineering, Polytechnic Institute of Brooklyn. Mem. ASME.

[3] Numbers in parentheses refer to the Bibliography at the end of the paper.

Contributed by the Applied Mechanics Division and presented at the Diamond Jubilee Annual Meeting, Chicago, Ill., November 13–18, 1955, of The American Society of Mechanical Engineers.

Discussion of this paper should be addressed to the Secretary, ASME, 29 West 39th Street, New York, N. Y., and will be accepted until April 10, 1956, for publication at a later date. Discussion received after the closing date will be returned.

Note: Statements and opinions advanced in papers are to be understood as individual expressions of their authors and not those of the Society. Manuscript received by ASME Applied Mechanics Division, October 13, 1954. Paper No. 55—A-4.

law. For an incompressible material, one of these relations furnishes the result (5)

$$M_\varphi = M_x/2 \quad \ldots\ldots [1d]$$

Since Equation [1*d*] holds until the onset of plastic behavior and since there is nothing in the plastic relations to predict a change in the value of M_φ, Equation [1*d*] may be taken to hold throughout. Therefore, if Equations [1*a*], [1*c*], [1*d*] are taken as defining N_x, Q_x, and M_φ, the problem may be stated in terms of the resultants M_x and N_φ, satisfying Equation [1*b*].

Since the principal stresses are σ_x and σ_φ, Tresca's yield condition may be written

$$\max\,[|\sigma_x|,\ |\sigma_\varphi|,\ |\sigma_x - \sigma_\varphi|] - 2k \leq 0 \quad \ldots\ldots [2]$$

Elastic behavior is characterized by the inequality sign in [2] and plastic, by the equality. This condition must be satisfied by the membrane stresses $\sigma_x{}^1$, $\sigma_\varphi{}^1$ in the top face and stresses $\sigma_x{}^2$, $\sigma_\varphi{}^2$ in the bottom face of the shell. In terms of reduced stress resultants defined by

$$m = M_x/4kht,\ n = N_\varphi/4kh \quad \ldots\ldots [3a]$$

where k is the yield stress in pure shear, these stresses may be written (3)

$$\left.\begin{aligned} \sigma_x{}^1 &= -2mk, \quad \sigma_\varphi{}^1 = (2n - m)k \\ \sigma_x{}^2 &= +2mk, \quad \sigma_\varphi{}^2 = (2n + m)k \end{aligned}\right\} \quad \ldots\ldots [3b]$$

The resulting stress distribution is symbolically pictured in Fig. 3.

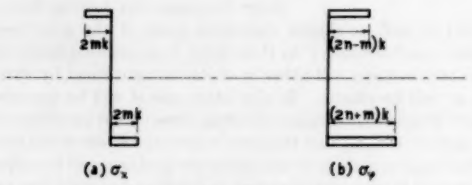

FIG. 3 STRESS DISTRIBUTION IN SHELL

It is now easy to justify the previous assertion that an element of the shell passes directly from the fully elastic to the fully plastic state. For the ideal shell here considered, the only alternative is that one face is plastic and the other elastic. However, if the top face is plastic, it follows from Expressions [2] and the first line of [3*b*] that at least one of

$$-2mk = \pm 2k,\ (2n-m)k = \pm 2k,\ \ (-2n-m)k = \pm 2k \quad [4]$$

must hold. Comparison with the second line of Equations [3*b*] then shows that in each case the bottom face is also plastic. Therefore there is no elastic-plastic state.

At a fully elastic element, Hooke's law must apply. If u and w represent the axial and inward radial displacements, respectively, of the center surface, the strains in the two faces are given by

$$\left.\begin{matrix} \epsilon_x{}^1 \\ \epsilon_x{}^2 \end{matrix}\right\} = \frac{du}{dx} \pm t\,\frac{d^2w}{dx^2}, \quad \left.\begin{matrix} \epsilon_\varphi{}^1 \\ \epsilon_\varphi{}^2 \end{matrix}\right\} = -\frac{w}{a}$$

where t/a is neglected in comparison with one. The substitution of these equations together with Equations [3] into Hooke's law

$$\sigma_x = (2E/3)(2\epsilon_x + \epsilon_\varphi), \quad \sigma_\varphi = (2E/3)(2\epsilon_\varphi + \epsilon_x)$$

leads finally to

$$\left.\begin{aligned} du/dx &= w/2a, \quad n = -(E/2k)(w/a) \\ m &= -(2E/3k)\,td^2w/dx^2 \end{aligned}\right\} \quad \ldots\ldots [5]$$

It is convenient to introduce further dimensionless quantities defined by

$$y = x/L, \quad W = (E/2k)w/a, \quad c = L/\sqrt{2at}, \quad P = pa/4kh \quad \ldots\ldots [6]$$

The substitution of Equations [3*a*] and [6] into Equations [5] and [1*b*] then leads to

$$n = -W,\ m = -(2/3c^2)W'' \quad \ldots\ldots [7]$$

$$m''/2c^2 + n + P = 0 \quad \ldots\ldots [8]$$

where primes indicate differentiation with respect to y. Equations [7] and [8] define the stresses and displacement in an elastic portion of the shell and lead to the well-known solution

$$W = C_1 \cosh dy \cos dy + C_2 \sinh dy \sin dy + C_3 \cosh dy \sin dy + C_4 \sinh dy \cos dy + P \quad \ldots\ldots [9]$$

where

$$d = \sqrt[4]{3/4}\,c \quad \ldots\ldots [10]$$

A fully plastic section is characterized by one of the six Equations [2]. These may be conveniently represented by a yield polygon in a stress-resultant space with co-ordinates n, m, Fig. 4. Although the plastic problem is statically determinate in

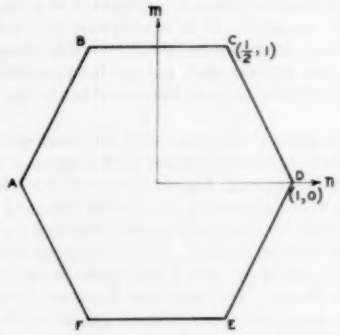

FIG. 4 YIELD POLYGON

the sense that there exist two equations to determine m and n, some of the boundary and continuity conditions are given in terms of the displacement W. Therefore it is necessary to introduce the stress-strain law.

In general, the total strain of a plastic element can be divided into an elastic component ϵ^e and a plastic component ϵ^p. The elastic part is still given by Hooke's law, while the plastic part must satisfy the plastic potential law. As used in (3), this may be most simply stated by the requirement that the plastic strain-rate vector, defined by

$$\dot{\mathbf{E}}_p = (-\dot{W}_p,\ -\dot{W}_p''/2c^2)$$

be normal and directed outward to the yield polygon at each point with a unique tangent and lie between the two defined limiting normals at a corner. The resulting equations for the plastic regimes of interest in the present problem are indicated in

Table 1. The parameters $\dot{\lambda}$, $\dot{\mu}$, $\dot{\nu}$, $\dot{\rho}$ represent the length of the vector and must be positive, but are otherwise arbitrary.

TABLE 1 EQUATIONS FOR PLASTIC REGIMES

Plastic regime	Stress relations	Velocity relations
EF	$-m = 1$	$\dot{W}_p = 0,\ \dot{W}_p'' = 2c^2\dot{\rho}$
F	$-2n - 1, -m = 1$	$\dot{W}_p = 2\dot{\lambda},\ \dot{W}_p'' = 2c^2(\dot{\lambda} + \dot{\nu})$
FA	$-2n - m = 2$	$\dot{W}_p = 2\dot{\lambda},\ \dot{W}_p'' = 2c^2\dot{\lambda}$
A	$-n = 1,\ m = 0$	$\dot{W}_p = 2\dot{\lambda} + 2\dot{\mu},\ \dot{W}_p'' = 2c^2(\dot{\lambda} - \dot{\mu})$
AB	$-2n + m = 2$	$\dot{W}_p = 2\dot{\mu},\ \dot{W}_p'' = -2c^2\dot{\mu}$
B	$-2n = 1,\ m = 1$	$\dot{W}_p = 2\dot{\mu},\ \dot{W}_p'' = -2c^2(\dot{\rho} + \dot{\mu})$
BC	$m = 1$	$\dot{W}_p = 0,\ \dot{W}_p'' = -2c^2\dot{\rho}$

The complete plastic stress-strain law may then be written

$$\dot{\mathbf{E}} = \dot{\mathbf{E}}_e + \dot{\mathbf{E}}_p = (-\dot{W}_e, -\dot{W}_e''/2c^2) + (-\dot{W}_p, -\dot{W}_p/2c^2) \quad \ldots\ldots[11]$$

where $\dot{\mathbf{E}}_e$ is given by Equations [7] and $\dot{\mathbf{E}}_p$ by Table 1. With Equation [8], this now determines the plastic solution.

The method of solution may be illustrated with reference to plastic regime AB. The substitution of the stress equation from line 5 of Table 1 into Equation [8] leads to

$$m = 2(A_1 \cos cy + A_2 \sin cy - P + 1) \quad \ldots\ldots[12a]$$

$$n = A_1 \cos cy + A_2 \sin cy - P$$

where A_1 and A_2 are constant in space but may vary with time Equations [11] and [7] and Table 1 then state that

$$\dot{\mathbf{E}} = (-\dot{W}, -\dot{W}''/2c^2) = (\dot{n}, 3\dot{m}/4) + \dot{\mu}(-2, 1)$$

This vector equation is equivalent to two scalar equations. The elimination of $\dot{\mu}$ between these equations and the use of Equations [12] leads to

$$\dot{W}''/c^2 + \dot{W} = -4(\dot{A}_1 \cos cy + \dot{A}_2 \sin cy - \dot{P})$$

If this equation is solved for $\dot{W}$ and then integrated with respect to time the result

$$W = (A_3 + 2cA_2y)\cos cy + (A_4 - 2cA_1y)\sin cy + 4P + f(y) \quad \ldots\ldots[12b]$$

is obtained where the A_k are all functions of time only and f depends only upon y.

Similarly, on plastic regime FA, it may be shown that

$$\left.\begin{aligned} m &= -2(B_1 \cosh cy + B_2 \sinh cy - P + 1) \\ n &= (B_1 \cosh cy + B_2 \sinh cy - P) \\ W &= (B_3 + 2cB_2y)\cosh cy + (B_4 + 2cB_1y)\sinh cy + 4P + g(y) \end{aligned}\right\} \quad \ldots[13]$$

It turns out that AB and FA are the only plastic regimes required for the problem to be considered.

The complete solution to the elastic-plastic problem now reduces to a suitable combination and determination of the constants of Equations [9], [12], and [13]. To this end it is necessary to consider the boundary and continuity conditions. At an elastic section direct stress, moment, shear, displacement, slope, and curvature must all be continuous and, in general, this is also true at an elastic-plastic boundary or in a plastic region. However, for a stress point in plastic regime B, BC, F, or EF, Table 1 shows that the curvature can become infinite with the displacement remaining finite. Such a point will be called a hinge circle, since a finite rotation is permissible. Thus the continuity conditions require that

$$\left.\begin{aligned} &n, m, m', W \text{ continuous} \\ \text{either } &W', W'' \text{ continuous or } m = \pm 1 \end{aligned}\right\} \quad \ldots[14]$$

The boundary conditions may be regarded as a special case of the continuity conditions. If the co-ordinate origin is taken at the center of the shell then symmetry at the center and the rigid supports at the ends lead to

$$\left.\begin{aligned} &m'(0) = 0 \\ \text{either } &W'(0) = 0 \text{ or } m(0) = +1 \end{aligned}\right\} \quad \ldots\ldots[15]$$

$$\left.\begin{aligned} &W(1) = 0 \\ \text{either } &W'(1) = 0 \text{ or } m(1) = -1 \end{aligned}\right\} \quad \ldots\ldots[16]$$

Example

If the load on the shell is sufficiently small, the shell will be entirely elastic. The solution in this case is well known and assumes a particularly simple form if $d = \pi/2$ ($c = 1.69$). This example will now be considered in detail

$$\left.\begin{aligned} -n = W &= -P \operatorname{csch} \pi/2\,[\cosh \pi y/2 \cos \pi y/2 + \sinh \pi y/2 \sin \pi y/2] + P \\ m &= (2/\sqrt{3})P \operatorname{csch} \pi/2\,[\cosh \pi y/2 \cos \pi y/2 - \sinh \pi y/2 \sin \pi y/2] \end{aligned}\right\} \quad \ldots[17]$$

Equations [17] will remain valid as long as the stress point with co-ordinates n, m lies everywhere within the yield polygon, Fig. 4. The proceedings at this point are facilitated by plotting the stress profile, i.e., the image curve of the stress state of the shell in the n, m-plane. The stress profile for $P = 0.5$ is shown in Fig. 5. The plotted points on each of the curves in Fig. 5 correspond to the stress resultants at the points $y = 0.1, 0.2,$

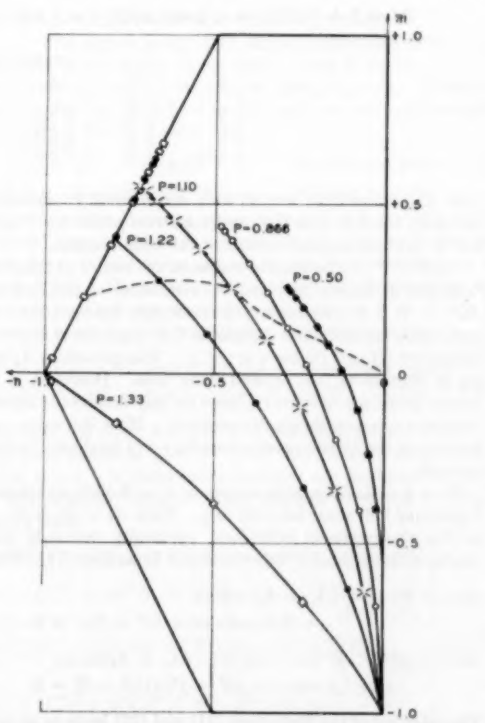

Fig. 5 Stress Profiles for $d = \pi/2$ Under Various Loads

..., 1.0 in the shell, and the various curves correspond to various values of the load P.

Since in the fully elastic range an increase in the load will change only the size of the stress profile and not its shape, it is evident from Fig. 5 that the shell will first become plastic at the end support $y = 1$. The maximum elastic load P^* can therefore be determined by setting $m(1) = -1$ in Equations [18] and solving for P

$$P^* = \sqrt{3}/2 = 0.866 \ldots\ldots\ldots\ldots [18]$$

If the pressure is slowly increased to a value greater than P^*, the resulting solution must be obtainable by a continuous transition from Equations [17]. After some consideration of the possible alternatives, it is seen that the plastic region at $y = 1$ does not spread, but is concentrated in a hinge circle. Therefore, during this second stage, the shell is everywhere elastic but the boundary condition of zero slope at $y = 1$ is to be replaced by the condition of minimum moment. The resulting solution is

$$\left.\begin{aligned} -n = W = -\operatorname{csch} \pi/2[(\sqrt{3}/2)\cosh \pi y/2 \cos \pi y/2 \\ - P \sinh \pi y/2 \sin \pi y/2] + P \\ m = \operatorname{csch} \pi/2[2P/\sqrt{3}\cosh \pi y/2 \cos \pi y/2 \\ - \sinh \pi y/2 \sin \pi y/2] \end{aligned}\right\} \ldots [19]$$

Equations [19] will remain valid until the stress profile touches the yield polygon at an additional point. Although the growth of the stress profile can no longer be predicted by inspection, it appears likely that this will happen when the end corresponding to $y = 0$ touches the side AB. The substitution of Equations [19] into the relation $m(0) - 2n(0) = 2$ shows that the corresponding load is

$$P' = 1 + (1/2)[1 + \sqrt{3}\sinh \pi/2]^{-1} = 1.100 \ldots [20]$$

That Equations [19] are, in fact, valid until P reaches P' is shown by the fact that the resulting stress profile for $P = 1.100$, Fig. 5, nowhere extends outside of the yield polygon.

For $P > P'$, an increasing region of the center of the shell will lie in plastic regime AB, and the remainder of the shell will be elastic. If $y = u$ represents the boundary between these elastic and plastic regions, then Equations [12] apply for $0 < y < u$ and Equations [7] and [9] for $u < y < 1$. The quantities A_k appearing in Equations [12] depend upon time. However, it is well known that time may be replaced by any monotonic function of time in a quasi-static plastic problem. Here the value u of the position of the elastic-plastic boundary will be chosen as the time variable.

Since the plastic region centers at $y = 0$ with no hinge circle, Equations [12] must be even in y. Thus $A_2 = A_4 = 0$. Next, at the elastic-plastic boundary, continuity demands that the plastic solution must satisfy the elastic Equations [7]. Therefore

$$n(u) + W(u) = (A_1 + A_3)\cos cu - 2cA_1 u \sin cu + 3P + f(u) = 0 \ldots\ldots [21]$$

$$m(u) + (2/3c^2)W''(u) = (2/3)[-(A_1 + A_3)\cos cu + 2cA_1 u \sin cu - 3P + f''(u)/c^2 + 3] = 0 \ldots\ldots [22]$$

The addition of the Equations [21] and [22] leads to an ordinary differential equation in $f(u)$ whose solution is

$$f(u) = a_1 \cos cu + a_2 \sin cu - 3 \ldots\ldots\ldots [23]$$

Since u increases from zero as the load is increased, Equation [23] gives the functional form of f for all $0 < y < u$. Since $a_2 = 0$ by symmetry and a_1 may be absorbed in the arbitrary function A_3, the particular solution $f(y) = -3$ is desired.

With $f(y)$ known, it is now a straightforward procedure to determine the remaining unknown functions of u. If A_3 is eliminated by means of the second independent relation inherent in Equations [22], and the conditions $W(1) = 0$, $m(1) = -1$ are used to determine C_3 and C_4 in Equations [11], the resulting solution may be written

$$\left.\begin{aligned} 0 < y < u\text{:}\quad W = [A_1(2cu\tan cu - 1) - 3(P-1)\sec cu] \\ \cos cy - 2cA_1 y \sin cy + 4P - 3 \\ m = 2(A_1 \cos cy - P + 1),\ n = A_1 \cos cy - P \\ u < y < 1\text{:}\ W = C_1 \cosh \pi y/2 \cos \pi y/2 + C_2 \sinh \pi y/2 \\ \sin \pi y/2 - [C_2 \tanh \pi/2 + P \operatorname{sech} \pi/2]\cosh \pi y/2 \\ \sin \pi y/2 - [C_1 \tanh \pi/2 + (\sqrt{3}/2)\operatorname{sech} \pi/2] \\ \sinh \pi y/2 \cos \pi y/2 + P \\ n = -W,\ m = -4/(\sqrt{3}\pi^2)W'' \\ c = \sqrt[4]{4/3}(\pi/2) = 1.69 \end{aligned}\right\} \ldots [24]$$

At $y = u$, the six continuity Conditions [14] must be satisfied. However, in view of Equations [21] and [22], two of these are no longer independent; and it is sufficient to demand continuity of W', n, m, m'. This will result in four linear algebraic equations which can be solved for A_1, C_1, C_2, and P as functions of u.

While the general solution of any set of linear equations can be expressed by means of Cramer's rule there appears to be no advantage in so doing. Instead, values of u were specified and the equations solved for numerical values of the unknowns. The results are given in Table 2.

TABLE 2 NUMERICAL VALUES

u	P	A_1	C_1	C_2	n at $y = 0$	n at $y = u$
0	1.10	—	—	—	−0.72	−0.72
0.2	1.14	0.428	−0.349	−0.503	−0.71	−0.74
0.4	1.22	0.539	−0.103	−0.628	−0.68	−0.80
0.6	1.31	0.655	+0.889	−1.155	−0.66	−0.97
0.625	1.33	0.666	+1.122	−1.292	−0.66	−0.997

For $P = 1.33$, the stress point $y = u$ is at point A on the yield polygon. As P increases still further, there will be two plastic regions corresponding to regimes AB and AF. While it is a simple matter to enumerate the necessary equations from the continuity and boundary conditions, their solution would be extremely difficult and laborious. However, an analysis of the plastic-rigid shell (3) shows that the collapse load for this case is $P = 1.36$; thus the preceding results are valid up to within 98 per cent of the collapse load.

For other values of d, still other difficulties can occur. For example, if $d = 2\pi$, it is readily verified that the stress profile "curls over" in such a way that a point a little away from the center becomes plastic while the center section of the shell is still elastic. Obviously, the analysis in this case becomes much more complex. For these reasons an approximate method for finding the center displacement just prior to collapse appears to be highly desirable, and such a method will be presented in the next section.

First, however, one may observe that for the example $d = \pi/2$, the complete stress picture (up to $P = 1.33$) is given in Fig. 5. Each curve represents the stress profile for a particular load, while the points on each curve represent the equal division points of the shell: $y = 0.0, 0.1, 0.2, \ldots, 1.0$. The stress history of a particular point on the shell can be found by connecting the corresponding points. The dashed curve shows the stress history

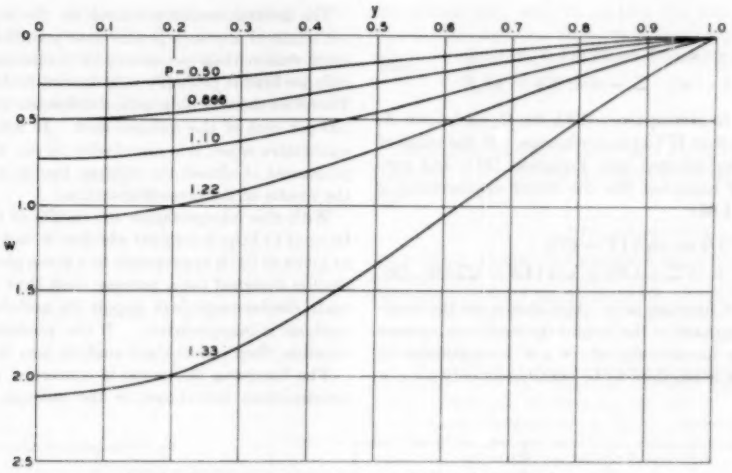

FIG. 6 DEFORMED SHAPE OF SHELL UNDER VARIOUS LOADS ($d = \pi/2$)

of the quarter point of the shell, $y = 0.5$. The corresponding displacements are shown in Fig. 6.

APPROXIMATE METHOD

The approximate method to be presented here presumes that the plastic-rigid problem has already been solved to determine the collapse load P^{**} and the final value of the point u which corresponds to the vertex A of the yield polygon. The details of this solution are given in (3) and the following equations defining $P = P^{**}$ and u are quoted from that reference.[4]

For $0 < c < 1.65$ $(0 < d < 1.54)$

$$P = 1 + (1/2)\cos cu/(1 - \cos cu) \quad [25]$$

$$\cos cu \cosh c(1-u) + \sin cu \sinh c(1-u) = 1 \quad [26]$$

For $1.65 < c$ $(1.54 < d)$

$$P = 1 + (1/2)/[2\cosh c(1-u) - 1] \quad [27]$$

$$\tan cu = \coth c(1-u) \quad [28]$$

The basic idea of the approximation is to neglect that part of the plastic deformation which occurs in plastic regime FA. Therefore the displacement will be computed as if the stress profile at collapse consisted of plastic regime AB for $0 < y < u$, and behaved elastically for $u < y < 1$. Since the values of u and P will be taken to be the collapse values, it will not, in general, be possible to satisfy all of the continuity conditions at $y = u$. Convenience suggests that continuity of shear and sometimes of slope be neglected.

The solution for $0 < y < u$ is given by Equations [12]. The conditions of zero shear at the center $[m'(0) = 1]$ and that u be at the point $A[m(u) = 0]$ show that

$$A_2 = 0, \quad A_1 = (P-1)/\cos cu$$

Next, the technique used in evaluating f in the previous section (see Equations [21] and [22]), yields the general result $f = -3$ and the relationship

$$A_3 \cos cu + A_4 \sin cu - 2(P-1)\, cu \tan cu + 4(P-1) = 0 \quad [29]$$

The plastic solution is thus given by

$$\left.\begin{aligned} m &= 2(P-1)(\cos cy/\cos cu - 1) \\ n &= (P-1)(\cos cy/\cos cu) - P \\ W &= A_3 \cos cy + [A_4 - 2(P-1)cy/\cos cu]\sin cy \\ &\quad + 4P - 3 \end{aligned}\right\} \quad [30]$$

where A_3 and A_4 must satisfy Equation [29]. In particular, the desired displacement at the center is given by

$$W(0) = A_3 + 4P - 3 \quad [31]$$

so that the problem reduces to the evaluation of A_3.

If $c > 1.65$ this is easily done, since in this case there is no hinge circle at the center of the shell. Thus $W'(0) = 0$, and it follows from the last Equation [30] that $A_4 = 0$. Therefore Equation [29] can be solved for A_3 and the result substituted into Equation [31] to furnish (for $c > 1.65$)

$$W(0) = 4P - 3 - 2(P-1)(2 - cu\tan cu)/\cos cu \quad [32]$$

Here P and u are defined by Equations [27] and [28].

For $0 < c < 1.65$, there is a hinge circle at $y = 0$, and the condition $W'(0)$ must be replaced by $m(0) = 1$. This condition can be solved for P and turns out to be merely a restatement of Equation [25]. Therefore it is necessary to use the complete elastic solution and the various continuities at $y = u$. It is convenient to express the general elastic solution in the form

$$W = \sin d(y-u)[C_1 \cosh d(y-u) + C_2 \sinh d(y-u)] + \sin d(1-y)[C_3 \cosh d(1-y) + C_4 \sinh d(1-y)] + P. \quad [33]$$

Since u is at the point A on the yield polygon, n must equal -1 and m must vanish at $y = u$. Also, at $y = 1$, W must vanish while $m = -1$. If these four conditions are expressed in terms of W and its second derivative, the resulting equations are easily solved to yield

$$\left.\begin{aligned} C_4 &= [C\Sigma(\Gamma - C)P/S + C^2\Sigma S + \sqrt{3}\,\Gamma^2/2]/(\Gamma^2 - C^2) \\ C_3 &= [-(C\Sigma^2 + S^2\Gamma)P/S + S\Gamma - \sqrt{3}\,\Gamma\Sigma/2]/(\Gamma^2 - C^2) \\ C_2 &= [C\Sigma(\Gamma - C)P/S - C\Gamma\Sigma/S - \sqrt{3}\,C\Gamma/2]/(\Gamma^2 - C^2) \\ C_1 &= [-(C\Sigma^2 + S^2\Gamma)P/S + C\,\Sigma^2/S + \sqrt{3}\,C\Sigma/2]/(\Gamma^2 - C^2) \end{aligned}\right\} \quad [34]$$

[4] See Equations [31], [32], [37b], [37c]. The notations are related by $u = 1 - y_0$.

Here the notations

$$\left.\begin{aligned} C &= \cos d(1-u), \quad S = \sin d(1-u) \\ \Gamma &= \cosh d(1-u), \quad \Sigma = \sinh d(1-u) \end{aligned}\right\} \quad \ldots\ldots [35]$$

have been introduced to save space. With the C_k all known A_3 may be determined so that $W'(u)$ is continuous. If the value of A_3 so determined is substituted into Equation [31], and convenient use is made of Equation [25] the center displacement is found to be $(0 < c < 1.65)$

$$W(0) = \cos cu + [\sqrt[4]{3/4} \sin cu/(\Gamma^2 - C^2)]$$
$$[P(\Gamma - C)(S - \Sigma) + (\Gamma\Sigma + CS) + \sqrt{3}\,(\Gamma S - C\Sigma)/2]\,. \quad [36]$$

Fig. 7 shows $W(0)$ as a function of c. Also shown are the maximum elastic values computed at the instant the shell first becomes plastic at $y = 1$. The discontinuity at $c = 1.65$ is explainable by the fact that the slope is required to be continuous only for $c < 1.65$.

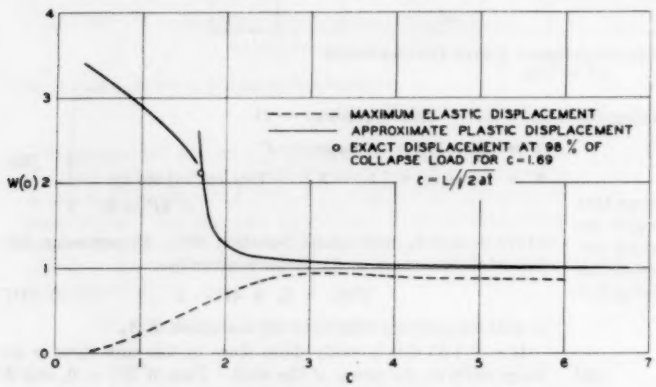
MAXIMUM ELASTIC DISPLACEMENT
APPROXIMATE PLASTIC DISPLACEMENT
o EXACT DISPLACEMENT AT 98 % OF COLLAPSE LOAD FOR c = 1.69
c = L/√2at
W(0)
c

FIG. 7 DISPLACEMENTS AT CENTER OF SHELL

DISCUSSION OF RESULTS

The foregoing analysis has given the exact solution for the displacements in a particular case and an approximate method for computing the maximum displacement for an arbitrary shell. In interpreting these results it is necessary to give some care to the precise meaning of the term "displacement at collapse." According to the theory of perfectly plastic solids, if the load is brought to its collapse value and maintained there, the displacements will increase indefinitely. Further, in problems which involve limiting stress discontinuities, such as torsion,[5] and also in other cases such as bending of beams,[6] the displacements tend to infinity as the load is slowly increased to collapse. Thus a literal interpretation of displacement at collapse is usually meaningless.

However, meaningful questions can be asked relating the collapse load and the displacement in terms of percentages. To this end Fig. 8 shows the ratio of the maximum displacement to the maximum elastic displacement as a function of the ratio of the load to the collapse load for the particular case $d = \pi/2$. One sees immediately that the maximum displacement at 98 per cent of the collapse load is less than 5 times the maximum elastic displacement. Alternatively, the load can reach about 89 per cent of the collapse load before the displacement is double the elastic displacement and 94 per cent before it is triple.

[5] Reference (7), chapter 3.
[6] Ibid., chapter 2.

The general results obtained by the approximate method do not admit of any such precise interpretation. However, if for no other reason than inaccuracy in measuring the yield stress, the collapse load is probably only known to within several per cent. Therefore there is no practical difference between 95 per cent and 100 per cent of the collapse load. It follows that, at least in a qualitative sense, it is permissible to say that the maximum displacement at almost the collapse load is approximately given by the results of the preceding section.

With this interpretation the results of the present paper may be used to help determine whether or not a plastic-rigid solution as given in (3) is appropriate to a given physical problem. If the shell is designed for a purpose such that the predicted approximate displacement will impair its usefulness, then plastic-rigid ana sis is inappropriate. If the predicted displacement is admissible, then plastic-rigid analysis may well be worth while.

The foregoing discussion is concerned primarily with the approximations introduced in the analysis. However, the basic

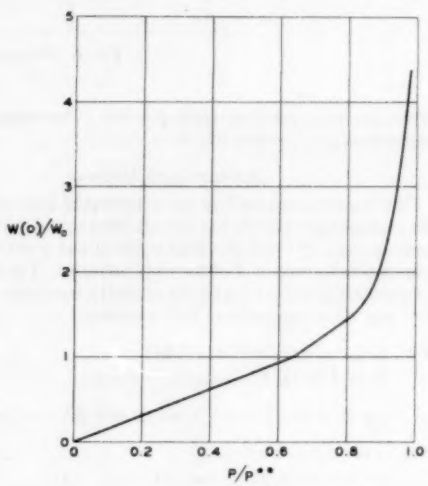

FIG. 8 ELASTIC-PLASTIC MAXIMUM DEFORMATION ($d = \pi/2$)

equations set up in the first part of the paper represent a considerable simplification of an actual cylindrical shell under excess pressure. It is also of interest to discuss the approximations which make up the basic theory.

First, if the material of the actual shell exhibits strain hardening, the analysis here presented will, of course, be conservative, in that the actual critical loads will be greater and the displacements less.

Concerning the use of the Tresca yield condition as opposed to some other type, little direct evidence is available. Hill (6) has given some examples where the predictions of the Tresca and Mises yield conditions showed considerable differences. However, in the present case the singular points (i.e. vertices) of the yield polygon do not figure prominently in the analysis and it would seem reasonable to expect only a slight smoothing of the results if a nonsingular yield condition were used.

The predicted magnitude of the displacements is certainly sufficiently small to justify the use of thin-shell small-deformation theory whenever t/a is reasonably small.

Finally, the relation between the ideal sandwich and a uniform shell may be considered. If the correspondence is such that the two shells have the same yield moment and force, the yield curve

will be as shown in Fig. 9. Since the sandwich-section yield curve (shown by the dashed line in Fig. 9) is everywhere inside the other, it follows from the first theorem of limit analysis that the collapse-load prediction will be conservative. However, the same will not necessarily be true of the deformations. Indeed,

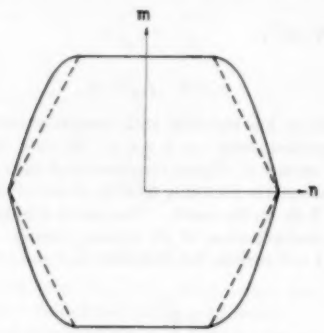

FIG. 9 YIELD CURVE FOR UNIFORM SECTION

since the uniform section becomes partially plastic under lower loads than it becomes fully plastic, and since the two sections are matched so as to give an equal full bending moment, it follows that the uniform section will be partially plastic under loads for which the sandwich section is fully elastic. Therefore the deformations may well be greater for the uniform section. Of course a conservative estimate of this factor could always be obtained by matching the maximum elastic moment of the uniform section with the ideal section.

ACKNOWLEDGMENT

The author wishes to thank Mr. Julian Gliksman-Felix for his assistance in computing the data for the tables and figures in this paper.

BIBLIOGRAPHY

1 "Limit Analysis of Cylindrical Shells Under Axially Symmetric Loading," by D. C. Drucker, Proceedings of the First Midwest Conference on Solid Mechanics, 1953, pp. 158–163.

2 "The Plastic Collapse of Cylindrical Shells Under Axially Symmetrical Loading," by E. T. Onat, *Quarterly of Applied Mathematics*, vol. 13, 1955, pp. 63–72.

3 "The Rigid-Plastic Analysis of Symmetrically Loaded Cylindrical Shells," by P. G. Hodge, Jr., JOURNAL OF APPLIED MECHANICS, Trans. ASME, vol. 76, 1954, pp. 336–342.

4 "Recent Progress in the Plastic Methods of Structural Analysis," by P. S. Symonds and B. G. Neal, *Journal of The Franklin Institute*, vol. 252, 1951, pp. 383–407, 469–492.

5 "Theory of Plates and Shells," by S. Timoshenko, McGraw-Hill Book Company, Inc., New York, N. Y., chapter 11.

6 Discussion by R. Hill in the JOURNAL OF APPLIED MECHANICS, Trans. ASME, vol. 76, 1954, p. 93, of "On the Use of Singular Yield Conditions and Associated Flow Rules," by W. Prager, JOURNAL OF APPLIED MECHANICS, Trans. ASME, vol. 75, 1953, pp. 317–320.

7 "Theory of Perfectly Plastic Solids," by W. Prager and P. G. Hodge, Jr., John Wiley & Sons, Inc., New York, N. Y., 1951.

Stress Concentration Caused by Multiple Punches and Cracks

By MICHAEL SADOWSKY,[1] TROY, N. Y.

The paper contains (*a*) a general theory of stress distribution under several punches in simultaneous action and of stress concentration caused by several cracks; (*b*) a complete evaluation for the case of two punches or two cracks. Considerable stress interference is found with punches (cracks) close to each other.

Nomenclature

The following nomenclature is used in the paper:

x, y = Cartesian co-ordinates
u, v = displacements in plane strain
$\sigma_x, \sigma_y, \tau_{xy}$ = Cartesian stress components in plane strain
G = shear modulus
ν = Poisson's ratio
sn, cn, dn = Jacobian elliptic functions
K, K', E, E' = complete elliptic integrals of the first and second kinds to moduli k and k'
P = force on a punch in plane strain (lb per in.)

History and Literature of Problem

The history of the punch problem dates back to 1881, since the Hertz solution of the contact problem (1, 2)[2] may be considered a precursor of the punch problems. The stress distribution under a single punch was determined in 1928 (3). A general theory was developed by Muskhelishvili (4) and first published in the Russian original treatise in 1933. The English translation (4) of Muskhelishvili's work appeared in 1953. An intensification of interest in the problem seems to manifest itself since about 1950, after the subject had become an accepted part of general expository books on elasticity; in (5) on a broad tensor basis prepared to go into finite strain; in (6) in the modern integral-transforms presentation; in (7) as a monograph of 264 pages. The affinity between punch and crack problems was recognized by Muskhelishvili (4) in 1933. In connection with the Griffith theory of fracture (8) crack problems with modified boundary conditions became prominent and have been solved (9).

Equivalence of Punch and Crack Problems

Fig. 1 shows the infinite xy-plane slit along the x-axis from $-\infty$ to $-a$ and from a to ∞. Stresses at infinity amount to two resultants pulling the upper and lower half-planes away from each other. The cuts are free from surface tractions, while the following is true for the segment $-a < x < a$ on the x-axis

$$v = 0, \quad \tau_{xy} = 0 \qquad [1]$$

These conditions are identical with boundary conditions for a semiplane punched along $-a < x < a$. In view of forthcoming mapping by means of elliptic functions and their integrals, we make the unusual (in punching figures) choice of the upper half-plane. Fig. 2 shows the result. The punch is pulling instead of pushing; a multiplication of all stresses, strains, and displacements by —1 will reverse the character and make it the pushing type.

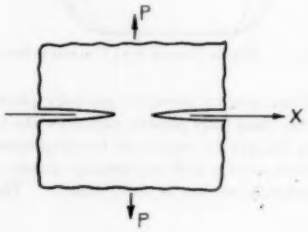

Fig. 1 Transition From Crack Interpretation to Punch Interpretation; Crack-Interpretation Stage

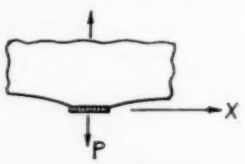

Fig. 2 Transition From Crack Interpretation to Punch Interpretation; Punch-Interpretation Stage

Inapplicability of Method of Superposition in Punch and Crack Problems

In a punch or crack problem, the boundary conditions on the x-axis are of mixed nature; on the entire axis $\tau_{xy} = 0$ is a common condition for both free and punched parts. Then, in addition, we have $\sigma_y = 0$ for free parts, v = const for punched parts. Should we superimpose two single-punch solutions (with punches not overlapping), we will have a variable v under the first punch contributed by the second-punch solution, and a variable v under the second punch contributed by the first-punch solution. The superposition will not represent any punch problem at all. As crack problems are equivalent to a multicontact single-punch problem, the same conclusion holds for the crack problem. This means that the multiple punch or crack problems are essential (nontrivial) extensions of the single-punch and single-crack problems.

General Theory of Punch and Crack Problems

We will formulate the problem in terms of the punch interpretation. The crack problem is then solved by a reinterpretation of the corresponding punch problem.

The basis for the solution is given by the following plane-strain displacement and stress field which was established by Nadai in 1927 (10)

[1] Professor of Mechanics, Rensselaer Polytechnic Institute. Mem. ASME.

[2] Numbers in parentheses refer to the Bibliography at the end of the paper.

Contributed by the Applied Mechanics Division and presented at the Diamond Jubilee Annual Meeting, Chicago, Ill., November 13–18, 1955, of The American Society of Mechanical Engineers.

Discussion of this paper should be addressed to the Secretary, ASME, 29 West 39th Street, New York, N. Y., and will be accepted until April 10, 1956, for publication at a later date. Discussion received after the closing date will be returned.

Note: Statements and opinions advanced in papers are to be understood as individual expressions of their authors and not those of the Society. Manuscript received by ASME Applied Mechanics Division, March 3, 1955. Paper No. 55—A-16.

$$\left.\begin{aligned} 2Gu &= y\frac{\partial\lambda}{\partial x} + (1-2\nu)\mu \\ 2Gv &= y\frac{\partial\lambda}{\partial y} - 2(1-\nu)\lambda \\ \sigma_x &= y\frac{\partial^2\lambda}{\partial x^2} - \frac{\partial\lambda}{\partial y} \\ \sigma_y &= y\frac{\partial^2\lambda}{\partial y^2} - \frac{\partial\lambda}{\partial y} \\ \tau_{xy} &= y\frac{\partial^2\lambda}{\partial x\partial y} \end{aligned}\right\} \quad \ldots\ldots\ldots\ldots [2]$$

In Equations [2]

$$\lambda + i\mu = f(x+iy)$$

is an analytic function of $x + iy$ which means that λ and μ are plane potential functions and μ is conjugate to λ.

The values on the boundary $y = 0$ of the upper half-plane are as follows

$$\left.\begin{aligned} 2Gu &= (1-2\nu)\mu \\ 2Gv &= -2(1-\nu)\lambda \\ \sigma_x &= \sigma_y = -\frac{\partial\lambda}{\partial y} = \frac{\partial\mu}{\partial x} \\ \tau_{xy} &= 0 \end{aligned}\right\} \quad \ldots\ldots\ldots\ldots [3]$$

Every stress field in which $\tau_{xy} = 0$ on the entire x-axis can be represented by the foregoing λ, μ solution with the only exception of the uniform uniaxial stress field in the x-direction

$$\sigma_x = \text{const}, \qquad \sigma_y = \tau_{xy} = 0 \ldots\ldots\ldots\ldots [4]$$

Such a uniaxial stress field can be superimposed on any λ, μ solution. This is important to comply with field conditions prescribed at infinity.

The entire infinite x-axis is subdivided into adjacent segments alternately representing the punched and the free sections. We number those sections consecutively $1, 2, \ldots, k, \ldots, n$. Two of these sections will be infinite. For a punched section the displacement v is constant. We may write

$$v = v_k \ldots\ldots\ldots\ldots [5]$$

where k is the number of the punched section. From this

$$\lambda = -\frac{Gv_k}{1-\nu} \ldots\ldots\ldots\ldots [6]$$

is seen to be constant on a punched section. On a free section, $\sigma_y = 0$, whence $\dfrac{\partial\mu}{\partial x} = 0$ or

$$\mu = \mu_k \ldots\ldots\ldots\ldots [7]$$

is constant.

The resultant of the stress σ_y on any interval from x_1 to x_2 of the x-axis (not necessarily one of the sections as defined and numbered $1, 2, 3, \ldots n$) is given by

$$\int_{x_1}^{x_2} \sigma_y dx = \int_{x_1}^{x_2} \frac{\partial\mu(x,0)}{\partial x}\, dx = \mu(x_2,0) - \mu(x_1,0) \ldots [8]$$

This result establishes the continuity of $\mu(x, 0)$ over the entire x-axis, since a stress distribution σ_y equivalent to forces concentrated at a point is ruled out in the theory of punching and thus the difference $\mu(x_2, 0) - \mu(x_1, 0)$ must approach zero in the limit if $(x_2 - x_1) \to 0$, which is seen to imply continuity of $\mu(x, 0)$. The only exception could be at $x = \infty$, where a force concentrated at a point must appear if

$$\int_{-\infty}^{\infty} \sigma_y dx \neq 0$$

In this case $\mu(\infty, 0) - \mu(-\infty, 0)$ will not vanish and $\mu(x, 0)$ will be discontinuous at ∞. $\lambda(x, 0)$ is continuous because $v(x, 0)$ is continuous in punching deformation by hypothesis and λ is proportional to v on the boundary $y = 0$. Again, $x = \infty$ may be an exception and $\lambda(\infty, 0)$ may differ from $\lambda(-\infty, 0)$. Altogether, the relation

$$\lambda + i\mu = f(x+iy)$$

maps the x-axis on a continuous rectangular broken line in the λ, μ plane, in which the sides $\lambda = c$ are the images of the punches and the sides $\mu = c$ are the images of the free sections. If either $\lambda(x, 0)$ or $\mu(x, 0)$ is discontinuous at ∞, the broken line will not close to form a polygon.

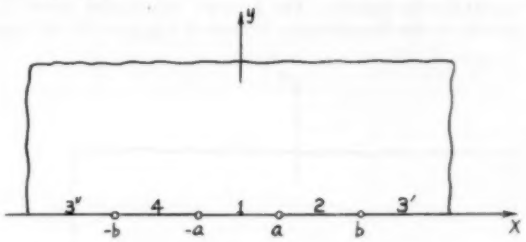

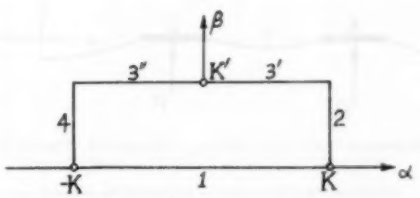

FIG. 3 MAPPING OF THE α, β RECTANGLE ON THE UPPER x, y HALF-PLANE—SHOWING CORRESPONDENT PARTS—BY MEANS OF $x + iy = a\,\mathrm{sn}(\alpha + i\beta)$

CASE OF FOUR SECTIONS

If $x = \infty$ is not a point at which two different sections meet, we will have four such meeting points with finite x-values, which we distribute symmetrically at $-b$, $-a$, a, b, $(0 < a < b)$. We number the sections 1, 2, 3, 4 as shown in Fig. 3. Section 3 is in two parts connected at ∞. The part $b < x < \infty$ is designated 3′, the part $-\infty < x < -b$ is designated 3″. 3′ and 3″ meet at ∞ and thus a discontinuity of λ or μ, if present at all, will be found at the point where 3′ and 3″ meet. The Jacobian elliptic functions with the modulus $k = a/b$ are the natural means to map the four segments of the x-axis on an orthogonal λ, μ broken line. We first introduce suitable orthogonal curvilinear co-ordinates α, β by writing

$$x + iy = a\,\mathrm{sn}(\alpha + i\beta, k) \ldots\ldots\ldots\ldots [9]$$

The rectangle in the $\alpha + i\beta$ plane

$$\left.\begin{aligned} -K \leq \alpha \leq K \\ 0 \leq \beta \leq K' \end{aligned}\right\} \quad \ldots\ldots\ldots\ldots [10]$$

is then mapped on the upper half-plane $y \geq 0$. Applying the equations of elasticity in orthogonal curvilinear co-ordinates to the present α, β system, it is possible to arrive at the solutions to the three problems as given later. As usually is the case with elliptic functions, the amount of formal computation is excessive, and no attempt is made to give a continuous exposition of the formal computations in this paper.

In the case of two punches the loads on them do not have to be equal. The penetrations of the punches also will be unequal. The best mathematical treatment of such an unsymmetric situation is by considering separately the symmetric and the antisymmetric ways of loading ($P_1 = P_2$ and $P_1 = -P_2$). By superposition, the general unsymmetric loading can be obtained. The coefficients of superposition are discussed at the end of the antisymmetric punch section.

Solution for Symmetric Double Punch

Fig. 4 shows the arrangement, which is symmetric about the y-axis. The displacements v in the y-direction computed and tabulated are not informative since the displacements at ∞ are logarithmically infinite. The pressure distribution under the punches is the characteristic feature of interest. If the ratio $a \div b$ is small, there is considerable stress-concentration interference between the two punches to the effect that the interior sides of the punches (near $x = a$ and $x = -a$) carry less of the load than the exterior sides (near $x = b$ and $x = -b$). The pressure distribution for $a/b = 0.1$ is shown in Fig. 5.

Symmetric Double Punch

$$\lambda + i\mu = \frac{P}{\pi} \log \frac{\mathrm{dn}(\alpha + i\beta) + k\,\mathrm{cn}(\alpha + i\beta)}{\mathrm{dn}(\alpha + i\beta) - k\,\mathrm{cn}(\alpha + i\beta)}$$

	$2Gv$	σ_x
1	$\frac{2(1-\nu)P}{\pi} \log \frac{\sqrt{b^2 - x^2} - \sqrt{a^2 - x^2}}{\sqrt{b^2 - x^2} + \sqrt{a^2 - x^2}}$	0
2	0	$-\frac{2Px}{\pi\sqrt{(x^2 - a^2)(b^2 - x^2)}}$
3	$\frac{2(1-\nu)P}{\pi} \log \frac{\sqrt{x^2 - a^2} - \sqrt{x^2 - b^2}}{\sqrt{x^2 - a^2} + \sqrt{x^2 - b^2}}$	0
4	0	$\frac{2Px}{\pi\sqrt{(x^2 - a^2)(b^2 - x^2)}}$

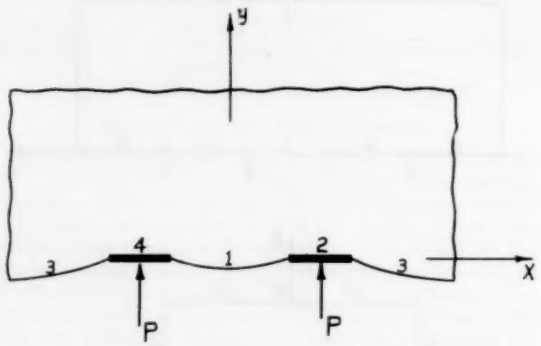

Fig. 4 Symmetric Double Punch—Bicontact Simple Punch

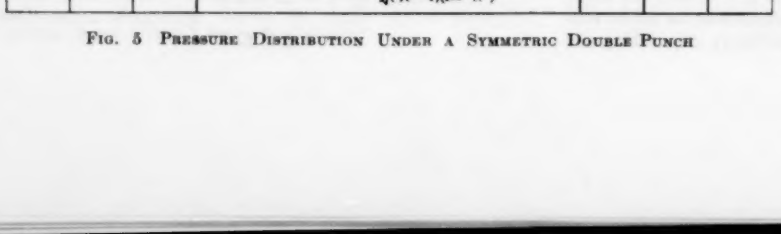

Fig. 5 Pressure Distribution Under a Symmetric Double Punch

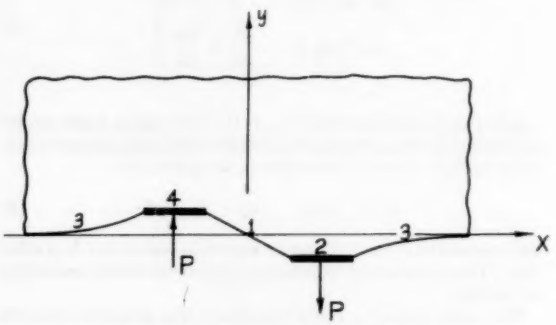

Fig. 6 Antisymmetric Double Punch

Solution for Antisymmetric Double Punch

Fig. 6 shows the arrangement which is antisymmetric about the y-axis. The displacements v in the y-direction are informative since v is zero at infinity. The vertical displacement of one punch relative to the other is

$$\frac{2(1-\nu)KP}{GK'} \quad \ldots\ldots [11]$$

which could serve as a characteristic measurement of stiffness of the elastic half-plane in the shown mode of loading by the opposite forces P. The pressure distribution under the punches is another characteristic feature of interest. If the ratio a/b is small, the stress-concentration interference is again considerable but has the opposite effect as compared with the symmetric case discussed first; i.e., the inner parts of the

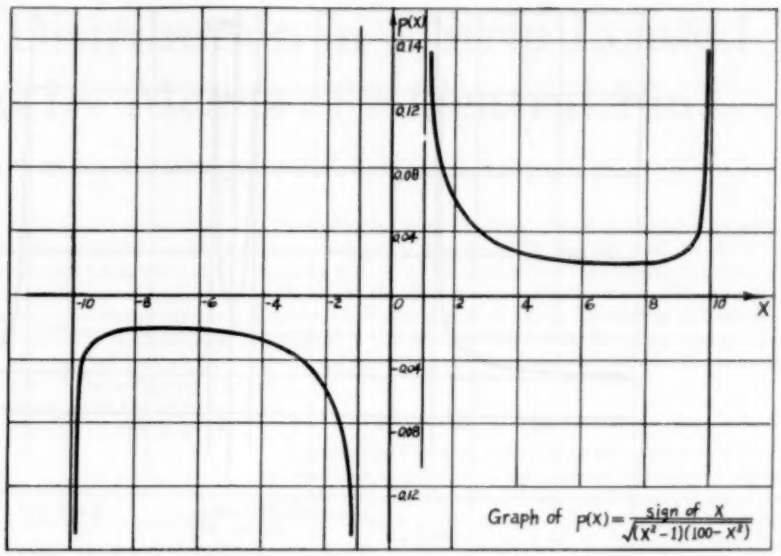

FIG. 7 PRESSURE DISTRIBUTION UNDER AN ANTISYMMETRIC DOUBLE PUNCH

punches now carry the bigger share of the load. The pressure distribution for $a/b = 0.1$ is shown in Fig. 7.

Both cases (symmetric and antisymmetric) with common values of a and b can be superimposed with arbitrary coefficients C_s and C_a, giving rise to a general nonsymmetric double punch with loads (positive in the sense of pressure) of $(C_s - C_a)P$ on the punch on section No. 2 and $(C_s + C_a)P$ on the punch on section No. 4.

ANTISYMMETRIC DOUBLE PUNCH

$$\lambda + i\mu = \frac{P}{K'}(\alpha + i\beta)$$

	$2Gv$	σ_y
1	$-\dfrac{2(1-\nu)\alpha P}{K'}$	0
2	$-\dfrac{2(1-\nu)KP}{K'}$	$\dfrac{Pb}{K'\sqrt{(x^2-a^2)(b^2-x^2)}}$
3	$-\dfrac{2(1-\nu)\alpha P}{K'}$	0
4	$\dfrac{2(1-\nu)KP}{K'}$	$-\dfrac{Pb}{K'\sqrt{(x^2-a^2)(b^2-x^2)}}$

SOLUTION FOR DOUBLE-LINE CRACK

Fig. 8 shows the location of the cracks. The displacements are single-valued; the region is triply connected. The stress field at infinity is

$$\left.\begin{aligned}\sigma_x &= \sigma_y = kK'\\ \tau_{xy} &= 0\end{aligned}\right\} \quad \ldots\ldots\ldots\ldots [12]$$

We may subtract the uniaxial field $\sigma_x = kK'$ which will leave σ_y unaltered. The stress σ_y is given by

$$\sigma_y = \frac{k[b^2E' - x^2K']}{\sqrt{(a^2-x^2)(b^2-x^2)}} \quad \ldots\ldots\ldots\ldots [13]$$

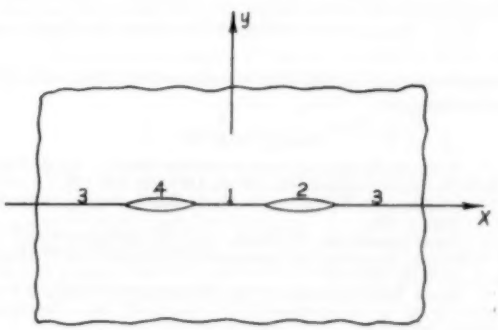

FIG. 8 DOUBLE CRACK—LOCATION DIAGRAM

on section 1, $-a < x < a$ and by

$$\sigma_y = \frac{k[x^2K' - b^2E']}{\sqrt{(x^2-a^2)(x^2-b^2)}} \quad \ldots\ldots\ldots\ldots [14]$$

on section 3 ($|x| > b$). Dividing σ_y by kK' we have ratios which represent the stress-concentration factors on 1 and 3. Fig. 9 shows the stress-concentration factor for the points on the x-axis for $a/b = 0.1$.

The complex function $\lambda + i\mu$ is given by

$$\lambda + i\mu = ia[K'E(\alpha + i\beta, k) - (K' - E')(\alpha + i\beta)] \quad \ldots [15]$$

ACKNOWLEDGMENT

The present investigation was carried out as part of a research program conducted at Rensselaer Polytechnic Institute under the sponsorship of the Office of Naval Research. The author is indebted to the Office of Naval Research for permission to publish the material.

The competent help received from Mr. Yih Hsing Pao of the Department of Mechanics at Rensselaer Polytechnic Institute in the task of the preparation of the manuscript is gratefully acknowledged. The interest shown by the reviewers has been ap-

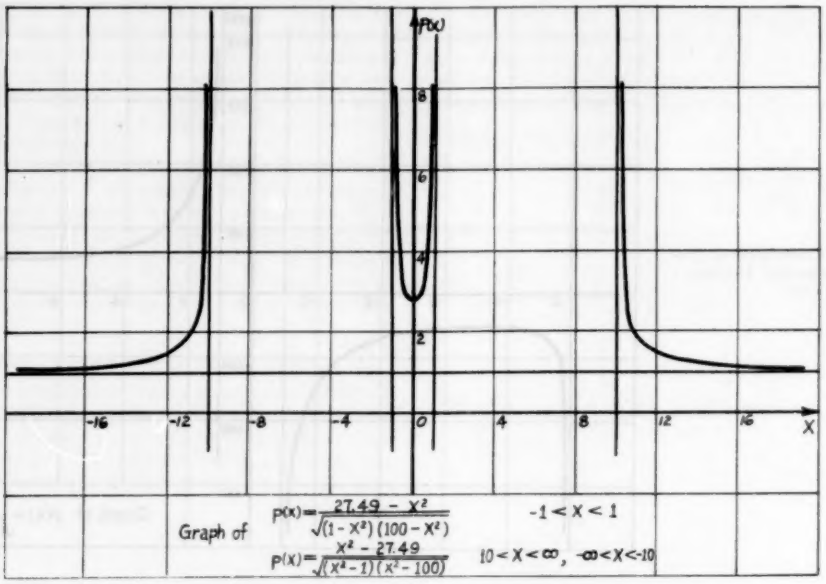

FIG. 9 DISTRIBUTION OF STRESS-CONCENTRATION FACTOR FOR σ_y IN PLANE UNDER TENSION IN PRESENCE OF A DOUBLE CRACK

preciated and their helpful suggestions have been used in the final draft of the paper.

BIBLIOGRAPHY

1 "Über die Berührung fester elastischer Körper," by H. Hertz, *Crelle's Journal of Mathematics*, vol. 92, 1881, pp. 157–171.

2 "Gesammelte Werke," by H. Hertz, Barth, Leipzig, Germany, vol. 1, 1895, p. 155.

3 "Zweidimensionale Probleme der Elastizilaetstheorie," by M. Sadowsky, *Zeitschrift für angewandte Mathematik und Mechanik*, vol. 8, 1928, pp. 107–121.

4 "Some Basic Problems of the Mathematical Theory of Elasticity," by N. I. Muskhelishvili, P. Noordhoff Ltd., Groningen, Holland, 1953.

5 "Theoretical Elasticity," by A. E. Green and W. Zerna, Oxford University Press, London, England, 1954.

6 "Fourier Transforms," by I. N. Sneddon, McGraw-Hill Book Company, Inc., New York, N. Y., 1951.

7 "Kontaktnye zadachi teorii uprugosti," by L. A. Galin, Moscow, Russia, 1953.

8 "The Phenomena of Rupture and Flow in Solids," by A. A. Griffith, Philosophical Transactions of the Royal Society of London, England, series A, vol. 221, 1920, p. 163.

9 "The Distribution of Stress in the Neighborhood of a Crack," by T. J. Willmore, *Quarterly Journal of Mechanics and Applied Mathematics*, vol. 2, 1949, pp. 53–63.

10 "Darstellung ebener Spannungszustände mit Hilfe von winkeltreuen Abbildungen," by A. Nadai, *Zeitschrift für Physik*, vol. 41, 1927, pp. 48–50.

The Stress Distribution in a Strip Loaded in Tension by Means of a Central Pin[1]

By P. S. THEOCARIS,[2] ATHENS, GREECE

It is the purpose of this paper to give an exact solution for the stress distribution resulting from loading a perforated strip in tension through a rigid pin filling the hole. The strip is regarded as of an infinite length and having a single axial hole. Stress distributions are found by an alternating approximation method and the stresses are tabulated in the form of stress-concentration factors for different values of diameter of the hole. The influence of size of the hole on the stress concentration in the strip is investigated and the optimum diameter of the hole is evaluated.

Introduction

THE problem of determining the stresses in a perforated strip loaded in tension through a close-fitting pin, filling the hole, is in close relation with the problem of the rivet in a strip which presents several difficulties. Among them, one is the evaluation of stress distribution around the hole and the effect on the stresses of the boundaries of strip.

In the present paper we shall be concerned with this difficulty and especially we deal with the following:

(*a*) The evaluation of the influence of the ratio of the diameter of the hole and the breadth of the strip on the stress distribution. We represent this ratio by λ and we consider the cases where λ does not exceed 0.5.

(*b*) The determination of the domain in the strip influenced by the presence of the hole.

(*c*) The definition of the optimum value of λ.

The problem can be considered as derived from the superposition of two distinct problems; i.e., the problem of a perforated strip stressed in tension by uniform traction, applied along its short edges and, on the other hand, the problem of the same strip charged, through a pin, in tension, by a longitudinal force, which is balanced by a uniform thrust and a uniform tension applied on its two short edges, respectively.

The solution for an unperforated infinite strip stressed by a longitudinal force acting in the middle of the strip was obtained by R. C. J. Howland (1).[3] The same author has studied the stress distribution in the neighborhood of a hole in a perforated strip under tension in the case when no load is applied in the hole (2).

The theoretical analysis of the problem is developed by adopting an alternating approximation method, used by R. C. J. Howland and A. C. Stevenson (3). The solution is obtained by the use of the stress function which satisfies all the boundary conditions in the strip, and the stress distribution is determined throughout the strip. At the end of the paper are given in tabular and graphical form the stress-concentration factors in the strip.

Statement of Problem

We consider a strip of an elastic, isotropic material and of uniform thickness, bounded in the x-y plane by the lines $y = \pm b$ and perforated by a circular hole of radius a. We suppose also a system of Cartesian co-ordinates ξ, η with their origin at the center of the hole and the η-axis perpendicular to the edges of the strip. Polar co-ordinates r, θ will also be used and, for convenience, we take their initial line along the y-axis and the positive direction of θ clockwise.

We define as unit of lengths the half of the width b of the strip. So, we write the relative co-ordinates

$$\xi = \frac{x}{b},\ \eta = \frac{y}{b},\ \rho = \frac{r}{b},\ \text{and}\ \lambda = \frac{a}{b} \qquad [1]$$

where λ is the radius of the hole measured with the same unit. We choose also as unit of stresses the uniform principal tension stress $\sigma_m = P/2b$ parallel to the ξ-axis.

We suppose the material to be in a state of generalized plane stress corresponding to a biharmonic stress function F.

We split this function into two parts as follows

$$F = F_1 + F_2 \qquad [2]$$

F_1 being a biharmonic function describing the case where the strip is stressed by a uniform tension, applied to its two short edges. This problem being examined by Howland (2), we are limited here to use the results already calculated.

In this paper we deal with the function F_2 which corresponds to the case where the applied longitudinal force at the origin is balanced half by a uniform tension and half by a uniform thrust applied in the two short edges of the strip, respectively. This function which is also biharmonic must give the stresses

(*a*) $\sigma_{x^2} = \pm\sigma_m,\ \sigma_{y^2} = \tau_{xy^2} = 0$

at the short edges of the strip ($\xi \to \pm\infty$).

(*b*) $\sigma_{y^2} = \tau_{xy^2} = 0$

along the lateral straight edges of the strip ($\eta = \pm 1$).

(*c*) The polar stresses σ_{r^2} and $\tau_{r\theta^2}$ at the rim of the hole, which must be even about the ξ-axis, must vanish along the part of the circle of the hole where $\pi \leq \theta \leq 2\pi$ and must give a resultant equal to the applied force P.

The function F_2 is split into three terms as follows

$$F_2 = F_2' + F_2'' + F_2''' \qquad [3]$$

where F_2' gives the stress distribution in a plate extended to an infinite distance from the center of the hole. If the hole is filled with a disk of elastic material and a force P acts in the center of the disk, then F_2' has the form

---

[1] The paper is based upon work forming part of the author's dissertation for a doctorate at Brussels University, March, 1953.

[2] Assistant Technical Adviser, Shell Petroleum (Hellas) Company; formerly, Assistant of Applied Mechanics, Athens National Technical University.

[3] Numbers in parentheses refer to the Bibliography at the end of the paper.

Contributed by the Applied Mechanics Division and presented at the Diamond Jubilee Annual Meeting, Chicago, Ill., November 13–18, 1955, of The American Society of Mechanical Engineers.

Discussion of this paper should be addressed to the Secretary, ASME, 29 West 39th Street, New York, N. Y., and will be accepted until April 10, 1956, for publication at a later date. Discussion received after the closing date will be returned.

Note: Statements and opinions advanced in papers are to be understood as individual expressions of their authors and not those of the Society. Manuscript received by ASME Applied Mechanics Division, September 15, 1954. Paper No. 55—A-34.

$$F_2' = \frac{Pb}{2\pi}\left[\frac{1-\mu}{2}\,\xi\log\rho + \eta\theta\right] \quad [4]$$

The term F_2'' added to F_2' must fulfill the conditions along the edges of the strip. This term has the form

$$F_2'' = \frac{Pb}{2\pi}\left[\int_0^\infty \frac{u\eta sS - (s+uc)C}{u^2\Sigma}\{u(1+\mu)-(1-\mu)\}\, e^{-u}\sin u\xi\, du + \int_0^\infty \frac{sC-\eta cS}{u\Sigma}\{2-u(1+\mu)\}\, e^{-u}\sin u\xi\, du\right] \quad [5]$$

where the different symbols have the meanings

$$s = \sinh u \qquad c = \cosh u \qquad \Sigma = \sinh 2u + 2u \quad [6]$$
$$S = \sinh \eta u \qquad C = \cosh \eta u$$

and μ is Poisson's ratio.

The term F_2''' must give zero stresses along the short edges of the strip, zero tractions along its lateral edges, and balance the tractions introduced from the first two terms at the rim of the hole so that the stresses obtained at the rim correspond to the conditions of the problem. In order to determine the term F_2''' so that it satisfies all these conditions, we use a process of alternating successive approximations and we write this term under the form

$$F_2''' = \sum_{r=0}^{\infty}(F_{2r}''' + F_{2r+1}''') \quad [7]$$

where the first term F_0''' is an even function giving stresses at the rim of the hole which have identical values over the right-hand half of the circle with those given from the functions $(F_2' + F_2'')$ and values of opposite sign over the left-hand half.

Each of the terms F_{2r}''' satisfies the conditions imposed by the problem at the rim of the hole but introduces tractions along the straight edges of the strip since the terms F_{2r+1}''' cancel the tractions introduced along the straight edges from every previous term F_{2r}''' but introduce, in their turn, residual stresses at the rim of the hole.

In requiring each time one of these functions to cancel the residual stresses introduced by its previous function we arrive, after some steps of this approximation, to a function which gives stresses of insignificant amount, provided that the series in Equation [7] and its derivatives up to the fourth degree are uniformly convergent.

If the method is to be practicable, it is necessary that the series expressing the function F_2''' very early gives the term corresponding to tractions of negligible amount. We truncate always the series at an even term in order to obtain a function fulfilling all the other conditions except those along the straight edges.

The formulas expressing the two groups of terms in the Series [7] are

$$F_{2r}''' = \frac{Pb}{2\pi}\left[-D_0^{(r)}\log\rho + \sum_{n=1}^{\infty}\left(\frac{D_{2n}^{(r)}}{\rho^{2n}} + \frac{E_{2n}^{(r)}}{\rho^{2n-2}}\right)\cos 2n\theta\right] \quad [8]$$

$$F_{2r+1}''' = \frac{Pb}{2\pi}\left[\int_0^\infty \frac{4\eta\, S\cos u\xi}{\Sigma}(s\phi^{(r)} + c\psi^{(r)})\, du - \int_0^\infty \frac{4C\cos u\xi}{\Sigma}\left\{\frac{s+uc}{u}\,\phi^{(r)} + s\psi^{(r)}\right\} du\right] \quad [9]$$

where $\phi^{(r)}$ and $\psi^{(r)}$ are given by the expressions

$$\phi^{(r)} = e^{-u}\left[\frac{D_0^{(r)}}{2} + \frac{1}{2}\sum_{n=1}^{\infty}(D_{2n}^{(r)} - E_{2n}^{(r)})\frac{u^{2n}}{(2n-1)!} + \sum_{n=1}^{\infty}E_{2n}^{(r)}\frac{u^{2n-1}}{(2n-2)!}\right] \quad [10]$$

$$\psi^{(r)} = e^{-u}\left[\frac{D_0^{(r)} - 2E_2^{(r)}}{2} + \sum_{n=1}^{\infty}\frac{nD_{2n}^{(r)} - (n+1)E_{2n+2}^{(r)}}{(2n)!}u^{2n} + \sum_{n=1}^{\infty}\frac{E_{2n}^{(r)}}{(2n-2)!}u^{2n-1}\right] \quad [11]$$

In order to obtain the first term F_0''' and to calculate the coefficients $D_{2n}^{(0)}$, $E_{2n}^{(0)}$ we must first express the boundary conditions in a suitable form. Thus we write the term F_2'' as follows

$$F_2'' = \frac{Pb}{2\pi}(1+\mu)\sum_{n=0}^{\infty}(a_n + b_n\rho^2)\rho^{2n+1}\sin(2n+1)\theta \quad [12]$$

where the coefficients a_n and b_n are given in a previous paper and can be calculated easily for $\mu = 0.365$ (see reference 3, p. 160).

We now express the stresses at the rim of the hole corresponding to the function $(F_2' + F_2'')$ under the form

$$(\sigma_{r2}' + \sigma_{r2}'') = \frac{P}{2\pi b}\sum_{n=0}^{\infty}p_n\sin(2n+1)\theta \quad [13]$$

$$(\sigma_{\theta 2}' + \sigma_{\theta 2}'') = \frac{P}{2\pi b}\sum_{n=0}^{\infty}q_n\sin(2n+1)\theta \quad [14]$$

$$(\tau_{r\theta 2}' + \tau_{r\theta 2}'') = \frac{P}{2\pi b}\sum_{n=0}^{\infty}r_n\cos(2n+1)\theta \quad [15]$$

where p_n, q_n, and r_n are functions of coefficients a_n, b_n, μ, and λ.

The polar stresses σ_{r2}''' and $\tau_{r\theta 2}'''$, due to the term F_0''', expanded in the form of a cosine and sine series, are (4)

$$\sigma_{r2}''' = -\frac{P}{2\pi b}\sum_{n=0}^{6}A_{2n}\cos 2n\theta \quad [16]$$

$$\tau_{r\theta 2}''' = -\frac{P}{2\pi b}\sum_{n=1}^{5}B_{2n}\sin 2n\theta \quad [17]$$

In order to have the Stresses [16] and [17] identical with those found by Equations [13] and [15], respectively, over the right-hand half of the rim of the hole, we equalize the corresponding coefficients and calculate the values of A_{2n} and B_{2n} for intervals of 15 deg of the angle θ and for the first quadrant only.

By identifying the corresponding coefficients of Equations [16] and [17] and of the stresses σ_r and $\tau_{r\theta}$, obtained by differentiation from Equation [8], we find for the coefficients $D_{2n}^{(0)}$ and $E_{2n}^{(0)}$

$$D_0 = \lambda^2 A_0 \quad [18]$$

$$D_{2n}^{(0)} = \frac{\lambda^{2n+2}\{(n+1)B_{2n} - nA_{2n}\}}{2n(2n+1)} \quad [19]$$

$$E_{2n}^{(0)} = \frac{\lambda^{2n}\{A_{2n} - B_{2n}\}}{2(2n-1)} \quad [20]$$

The coefficients $D_0^{(r+1)}$, $D_{2n}^{(r+1)}$, and $E_{2n}^{(r+1)}$ can be calculated:

(*a*) By equalizing each time the corresponding coefficients of stresses σ_y and τ_{xy} at the straight edges of the strip, due to the functions F_{2r}''' and F_{2r+1}''', in order to cancel those stresses along these edges.

(*b*) By requiring the stresses σ_r and $\tau_{r\theta}$ due to functions F_{2r+2}''' to cancel those due to functions F_{2r+1}''' along the left-hand half of the circle.

In this way the coefficients $D_0^{(r+1)}$, $D_{2n}^{(r+1)}$, and $E_{2n}^{(r+1)}$ are determined by the expressions

$$D_0^{(r+1)} = 4\lambda^2 \int_0^\infty \frac{s\phi^{(r)} + c\psi^{(r)}}{\Sigma}\, u du \quad \ldots\ldots [21]$$

$$D_{2n}^{(r+1)} = \lambda^{4n}\left[\frac{4(2n-1)}{(2n)!}\int_0^\infty [s\{(n-1)\phi^{(r)} - u\psi^{(r)}\} + c(n\psi^{(r)} - u\phi^{(r)})]\frac{u^{2n-1}}{\Sigma}\, du + \frac{4n\lambda^2}{(2n+1)!}\int_0^\infty \frac{s\phi^{(r)} + c\psi^{(r)}}{\Sigma}\, u^{2n+1}\, du\right] \quad \ldots\ldots [22]$$

$$E_{2n}^{(r+1)} = -\lambda^{4n-2}\left[\frac{4}{(2n-1)!}\int_0^\infty \left[s\{(n-1)\phi^{(r)} - u\psi^{(r)}\} + c(n\psi^{(r)} - u\phi^{(r)})\right]\frac{u^{2n-1}}{\Sigma}\, du + \frac{2\lambda^2}{(2n)!}\int_0^\infty \frac{s\phi^{(r)} + c\psi^{(r)}}{\Sigma}\, u^{2n+1}\, du\right] \quad \ldots\ldots [23]$$

The number of steps in the approximation process is carried out until the greatest residual stresses in the one boundary are of negligible amount. Since the importance of stresses near the hole is greater than in any other place, we choose to end the approximation process with a stress function of even order, so that the hole shall be free from residual tractions.

By using the notations

$$d_{2n} = \sum_{r=0}^{\infty} D_{2n}^{(r)} \qquad e_{2n} = \sum_{r=0}^{\infty} E_{2n}^{(r)}$$

we can express the general stress function as follows

$$F_2 = \frac{Pb}{2\pi}\left\{\frac{1-\mu}{2}\,\xi\log\rho + \eta\theta + \int_0^\infty \frac{u\eta sS - (s+uc)C}{u^2\Sigma}\,[u(1+\mu) - (1-\mu)]\,e^{-u}\sin u\xi du + \int_0^\infty \frac{sC + \eta cS}{u\Sigma}\,[2 - u(1+u)]e^{-u}\sin u\xi du - d_0\log\rho + \sum_{n=1}^{\infty}\left(\frac{d_{2n}}{\rho^{2n}} + \frac{e_{2n}}{\rho^{2n-2}}\right)\cos 2n\theta + \int_0^\infty \frac{4\eta\, S\cos u\xi}{\Sigma}(s\bar{\phi} + c\bar{\psi})du - \int_0^\infty \frac{4C\cos u\xi}{\Sigma}\left(\frac{s+uc}{u}\,\bar{\phi} + s\bar{\psi}\right)du\right\} \quad \ldots\ldots [24]$$

where the new symbols $\bar{\phi}$ and $\bar{\psi}$ are defined by

$$\bar{\phi} = \sum_{r=0}^{\infty}\phi^{(r)} \qquad \bar{\psi} = \sum_{r=0}^{\infty}\psi^{(r)} \quad \ldots\ldots [25]$$

and the coefficients d_{2n} and e_{2n} are tabulated in Table 1.

Owing to the fluctuation in the sign of the factors containing the trigonometric amounts, the trigonometric integrals of the form

$$I = \int_0^\infty f(u)\sin u\xi du \qquad J = \int_0^\infty f(u)\cos u\xi du$$

can be conveniently calculated from the ordinary quadrature formulas in the case when ξ is very small. For large values of ξ we use Filon's adaptation of Simpson's formula, convenient to be used with trigonometric integrals (5).

From Equation [24], expressing the general stress function F_2, we obtain the stresses in rectangular co-ordinates

$$\sigma_{x2} = \frac{P}{2\pi b}\left[\frac{\xi}{\rho^2}\left\{(1+\mu)\,\frac{\eta^2}{\rho^2} - \frac{\mu+3}{2}\right\} + \frac{d_0 - 2e_2}{\rho^2}\cos 2\theta + 2\sum_{n=1}^{\infty}\left\{\frac{(2n+1)(nd_{2n} - e_{2n+2})}{\rho^{2n+2}} + \frac{n(2n-1)}{\rho^{2n}}\,e^{2n}\right\}\cos(2n+2)\theta + \int_0^\infty \frac{(s-uc)C + u\eta sS}{\Sigma}\,\{u(1+\mu) - (1-\mu)\}e^{-u}\sin u\xi du + \int_0^\infty \frac{(su-2c)C - \eta ucS}{\Sigma}\,\{2 - u(1+\mu)\}e^{-u}\sin u\xi du + \int_0^\infty \frac{4u(2C+\eta uS)}{\Sigma}\,(s\bar{\phi} + c\bar{\psi})\cos u\xi du - \int_0^\infty \frac{4uC}{\Sigma}\,\{(s+uc)\bar{\phi} + su\bar{\psi}\}\cos u\xi du\right] \quad \ldots\ldots [26]$$

$$\sigma_{y2} = \frac{P}{2\pi b}\left[\frac{\xi}{\rho^2}\left\{\frac{1-\mu}{2} - \frac{(1+\mu)\eta^2}{\rho^2}\right\} - \frac{d_0 + 2e_2}{\rho^2}\cos 2\theta - 2\sum_{n=1}^{\infty}\left\{\frac{(2n+1)(nd_{2n} + e_{2n+2})}{\rho^{2n+2}} + \frac{n(2n-1)}{\rho^{2n}}\,e_{2n}\right\}\cos(2n+2)\theta - \int_0^\infty \frac{u\eta sS - (s+uc)C}{\Sigma}\,\{u(1+\mu) - (1-\mu)\}\,e^{-u}\sin u\xi du - \int_0^\infty \frac{sC - \eta cS}{\Sigma}\,\{2u - u^2(1+\mu)\}\,e^{-u}\sin u\xi du - \int_0^\infty \frac{4\eta u^2 S}{\Sigma}\,(s\bar{\phi} + c\bar{\psi})\cos u\xi du + \int_0^\infty \frac{4uC}{\Sigma}\,\{(s+uc)\bar{\phi} + su\bar{\psi}\}\cos u\xi\, du\right] \quad \ldots\ldots [27]$$

$$\tau_{xy2} = -\frac{P}{2\pi b}\left[\frac{\eta}{\rho^2}\left\{(1+\mu)\,\frac{\xi^2}{\rho^2} + \frac{(1-\mu)}{2}\right\} + \frac{d_0}{\rho^2}\sin 2\theta + 2\sum_{n=1}^{\infty}\left\{\frac{n(2n+1)d_{2n}}{\rho^{2n+2}} + \frac{n(2n-1)}{\rho^{2n}}\,e^{2n}\right\}\sin(2n+2)\theta + \int_0^\infty \frac{u\eta sC - ucS}{\Sigma}\,\{u(1+\mu) - (1-\mu)\}\,e^{-u}\cos u\xi du + \int_0^\infty \frac{(su-c)S - \eta ucC}{\Sigma}\,\{2 - u(1+\mu)\}\,e^{-u}\cos u\xi du + \int_0^\infty \frac{4uS}{\Sigma}\,\{(s+uc)\bar{\phi} + us\bar{\psi}\}\,\sin u\xi du - \int_0^\infty \frac{4u(S+\eta uC)}{\Sigma}\,(s\bar{\phi} + c\bar{\psi})\sin u\xi du\right] \quad \ldots\ldots [28]$$

All the trigonometric integrals contained in Equations [24] to [28], being rapidly convergent, can be easily evaluated by Filon's formula. In these integrals, instead of infinity, we take as an effective upper limit, the numbers 6 to 8, and as interval for u the value 0.5. Furthermore, to facilitate the calculation, we take as values of ξ submultiples of π.

Since the terms contained in the foregoing formulas are finite all over the strip they can be extended for the evaluation of stresses throughout the strip.

By using the Equations [26] to [28] we calculate the stresses

TABLE 1 VALUES OF COEFFICIENTS d_{2n} AND e_{2n}

η	λ=0.2	λ=0.3	λ=0.4	λ=0.5	λ=0.2	λ=0.3	λ=0.4	λ=0.5
	d_{2n}				e_{2n}			
0	$2.15\cdot10^{-1}$	$3.31\cdot10^{-1}$	$4.52\cdot10^{-1}$	$5.89\cdot10^{-1}$				
1	$1.82\cdot10^{-3}$	$6.81\cdot10^{-3}$	$2.05\cdot10^{-2}$	$4.71\cdot10^{-2}$	$-1.06\cdot10^{-1}$	$-1.76\cdot10^{-1}$	$-2.88\cdot10^{-1}$	$-4.23\cdot10^{-1}$
2	$8.45\cdot10^{-6}$	$5.87\cdot10^{-5}$	$2.52\cdot10^{-4}$	$9.95\cdot10^{-4}$	$-3.18\cdot10^{-4}$	$-9.14\cdot10^{-4}$	$-2.31\cdot10^{-3}$	$-5.51\cdot10^{-3}$
3	$1.19\cdot10^{-7}$	$1.93\cdot10^{-6}$	$1.27\cdot10^{-5}$	$5.71\cdot10^{-5}$	$-3.35\cdot10^{-6}$	$-2.70\cdot10^{-5}$	$-2.91\cdot10^{-5}$	$-2.89\cdot10^{-4}$
4	$2.50\cdot10^{-9}$	$1.10\cdot10^{-7}$	$9.13\cdot10^{-7}$	$6.39\cdot10^{-6}$	$-1.60\cdot10^{-7}$	$-1.60\cdot10^{-6}$	$-7.16\cdot10^{-6}$	$-2.93\cdot10^{-5}$
5	$4.15\cdot10^{-11}$	$2.85\cdot10^{-9}$	$8.36\cdot10^{-8}$	$8.37\cdot10^{-7}$	$-1.20\cdot10^{-9}$	$-4.00\cdot10^{-8}$	$-5.71\cdot10^{-7}$	$-4.06\cdot10^{-6}$
6	$6.30\cdot10^{-13}$	$1.30\cdot10^{-10}$	$3.80\cdot10^{-9}$	$6.00\cdot10^{-8}$	$-1.30\cdot10^{-11}$	$-1.60\cdot10^{-9}$	$-2.70\cdot10^{-8}$	$-2.81\cdot10^{-7}$

throughout the strip. Thus, by putting $\rho = \xi, \eta = 0, \theta = \pm\pi/2$, we obtain the stresses along the ξ-axis. Putting $\rho = \eta$, $\xi = 0$, $\theta^0 = 0$ or π, we have formulas for stresses along the η-axis.

In order to calculate the stresses at the rim of the hole we use the polar components of stresses. The formulas of these stresses are omitted. Only the values of principal stresses at the rim are given in Table 2 for different values of λ.

For the stress σ_{zz} at the edges of the strip, we introduce in Equation [26]

$$\eta = \pm 1, \quad \rho = \sqrt{1 + \xi^2}, \quad \text{and} \quad \theta = \arctan \xi$$

which after a slight reduction takes the form

$$\sigma_{zz} = \frac{P}{2\pi b}\left[(1+\mu)\left\{\frac{4\xi}{(1+\xi^2)^2} - \int_0^\infty \frac{u(4u - e^{-2u} + 1)}{\Sigma} e^{-u}\sin u\xi\, du\right\} - 2\left\{\frac{2\xi}{1+\xi^2} - \int_0^\infty \frac{4u - 1 - e^{-2u}}{\Sigma} e^{-u}\sin u\xi\, du\right\} + \frac{2(2d_0 - 3e_2)}{(1+\xi^2)}\cos 2\theta + 2\sum_{n=1}^{\infty}\left\{\frac{(2n+1)[4nd_{2n} - (3n+1)e_{2n+2}]}{(1+\xi^2)^{(n+1)}} + \frac{n(2n-1)e_{2n}}{(1+\xi^2)^n}\right\}\cos(2n+2)\theta + 6\sum_{n=1}^{\infty}\frac{2n(2n-1)e_{2n}\cos(2n+1)\theta}{(1+\xi^2)^{\frac{2n+1}{2}}} - 4\int_0^\infty \{2u(\bar{\phi} + \bar{\psi}) - (1 - e^{-2u})\bar{\psi}\}\frac{u\cos u\xi}{\Sigma}\, du\right] \quad \ldots\ldots [29]$$

Finally, in order to have the stress distribution in the perforated strip stressed in tension by a close-fitting pin filling the hole, we must add to the stress components, obtained by the stress function F_2, those resulting from the stress function F_1, which has already been calculated by Howland (2).

In Tables 2, 3, and 4 are tabulated the values of stresses along the principal lines of the strip. Figs. 1, 2, and 3 represent the graphs of the same stresses.

Discussion of Results and Remarks

From the theoretical analysis of the problem we obtain:

1 The influence of the hole on the stress distribution is extended to a circle of diameter equal to the width of the strip multiplied by 1.5.

2 At the rim of the hole both principal stresses exist. From these the circumferential stress σ_I takes its maximum value when $\theta = 0$ deg. This maximum value is equal to 6.5 σ_m for $\lambda = 0.2$. When λ is increasing this stress is diminishing and after it has passed through a minimum, located at λ between 0.4 and 0.5, it takes the value of $5\sigma_m$ for $\lambda = 0.5$.

TABLE 2 VALUES OF PRINCIPAL STRESSES AT RIM OF HOLE

θ^0	λ=0.2		λ=0.3		λ=0.4		λ=0.5	
	$\frac{1}{\sigma_m}\cdot\sigma_I$	$\frac{1}{\sigma_m}\cdot\sigma_{II}$	$\frac{1}{\sigma_m}\cdot\sigma_I$	$\frac{1}{\sigma_m}\cdot\sigma_{II}$	$\frac{1}{\sigma_m}\cdot\sigma_I$	$\frac{1}{\sigma_m}\cdot\sigma_{II}$	$\frac{1}{\sigma_m}\cdot\sigma_I$	$\frac{1}{\sigma_m}\cdot\sigma_{II}$
90°	-0.13	-5.27	-0.50	-3.65	-0.96	-2.80	-1.21	-2.32
75°	0.14	-5.24	-0.28	-3.52	-0.64	-2.70	-0.95	-2.21
60°	1.01	-4.75	0.58	-3.12	0.22	-2.38	-0.10	-1.92
45°	2.31	-3.83	1.82	-2.50	1.45	-1.87	1.16	-1.46
30°	3.73	-2.69	3.05	-1.75	2.86	-1.26	2.73	-0.91
15°	5.44	-1.44	4.36	-0.94	4.18	-0.60	4.26	-0.42
0°	6.62	0	5.26	0	4.84	0	5.10	0
-15°	5.00	0	4.13	0	4.03	0	4.19	0
-30°	3.11	0	2.66	0	2.60	0	2.55	0
-45°	1.53	0	1.30	0	1.06	0	0.86	0
-60°	0.07	0	-0.04	0	-0.27	0	-0.48	0
-75°	-0.85	0	-0.93	0	-1.16	0	-1.31	0
-90°	-1.14	0	-1.17	0	-1.47	0	-1.63	0

TABLE 3 VALUES OF PRINCIPAL STRESSES ALONG η-AXIS AND EDGES OF STRIP

η	λ=0.2		λ=0.3		λ=0.4		λ=0.5	
	$\frac{1}{\sigma_m}\cdot\sigma_I$	$\frac{1}{\sigma_m}\cdot\sigma_{II}$	$\frac{1}{\sigma_m}\cdot\sigma_I$	$\frac{1}{\sigma_m}\cdot\sigma_{II}$	$\frac{1}{\sigma_m}\cdot\sigma_I$	$\frac{1}{\sigma_m}\cdot\sigma_{II}$	$\frac{1}{\sigma_m}\cdot\sigma_I$	$\frac{1}{\sigma_m}\cdot\sigma_{II}$
±0.2	6.55	0						
±0.3	2.04	0.69	5.25	0				
±0.4	1.26	0.47	2.29	0.58	4.96	0		
±0.5	0.99	0.30	1.49	0.47	2.61	0.51	5.06	0
±0.6	0.85	0.20	1.17	0.32	1.81	0.47	2.95	0.45
±0.7	0.77	0.12	0.96	0.19	1.42	0.29	2.07	0.38
±0.8	0.69	0.06	0.85	0.10	1.05	0.14	1.50	0.24
±0.9	0.64	0.04	0.71	0.02	0.91	0.03	1.08	0.15
±1.0	0.51	0	0.50	0	0.45	0	0.42	0
ξ	$\frac{1}{\sigma_m}\cdot\sigma_x$		$\frac{1}{\sigma_m}\cdot\sigma_x$		$\frac{1}{\sigma_m}\cdot\sigma_x$		$\frac{1}{\sigma_m}\cdot\sigma_x$	
	$\xi>0$	$\xi<0$	$\xi>0$	$\xi<0$	$\xi>0$	$\xi<0$	$\xi>0$	$\xi<0$
0	0.51	0.51	0.49	0.49	0.45	0.45	0.42	0.42
±0.17	0.62	0.52	0.63	0.53	0.65	0.55	0.72	0.62
±0.35	0.74	0.65	0.86	0.77	1.02	0.93	1.25	1.16
±0.52	0.75	0.79	0.94	0.98	1.21	1.18	1.56	1.61
±0.70	0.66	0.90	0.88	1.11	1.17	1.41	1.55	1.78
±0.87	0.52	0.96	0.70	1.14	1.09	1.43	1.31	1.76
±1.05	0.37	1.00	0.51	1.15	0.74	1.41	1.02	1.65
±1.57	0.09	1.02	0.13	1.06	0.21	1.14	0.31	1.25

This stress represents the maximum stress concentration all over the strip. Fig. 1 gives the values of σ_I at the rim of the hole. We remark that σ_I is equal to zero for $\theta_1 = 50$ to 80 deg and $\theta_2 = -50$ to -60 deg. For values of θ absolutely greater than θ_1 and θ_2, σ_I becomes a compression stress. The stress σ_{II} vanishes along all the lower half of the hole. Between $\theta = 0$ deg and $\theta = 90$ deg it becomes a compression stress and its maximum is at

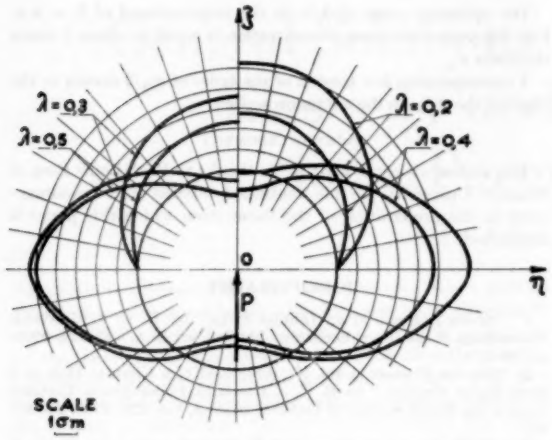

FIG. 1 VALUES OF PRINCIPAL STRESSES σ_I AND σ_{II} AT RIM OF HOLE FOR DIFFERENT VALUES OF λ

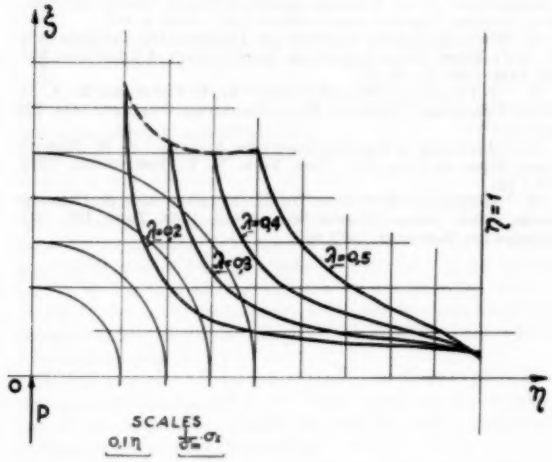

FIG. 2 VALUES OF STRESS σ_I ALONG MINIMUM SECTION OF STRIP

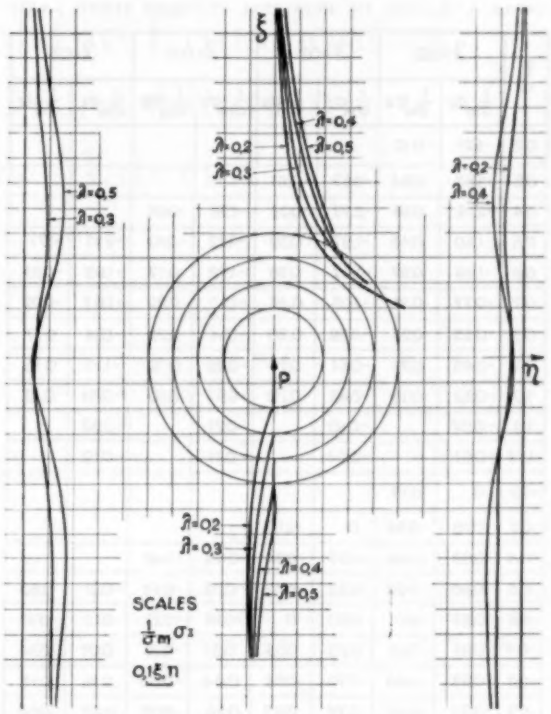

FIG. 3 VALUES OF STRESS σ_I ALONG LONGITUDINAL AXIS AND EDGES OF STRIP

$\theta = 90$ deg. This maximum stress remains always smaller than the corresponding maximum of σ_I.

3 Along the η-axis, σ_I is diminishing very rapidly, Fig. 2, when η is increasing and after a certain distance from the hole it becomes smaller than σ_∞. A check of the results obtained is provided by the conditions of statical equilibrium along the η-axis. Obviously, the resultant of σ_I stresses along this axis must be equal to P. The errors found by this check do not exceed 1.6 per cent. The values of the other stress σ_{II} along the η-axis are insignificant.

4 Fig. 3 gives the stresses along ξ-axis. Along $\xi > 0$, σ_I tends rapidly to its asymptotic value which is zero. The other stress σ_{II} passes through a zero value and then tends also asymptotically to zero.

5 At the straight edges of the strip and on the minimum section the only existing stress σ_I is about $^1/_2\sigma_\infty$ for all values of λ. At a short distance along the edges the tension stress σ_I rises to a maximum value and then it tends asymptotically to zero, for $\xi > 0$, or to σ_∞, for $\xi < 0$.

6 Since the strip is a doubly connected body and the resultant of the forces applied to its boundaries do not vanish, the stress distribution depends on the elastic constants of the material and especially on Poisson's ratio. Thus the results obtained by taking $\mu = 0.365$ can be transposed rigorously only to materials having the same constant. However, the effect of the variation of Poisson's ratio influences insignificantly the stress distribution and the influence is particularly negligible on the domain of maximum stress concentration. Therefore the values of the calculated stresses can be transposed, without great error, to other technical materials having different values of Poisson's ratio.

CONCLUSIONS

An exact solution of the problem of determining the stresses in a perforated strip loaded by a tension force applied through a close-fitting pin, filling the hole, is obtained by Equations [26] to [28] throughout the strip.

The solution obtained depends upon the shape ratio $\lambda = a/b$ and furthermore involves Poisson's ratio μ. The stresses within the strip are tabulated, through extensive numerical computations, for values of λ between 0.2 and 0.5. The values of stresses given in Tables 2 to 4 are calculated by taking the uniform principal tension stress

$$\sigma_\infty = \frac{P}{2b}$$

as unit of measure. Hence they are independent of the applied forces and the width of the strip.

The maximum stress concentration is located at the rim of the hole and of the minimum section of the strip. The region influenced by the hole is limited by a circle of diameter equal 1.5 times the width of the strip.

TABLE 4 VALUES OF PRINCIPAL STRESSES ALONG ξ-AXIS

ξ	λ=0.2		λ=0.3		λ=0.4		λ=0.5	
	$\frac{1}{\sigma_m}\cdot\sigma_I$	$\frac{1}{\sigma_m}\cdot\sigma_{II}$	$\frac{1}{\sigma_m}\cdot\sigma_I$	$\frac{1}{\sigma_m}\cdot\sigma_{II}$	$\frac{1}{\sigma_m}\cdot\sigma_I$	$\frac{1}{\sigma_m}\cdot\sigma_{II}$	$\frac{1}{\sigma_m}\cdot\sigma_I$	$\frac{1}{\sigma_m}\cdot\sigma_{II}$
0.2	-5.21	-0.15						
0.3	-3.38	0.34	-3.67	-0.51				
0.4	-2.18	0.55	-2.73	0.28	-2.76	-0.96		
0.5	-1.50	0.48	-1.97	0.39	-2.32	-0.10	-2.31	-1.21
0.6	-1.05	0.37	-1.42	0.38	-1.78	0.17	-1.98	-0.33
0.7	-0.77	0.31	-1.05	0.35	-1.37	0.22	-1.67	-0.02
0.8	-0.55	0.25	-0.78	0.30	-1.04	0.22	-1.34	0.17
0.9	-0.45	0.21	-0.61	0.27	-0.82	0.19	-1.10	0.16
1.0	-0.32	0.15	-0.43	0.20	-0.61	0.10	-0.84	0.12
1.4	-0.07		-0.10		-0.21		-0.32	
1.57	-0.01		-0.04		-0.11		-0.19	
-0.2	0	-1.17						
-0.3	0.28	-0.34	0	-1.19				
-0.4	0.62	0.03	0.07	-0.24	-0.04	-1.48		
-0.5	0.80	0.02	0.33	-0.03	-0.02	-0.52	-0.01	-1.63
-0.6	0.87	-0.01	0.50	0	+0.14	-0.21	-0.12	-0.71
-0.7	0.91	-0.01	0.63	0.03	0.31	-0.10	0.01	-0.34
-0.8	0.93	-0.03	0.70	0.03	0.44	-0.06	0.14	-0.11
-0.9	0.93	-0.03	0.77	0.03	0.56	-0.05	0.28	-0.08
-1.0	0.95	-0.05	0.83	0	0.65	-0.04	0.42	-0.06

The optimum value of λ is in the neighborhood of $\lambda = 0.4$. For this value the stress concentration is equal to about 5 times the stress σ_m.

A corresponding low tension of the order of $\sigma_m/2$ occurs at the edges of the strip on the minimum section.

Acknowledgment

The author wishes to express his thanks to Prof. Louis Baes of Brussels University for his continued interest and encouragement in the preparation of the thesis from which this paper is abstracted.

BIBLIOGRAPHY

1 "Stress Systems in an Infinite Strip," by R. C. J. Howland, Proceedings of the Royal Society of London, series A, vol. 124, 1929, pp. 89–119.

2 "On the Stresses in the Neighborhood of a Circular Hole in a Strip Under Tension," by R. C. J. Howland, Philosophical Transactions of the Royal Society of London, series A, vol. 229, 1930, pp. 49–86.

3 "Bi-Harmonic Analysis in a Perforated Strip," by R. C. J. Howland and A. C. Stevenson, Philosophical Transactions of the Royal Society of London, series A, vol. 232, 1933, pp. 155–222.

4 "The Calculus of Observations. A Treatise on Numerical Mathematics," by E. Whittaker and G. Robinson, Blackie and Sons, Ltd., London, England, fourth edition, vol. 1, 1949, p. 397.

5 "On a Quadrature Formula for Trigonometric Integrals," by L. N. G. Filon, Proceedings of the Royal Society of Edinburgh, vol. 49, 1928–1929, pp. 38–47.

6 "A Treatise on Photoelasticity," by E. Coker and L. N. G. Filon, Cambridge University Press, Cambridge, England, 1931, 726 pp.

7 "Handbook of Experimental Stress Analysis," by M. Hetényi, John Wiley & Sons, Inc., New York, N. Y., first edition, 1950, 1077 pp.

8 "Méchanique Technique," by K. Georgikopoulos, K. Papadoyannis, editor, Athens, Greece, first edition, 1949, Tome III, "Résistance des Matériaux," 232 pp.

General Solutions of the Equations of Elasticity and Consolidation for a Porous Material[1]

By M. A. BIOT,[2] NEW YORK, N. Y.

Equations of elasticity and consolidation for a porous elastic material containing a fluid have been previously established (1, 5).[3] General solutions of these equations for the isotropic case are developed, giving directly the displacement field or the stress field in analogy with the Boussinesq-Papkovitch solution and the stress functions of the theory of elasticity. General properties of the solutions also are examined and the viewpoint of eigenfunctions in consolidation problems is introduced.

1 Introduction

THE theory of deformation of an elastic porous material containing a compressible fluid has been established by the author in previous publications. Reference (1) deals with the case of an isotropic material. In reference (5) the theory has been generalized to anisotropic materials. The model of a porous elastic body was suggested by Terzaghi (8) to represent the consolidation and settlement of fluid saturated soils. Hence the theory also has been referred to as a consolidation theory. Another category of problems covered by this theory is that of the flow of a compressible fluid in a porous material from the standpoint of determining the flow pattern of the fluid or the stresses set up by the fluid seepage through the elastic solid. Such a theory is applicable, for instance, to the problem associated with the loading process of a dam and in certain fundamental problems of petroleum geology.

Several problems of two-dimensional consolidation have been treated by the author (2, 3, 4). These papers make extensive use of the operational calculus and develop certain numerical methods appropriate to the problem.

The object of the present paper is to furnish general solutions of the equations for the isotropic case by means of functions satisfying the Laplace and the heat-conduction equation. The solutions developed in Section 3 are analogous to the Boussinesq-Papkovitch functions of the theory of elasticity (9, 10, 11). They yield directly the displacement field. Stress functions introduced in Section 4 express directly the stress field. In Section 5 general properties of the solutions are examined.

The concept of "consolidation mode" is introduced in Section 6, and it is pointed out that solutions expressed in this form are a consequence of a general property of relaxation phenomena (7).

2 The Elasticity and Consolidation Theory for a Porous Solid

In references (1) and (5) we have established a theory for the deformation of a porous elastic material containing a fluid. The equations obtained in the case of isotropy are reviewed briefly in the present section. The stress field of the porous material is denoted by

$$\begin{Bmatrix} \sigma_{xx} + \sigma & \sigma_{xy} & \sigma_{xz} \\ \sigma_{yx} & \sigma_{yy} + \sigma & \sigma_{yz} \\ \sigma_{zx} & \sigma_{zy} & \sigma_{zz} + \sigma \end{Bmatrix} \quad \ldots\ldots [1]$$

The $\sigma_{xx}\sigma_{xy}$, etc., components represent the forces acting on the solid part of the faces of a unit cube of bulk material while σ represents the force applied to the fluid part. Introducing the porosity f, the pressure p in the fluid is related to σ by

$$\sigma = -fp \quad \ldots\ldots [2]$$

The average displacement vector of the solid has components $u_x u_y u_z$ and that of the fluid $V_x V_y V_z$. We introduce the following strain components for the solid

$$e_{xx} = \frac{\partial u_x}{\partial x} \quad e_{xy} = \frac{\partial u_y}{\partial x} + \frac{\partial u_x}{\partial y} \quad \ldots \text{ etc.} \quad \ldots\ldots [3]$$

The only relevant strain component of the fluid is the dilation

$$\epsilon = \frac{\partial U_x}{\partial x} + \frac{\partial U_y}{\partial y} + \frac{\partial U_z}{\partial z} \quad \ldots\ldots [4]$$

We also introduce the dilation of the solid

$$e = e_{xx} + e_{yy} + e_{zz} \quad \ldots\ldots [5]$$

The stress-strain relations are

$$\left.\begin{aligned} \sigma_{xx} &= 2Ne_{xx} + Ae + Q\epsilon \\ \sigma_{yy} &= 2Ne_{yy} + Ae + Q\epsilon \\ \sigma_{zz} &= 2Ne_{zz} + Ae + Q\epsilon \\ \sigma_{yz} &= Ne_{yz} \\ \sigma_{zx} &= Ne_{zx} \\ \sigma_{xy} &= Ne_{xy} \\ \sigma &= Qe + R\epsilon \end{aligned}\right\} \quad \ldots\ldots [6]$$

There are in this case four elastic constants, A, N, Q, and R.

If we neglect the body force, which is irrelevant to our problem, the stress field must satisfy the following equilibrium relations

$$\left.\begin{aligned} \frac{\partial(\sigma_{xx} + \sigma)}{\partial x} + \frac{\partial \sigma_{xy}}{\partial y} + \frac{\partial \sigma_{xz}}{\partial z} &= 0 \\ \frac{\partial \sigma_{yx}}{\partial x} + \frac{\partial(\sigma_{yy} + \sigma)}{\partial y} + \frac{\partial \sigma_{yz}}{\partial z} &= 0 \\ \frac{\partial \sigma_{zx}}{\partial x} + \frac{\partial \sigma_{zy}}{\partial y} + \frac{\partial(\sigma_{zz} + \sigma)}{\partial z} &= 0 \end{aligned}\right\} \quad \ldots\ldots [7]$$

[1] This investigation was carried out for the Exploration and Production Research Division of the Shell Development Company, Houston, Texas.

[2] Consultant, Shell Development Company. Mem. ASME.

[3] Members in parentheses refer to the Bibliography at the end of the paper.

Contributed by the Applied Mechanics Division and presented at the Diamond Jubilee Annual Meeting, Chicago, Ill., November 13–18, 1955, of The American Society of Mechanical Engineers.

Discussion of this paper should be addressed to the Secretary, ASME, 29 West 39th Street, New York, N. Y., and will be accepted until April 10, 1956, for publication at a later date. Discussion received after the closing date will be returned.

Note: Statements and opinions advanced in papers are to be understood as individual expressions of their authors and not those of the Society. Manuscript received by ASME Applied Mechanics Division, January 31, 1955. Paper No. 55—A-7.

The equations of flow for the fluid in the porous solid are written

$$\left.\begin{aligned}\frac{\partial \sigma}{\partial x} &= b\,\frac{\partial}{\partial t}\,(U_x - u_x)\\ \frac{\partial \sigma}{\partial y} &= b\,\frac{\partial}{\partial t}\,(U_y - u_y)\\ \frac{\partial \sigma}{\partial z} &= b\,\frac{\partial}{\partial t}\,(U_z - u_z)\end{aligned}\right\} \quad \ldots\ldots\ldots\ldots [8]$$

Substituting Equations [6] into the equilibrium Equations [7] and the flow Equations [8] yields the six equations

$$N\nabla^2\bar{u} + (P - N + Q)\,\text{grad}\,e + (Q + R)\,\text{grad}\,\epsilon = 0$$

$$\text{grad}\,(Qe + R\epsilon) = b\,\frac{\partial}{\partial t}\,(\bar{U} - \bar{u}) \quad \ldots\ldots [9]$$

We have put

$$P = A + 2N \quad \ldots\ldots [10]$$

The vectors $\bar{u}$ and $\bar{U}$ are the displacement of solid and fluid, respectively

$$\left.\begin{aligned}\bar{u} &= (u_x, u_y, u_z)\\ \bar{U} &= (U_x, U_y, U_z)\end{aligned}\right\} \quad \ldots\ldots [11]$$

Also, by definition we have

$$\left.\begin{aligned}\epsilon &= \text{div}\,\bar{u}\\ e &= \text{div}\,\bar{U}\end{aligned}\right\} \quad \ldots\ldots [11a]$$

We shall now formulate general solutions of Equations [9].

3 Solutions by Means of Displacement Functions

Since the relative displacement $\bar{U} - \bar{u}$ of the fluid is initially zero, the second Equation [9] shows that it must be irrotational; hence we put

$$\bar{U} - \bar{u} = \text{grad}\,\varphi \quad \ldots\ldots [12]$$

Then we introduce the new unknowns u_1 and φ in the differential Equations [9] by the substitution

$$\left.\begin{aligned}\bar{u} &= \bar{u}_1 - \frac{R + Q}{H}\,\text{grad}\,\varphi\\ \bar{U} &= \bar{u}_1 + \frac{P + Q}{H}\,\text{grad}\,\varphi\end{aligned}\right\} \quad \ldots\ldots [13]$$

with $H = P + R + 2Q$ we find

$$\left.\begin{aligned}N\nabla^2 u_1 + (H - N)\,\text{grad}\,e_1 &= 0\\ (Q + R)e_1 + K\nabla^2\varphi &= b\,\frac{\partial \varphi}{\partial t}\end{aligned}\right\} \quad \ldots\ldots [14]$$

with

$$e_1 = \text{div}\,\bar{u}_1$$

$$K = \frac{PR - Q^2}{H} \quad \ldots\ldots [15]$$

We note that $\bar{u}_1$, at the instant of loading, is equal to the displacement of the solid. Hence we may assume that $\varphi = 0$ at $t = 0$. The advantage of Equations [14] is that the first equation is the same as for the displacement vector in the theory of elasticity. They are solved by the introduction of the Boussinesq-Papkovitch functions (9, 10); namely, a scalar ψ_0 and a vector $\bar{\psi}$ satisfying Laplace's equation in Cartesian co-ordinates

$$\nabla^2\psi_0 = \nabla^2\bar{\psi} = 0 \quad \ldots\ldots [16]$$

We may then write for a complete solution of the first Equation [14] the expression

$$\bar{u}_1 = -\text{grad}\,(\psi_0 + \bar{r}\cdot\bar{\psi}) + \frac{2H}{H - N}\,\bar{\psi} \quad \ldots\ldots [17]$$

where

$$\bar{r} = (x, y, z)$$

Because of the property which is derived from the first Equation [14] that

$$\nabla^2 e_1 = 0 \quad \ldots\ldots [18]$$

the solution of the second Equation [14] is

$$\varphi = \frac{Q + R}{b}\int_0^t e_1 dt + \phi \quad \ldots\ldots [19]$$

where ϕ now satisfies the heat-conduction equation

$$K\nabla^2\phi = b\,\frac{\partial \phi}{\partial t} \quad \ldots\ldots [20]$$

We may write e_1, in terms of the functions $\bar{\psi}$

$$e_1 = \text{div}\,u_1 = \frac{2N}{H - N}\,\text{div}\,\bar{\psi} \quad \ldots\ldots [21]$$

Then using Equations [13], [19], and [21], the solid displacement $\bar{u}$ is given by the expression

$$\bar{u} = -\text{grad}\,(\psi_0 + \bar{r}_0\bar{\psi}) + \frac{2H}{H - N}\,\bar{\psi} - \frac{2N(Q + R)^2}{bH(H - N)}\int_0^t \text{grad div}\,\bar{\psi}dt - \frac{Q + R}{H}\,\text{grad}\,\phi \quad \ldots\ldots [22]$$

A similar expression may be written for $\bar{U}$.

Completeness of the solution, Equation [17], was established by Mindlin (11). Hence Equation [22] is also a complete solution of Equation [9] in terms of a scalar ψ_0 and a vector $\bar{\psi}$ satisfying Laplace's Equation [16] and a scalar ϕ satisfying the heat-conduction Equation [20].[4] Since the Boussinesq-Papkovitch solution is the same as that used in the theory of elasticity it appears therefore that from a mathematical standpoint what distinguishes the consolidation problem from an elasticity problem is the addition of the function ϕ satisfying a heat-conduction-type equation.

The settlement is found by subtracting from $\bar{u}$ the value of $\bar{u}$ at the instant immediately after loading found by putting $t = 0$ and $\phi = 0$ in Expression [22].

Substitution of the values of $\bar{u}$ and $\bar{U}$ in Expression [6] yields the stresses in the solid and the pressure in the fluid.

Particular problems may be solved conveniently by the operational methods as exemplified in references (2, 3, 4). The foregoing solutions have the advantage of mathematical symmetry. However, in some problems it may be advantageous to introduce a different set of variables. We write the stress-strain relations as

$$\left.\begin{aligned}\sigma_{\mu\mu} + \sigma &= 2Ne_{\mu\mu} + Se - \alpha p\\ \sigma_{\mu\nu} &= Ne_{\mu\nu} \quad (\mu \neq \nu)\end{aligned}\right\} \quad \ldots\ldots [23]$$

with

$$\alpha = \frac{Q + R}{R}\,f \quad S = A - \frac{Q^2}{R}$$

[4] It will be noted that the grad operator which was dropped in the second Equation [14] is re-established in Expression [22].

The coefficients N and S are Lamé constants in the absence of fluid pressure p. We also introduce a constant

$$M = R/f^2 \quad [24]$$

and a variable

$$\zeta = -f(\epsilon - e) = \frac{1}{M} p + \alpha e \quad [25]$$

The variable ζ is the change of fluid content in volume per unit volume. It is interesting to note the relation between ζ and φ. We find

$$\zeta = -f\nabla^2\varphi \quad [26]$$

Also, we introduce a permeability

$$k = f^2/b \quad [27]$$

such that

$$-k \text{ grad } p = f \frac{\partial}{\partial t} (\bar{U} - \bar{u}) \quad [28]$$

These variables were used originally in reference (1).

Introducing the variable ζ instead of σ, Equations [9] may be written

$$N\nabla^2\bar{u} + (N + S + \alpha^2M) \text{ grad } e - \alpha M \text{ grad } \zeta = 0$$

$$kK_1\nabla^2\zeta = \frac{\partial\zeta}{\partial t} \quad [29]$$

with

$$K_1 = \frac{(2N + S)M}{2N + S + \alpha^2M} = \frac{PR - Q^2}{Hf^2} = \frac{K}{f^2}$$

The second equation is independent of the deformation field and expresses the remarkable property that the fluid content ζ satisfies the diffusion equation. This property is also expressed below by Equation [53]. Proceeding as for Equations [14] it is seen that the general solution for $\bar{u}$ is

$$\bar{u} = -\text{grad } (\psi_0 + r\bar{\psi}) + \frac{2(2N + S + \alpha^2M)}{N + S + \alpha^2M} \bar{\psi} \quad [30]$$

with $\bar{\psi}$ satisfying

$$\nabla^2\bar{\psi} = 0 \quad [31]$$

and

$$(2N + S + \alpha^2M)\nabla^2\psi_0 + \alpha M\zeta = 0 \quad [31a]$$

Actually, the last equation contains a grad operator. However, it can be dropped since it adds to ψ_0 a quadratic function of the co-ordinates which may be included in the Solution [30] by adding a linear function of the co-ordinates in the value of $\bar{\psi}$.

4 Solution by Means of Stress Functions

In some problems the emphasis is on the calculation of the stress rather than the displacement. It is therefore useful to investigate the possibility of expressing solutions by means of stress functions rather than displacement functions. We consider the problem of two-dimensional strain where the strain components $e_{xz}e_{yz}$ and e_{zz} all vanish and the displacement vectors $\bar{u}$ and $\bar{U}$ have only (x, y) components independent of z. The stress-strain relations are

$$\left.\begin{aligned} \sigma_{xx} &= 2Ne_{xx} + Ae + Q\epsilon \\ \sigma_{yy} &= 2Ne_{yy} + Ae + Q\epsilon \\ \sigma_{xy} &= Ne_{xy} \\ \sigma &= Qe + R\epsilon \end{aligned}\right\} \quad [32]$$

In addition

$$\sigma_{zz} = Ae + Q\epsilon \quad [33]$$

All quantities are independent of z.

The equations of equilibrium, Equations [7], may be satisfied by introducing a stress function F

$$\left.\begin{aligned} \sigma_{xx} + \sigma &= \frac{\partial^2F}{\partial y^2} \\ \sigma_{yy} + \sigma &= \frac{\partial^2F}{\partial x^2} \\ \sigma_{xy} &= -\frac{\partial^2F}{\partial x\partial y} \end{aligned}\right\} \quad [34]$$

This represents the total stress field in the bulk material. If we eliminate ϵ between Equations [32] we find

$$\left.\begin{aligned} \sigma_{xx} &= 2Ne_{xx} + Se + \frac{Q}{R}\sigma \\ \sigma_{yy} &= 2Ne_{yy} + Se + \frac{Q}{R}\sigma \\ \sigma_{xy} &= Ne_{xy} \end{aligned}\right\} \quad [35]$$

with

$$S = A - \frac{Q^2}{R} \quad [36]$$

Introducing Equations [34] this becomes

$$\left.\begin{aligned} \frac{\partial^2F}{\partial y^2} &= 2Ne_{xx} + Se + \frac{Q + R}{R}\sigma \\ \frac{\partial^2F}{\partial x^2} &= 2Ne_{yy} + Se + \frac{Q + R}{R}\sigma \\ \frac{\partial^2F}{\partial x\partial y} &= -Ne_{xy} \end{aligned}\right\} \quad [37]$$

Adding the two first Equations [37] and taking into account that

$$e = e_{xx} + e_{yy} \quad [38]$$

we find

$$\frac{1}{2}\nabla^2F = (N + S)e + \frac{(Q + R)}{R}\sigma \quad [39]$$

We now introduce the well-known compatibility relation of the strain tensor. This relation is the following identity

$$\frac{\partial^2e_{xx}}{\partial y^2} + \frac{\partial^2e_{yy}}{\partial x^2} - \frac{\partial^2e_{xy}}{\partial x\partial y} = 0 \quad [40]$$

It may be used to eliminate the strain components from Equations [37] if we add these three equations after applying to each the proper differential operator. This gives

$$\nabla^4F = S\nabla^2e + \frac{Q + R}{R}\nabla^2\sigma \quad [41]$$

Finally, eliminating e between Equations [39] and [41] gives a relation between F and σ

$$(PR - Q^2)\nabla^4F = 2N(Q + R)\nabla^2\sigma \quad [42]$$

In order to solve the problem we need another equation with F

and σ. This may be obtained from the second Equation [9] which expresses Darcy's law. By forming the divergence we have

$$\nabla^2(Qe + R\epsilon) = b\frac{\partial}{\partial t}(\epsilon - e) \quad [43]$$

The quantities e and ϵ may be expressed in terms of F and σ from the last Equation [32] and Equation [39]. Introducing these values in Equation [43] it becomes

$$(PR - Q^2 - NR)\nabla^2\sigma = b(H - N)\frac{\partial\sigma}{\partial t} - \frac{b}{2}(Q + R)\frac{\partial}{\partial t}\nabla^2 F \quad [44]$$

This last equation may be given a more convenient form by combining with Equation [42]. If we multiply Equation [42] by $Q + R$ and Equation [44] by $-H$, then add these equations, we obtain after dividing by H

$$\left(K\nabla^2 - b\frac{\partial}{\partial t}\right)[(Q + R)\nabla^2 F - 2(H - N)\sigma] = 0 \quad [45]$$

Equations [42] and [45] constitute a system of two simultaneous equations for the stress function and the fluid pressure.

A primary inconvenience in using the stress function is that boundary conditions involving displacements require evaluation of these displacements from the stress. Also, it is well known that if the body contains cavities, single-valued stress functions may lead to multivalued displacements or dislocations. The condition that displacements be single-valued requires the use of an additional condition (6). In such cases it will generally be simpler to solve the problem by means of displacement functions. However, when the boundary conditions are given in terms of stresses and if the field contains no cavities, the problem should be conveniently solved by the use of stress functions.

It is interesting to note that elimination of F between Equations [42] and [45] leads to

$$K\nabla^4\sigma = b\frac{\partial}{\partial t}\nabla^2\sigma \quad [46]$$

The fluid pressure is therefore the sum of two functions satisfying, respectively, the two equations

$$\left.\begin{aligned} K\nabla^2\sigma &= b\frac{\partial\sigma}{\partial t} \\ \nabla^2\sigma &= 0 \end{aligned}\right\} \quad [47]$$

Also, elimination of σ between the same Equations [42] and [45] yields

$$K\nabla^6 F = b\frac{\partial}{\partial t}\nabla^4 F \quad [48]$$

Similarly, F is the sum of two functions satisfying, respectively, the two equations

$$\left.\begin{aligned} K\nabla^2 F &= b\frac{\partial F}{\partial t} \\ \nabla^4 F &= 0 \end{aligned}\right\} \quad [49]$$

5 General Properties of Solutions

It is possible to derive certain general properties of the solutions. Starting from Expression [13] for $\vec{u}$ and $\vec{U}$ we find by applying the divergence operator

$$\left.\begin{aligned} e &= e_1 - \frac{R + Q}{H}\nabla^2\varphi \\ \epsilon &= e_1 + \frac{P + Q}{H}\nabla^2\varphi \end{aligned}\right\} \quad [50]$$

Elimination of $\nabla^2\varphi$ or e_1 gives, respectively

$$\left.\begin{aligned} (P + Q)e + (R + Q)\epsilon &= He_1 \\ \epsilon - e &= \frac{P + R}{H}\nabla^2\varphi \end{aligned}\right\} \quad [51]$$

Applying the Laplace operator to the first equation and taking Equation [18] into account

$$\nabla^2[(P + Q)e + (R + Q)\epsilon] = 0 \quad [52]$$

Applying the operator

$$K\nabla^2 - b\frac{\partial}{\partial t}$$

to the second Equation [51] and taking Equations [14] and [18] into account

$$\left(K\nabla^2 - b\frac{\partial}{\partial t}\right)(\epsilon - e) = 0 \quad [53]$$

Similar relations exist for the stresses in the solid. To show this let us introduce the hydrostatic stress σ_h in the solid

$$\sigma_h = \frac{1}{3}(\sigma_{xx} + \sigma_{yy} + \sigma_{zz}) \quad [54]$$

From the stress-strain Relation [6] we derive

$$\left.\begin{aligned} \sigma_h &= Be + Q\epsilon \\ \sigma &= Qe + R\epsilon \end{aligned}\right\} \quad [55]$$

with

$$B = P - \frac{4}{3}N \quad [56]$$

Solving Equation [55] for e and ϵ and substituting in Relations [52] and [53] yields

$$\left.\begin{aligned} &\nabla^2\left\{\sigma_h(PR - Q^2) + \sigma\left[PR - Q^2 - \frac{4}{3}N(Q + R)\right]\right\} = 0 \\ &\left(K\nabla^2 - b\frac{\partial}{\partial t}\right)[\sigma_h(Q + R) - \sigma(B + Q)] = 0 \end{aligned}\right\} \quad [57]$$

Finally, by applying the operator

$$\nabla^2\left(K\nabla^2 - b\frac{\partial}{\partial t}\right)$$

to Expression [50] and taking into account Equations [14] and [18], we find

$$\left.\begin{aligned} \nabla^2\left(K\nabla^2 - b\frac{\partial}{\partial t}\right)e &= 0 \\ \nabla^2\left(K\nabla^2 - b\frac{\partial}{\partial t}\right)\epsilon &= 0 \end{aligned}\right\} \quad [58]$$

Also, from Equations [55] and [58]

$$\left.\begin{aligned}\nabla^2\left(K\nabla^2 - b\frac{\partial}{\partial t}\right)\sigma_h &= 0\\ \nabla^2\left(K\nabla^2 - b\frac{\partial}{\partial t}\right)\sigma &= 0\end{aligned}\right\} \quad \ldots\ldots [59]$$

It is interesting to note that Equation [45] may be derived from the second Equation [57].

We write

$$X = (B + Q)\sigma - (R + Q)\sigma_h \quad \ldots\ldots [60]$$

and substitute the value of σ_h in terms of $\nabla^2 F$ and σ by the relation

$$\left.\begin{aligned}D\nabla^2 F &= 2\sigma_h\left(D + \frac{1}{3}NR\right) + 2\sigma\left(D - \frac{1}{3}QN\right)\\ &\text{with}\\ D &= BR - Q^2 = PR - Q^2 - \frac{4}{3}NR\end{aligned}\right\} \quad \ldots\ldots [61]$$

We find

$$2X\left(D + \frac{1}{3}NR\right) = D[2\sigma(H - N) - (R + Q)\nabla^2 F] \quad \ldots\ldots [62]$$

Applying the operator

$$K\nabla^2 - b\frac{\partial}{\partial t}$$

to the equation and taking into account that, from Equation [57]

$$\left(K\nabla^2 - b\frac{\partial}{\partial t}\right)X = 0 \quad \ldots\ldots [63]$$

we find Equation [45].

One interesting particular case of the general solution is when the displacement vector in the solid is the gradient of a scalar, i.e., when the rotation vanishes. Such a case occurs if we put

$$\vec{\psi} = 0 \quad \ldots\ldots [64]$$

in Equation [22]. The solid and fluid displacements are

$$\left.\begin{aligned}\vec{u} &= -\text{grad}\left[\psi_0 + \frac{Q + R}{H}\phi\right]\\ \vec{U} &= -\text{grad}\left[\psi_0 - \frac{P + Q}{H}\phi\right]\end{aligned}\right\} \quad \ldots\ldots [65]$$

with

$$\left.\begin{aligned}\nabla^2\psi_0 &= 0\\ \left(K\nabla^2 - b\frac{\partial}{\partial t}\right)\phi &= 0\end{aligned}\right\} \quad \ldots\ldots [66]$$

We have

$$\left.\begin{aligned}e &= \text{div } \vec{u} = -\frac{Q + R}{H}\nabla^2\phi\\ \epsilon &= \text{div } \vec{U} = \frac{P + Q}{H}\nabla^2\phi\end{aligned}\right\} \quad \ldots\ldots [67]$$

The fluid pressure is given by the last Equation [6]

$$\sigma = Qe + R\epsilon \quad \ldots\ldots [68]$$

Substituting Equation [67]

$$\sigma = K\nabla^2\phi \quad \ldots\ldots [69]$$

Because of Equation [66] we may write

$$\left(K\nabla^2 - b\frac{\partial}{\partial t}\right)\sigma = 0 \quad \ldots\ldots [70]$$

The pore pressure in this case satisfies the heat-conduction equation.

By substituting Equations [65] and [69] into Expression [6] for the stress we find

$$\left.\begin{aligned}\sigma_{zz} &= -2N\frac{\partial^2}{\partial x^2}\left[\psi_0 + \frac{R + Q}{H}\phi\right] - \left[\frac{2N(Q + R)}{PR - Q^2} - 1\right]\sigma\\ \sigma_{xy} &= -2N\frac{\partial^2}{\partial x\partial y}\left[\psi_0 + \frac{R + Q}{H}\phi\right], \text{ etc.}\end{aligned}\right\} \quad \ldots\ldots [71]$$

The function ϕ may be determined from σ by taking into account Equations [66] and [69], i.e.

$$\sigma = b\frac{\partial\phi}{\partial t} \quad \ldots\ldots [72]$$

Since $\phi = 0$ at the instant of loading we have

$$\phi = \frac{1}{b}\int_0^t \sigma\, dt \quad \ldots\ldots [73]$$

These expressions are particularly useful in solving problems with spherical symmetry or cylindrical problems with circular symmetry.

For instance, the problem of loading of a spherical cavity in an infinite porous material is easily solved by putting

$$\psi_0 = \frac{C}{r} \quad \ldots\ldots [74]$$

with

$$r = \sqrt{x^2 + y^2 + z^2}$$

while σ is given by the well-known expression for heat conduction with spherical symmetry. Similarly, for a cylindrical cavity we put

$$\psi_0 = C \log r \quad \ldots\ldots [75]$$

with $r = \sqrt{x^2 + y^2}$ and the corresponding heat-conduction expressions for σ.

More general irrotational solutions are obtained by adding to the foregoing the trivial case of uniform hydrostatic pressure in the pores along with a state of uniform isotropic stress in the solid. This amounts to putting $\vec{\psi}$ equal to the gradient of a scalar. With these additional solutions we can solve the case of the sphere or cylinder with finite thickness.

6 Eigenfunctions and Modes of Consolidation

Another procedure in the solution of consolidation problems is to introduce eigenfunctions and the concept of consolidation modes. This is best illustrated by an example:

Consider the one-dimensional consolidation problem when a column of height h is under a vertical load γ per unit area. The load is applied through a porous slab so that the fluid pressure at the top boundary is zero. The z-co-ordinate is along the vertical direction, the bottom of the column being at $z = 0$ and the top at $z = h$.

Equation [9] becomes in this case

$$\left.\begin{aligned}(P+Q)\frac{\partial^2 u_s}{\partial z^2}+(Q+R)\frac{\partial^2 U_s}{\partial z^2}&=0\\ Q\frac{\partial^2 u_s}{\partial z^2}+R\frac{\partial^2 U_s}{\partial z^2}&=b\frac{\partial}{\partial t}(U_s-u_s)\end{aligned}\right\}\quad\ldots\ldots[76]$$

These equations are solved by Expressions [13] which in the present case take the form

$$\left.\begin{aligned}u_s&=u_1-\frac{R+Q}{H}\frac{\partial\varphi}{\partial z}\\ U_s&=u_1+\frac{P+Q}{H}\frac{\partial\varphi}{\partial z}\end{aligned}\right\}\quad\ldots\ldots[77]$$

Substituting in Equations [76] leads to

$$\frac{\partial^2 u}{\partial z^2}=0$$

$$(Q+R)\frac{\partial^2 u_1}{\partial z^2}+K\frac{\partial^2\varphi}{\partial z^2}=b\frac{\partial\varphi}{\partial t}\quad\ldots\ldots[78]$$

In order to introduce the boundary condition let us express the stress

$$\left.\begin{aligned}\sigma_{zz}&=(P+Q)\frac{\partial u_1}{\partial z}-K\frac{\partial^2\varphi}{\partial z^2}\\ \sigma&=(Q+R)\frac{\partial u_1}{\partial z}+K\frac{\partial^2\varphi}{\partial z^2}\end{aligned}\right\}\quad\ldots\ldots[79]$$

We separate the solution into a part independent of time and a variable one. We consider u_1 independent of time and we put

$$\varphi=\varphi_1+\phi\quad\ldots\ldots[80]$$

where ϕ is the time-dependent part of φ.

Because of Equation [78] and the boundary condition $\sigma=0$ at $z=h$ we find

$$\frac{\partial u_1}{\partial z}=C_1\quad\frac{\partial^2\varphi_1}{\partial z^2}=C_2\quad\ldots\ldots[81]$$

with

$$\left.\begin{aligned}(Q+R)C_1+KC_2&=0\\ (P+Q)C_1-KC_2&=-\gamma\end{aligned}\right\}\quad\ldots\ldots[82]$$

Hence

$$\left.\begin{aligned}C_1&=-\gamma/H\\ C_2&=\frac{\gamma(Q+R)}{PR-Q^2}\end{aligned}\right\}\quad\ldots\ldots[83]$$

The time-dependent part ϕ satisfies the equation

$$\frac{\partial^2\phi}{\partial z^2}=\frac{1}{a}\frac{\partial\phi}{\partial t}\quad\ldots\ldots[84]$$

with $a=b/K$. Solutions of this equation are

$$\phi=\cos z\sqrt{\frac{\alpha}{a}}\,e^{-\alpha t}\quad\ldots\ldots[85]$$

The boundary condition that $u_s=U_s=0$ at $z=0$ is not disturbed since $\partial\phi/\partial z=0$ at that point. The stresses at the upper boundary are not disturbed if we have $\partial^2\phi/\partial z^2=0$ at $z=h$; hence

$$h\sqrt{\frac{\alpha}{a}}=\frac{\pi}{2},\ \frac{3\pi}{2},\ \frac{5\pi}{2}\ldots\left(\frac{2n+1}{2}\right)\pi\quad\ldots\ldots[86]$$

These lead to the eigenfunctions

$$\phi_n=\cos z\sqrt{\frac{\alpha_n}{a}}\,e^{-\alpha_n t}\quad\ldots\ldots[87]$$

with the characteristic values for α

$$\alpha_n=\left(\frac{2n+1}{2}\right)^2\frac{\pi^2 a}{h^2}\quad\ldots\ldots[88]$$

The consolidation problem is then solved by a series of eigenfunctions

$$\phi=\sum^{n}A_n\phi_n\quad\ldots\ldots[89]$$

when A_n are Fourier coefficients determined by the initial condition

$$\varphi=0\text{ for }t=0$$

or

$$\frac{\partial^2\phi}{\partial z^2}=-\frac{\partial^2\varphi_1}{\partial z^2}=-C_2\quad\ldots\ldots[90]$$

The time-dependent part of the deformation is then expressed as the sum of an infinite number of "modes of consolidation," such that for each of these functions the displacements are proportional to the same decreasing exponential $e^{-\alpha t}$. This procedure may be generalized to the three-dimensional case. The existence of consolidation modes is a consequence of a general property of relaxation phenomena as shown by the author in reference (7).

BIBLIOGRAPHY

1 "General Theory of Three Dimensional Consolidation," by M. A. Biot, *Journal of Applied Physics*, vol. 12, 1941, pp. 155–165.

2 "Consolidation Settlement Under a Rectangular Load Distribution," by M. A. Biot, *Journal of Applied Physics*, vol. 12, 1941, pp. 426–430.

3 "Consolidation Settlement of a Soil With an Impervious Top Surface," by M. A. Biot and F. M. Clingan, *Journal of Applied Physics*, vol. 12, 1941, pp. 578–581.

4 "Bending Settlement of a Slab Resting on a Consolidating Foundation," by M. A. Biot and F. M. Clingan, *Journal of Applied Physics*, vol. 13, 1942, pp. 35–40.

5 "Theory of Elasticity and Consolidation for a Porous Anisotropic Solid," by M. A. Biot, *Journal of Applied Physics*, vol. 26, 1955, pp. 182–185.

6 "A Treatise on the Mathematical Theory of Elasticity," by A. E. H. Love, Dover Publications, New York, N. Y., 1944, chapter IX.

7 "Theory of Stress Strain Relations in Anisotropic Visco-Elasticity and Relaxation Phenomena," by M. A. Biot, *Journal of Applied Physics*, vol. 25, 1954, pp. 1385–1391.

8 "Endbaumechanik auf Bodenphysikalischer Grundlage," by K. Terzaghi, F. Denticke, Leipzig, Germany, 1925.

9 "Application des Potentiels a l'Étude de l'Equilibre et des Mouvements des Solides Élastiques," by J. Boussinesq, Gauthier-Villars, Paris, France, 1885, pp. 65–72.

10 "Solution Générale des Equations Fondamentales d'Élasticité, Exprimée par Trois Fonctions Harmoniques," by P. F. Papkovitch, Comptes-Rendus Academie des Sciences, vol. 195, 1932, pp. 513–515, 754–756.

11 "Note on the Gallerkin and Papkovitch Stress-Functions," by R. D. Mindlin, Bull. American Mathematical Society, vol. 42, 1936, pp. 373–376.

Determination of Natural Frequencies of Continuous Plates Hinged Along Two Opposite Edges

By A. S. VELETSOS[1] and N. M. NEWMARK,[2] URBANA, ILL.

A numerical procedure is presented for computing the undamped natural frequencies of bending vibration of rectangular plates which are hinged along two opposite edges and continuous over rigid supports transverse to the hinged edges. Along the hinged edges, there are assumed to be uniformly distributed forces acting in the middle plane of the plate. The procedure is illustrated by two examples.

Introduction

THE procedure described herein is an extension of Holzer's method (1)[3] for calculating the natural frequencies of torsional vibration of shafts. Like Holzer's method it is reduced to a straightforward scheme of numerical computations which, when repeated a sufficient number of times, will give the natural frequencies of the system to any desired degree of accuracy.

The procedure is applicable to any plate which is hinged along two opposite edges and is continuous over rigid supports transverse to the hinged edges; along the hinged edges the plate may be subjected to distributed forces acting in the middle plane of the plate. The mass per unit of the area, the flexural rigidity of the plate, and the magnitude of the distributed forces may vary from one panel to the next, but in any one panel these quantities are considered constant. The assumptions made are those embodied in the ordinary theory of flexure of medium-thick elastic plates; it is further assumed that the supports offer no torsional restraint and that no frictional forces or horizontal shearing forces develop between the plate and the supports. The effects of damping, rotatory inertia, shearing deformation, and vibrations in the plane of the plate are neglected.

Sign Convention. Downward deflection and clockwise rotations are taken as positive. Internal bending moments at the ends of a panel and external couples are taken as positive when acting in a clockwise direction.

Basic Principles

Fig. 1 shows the type of continuous plate considered. The coordinate axes are taken along the two adjacent edges with the origin of the axes at the upper left-hand corner, as shown in Fig. 1. The hinged edges are taken parallel to the y-axis. The transverse rigid supports are numbered consecutively starting with 1 at the extreme left end and terminating with z at the extreme right end. The symbol j denotes an interior support.

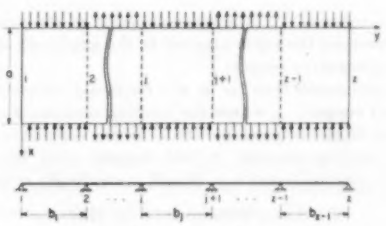

FIG. 1 TYPE OF CONTINUOUS PLATE CONSIDERED

Consider first that the plate oscillates in one of its natural modes. Then the solution of the governing differential equation reveals that the deflections, rotations, shears, and bending moments along sections perpendicular to the simply supported edges are proportional to

$$\sin \frac{n\pi x}{a} \cos \omega_{n,i} t$$

where $\omega_{n,i}$ is a circular natural frequency, t is time, a is the width of the plate, and n is an integer designating the number of half-sine waves, alternately upward and downward, in the distribution of the deflection, slope, shear, or bending moment along the plate width. Corresponding to each value of n there is an infinite number of natural frequencies ω_n corresponding to $i = 1, 2, 3, \ldots$.

Consider next that the plate undergoes a steady-state forced vibration, such that its rotation at the extreme left support is

$$\theta_1(x, t) = \theta_1 \sin \frac{n\pi x}{a} \cos \omega t \ldots\ldots\ldots\ldots [1a]$$

where ω is the circular frequency of the forced vibration, n is the same integer as that used previously, and θ_1 is the maximum amplitude of rotation at the left support. The quantity θ_1 is assumed to have a prescribed finite value. If the left support is fixed, θ_1 is equal to zero, but the amplitude of the corresponding internal bending moment is finite. In this case, consider that the moment is given by the relation

$$M_1(x, t) = M_1 \sin \frac{n\pi x}{a} \cos \omega t \ldots\ldots\ldots\ldots [1b]$$

and that the amplitude M_1 has a prescribed finite value. In either case, imagine that the vibration is maintained by an exciting couple applied at the extreme right-hand support. As before, the solution of the governing differential equation reveals that the deflections, rotations, shears, and bending moments along sections perpendicular to the simply supported edges, and the exciting couple, are proportional to, and either in phase with, or 180 deg

---

[1] Research Assistant Professor of Civil Engineering, University of Illinois. Assoc. Mem. ASME.

[2] Research Professor of Structural Engineering, University of Illinois. Mem. ASME.

[3] Numbers in parentheses refer to the Bibliography at the end of the paper.

Contributed by the Applied Mechanics Division and presented at the Diamond Jubilee Annual Meeting, Chicago, Ill., November 13–18, 1955, of THE AMERICAN SOCIETY OF MECHANICAL ENGINEERS.

Discussion of this paper should be addressed to the Secretary, ASME, 29 West 39th Street, New York, N. Y., and will be accepted until April 10, 1956, for publication at a later date. Discussion received after the closing date will be returned.

NOTE: Statements and opinions advanced in papers are to be understood as individual expressions of their authors and not those of the Society. Manuscript received by ASME Applied Mechanics Division, December 14, 1954. Paper No. 55—A-11.

out of phase with, the rotation (or bending moment) at the extreme left support. The exciting couple may be written as

$$\bar{M}_s(x, t) = \bar{M}_z \sin \frac{n\pi x}{a} \cos \omega t \quad [2]$$

The amplitude $\bar{M}_z$ depends upon the frequency of vibration. For the limiting case of zero frequency, $\bar{M}_z$ is finite. For frequencies greater than zero, the value of $\bar{M}_z$ may be smaller or larger than that for the static case, depending on whether the resulting inertia forces are in phase with, or 180 deg out of phase with, the exciting couple. For a frequency equal to a natural frequency of the plate ($\omega = \omega_{n,i}$), $\bar{M}_z$ becomes identically equal to zero, and the deflection of the plate, which represents a natural mode of vibration, is given by the expression

$$w(x, y, t) = Y_n \sin \frac{n\pi x}{a} \cos \omega_{n,i} t, \quad [3]$$

where the value of Y_n, which is a function of the y-co-ordinate only, depends on the value assigned to the amplitude of slope (or bending moment) at support 1.

In the discussion thus far, it was implicitly assumed that the right-hand support, z, where the exciting moment was applied, was either hinged or partially fixed. If this support is fixed, the internal bending moment at that support must have such a value, at a natural frequency, that θ_z is identically equal to zero.

General Description of Method

The foregoing facts suggest the following procedure for computing natural frequencies of vibration of the type of plate considered.

1 Imagine that the plate oscillates in a steady state at an assumed frequency of vibration and with a specified number of half-sine waves along sections perpendicular to the hinged edges. Let $n = \bar{n}$ be the number of half-sine waves. Consider further that the amplitude of the sinusoidally distributed rotation (or internal bending moment) at the left-hand support has a prescribed finite value.

2 Determine the amplitude of the exciting couple at the right-hand support necessary to maintain this vibration.

3 Repeat these steps for different frequencies and plot the magnitude of the exciting moment as a function of the frequency of vibration. The desired natural frequencies are those frequencies for which the exciting couple[4] vanishes.

4 The natural frequencies determined in step 3 correspond to a value of $n = \bar{n}$. In general, steps 1 through 3 must be repeated for as many values of n as may be necessary in a given problem.

The principal computational task in this method is the evaluation of the exciting couple. This may be accomplished by a number of different procedures. The conditions to be satisfied are simply those of equilibrium and continuity at each support. These may be expressed in equation form in a number of different ways, and the equations may be solved by a variety of procedures. In the procedure presented herein, these conditions are expressed in the form of a dynamic three-slope equation, and the distortions of the plate, from which the exciting moment is evaluated, are computed by the repeated application of this equation, progressing from one end of the plate to the other. The details of the procedure are explained in a later section.

Elastic Constants for a Plate Panel

Consider the rectangular plate shown in Fig. 2 which is hinged on three edges, fixed on the fourth, and subjected to uniformly distributed forces along the two opposite hinged edges. The magnitude of these forces per unit of length will be denoted by p_x. A positive value of p_x corresponds to a compressive force, whereas a negative value corresponds to a tensile force. Let edge f be subjected to a rotation without deflection, such that the magnitude of the rotation is given by the relation

$$\theta_f(x, t) = \theta_f \sin \frac{n\pi x}{a} \cos \omega t \quad [4]$$

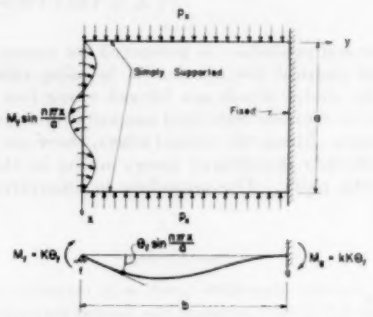

FIG. 2 STIFFNESS AND CARRY-OVER FACTOR

The moment at edge f necessary to produce this rotation is proportional to $\sin (n\pi x/a) \cos \omega t$, and its maximum amplitude is

$$M_f = K\theta_f \quad [5]$$

The quantity K is defined as the "dynamic flexural stiffness" of edge f.

The moment induced at the fixed edge is also proportional to $\sin (n\pi x/a) \cos \omega t$, and its maximum amplitude may be written as

$$M_g = kK\theta_f = kM_f \quad [6]$$

The quantity k, which represents the ratio of the moment at the fixed edge and the applied moment, is defined as the "dynamic flexural carry-over factor" for edge f.

These quantities are generalizations of those introduced by Hardy Cross (2) and extended later by James (3), Lundquist (4, 5), Newmark (6), and Gaskell (7).

The stiffness K may be expressed as

$$K = C_K \frac{D}{b} \quad [7]$$

where C_K is a dimensionless factor, D is the flexural rigidity per unit width of the plate, and b is its span length in a direction parallel to the hinged edges.

For the special case of a plate which does not vibrate but is subjected only to compressive forces p_x, the quantity C_K and the carry-over factor k are functions of the ratio a/nb and of the dimensionless parameter

$$\xi_p = \frac{b^2 p_x}{\pi^2 D} \quad [8]$$

For this case, numerical values of C_K and k have been tabulated by Kroll (8).[5] By comparing the differential equation for flexural vibration with that for buckling, it can readily be shown that, for a vibrating plate of the type considered in this paper, the values of C_K and k can be obtained from Kroll's tables merely by replacing the value of ξ_p by $\bar{\xi}$, where

[4] It is assumed that support z is not fixed. If this support is fixed, the desired natural frequencies are those frequencies for which θ_z vanishes.

[5] Kroll uses the symbols λ for a/n, k for ξ_p, S for K, and C for k. The symbols used herein conform, in general, to those used in reference (6).

$$\bar{\xi} = \xi_p + \xi_\omega \quad [9]$$

The quantity ξ_ω accounts for the inertia effects and is given by

$$\xi_\omega = \left(\frac{a}{nb}\right)^2 \frac{b^4}{\pi^4} \frac{m\omega^2}{D} \quad [10]$$

The analogy defined by Equation [9] may be arrived at in a manner similar to that used by Lurie (9) for the special case of a vibrating plate for which $p_x = 0$.

It should be noted that Kroll defines stiffness as the moment necessary to produce a maximum rotation amplitude of $^1/_4$ radian, instead of 1 radian. Consequently, the stiffness values obtained from Kroll's tables must be multiplied by four to make them conform to the definition given in this paper.

Fundamental Equations

Fig. 3 shows, to an exaggerated scale, the extreme deflected position of panels $j-1$ and j of a continuous plate undergoing steady-state forced vibration. As previously remarked, the vibration is assumed to be maintained by a single exciting couple, $\bar{M}_j(x, t)$, applied at the extreme right-hand support. In the following, the quantities b_j, D_j, $(\xi_p)_j$, $(\xi_\omega)_j$, $\bar{\xi}_j$, K_j, and $(kK)_j$ refer to the panel between supports j and $j+1$. The rotations and bending moments at the ends of the panels are indicated in their positive directions. Their values at a time t for support j are

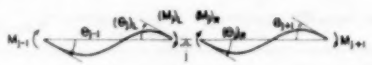

Fig. 3 Spans $j-1$ and j of a Continuous Plate

$$\left.\begin{aligned} \theta_j(x, t) &= \theta_j \sin\frac{n\pi x}{a}\cos\omega t \\ M_j(x, t) &= M_j \sin\frac{n\pi x}{a}\cos\omega t \end{aligned}\right\} \quad [11]$$

In the equations to be used, the term $\sin(n\pi x/a)\cos\omega t$ appears as a common factor; for convenience, this will be omitted, and in the remainder of this discussion, the terms "maximum amplitude of rotation" and "rotation" and the terms "maximum amplitude of moment" and "moment" will be used interchangeably.

The equations expressing the conditions of continuity and equilibrium at the j-th support are

$$(\theta_j)_L = (\theta_j)_R = \theta_j \quad [12]$$

$$(M_j)_L + (M_j)_R = 0 \quad [13]$$

where the subscripts L and R refer to sections just to the left and just to the right of the support.

The moments $(M_j)_L$ and $(M_j)_R$ can be expressed in terms of the end rotations of spans $j-1$ and j as follows

$$(M_j)_L = K_{j-1}\theta_j + (kK)_{j-1}\theta_{j-1} \quad [14a]$$

$$(M_j)_R = K_j\theta_j + (kK)_j\theta_{j+1} \quad [14b]$$

Substitution of the last two equations into Equation [13] yields

$$(kK)_{j-1}\theta_{j-1} + [K_{j-1} + K_j]\theta_j + (kK)_j\theta_{j+1} = 0 \quad [15]$$

For convenience in later use, this equation is rewritten as

$$\theta_{j+1} = -\frac{(kK)_{j-1}\theta_{j-1} + \bar{K}_j\theta_j}{(kK)_j} \quad [16a]$$

where $\bar{K}_j$ denotes the total flexural stiffness at support j

$$\bar{K}_j = K_{j-1} + K_j \quad [16b]$$

Strictly speaking, Equation [16] is applicable to interior supports only. For the end supports the following specialized relations must be used. Consider the general case in which the ends are subjected to rotational restraints of constant stiffness. Let the relationship between the end moments and the corresponding rotations be given by

$$M_1 = -R_1\theta_1 \text{ and } M_s = -R_s\theta_s \quad [17]$$

where R_1 and R_s are the stiffnesses of the restraints at the left and right ends, respectively. For a hinged end $R = 0$ and for a fixed end $R =$ infinity. The negative signs in these expressions denote that for a positive restraint (positive value of R) the moment acts in a direction opposite to the direction of rotation of the panel.

Consider first the left end. For a hinged or partially fixed condition, Equation [16a] reduces to

$$\theta_2 = -\frac{\bar{K}_1}{(kK)_1}\theta_1 \quad [18a]$$

where

$$\bar{K}_1 = R_1 + K_1 \quad [18b]$$

For a fixed condition $\theta_1 = 0$, and the relation between the internal bending moment at the fixed end and the rotation at the second support is obtained from Equation [14b] as

$$M_1 = (kK)_1\theta_2 \quad [19]$$

Consider next the right end of the plate. For a hinged or partially fixed condition, the exciting couple is found from a specialized form of Equation [14a] as

$$\bar{M}_s = (K_{s-1} + R_s)\theta_s + (kK)_{s-1}\theta_{s-1} \quad [20]$$

For a fixed condition $\theta_s = 0$. In this case, the internal bending moment M_s is of no practical interest but, if desirable, it can be calculated from Equation [20] by taking $\theta_s = 0$.

Outline of Procedure

The principal computational task of the procedure, as previously described, is the determination of the exciting couple at the right end of the plate necessary to maintain a prescribed amplitude of rotation (or internal bending moment) at the left end. Since the natural frequencies of a system depend on the relative rather than the absolute values of the deflection, any arbitrary amplitude, consistent with the actual boundary conditions, may be chosen for the amplitude of vibration at support 1. For a hinged edge and for a partially fixed edge, take

$$\theta_1(x) = 1.00 \sin\frac{n\pi x}{a}$$

For a fixed edge, take

$$M_1(x) = -1.00 \sin\frac{n\pi x}{a}$$

The procedure is initiated by specifying the value of n and by assuming a value of ξ_ω for some reference panel r; let $n = \bar{n}$. This step is equivalent to assuming a frequency of vibration

$$\omega = \sqrt{(\xi_\omega)_r}\,\frac{\bar{n}b_r}{a_r}\,\frac{\pi^2}{b_r^2}\sqrt{\frac{D_r}{m_r}} \quad [21]$$

The values of ξ_ω for the remaining panels are computed from the expression

$$(\xi_\omega)_j = \frac{m_j}{m_r}\left(\frac{b_j}{b_r}\right)^2 \frac{D_r}{D_j}(\xi_\omega)_r \quad [22]$$

and the corresponding values of $\bar{\xi}$ are determined from

$$\bar{\xi}_j = (\xi_p)_j + (\xi_\omega)_j \quad [23]$$

The term $(\xi_p)_j$ is independent of the frequency of vibration. Using the values of $\bar{\xi}_j$ determined in Equation [23], the values of K_j and $(kK)_j$ for the various panels are next obtained from Kroll's tables (8), in terms of $4D_j/b_j$, where the subscript j refers to the particular panel considered. Before using them in the fundamental equations, it is convenient to express these quantities in terms of the properties of the reference panel. This is accomplished by multiplying them by the dimensionless factor

$$\alpha_j = \frac{D_j}{D_r}\frac{b_r}{b_j} \quad [24]$$

The rotations at the supports are finally evaluated as follows: The rotation θ_2 is computed from Equation [18], and the rotations θ_3 through θ_s are evaluated by the successive application of Equation [16] to supports 2 through 4. A convenient scheme for arranging the computations is described in the second illustrative example. If support z is fixed, the determination of the rotation θ_s completes one cycle of the procedure. However, if this support is hinged or only partially fixed, it is necessary to evaluate also Equation [20].

The foregoing steps are repeated for different values of $(\xi_\omega)_r$ and for as many values of n as necessary, and the exciting moment (or slope) at the right end is plotted as a function of $(\xi_\omega)_r$. The desired natural frequencies are those frequencies for which the quantity plotted becomes equal to zero.

Illustrative Examples

Example 1. Consider a rectangular plate simply supported along two opposite edges and continuous over five rigid supports spaced equidistantly. The plate is simply supported at the left end and fixed at the right end, as shown in Fig. 4. All panels are square and their flexural rigidity D, and mass per unit of area m, are assumed to be constant. There are no forces acting in the plane of the plate ($p_x = 0$); accordingly, $\xi_\omega = \bar{\xi}$. It is desired to calculate all natural frequencies comprised within a range of frequencies corresponding to values of ξ_ω from zero to 7.0.

Since all panels are identical, rather than repeating the procedure outlined for each assumed frequency of vibration, it is more convenient, in this particular case, to obtain a general expression for θ_5 and determine directly from this expression the desired natural frequencies.

Let K be the flexural stiffness and k the flexural carry-over factor for each panel. Take $\theta_1 = 1.00$; then from Equation [18] one obtains

$$\theta_2 = -\frac{K}{kK} = -\frac{1}{k}$$

Applying Equation [16] successively to joints 2, 3, and 4, one obtains

$$\theta_3 = -\frac{K\left[2\left(-\frac{1}{k}\right)+k\right]}{kK} = \frac{2-k^2}{k^2}$$

$$\theta_4 = -\frac{K\left[2\frac{2-k^2}{k^2}+k\left(-\frac{1}{k}\right)\right]}{kK} = \frac{3k^2-4}{k^3}$$

$$\theta_5 = -\frac{K\left[2\frac{3k^2-4}{k^3}+k\frac{2-k^2}{k^2}\right]}{kK} = \frac{k^4-8k^2+8}{k^4}$$

The expression for θ_5 has been evaluated for $n = 1$ and $n = 2$ over the entire range of values of ξ_ω considered. The results are presented in Fig. 4. The values of K corresponding to the various values of ξ_ω and n were obtained from Kroll's tables. The values of ξ_ω corresponding to natural frequencies are recorded on the figure.

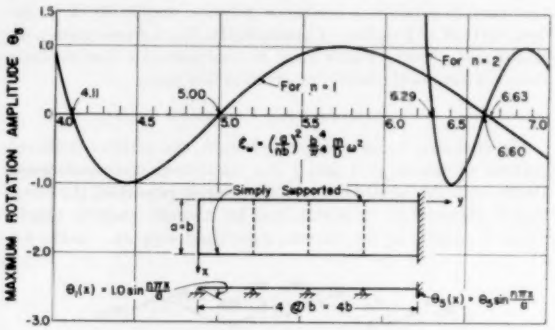

Fig. 4 Natural Frequencies for Example 1

The lowest circular natural frequencies for $n = 1$ and $n = 2$ are

$$\omega_{1,1} = \sqrt{4.11}\,\frac{\pi^2}{b^2}\sqrt{\frac{D}{m}} = \frac{20.01}{b^2}\sqrt{\frac{D}{m}}$$

$$\omega_{2,1} = 2\sqrt{6.29}\,\frac{\pi^2}{b^2}\sqrt{\frac{D}{m}} = \frac{49.51}{b^2}\sqrt{\frac{D}{m}}$$

Example 2. To illustrate the application of the method to a general case in which the properties of the plate change from one panel to the next, and to present a convenient scheme for arranging the computations, we shall calculate the fundamental natural frequency of the hypothetical 4-panel continuous plate shown in Fig. 5(*a*). The plate is elastically restrained against rotation at the left end and simply supported at the right end. The stiffness of the end restraint R_1, the magnitudes of the axial forces, and the properties of the various panels are shown in Fig. 5(*a*). In this case, panel 2 is taken as the reference span.

The quantities $(\xi_\omega)_j/(\xi_\omega)_r$, $(\xi_p)_j$, and α_j are evaluated in Table 1. It should be noted that these quantities are independent of the frequency of vibration and are computed but once.

A complete cycle of the procedure is presented for a trial value of $(\xi_\omega)_r = 1.7$, considering that $n = 1$; this value corresponds to a circular frequency of vibration

$$\omega = \sqrt{1.7}\,\frac{\pi^2}{b^2}\sqrt{\frac{D}{m}}$$

The appropriate calculations are carried out in Figs. 5(*b*) and 5(*c*). The values of a_j/nb_j and $\bar{\xi}_j$ (see Equation [9]) are given at the top of the diagram in Fig. 5(*b*). The numbers in parentheses in the same diagram represent the values of α determined in column 10 of Table 1. The numbers directly above the values of α_j give the stiffnesses of the panels and those below the values of α give the corresponding products of the stiffnesses and carry-over factors. These quantities are expressed in terms of $4D_j/b_j$ and they are obtained directly from Kroll's tables.

On the diagram in Fig. 5(*c*) are given the values of $\bar{K}_j$ and $(kK)_j$ in terms of $4D_r/b_r$, where the subscript r designates the reference panel (in this case, $r = 2$). The values of $\bar{K}_j$ are represented by

TABLE 1 CALCULATIONS FOR EXAMPLE 2

Panel	(1) $\frac{b_j}{b_r}$	(2) $\frac{D_j}{D_r}$	(3) $\frac{m_j}{m_r}$	(4) $\frac{(p_z)_j}{(p_z)_r}$	(5) (1)[2]	(6) (5)/(2)	(7) $\frac{(\xi\omega)_j}{(\xi\omega)_r}$ (3)(6)	(8) $\frac{(\xi_p)_j}{(\xi_p)_r}$ (4)(6)	(9) $(\xi_p)_j$ $(\xi_p)_r$(8)	(10) α_j (2)/(1)
1	1.25	1.00	0.80	−0.50	1.5625	1.5625	1.25	−0.78125	−0.625	0.80
2 = r	1.00	1.00	1.00	1.00	1.00	1.00	1.00	1.00	0.80	1.00
3	1.00	0.50	1.00	0.50	1.00	2.00	2.00	1.00	0.80	0.50
4	0.8333	0.50	2.16	−0.36	0.6944	1.389	3.00	−0.50	−0.40	0.60

$(\xi_p)_r = 0.80$

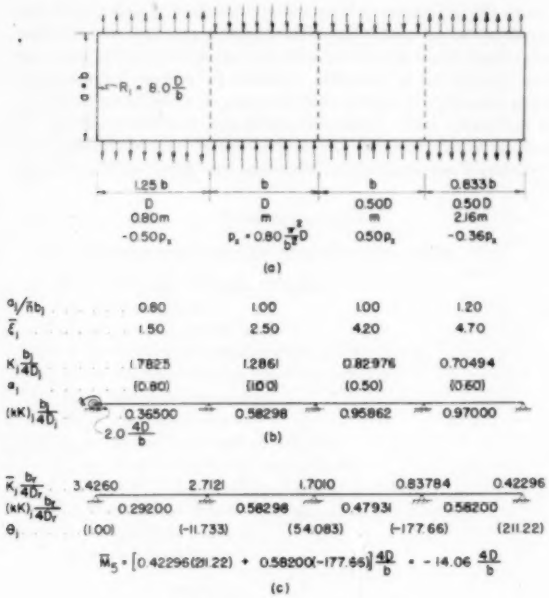

FIG. 5 ILLUSTRATIVE EXAMPLE 2

the numbers directly above the supports and those of $(kK)_j$ are represented by the numbers at the middle of the panels. The former are determined from Fig. 5(*b*) by taking the sum of the products of the values of α and K for spans $j-1$ and j. Thus

$$\bar{K}_2 = [1.7825\ (0.80) + 1.2861\ (1.00)]\ \frac{4D}{b} = 2.7121\ \frac{4D}{b}$$

Similarly, the values of $(kK)_j$ are obtained by multiplying the values of α by the values of $(kK)_j$ given in Fig. 5(*b*).

The rotations of the plate over the supports are represented by the numbers in parentheses in Fig. 5(*c*) and they are computed as follows: The rotation θ_1 is taken equal to unity. The rotation θ_2 is evaluated from Equation [18]

$$\theta_2 = -\frac{3.426(1.00)}{0.29200} = -11.733$$

The rotations θ_3, θ_4, and θ_5 are determined by application of Equation [16] to supports 2, 3, and 4, respectively. Thus

$$\theta_3 = -\frac{0.29200\ (1.00) + 2.7121\ (-11.733)}{0.58298} = 54.083$$

$$\theta_4 = -\frac{0.58298\ (-11.733) + 1.7010\ (54.083)}{0.47931} = -177.66$$

$$\theta_5 = -\frac{0.47931\ (54.083) + 0.83784\ (-177.66)}{0.58200} = 211.22$$

These results are recorded on the diagram as they are computed.

The maximum amplitude of the exciting couple, evaluated at the bottom of Fig. 5(*c*) by use of Equation [20], is found to be equal to $-14.06\ 4D/b$. Since this is different from zero, the assumed value of ξ_ω does not correspond to a natural frequency. By repeating such cycles of computation for two additional values of ξ_ω and by plotting the magnitude of the exciting couple as a function of ξ_ω, the first characteristic value of ξ_ω was found to be equal to 1.66. Thus the fundamental frequency of the plate, in radians per second, is

$$\omega_{1,1} = \sqrt{1.66}\ \frac{\pi^2}{b^2}\sqrt{\frac{D}{m}} = \frac{12.7}{b^2}\sqrt{\frac{D}{m}}$$

It should be noted that in some cases, particularly in evaluating the higher natural frequencies of a plate, the computations may involve small differences between large quantities. Under such conditions, it may be necessary to retain a minimum of five significant figures throughout the computations.

CONCLUSION

The procedure presented is suitable for computing all natural frequencies of bending vibration of the type of continuous plate considered. However, it is practically restricted by the fact that the available tables of stiffness and carry-over factor (8) cover a restricted range of values of $\bar{\xi}$ and a/nb. Thus, until more extensive tables are prepared, it may be practicable to determine only the first few natural frequencies of the plate.

The extension of the procedure to the case of plate structures involving closed panels may be accomplished in the manner described in reference (10) for the case of closed frames. Without much additional work, the procedure may be extended also to the analysis of the steady-state forced vibration of plates.

ACKNOWLEDGMENT

This paper is based upon part of a thesis by A. S. Veletsos (10). The work was carried out under the supervision of N. M. Newmark in the Structural Research Laboratory, Department of Civil Engineering, University of Illinois, in the course of a research program sponsored by the Mechanics Branch of the Office of Naval Research.

BIBLIOGRAPHY

1 "Die Berechnung der Drehschwingungen," by H. Holzer, J. Springer, Berlin, 1921.

2 "Analysis of Continuous Frames by Distributing Fixed-End

Moments," by Hardy Cross, Trans. ASCE, vol. 96, 1932, pp. 1–10.

3 "Principal Effects of Axial Load on Moment-Distribution Analysis of Rigid Structures," by B. W. James, NACA Technical Note No. 534, 1935.

4 "Stability of Structural Members Under Axial Load," by E. E. Lundquist, NACA Technical Note No. 617, 1937.

5 "Principles of Moment Distribution Applied to Stability of Structures Composed of Bars or Plates," by E. E. Lundquist, E. Z. Stowell, and E. H. Schuette, NACA Wartime Report L-326, 1943.

6 "A Distribution Procedure for the Analysis of Slabs Continuous Over Flexible Beams," by N. M. Newmark, University of Illinois, Bulletin No. 304, 1938.

7 "On Moment Balancing in Structural Dynamics," by R. E. Gaskell, *Quarterly of Applied Mathematics*, vol. 1, 1943, pp. 237–249.

8 "Tables of Stiffness and Carry-Over Factor for Flat Rectangular Plates Under Compression," by V. D. Kroll, NACA Wartime Report L-398, 1943.

9 "Vibrations of Rectangular Plates," by H. Lurie, *Journal of the Aeronautical Sciences*, vol. 18, 1951, pp. 139–140.

10 "A Method for Calculating the Natural Frequencies of Continuous Beams, Frames, and Certain Types of Plates," by A. S. Veletsos, Doctoral Dissertation, Civil Engineering Department, University of Illinois, 1953.

Bending Vibrations of Variable Section Beams[1]

By E. T. CRANCH[2] and ALFRED A. ADLER[3]

Using simple beam theory, solutions are given for the vibration of beams having rectangular cross section with (*a*) linear depth and any power width variation, (*b*) quadratic depth and any power width variation, (*c*) cubic depth and any power width variation, and (*d*) constant depth and exponential width variation. Beams of elliptical and circular cross section are also investigated. Several cases of cantilever beams are given in detail. The vibration of compound beams is investigated. Several cases of free double wedges with various width variations are discussed.

Nomenclature

The following nomenclature is used in the paper:

EI = bending stiffness of beam
ρ = mass density
A = cross-sectional area
$y(x, t)$ = transverse displacement of bent beam
$Y(x)$ = normal mode shape of bent beam
ω = circular frequency
R, S = functions of x
J_n, J_{-n} = Bessel functions of first kind
Y_n = Bessel function of second kind
I_n, I_{-n} = modified Bessel functions of first kind
K_n = modified Bessel function of second kind
b = width of beam
h = depth of beam
$f = \dfrac{\omega}{2\pi}$ = frequency
L = length of beam

Introduction—Bending

According to simple beam theory, the equation of motion of a beam in bending is

$$\frac{\partial^2}{\partial x^2} EI \frac{\partial^2 y}{\partial x^2} + \rho A \frac{\partial^2 y}{\partial t^2} = 0 \quad [1]$$

The normal modes are found by a solution of the form

$$y(x, t) = Y(x)e^{j\omega t} \quad [2]$$

which, when substituted in Equation [1], gives

$$\frac{d^2}{dx^2} EI \frac{d^2 Y}{dx^2} - \rho A \omega^2 Y = 0 \quad [3]$$

If EI and ρA are constants, the normal modes and corresponding frequencies for various boundary conditions are well known. If EI and ρA are variable along the beam, then the solution of Equation [3] is more complicated. Exact solutions of Equation [3] have been obtained in some particular cases (1, 2)[4] by power series or Bessel functions. The solutions given here are more general and include some interesting shapes as special cases.

Method of Approach

Consider the fourth-order equation obtained by repeated operation of two second-order operators

$$\left[\frac{1}{R}\frac{d}{dx}\left(S\frac{d}{dx}\right) + C\right]\left[\frac{1}{R}\frac{d}{dx}\left(S\frac{d}{dx}\right) - C\right] Y = 0 \quad [4]$$

where R and S are functions of x. If Equations [3] and [4] are written out and the coefficients equated, the following conditions are obtained

$$R = \rho A \quad [5]$$

$$S^2 = (\rho A)(EI) \quad [6]$$

$$\frac{dS}{dx} = KR \text{ when } \frac{dS}{dx} \neq 0 \quad [7a]$$

or

$$S = K \text{ when } \frac{dS}{dx} = 0 \quad [7b]$$

where K is a constant. Equation [3] written in the form of Equation [4] is

$$\left[\frac{1}{\rho A}\frac{d}{dx}\left(\sqrt{(\rho A)(EI)}\,\frac{d}{dx}\right) + \omega\right]\left[\frac{1}{\rho A}\frac{d}{dx}\left(\sqrt{(\rho A)(EI)}\,\frac{d}{dx}\right) - \omega\right] Y = 0 \quad [8]$$

Equations [5] and [6] when put in Equations [7*a*] and [7*b*] give

$$EI = \frac{(K \int \rho A\, dx)^2}{\rho A} \quad [9a]$$

or

$$EI = \frac{K^2}{\rho A} \quad [9b]$$

Equation [9*a*] or [9*b*] gives the relation which must exist between ρA and EI if Equation [3] is to be written in the form of Equation [8]. Further, if Equation [4] is to represent a vibrating beam, then Equation [7*a*] or [7*b*] shows the necessary relation between S and R.

Thus the equation of motion of the beam is written in the form of Equation [4]. The solution of Equation [4] is obtained

[1] Part of this work is from a thesis submitted in partial fulfillment of the requirements for the degree of Master of Science at Cornell University, Ithaca, N. Y., by A. A. Adler.

[2] Associate Professor, Department of Engineering Mechanics and Materials, Cornell University, Ithaca, N. Y.

[3] Associate Aerodynamicist, Cornell Aeronautical Laboratory, Buffalo, N. Y.

Contributed by the Applied Mechanics Division and presented at the Diamond Jubilee Annual Meeting, Chicago, Ill., November 13–18, 1955, of The American Society of Mechanical Engineers.

Discussion of this paper should be addressed to the Secretary, ASME, 29 West 39th Street, New York, N. Y., and will be accepted until April 10, 1956, for publication at a later date. Discussion received after the closing date will be returned.

Note: Statements and opinions advanced in papers are to be understood as individual expressions of their authors and not those of the Society. Manuscript received by ASME Applied Mechanics Division, March 14, 1955. Paper No. 55—A-19.

[4] Numbers in parentheses refer to the Bibliography at the end of the paper.

by solving the two second-order equations contained in the fourth-order equation.

Bessel-Function Solutions

It can be shown (3) that Equation [4] has Bessel-function solutions if $R \sim x^n$ and $S \sim x^m$, where $m \neq n + 2$. Thus Equation [5] becomes

$$\rho A = \frac{\rho_0 A_0}{L^n} x^n \quad \ldots\ldots [10]$$

and Equation [9a] gives

$$EI = \frac{E_0 I_0}{L^{n+2}} x^{n+2} \quad \ldots\ldots [11]$$

and Equation [8] is

$$\left[\frac{1}{x^n}\frac{d}{dx}\left(x^{n+1}\frac{d}{dx}\right) + \sqrt{\frac{\rho_0 A_0}{E_0 I_0}}\, L\omega\right] \left[\frac{1}{x^n}\frac{d}{dx}\left(x^{n+1}\frac{d}{dx}\right) - \sqrt{\frac{\rho_0 A_0}{E_0 I_0}}\, L\omega\right] Y = 0 \quad \ldots\ldots [12]$$

The sum of the solutions of each second-order equation contained in Equation [12] gives the solution of Equation [12]

$$Y(x) = x^{-n/2}[C_1 J_n(z) + C_2 Y_n(z) + C_3 I_n(z) + C_4 K_n(z)] \quad \ldots [13a]$$

if n is an integer, and

$$Y(x) = x^{-n/2}[C_1 J_n(z) + C_2 J_{-n}(z) + C_3 I_n(z) + C_4 I_{-n}(z)] \quad \ldots [13b]$$

if n is not an integer, where

$$z = 2x^{1/2} L^{1/2} \omega^{1/2} \left(\frac{\rho_0 A_0}{E_0 I_0}\right)^{1/4}$$

Consider the case of a cantilever beam with boundary conditions

$$EI\frac{d^2Y}{dx^2} = \frac{d}{dx}\left(EI\frac{d^2Y}{dx^2}\right) = 0$$

at $x = 0$ and $Y = dY/dx = 0$ at $x = L$. The boundary conditions at the free end require $C_2 = C_4 = 0$ in Equations [13a] and [13b]. The boundary conditions at the clamped end give the frequency equation

$$J_n(\gamma) I_{n+1}(\gamma) + J_{n+1}(\gamma) I_n(\gamma) = 0 \quad \ldots\ldots [14]$$

where $\gamma = z(L)$.

The roots of Equation [14] are readily calculated and Airey (4) has computed the first ten roots for $n = 0, 1, 2, 3$. Equation [14] is also applicable for nonintegral values of n. From the definition of γ, the natural frequency $f = \omega/2\pi$ is

$$f = c\,\frac{1}{L^2}\left(\frac{E_0 I_0}{\rho_0 A_0}\right)^{1/2} \quad \ldots\ldots [15]$$

where

$$c = \frac{\gamma^2}{8\pi}$$

Equations [13a] and [13b] give the normal mode configurations

$$Y(x) = Cx^{-n/2}\left\{I_n[\gamma] J_n\left[\gamma\left(\frac{x}{L}\right)^{1/2}\right] - J_n[\gamma] I_n\left[\gamma\left(\frac{x}{L}\right)^{1/2}\right]\right\} \quad \ldots\ldots [16]$$

Although in the foregoing work the beam comes to a point, the case of a truncated beam also can be solved. The boundary conditions for a truncated beam are

$$Y(L_2) = \frac{dY}{dx}(L_2) = 0$$

at the clamped end and

$$EI\frac{d^2Y}{dx^2} = \frac{d}{dx}\left(EI\frac{d^2Y}{dx^2}\right) = 0$$

at $x = L_1$, the free end. In the truncated cases, Bessel functions of both the first and second kinds appear. It also is possible to use other boundary conditions in Equations [13a] and [13b] and proceed in an identical manner.

Case 1 Rectangular Cross Section

Consider ρ and E constant and from Equations [10] and [11] it is found that beam width b and depth h vary as

$$b = b_0\left(\frac{x}{L}\right)^{n-1} \quad \ldots\ldots [17]$$

$$h = h_0\left(\frac{x}{L}\right) \quad \ldots\ldots [18]$$

Thus, with Bessel-function solutions and the relation between ρA and EI of Equation [9a], the beam depth has a linear taper and the width can vary as x^{n-1}.

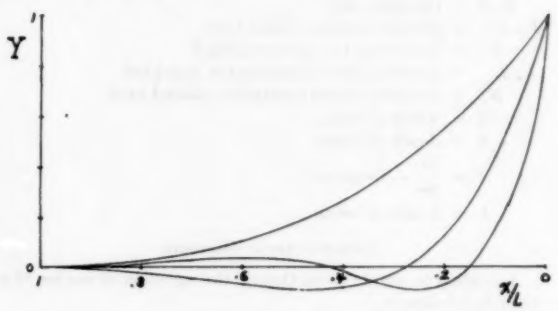

Fig. 1

Example 1. If $n = 1$ then the width is constant. For the cantilever the normal mode shape is given by Equation [16] and the frequency equation is Equation [14]. The results are summarized in Table 1. This example has been solved previously (1).

Example 2. If $n = 2$ both the width and depth have a linear taper (pyramid). A truncated, pyramid cantilever with a square cross section has been investigated previously (2), using power series. It is interesting that the solution is valid for a pyramid with rectangular cross section. The results are given in Table 1.

Some interesting examples follow from considering the values of n in Equation [17] that give the width a blunt end at $x = 0$. If $1 < n < 2$ then cases of this character result.

Example 3. If $n = 3/2$ then Equation [17] gives a parabolic width variation. The results are given in Table 1. The first three normal modes are shown in Fig. 1. These were computed from Equation [16] by writing the Bessel functions of order three halves in terms of trigonometric and hyperbolic functions. It can be seen that in the higher modes the maximum stress does not occur at the root of the cantilever. The effect of tapered depth is to move the maximum-stress region toward the free end.

TABLE 1 RESULTS OF EXAMPLE CALCULATIONS

EXAMPLE	b/b_0	h/h_0	FREQUENCY EQUATION	ROOTS OF FREQUENCY EQUATION	C OF EQ. (15)	NORMAL MODE CONFIGURATION $Y(x)$	BEAM SHAPE
	1	1	$\cos\gamma \cosh\gamma = -1$	1.875 4.694 7.855	0.560 3.51 9.82		
1	1	x/L	$J_1(\gamma)I_2(\gamma)+J_2(\gamma)I_1(\gamma)=0$	4.61 7.80 11.0	0.846 2.42 4.78	EQ. (16) $n=1$	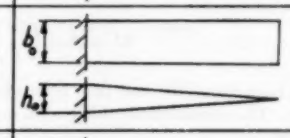
2	x/L	x/L	$J_2(\gamma)I_3(\gamma)+J_3(\gamma)I_2(\gamma)=0$	5.91 9.20 12.4	1.39 3.37 6.12	EQ. (16) $n=2$	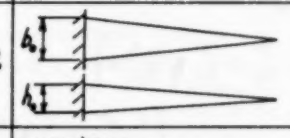
3	$(x/L)^{1/2}$	x/L	$\gamma(\tanh\gamma+\tan\gamma)=$ $2\tan\gamma\tanh\gamma$	5.27 8.51 11.7	1.104 2.88 5.44	EQ. (16) $n=3/2$	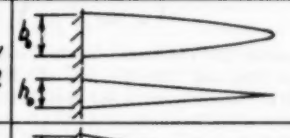
4	$e^{\frac{x}{L}}$	1	EQ. (31)	18.94 96.81 255.4	0.754 3.85 10.2	EQ. (29) $\alpha=\frac{1}{2L}$	
5	1	x/L	SYMMETRIC $J_2(\gamma)=0$ ANTISYMMETRIC EQ. (51) $n=1$	5.135 8.417 6.604	1.05 2.82 1.735	EQ. (50) $n=1$ EQ. (52) $n=1$	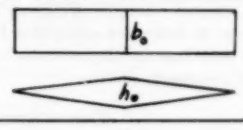
6	x/L	x/L	SYMMETRIC $J_3(\gamma)=0$ ANTISYMMETRIC EQ. (51) $n=2$	6.39 9.76 7.85	1.62 3.79 2.45	EQ. (50) $n=2$ EQ. (52) $n=2$	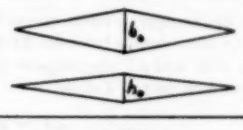
7	$(x/L)^{1/2}$	x/L	SYMMETRIC $J_{5/2}(\gamma)=0$ ANTISYMMETRIC EQ. (51) $n=3/2$	5.65 9.07 7.23	1.27 3.27 2.08	EQ. (50) $n=3/2$ EQ. (52) $n=3/2$	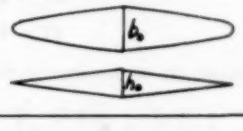

As explained previously, truncated beams of parabolic width also can be solved by using Equation [13b] with $n = 3/2$.

Case 2 Elliptical Cross Section

Consider ρ and E constant (see Fig. 2) and from Equations [10] and [11] the width b and depth h vary as

$$b = b_0\left(\frac{x}{L}\right)^{n-1} \quad \ldots\ldots [19]$$

$$h = h_0\left(\frac{x}{L}\right) \quad \ldots\ldots [20]$$

where $A_0 = \frac{\pi}{4} b_0 h_0$; $I_0 = \frac{\pi}{64} b_0 h_0^3$

Equations [19] and [20] are the same as Equations [17] and [18] for the rectangular cross section. All the results given in Case 1 are directly applicable to the elliptical cross section. The mode shapes and frequency equations are identical. To compute the frequencies it is only necessary to use the appropriate expressions for A_0 and I_0 in Equation [15].

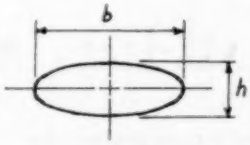

FIG. 2

Case 3 Circular Cross Section

Consider ρ and E constant and from Equations [10] and [11] the radius r varies as

$$r = r_0\left(\frac{x}{L}\right) \quad \ldots\ldots [21]$$

where

$$A_0 = \pi r_0^2 \text{ and } I_0 = \frac{\pi}{4} r_0^4$$

In this case $n = 2$ and the results are identical to those obtained for the pyramid in Case 1, example 2.

In the results given in Cases 1, 2, 3, Equation [9a] gives the relation between ρA and EI. The other relation between ρA and EI is given by Equation [9b]. Using Equations [10] and [9b] gives

$$EI = E_0 I_0 \left(\frac{x}{L}\right)^{-n} \quad \ldots\ldots [22]$$

and Equations [10] and [22] determine the cross-section variation. The normal-mode differential equation, Equation [8], becomes

$$\left(\frac{1}{x^n}\frac{d^2}{dx^2} + \frac{1}{L^n}\sqrt{\frac{\rho_0 A_0}{E_0 I_0}}\,\omega\right)\left(\frac{1}{x^n}\frac{d^2}{dx^2} - \frac{1}{L^n}\sqrt{\frac{\rho_0 A_0}{E_0 I_0}}\,\omega\right) Y = 0 \quad \ldots\ldots [23]$$

Equation [23] has Bessel-function solutions analogous to Equations [13a] and [13b] if $n \neq -2$. For rectangular or elliptical cross sections of width b and depth h Equations [10] and [22] give

$$b = b_0 \left(\frac{x}{L}\right)^{2n} \quad \ldots\ldots [24]$$

$$h = h_0 \left(\frac{x}{L}\right)^{-n} \quad \ldots\ldots [25]$$

No detailed examples are given because the sectional variations appear to have less immediate interest. However, Bessel-function solutions are theoretically obtainable in a manner similar to that previously shown.

Exponential Solutions

It can be seen by inspection of the original differential Equation [3] or the relation between EI and ρA, given in Equation [9a], that if EI and ρA vary exponentially then Equation [3] has constant coefficients. Taking

$$\rho A = \rho_0 A_0 e^{ax/L} \quad \ldots\ldots [26]$$

$$EI = E_0 I_0 e^{ax/L} \quad \ldots\ldots [27]$$

Equation [3], when written in the form of Equation [8], yields

$$\left(\frac{d^2}{dx^2} + \frac{a}{L}\frac{d}{dx} + \sqrt{\frac{\rho_0 A_0}{E_0 I_0}}\,\omega\right)\left(\frac{d^2}{dx^2} + \frac{a}{L}\frac{d}{dx} - \sqrt{\frac{\rho_0 A_0}{E_0 I_0}}\,\omega\right) Y = 0 \quad \ldots\ldots [28]$$

The solution of Equation [28] is

$$Y(x) = e^{-\alpha x}\left(C_1 \sin \alpha\sqrt{\gamma - 1}\,x + C_2 \cos \alpha\sqrt{\gamma - 1}\,x + C_3 \sinh \alpha\sqrt{\gamma + 1}\,x + C_4 \cosh \alpha\sqrt{\gamma + 1}\,x\right) \quad \ldots\ldots [29]$$

where

$$\alpha = \frac{a}{2L};\quad \beta^2 = \omega\sqrt{\frac{\rho_0 A_0}{E_0 I_0}};\quad \gamma = \beta^2/\alpha^2$$

If the beam is a cantilever such that

$$\frac{d}{dx}\left(EI\frac{d^2Y}{dx^2}\right) = EI\frac{d^3Y}{dx^3} = 0$$

at $x = 0$ and

$$Y = \frac{dY}{dx} = 0$$

at $x = L$ then the frequency equation is

$$(\gamma^2 - 1)^{1/2} + (\gamma^2 - 1)^{1/2}\cos \alpha L(\gamma - 1)^{1/2}\cosh \alpha L(\gamma + 1)^{1/2} + 3\sin \alpha L(\gamma - 1)^{1/2}\sinh \alpha L(\gamma + 1)^{1/2} + 2(\gamma + 1)^{1/2}\sin \alpha L(\gamma - 1)^{1/2}\cosh \alpha L(\gamma + 1)^{1/2} + 2(\gamma - 1)^{1/2}\cos \alpha L(\gamma - 1)^{1/2}\sinh \alpha L(\gamma + 1)^{1/2} = 0 \quad \ldots [30]$$

where $\gamma > 1$.

Example 4. The case when $a = 1$ is shown by the diagram in Table 1. For a beam with rectangular cross section, Equations [26] and [27] give

$$h = h_0$$

$$b = b_0 e^{x/L}$$

The frequency Equation [30] is

$$(\gamma^2 - 1)^{1/2} + (\gamma^2 - 1)^{1/2}\cos 1/2(\gamma - 1)^{1/2}\cosh 1/2(\gamma + 1)^{1/2} + 3\sin 1/2(\gamma - 1)^{1/2}\sinh 1/2(\gamma + 1)^{1/2} + 2(\gamma + 1)^{1/2}\sin 1/2(\gamma - 1)^{1/2}\cosh 1/2(\gamma + 1)^{1/2} + 2(\gamma - 1)^{1/2}\cos 1/2(\gamma - 1)^{1/2}\sinh 1/2(\gamma + 1)^{1/2} = 0 \quad \ldots [31]$$

The first three roots of Equation [31] are

$$\gamma = 18.94;\ 96.81;\ 255.4 \quad \ldots\ldots [32]$$

and from the definitions of α, β, and γ, the corresponding values of c in Equation [15] are

$$c = 0.754;\ 3.85;\ 10.2 \quad \ldots\ldots [33]$$

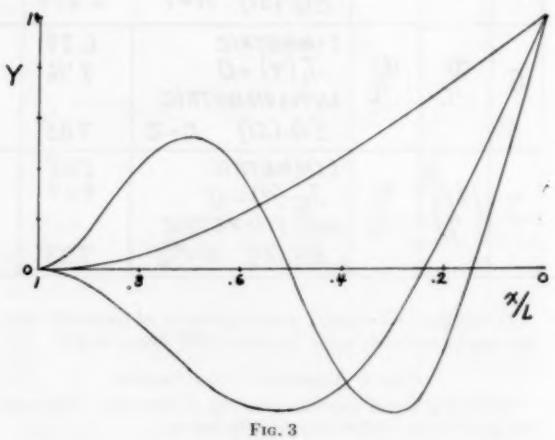

Fig. 3

The normal modes are obtained from Equation [29] in conjunction with the boundary conditions. The first three normal modes are shown in Fig. 3. Other exponential width variations can be obtained by using different positive or negative values of a in Equations [26] and [27].

Additional Solutions

There are some additional Bessel-function solutions of Equation [3]. Let

$$\rho A = \rho_0 A_0 \left(\frac{x}{L}\right)^m \quad [34]$$

$$EI = E_0 I_0 \left(\frac{x}{L}\right)^n \quad [35]$$

If $m = n - 6$ it can be shown (8) that Equation [3] has a solution

$$Y(x) = x^{\frac{4-n}{2}} [C_1 J_{n-2}(\beta x^{-1/2}) + C_2 Y_{n-2}(\beta x^{-1/2}) + C_3 I_{n-2}(\beta x^{-1/2}) + C_4 K_{n-2}(\beta x^{-1/2})] \quad [36]$$

where $$\beta = 2\omega^{1/2} L^{3/2} \left(\frac{\rho_0 A_0}{E_0 I_0}\right)^{1/4}$$

If $m = 3n - 8$ and $n \neq 2$ it can be shown (8) that Equation [3] has a solution

$$Y(x) = x^{\frac{5-2n}{2}} \left[C_1 J_{\frac{1}{n-2}}\left(\beta x^{\frac{n-2}{2}}\right) + C_2 Y_{\frac{1}{n-2}}\left(\beta x^{\frac{n-2}{2}}\right) + C_3 I_{\frac{1}{n-2}}\left(\beta x^{\frac{n-2}{2}}\right) + C_4 K_{\frac{1}{n-2}}\left(\beta x^{\frac{n-2}{2}}\right)\right] \quad [37]$$

where

$$\beta = \frac{2\omega^{1/2} L^{\frac{4-n}{2}}}{(n-2)} \left(\frac{\rho_0 A_0}{E_0 I_0}\right)^{1/4}$$

Rectangular Cross Section. When $m = n - 6$ then Equation [36] is the solution for a beam whose depth increases as the third power

$$h = h_0 \left(\frac{x}{L}\right)^3 \quad [38]$$

$$b = b_0 \left(\frac{x}{L}\right)^{n-9} \quad [39]$$

When $m = 3n - 8$ and $n \neq 2$ then Equation [37] is the solution for a beam with

$$h = h_0 \left(\frac{x}{L}\right)^{4-n} \quad [40]$$

$$b = b_0 \left(\frac{x}{L}\right)^{4n-12} \quad [41]$$

Although the depth variation can take on different powers, the width is not then arbitrary as it is in the cases of linear and cubic depth variation.

Circular Cross Section. When $m = n - 6$ then $n = 12$ and the radius varies as

$$r = r_0 \left(\frac{x}{L}\right)^3 \quad [42]$$

When $m = 3n - 8$ then $n = 16/5$ and the radius varies as

$$r = r_0 \left(\frac{x}{L}\right)^{6/5} \quad [43]$$

If the area and inertia vary as in Equations [34] and [35] then when $m = n - 4$ Equation [3] reduces to

$$x^4 \frac{d^4Y}{dx^4} + 2nx^3 \frac{d^3Y}{dx^3} + n(n-1)x^2 \frac{d^2Y}{dx^2} - \frac{\omega^2 L^4 \rho_0 A_0}{E_0 I_0} Y = 0 \quad [44]$$

which is a homogeneous linear equation

Rectangular Cross Section. When $m = n - 4$ then Equations [34] and [35] give

$$h = h_0 \left(\frac{x}{L}\right)^2 \quad [45]$$

$$b = b_0 \left(\frac{x}{L}\right)^{n-6} \quad [46]$$

In this case the depth varies as the second power and the width variation is arbitrary.

Circular Cross Section. When $m = n - 4$ then

$$r = r_0 \left(\frac{x}{L}\right)^2 \quad [47]$$

and the radius varies as the second power.

Compound Beams

Consider a beam consisting of several parts joined together. If the characteristic functions for each part are known, then it is possible to find the normal modes and frequencies for the combined beam. As examples, consider beams compounded of similar halves as shown in Examples 5, 6, 7 of Table 1. Assume ρA and EI are given by Equations [10] and [11] so that the solution will be in terms of Bessel functions. The characteristic function for each half is given by Equation [13*a*] or [13*b*]. Consider the region $0 \leq x \leq L$. As before, the free end conditions at $x = 0$ give $C_2 = C_4 = 0$ in Equations [13*a*] and [13*b*]. The characteristic function is

$$Y(x) = x^{-n/2}[C_1 J_n(z) + C_3 I_n(z)] \quad [48]$$

where

$$z = 2x^{1/2} L^{1/2} \omega^{1/2} \left(\frac{\rho_0 A_0}{E_0 I_0}\right)^{1/4}$$

For the symmetric modes of vibration

$$\frac{dY}{dx} = \frac{d}{dx} EI \frac{d^2Y}{dx^2} = 0$$

at $x = L$ and the frequency equation is

$$J_{n+1}(\gamma) = 0 \quad [49]$$

where $\gamma = z(L)$.

The symmetric normal-mode configurations are

$$Y(x) = Cx^{-\frac{n}{2}} J_n\left[\gamma\left(\frac{x}{L}\right)^{1/2}\right] \quad [50]$$

For the antisymmetric modes of vibration

$$Y(x) = EI \frac{d^2Y}{dx^2} = 0$$

at $x = L$ and the frequency equation is

$$\gamma J_n(\gamma) I_n(\gamma) + (n+1)[J_{n-1}(\gamma) I_n(\gamma) - J_n(\gamma) I_{n-1}(\gamma)] = 0 \quad [51]$$

The antisymmetric normal-mode configurations are

$$Y(x) = Cx^{-\frac{n}{2}} \left\{ I_n[\gamma] J_n\left[\gamma\left(\frac{x}{L}\right)^{1/2}\right] - J_n[\gamma] I_n\left[\gamma\left(\frac{x}{L}\right)^{1/2}\right]\right\} \quad [52]$$

If beams of rectangular or elliptical cross section are considered, then the width and depth vary as in Equations [17] and [18].

Example 5. If $n = 1$ then the compound beam shown in Table 1 has constant width and linearly varying depth (double wedge). The first two roots (5) of the symmetric frequency Equation [49] and the first root of the antisymmetric frequency Equation [51] are given in Table 1. Mindlin and Forray (6) previously solved this example.

Example 6. If $n = 2$ then the compound beam has linearly varying width and depth (double pyramid or double cone). Nicholson (7) investigated the double cone. The results are given in Table 1.

Example 7. If $n = 3/2$ then the compound beam has linearly varying depth and parabolic width variation. The results are given in Table 1.

If the parts of the compound beam are not the same, or are more than two in number, the method can still be used. At each junction the deflection, slope, bending moment, and shearing force are made continuous.

BIBLIOGRAPHY

1 "A Theoretical and Experimental Study of the Vibrations of Non-Uniform Cantilevers," by H. P. Koehler, presented at the Semi-Annual Meeting, Toronto, Canada, June 11–14, 1951, of THE AMERICAN SOCIETY OF MECHANICAL ENGINEERS.

2 "Calculation of Frequencies of Truncated Pyramids," by H. D. Conway, *Aircraft Engineering*, vol. 20, 1948, p. 148.

3 "Mathematical Methods in Engineering," by Th. von Kármán and M. A. Biot, McGraw-Hill Book Company, Inc., New York, N. Y., 1940, p. 66.

4 "The Vibrations of Circular Plates and Their Relation to Bessel Functions," by J. Airey, Proceedings of the Physical Society of London, vol. 23, 1910–1911, p. 227.

5 "Bessel Functions," by A. Gray, G. B. Mathews, and T. M. MacRobert, The Macmillan Company, New York, N. Y., 1931.

6 "Thickness-Shear and Flexural Vibrations of Contoured Crystal Plates," by R. D. Mindlin and M. Forray, *Journal of Applied Physics*, vol. 25, January, 1954, pp. 18–20.

7 "The Lateral Vibrations of Bars of Variable Section," by J. Nicholson, Proceedings of the Royal Society of London, England, vol. 93, series A, 1916–1917, p. 506.

8 "Handbuch der Theorie der Cylinderfunctionen," by N. Nielsen, B. G. Teubner, Germany, 1904, pp. 137–138.

A Matrix Solution for the Vibration Modes of Nonuniform Disks

By F. F. EHRICH,[1] PHILADELPHIA, PA.

An arbitrary disk is represented by a simulated disk composed of circumferential strips. Alternate strips are considered to be massless, constant-thickness elements with the average local elastic properties of the actual disk. Intermediate strips are considered to have the properties of local mass and polar moment of inertia, but to have no physical dimensions or elasticity. A matrix vector, formed of the local antinodal value of deflection, slope, moment, and transverse force, may be operated on by matrices representative of the elastic strips and by matrices representative of the vibratory inertia loading, centrifugal inertia loading, internal stress, and external supports at the mass strips. Thus the influence of boundary conditions at the outer edge on conditions at the inner edge may be calculated in a simple efficient manner. Successive guesses of vibration frequency lead to final satisfaction of all boundary conditions. Concise treatment of all types of boundary conditions and numerical values of required matrices are given in tables. The results of a sample calculation are compared with exact analytic results.

Nomenclature

The following nomenclature is used in the paper:

- A = homogeneous solution coefficient
- $\mathbf{A}$ = matrix vector of homogeneous solution coefficients
- $\mathbf{C}$ = matrix of coefficients
- D = local plate stiffness
- $\mathbf{D}$ = matrix of plate stiffness
- E = Young's modulus of elasticity
- $\mathbf{E}$ = elasticity matrix
- F = elastic foundation spring coefficient
- h = element of $\mathbf{H}$
- $\mathbf{H}$ = complete influence matrix
- j = homogeneous solution exponent
- J = local mass moment of inertia per unit length of circumference
- k = station index (just before mass strip)
- k' = station index (just after mass strip)
- K = number of stations
- $\mathbf{L}$ = loading matrix
- m = moment on radial antinode
- M = moment
- n = number of diametral nodes
- p = number of circumferential nodes
- Q = hoop-stress (force representation)
- r = radial co-ordinate
- $\mathbf{R}$ = matrix of radii
- S = radial stress (force representation)
- t = local plate thickness
- T = elastic hinge constant
- v = internal transverse force on radial antinode
- V = internal tranverse force
- $\mathbf{X}$ = matrix vector of deflection, slope, moment, and transverse force
- y = deflection on radial antinode
- Y = deflection
- α = frequency factor
- β_k = radius ratio r_{k+1}/r_k
- $\mathbf{B}$ = radius ratio matrix
- ϵ = residual determinant
- θ = radial slope on radial antinode
- Θ = radial slope
- μ = mass per unit length of circumference
- ν = Poisson's elastic ratio
- ρ = material mass density
- σ_r = radial stress
- σ_t = tangential stress
- ϕ = tangential-angle co-ordinate
- ω = radian vibration frequency of disk
- Ω = radian rotational velocity of disk

Introduction

The Myklestad (1)[2] technique is a very convenient numerical method for finding all the natural frequencies of one-dimensional beams. Thomson (2) has shown how the method may be stated concisely in matrix form. Rossard (3) has dealt with the disk problem by reducing it to the approximately equivalent beam problem. With this background we can approach the problem of vibration of axisymmetric, nonuniform thickness, thin disks.

The Simulated Disk

The basic manipulation preparatory to analysis and calculation of the vibration of an axially symmetric disk, is the reduction of the actual disk to an equivalent model which retains the essential properties of the real problem but is simple enough to be amenable to straightforward analysis and computation. The Myklestad (1) approach suggests that, in the case of a disk, we reduce it to a series of K, circumferential strips each of which is located at a position indicated by the subscript k. Each of these strips incorporates the local surrounding mass of the disk but has no elastic properties or physical dimensions. This mass strip also may include the local mass moment of inertia which contributes to the vibration problem by exerting a dynamic reaction moment at the point k as the disk vibrates.

Connecting any two adjacent mass strips is a circumferential strip of plate having the average local bending properties of the disk (that is, constant thickness) but having no mass. A typical

[1] Supervisor, Analytical and Mechanical Development Section, Aviation Gas Turbine Division, Westinghouse Electric Corporation. Assoc. Mem. ASME.

Contributed by the Applied Mechanics Division and presented at the Diamond Jubilee Annual Meeting, Chicago, Ill., November 13–18, 1955, of The American Society of Mechanical Engineers.

Discussion of this paper should be addressed to the Secretary, ASME, 29 West 39th Street, New York, N. Y., and will be accepted until April 10, 1956, for publication at a later date. Discussion received after the closing date will be returned.

Note: Statements and opinions advanced in papers are to be understood as individual expressions of their authors and not those of the Society. Manuscript received by ASME Applied Mechanics Division, November 24, 1954. Paper No. 55—A-17.

[2] Numbers in parentheses refer to the Bibliography at the end of the paper.

simulation along these lines is represented schematically in Fig. 1.

A reasonable assurance of the pertinence of this model is had by the realization that it reduces to the actual disk asymptotically as K goes to infinity.

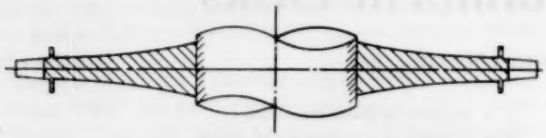

FIG. 1(a) ACTUAL DISK CROSS SECTION

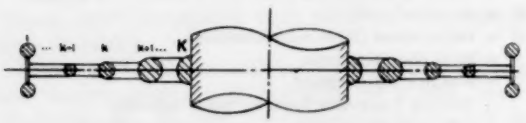

FIG. 1(b) SIMULATED DISK CROSS SECTION

In terms of local parameters, we may set for the bending stiffness of the kth elastic strip (following the kth mass strip)

$$D_k = \frac{E(t_k + t_{k+1})^3}{(1 - \nu^2)96} \quad \ldots\ldots [1]$$

It is convenient to associate with the mass strip at point k, all the mass lying between the root mean radius of k to $(k + 1)$ and the root mean radius of k to $(k - 1)$ as in Fig. 2. So that

$$\text{Mass} = \rho t_k \pi \left[\sqrt{r_k r_{k-1}}^2 - \sqrt{r_k r_{k+1}}^2 \right] \quad \ldots\ldots [2]$$

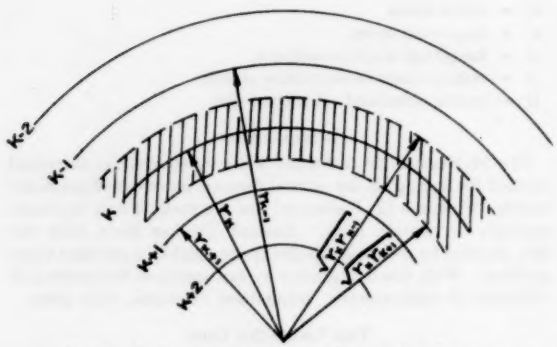

FIG. 2 APPORTIONING OF DISK MASS AT kTH STATION

To find the required mass per unit length of circumference then

$$\mu_k = \text{mass}/2\pi r_k = \rho t_k [r_{k-1} - r_{k+1}]/2 \quad \ldots\ldots [3]$$

Added to (μ_k) should be any superposed masses such as the contribution of blades at the edge of a turbine disk.

ELASTICITY MATRIX

The equation governing the deflection of the circumferential strip of elastic, massless, constant-thickness plate between any two stations is

$$\nabla^4 Y = 0 \quad \ldots\ldots [4]$$

or for polar co-ordinates

$$\left(\frac{\partial^2}{\partial r^2} + \frac{1}{r}\frac{\partial}{\partial r} + \frac{1}{r^2}\frac{\partial^2}{\partial \phi^2} \right)\left(\frac{\partial^2}{\partial r^2} + \frac{1}{r}\frac{\partial}{\partial r} + \frac{1}{r^2}\frac{\partial^2}{\partial \phi^2} \right) Y = 0. \quad [5]$$

We shall investigate modes of vibration described by diametral and radial nodes as in Fig. 3. These modes are adequately described if we choose a deflection function of the separated form

$$Y = y(r) \cos n\phi \quad \ldots\ldots [6]$$

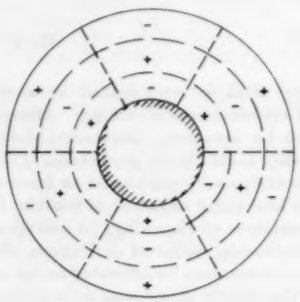

FIG. 3 TYPICAL DISK VIBRATION; $n = 3$, $p = 2$

Substitution of Equation [6] in Equation [5] yields the ordinary differential equation

$$\frac{d^4y}{dr^4} + \frac{1}{r}\frac{d^3y}{dr^3}(2) + \frac{1}{r^2}\frac{d^2y}{dr^2}(-2n^2 - 1) + \frac{1}{r^3}\frac{dy}{dr}(2n^2 + 1) + \frac{1}{r^4}y(n^4 - 4n^2) = 0 \quad \ldots\ldots [7]$$

It is seen that this equation is of the equidimensional form (4) and hence has solutions of the type

$$y = Ar^j \quad \ldots\ldots [8]$$

Substitutions of Equation [8] in Equation [7] yields the indicial equation

$$j(j-1)(j-2)(j-3) + j(j-1)(j-2)(2) + j(j-1)(-2n^2 - 1) + j(2n^2 + 1) + (n^4 - 4n^2) = 0 \quad [9]$$

It can be verified that this equation has the roots

$$j = \pm n;\ 2 \pm n \quad \ldots\ldots [10]$$

which gives four distinct homogeneous solutions except in the case of $(n = 0)$ and $(n = 1)$. In general then

$$y = A_1 r^n + A_2 r^{-n} + A_3 r^{2+n} + A_4 r^{2-n} \qquad (n \geq 2) \quad \ldots\ldots [11a]$$

and, in the two cases where repeated roots appear

$$y = A_1 + A_2 \ln r + A_3 r^2 + A_4 r^2 \ln r \qquad (n = 0) \quad \ldots\ldots [11b]$$

$$y = A_1 r + A_2 r^{-1} + A_3 r^3 + A_4 r \ln r \qquad (n = 1) \quad \ldots\ldots [11c]$$

With this equation of the deflection curve for the elastic-disk element, it is possible to solve for the other quantities of necessary interest. The radial slope of the disk at any point

$$\Theta = \theta(r) \cos n\phi = \partial Y/\partial r \quad \ldots\ldots [12]$$

gives, for the general case of Equation [6] and Equation [11a]

$$\theta = (n)A_1 r^{n-1} + (-n)A_2 r^{-n-1} + (2 + n)A_3 r^{1+n} + (2 - n)A_4 r^{1-n} \quad \ldots\ldots [13]$$

The magnitude per unit circumferential length of the moment vector in the tangential direction is given by (5)

$$M = m(r) \cos n\phi = -D\left[\frac{\partial^2 Y}{\partial r^2} + \frac{\nu}{r}\frac{\partial Y}{\partial r} + \frac{\nu}{r^2}\frac{\partial^2 Y}{\partial \phi^2} \right] \quad [14]$$

where ν is Poisson's ratio.

Substituting Equations [6] and [11a] in Equation [14] we find

$$m = D\{(-n)(n-1)(1-\nu)A_1r^{n-2} + (-n)(n+1)(1-\nu)A_2r^{-n-2} + (n+1)[-4-(n-2)(1-\nu)]A_3r^n + (n-1)[4-(n+2)(1-\nu)]A_4r^{-n}\} \quad [15]$$

The last quantity of interest is the net transverse force acting on the edge of the plate at any circumferential cut per unit circumferential length (5)

$$V = v(r)\cos n\phi = -D\left[\frac{\partial^3 Y}{\partial r^3} + \frac{1}{r}\frac{\partial^2 Y}{\partial r^2} - \frac{1}{r^2}\frac{\partial Y}{\partial r} - \frac{2}{r^2}\frac{\partial^3 Y}{\partial \phi^2} + \frac{1}{r^2}\frac{\partial^3 Y}{\partial r \partial \phi^2}\right] - D(1-\nu)\left[\frac{1}{r^2}\frac{\partial^3 Y}{\partial r \partial \phi^2} - \frac{1}{r^3}\frac{\partial^2 Y}{\partial \phi^2}\right] \quad [16]$$

Substitution of Equations [6] and [11a] yields

$$v = D\{(n^2)(n-1)(1-\nu)A_1r^{n-3} + (-n^2)(n+1)(1-\nu)A_2r^{-n-3} + (n)(n+1)[-4+n(1-\nu)]A_3r^{n-1} + (-n)(n-1)[4+n(1-\nu)]A_4r^{-n-1}\} \quad [17]$$

Then these equations fully describe the states of deflection, slope, moment, and transverse force in any circumferential disk element.

These four Equations [11a], [13], [15], and [17] are more conveniently factored and written in matrix form giving

$$\mathbf{X} = \mathbf{DC}_n\mathbf{RA} \quad [18]$$

where

$$\mathbf{X} = \begin{pmatrix} y \\ \theta r \\ mr^2 \\ vr^3 \end{pmatrix} \quad [19]$$

and

$$\mathbf{R} = \begin{bmatrix} r^n & 0 & 0 & 0 \\ 0 & r^{-n} & 0 & 0 \\ 0 & 0 & r^{2+n} & 0 \\ 0 & 0 & 0 & r^{2-n} \end{bmatrix} \quad [20]$$

Also

$$\mathbf{C}_n = \begin{bmatrix} 1 & 1 & 1 & 1 \\ n & -n & 2+n & 2-n \\ -n(n-1)(1-\nu) & -n(n+1)(1-\nu) & (n+1)[-4-(n-2)(1-\nu)] & (n-1)[4-(n+2)(1-\nu)] \\ n^2(n-1)(1-\nu) & -n^2(n+1)(1-\nu) & -n(n+1)[4-n(1-\nu)] & -n(n-1)[4+n(1-\nu)] \end{bmatrix} \quad [21]$$

which is simply a function of n, the number of diametral nodes and ν, Poisson's ratio. Furthermore

$$\mathbf{A} = \begin{pmatrix} A_1 \\ A_2 \\ A_3 \\ A_4 \end{pmatrix} \quad [22]$$

and

$$\mathbf{D} = \begin{bmatrix} 1 & 0 & 0 & 0 \\ 0 & 1 & 0 & 0 \\ 0 & 0 & D & 0 \\ 0 & 0 & 0 & D \end{bmatrix} \quad [23]$$

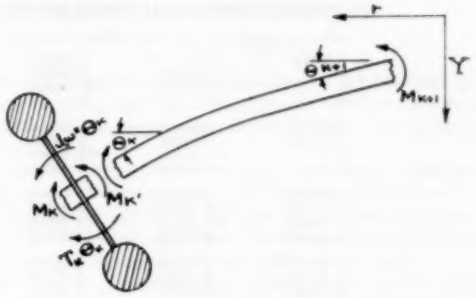

FIG. 4(a) MOMENT BALANCE

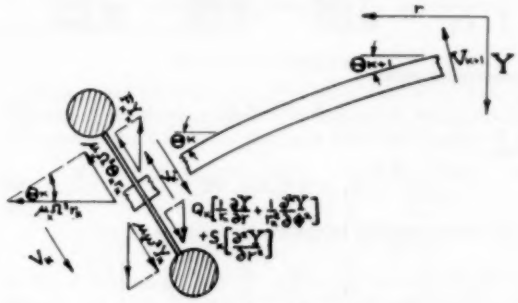

FIG. 4(b) FORCE BALANCE

For the kth elastic circumferential element, located after the kth point, we may write the four equations at the point k' next to the kth mass strip (where the prime is used to signify the difference from the point k which is just before the kth mass strip as in Fig. 4). At this point ($r = r_k$), the elasticity constant D and the equation constants A must be identified with the subscript k to signify their association with the kth elastic strip. Thus, in matrix notation

$$\mathbf{X}_{k'} = \mathbf{D}_k\mathbf{C}_n\mathbf{R}_k\mathbf{A}_k \quad [24]$$

At the other edge of the same elastic strip where ($r = r_{k+1}$)

$$\mathbf{X}_{k+1} = \mathbf{D}_k\mathbf{C}_n\mathbf{R}_{k+1}\mathbf{A}_k \quad [25]$$

Eliminating ($\mathbf{A}_k$) from Equations [24] and [25] we find

$$\mathbf{X}_{k+1} = \mathbf{D}_k\mathbf{C}_n\mathbf{R}_{k+1}\mathbf{R}_k^{-1}\mathbf{C}_n^{-1}\mathbf{D}_k^{-1}\mathbf{X}_{k'} \quad [26]$$

A slight simplification is had by writing

$$\mathbf{B}_k = \mathbf{R}_{k+1}\mathbf{R}_k^{-1} = \begin{bmatrix} \beta_k^n & 0 & 0 & 0 \\ 0 & \beta_k^{-n} & 0 & 0 \\ 0 & 0 & \beta_k^{2+n} & 0 \\ 0 & 0 & 0 & \beta_k^{2-n} \end{bmatrix} \quad [27]$$

where

$$\beta_k = r_{k+1}/r_k \quad [28]$$

TABLE 1 NUMERICAL EVALUATIONS OF COEFFICIENT MATRIX AND ITS INVERSE

	C_n				C_n^{-1}			
	1.00000	$\ln \beta_k$	1.00000	$\ln \beta_k$	1.00000	−0.17500	0.25000	−0.25000
	0	1.00000	2.00000	$1 + 2 \ln\beta_k$	0	0.65000	0.50000	−0.25000
$n = 0$	0	0.70000	−2.60000	$-3.3-2.6 \ln\beta_k$	0	0.17500	−0.25000	0.25000
$\nu = 0.3$	0	0	0	−4.00000	0	0	0	−0.25000
	1.00000	1.00000	1.00000	$\ln\beta_k$	0.67500	0.32500	0.25000	0
	1.00000	−1.00000	3.00000	$1 + \ln\beta_k$	0.41250	−0.41250	−0.18750	0.06250
$n = 1$	0	−1.40000	−6.60000	−1.30000	−0.08750	0.08750	−0.06250	−0.06250
$\nu = 0.3$	0	−1.40000	−6.60000	2.70000	0	0	−0.25000	0.25000
	1.00000	1.00000	1.00000	1.00000	0.67500	0.07500	0	0.06250
	2.00000	−2.00000	4.00000	0	0.32500	−0.25000	−0.08333	0.02083
$n = 2$	−1.40000	−4.20000	−12.00000	1.20000	−0.17500	0.08750	−0.04167	−0.02083
$\nu = 0.3$	2.80000	−8.40000	−15.60000	−10.80000	0.17500	0.08750	0.12500	−0.06250
	1.00000	1.00000	1.00000	1.00000	0.76250	0.02083	0.02083	0.02083
	3.00000	−3.00000	5.00000	−1.00000	0.23750	−0.19583	−0.05208	0.01042
$n = 3$	−4.20000	−8.40000	−18.80000	1.00000	−0.26250	0.08750	−0.03125	−0.01042
$\nu = 0.3$	12.60000	−25.20000	−22.80000	−36.60000	0.02650	0.08750	0.06250	−0.02083
	1.00000	1.00000	1.00000	1.00000	0.85000	−0.00625	0.02083	0.01042
	4.00000	−4.00000	6.00000	−2.00000	0.15000	−0.16875	−0.03750	0.00625
$n = 4$	−8.40000	−14.00000	−27.00000	−0.60000	−0.35000	0.08750	−0.02500	−0.00625
$\nu = 0.3$	33.60000	−56.00000	−24.00000	−81.60000	0.35000	0.08750	0.04167	−0.01042

Summarizing, we have

$$\mathbf{X}_{k+1} = \mathbf{E}_k \mathbf{X}_k' \quad [29]$$

where

$$\mathbf{E}_k = \mathbf{D}_k \mathbf{C}_n \mathbf{B}_k \mathbf{C}_n^{-1} \mathbf{D}_k^{-1} \quad [30]$$

The other necessary inversions can be made, giving

$$\mathbf{D}_k^{-1} = \begin{bmatrix} 1 & 0 & 0 & 0 \\ 0 & 1 & 0 & 0 \\ 0 & 0 & 1/D_k & 0 \\ 0 & 0 & 0 & 1/D_k \end{bmatrix} \quad [31]$$

and

$$\mathbf{C}_n^{-1} = (1/8) \begin{bmatrix} [4 + n(1-\nu)] & [4 - (n+2)(1-\nu)]/n & (n-2)/(n-1)n & 1/(n-1)n \\ [4 - n(1-\nu)] & [-4 - (n-2)(1-\nu)]/n & -(n+2)/(n+1)n & 1/(n+1)n \\ -n(1-\nu) & (1-\nu) & -1/(n+1) & -1/(n+1)n \\ n(1-\nu) & (1-\nu) & 1/(n-1) & -1/(n-1)n \end{bmatrix} \quad [32]$$

Numerical evaluations of the matrices $(\mathbf{C}_n)$ and $(\mathbf{C}_n)^{-1}$ are given in Table 1 for values of $(n = 2, 3, 4)$ and $(\nu = 0.3)$. Also

$$\mathbf{X}_{k+1} = \begin{Bmatrix} y_{k+1} \\ \theta_{k+1} r_{k+1} \\ m_{k+1} r_{k+1}^2 \\ v_{k+1} r_{k+1}^3 \end{Bmatrix} \qquad \mathbf{X}_k' = \begin{Bmatrix} y_k' \\ \theta_k' r_k \\ m_k' r_k^2 \\ v_k' r_k^3 \end{Bmatrix} \quad [33]$$

Special Cases of Zero and One Diametral Node

Because of the redundant roots of the indicial equation when $(n = 0)$ and $(n = 1)$, we get for the homogeneous solutions the special forms of Equations [11b] and [11c]. They can be written also, with modification of the arbitrary coefficients

$$y = A_1 + A_2 \ln (r/r_k) + A_3 r^2 + A_4 r^2 \ln (r/r_k) \quad [34]$$

for $(n = 0)$ and similarly

$$y = A_1 r + A_2 r^{-1} + A_3 r^2 + A_4 r \ln (r/r_k) \quad [35]$$

for $(n = 1)$. The factorization of the set of equations giving deflection, slope, moment, and transverse force are accomplished in a manner analogous to Equation [18] but the matrix $(\mathbf{C})$ contains terms in $\ln (r/r_{k+1})$ as well as n and ν.

In writing the set of equations at points k' and $(k + 1)$ then, we must associate with the $(\mathbf{C}_n)$ matrix the proper index to identify the correct value of r implied. Thus

$$\mathbf{X}_k' = \mathbf{D}_k \mathbf{C}_{n,k} \mathbf{R}_k \mathbf{A}_k \quad [36]$$

$$\mathbf{X}_{k+1} = \mathbf{D}_k \mathbf{C}_{n,k+1} \mathbf{R}_{k+1} \mathbf{A}_k \quad [37]$$

Elimination of $(\mathbf{A}_k)$ as before gives

$$\mathbf{X}_{k+1} = \mathbf{D}_k \mathbf{C}_{n,k+1} \mathbf{B}_k \mathbf{C}_{n,k}^{-1} \mathbf{D}_k^{-1} \mathbf{X}_k' \quad [38]$$

Some simplification results in that substitution of $(r = r_k)$ in $(\mathbf{C}_{n,k})^{-1}$ eliminates the logarithmic terms and achieves the simple function of n and ν. But $(\mathbf{C}_{n,k+1})$ must carry along the terms in $\ln (\beta_k)$. Thus

$$\mathbf{C}_{0,k+1} = \begin{bmatrix} 1 & \ln \beta_k & 1 & \ln \beta_k \\ 0 & 1 & 2 & 1 + 2 \ln\beta_k \\ 0 & (1-\nu) & -2(1+\nu) & -3 - \nu - 2(1+\nu) \ln \beta_k \\ 0 & 0 & 0 & -4 \end{bmatrix} \quad [39]$$

$$\mathbf{C}_{0,k}^{-1} = (1/4) \begin{bmatrix} 4 & -(1-\nu) & 1 & -1 \\ 0 & 2(1+\nu) & 2 & -1 \\ 0 & (1-\nu) & -1 & 1 \\ 0 & 0 & 0 & -1 \end{bmatrix} \quad [40]$$

$$\mathbf{C}_{1,k+1} = \begin{bmatrix} 1 & 1 & 1 & \ln \beta_k \\ 1 & -1 & 3 & 1 + \ln \beta_k \\ 0 & -2(1-\nu) & -2(3+\nu) & -(1+\nu) \\ 0 & -2(1-\nu) & -2\,3+\nu) & (3-\nu) \end{bmatrix} \quad [41]$$

$$\mathbf{C}_{1,k}^{-1} = (1/16) \begin{bmatrix} 4(3-\nu) & 4(1+\nu) & 4 & 0 \\ 2(3+\nu) & -2(3+\nu) & -3 & 1 \\ -2(1-\nu) & 2(1-\nu) & -1 & -1 \\ 0 & 0 & -4 & 4 \end{bmatrix} \quad [42]$$

Evaluations of the matrices and their inverses are included in Table 1 for these special cases.

Loading Matrix

The mass circumferential strip at point k has the effect of changing certain of the quantities in the matrix vector $\mathbf{X}$ at k just before the mass to other values at k' just after the mass, as in Fig. 4.

The simple assumptions of the simulated disk which state that the mass strip has no physical size give immediately

$$y_k' = y_k \quad [43]$$

and

$$\theta_k' = \theta_k \quad [44]$$

If the mass has a mass moment of inertia per unit circumferential length J, and a torsional restraint T, then the moment balance as in Fig. 4(a) gives

$$M_k' = M_k - J_k\omega^2\Theta_k + T_k\Theta_k \quad [45]$$

or, in terms of amplitudes

$$m_k' = m_k - J_k\omega^2\theta_k + T_k\theta_k \quad [46]$$

Fig. 4(b) describes the contributions to the transverse force V_k made by the following:

(a) Vibratory inertia loading from the mass of the strip (μ) for a radian frequency ω.

(b) Elastic loading if the disk is externally supported with an elastic foundation represented by the elastic coefficient F.

(c) Contribution of centrifugal force on the strip if the disk is rotating with a radian velocity of Ω.

(d) Restoring force contributed by the curvature in the tangential direction acting on a hoop stress represented by the hoop force Q.

A satisfactory representation in terms of tangential stress is given by

$$Q_k = \sigma_{\theta k} l_k (r_{k-1} - r_{k+1})/2 \quad [47]$$

(e) Restoring force contributed by the curvature in the radial direction acting on a radial stress represented by the radial force S.

A satisfactory representation in terms of the radial stresses is given by

$$S_k = \sigma_{r k} l_k (r_{k-1} - r_{k+1})/2 \quad [48]$$

These give

$$V_k' = V_k + \mu_k\omega^2 Y_k - F_k Y_k - \mu_k\Omega^2\Theta_k r_k + Q_k\left[\frac{1}{r_k}\frac{\partial Y}{\partial r} + \frac{1}{r_k^2}\frac{\partial^2 Y}{\partial\phi^2}\right] + S_k\left[\frac{\partial^2 Y}{\partial r^2}\right] \quad [49]$$

or

$$v_k' = v_k + \mu_k\omega^2 y_k - F_k y_k - \mu_k\Omega^2\theta_k r_k + Q_k\left[\frac{1}{r_k}\theta_k - \frac{n^2}{r_k^2}\,y_k\right] + S_k\left[-\frac{m_k}{D_k} - \nu\frac{\theta_k}{r_k} + \nu\frac{n^2}{r_k^2}\,y_k\right] \quad [50]$$

Equations [43], [44], [46], and [50] may be written in the matrix form

$$\mathbf{X}_k' = \mathbf{L}_k\mathbf{X}_k \quad [51]$$

where

$$\mathbf{L}_k = \begin{bmatrix} 1 & 0 & 0 & 0 \\ 0 & 1 & 0 & 0 \\ 0 & [-J_k\omega^2 r_k + T_k r_k] & 1 & 0 \\ \left\{\begin{matrix}\mu_k\omega^2 r_k^3 - F_k r_k^3 \\ -(Q_k - \nu S_k)n^2 r_k\end{matrix}\right\} & \left\{\begin{matrix}-\mu_k\Omega^2 r_k^3 \\ +(Q_k - \nu S_k)r_k\end{matrix}\right\} & [-S_k r_k/D_k] & 1 \end{bmatrix} \quad [52]$$

We then have the simple recurrence formula

$$\mathbf{X}_{k+1} = \mathbf{E}_k\mathbf{L}_k\mathbf{X}_k \quad [53]$$

where ($\mathbf{L}_k$) represents the loading effect of the kth mass strip on the vector ($\mathbf{X}_k$) and ($\mathbf{E}_k$) represents the effect of the kth elastic strip to give, in combination, the vector ($\mathbf{X}_{k+1}$) at the next point along the disk.

It should be noted that the effect of centrifugal forces enters in two roles in this treatment. The direct contribution of the dynamic force normal to the disk has been included but the secondary effect of the centrifugally induced hoop stress and radial-stress field in the plane of the disk also will come into play in conjunction with the curvatures of the plate implicit in the vibration mode. This may be accounted for completely by calculation of the centrifugal-stress field in the nonvibratory disk and inclusion of the resultant hoop stresses in the term Q_k, and the resultant radial stresses in the term S_k.

Boundary Conditions

Starting with the first strip at the outer edge of the disk, and applying the recurrence formula of Equation [53], we may deduce the value of the X-vector at the inner boundary at point K as

$$\mathbf{X}_K = \mathbf{L}_K\mathbf{E}_{K-1}\mathbf{L}_{K-1}\ldots\mathbf{E}_k\mathbf{L}_k\ldots\mathbf{E}_1\mathbf{L}_1\mathbf{X}_1 = \mathbf{H}\mathbf{X}_1 \quad [54]$$

where

$$\mathbf{H} = \mathbf{L}_K\mathbf{E}_{K-1}\mathbf{L}_{K-1}\ldots\mathbf{E}_k\mathbf{L}_k\ldots\mathbf{E}_1\mathbf{L}_1 \quad [55]$$

so that H represents a succinct summary of the influence of conditions at the outer edge of the disk on conditions at the inner edge of the disk.

The application of the Myklestad approach to the disk-vibration problem involves the setting of the boundary conditions at the outer edge, the guessing of a frequency, and the calculation of resultant conditions at the inner edge to see if they are compatible with boundary conditions stipulated by the problem.

Nonsatisfaction of boundary conditions necessitates an improved guess of the natural frequency and recalculation until inner-edge boundary conditions are satisfied.

Thus Equation [54] represents

$$\begin{Bmatrix} y_K \\ \theta_K r_K \\ m_K r_K^2 \\ v_K r_K^2 \end{Bmatrix} = \begin{bmatrix} h_{11} & h_{12} & h_{13} & h_{14} \\ h_{21} & h_{22} & h_{23} & h_{24} \\ h_{31} & h_{32} & h_{33} & h_{34} \\ h_{41} & h_{42} & h_{43} & h_{44} \end{bmatrix} \begin{Bmatrix} y_1 \\ \theta_1 r_1 \\ m_1 r_1^2 \\ v_1 r_1^2 \end{Bmatrix} \quad [56]$$

If a disk were free at the outer edge we would have the conditions to set

$$m_1 = v_1 = 0 \quad [57]$$

If the disk were clamped at the inner edge we would have the conditions to satisfy

$$y_K = \theta_K = 0 \quad [58]$$

Insertion of the conditions into Equation [56] implies that the single condition

$$\epsilon = \begin{vmatrix} h_{11} & h_{12} \\ h_{21} & h_{22} \end{vmatrix} \to 0 \quad [59]$$

Here ϵ is the determinant of the particular terms in H. In the case of an arbitrarily chosen frequency, ϵ will not be zero. The

TABLE 2 FORMULATION OF RESIDUAL DETERMINANT FOR VARIOUS TYPES OF BOUNDARY CONDITIONS

	Outer edge free	Outer edge hinged	Outer edge clamped
Inner edge free	$\begin{matrix} h_{31} & h_{32} \\ h_{41} & h_{42} \end{matrix}$	$\begin{matrix} h_{31} & h_{34} \\ h_{41} & h_{44} \end{matrix}$	$\begin{matrix} h_{31} & h_{34} \\ h_{41} & h_{44} \end{matrix}$
Inner edge hinged	$\begin{matrix} h_{13} & h_{12} \\ h_{23} & h_{22} \end{matrix}$	$\begin{matrix} h_{32} & h_{34} \\ h_{42} & h_{44} \end{matrix}$	$\begin{matrix} h_{32} & h_{34} \\ h_{42} & h_{44} \end{matrix}$
Inner edge clamped	$\begin{matrix} h_{11} & h_{12} \\ h_{21} & h_{22} \end{matrix}$	$\begin{matrix} h_{12} & h_{14} \\ h_{22} & h_{24} \end{matrix}$	$\begin{matrix} h_{12} & h_{14} \\ h_{22} & h_{24} \end{matrix}$
USING SPECIAL DEFINITION OF LAST MATRICES EQUATION [63]			
Inner edge at disk center	$\begin{matrix} h_{31} & h_{32} \\ h_{41} & h_{42} \end{matrix}$	$\begin{matrix} h_{32} & h_{34} \\ h_{42} & h_{44} \end{matrix}$	$\begin{matrix} h_{32} & h_{34} \\ h_{42} & h_{44} \end{matrix}$
Inner edge at disk center $n = 0$ Center fixed	$\begin{matrix} h_{11} & h_{12} \\ h_{21} & h_{22} \end{matrix}$	$\begin{matrix} h_{12} & h_{14} \\ h_{22} & h_{24} \end{matrix}$	$\begin{matrix} h_{12} & h_{14} \\ h_{22} & h_{24} \end{matrix}$

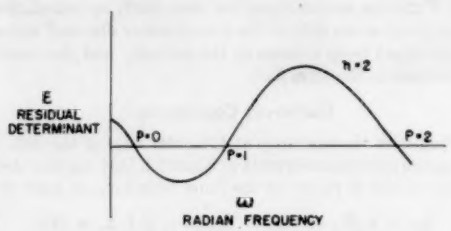

FIG. 5 GENERAL FORM OF RESIDUAL CURVE

particular values of ω where ϵ is zero (for a chosen value of n) are natural frequencies of the disk. The various solutions represent the various possible modal shapes with different numbers of circumferential nodes as in Fig. 5.

The formulation of the residual determinant from terms of the influence matrix **H** for various combinations of boundary conditions is given in Table 2. If the inner or outer edge is elastically hinged such that the angular deflection is proportional to the moment by the torsional spring constant T, then the T term in the appropriate matrix **L** may be used along with the boundary condition for simple hinge.

In any given problem, computation effort may be spared by recognition of the fact that it is not necessary to generate all the terms in **H** since, for example, in order to generate the terms needed in Equation [59] we need only calculate

$$\begin{bmatrix} h_{11} & h_{13} \\ h_{21} & h_{23} \\ h_{31} & h_{33} \\ h_{41} & h_{43} \end{bmatrix} = \mathbf{L}_K\mathbf{E}_{K-1}\mathbf{L}_{K-1}\ldots\mathbf{E}_k\mathbf{L}_k\ldots\mathbf{E}_1\mathbf{L}_1\begin{bmatrix} 1 & 0 \\ 0 & 1 \\ 0 & 0 \\ 0 & 0 \end{bmatrix} \quad \ldots [60]$$

BOUNDARY AT ZERO INNER RADIUS

If the disk extends all the way to the center ($r_K = 0$), some difficulty is encountered due to the singular nature of the matrices there. A special formulation must then be used. The boundary condition to be satisfied is not expressed directly in terms of required values of deflection, slope, moment, and transverse force, but in terms of the coefficients of the homogeneous solution. Examination of the general homogeneous solution of Equations [11 (*a*), (*b*), (*c*)] indicates that a finite solution with finite derivatives requires that

$$(A_3)_{K-1} = (A_4)_{K-1} = 0 \qquad (r_K = 0) \ldots\ldots [61]$$

Since, from Equation [24]

$$\mathbf{R}_{K-1}\mathbf{A}_{K-1} = \mathbf{C}_n^{-1}\mathbf{D}_{K-1}^{-1}\mathbf{L}_{K-1}\mathbf{X}_{K-1}' \ldots\ldots [62]$$

we may use the special definition when ($r_K = 0$) of the last elasticity and loading matrices

$$\mathbf{L}_K\mathbf{E}_{K-1} = \mathbf{C}_n^{-1}\mathbf{D}_{K-1}^{-1} \ldots\ldots [63]$$

and using the conventional definition of **H** arrive at the over-all problem stated as

$$\begin{Bmatrix} r_{K-1}^n A_1 \\ 0 \\ r_{K-1}^{n+2} A_2 \\ 0 \end{Bmatrix} = \begin{bmatrix} h_{11} & h_{12} & h_{13} & h_{14} \\ h_{21} & h_{22} & h_{23} & h_{24} \\ h_{31} & h_{32} & h_{33} & h_{34} \\ h_{41} & h_{42} & h_{43} & h_{44} \end{bmatrix} \begin{Bmatrix} y_1 \\ \theta_1 r_1 \\ m_1 r_1^2 \\ v_1 r_1^3 \end{Bmatrix} \ldots\ldots [64]$$

allowing us to formulate the residual determinant for various types of boundary conditions. For instance, if the outer edge is free then the conditions of Equation [57] imply

$$\epsilon = \begin{vmatrix} h_{21} & h_{22} \\ h_{41} & h_{42} \end{vmatrix} \to 0 \ldots\ldots [65]$$

In the case of ($n = 0$), the foregoing treatment gives a nonzero deflection at the center. If we stipulate that the center is restrained from motion, we must set

$$(A_1)_{K-1} = (A_2)_{K-1} = 0 \qquad (r_K = 0) \ldots\ldots [66]$$

which gives

$$\epsilon = \begin{vmatrix} h_{11} & h_{12} \\ h_{21} & h_{22} \end{vmatrix} \to 0 \ldots\ldots [67]$$

Other combinations of boundary conditions are included in Table 2.

DISCUSSION AND CONCLUSION

A calculation was performed to solve for the mode shape and natural frequency of a uniform thickness disk with free edges vibrating in the mode which has two nodal diameters and no nodal circles. Rayleigh (6) has treated this problem analytically and gives the result in terms of Bessel functions. Timoshenko (7) tabulates the actual numerical solutions to the frequency. A full comparison is given in Fig. 6 with

$$\omega = \alpha\sqrt{D/\rho t r^4} \ldots\ldots [68]$$

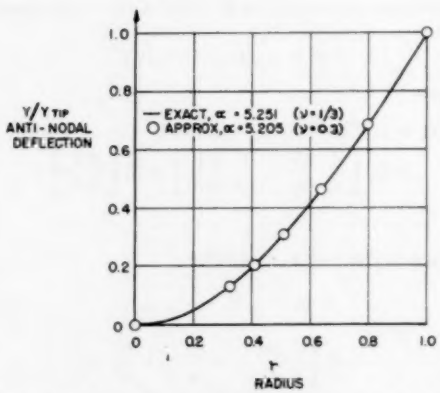

FIG. 6 MODAL SHAPE OF A VIBRATING DISK; $n = 2$, $p = 0$ (Constant thickness)

It is felt that the procedure described in the report provides a simple, straightforward, and accurate general technique for computation of the natural frequencies of nonuniform thickness disks, including effects of superposed masses, moments of inertia, and the effects of residual stresses, centrifugal stresses, and elastic restraints.

The procedure outlined here may be used to develop results identical to those of Thomson (2) for one-dimensional beams.

ACKNOWLEDGMENT

The author wishes to express his appreciation to Arthur Simmons for assistance in the computations and preparation of the paper.

BIBLIOGRAPHY

1 "New Method of Calculating Natural Modes of Uncoupled Bending Vibrations," by N. O. Myklestad, *Journal of the Aeronautical Sciences*, vol. 11, April, 1944, pp. 153–162.

2 "Matrix Solution for the Vibration of Nonuniform Beams," by W. T. Thomson, JOURNAL OF APPLIED MECHANICS, Trans. ASME, vol. 72, 1950, pp. 337–339.

3 "Vibration Characteristics of a Bladed Disc," by D. Rossard, Philadelphia, Pa., 1954 (unpublished).

4 "Advanced Calculus for Engineers," by F. B. Hildebrand, Prentice-Hall, Inc., New York, N. Y., first edition, 1949, pp. 14 and 420.

5 "Theory of Plates and Shells," by S. Timoshenko, McGraw-Hill Book Company, Inc., New York, N. Y., first edition, 1940, pp. 257 ff.

6 "The Theory of Sound," by Lord Rayleigh, Dover Publications, New York, N. Y., second edition, 1945, pp. 352 ff.

7 "Vibration Problems in Engineering," by S. Timoshenko, D. Van Nostrand Company, Inc., New York, N. Y., second edition, 1948, p. 431.

Studies in Dynamic Photoelasticity[1]

By M. M. FROCHT,[2] and P. D. FLYNN[3]

Equipment and techniques are described for obtaining dynamic photoelastic stress patterns from arbitrary lines in plane-stress systems by means of streak photography. Streak-type stress patterns of such lines were obtained which provide continuous records throughout the entire period of impact (of the order of milliseconds) at times of exposure of 2/3 microsec. This is thirty times faster than the time of exposure (20 microseconds) obtained by Tuzi and Nisida in 1935. Dynamic photoelastic stress patterns showing stress-wave propagation are given for a bar struck axially by a rigid mass, and these patterns show that a uniform state of stress was obtained. Theoretical stress patterns based on the Boussinesq solution are in essential agreement with the experimental results.

Introduction

THE subject of stress-wave propagation is receiving much attention. Elasticians are concerned with improvements and refinements in existing solutions as well as with new problems. Because of the mathematical complications, relatively few impact problems have thus far been solved theoretically. Also, the more exact solutions are not readily usable even in such simple cases as the compression bar. These circumstances as well as the need for verifying the theoretical solutions make experimental approaches desirable, if not imperative.

Most of the experimental work on impact stresses has been done by means of strain gages. The present paper is a report of progress on our attempts to extend the photoelastic method to the study of stress-wave propagation.

A survey of the literature[4] shows that the first attempts in the application of photoelasticity to dynamic stress problems were made by means of conventional kinematography. Pictures showing the formation of stress patterns in beams, disks, rings, angles, and frames under slow impact conditions were taken at rates up to 64 frames per sec by Tuzi (2)[5] and Frocht (3).

The first work of major importance in dynamic photoelasticity was published in 1935 by Tuzi and Nisida (4). Using a drum camera and a narrow open slit or transparent window, they obtained continuous stress patterns for strips or line elements of models subjected to impact loads. This type of photography is called "streak photography."

Findley (5) used full-image photography in an attempt to study the dynamic stress-optic law. In 1949 Foeppl (6) obtained full-stress patterns for a simply supported beam subjected to central impact at a rate of 3020 frames per sec.

Numerous examples of full-image stress patterns, one or two from a single test, have been obtained by means of spark photography, e.g., Edgerton and Barstow (7). If a given set of experimental conditions can be reproduced accurately, a sequence of spark pictures of the same phenomena can be obtained by using different delay times in successive tests. This technique is equivalent to high-speed motion-picture photography and has been used by Senior and Wells (8) and others. Christie (9) used a multiple-spark, multiple-lens camera to take a total of nine successive frames from a single test on a stationary piece of film.

From our study of the literature we concluded that streak photography would seem to be the most practical approach to the photoelastic study of stress-wave propagation.

Equipment and Techniques for Streak Photography

The equipment described in this section is the result of numerous modifications and improvements. Only the present form and operating characteristics are given. Additional information may be found in reference (10).

Drum Camera. The camera shown in Fig. 1 has two lenses for the simultaneous recording of data on separate strips of 35-mm film. The film strips are carried on the inside cylindrical surfaces of two concentric drums, 16 and 11 1/2 in. diam, respectively, with the emulsion side inward. Rotational speeds of 2100 rpm, 3100 rpm, and 3600 rpm, approximately, are obtained by means of a 1/2-hp, 1725-rpm motor acting through a system of belts and pulleys. In the work reported in this paper, only the 16-in. drum was used.

The lenses are fastened to arms which are free to rotate about the axis of the camera so that each lens can be moved along a circular arc of fixed radius, C, in Fig. 1. Inside of the camera, 45-deg mirrors are attached to the same arms so that they reflect the image from the lenses onto the emulsion side of the film. When the line element of the model under observation is parallel to the radius of the drum which passes through the center of the lens the image of that line element is transverse to the direction of the motion of the film. For all other directions of the line element the direction of the reflected image on the film is oblique. Thus, by proper adjustment of the lens arm the image can be placed at any desired angle relative to the direction of the film motion. In the work reported, only the transverse position was used.

The camera is loaded in daylight through an opening in the front cover which is protected by cloth flaps. Alignment of the image and focusing is accomplished by viewing the image through windows in the side of the camera. After selecting a speed of operation, the mechanical shutter of the lens is set for a period of time slightly less than the time taken for one revolution of the drum. This utilizes nearly the full length of the film. The shutter is tripped by a solenoid in synchronization with the impact. The solenoids and cloth flaps may be seen in Fig. 1.

The isolation of a line element in the model was accomplished by means of an opaque diaphragm with a transparent slit which was placed as close as possible to the model.

Loading Mechanism and Model Support. The impact loads

[1] For a more complete account see "Studies in Dynamic Photoelasticity," by P. D. Flynn, PhD thesis, Illinois Institute of Technology, Chicago, Ill., June, 1954.

[2] Research Professor of Mechanics, Director of Experimental Stress Analysis, Illinois Institute of Technology, Chicago, Ill. Mem. ASME.

[3] Formerly, Research Corporation Fellow, Illinois Institute of Technology; now, Development Engineer, General Engineering Laboratory, General Electric Company, Schenectady, N. Y. Assoc. Mem. ASME.

[4] A more complete and critical review of previous work in dynamic photoelasticity, as well as a survey of modern equipment for high-speed photography, can be found in reference (1).[5]

[5] Numbers in parentheses refer to Bibliography at end of paper.

Contributed by the Applied Mechanics Division and presented at the Diamond Jubilee Annual Meeting, Chicago, Ill., November 13–18, 1955, of The American Society of Mechanical Engineers.

Discussion of this paper should be addressed to the Secretary, ASME, 29 West 39th Street, New York, N. Y., and will be accepted until April 10, 1956, for publication at a later date. Discussion received after the closing date will be returned.

Note: Statements and opinions advanced in papers are to be understood as individual expressions of their authors and not those of the Society. Manuscript received by ASME Applied Mechanics Division, July 9, 1954. Paper No. 55—A-1.

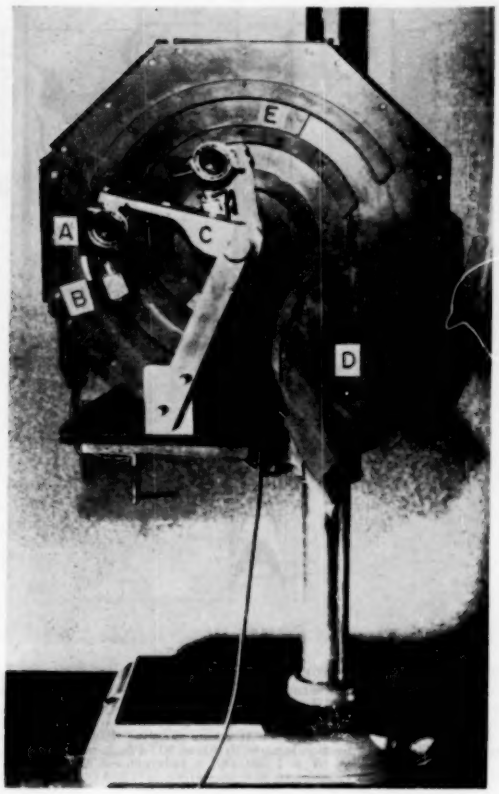

FIG. 1 DRUM CAMERA FOR STREAK PHOTOGRAPHY
(A, Lens; B, solenoid; C, lens arm; D, daylight loading flaps; E, circular slides.)

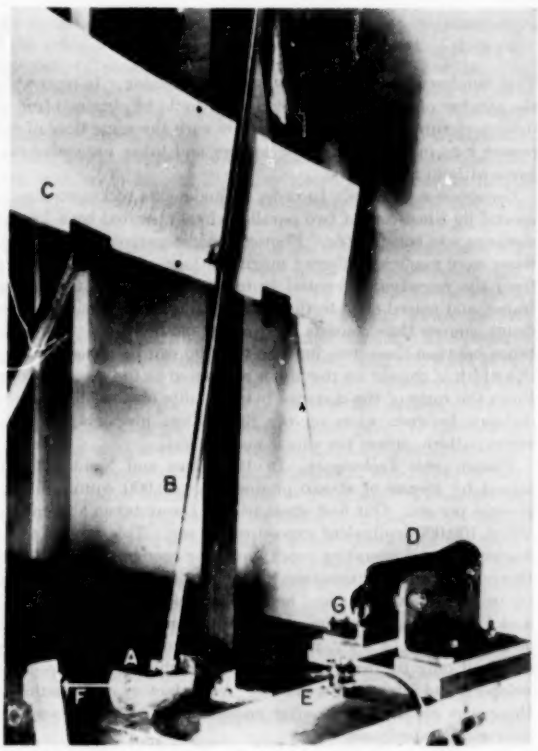

FIG. 2 PENDULUM LOADING MECHANISM AND MODEL SUPPORT
(A, Hammer; B, tube; C, angular scale; D, model support; E, switch; F, restraining string; G, model.)

were produced by means of a pendulum consisting of a steel hammer attached to a long tube, Fig. 2. An angular scale was used to measure the position of the pendulum at the points of release and impact. Release of the pendulum was accomplished by cutting a restraining string which can be seen in the figure.

The model rests against a 3-in. × 12-in. solid steel cylinder supported between heavy angle sections in such a way that it can be aligned relative to the striking face of the pendulum hammer. The chief features of this support or anvil are its relatively large mass, rigidity, simplicity of construction, and ease of alignment. The hammer and model are adjusted so that the resulting impact force passes approximately through the center of percussion of the pendulum.

Synchronization and Light Source. The operation of the camera shutter must be synchronized with the impact between the hammer and model. This is accomplished by having the moving pendulum actuate a small toggle switch just before striking the model, Fig. 2. When the switch closes, the solenoid on the camera is energized from a d-c source and trips the shutter. The time interval between shuttering and impact is regulated by varying the position of the switch along the arc of the swing of the pendulum.

After much experimentation with lamps, a No. 22 photoflash bulb was found to give satisfactory results when operated from the same switch as the shutter.

Polariscope. The polarizer and analyzer were made from a sheet of polaroid circular polarizer, which gives a polariscope with a bright background. A condenser lens was used to produce a parallel beam of light, and a collector lens was used to converge the beam into the camera lens. Since all lenses were placed outside of the polarized field, they did not have to be stress-free. The lenses used in a particular test were selected to give a field large enough to illuminate the entire slit and to produce an image of maximum size on the film. A 60-watt incandescent lamp, which has approximately the same dimensions as the No. 22 photoflash bulb, was used as a modeling lamp during the alignment of the optical system.

Exposure Time and Number of Equivalent Exposures per Second. In high-speed motion-picture photography, the film is stationary relative to the image and blurring results from the motion of the object which is being photographed. In streak photography, the film moves relative to the image of the slit and blurring occurs because of this motion and because of the changes of the stress pattern along the slit.

In streak photography, the time τ during which a point on the film is exposed to light is given by

$$\tau = \frac{d}{V} \qquad [1]$$

where d is the width of the image of the slit on the film and V is the velocity of the film. The time τ is called the exposure time.

For purposes of comparison of streak photography with kinematography, it may perhaps be useful to introduce the reciprocal of the exposure time, which we will denote by N and refer to as the "number of equivalent exposures per second." Thus

$$N = \frac{1}{\tau} = \frac{V}{d} \quad \ldots\ldots\ldots\ldots\ldots\ldots [2]$$

This number N can be given a physical meaning. It represents the number of pictures per second that would be obtained from a motion-picture camera which operates with the same time of exposure τ as in the streak-type camera and takes successive pictures without loss of time.

Construction of Slits. In order to make slits of known size, a special jig consisting of two parallel wires separated by a known distance was constructed. Photographic negatives of these two wires were made at different magnifications. Portions were cut from the negative, cemented to one face of a thin supporting frame, and placed close to the model. The image received in the drum camera thus consists of two fine parallel lines. The distance between these two lines on the film can be measured, and the width of the slit on the film is computed as the wire diameter times the ratio of the distance between slits on the film and the distance between wires on the jig. When photographing the stress pattern, one of the slits is masked out.

Photographic Techniques. In 1935 Tuzi and Nisida (4) obtained by means of streak photography 50,000 equivalent exposures per sec. Our first stress patterns were taken at a rate of about 100,000 equivalent exposures per sec. This proved to be inadequate and operating conditions have been improved to raise this number to approximately 1,500,000. This was accomplished by using narrower slits and higher film velocities (d = 0.002 in. and V = 250 fps are typical operating conditions). With such short exposures (τ = $^2/_3$ microsec), photographic records can be obtained only by using sensitive films, high-emulsion-speed developers, and intense light sources. A satisfactory combination of these was obtained only after considerable, and at times discouraging, experimentation.

Fig. 3 shows typical streak-type dynamic stress patterns for the load line of a circular disk under diametral loads which illustrate our progress in obtaining stress patterns under impact. The disk was chosen as a convenient model for the development of technique and not for quantitative studies. Figs. 3 (a, b, c) are the records of the change of stress pattern of the loaded diameter of a disk with time. The width of these photographs is the length of the diameter, and their lengths represent the time co-ordinate, so that the fringes on any line at right angles to the length of the photographs represent the fringe pattern of the loaded diameter at the corresponding time.

Three types of Kodak 35-mm film have been tried: Super XX, Linagraph Pan, and Linagraph Ortho, with the last one giving the best results. At first the film was developed in D-72 but at increased operating speeds a high-contrast developer, D-11, was used. For very high rates of exposure, such as we are now using, it became necessary to resort to a new high-emulsion-speed developer, Kodak SD-19a, which was recommended by the Eastman Kodak Company.

In order to approximate a monochromatic source of light, filters are employed. Various glass filters as well as a "Baird high-transmission narrow-band filter" were tried. The best combination was determined experimentally on the basis of the clarity of the dynamic records. Satisfactory results were obtained by using the orange and the didymium elements from a three-element Corning glass monochromatic filter (Hg 5461 Å) in combination with Linagraph Ortho film and photoflash bulbs. The exact range of wave lengths of the resulting light was not determined.

Elastic Stress Waves in a Compression Bar Struck by a Rigid Mass

Introduction. For the first quantitative study of stress-wave propagation, we chose a compression bar fixed at one end, i.e.,

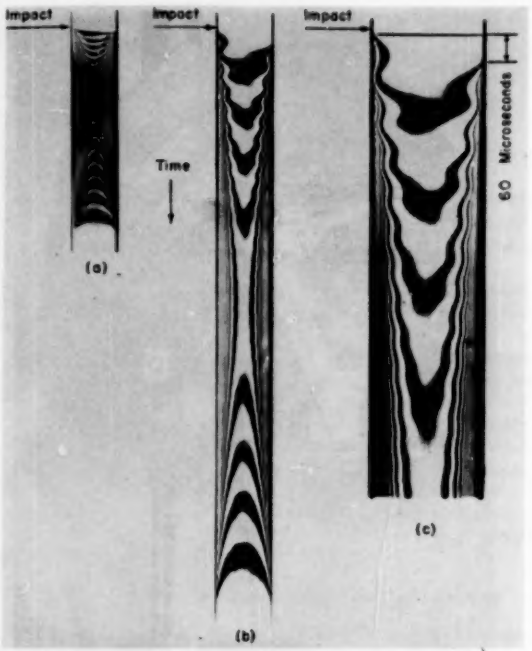

Fig. 3 Dynamic Photoelastic Stress Patterns for the Load Line of a Castolite Circular Disk Under Diametral Loads

(a, Diameter 1.201 in., thickness 0.183 in., camera speed 1,430 rpm, Linagraph pan film, 1000-watt projection lamp, D-11 developer, N = 100,000; b, diameter 1.200 in., thickness 0.238 in., camera speed 3800 rpm, Linagraph pan film, 1000-watt projection lamp with filters, SD-19a developer. Width of slit = 0.002 in., N = 1,600,000; c, enlargement of b, 2:1.)

resting against a rigid wall, and struck by a heavy rigid mass at the other end, Fig. 4(a). This problem has been treated theoretically by several investigators on the basis of the elementary theory of the longitudinal vibrations of bars, and the solution is credited[6] to Boussinesq (11).

Attempts to improve the elementary treatment of longitudinal waves in a bar have been the subject of much mathematical work. Pochhammer (13) gave an exact solution of the equations of the theory of elasticity for the waves in an infinite bar of uniform circular section which shows the dispersive nature of the medium. In a recent paper, Mindlin and Herrmann (14) pointed out the impracticability of attempting to employ the general equations of elasticity for finite bars, summarized some of the previous refinements to the elementary theory, and presented an approximate theory which is intermediate between the elementary and the exact theories. However, for the case of a compression bar struck by a rigid mass, it appears that the only explicit solution available is the Boussinesq solution which is based on the elementary theory.

Brief Summary of the Boussinesq Solution (11, 12, 15). The Boussinesq solution states that a compressive stress wave having an initial stress amplitude

$$\sigma_0 = v_0(E_d\rho)^{1/2} \quad \ldots\ldots\ldots\ldots\ldots\ldots [3]$$

will propagate along a bar at a velocity

$$c = (E_d/\rho)^{1/2} \quad \ldots\ldots\ldots\ldots\ldots\ldots [4]$$

where v_0 is the initial velocity of the hammer, E_d is the dynamic modulus of elasticity, and ρ is the mass per unit volume of the

[6] See reference (12), p. 446.

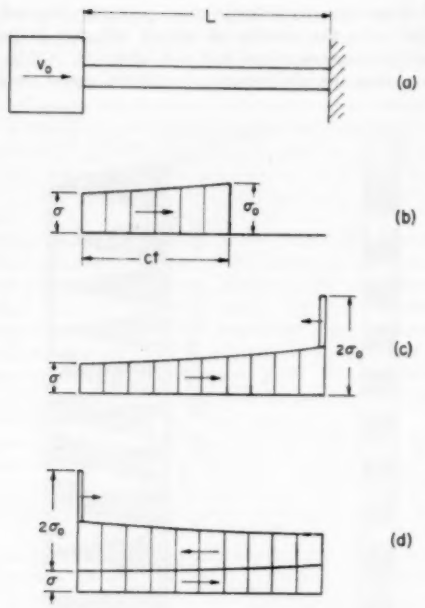

FIG. 4 IMPACT OF A RIGID MASS WITH A BAR

bar, Fig. 4(*b*). According to the laws of reflection the wave will reflect from the fixed end as a compressive wave, so that the stress abruptly increases from zero to $2\sigma_0$, Fig. 4(*c*).

The strut will retard the motion of the hammer so that the stress wave being sent into the bar will gradually decrease, and the compressive stress σ acting at the end of the bar is

$$\sigma = \sigma_0 \exp\left(-\frac{2\alpha t}{T}\right) \quad \ldots\ldots\ldots\ldots\ldots [5]$$

for $t < T$, where t is the time measured from the instant of impact, T is the time taken for the stress wave to travel twice the length of the bar, and α is the ratio of the mass of the strut to the mass of the hammer. At $t = T$ the stress wave will have returned to the hammer. Since the hammer cannot change its velocity suddenly, the stress wave will reflect as from a fixed end, and the stress will increase abruptly by $2\sigma_0$, Fig. 4(*d*).

This process of repeated reflections and abrupt increases in stress keeps repeating itself. The stress builds up to a maximum and then, because of the increasing effects of decay associated with the slowing down and reversal of the hammer, the stress falls off to zero and contact ends.

For the case of small values of α, approximate expressions for the duration of impact t_i and the maximum stress σ_{max} are available. These are

$$t_i = \frac{\pi L}{c}\left(\frac{1}{\alpha}\right)^{1/2} \quad \ldots\ldots\ldots\ldots\ldots [6]$$

where L is the length of the bar, and

$$\sigma_{max} = v_0(E_d\rho)^{1/2}\left[\left(\frac{1}{\alpha}\right)^{1/2} + 1\right] \quad \ldots\ldots\ldots [7]$$

Theoretical Stress Patterns on Basis of Boussinesq Solution. Theoretical stress patterns, on the basis of the Boussinesq solution, will now be constructed for both transverse and longitudinal slits assuming the following aspects of the solution: (*a*) constancy of the velocity of propagation; (*b*) steep wave front as shown in Fig. 4(*b*); (*c*) constancy of stress behind the wave front, i.e. α is small so that the decay is negligible, Equation [5]; and (*d*) uniform stress across transverse sections. In addition, we shall assume the laws of stress-wave reflection and a linear stress-optic law, i.e., a constant fringe value. Also, it will be convenient to work with an initial velocity v_0, adjusted to produce an initial stress σ_0, which develops a birefringence n_0, of one half of a fringe.

Let us now consider the nature of the stress pattern which will be obtained by means of streak photography for a transverse slit, A-A, located as shown in Fig. 5(*a*). For a polariscope with a bright background, the stress pattern is initially white and remains white until the stress wave reaches the slit. The pattern should turn black and should remain black until the wave is reflected from the anvil and returns to the slit. The stress at the slit should then abruptly rise to $2\sigma_0$ so that the pattern will turn white ($n = 1$) and remain unchanged for the period of time that it takes for the wave to reach the hammer and for the reflected wave to reach the slit once again. The stress should now be $3\sigma_0$ so that the pattern turns black again, ($n = 1^1/_2$), etc. These results have been sketched partially in Fig. 5(*b*). The bases of the white rectangles correspond to a period of time t_1, needed for the wave to travel a distance $2a$, Fig. 5(*a*). Similarly, the bases of the black rectangles correspond to a period of time t_2, needed for the wave to travel $2b$. The ratio of the bases of the white and black rectangles is a/b and is thus determined by the location of the slit. The total time, $T = t_1 + t_2$, represents the time it takes for the wave to travel across the full length of the bar and to return to the hammer.

Consider now the stress pattern resulting from a longitudinal slit, such as B-B in Fig. 5(*a*). The locus of the wave front recorded on the film will depend on the ratio of the film velocity V to the velocity of stress wave propagation c. Since these velocities are constant, the locus should be a straight line inclined at an

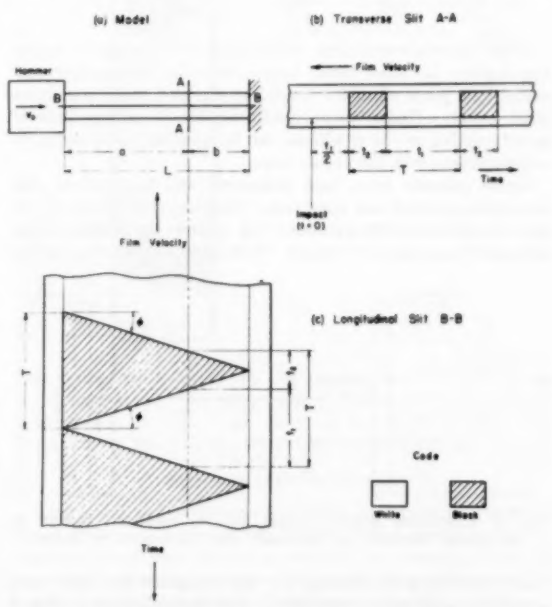

FIG. 5 THEORETICAL STRESS PATTERNS ON THE BASIS OF THE BOUSSINESQ SOLUTION

angle ϕ such that $\phi = \tan^{-1} V/c$, Fig. 5(*c*). The initial stress wave is of intensity $n = 1/2$ so that the stressed region should appear black. Upon reflection at the anvil, the returning compression wave causes the stress to double. Hence the stress pattern at an arbitrary point along B-B should remain black until the reflected wave reaches it, at which time it should turn white. The locus of this returning wave also should appear as a straight line inclined at an angle minus ϕ. This would give the triangular pattern sketched in Fig. 5(*c*). The bases of these triangles represent the time T which it takes for the stress wave to travel twice the length of the bar.

Since no explicit exact solution exists for a bar struck by a rigid mass, no precise statement can be made about the modifications in the stress patterns of Fig. 5 which such solutions would introduce.

In general, it is known that in the region of the wave front the longitudinal compressive stresses are accompanied by transverse compressive and shearing stresses. Qualitatively speaking, the wave front would be modified to show dispersion. Also, variations in stress intensity, or wiggles, would appear behind the wave front. The resulting stress pattern would under such conditions show gray fronts instead of sharp black or white fronts as well as transverse streaks of gray in the uniform black and white rectangles of Fig. 5(*b*).

Photoelastic Models and Stress Patterns. Impact between a compression bar fixed at one end and struck by a heavy rigid mass at the other end was produced by means of the pendulum loading mechanism and model support shown in Fig. 2. The hammer and support were made of steel so that they can be considered as rigid relative to the plastic photoelastic models. Three compression bars made of Castolite (16) were tested. Their dimensions are given in Table 1.

TABLE 1 DIMENSIONS OF CASTOLITE COMPRESSION BARS

Model	Length in.	Depth in.	Thickness in.	$1/\alpha$
1	2.26	0.692	0.187	795
2	4.62	0.736	0.251	244
3	4.34	0.324	0.251	591

These models were chosen to illustrate the influence of length and depth. In these tests, impact between the hammer and model took place when the pendulum was at a small angle past dead center. Under these conditions the retarding force of gravity acting on the pendulum can be assumed to be negligible in comparison with the impact force.

Stress patterns from both transverse and longitudinal slits were photographed and examined. The long, thin model, No. 3, gave the clearest stress patterns. Fig. 6 shows the location of the slits and the method of support. It should be noted that several

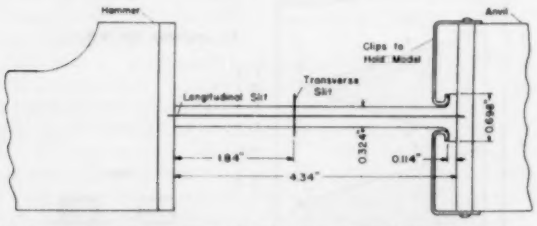

FIG. 6 CASTOLITE STRUT, MODEL NO. 3, SHOWING IMPACT OF HAMMER, METHOD OF SUPPORT, AND LOCATION OF SLITS

other procedures for holding the model against the anvil were considered and some were tried. The design shown in Fig. 6 proved to be the most satisfactory. Tests were made with and without lubrication. The results showed no visible difference.

Fig. 7 shows the photoelastic stress patterns obtained from model No. 3 for the velocity of impact adjusted to produce an initial birefringence of one half of a fringe ($n_0 = 1/2$). Fig. 7(*a*) shows that the birefringence is uniform across transverse

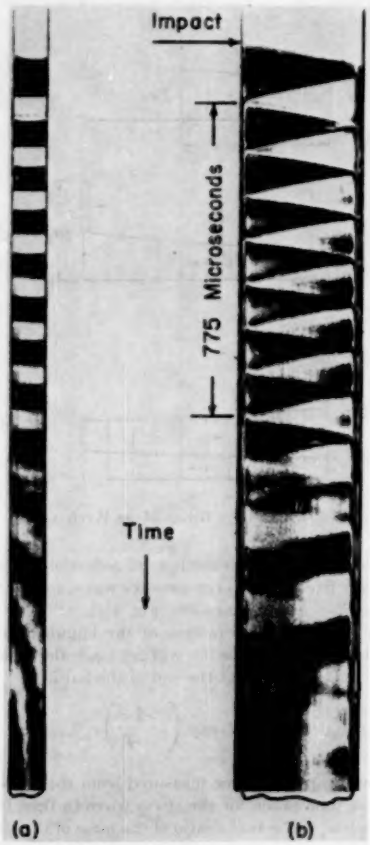

FIG. 7 DYNAMIC PHOTOELASTIC STRESS PATTERNS FOR CASTOLITE STRUT, MODEL NO. 3

$\alpha = 1/591$ $n_0 = 46.4$ ips

Linagraph ortho film, photoflash bulb with filters, 8D-19a developer.
(*a*) Transverse slit 0.0043 in.; camera speed, 3320 rpm; $N = 650{,}000$
(*b*) Longitudinal slit 0.0020 in.; camera speed, 3370 rpm; $N = 1{,}400{,}000$

sections of the bar and that it remains essentially uniform up to its maximum value. Hence the stress distribution at transverse sections is uniform. This uniformity in the state of stress was obtained by careful alignment of all the elements in the test[7] and was reproducible for all models.

The stress pattern in Fig. 7(*b*) shows that the footing or protrusions of the model at the anvil end of the bar had a negligible effect on the results. Perhaps this can be seen best by noting that the differences in the stress pattern at the two ends of the bar are small; i.e., the anvil with the footing produced essentially the same effect as the hammer end with no footing.

The experimental procedure used and the resulting stress patterns show that the boundary conditions in these tests were essentially the same as those in the Boussinesq solution.

Interpretation of Photoelastic Stress Patterns. The photoelastic patterns of Fig. 7 establish directly the following facts: (*a*) Since

[7] Details of this alignment can be found in the thesis by P. D. Flynn. See footnote 1.

the sides of the triangles are straight lines, the velocity of propagation is a constant; (*b*) the abrupt changes in the fringe order indicate that the wave front is relatively steep; (*c*) the uniformity of fringe order behind the wave front indicates the constancy of stress; (*d*) the stress distribution across transverse sections is uniform; and (*e*) the birefringence develops in integral multiples of n_0. In addition, the stress patterns provide data for the direct determination of the velocity of propagation c, the duration of impact t_i, and the birefringence n at any time during impact.

Comparison of Experimental With Theoretical Stress Patterns. The theoretical stress patterns of Fig. 5 and the photoelastic patterns of Fig. 7 are for the case of small α and for an initial birefringence n_0 of one half of a fringe. Comparison shows that rectangles were obtained from transverse slits and isosceles triangles from longitudinal slits, as predicted by the theory. This agreement provides experimental proof of assumptions (*a*) through (*d*) which were made in constructing the theoretical stress patterns on the basis of the Boussinesq solution.

Some deviations between the photoelastic and the theoretical stress patterns may be noted. The first triangle in Fig. 7(*b*) has a somewhat flat apex and a slightly broader base than the succeeding triangles. Also, the sides of some triangles appear to have a slight curvature, and there are a few white and black "islands" indicating disturbances in the otherwise regular triangular pattern. Work with a bakelite bar shows evidence of dispersion in the wave front which is confined to a narrow zone. Higher speeds than those attained in the present experiments are necessary in order to obtain clear stress patterns of the wave front itself.

The differences between the Boussinesq theory and the experiment may be a result of the limitations of this theory, which neglects the transverse compressive and shearing stresses in the region of the wave front, or of the imperfections in the experimental technique and equipment, or both. In the main, however, the agreement is believed to be satisfactory up to the maximum value of the birefringence. Beyond that, the patterns show evidence of bending which is believed to be due to disturbances in the alignment.

Velocity of Propagation, Duration of Impact, Initial Stress Wave, and Modulus of Elasticity. The bases of the triangles of Fig. 7(*b*) and the sum of the bases of a pair of adjacent black and white rectangles in Fig. 7(*a*) represent the time T that it takes for the stress wave to travel a distance $2L$ equal to twice the length of the bar. The velocity of propagation is given by

$$c = \frac{2L}{T} \quad \ldots\ldots\ldots\ldots\ldots\ldots\ldots\ldots [8]$$

and can be determined with good accuracy.

A series of tests at different impact velocities was made on model No. 3. Fig. 8 shows that the duration of impact is independent of the striking velocity and that its magnitude is in good agreement with Equation [6].

Fig. 9 provides experimental corroboration for Equation [3] which states that the amplitude of the initial stress wave is independent of the cross-sectional area of the strut. This stress pattern was obtained from a longitudinal slit with model No. 2 which has the same thickness as model No. 3 but a greater depth. The impact velocity and the initial birefringence are essentially the same as in Fig. 7(*b*).

Also, the dynamic modulus of elasticity may be computed from Equation [4], i.e.

$$E_d = \rho c^2 \quad \ldots\ldots\ldots\ldots\ldots\ldots\ldots\ldots [9]$$

The values of c and E_d have been computed from Fig. 7(*b*) by omitting the first triangle and taking the average length of the bases of the next seven triangles. For Castolite, the weight per unit volume ρg is 0.0438 pci. The results are: c = 78,500 ips, E_d = 698,000 psi. The static value of E given for this material in reference (16) is 705,000 psi. The velocity of propagation from Equation [4] based on the static modulus is 78,900 ips.

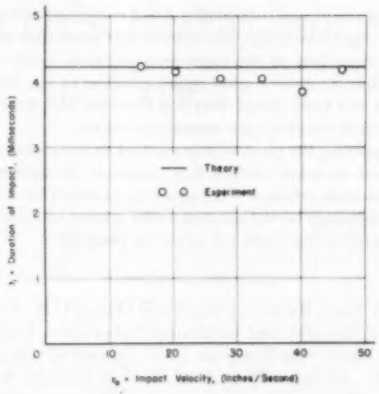

FIG. 8 DURATION OF IMPACT VERSUS IMPACT VELOCITY. CASTOLITE STRUT, MODEL NO. 3

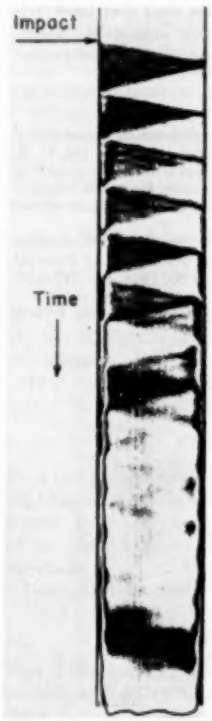

FIG. 9 DYNAMIC PHOTOELASTIC STRESS PATTERN FOR CASTOLITE STRUT, MODEL NO. 2

α = 1/164 v_0 = 46.1 ips
Linagraph ortho film, photoflash bulb with filters, SD-19a developer
Longitudinal slit 0.0020 in.; camera speed, 3510 rpm; N = 1,500,000

SUMMARY AND CONCLUSIONS

Equipment and techniques have been developed for obtaining stress patterns from arbitrary lines in bodies under impact by means of streak photography at rates of approximately 1,500,000 equivalent exposures per sec. This is 30 times faster than the highest rate (50,000) obtained by Tuzi and Nisida in 1935.

Theoretical stress patterns based on the Boussinesq solution are in essential agreement with the results obtained with the

present equipment and techniques for a compression bar struck by a heavy rigid hammer. The results also show that the initial stress is independent of the cross-sectional area of the bar, and that Equation [6] gives a good approximation to the duration of impact. It has been found that for Castolite the dynamic and static moduli of elasticity are essentially equal.

Before applying the photoelastic method to structural problems under impact or shock loading it is necessary to explore the dynamic stress-optic relation. It cannot be assumed that this relation will necessarily be the same as under static conditions. Work on the dynamic stress-optic law is now in progress.

Acknowledgments

The U. S. Navy Bureau of Yards and Docks, U. S. Naval Civil Engineering Research and Evaluation Laboratory, Construction Battalion Center, Port Hueneme, Calif., sponsored this investigation, and we are sincerely grateful for their financial assistance. At the present time, this work is under the sponsorship of the Office of Ordnance Research, U. S. Army. The Research Corporation provided the funds for the fellowship held by Paul D. Flynn. Lastly, the authors wish to express their deep indebtedness to David Landsberg[8] for his invaluable suggestions, assistance, and wholehearted co-operation throughout the investigation.

BIBLIOGRAPHY

1 "A Photoelastic Study of Dynamic Stresses in Structures," by M. M. Frocht and P. D. Flynn, Technical Report to the U. S. Navy Bureau of Yards and Docks, U. S. Naval Civil Engineering Research and Evaluation Laboratory, Structures Research Department, Port Hueneme, Calif., Contract NOy-28149, Project Order 10703, June 30, 1952.

2 "Photographic and Kinematographic Study of Photo-elasticity," by Ziro Tuzi, Scientific Papers of the Institution of Physical and Chemical Research, vol. 8, no. 149, June 20, 1928, pp. 247–267.

3 "Kinematography in Photoelasticity," by M. M. Frocht, Trans. ASME, vol. 54, 1932, pp. 83–96.

4 "Photoelastic Study of Stresses Due to Impact," by Ziro Tuzi and M. Nisida, Scientific Papers of the Institution of Physical and Chemical Research, vol. 26, no. 566, April, 1935, pp. 277–309; also, *Philosophical Magazine*, series 7, vol. 21, 1936, pp. 448–473.

5 "The Fundamentals of Photoelastic Stress Analysis Applied to Dynamic Stresses," by W. N. Findley, Proceedings of the Ninth Semi-Annual Eastern Photoelasticity Conference, May 13, 1939, pp. 1–11.

6 "Slow-Motion Pictures of Impact Tests by Means of Photoelasticity," by Ludwig Foeppl, JOURNAL OF APPLIED MECHANICS, Trans. ASME, vol. 71, 1949, pp. 173–177.

7 "Further Studies of Glass Fracture With High-Speed Photography," by H. E. Edgerton and F. E. Barstow, *Journal of the American Ceramic Society*, vol. 24, 1941, pp. 131–137.

8 "A Photoelastic Study of Stress Waves," by D. A. Senior and A. A. Wells, *Philosophical Magazine*, series 7, vol. 37, July, 1946, pp. 463–469.

9 "An Investigation of Cracks and Stress Waves in Glass and Plastics by High-Speed Photography," by D. G. Christie, Trans. of the Society of Glass Technology, vol. 36, 1952, pp. 74–89.

10 "A Photoelastic Study of Dynamic Stresses in Structures," by M. M. Frocht, P. D. Flynn, and D. Landsberg, Technical Report as in reference (1), June 30, 1953.

11 "Du choc longitudinal d'une barre prismatique fixée à un bout et heurtée à l'autre," by J. Boussinesq, Comptes Rendus, vol. 97, 1883, pp. 154–157.

12 "Theory of Elasticity," by S. Timoshenko and J. N. Goodier, McGraw-Hill Book Company, Inc., New York, N. Y., second edition, 1951, chapter 15, pp. 446–452.

13 "Über die Fortpflanzungsgeschwindigkeiten kleiner Schwingungen in einem unbegrenzten isotropen Kreiscylinder," by L. Pochhammer, *Journal für die reine und angewandte Mathematik*, (Crelle), vol. 81, 1876, pp. 324–336.

14 "A One-Dimensional Theory of Compressional Waves in an Elastic Rod," by R. D. Mindlin and G. Herrmann, Proceedings of the First U. S. National Congress of Applied Mechanics, December, 1952, pp. 187–191.

15 "Longitudinal Wave Transmission and Impact," by L. H. Donnell, Trans. ASME, vol. 52, 1930, pp. 153–167.

16 "A New Cementable Material for Two- and Three-Dimensional Photoelastic Research," by M. M. Frocht and Hui Pih, Proceedings of the Society of Experimental Stress Analysis, vol. 12, no. 1, 1954, pp. 55–64.

[8] Associate Research Engineer, Mechanics Department, Illinois Institute of Technology, Chicago, Ill.

The Effect of the Earth's Rotation on Laminar Flow in Pipes

By G. S. BENTON,[1] BALTIMORE, MD.

The theory of laminar pipe flow has been developed, retaining the effect of the earth's rotation. A secondary flow is set up in the pipe cross section which results in distortion of the usual parabolic profile. The distortion may be significant in pipes of moderate diameter. Laboratory studies tend to substantiate these conclusions.

Introduction

IT IS well known that the steady-state equations of motion of an incompressible fluid in laminar flow relative to a co-ordinate system rotating at a constant angular velocity ω, may be written in the form

$$\underline{c} \cdot \nabla \underline{c} = -2\underline{\omega} \times \underline{c} - \nabla\Phi + \nu\nabla^2\underline{c} \quad \ldots\ldots [1]$$

where

$$\Phi = \frac{p}{\gamma} + \varphi + \frac{\omega^2 a^2}{2} \quad \ldots\ldots [2]$$

Here $\underline{c}$ is the velocity; p is the pressure and γ the density; φ is the gravitational geopotential; a is the distance from the axis of rotation; and ν is the kinematic viscosity. When the co-ordinate system in Equation [1] is fixed relative to the surface of the earth, ω becomes the angular velocity of the earth's rotation.

In any given problem the Coriolis terms ($2\underline{\omega} \times \underline{c}$), and hence the effect of the earth's rotation, may or may not be of significance depending on the nondimensional ratio of the inertia forces to the Coriolis forces. This ratio takes the form $V/2\omega D \sin \alpha$, where V and D are, respectively, a fluid speed and length characteristic of the system under consideration, and α is the angle between the axis of the earth's rotation and the direction of fluid motion. This nondimensional ratio has been named the Rossby number by Fultz,[2] in honor of Prof. C.-G. Rossby who used this number in comparing the circulations of the terrestrial and solar atmospheres. Apparently, when the Rossby number is sufficiently large, the effect of the rotation of the co-ordinate system on fluid-flow patterns will be negligible; when the Rossby number is sufficiently small, this no longer will be true.

Because of the appearance of the characteristic length D in the Rossby number, the importance of the earth's rotation is closely related to the scale of the phenomenon under consideration. In meteorology and oceanography, typical values of the Rossby number would be of the order of magnitude of 10^{-1}. For these sciences, the rotation of the earth is of prime importance in determining flow characteristics. In the analysis of flow of fluids in estuaries, rivers, and canals, the Rossby number is of the order of 10^2. For these fields, it has often been suggested that the rotation of the earth may not be negligible. However, verification of this hypothesis has only recently been forthcoming.[3] In the analysis of laboratory problems in hydraulics (such as pipe or small-scale channel flows) typical values of the Rossby number would be of the order of 10^6. Heretofore it has been assumed implicitly that in such cases the effect of the earth's rotation may be completely ignored.

One purpose of the present study is to test the validity of this assumption. To do this, the equations of motion for the laminar flow of a fluid in a circular pipe are examined with the Coriolis terms retained. A theoretical solution for the flow, including secondary motions due to the rotation of the earth, is obtained. The magnitude of the effects of the earth's rotation is evaluated, and the results of laboratory investigations seeking to measure these effects are presented. It is shown that in certain specific cases the assumption that the earth's rotation is of negligible importance in the laboratory is open to serious question.

The Equations of Motion for Laminar Flow in Pipes

In considering steady-state laminar flow in a pipe with the Coriolis terms retained, it will be assumed that with the exception of Φ, none of the dependent variables in Equation [1] varies in the direction of the pipe axis. Therefore Φ must vary linearly in this direction.

In cylindrical co-ordinates with the z-axis coinciding with the axis of the pipe, the fluid velocity $\underline{c}$ may be written

$$\underline{c}(r, \theta) = \underline{u}(r) + \underline{v}(r, \theta) \quad \ldots\ldots [3]$$

Here $u(r)$ is the conventional solution for laminar flow neglecting the effect of the earth's rotation, while $\underline{v}(r, \theta)$ are small secondary terms. Obviously, $\underline{u}$ is directed everywhere parallel to the axis of the pipe; $\underline{v}$ may have components in all three co-ordinate directions.

Similarly, it is possible to write

$$\Phi(r, \theta, z) = \overline{\Phi}(z) + \Phi'(r, \theta) \quad \ldots\ldots [4]$$

Here $\overline{\Phi}$ is a linear function of z and $\partial\overline{\Phi}/\partial z$ is proportional to the imposed hydraulic gradient; Φ' represents the variation of Φ in the r, θ-plane associated with the secondary velocities $\underline{v}$. The equation of motion in an inertial co-ordinate system is then

$$\nu\nabla^2\underline{u} = \nabla\overline{\Phi} \quad \ldots\ldots [5]$$

Rewriting the complete equations of motion using Equations [3], [4], and [5]

$$\underline{v} \cdot \nabla(\underline{u} + \underline{v}) = -2\underline{\omega} \times (\underline{u} + \underline{v}) - \nabla\Phi' + \nu\nabla^2\underline{v} \quad \ldots\ldots [6]$$

Equation [6] may be linearized with negligible error, since it is safe to assume that the components and the derivatives of $\underline{v}$ will

---

[1] Associate Professor of Civil Engineering, The Johns Hopkins University.

[2] "Non-Dimensional Equations and Modeling Criteria for the Atmosphere," by D. Fultz, *Journal of Meteorology*, vol. 9, 1951, pp. 262–267.

Contributed by the Applied Mechanics Division and presented at the Diamond Jubilee Annual Meeting, Chicago, Ill., November 13–18, 1955, of The American Society of Mechanical Engineers.

Discussion of this paper should be addressed to the Secretary, ASME, 29 West 39th Street, New York, N. Y., and will be accepted until April 10, 1956, for publication at a later date. Discussion received after the closing date will be returned.

Note: Statements and opinions advanced in papers are to be understood as individual expressions of their authors and not those of the Society. Manuscript received by ASME Applied Mechanics Division, September 29,1954. Paper No. 55—A-9.

[3] For example, see "Rational Theory of Delta Formation," by C. C. Bates, *Bulletin of the American Association of Petroleum Geologists*, vol. 37, 1953, pp. 2119–2162.

be very small compared to $\underline{u}$. In addition, the term $2\underline{\omega} \times \underline{v}$ is second order, since the earth's angular velocity is small. Thus the equations of motion become

$$\underline{v} \cdot \nabla \underline{u} = -2\underline{\omega} \times \underline{u} - \nabla \Phi' + \nu \nabla^2 \underline{v} \quad \ldots\ldots [7]$$

The problem at hand is to obtain a solution of Equation [7] which satisfies the necessary boundary conditions and which also satisfies the continuity equation

$$\nabla \cdot \underline{v} = 0 \quad \ldots\ldots [8]$$

The dependent variables are the secondary velocity $\underline{v}$, and Φ'. Since laminar flow is assumed $\underline{u}(r)$ is a known function.

A Solution for the Secondary Circulation Normal to the Pipe Axis

The first step in solving Equations [7] and [8] is to determine the secondary circulation normal to the pipe axis. It should be noted that $\underline{v}$ may have components in the direction of the pipe axis, as well as in the r,θ-plane. However, since $\underline{v} = \underline{v}(r, \theta)$ a stream function can be introduced for the components of the secondary flow in the r,θ-plane. Thus

$$\underline{v} = \underline{k} v_z - \nabla \times \underline{\psi} \qquad (\underline{\psi} = \underline{k}\psi) \quad \ldots\ldots [9]$$

where the unit vector $\underline{k}$ is in the direction of the pipe axis. Substituting in Equation [7] and taking the curl of the equation of motion in the cross-sectional plane, one obtains the vorticity equation for secondary motion in the r,θ-plane in terms of the stream function

$$\nabla^4 \psi = -\frac{2\omega \cdot \nabla u}{\nu} \quad \ldots\ldots [10]$$

It will be helpful to recast Equation [10] in nondimensional form. Let V be the mean velocity in a pipe of diameter D. Also, let α be the angle between ω and the pipe axis, and orient the direction $\theta = 0$ parallel to the component of ω lying in the r,θ-plane. Then, in terms of the nondimensional co-ordinates $\rho,\theta (\rho = 2r/D)$

$$\nabla^4 \psi^* = -\frac{1}{4} \frac{\mathrm{Re}}{\mathrm{Ro}} \cos\theta \frac{\partial (u/V)}{\partial \rho} \quad \ldots\ldots [11]$$

Here Re is the Reynolds number ($\mathrm{Re} = VD/\nu$); Ro is the Rossby number ($\mathrm{Ro} = V/2\omega D \sin\alpha$); and ψ^* is a nondimensional stream function ($\psi^* = 2\psi/VD$) whose curl yields the ρ,θ-components of the velocity ratio $\underline{v}/V$.

From the solution for laminar flow in an inertial system

$$\frac{u}{V} = 2(1 - \rho^2) \quad \ldots\ldots [12]$$

Therefore the equation for the nondimensional stream function in the ρ,θ-plane becomes

$$\nabla^4 \psi^* = \frac{\mathrm{Re}}{\mathrm{Ro}} \rho \cos\theta \quad \ldots\ldots [13]$$

Boundary conditions require that $\psi^* = 0$ and $\partial\psi^*/\partial\rho = 0$ at $\rho = 1$. The appearance of the ratio of the Reynolds and Rossby numbers on the right side of Equation [13] is significant. This term is proportional to the ratio of the Coriolis and frictional forces. When Coriolis effects are truly negligible $\nabla^4\psi^* = 0$; the solution is $\psi^* = 0$; and there is no secondary flow in the ρ,θ-plane. As Coriolis forces increase in magnitude relative to molecular friction, the secondary flow appears and strengthens.

Equation [13] and its boundary conditions are identical in form to those encountered in determining the deflection of a circular plate, clamped at the periphery and subjected to a load which is zero at the center and varies linearly with distance from a neutral axis. The solution, cited by Love,[4] is not difficult and in the present problem gives

$$\psi^* = \frac{\mathrm{Re}}{192\mathrm{Ro}} \rho (1 - \rho^2)^2 \cos\theta \quad \ldots\ldots [14]$$

whence from the definition of ψ^*

$$\left.\begin{aligned} \frac{v_r}{V} &= \frac{\mathrm{Re}}{192\mathrm{Ro}} (1 - \rho^2)^2 \sin\theta \\ \frac{v_\theta}{V} &= \frac{\mathrm{Re}}{192\mathrm{Ro}} (1 - \rho^2)(1 - 5\rho^2) \cos\theta \end{aligned}\right\} \quad \ldots\ldots [15]$$

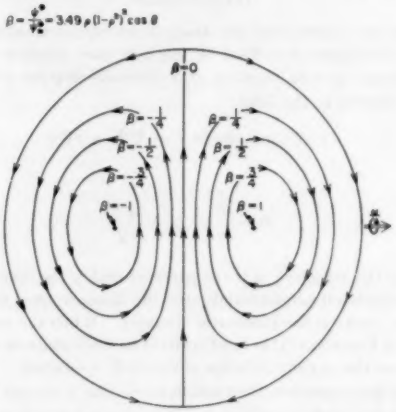

Fig. 1 Stream Function for Secondary Flow in Plane of Pipe Cross Section, Expressed in Nondimensional Form

Fig. 1 shows the nondimensional streamlines in the ρ,θ-plane. The basic flow is out of the page. The maximum value of ψ^* is

$$\psi_m^* = 1.49 \frac{\mathrm{Re}}{\mathrm{Ro}} \, 10^{-3}$$

at $\theta = 0$, $\rho = \sqrt{5}/5$. The streamlines are drawn for $-\psi_m^* \leq \psi^* \leq \psi_m^*$ at intervals of $\psi_m^*/4$.

The magnitude of the velocities in the secondary circulation may now be appraised. The highest velocity in the ρ,θ-plane occurs at $\rho = 0$, where the flow is in the $\theta = \pi/2$ direction and the relative speed is

$$\frac{(v_r^2 + v_\theta^2)^{1/2}}{V} = \frac{\mathrm{Re}}{192\mathrm{Ro}} \quad \ldots\ldots [16]$$

The absolute speed is

$$(v_r^2 + v_\theta^2)^{1/2} = \frac{\omega D \sin\alpha}{96} \mathrm{Re} \quad \ldots\ldots [17]$$

and therefore is a function only of the Reynolds number, the diameter of the pipe, and the component of the earth's rotation normal to the pipe. Even for laminar flow at a Reynolds number as high as 6000, the cross-axial flow in a 2-cm pipe cannot exceed 0.01 cm/sec.

[4] "The Mathematical Theory of Elasticity," by A. E. H. Love, Dover Publications, New York, N. Y., fourth edition, 1944.

This velocity (and therefore all of the circulation in the ρ,θ-plane) is too small to measure directly. However, the secondary circulation may be indirectly measurable from its effect on the velocity profile in the direction of the pipe axis. The extent to which the usual parabolic profile is distorted by the crossflow is examined in the next section.

Anomalies in the function Φ associated with the secondary flow in the ρ,θ-plane will now be considered. Taking the divergence of Equation [7], one obtains

$$\nabla^2\Phi' = 2\underline{\omega}\cdot(\nabla \times \underline{u}) \quad [18]$$

It will be convenient to write this equation in terms of the nondimensional function

$$E = \frac{2\Phi'}{V^2} \quad [19]$$

Whence, after making use of Equation [12]

$$\nabla^2 E = -\frac{4}{\mathrm{Ro}}\rho \sin\theta \quad [20]$$

This, together with Equation [7], leads to the solution

$$E = \frac{1}{6\mathrm{Ro}}\rho\,(10 - 3\rho^2)\sin\theta \quad [21]$$

The maximum value of E occurs at $\rho = 1$, $\theta = \pi/2$, at which point $E = E_m = 7/(6\ \mathrm{Ro})$. Fig. 2 shows the distribution of E in the ρ,θ-plane for $-E_m \leq E \leq E_m$ at intervals of $E_m/4$. For

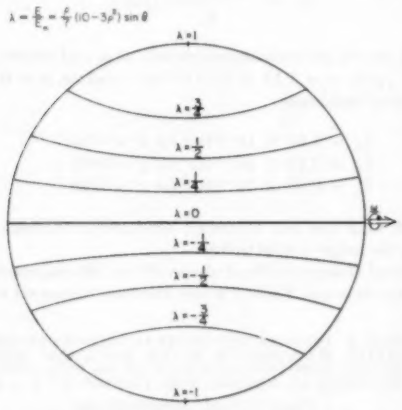

FIG. 2 PRESSURE DISTRIBUTION IN PLANE OF PIPE CROSS SECTION, EXPRESSED IN NONDIMENSIONAL FORM

laminar flow it would be difficult to detect E by direct measurement. The maximum value of Φ' for water flowing in a 2-cm pipe at a Reynolds number of 6000 would be 7×10^{-2} ergs/gm. This would correspond to a pressure increment across the pipe of only 1.4×10^{-2} dynes/cm^2. Although this figure would be increased for more viscous fluids, it again would appear that anomalies in the ρ,θ-plane due to the earth's rotation would not be directly measurable in the laboratory. The effect of these anomalies on fluid flow in the axial direction must now be considered.

SECONDARY VELOCITIES IN THE DIRECTION OF THE PIPE AXIS

Secondary velocity components in the direction of the pipe axis can be obtained from a solution of the component of Equation [7] parallel to the pipe axis. In nondimensional notation, this equation becomes

$$\nabla^2 w = -\frac{\mathrm{Re}^2}{96\mathrm{Ro}}\rho(1-\rho^2)^2 \sin\theta \qquad w = \frac{v_s}{V} \quad [22]$$

Boundary conditions require that $w = 0$ for $\rho = 1$. The solution is

$$w = \frac{\mathrm{Re}^2}{2^6 3^2 \mathrm{Ro}}\rho(1-\rho^2)(3 - 3\rho^2 + \rho^4)\sin\theta \quad [23]$$

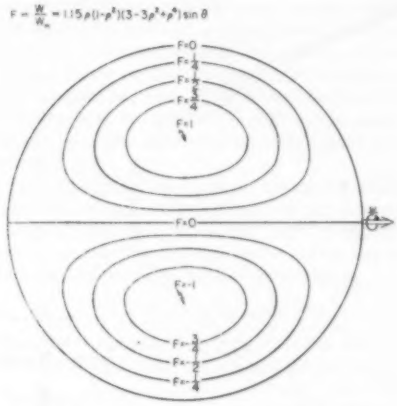

FIG. 3 ISOLINES OF SECONDARY FLOW IN AXIAL DIRECTION, EXPRESSED IN NONDIMENSIONAL FORM

Fig. 3 shows isolines of w plotted on the ρ,θ-plane. The maximum value of w occurs at $\theta = \pi/2$, $\rho = 0.46$. At this point

$$w = w_m = 1.9\frac{\mathrm{Re}^2}{\mathrm{Ro}} \times 10^{-4}$$

Curves are drawn for $-w_m \leq w \leq w_m$ at intervals of $w_m/4$. It is significant that the absolute magnitude of the secondary velocity in the axial direction increases with the square of the Reynolds number. For an arbitrary fluid

$$v_s)_{\max} = 3.8\omega D \sin\alpha\ \mathrm{Re}^2\ 10^{-4} \quad [24]$$

Hence at a Reynolds number of 6000, for laminar flow in a 2-cm pipe oriented east-west, the maximum increase in axial velocity is about 2 cm/sec. For water, this would be approximately 7 per cent of the mean velocity. The resulting distortion of the normal parabolic profile might therefore be detected with careful observation.

A nondimensional presentation of the distortion of the parabolic profile is shown in Fig. 4. Here the parameter $(u + v_s)/V$ is plotted as a function of $\mathrm{Re}^2/\mathrm{Ro}$ for the cross section $\theta = \pi/2$, $3\pi/2$. It can be seen that the distortion is substantial only when $\mathrm{Re}^2/\mathrm{Ro}$ is about 5×10^3 or greater. In the previous numerical example this ratio was approximately 3.5×10^2. It is also clear that for $\mathrm{Re}^2/\mathrm{Ro} \gg 5 \times 10^3$, v_s is no longer small compared to u. Thus $2\underline{\omega} \times \underline{k}\, v_s$ is no longer small compared to $2\underline{\omega} \times \underline{u}$ and neither the cross-sectional flow nor the axial flow can be accurately computed from Equations [15] and [23].

For water at 20 C flowing in a pipe oriented east-west, the nondimensional value of the maximum secondary velocity in the axial direction (w_m) is shown in Table 1. For a pipe 4 cm diam the effect of the earth's rotation is already appreciable at a Reynolds number of 2000; for small pipes the rotation becomes

TABLE 1 RATIO OF MAXIMUM SECONDARY VELOCITY TO MEAN AXIAL VELOCITY FOR LAMINAR FLOW OF WATER IN AN EAST-WEST PIPE, EXPRESSED AS A FUNCTION OF REYNOLDS NUMBER AND PIPE DIAMETER

	Pipe diameter, cm				
Re	1	2	3	4	5
2000	0.01	0.02	0.05	0.09	0.15
4000	0.01	0.05	0.10	0.19	>0.25[a]
6000	0.02	0.07	0.16	>0.25[a]	>0.25[a]
10000	0.03	0.12	>0.25[a]	>0.25[a]	>0.50[a]
20000	0.06	0.24	>0.50[a]	>0.50[a]	>1.00[a]

[a] For these conditions the first-order approximation used in this study cannot be accurate.

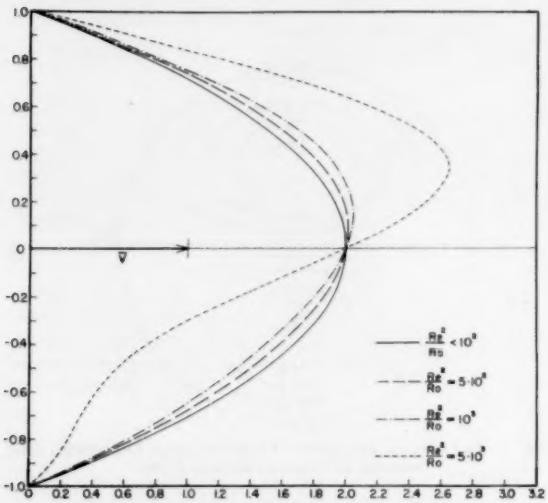

FIG. 4 NONDIMENSIONAL PROFILE OF AXIAL FLOW ALONG CROSS SECTION $\theta = \pi/2, 3\pi/2$, AS A FUNCTION OF RATIO OF REYNOLDS NUMBER SQUARED TO ROSSBY NUMBER

important at Reynolds numbers above the usual critical range. However, it is clear that under certain circumstances the rotation of the earth may play a significant role in the breakdown of laminar flow into turbulence.

LABORATORY INVESTIGATIONS

An effort was made to measure experimentally the effect of the earth's rotation in laminar pipe flow. At the outset, several difficulties were encountered. Owing to space limitations a system only 35 ft in length oriented north-south could be used. There was considerable doubt whether this distance would be sufficient to establish fully both the primary and secondary flows in a pipe of moderate diameter. In addition, at the latitude of Baltimore the north-south orientation reduced the maximum possible effect of the earth's rotation by about 35 per cent. It was decided, therefore, to concentrate on detecting the secondary axial flow rather than on determining its cross-sectional distribution.

Two sections of pipe were used. A 21-ft 2-in-diam pipe formed the first section. Near the end of this section, a smooth bell-shaped transition led into an 11-ft length of 1-in. brass tubing which was free to rotate about its axis. Head and outlet tanks were constructed. Screening and a smooth entrance to the 2-in. section were designed to secure laminar flow, although at the Reynolds numbers considered this posed no serious problem. A screened overflow pipe was centered at the rear of the outlet tank. Discharge was determined volumetrically and the total drop in head through the system also was measured.

Two probes were mounted securely on drilled aluminum carriers which could be clamped to the end of the 1-in. pipe. The probes extended 4 in. into the pipe, and their position could be adjusted across the pipe diameter. The probes led to a differential manometer filled with distilled water and a fluid with a specific gravity of 1.027.

The following procedure was employed for each run: (1) The discharge was measured accurately. (2) The probes were adjusted carefully along the horizontal pipe diameter until the differential manometer showed a near-zero reading. The probes were then clamped securely to the pipe, and another manometer reading was taken. The probes were not adjusted in any way during the remainder of the run. (3) The 1-in. pipe was rotated an angle φ about its axis and after equilibrium was established new discharge and manometer measurements were taken. (4) This procedure was repeated until the pipe was back in its original position. The final discharge and manometer readings were checked with the first measurements to make certain no change occurred. Discharge was compared with total drop in head to verify the existence of laminar flow.

If the flow in the 1-in. pipe was symmetrical, or if the asymmetry was associated with irregularities in the pipe or with the probe system, the differential manometer readings should not change with pipe rotation. On the other hand, if an asymmetry existed as a result of the earth's rotation, it can be shown readily that the change in head (δ) recorded by the manometer should vary as the cosine of rotation angle since the experiments were all started with the probes in the horizontal plane (i.e., along the cross section $\theta = \pi/2, 3\pi/2$). The maximum change (δ_m) occurs with a rotation of 180 deg, and is given by

$$\delta_m = \frac{4u(\rho)v_z(\rho,\pi)}{g} \text{ (feet)} \quad \ldots\ldots [25]$$

where the probes are both approximately at ρ, and where $v_z \ll u$. For $D = 1/12$ ft; $\nu = 1.13 \times 10^{-5}$ ft²/sec; and $\sin \alpha = 0.632$ (α = latitude of Baltimore)

$$\left.\begin{aligned} \delta_m &= 3.61 \times 10^{-14}\mathrm{Re}^3 \text{ for } \rho = 0.50 \\ \delta_m &= 2.23 \times 10^{-14}\mathrm{Re}^3 \text{ for } \rho = 0.65 \\ \delta_m &= 0.86 \times 10^{-14}\mathrm{Re}^3 \text{ for } \rho = 0.80 \end{aligned}\right\} \quad \ldots\ldots [26]$$

The value of ρ was not measured accurately, although it was always in the range of 0.50 to 0.80.

The actual changes in head observed for 180-deg rotations of the pipe are shown in Table 2 where they are compared with the theoretical values for $\rho = 0.65$. Higher velocities were observed to the right facing down the pipe, as called for by theory. However, it can be seen readily that the observed differences in head are about one third as large as expected. The variations of the ratio from one run to the next are not necessarily significant since ρ did not remain exactly constant.

TABLE 2 DIFFERENCE IN HEAD RECORDED IN DIFFERENTIAL MANOMETER AFTER ROTATING PIPE AND PROBE SYSTEM THROUGH AN ANGLE OF 180 DEG, COMPARED TO THEORETICAL VALUES, FOR PROBES AT $\rho = 0.65$

Reynolds number	Observed head difference (10^{-4} ft)	Theoretical head difference (10^{-4} ft)	Ratio observed to theoretical
2950	1.8	5.8	0.31
3500	2.7	9.5	0.28
3500	3.6	9.5	0.37
3700	5.0	11.3	0.45
4900	4.5	26.3	0.17

The problem arises of course whether the observed asymmetry in the axial flow occurred due to the rotation of the earth. The results are certainly not conclusive, but they point strongly in this direction. It is entirely probable that the secondary flow associated with the earth's rotation would not be established fully over such a short distance and time. It is gratifying that any

consistent effect was observed at all, and that the effect was of the proper sign and order of magnitude.

Another substantiating feature was that the manometer change increased regularly with angle of rotation up to 180 deg, and then decreased to zero at 360 deg. This showed that the asymmetry was an even function of rotation angle, and within observational error could well have been the cosine function called for by the theory.

The observed asymmetry could not have been due to entrance conditions, irregularities of the pipe, or flow interference associated with the probes since the entire system was rotated as a unit. Other than the earth's rotation, the only possible cause might have been a cross circulation in the outlet tank. No such circulation was observed and every effort was made to avoid its occurrence. It seems highly unlikely that such a circulation could have existed unobserved and could by chance have resulted in a flow asymmetry near the end of the pipe which was of the proper order of magnitude and in the direction called for by the foregoing theory. Although further research is warranted, the author believes that laboratory experiments have tended to substantiate the previous conclusion that the effect of the rotation of the earth on pipe flow may not be negligible, as has heretofore been implicitly assumed.

Summary

The theory of laminar pipe flow has been developed retaining the effect of the earth's rotation. It is shown that this effect depends on the component of the earth's rotation normal to the pipe, and is thus a maximum for flow in the east-west direction. Weak secondary circulations form in the cross-sectional plane. The intensity of these circulations, expressed nondimensionally, is proportional to the ratio of the Reynolds number and the Rossby number.

The cross circulations and the associated pressure field are extremely weak, even for flow at high Reynolds numbers. However, this flow tends to cause an asymmetry in the axial velocity distribution which can be significant, especially when the ratio of the square of the Reynolds number to the Rossby number exceeds 5×10^2. High velocities are displaced from the pipe axis in a direction specified by the negative cross product of the vectors parallel to the earth's axis and to the direction of fluid discharge.

Laboratory experiments indicate the existence of such asymmetric flows. However, the measured asymmetry is about one third of the theoretical value. This is attributed to the fact that the pipe system used was probably insufficient in length to allow the secondary flow associated with the earth's rotation to become fully developed.

Theory and experiment both indicate that under certain circumstances the effect of the earth's rotation on pipe flow is not negligible. In particular, this factor may be of importance in the breakdown of laminar flow into turbulence at high Reynolds numbers. This subject warrants further investigation.

Acknowledgments

The laboratory experiments described herein were conducted by Mr. George Walder under the supervision of the author.

Unsteady Radial Flow of Gas Through Porous Media—Variable Viscosity and Compressibility

By J. S. ARONOFSKY[1] and J. D. PORTER[2]

Calculations of pressure-time histories and flow rates are presented for radial unsteady flow of gases through porous media. Some nonideal gas properties are considered by expressing gas viscosity and gas compressibility (z-factor) as simple functions of pressure. These calculations were obtained by using the high-speed, electronic computer called "Whirlwind" which is located at the Digital Computer Laboratory of the Massachusetts Institute of Technology. The results demonstrate that variable viscosity and compressibility can exert a substantial effect on transient gas-flow systems. A simple means is suggested for estimating the velocity of gas flowing across an inner radial boundary into a hole when the gas pressure is held constant at that boundary.

Nomenclature

The following nomenclature is used in the paper:

d = constant representing intercept on viscosity-pressure plot, centipoises
h = thickness of formation, cm
k = permeability, darcys
m = slope of straight line on compressibility-pressure plot, atm^{-1}
n = slope of straight line of viscosity-pressure plot, centipoises $(atm)^{-1}$
P = pressure, atm
P_m = initial pressure in system, atm
P_w = pressure at well, atm
$P(r_e)$ = pressure at outer radius, atm
P_s = pressure at standard conditions, atm
p = pressure ratio, P/P_m
p_a = average pressure, atm
Q = flow rate at standard conditions, cm^3/sec
r = radius, cm
r_w = well radius, cm
r_e = reservoir radius (outer boundary), cm
r_d = effective drainage radius, cm
t = time, sec
$\bar{v}$ = velocity, cm/sec
z = compressibility factor, dimensionless
α = dimensionless ratio, $(nP_m)/d$
β = dimensionless ratio, mP_m
μ = viscosity, centipoises
ξ = dimensionless length parameter
ρ = density, $grams/cm^3$
ρ_s = density at standard conditions, $grams/cm^3$
τ = dimensionless time parameter
$\bar{\tau}$ = dimensionless time for pressure ratio, $[P(r_e) - P_m]/(P_w - P_m)$, to become equal to 0.25
ϕ = porosity fraction

Introduction

The previously obtained solutions[3] of a transient gas-flow problem in a radial system have been extended to gases which do not obey the ideal gas law, and which have pressure-dependent viscosities. This study is concerned with a hole passing through the center of a disk-shaped porous body of uniform thickness, such as is shown in Fig. 1, containing gas at an initial uniform pressure P_m. Gas flows across the inner radial boundary as the pressure at that boundary is held at a constant value, P_w. In the work described in this paper, P_w is always held at $0.1P_m$.

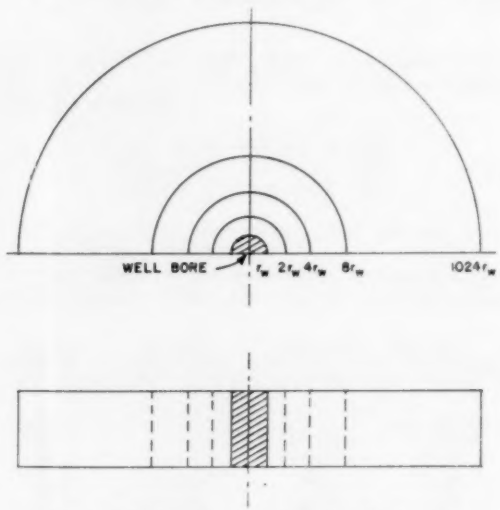

Fig. 1 Schematic Section of Radial Reservoir

The computational procedure used in this work was to reduce the basic differential equation to a difference equation and then to solve the difference equation by means of a digital computing machine. These numerical solutions were obtained on the Whirl-

[1] Research Associate, Field Research Laboratories, Magnolia Petroleum Company, Dallas, Texas. Mem. ASME.

[2] Digital Computer Laboratory, Massachusetts Institute of Technology, Cambridge, Mass.

Contributed by the Applied Mechanics Division and presented at the Diamond Jubilee Annual Meeting, Chicago, Ill., November 13–18, 1955, of The American Society of Mechanical Engineers.

Discussion of this paper should be addressed to the Secretary, ASME, 29 West 39th Street, New York, N. Y., and will be accepted until April 10, 1956, for publication at a later date. Discussion received after the closing date will be returned.

Note: Statements and opinions advanced in papers are to be understood as individual expressions of their authors and not those of the Society. Manuscript received by ASME Applied Mechanics, Division, September 17, 1954. Paper No. 55—A-13.

[3] "Unsteady Radial Flow of Gas Through Porous Media," by R. Jenkins and J. S. Aronofsky, Journal of Applied Mechanics, Trans. ASME, vol. 20, 1953, pp. 210–214.

wind computer, a project supported by the Office of Naval Research. (The Whirlwind computer is part of the Digital Computer Laboratory of Massachusetts Institute of Technology.)

A direct application of the results obtained is in the interpretation of well pressure tests in natural-gas fields for evaluating such engineering quantities as estimated total mass of gas in place (predicting the extent of the outer radial boundary), or predicting gas-flow rates into the well bore. Thus it is important to determine to what extent the variations of gas viscosity and gas compressibility with pressure can influence pressure-time histories and flow rates for the radial-flow problem stated. Such effects are described in this paper as well as a simple means of predicting the relationship between flow rate and average gas pressure in the porous body.

Equations of Gas Flow

The continuity equation for single-phase flow of any fluid through a porous medium may be expressed as[4]

$$\nabla(\rho \bar{v}) = -\phi \frac{\partial \rho}{\partial t} \quad \ldots\ldots [1]$$

In the viscous-flow region Darcy's law is valid and, when gravity forces are neglected, it can be expressed in the form of a velocity potential

$$\bar{v} = -\frac{k}{\mu} \nabla P \quad \ldots\ldots [2]$$

Substituting Equation [2] into Equation [1] gives

$$\nabla \left(\rho \frac{k}{\mu} \nabla P \right) = \phi \frac{\partial \rho}{\partial t} \quad \ldots\ldots [3]$$

which is considered as the basic equation of gas flow in a porous[4] body.

In this investigation k and ϕ are assumed to be constant, whereas both the viscosity μ, and the density ρ, are considered to be pressure-dependent. The pressure dependency of the viscosity for some gases (particularly hydrocarbon gases) can be reasonably approximated by an equation of the form

$$\mu = nP + d \quad \ldots\ldots [4]$$

where n represents the slope of the viscosity-pressure curve and d represents the intercept on the μ-axis.

It is further assumed that gases can be represented by the following density-pressure relationship, $(PV)/Z = RT$, which also may be expressed as[5]

$$\rho = \left(\frac{\rho_s Z_s}{P_s} \right) \left(\frac{P}{z} \right) \quad \ldots\ldots [5]$$

under constant temperature conditions. The dimensionless quantity, z, describes the deviation from the ideal-gas law and, therefore, is referred to as the deviation factor or compressibility factor, z. This factor approaches unity in the vicinity of P_s (a low pressure used as a standard), hence Z_s is assumed equal to unity. Fig. 2 shows the deviation factor for ethane, as a function of pressure, for various temperatures.[5] The curves for ethane are presented merely as a typical illustration. Note that in the region of lower pressures (e.g., below 1200 psi on a constant-temperature curve) a straight-line representation is a reasonable first approximation to the curve. Thus in this investigation Z is assumed to vary linearly with pressure

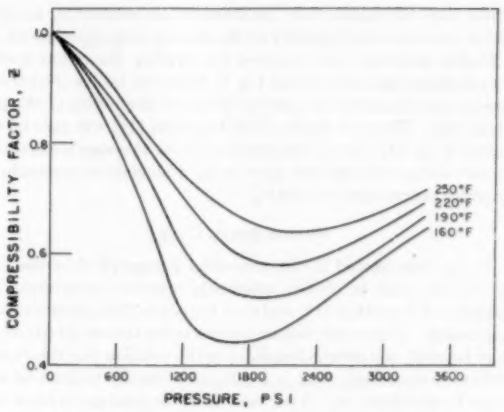

Fig. 2 Deviation Factor Versus Pressure for Ethane

$$Z = 1 - mp \quad \ldots\ldots [6]$$

Equation [3] may now be expressed in the following form

$$\nabla \left[\frac{P}{(d + nP)(1 - mP)} \nabla P \right] = \frac{\phi}{k} \frac{\partial}{\partial t} \left(\frac{P}{1 - mP} \right) \quad \ldots [7]$$

where a particular gas is characterized by specific values of the parameters d, n, and m. For a system with radial symmetry Equation [7] takes on the form

$$F_1(p) \left(\frac{\partial^2 p}{\partial r^2} + \frac{1}{r} \frac{\partial p}{\partial r} \right) + F_2(p) \left(\frac{\partial^2 p^2}{\partial r^2} + \frac{1}{r} \frac{\partial p^2}{\partial r} \right) = F_3(p) \frac{\partial p}{\partial t} \quad \ldots\ldots [8]$$

where
$$F_1(p) = 2p^2[(\alpha - \beta) - 2\alpha\beta p]$$
$$F_2(p) = (1 + \alpha\beta p^2)$$
$$F_3(p) = (\phi d / k P_m) 2(1 + \alpha p)^2$$

and P_m is the initial pressure, $p = P/P_m$, $\alpha = (nP_m)/d$, and $\beta = mP_m$. The dimensionless quantities p, α, and β were introduced to simplify the calculation procedure.

The differential Equation [8] is further simplified by introducing the new variable

$$\xi = \ln \frac{r}{r_w} \quad \ldots\ldots [9]$$

The differential equation written in terms of the new variable becomes

$$F_1(p) \frac{\partial^2 p}{\partial \xi^2} + F_2(p) \frac{\partial^2 p^2}{\partial \xi^2} = F_3(p)[r_w^2 e^{2\xi}] \frac{\partial p}{\partial t} \quad \ldots\ldots [10]$$

The step-by-step calculations of pressure change have been performed on the finite-difference form of this equation, which is

$$p_{\xi,t+\Delta t} = p_{\xi,t} + \frac{\Delta t}{(\Delta \xi)^2 r_w^2 e^{2\xi} F_3(p_\xi)} \{ F_1(p_\xi)[p_{\xi-\Delta\xi} + p_{\xi+\Delta\xi} - 2p_\xi] + F_2(p_\xi)[p_{\xi-\Delta\xi}^2 + p_{\xi+\Delta\xi}^2 - 2p_\xi^2] \}_t \quad \ldots\ldots [11]$$

It is convenient in the calculations to choose time increments Δt, such that

$$\frac{\Delta t P_m k}{2(\Delta \xi)^2 r_w^2 \phi d} = \frac{(1 + \alpha)^2}{(1 + \alpha + \beta + 3\alpha\beta)} \quad \ldots\ldots [12]$$

[4] "Flow of Homogeneous Fluids Through Porous Media," by M. Muskat, Edwards Bros., Inc., Ann Arbor, Mich., 1946.

[5] "Chemical Engineering Thermodynamics," by B. F. Dodge, McGraw-Hill Book Company, Inc., New York, N. Y., 1944.

These time increments may be shown to be sufficiently small to insure the numerical stability of the step-by-step calculations.

Radial positions were selected by dividing the radial system into annular rings as shown in Fig. 1, where the radius of each successive ring increases by a factor of 2 over the radius of the previous ring. Thus the factor $e^{2\xi}$ in Equation [11] will take on the values 4, 16, 64, ... , respectively, as the pressure is calculated at each successive ring and $\Delta\xi = \ln 2$. Calculations are made for an outer radius equal to $1024r_w$.

Steady-State Core

It has been stated in the preceding paragraph that the time increments must be chosen sufficiently small to insure numerical stability of Equation [11] and that Equation [12] satisfies this requirement. This restriction on the size of the time step (Δt), which may be used, is a serious handicap to the solution (for this type of difference equation), since it would take literally millions of time steps to withdraw, say, 5 per cent of the original gas in place with Equation [11] as it now stands.[6] This difficulty was overcome by means of a simple device, called the "steady-state core" which reduces the number of time increments required to a quantity easily handled by the electronic computing machine. The steady-state core may be explained as follows:

The first gas withdrawn from a well originates very close to the well. As more gas is removed from the system, the area from which the gas is being removed has an increasingly larger outer radius. A short time after flow into the well begins, an area close to the well is essentially under steady-state conditions. Therefore the steady-state radial flow formula can be used to relate the pressure drop in this region to the well-flow rate, and the difference Equation [11] need not be applied to this region of steady-state flow. This gives a new and larger, "fictitious," well radius to use in Equation [11] to determine the size of the time steps. The calculations described in this paper were made with a steady-state core having a radius as large as 64 times the well radius. This value of the radius for the steady-state core permitted an increase in the size of the time increment by a factor 4096 since the time step in Equation [12] is directly proportional to $(r_w)^2$.[9]

Results

Results of numerical calculations are presented for the problem of Fig. 1 which shows a well bore passing through the center of a disk-shaped sand body of uniform thickness containing gas at a uniform pressure P_m. The top, bottom, and outer boundary of this sand body are impervious to the gas, which can escape only through the well bore. At time $t = 0$, withdrawal of gas through the well is begun and the well pressure is maintained at $P_w = 0.1 P_m$. The problem then is to determine both the radial pressure distribution as a function of time and, more particularly, the flow rates at the well at any later time. Such solutions were obtained for various values of α and β where the ratio β/α is held constant. Although the expressions for α and β each involve P_m the ratio β/α is independent of P_m and is determined solely by the parameters n, d, and m which characterize the pressure dependency of the gas viscosity and compressibility. Hence solutions of the equations expressed in terms of the ratio β/α clearly demonstrate the influence of variability in gas properties on the transient pressure behavior of the system.

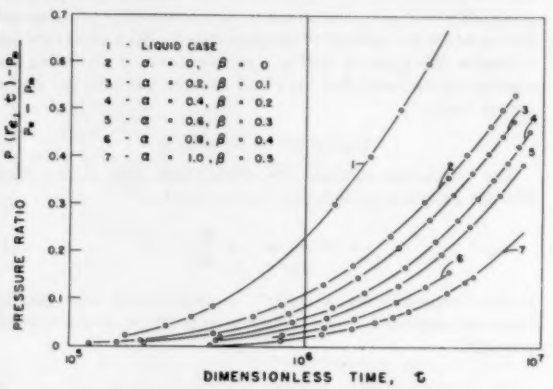

Fig. 3 Pressure-Time Curves for $\beta/\alpha = 0.5$

Curves are shown in Fig. 3 for the pressure ratio

$$[P(r_e) - P_m]/(P_w - P_m)$$

versus the dimensionless time τ for various values of α and β where the outer radius $r_e = 1024r_w$. The dimensionless time τ is defined as equal to

$$(kP_m t/(\phi d r_w^2)$$

Curves 3, 4, 5, 6, and 7 of Fig. 3 illustrate how the pressure at the outer boundary of the sand body will vary with time (dimensionless) for various values of α and β when the ratio $(\beta/\alpha) = 0.5$ and $P_w = 0.1P_m$. It is clear from Fig. 3 that the parameters α and β can influence greatly the time dependency of the pressure observed at the outer boundary in the system just described. Curve 2 of Fig. 3 corresponds to a previously investigated case[3] for $\alpha = \beta = 0$, where the viscosity and compressibility are assumed to be independent of pressure and $P_w = 0.1P_m$. It was stated in the previous paper[3] that the transient gas-flow system may be represented by the transient liquid-flow equations when the ratio P_w/P_m approaches 1.0. Curve 1 of Fig. 3, therefore, is such a solution of the liquid-flow equations for the same geometrical boundaries as the gas case. This particular liquid solution was obtained on an analog computer of the resistance-capacitance type.

It is emphasized that curves 3, 4, 5, 6, and 7 of Fig. 3 were calculated for various values of α and β when the ratio β/α is held at the constant value of 0.5. These solutions correspond to a set of experiments using the same porous medium and gas where each value of α (or β) is obtained by starting a new experiment at a different initial pressure, P_m.

Additional curves are given in Figs. 4 and 5 for the pressure ratios, $[P(r_e) - P_m]/(P_w - P_m)$, versus dimensionless time τ, when the ratio β/α is equal to 1 and 2, respectively, and $P_w = 0.1P_m$ as in Fig. 3. A comparison of the curves of Figs. 3, 4, and 5 demonstrates that the pressure-time distributions are also dependent upon the dimensionless ratio β/α.

[6] Considerable progress has been made in recent years in devising more elaborate difference equations of the so-called "implicit type" which permit the use of large time steps while still retaining numerical stability.[7] Such a difference equation has been applied to the transient gas-flow problem in a radial system for an ideal gas.[8]

[7] "A Study of the Numerical Solution of Partial Differential Equations," by G. O'Brien, M. Hyman, and S. Kaplan, *Journal of Mathematics and Physics*, vol. 29, 1951, pp. 223–251.

[8] "Calculations of Unsteady-State Gas Flow Through Porous Media," by G. Bruce, D. Peaceman, H. Rachford, and J. Rice, *Journal of Petroleum Technology*, Trans. AIME, vol. 198, March, 1953, pp. 79–92.

[9] An analogous problem is discussed[3] where calculations were repeated for various size steady-state cores and a correction was made in the time scale (for each size core) by fitting together pressure-history curves for the true well radius that overlap those made with the fictitious radius. This time correction was found to be small.

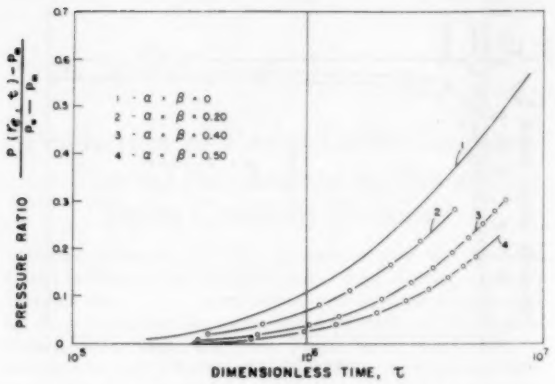

FIG. 4 PRESSURE-TIME CURVES FOR $\beta/\alpha = 1.0$

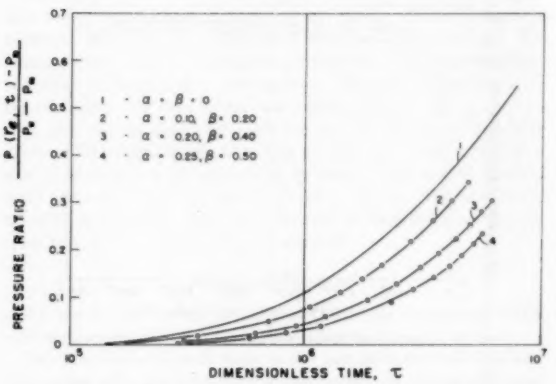

FIG. 5 PRESSURE-TIME CURVES FOR $\beta/\alpha = 2.0$

To afford a better view of the effects of α and β-values on decline times of the pressure at the outer boundary, the curves shown in Fig. 6 were plotted. Here the time ($\bar{\tau}$) for the dimensionless pressure

$$[P(r_e) - P_m]/(P_w - P_m)$$

at the outer boundary to become 0.25 is plotted against the ratio β/α for various values of β. Thus any one curve illustrates how changes in $1/\alpha$ affect the decline time for any given β. The horizontal straight line represents the limit which is approached as both α and β approach zero.

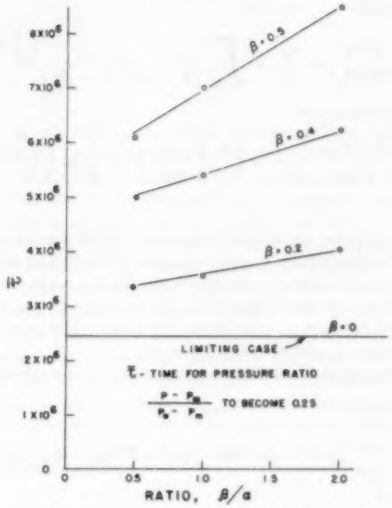

FIG. 6 EFFECT OF α AND β ON PRESSURE-DECLINE CURVES

Curves are given in Fig. 7 for the dimensionless flow rate

$$QP_e d/2\pi khP_m^2)$$

versus the dimensionless time τ for various values of α and β where again the outer radius $r_e = 1024r_w$ and the ratio β/α is 1.0. These curves also indicate that the parameters α and β can influence the flow rate into the well bore. There are a number of physical problems where it is important to estimate the gas velocity flowing across the inner boundary at any specified time. A mechanism is proposed in the following section that provides a means for estimating the flow rate by using the concept of a stabilized drainage radius.

EFFECTIVE DRAINAGE RADIUS

The concept of the effective drainage radius was developed and explained in a previous paper;[2] however, the picture presented there requires modification to permit consideration of variations of both viscosity and compressibility with pressure. This is done as follows: The steady-state formula for radial gas flow may be written as

$$\frac{QP_e d}{2\pi kh} \ln \frac{r_d}{r_w} = \int_{P_w}^{P_e} \frac{P}{(d + np)(1 - mp)}\, dP \ldots\ldots [13]$$

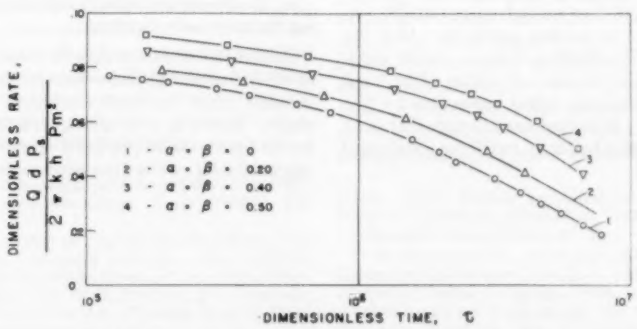

FIG. 7 DIMENSIONLESS RATE-TIME CURVES FOR $\beta/\alpha = 1.0$

or in the form

$$\frac{QP_s d}{2\pi khP_m^2} \ln \frac{r_d}{r_w} = \int_{p_w}^{p_e} \frac{p}{(1+\alpha p)(1-\beta p)}\, dp \quad \ldots\ldots [14]$$

which integrates into

$$\ln \frac{r_d}{r_w} = \left[\frac{P_m^2 2\pi kh}{P_s Qd}\right]\left[\frac{1}{\alpha} \ln\left(\frac{1+\alpha p_w}{1+\alpha p_e}\right) + \frac{1}{\beta} \ln\left(\frac{1-\beta p_w}{1-\beta p_e}\right)\right] \quad \ldots\ldots [15]$$

Equation [15] may be interpreted so that it will always represent properly the flowing well pressure p_w, and the well-flow rate Q, for the entire time history of the problem. This is accomplished by forcing the steady-state Equation [15] to represent the transient relationship between p_w and Q through proper definition of the remaining terms p_e and r_d in Equation [15].

Let p_e represent the bulk average pressure in the system at any instant of time. The bulk average pressure p_e is defined to be the pressure which would be found if flow at the well were interrupted and the pressure in the system allowed to stabilize. The remaining term that has not yet been defined is the effective drainage radius r_d, which must be allowed to take on any value required to force the steady-state Equation [15] to represent the transient solution.

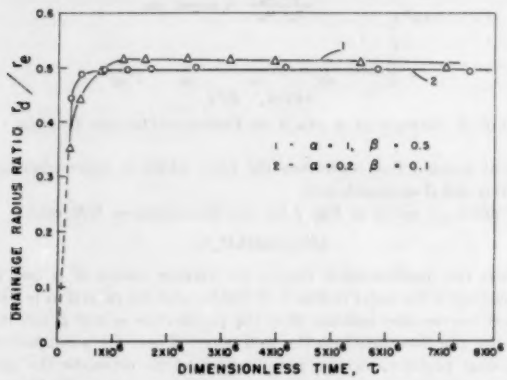

FIG. 8 DRAINAGE RADIUS VERSUS TIME FOR $\beta/\alpha = 0.5$

It is instructive to construct plots to determine how the effective drainage radius, so defined, will vary with time. Such plots are shown in Figs. 8, 9, and 10. Fig. 8 shows a series of plots of the drainage radius ratio, r_d/r_e, versus dimensionless time τ for various values of α and β for $\beta/\alpha = 1/2$, and $r_e = 1024 r_w$. These plots emphasize the condition that, initially, the effective drainage radius r_d, starts out near the well bore and advances radially outward away from the well bore as the flow continues. After the early transients have passed, the effective drainage radius stabilizes at a value roughly one half the reservoir radius. Figs. 9 and 10 illustrate plots of effective drainage radius versus time for β/α equal to 1 and 2, respectively. It is significant to note that in all cases the effective drainage radius builds up rapidly to a stabilized value near $0.5r_e$.

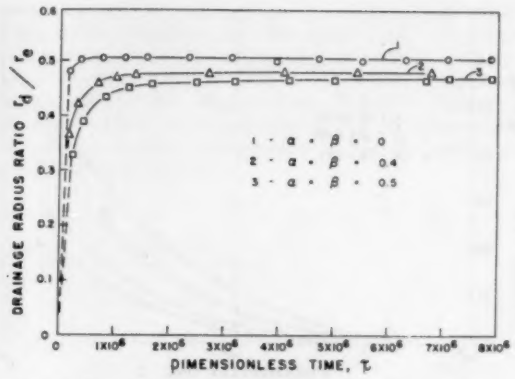

FIG. 9. DRAINAGE RADIUS VERSUS TIME FOR $\beta/\alpha = 1.0$

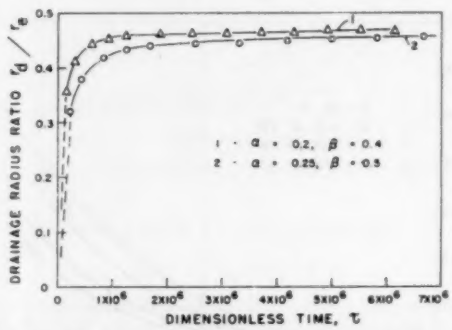

FIG. 10 DRAINAGE RADIUS VERSUS TIME FOR $\beta/\alpha = 2.0$

The significant features of this section are summarized below:

1 A relationship between the well pressure and flow rate can be determined from Equation [15] if the effective drainage radius, as defined in the foregoing, is known for any dimensionless time τ, and if the average pressure is known or can be determined.

2 The effective drainage radius stabilizes at a value roughly equal to one half the outer radius after only a small percentage of fluid in place has been withdrawn. Thus it may be assumed that $r_d = 0.5r_e$ in Equation [15], except for the early transients.

3 An estimate can be made of the relationship between production rate and average reservoir pressure by using the stabilized value of the effective drainage radius, well pressure, original gas pressure, outer radius, and well radius.

4 No attempt is made in this paper to predict flow rates during the very early transients.

Similar sets of curves may be prepared for constant-rate cases or other constant-pressure cases for different well pressure-initial pressure ratios, but such conditions are not considered in this paper. However, it is anticipated that effective drainage radii for such cases would also build up rapidly to a stabilized value of approximately one half the outer radius of the reservoir.

Discussion

Prediction of Creep-Deflection and Stress Distribution in Beams From Creep in Tension[1]

JOSEPH MARIN.[2] The discrepancies between the creep-test results in bending and the prediction of creep bending by theory based on tension creep is subject to error since the samples used for the bending tests are taken from a different part of the sheet than those for the tension tests. Test data have shown that for the material tested, considerable variation in mechanical properties may occur, depending upon the location of the specimen in the sheet of plastic from which the specimen was cut.

The author assumes in the theory proposed that the tension and compression-creep behavior is the same. Tests of various plastics, including the laminated plastics considered by the author, indicate that considerable difference can occur between the creep in tension and compression. Theories are available in the literature that take into account these differences.

It also should be noted that the use of the hyperbolic sine relation for creep, which is of the same form as the activation energy, should not be interpreted to mean that the relationship used for creep is a fundamental one; that is, the hyperbolic creep-strain relation used still remains an empirical one in the same way as other relationships proposed.

AUTHORS' CLOSURE

We would like to thank Dr. Marin for his comments. The questions raised may be clarified as follows:

The possible sources of error in the test data and assumptions made were fully acknowledged in the paper. It will be observed that the consistency of creep data is excellent when the selection of samples and testing techniques are carefully controlled as in the tension creep tests performed in our own laboratory (see Fig. 2 of the paper). Whether the inconsistencies in data for bending creep obtained from another laboratory (see Fig. 3 of the paper) are due to the causes suggested by Dr. Marin is not known. The questions posed by differences between creep in tension and compression were considered by the authors in the present paper and form part of a subsequent report.[3] Usable creep data in compression, however, were not available, as described in the present paper. Theories available in the literature for creep in bending when the creep in tension and compression are not equal were cited and reviewed in the paper.

The hyperbolic sine-stress functions were based on the activation-energy theory—the time function was based on the observation of many creep curves. The authors have not claimed that the creep relation employed is fundamental. However, it does seem that a form of creep equation which closely describes test data of several materials, which contains a function derived from a broadly based concept such as activation energy, which has a minimum of constants, and which predicts known behavior at small values of the variables is a more significant relation than relations which do not have all of these attributes. There seems to be a tendency to try to avoid using empirical relations as though there were some stigma attached to them. If we did avoid them we would be completely at a loss to describe most physical phenomena. Surely the method of observing a physical behavior and seeking a mathematical relation to describe the behavior may be called empirical. However, if one continues to observe this behavior in all possible or available settings and finds the chosen relation to be applicable then the relation may be described as a law of the available universe. One relation so derived is Newton's second law of motion—an empirical relation. It is upon such basic empirical laws that many rational relations describing physical phenomena are derived, such as the whole of Newtonian mechanics.

[1] By W. N. Findley and J. J. Pocsatek, published in the June, 1955, issue of the JOURNAL OF APPLIED MECHANICS, Trans. ASME, vol. 77, pp. 165–171.

[2] Professor and Head, Department of Engineering Mechanics, The Pennsylvania State University, University Park, Pa. Mem. ASME.

[3] "Prediction of Creep in Bending From Tension Creep Data When Creep Coefficients Are Unequal," by W. N. Findley, J. J. Pocsatek, and P. N. Mathur, Interim Report No. 3 to Picatinny Arsenal, Contract No. DA-11-022-ORD-401, February, 1954.

Frictional Vibrations[1]

J. J. BIKERMAN.[2] Erroneous statements on friction have been published so often in the last 30 years that it is a particular pleasure to welcome an investigation based on sound scientific principles.

In the writer's opinion all six conclusions of the author are correct and well substantiated by the experimental results reported in the paper. It is clear that the author knows his apparatus; when he observed (Fig. 13) an unexpected series of short oscillations, he did not attribute it to a fancy molecular mechanism but rather looked into its mechanical origin and thus traced it to vibration of the cast-iron base of the instrument.

However, the Bibliography can be improved upon. The first three conclusions were stated by Kaidanovskii and Khaikin[3] in 1933, and Equations [4] and [5] were derived by Bock[4] in 1936. That "time is required for the static friction to develop" was known to Coulomb.

After a step has been made in the right direction, the onlookers naturally wonder what the next step will be. Perhaps the writer will be allowed to make a few suggestions in this respect.

It would seem that elimination of brake squeal by making friction coefficient to increase with speed is not at all impossible. It is hoped that research in this direction will continue.

It also is hoped that time will be found to study the mechanism of friction between metal and brake surfaces. The author mentions only two possible mechanisms, namely, adhesion and lifting over surface asperities. These two phenomena do not exhaust all possibilities. Probably the elastic deformation of the brake is the main cause of the high resistance to its sliding over the metal surface. When rubber is used as rubber, i.e., as eraser of pencil marks, the main work of friction is spent not on overcoming surface roughness and, of course, not on the nonexisting welding, but rather on elastically deforming the eraser.

[1] By David Sinclair, published in the June, 1955, issue of the JOURNAL OF APPLIED MECHANICS, Trans. ASME, vol. 77, pp. 207–214.

[2] Woodside, Long Island, N. Y.

[3] "Mekhanicheskie relaksatsionnye kolebaniya" (Mechanical Relaxation Oscillations), by N. L. Kaidanovskii and S. E. Khaikin, *Journal of Technical Physics*, USSR, vol. 3, 1933, pp. 91–109.

[4] "Vibration bei Gleitreibung," by H. Bock, *Zeitschrift für Instrumentenkunde*, vol. 56, 1936, pp. 71–74.

TABLE 1 VARIATION OF COEFFICIENT OF SLIDING WITH INCREASING VALUES OF PARAMETER

Parameter	Normal load	Geometrical area of contact	Speed of sliding	Roughness of solids	Hardness of solids	Viscosity of lubricant
Type of sliding						
Petroff	{Inversely {Proportional	Proportional	Proportional	Independent	Independent	Proportional
Transitional	Independent	Independent	{Almost {Independent	{Little {Depends	Independent	Depends
Dry friction	Independent	Independent	Independent	Increases	Independent	—
Scratching	Depends	Depends	?	Independent	Depends	

Several years ago the writer compiled a table[5] which indicates what kind of experiments can be used to find the mechanism of the sliding resistance in every given instance, Table 1. Perhaps it will assist the author in his future work, although the resistance due to elastic deformation is not included in it, because it has not been sufficiently studied.

H. Blok.[6] As an extension to the author's method of determining the motion of the block mathematically, attention is drawn to the convenient method of isoclines in the phase plane, which was used by B. van der Pol[7] as early as 1926. This method provides a graphical solution to the most general case where the kinetic friction force varies with velocity in an arbitrary but known manner (see curve c in Fig. 7 and curve b in Fig. 9).

For the special case that the kinetic friction force is constant, that is, independent of velocity, and that it is smaller than, or equal to, the static friction force, a solution was given in a paper of the writer.[8] The solution is represented in Fig. 9 of that paper, and clearly brings out the combined effects of inertia, stiffness, damping, sliding velocity, and difference between kinetic and static friction force, as regards the demarcation line between the region where the stick-slip type of vibrations does occur and the region where it does not occur. Properly, the afore-mentioned figure refers to the limiting case where the kinetic friction force F_{kin} vanishes altogether, but it is easily proved that it can be generalized, so as to cover the case where F_{kin} is finite, simply by replacing the denominator F_{stat} by $(F_{stat} - F_{kin})$ in the expression ψ that defines the values on the abscissa of the figure. (Owing to an oversight of the writer, the proof was omitted when he had to abridge the paper concerned.)

Author's Closure

The author wishes to thank the writers for their discussion and, in particular, Mr. Bikerman for his praise. As they point out, friction and frictional vibrations have been studied diligently for 30 years and more. In spite of the fact that many mechanisms such as adhesion, lifting-over surface asperities, shearing, plowing, welding, etc. have been considered, the phenomenon of friction is still only poorly understood. No doubt all mechanisms contribute their part. The references cited by the discussers contain some of the best work on the subject, but are only a few samples from hundreds of papers. A very extensive bibliography is contained in the book by Bowden and Tabor cited by the author.

The aim of this work was to learn the cause and cure of intermittent sliding, particularly brake squeal. The importance of the mechanical properties of the moving parts and their interaction with the frictional properties of the rubbing surfaces is clearly understood by many but appeared not so well understood by some workers in this field. The possible numerous degrees of freedom of the system may produce superposition of vibrations more complicated than in Fig. 13 referred to by Mr. Bikerman. To paraphrase Dean Swift:

> As auto engineers observe, a squeal
> Has smaller squeals that on it play,
> And these have smaller still to 'cite 'em,—
> And so proceed *ad infinitum*.

We are continuing the work along a different line, namely, a study of the effect of inertia, stiffness, damping, sliding velocity, and difference between static and sliding friction using as a basis equations similar to those derived by Professor Blok.

[5] "The Mechanism of Friction and Lubrication," by J. J. Bikerman, *Lubrication Engineering*, vol. 4, 1948, pp. 208–214.

[6] Professor of Mechanical Engineering, Technological University, Delft, Holland.

[7] "On Relaxation Vibrations," by B. van der Pol, *Philosophical Magazine*, vol. 2, 1926, p. 978, etc.

[8] See the Appendix to "Fundamental Mechanical Aspects of Boundary Lubrication," by H. Blok, *Journal of the Society of Automotive Engineers*, vol. 46, February, 1940, pp. 54–68 (see especially, pp. 63–68).

Further Work on the General Three-Dimensional Photoelastic Problem[1]

A. J. Durelli[2] and J. M. Barriage.[3] The authors should be congratulated for their efforts to develop three-dimensional photoelastic techniques. The following observations may help in a better understanding of some phases of the problems involved:

1 The authors explain discrepancies between their results and the results of a theoretical solution by assuming that the thermal cycle used in the "freezing" (heating and cooling) process by itself produces a system of self-balancing (residual) stresses. This seems to be a very important statement which if it were correct may raise doubts about the accuracy of many of the already published results obtained using the "freezing" technique. Since nothing similar to this residual-stress system has been considered in the analysis of three-dimensional stresses by previous investigators, it may be advisable to look for the source of the discrepancy among other possible causes, such as errors in birefringence measurements, or the influence of the distortion of the sphere at the point of contact on the stress distribution.

2 We would like to point out that the "creeping" method for the determination of three-dimensional stresses may be better-suited to the solution of stress problems in specimens where it is important to minimize the deformation of the loaded specimen. To illustrate this point a fringe pattern was "crept" into, the same size parallelepiped, loaded in the same manner as by the authors: A slice from this model is shown in Fig. 1 of this discussion. It is obvious in this test, that the upper boundary is permanently deformed much less than the one shown by the authors. Some of the large permanent deformation in the authors' test could be reduced by decreasing the amount of load and still maintain sufficient optical response for accurate birefringence measurements. The main point, however, is that the figure of merit (ratio of modulus of elasticity to fringe value in

[1] By M. M. Frocht and Roscoe Guernsey, Jr., published in the June, 1955, issue of the Journal of Applied Mechanics, Trans. ASME, vol. 77, pp. 183–189.

[2] Supervisor, Stress Analysis Section, Armour Research Foundation of Illinois Institute of Technology, Chicago, Ill. Assoc. Mem. ASME.

[3] Assistant Engineer, Stress Analysis Section, Armour Research Foundation of Illinois Institute of Technology, Chicago, Ill.

tension) of the phenolformaldehyde used in the creeping method is of the order of 1000.

Details of the creeping method for three-dimensional photoelasticity can be found in a paper by one of the discussers.[4] The photograph shown in Fig. 1 represents a test conducted for the purpose of this discussion to show the advantages of a high figure of merit obtainable with commercially available non-annealed materials.

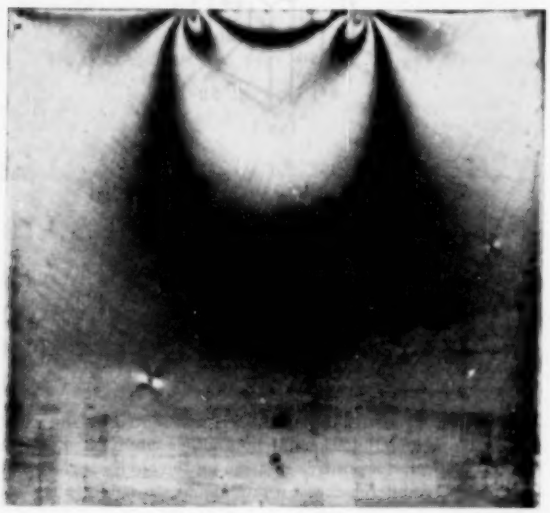

FIG. 1 ISOCHROMATIC PATTERN OF A SLICE (IDENTIFIED BY NUMBER 1 IN THE AUTHORS' PAPER) FROM A "CREPT-IN" PHENOLFORMALDEHYDE SPECIMEN OF SAME DIMENSIONS AND ORIGINAL LOADING CONDITIONS AS IN AUTHORS' PAPER

(It should be noted that deformation of loaded boundary is negligible.)

3 The authors could have used another slice on the plane of symmetry going through the corner of the square cross section. We believe this would have required relatively few extra computations and allowed good checks. We have some evidence from brittle failures showing that the maximum tensile stresses are perpendicular to this diagonal plane of symmetry, which may indicate that the authors did not find the maximum tensile stress in the specimen.

P. D. FLYNN.[5] While studying with Dr. Frocht at Illinois Institute of Technology, the writer became interested in the discrepancy between the photoelastic results and the theoretical values obtained by Sternberg and Rosenthal (3)[6] for the stresses at the free surface of a sphere under diametral loads. The experimental work performed on an aluminum sphere by means of strain gages showed surface stresses of the magnitude predicted in (3) and has already been cited (13).

Additional work was done which has not been reported previously. An uncut and unloaded sphere which had received the same thermal cycle as those tested was available. This was sliced and examined. Birefringence due to body forces and the presence of "skin" effects were readily apparent. This can be considered as supporting evidence that the differences between the photoelastic and theoretical values are due to extraneous stresses introduced during the thermal cycle employed in the freezing process.

M. M. LEVEN.[7] The authors are to be commended for their fine work in extending three-dimensional photoelasticity to the general solution. Heretofore, most practical investigations have been confined to free surface stresses or to stresses in planes of symmetry.

The authors have confined their experiments to symmetrical models or to the two-model method, but as better photoelastic materials are developed, larger models can be made and the one-model method using subslices will be quite feasible. Furthermore, as materials are developed with less residual stresses and/or higher strain-optic sensitivities, photoelastic solutions of a multitude of important contact problems will be possible. In these problems, stresses beneath the loaded surface may be quite significant.

In Fig. 6 of the paper, which shows the stress distribution for the two spheres of different loads along a section near the load, it would be desirable to show the theoretical solution (if available) to see how much further reduction in load may be necessary to approach the theoretical solution. If three different loads were used, perhaps an extrapolation could be made to the prototype P/E ratio.

Recently, the Cartesian graphical solution proposed by the authors has been extended to cylindrical co-ordinates by Smith and Cooper[8] in the determination of the stresses in conical-head pressure vessels.

The definition of F_{θ_y} in Equation [4] of the paper obviously is incorrect and is presumed to be a typographical error.

AUTHORS' CLOSURE

The authors wish to thank the discussers for their comments and suggestions. With respect to the points raised by Durelli and Barriage, it should be noted that the difference between the theoretical and the experimental solutions is a system of stresses which has two salient characteristics. These stresses constitute a self-balancing system across the equatorial plane and become isotropic tensions on the surface. Moreover, such stress systems also have been found in an unloaded sphere by Flynn as reported in his discussion. Also, Fig. 5 shows that on line A-A the distribution of σ_y is essentially the same for two different loads whereas on line B-B, Fig. 6, it is markedly different, thus indicating that the equatorial plane is far enough away from the loads for Saint Venant's principle to be effective. These facts would seem to rule out distortion of the sphere and errors in the measurements of birefringence as the primary causes of the discrepancy between theory and experiment and point to thermal stresses. The available data indicate that the thermal stresses are small, even on the surface. This subject is receiving further attention.

The authors agree with Durelli and Barriage that a higher figure of merit is desirable. However, they believe that the answer lies in improved materials, such as Leven refers to in his discussion of this paper, rather than in the "creeping" method. Incidentally, the present paper deals with methods rather than techniques which are described in references (2) and (7) of the paper.

The work reported by Flynn is of basic importance. The stresses which he found in the unloaded sphere were also isotropic tensions on the surface and a system of self-balancing stresses on the equatorial plane.

---

[4] "Some Unorthodox Procedures in Photoelasticity," by A. J. Durelli and R. L. Lake, Proceedings of the Society for Experimental Stress Analysis, vol. 9, no. 1, 1951, pp. 97–122.

[5] Development Engineer, General Engineering Laboratory, General Electric Company, Schenectady, N. Y. Assoc. Mem. ASME.

[6] Numbers in parentheses refer to the authors' Bibliography.

[7] Research Engineer, Westinghouse Research Laboratories, E. Pittsburgh, Pa.

[8] "Photoelastic Investigation of Stresses in Conical Head Pressure Vessels," by L. W. Smith and G. K. Cooper, presented at the fall meeting of SESA, Philadelphia, Pa., September, 1954.

The authors note with interest the points made by Mr. Leven. With reference to Fig. 6, no theoretical values were available for line *B-B*.

We wish to thank Mr. Leven for calling our attention to the typographical error. The line under Equation [4] should read, "where F_{σ_y} is the model fringe value, n_{σ_y} is the fringe order, ϕ_{σ_y} is the isoclinic parameter, and θ_y is the angle of rotation."

Since the writing of this paper the one-model, or subslice, method has been developed to a point where it is now a practical and effective tool. Several problems have been solved by this method. Consideration is also being given to a suggestion which may possibly lead to a one-model method not requiring the use of a subslice. In this procedure the $\Delta\tau$ would be determined from the shears on oblique planes which are parallel and close to the line of integration and inclined at suitable angles to the face of the slice. Birefringence and isoclinics would be obtained from observations in planes which are normal to the line of integration, the direction of the rays making suitable angles with the face of the full slice.

Representation of Three-Dimensional Stress Distributions by Mohr Circles[1]

C. M. FRIEDRICH.[2] It might be of interest to note that the two-dimensional Mohr's circle has been used by the writer to determine approximately the three principal stresses for any given stress distribution. The following device was developed independently before the writer read the author's paper. The following nomenclature is used in this discussion:

- (i, j, k) = subscripts having the possible values (1, 2, 3), (2, 3, 1) or (3, 1, 2)
- $'$, $''$, $'''$ = superscripts denoting successive rotations of axes
- x_i, x_j, x_k = Cartesian co-ordinates, arranged by the right-hand rule of this discussion, Fig. 1.
- θ_k = angle of rotation about the x_k-axis, positive counterclockwise
- S_{ii} = normal stress acting on surface perpendicular to x_i-axis, positive if tension
- S_{ij} = shear-stress component parallel to x_j-axis acting on surface perpendicular to x_i-axis; positive of it has a counterclockwise moment about x_k-axis on element $dx_i\,dx_j\,dx_k$ as shown. Thus $S_{ij} = -S_{ji}$ for equilibrium

The location of the axes x_i', x_j', x_k' after a rotation about the x_k-axis is given by

$$x_i' = +x_i \cos\theta_k' + x_j \sin\theta_k' \quad [1a]$$

$$x_j' = -x_i \sin\theta_k' + x_j \cos\theta_k' \quad [1b]$$

$$x_k' = +x_k \quad [1c]$$

and the stress components after rotation are

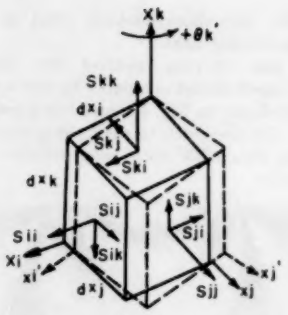

FIG. 1

$$S_{ii}' = +\frac{S_{ii}+S_{jj}}{2} + \frac{S_{ii}-S_{jj}}{2}\cos 2\theta_k' + S_{ij}\sin 2\theta_k' \quad [2a]$$

$$S_{ij}' = -\frac{S_{ii}-S_{ij}}{2}\sin 2\theta_k' + S_{ij}\cos 2\theta_k' \quad [2b]$$

$$S_{jj}' = S_{ii} + S_{jj} - S_{ii}' \quad [2c]$$

$$S_{ki}' = +S_{ki}\cos\theta_k' + S_{jk}\sin\theta_k' \quad [3a]$$

$$S_{jk}' = -S_{ki}\sin\theta_k' + S_{jk}\cos\theta_k' \quad [3b]$$

$$S_{kk}' = S_{kk} \quad [4]$$

Equations [2] of this discussion are represented by the usual Mohr's circle and Equation [3] by another circle, as shown in Fig. 2. Note that a positive rotation on the circles is clockwise for a positive counterclockwise rotation of axes x_i and x_j about x_k.

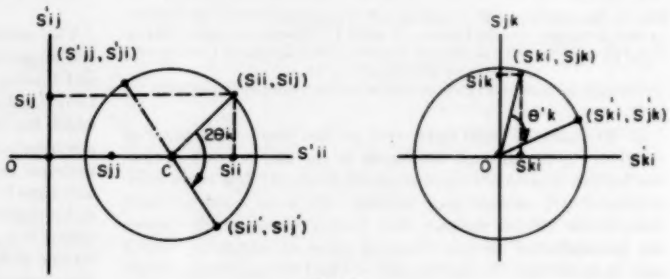

FIG. 2

If desired, Equations [1] could be represented by a third circle.

Suppose it is required to determine the principal stresses for this stress distribution

$S_{11} = +5$	$S_{22} = +2$	$S_{12} = 0$
$S_{12} = -4$	$S_{22} = +3$	$S_{21} = -2$

Table 1 summarizes graphical results of three rotations performed to minimize shears. Superscript P denotes the true principal stresses determined analytically.

TABLE 1 SUMMARY OF GRAPHICAL RESULTS OF THREE ROTATIONS TO MINIMIZE SHEARS

Superscript		'	''	'''	P
i		1	3	2	
j		2	1	3	
k		3	2	1	
θ_k°		−35	20	41.5	
S_{11}	5	7.8	9.0	9.0	9.0
S_{22}	2	−0.8	−0.8	0.4	0.2
S_{33}	0	0.0	−1.2	−2.4	−2.3
S_{12}	−4	0.0	−0.5	−0.4	0
S_{23}	3	+1.3	1.3	0.0	0
S_{31}	−2	−3.3	0.0	0.4	0

Figs. 3, 4, and 5, herewith, show the rotations. Since S_{12} is larger in magnitude than S_{23} or S_{31}, the first rotation is about the

[1] By G. A. Zizicas, published in the June, 1955, issue of the JOURNAL OF APPLIED MECHANICS, Trans. ASME, vol. 77, pp. 273–275.

[2] Engineer, Westinghouse Atomic Power Division, Westinghouse Electric Corporation, Pittsburgh, Pa.

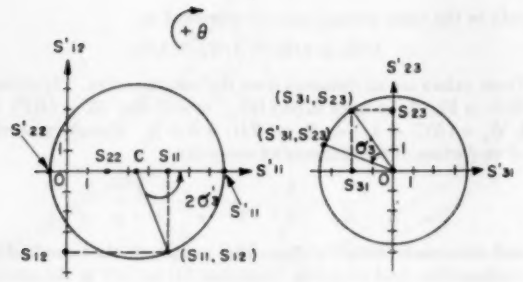

FIG. 3

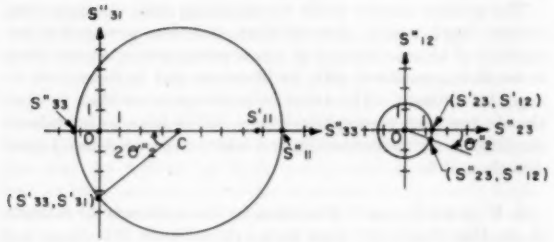

FIG. 4

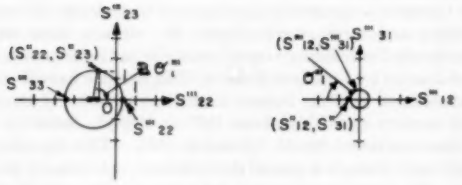

FIG. 5

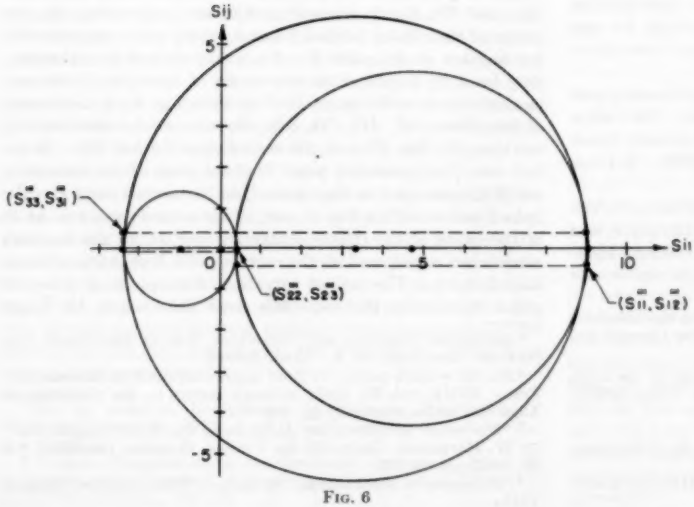

FIG. 6

x_3-axis to make $S_{12}' = 0$. Three rotations are enough to bring the stresses very close to the principal stresses, as shown by the negligible overlap of the three Mohr's circles for the (''') stress distribution drawn in Fig. 6.

AUTHOR'S CLOSURE

The author wishes to express his appreciation to Mr. Friedrich for his comments on the paper.

Mr. Friedrich, in discussing the author's paper, developed the interesting idea of using successive rotations of axes in order to approximate graphically the principal stresses. Such a procedure is valuable for three-dimensional stress distributions in view of the fact that for them the classical evaluation of principal stresses depends on the solution of a cubic equation. For such an equation, neither a general method of graphical solution by rule and compass nor a corresponding simple analytical solution exists, although both are available for the case of two-dimensional stress distributions.

As shown in the author's paper, the rotation of an element around any axis introduces a transformation according to two-dimensional stress distributions and is readily representable graphically by a Mohr circle. Mr. Friedrich uses this representation for a step-by-step reduction of the shearing stresses. Thus he brings the normal stress components close to the values of the principal stresses for which the associated shearing stresses are exactly zero.

The Effect of a Surrounding Fluid on Pressure Waves in a Fluid-Filled Elastic Tube[1]

G. W. MORGAN.[2] It may be of interest to point out a limitation of the validity of the analysis presented in this paper which restricts the range of frequency (and hence of wave number) within which the theoretical curves of phase velocity versus wave number may be expected to hold. As the frequency increases beyond the value for which the minimum phase velocity is obtained, the influence of inertia associated with rotation of the elements of the tube wall, as well as the influence of shear on the bending terms, become increasingly important. Their effect is to decrease the phase velocity. An analysis incorporating these effects has recently been carried out by T. C. Lin and the writer and will be published shortly.

AUTHOR'S CLOSURE

Professor Morgan's remark is well taken. The analysis assumes implicitly that the tube is a "thin" cylindrical shell, i.e., that its wall thickness is small in terms of wave lengths. Only if this condition is satisfied, the effects of rotary inertia and shear are negligible. The frequency range in which the "thin-shell" assumption is valid can be found in a recent paper by Hermann and Mirsky,[3] where more exact analyses of the dynamics of cylindrical shells are presented.

This seems a good opportunity for mention-

[1] By M. C. Junger, published in the June, 1955, issue of the JOURNAL OF APPLIED MECHANICS, Trans. ASME, vol. 77, pp. 227–231.

[2] Associate Professor of Applied Mathematics, Brown University, Providence, R. I.

[3] "Three-Dimensional and Shell-Theory Analysis of Axially Symmetric Motions of Cylinders," by G. Hermann and I. Mirsky, Technical Note No. 1, CU-3-55-AF-1247-CE, Office of Scientific Research, Columbia University, April, 1955.

ing a little-known paper by Lamb, which Prof. J. N. Goodier of Stanford University has kindly pointed out to the author. In this paper,[4] which deals with a variety of problems related to sound propagation in tubes, Lamb considers briefly the subject of the paper under discussion, as well as more refined analyses of the dynamics of the cylindrical shell.

Acceleration in Mechanisms[1]

ALLAN H. CANDEE.[2] Although the title refers to "acceleration," the paper is concerned mainly with determining radii of curvature and centers of curvature. The writer had difficulty in understanding what was being discussed in the opening paragraphs until he had studied the subsequent pages. For instance, "path of relative motion" is not easy to grasp when there is no statement as to *the path of what* or *relative to what*. And no reason is given for choosing the paths that were identified later, when there was already sufficient given information to determine the accelerations.

It has been universally accepted that for any mechanism in plane motion there is an "equivalent linkage" that will produce the same infinitesimal displacements. This being so, the instantaneous velocities and accelerations are also equal in the linkage and the original mechanism. We do not today require mathematical analysis to confirm what already has been proved and accepted. A list of references to the equivalent linkage would probably include much of the bibliography of kinematics.

Referring to Fig. 2, the linkage $ABDC$ is equivalent to the links 2 and 4 acting against each other by direct contact. And it can be seen also that the second linkage $ABPG_{42}$ is equivalent to the first, and has the effect of complicating the picture unnecessarily.

Various ASME papers have shown how radii and centers of curvature can be determined. To the writer the most important is by A. E. R. de Jonge,[3] which contains an extensive bibliography.

It is not necessary to use advanced kinematics or mathematics to find centers of curvature. In fact, the writer arrived at a method almost 30 years ago, that requires merely such a simple idea as the theorem of three instant centers on the same straight line, that is, the Aronhold-Kennedy theorem. He has not seen that particular method among those described in the publications to which he has had access; but it cannot be given here because of the space restriction. However, all constructions for the center of curvature of the path of a moving point must have similarities.

The authors are to be complimented for having devised a construction that requires the fewest lines possible. The same construction with different explanations, however, is to be found in Hartmann (1913), Hütte (1923), and Hain[4] (1952). It is ascribed to Bobillieri (1870).

The radius of curvature $R_{42} = (PG_{42})$ in Fig. 2 of the paper can be determined more easily than by the method in the paper, and Theorem II, by using one of the forms of the Euler-Savary equation. The relationships between pairs of conjugate centers and radii in the same normal line are expressed as

$$1/R_1 \pm 1/R_2 = 1/R_a \pm 1/R_b$$

These values are all distances from the instant center. Applying them in Fig. 2, we have $R_1 = (HG_{42}) = h - R_{42}$; $R_2 = (HP) = h$; $R_a = (HC) = h - r$; $R_b = (HD) = h + \rho$. Therefore merely by inspection of the diagram we can write

$$\frac{1}{h - R_{42}} - \frac{1}{h} = \frac{1}{h - r} - \frac{1}{h + \rho}$$

and then easily solve for R_{42}. This avoids all the complicated mathematics used to obtain Equations [1] to [13] in the paper.

As showing further that the results reported in the paper have all been known previously, the statement in Theorem III about the harmonic mean is to be found in Hain, p. 57,[4] and seemingly goes back to Aronhold (1872).

The authors deserve credit for obtaining their solutions even by the "hard way." Two of them, however, presumably are teachers of kinematics, and it seems reasonable to expect them to be well acquainted with its literature and to know how to apply its methods. The writer believes that in addition to what already has been accomplished there still is more to be done in simplifying our understanding and methods to make them more directly useful.

A. E. R. DE JONGE.[5] The paper by the authors is an example of one that should not have been written in the first place, and probably would not have been written had the authors been acquainted even only a little with the literature on kinematics, and it should not have been accepted by the ASME for publication in the second place.

By means of a formidable apparatus of the calculus of complex quantities and series developments, the authors have arrived at the simple Euler-Savary equation which has been known since its publication by Leonhard Euler in 1765, or since its rediscovery and derivation by Felix Savary in the late twenties of the nineteenth century (probably about 1827 or 1828).[6] Savary's work was first mentioned by M. Chales in 1845. This equation, although here given in a special derived form, can actually be read off from the simple Hartmann construction for the radii of curvature.[7] The four "theorems" stated by the authors have, likewise, been known for over a century.[8]

The authors start out with a mechanism of three links, AB, AP_2, and BP_4, Fig. 2, where P_2 and P_4 are, respectively, the two points of their links, labeled 2 and 4, which are in contact with one another at the point P. From this three-link mechanism, they form, by means of the two circles of curvature of the contacting curves at the point P (O in their Fig. 1), a mechanism of four links, AB, AC, CD, DB. In this mechanism they fix, one time, the link AC, and, the second time, the link BD. In the first case, they consider a point P_4 of the plane of the connecting rod BD, superposed, at that instant, on the contact point P of the links 2 and 4 of their Fig. 2, and, in the second case, a point P_2 of the plane of the (then) connecting rod AC of the four-link mechanism, superposed on the contact point P of the two former links 2 and 4. The radii of curvature of the paths of these two points relative to the respective fixed links are to be found.

[4] "On the Velocity of Sound in a Tube, as Affected by the Elasticity of the Walls," by H. Lamb, Memoirs of the Manchester Literary and Philosophical Society, vol. 42, no. 9, 1898, p. 1.

[1] By R. T. Hinkle, C. Ip, and J. S. Frame, published in the June, 1955, issue of the JOURNAL OF APPLIED MECHANICS, Trans. ASME, vol. 77, pp. 222–226.

[2] Rochester, N. Y. Fellow ASME.

[3] "A Brief Account of Modern Kinematics," by A. E. R. de Jonge, Trans. ASME, vol. 65, 1943, pp. 663–683.

[4] "Angewandte Getriebelehre," by Kurt Hain, Hannover-Darmstadt, 1952.

[5] Mechanical Engineer and Consultant, Reeves Instrument Corporation, New York, N. Y. Mem. ASME.

[6] See the writer's paper, "A Brief Account of Modern Kinematics," Trans. ASME, vol. 65, 1943; author's closure to the discussion by Allan H. Candee, especially pp. 679–682.

[7] "Ein neues Verfahren zur Aufsuchung des Krümmungskreises," by W. Hartmann, *Zeitschrift des Vereines deutscher Ingenieur*, vol. 37, 1893, pp. 95–101.

[8] "Principles of Mechanisms," by Robert Willis, London, England, 1841.

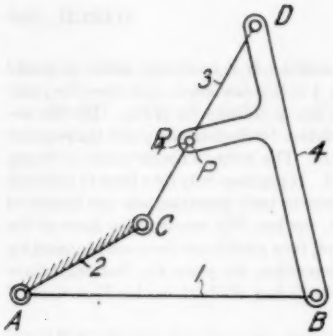

FIG. 1 EXPLAINING PROBLEM TO BE SOLVED

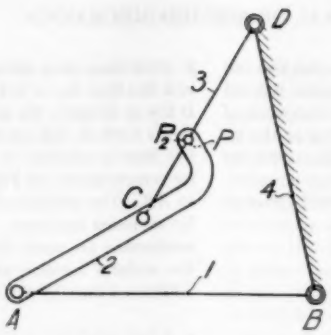

FIG. 2 EXPLAINING PROBLEM TO BE SOLVED

The problems outlined here are shown in the writer's Figs. 1 and 2 accompanying this discussion.

These are the two problems which the authors wish to solve, but which they have not even clearly stated.

The analytical derivations of the authors were quite unnecessary, as their Equations [13], [15], and [13a] can be obtained directly from the Euler-Savary equation by simple transformations. In fact, much simpler equations can be obtained for R and R' in that way. In setting up their geometrical construction, the authors have used one of Bobillier's constructions,[9] and in duplicating it for the two cases, they have used as many lines of one case as could be used for the second case. Thus they arrived at the simple construction shown in their Fig. 2, the construction requiring six lines for one case and two additional, or eight, lines for both cases. The eight lines in their Fig. 2 are AB, HL_2, PS', CEQ, QD, PFS, SEG_{42}, and $FS'G_{24}$. This is the minimum number of lines by which the two problems stated can be solved. The reason for this is that the method used is one of projective geometry. Actually, it is the complete quadrilateral that they have used and its projective properties.

The writer wishes to draw attention here to the Hartmann method[7] which also permits the solution of the two cases. However, the Hartmann method uses velocity vectors which, of necessity, must be perpendicular to the rays to which they belong, in this case to the ray on which the points and their conjugate centers of curvature lie, that are to be found. This imposes a serious restriction, a fact which Hartmann did not realize. The writer has found that this restriction is quite unnecessary and, if dropped, results in a far more general construction. With the writer's construction, it is possible to solve the two problems by means of nine lines. A special case of the writer's new general construction is shown in his accompanying Fig. 3, and, for purposes of comparison, the method used by the authors is also given in dashed lines. The designations are, as far as possible, those employed by the authors in their Fig. 2, although they are not in agreement with those commonly used in kinematics.

In the writer's new method, it is not necessary, as in the Hartmann method, to use velocity vectors perpendicular to the respective rays, but only to draw through the various points on the ray on which centers of curvature are to be found, lines converging toward any point in the plane. In the special case shown in his Fig. 3, the point of convergence is located at infinity on the line AB, so that the lines become parallel. The derivation for the general case has been published in the Transactions of the New York Academy of Science.[10]

[9] See for instance, Kurt Hain, "Angewandte Getriebelehre." Hannover-Darmstadt, 1952, p. 39, in particular fig. 95 and description thereto.

[10] "A New Construction for the Center of Curvature," by A. E. Richard de Jonge, Trans. N. Y. Academy of Science, series II, vol. 17, no. 7, May, 1955, pp. 541–546.

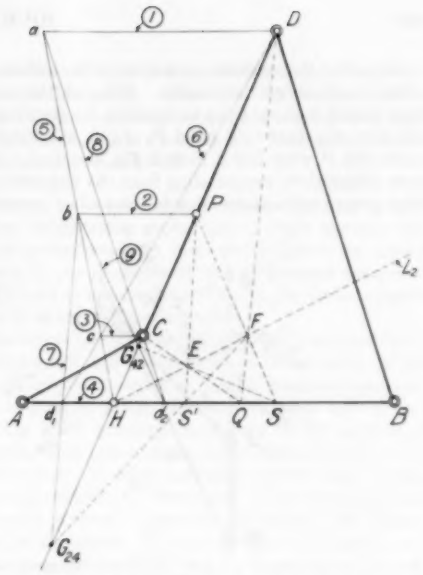

FIG. 3 COMPARISON OF THE WRITER'S NEW METHOD WITH THAT OF THE AUTHORS'

Inasmuch as the authors have saved one line in their construction, namely $AB = L_1$, by using this line which already exists, the writer, similarly, uses AB by drawing the parallel lines parallel to it. These parallels, including AB, have been designated by encircled numbers 1 to 4. Then, any line 5 (encircled) is drawn through the rotopole H (instantaneous center), which line intersects the parallels with encircled numbers 1 in a, 2 in b, and 3 in c. Next, D and c are joined by a straight line which meets AB in d_1. The line bd_1 intersects DH in G_{24}. If a is joined with C, the point d_2 on AB is obtained and, as a check, $d_2H = Hd_1$. Joining b with d_2 yields G_{42} on DH.

The proof for the correctness of the writer's method is given easily by considering an infinitesimal motion of the system including the radii of curvature to be found, and by projecting the elementary displacements by parallel affine projection in any constant ratio and direction. The radii of curvature thus obtained are, in the affine figure, bG_{24} and bG_{42} which no longer are equal to the radii of curvature sought, but since G_{24} and G_{42} still lie on the ray DH, these points are thus the actual centers of curvature of the paths of the points P_2 and P_4, respectively, and the radii of curvature are PG_{42} and PG_{24}.

This method, published for the first time in reference 10, is simple and requires but nine lines. In the writer's Fig. 3 they are shown by encircled numbers 1 to 9, four of which are parallel to one another. This is only one line more than the authors have used, but since four lines are parallel, the diagram is much more readily drawn and the accuracy is greater, because the respective segments used are, in general, longer and more suitably located than those used by the authors. In particular, the point G_{24} in the configuration shown by the authors in their Fig. 2, is obtained more accurately, because the segment bd_1 is much longer than the segment FS' used by the authors. Since $Hd_1 = d_1H$, the line ad_2 may be dispensed with by simply transferring d_1H to Hd_2. In some cases, this new construction reduces to but eight lines or less as will be shown hereinafter. Even this special case of the new construction is more general than the Hartmann method, because the restriction to perpendicular velocity vectors has been removed and has been replaced by displacements in any direction.

Regarding the examples presented by the authors, the first one refers to a four-link mechanism. Although the purpose has not been stated, it seems to be to establish the center of curvature of the path described by a point P_4 of link 4, coinciding at the instant with P, when link 2, in their Fig. 3, is fixed. The result has been obtained by computation from the Euler-Savary equation. The geometrical construction has not been presented although it could have been given easily. If it had been given, it would look like that shown in Fig. 4 of this discussion, and since the point D lies at infinity, G_{24} also lies at infinity on HPD. By the author's method, the construction for finding the point Q_{42} requires five lines in addition to AB. The writer's construction is shown for comparison in his Fig. 5. It requires only four lines in addition to AB. The additional lines in both constructions are indicated by encircled numbers. If, further, the construction lines of the mechanism are made use of, four additional lines are required by the authors' method to determine the point G_{42}, but only three additional lines by the writer's new method, see his Figs. 6 and 7

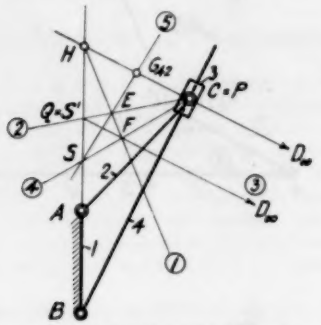

FIG. 4 APPLICATION OF THE AUTHORS' METHOD FOR OBTAINING POINT P

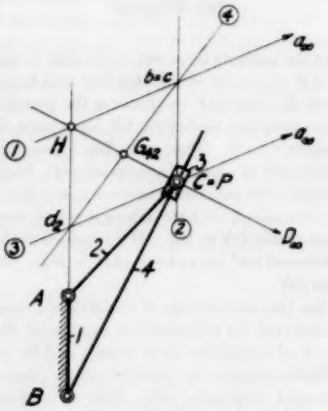

FIG. 5 APPLICATION OF WRITER'S METHOD FOR OBTAINING POINT P

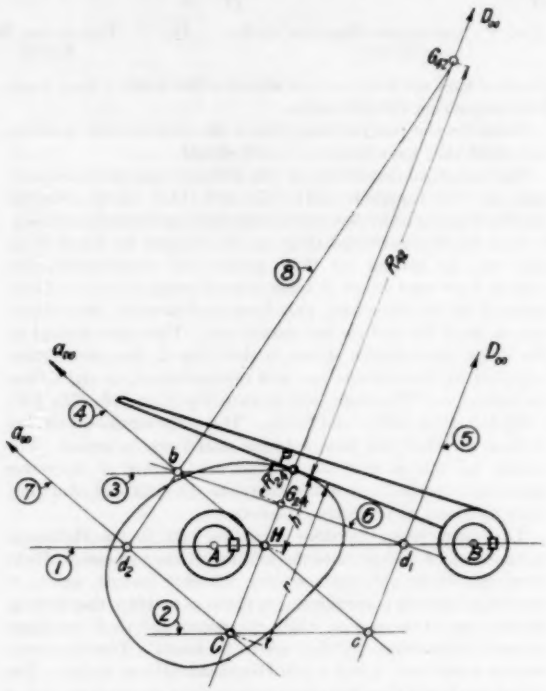

FIG. 8 COMPARISON WITH AUTHORS' FIG. 4a

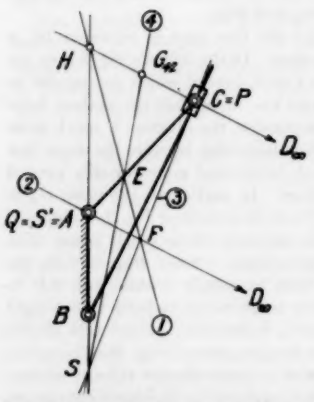

FIG. 6 SAME AS FIG. 4, BUT USING LINES OF THE MECHANISM SKELETON

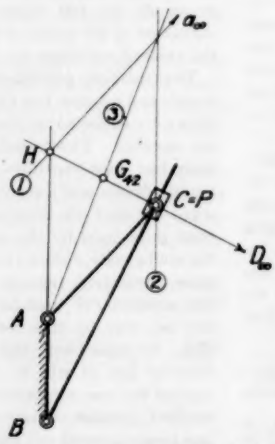

FIG. 7 SAME AS FIG. 5, BUT USING LINES OF THE MECHANISM SKELETON

respectively. The $\frac{1}{2}HP = PG_{42}$ relationship is here obvious.

For their example 2, the authors, likewise, do not state the purpose that they wish to achieve. Since the paper is entitled "Acceleration in Mechanisms," it may be inferred that the determination of the accelerations is their objective. These can be obtained only when the radii of curvature, R_{42} for the path of P_4 of the oscillating level 4—now the connecting rod (or coupler) relative to the fixed cam 2—and R_{24} for the path of P_2 of the cam 2 relative to the oscillating lever 4—which is then fixed—are known. They have been determined by the authors in their Fig. 4(a). However, owing to the very small segment SE used by them, the location of G_{42} is uncertain and in error in their Fig. 4(a). To show this, the writer's construction has been carried out in his Fig. 8 for the same configuration as in Fig. 4(a). It requires but eight lines, that is, just as many as were used in the authors' construction. The lines have been indicated by encircled numbers. The writer's graphical method yields $R_{42} = 3.46$ in. and $R_{24} = 0.28$ in. These values can be calculated by means of similar

triangles. For R_{42}, we have, with the values indicated in Fig. 8

$$\frac{R_{42}+h}{R_{42}} = 1 + \frac{h}{R_{42}} = \frac{d_2H}{bP} = \frac{Cc}{bP} = \frac{r-h}{h} = \frac{r}{h} - 1$$

or

$$\frac{h}{R_{42}} = \frac{r}{h} - 2$$

whence

$$\frac{1}{R_{42}} = \frac{1}{h}\left(\frac{r}{h} - 2\right)$$

From the authors' Fig. 4(*a*), we measure $r = 1.375$ in. and $h = 0.63$ in. With these values, we find

$$\frac{1}{R_{42}} = \frac{1}{0.63}\left(\frac{1.375}{0.63} - 2\right) = \frac{2.1825-2}{0.63} = \frac{0.1825}{0.63}$$

or

$$R_{42} = \frac{0.63}{0.1825} = 3.452 \text{ in.}$$

From the authors' drawing, $PG_{42} = R_{42}$ scales 2.53 in., that is, only about 73.3 per cent of the value found by the writer's construction and calculation, or is about 26.7 per cent in error.

The lines required in the writer's construction are self-explanatory if reference to his Fig. 3 is made.

For R_{24}, both the authors' and the writer's constructions give about the same value which scales 0.29 in. By calculation, we find

$$\frac{h-R_{24}}{R_{24}} = \frac{Hd_1}{bP} = \frac{Cc}{bP} = \frac{r-h}{h} = \frac{r}{h} - 1 = \frac{h}{R_{24}} - 1$$

whence

$$R_{24} = \frac{h^2}{r} = \frac{0.63^2}{1.375} = 0.288 \text{ in.}$$

or essentially the same value as found by the construction.

After the two radii of curvature R_{42} and R_{24} have been found, the computation of the accelerations presents no difficulty and can be carried out by the method shown by the authors or, even simpler, by any of the well-known standard graphical procedures.

Finally, a few words on the consideration of "equivalent linkages." By that, the authors mean the replacement of a so-called higher element pair by a link with two so-called lower element pairs. This, however, is only a small part of the meaning of the term "equivalent mechanisms." Furthermore, this method has been known for over a century[8] and has been used widely during that period. A discussion of it and the properties it entails was, therefore, quite unnecessary.

To sum up: Except for using the Bobillier construction for the radius of curvature of points on the same ray and duplicating it, using as many lines for the construction of the first to serve also for that of the second center of curvature, the paper has brought forth nothing new. It has only shown that a well-known formula which may be derived in a simple way can also be obtained in a very complicated way. This reminds one of the well-known German saying which, translated into English, reads "Why make it simple when it can also be made complicated." However, it also brings back to one's mind the advice by Lord Kelvin, "A problem is never solved until it has been reduced to its simplest terms."

Nevertheless, the writer wishes to thank the authors for having afforded him the opportunity to publish here, for the first time, applications of his hitherto unknown, and thus new, construction for obtaining the centers of curvature by means of a method involving parallel affine projection, in *any* direction and in *any* ratio, of elementary displacements. This new construction can be generalized still further by using perspective instead of parallel affine projection, as has been shown in the Transactions of the New York Academy of Science.

J. W. Huckert.[11] The authors are to be commended for a stimulating and enlightening paper upon a topic dealing with motion transfer in mechanisms. More papers like it are needed to uproot some of our ill-contrived and antiquated notions of motion transfer and to advance our thinking on the kinematics of mechanisms in step with a modern world.

So far as the writer's knowledge extends this consideration of inversion provides new and additional radii of curvature to the several already known and commonly used in kinematic analysis. The writer's thinking for many years has regarded radii of curvature as having solely geometric properties in the analysis of motions in mechanisms, and consequently independent of velocities and accelerations. In other words, the introduction of time rates of change is redundant. When radii of curvature only are wanted, the writer generally forms the derivatives with respect to an angle or an arc length. There is no loss of generality and the mathematics is simplified.

Why did the authors feel that radii of curvature of the path of relative motion might behave differently, say, than the radii of curvature of an ellipse, or an envelope, or a path of contact? And, wouldn't the mathematics be simplified and equally as general if the differentiations were made with respect to the arc length rather than time?

Equivalent mechanisms, in the writer's opinion, are truly a subterfuge. He would like to see them banned altogether as a method of kinematic analysis. The authors make a step in that direction in Theorem IV. Unfortunately, they do not illustrate the application of the theorem when the profile of a member has a continuously changing curvature, and which, naturally, is the case for which a method of analysis is needed.

As soon as time permits, the writer will try out the theorem on a cam mechanism consisting of an ellipse driving a pivoted roller follower. The theorem, as he views it, shifts the difficult part of the mathematical transformation from the point of contact to the variable center of curvature of the ellipse. In short, if the ellipse as a rigid body is considered as rotating at constant angular speed, the crank arm to the center of curvature could not have continuously an angular acceleration of magnitude zero.

As a substitute for the method of equivalent linkages the writer suggests the method of parallel curves. Involutes are basically parallel curves. Envelopes for cam profiles can be studied as parallel curves. And the center of the roller that makes contact with an ellipse traces a curve parallel to the ellipse. The use of parallel curves, therefore, seems to me to represent a more natural and logical approach than equivalent linkages. The simplification, of course, comes about through the replacement of an unknown path of contact by one that is known. The solution of specific problems by the method of parallel curves, while differing from that by equivalent linkages, is comparable in difficulty and in time required to make solutions.

M. F. Spotts.[12] The authors are to be commended for supplying additional information on one of the more difficult aspects of the science of kinematics. In order to obtain solutions to certain types of problems in this field, notably for bodies in direct contact, the radius of curvature R for the path of relative motion

[11] Professor of Machine Design, Mechanical Engineering Department, Robinson Laboratory, Ohio State University, Columbus, Ohio.

[12] Professor of Mechanical Engineering, Northwestern University, Evanston, Ill. Mem. ASME.

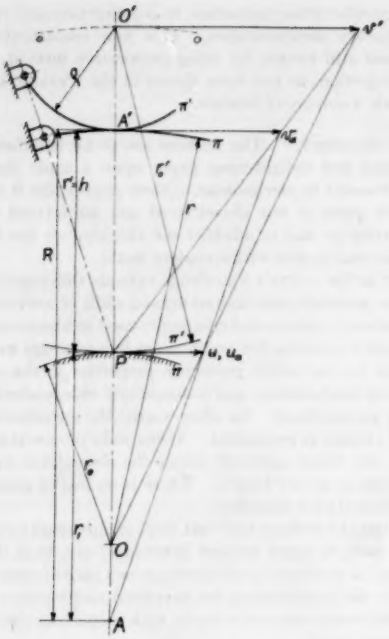

FIG. 9

must be known. The value of R can be easily computed by means of the authors' Equation [13]. It should be noted, however, that this equation can be derived from the well-known Euler-Savary equation.

Fig. 9, herewith, is similar to Fig. 2 as given in an earlier paper by de Jonge[13] except that angle φ becomes 90 deg. The bodies have radii of curvature ρ and r with centers O and O' when contact is made at A'. The instant center for the two bodies is at P. De Jonge has shown, by his Equation [7], that the following relationship holds

$$\frac{1}{r'} + \frac{1}{r_1} = \frac{1}{r_0'} + \frac{1}{r_0}$$

In this equation r_1 is used for the unknown instead of r to prevent subsequent conflict of notation. Reference to Fig. 9 indicates the following

$$r' = h$$

$$r_1 = R - h$$

$$r_0' = h + \rho$$

$$r_0 = r - h$$

These are substituted in the foregoing equations and the subsequent algebraic transformations performed which are self-evident

$$\frac{1}{h} + \frac{1}{R-h} = \frac{1}{h+\rho} + \frac{1}{r-h}$$

$$\frac{R}{hR - h^2} = \frac{r+\rho}{hr - h^2 + r\rho - h\rho}$$

$$h^2R - h^2r - h^2\rho = rR\rho - 2hR\rho$$

$$h^2R\rho + h^2rR - h^2r^2 - h^2r\rho = h^2R\rho + r^2R\rho - 2hrR\rho$$

$$h^2(R\rho + rR - r^2 - r\rho) = R\rho(h^2 - 2hr + r^2)$$

$$\frac{R\rho + rR - r^2 - r\rho}{r^2R\rho} = \frac{(h-r)^2}{h^2r^2}$$

$$\left(\frac{R-r}{rR}\right)\left(\frac{r+\rho}{r\rho}\right) = \left(\frac{h-r}{hr}\right)^2$$

$$\left(\frac{1}{r} - \frac{1}{R}\right)\left(\frac{1}{r} + \frac{1}{\rho}\right) = \left(\frac{1}{r} - \frac{1}{h}\right)^2$$

The foregoing equation agrees with the previously mentioned Equation [13] except that radius ρ in Fig. 9 is a negative number.

D. K. WRIGHT, JR.[14] If relative motion occurs between two links A and B, Fig. 10 of this discussion, a point X on link A will describe some path relative to link B. The center of curvature of this path is a point Y on link B lying on the straight line drawn through X and the instant center O_{AB}.

The Euler-Savary equation states that the distances to these points from the instant center have the relation

$$\frac{1}{r_x} - \frac{1}{r_y} = \text{const}$$

As shown in Fig. 10, if r_x is taken positive, r_y is negative.

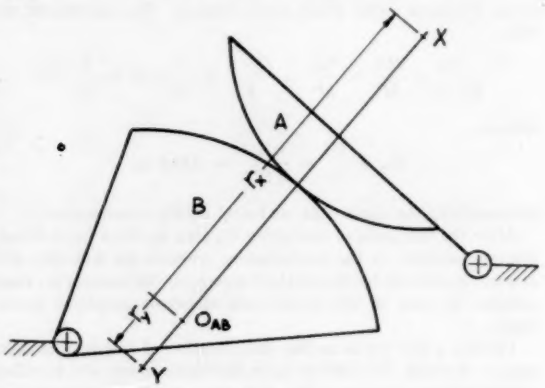

FIG. 10

Points X and Y are called conjugate points and each is the center of curvature of the path which the other describes. A particular point on the line will have its center of curvature at infinity. This point is describing a curve which is passing through an inflection; hence it is called the inflection point, I. If we write the Euler equation for this point and its conjugate at infinity, we obtain

$$\frac{1}{r_i} - \frac{1}{\infty} = \text{const}$$

which evaluates the constant and gives the equation for all conjugate pairs on that line as

$$\frac{1}{r_x} - \frac{1}{r_y} = \frac{1}{r_i}$$

If we deal with distances from point X (per Fig. 11) rather

[13] "A Brief Account of Kinematics," by A. E. R. de Jonge, Trans. ASME, vol. 65, 1943, p. 663.

[14] Professor of Machine Design, Case Institute of Technology, Cleveland, Ohio. Assoc. Mem. ASME.

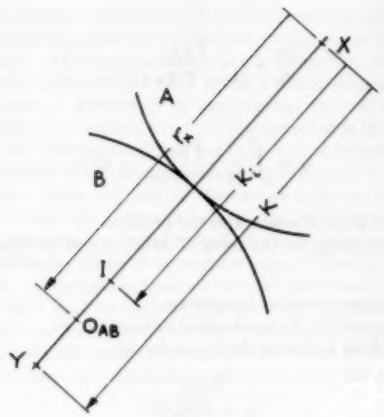

FIG. 11

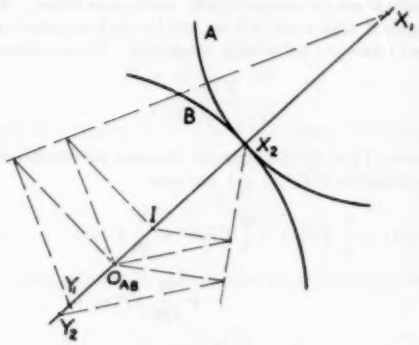

FIG. 12

than from the instant center, the equation can be rewritten in a form more suitable for graphical solution

$$r_x^2 = K K_i$$

or

$$\frac{K_i}{r_x} = \frac{r_x}{K}$$

When a cam and its follower are the links A and B, the cam profile is the envelope of the family of curves represented by all possible positions of the follower profile. At any position, the centers of curvature of the contacting profiles corresponding to the points in contact are conjugate points, as defined by the Euler equation. This property, in conjunction with the fact that nowhere in the evaluation of acceleration components do we find terms involving the rate of change of the radius of curvature, permits us to use the equivalent linkage shown by the authors when both profiles are curved.

Since the centers of curvature of the contacting profiles are conjugate points, we may use them with the instant center to solve the problem at hand in two steps:

1 We take the centers of curvature as points X_1 and Y_1, which with the instant center give us r_x and K and we solve the Euler equation graphically to locate the inflection point, Fig. 12(*a*).

2 Having the inflection point I, and the instant center, we choose the point of contact on link A as X_2, which gives us new values for r_x and K_i, and we solve for K which gives us the location of Y_2, the center of curvature on link B of the path described by the contact point on A, Fig. 12(*b*).

For the case of two curved profiles, this graphical construction involves about the same amount of work as that proposed by the authors. If one of the profiles is straight, the work is cut in half. In this case the center of curvature of the straight profile is at infinity and the center of curvature of the curved profile is itself an inflection point. Only one application of the Euler equation is necessary to locate the desired center of curvature.

Further consideration of the case of a straight profile in contact with a curved profile leads to the substitution of an equivalent mechanism in which the flat profile on, say, link A is moved parallel to itself until it passes through the center of curvature I of the curved profile on link B, Fig. 13. We then deal with the simple case in which I slides along the straight line located on A. The relative acceleration at the point of contact then involves, at most, a Coriolis component and a tangential component.

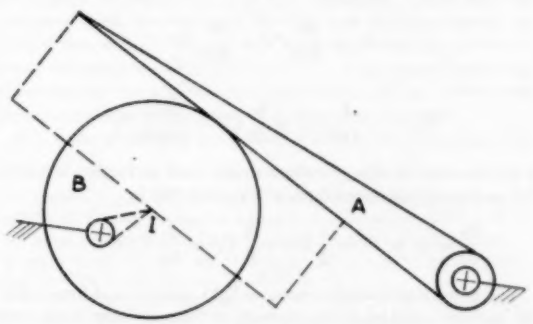

FIG. 13

There may be situations in which it is desired to locate the centers of curvature which are the subjects of this paper, in which case either the authors' or the Euler-Savary construction is available. If the ultimate problem is to solve for accelerations, the writer would choose every time the equivalent-mechanism method. It is exact theoretically, it involves negligible preliminary graphical construction, eliminating a possible source of errors, and the acceleration analysis itself is simplified.

AUTHORS' CLOSURE

In this paper the authors developed an analytical and a graphical method for determining the radii of curvature of the relative paths of contact points in direct contact mechanisms. If this work has stimulated others to develop their own methods, or to extend the work of earlier writers, the paper has served a dual purpose. Messrs. Candee, de Jonge, Spotts, and Wright have presented other methods.

Mr. Candee states that the proof for the equivalent linkage is unnecessary. The authors are aware that the equivalent linkage is described without proof in many books. However, there are some who believe that it is not valid. Since the development of the work for the radii of curvature laid the ground work for a rigorous proof, the authors felt justified in including it.

Professor Huckert suggests the use of parallel curves. This is a valuable concept and should be investigated further but the authors doubt if it can be applied to a mechanism of the type shown in Fig. 4 of the paper.

An attempt to determine the acceleration of member 4 in Fig. 4, using the conventional equivalent linkage, will involve an indeterminate ratio. For this problem, Professor Wright proposes a different type of equivalent mechanism. He is correct when he states that the simplest solution is obtained by using an equivalent linkage.

On the Nonlinear Differential Equation for Beam Deflection[1]

N. J. Huffington, Jr.[2] Although the authors are to be complimented on their application of the reversion method to a problem of interest in mechanics, attention should be called to certain errors which appear in the paper. The authors' Equation [10] should appear as

$$\Phi_1 y_6 = -\Phi_6 y_1^6 - 5\Phi_5 y_1^4 y_2 - \Phi_4(6y_1^2 y_2^2 + 4y_1^3 y_3) - \Phi_3(y_2^3 + 3y_1^2 y_4 + 6y_1 y_2 y_3) - \Phi_2(y_3^2 + 2y_1 y_5 + 2y_2 y_4)$$

Also, the coefficient of the term involving Y_1^7 in Equation [25] is incorrect. By use of Equation [9] and the revised form of Equation [10] one obtains

$$Y_5 = \frac{39}{280} Y_1^7 + \frac{31}{280} Y_1^9$$

$$Y_6 = -\frac{1}{112} Y_1^7 + \frac{6}{35} Y_1^9 + \frac{2073}{30800} Y_1^{11}$$

A continuation of this procedure would yield no further terms in Y_1^7, so that the corrected form of Equation [25] is

$$\frac{dy}{dx} = Y = Y_1 + \frac{1}{2} Y_1^3 + \frac{3}{8} Y_1^5 + \frac{5}{16} Y_1^7 + \ldots.$$

The noted discrepancies came to light when it was found that the authors' solution of the example of the cantilever beam with a couple applied at the free end did not agree with the series expansion of the closed-form solution of this problem. Since the rate of convergence of power-series solutions of such problems is frequently slow, mention should be made of a related paper[3] in which results useful for computational purposes are presented.

George Luchak.[4] The solution of the equation

$$EI\, d^2y/dx^2 = M(x)\,[1 + (dy/dx)^2]^{3/2}$$

is given in closed form. From the solution can be obtained a variety of representations in infinite series. One of these, obtained by the authors, is discussed and its limits of convergence are stated.

To solve

$$EId^2y/dx^2 = M(x)\,[1 + (dy/dx)^2]^{3/2} \ldots\ldots\ldots [1]$$

put $dy/dx = s$ and get

$$EI\, ds/dx = M(x)\,(1 + s^2)^{3/2}$$

Then

$$\int \frac{ds}{(1+s^2)^{3/2}} = \int \frac{M(x)}{EI}\, dx = Y_1(x) \ldots\ldots\ldots [2]$$

in the notation of the authors, and

$$\frac{s}{(1 + s^2)^{1/2}} = Y_1(x)$$

Thus

$$\frac{dy}{dx} = \frac{Y_1(x)}{[1 - Y_1^2(x)]^{1/2}} \ldots\ldots\ldots [3]$$

and finally

$$y = \int \frac{Y_1(x)}{[1 - Y_1^2(x)]^{1/2}}\, dx \ldots\ldots\ldots [4]$$

which is the general solution to the problem.

Now, depending on the form of $M(x)$, y can be obtained as follows:

(*a*) In closed form by integration,
(*b*) Numerically by mechanical integration, or
(*c*) In other forms by the expansion of

$$\frac{Y_1(x)}{[1 - Y_1^2(x)]^{1/2}}$$

into infinite series or asymptotically convergent series. Nothing will be gained and much will be lost by such expansions if the individual terms are not readily integrable. If one expands

$$\frac{Y_1(x)}{[1 - Y_1^2(x)]^{1/2}}$$

in powers of $Y_1(x)$ by the binomial theorem, an expansion which is only admissible if $Y_1^2(x) < 1$, one gets

$$\frac{dy}{dx} = Y_1(x) + \frac{1}{2} Y_1^3(x) + \frac{3}{8} Y_1^5(x) + \frac{5}{16} Y_1^7(x) + \frac{35}{128} Y_1^9(x) + \ldots\ldots\ldots [5]$$

Equation [5], differs from Equation [25] of the author's paper to which it corresponds, by having a larger coefficient for $Y_1^7(x)$. The authors, it is presumed, would have obtained the correct coefficient by solving the next equation in their series of Equations [17] to [20].

It would appear that in most practical problems, the Taylor series expansion of

$$\frac{Y_1(x)}{[1 - Y_1^2(x)]^{1/2}}$$

would probably be used if the evaluation of the integral in closed form in Equation [4] of this discussion is impossible and if a numerical evaluation is undesirable.

M. E. Raville.[5] The authors have presented a formal solution to the classical nonlinear beam equation which is applicable in all cases in which the bending moment may be expressed in terms of the independent variable. Various authors have solved specific problems concerning beam deflections using the exact expression for the curvature; for example, L. Euler, who was the first to make extensive use of the beam equation, is credited with having discussed problems in which he retained the term $(y')^2$ in the denominator and performed the subsequent integration by the use of series.[6] However, the writer is not aware of the existence of a solution which is as general in nature as this.

---

[1] By E. J. Scott and D. R. Carver, published in the June, 1955, issue of the Journal of Applied Mechanics, Trans. ASME, vol. 77, pp. 245–248.

[2] Associate Professor of Applied Mechanics, Virginia Polytechnic Institute, Blacksburg, Va. Assoc. Mem. ASME.

[3] "Solution of Nonlinear Differential Equations by the Reversion Method Through the First Thirteen Terms," by G. I. Cohn and B. Saltzberg, *Journal of Applied Physics*, vol. 25, 1954, pp. 252–254.

[4] Defense Service Scientific Officer, Defence Research Board of Canada, Ralston, Alta., Canada.

[5] Department of Mechanics, College of Engineering, University of Wisconsin, Madison, Wis.

[6] "History of Strength of Materials," by S. Timoshenko, McGraw-Hill Book Company Inc. New York, N. Y., 1953, p. 32.

From a practical standpoint, it should be mentioned that the use of the solution presented by the authors appears to be a rather tedious task. The fact that the horizontal projection of the beam length must be substituted for L in the authors' equations is the primary cause of difficulty. It appears that the use of a value for L less than the original length of the beam tends to produce a value for the deflection which is less than that obtained from the usual elementary formula, while the additional terms in the series which result from the use of the exact expression for the curvature have the opposite effect. Some numerical computations showing how much effect the correction terms have on the elementary solution for various cases of loading would be of interest. Although, in practice, a beam is seldom loaded and supported in a manner such as to satisfy the requirements laid down by the authors, the writer feels that they have provided a possible means for evaluating the effect of one of the several factors not taken into account by the elementary theory.

C. J. Thorne.[7] In the authors' Equation [13] let $y' = w$. We have

$$\frac{dw}{(1 + w^2)^{3/2}} = \frac{M(x)}{EI}$$

The usual substitution $w = \tan \theta$ will make the integration obvious. We find

$$y' = \frac{\pm Y_1}{(1 - Y_1^2)^{1/2}}$$

in terms of the authors' Y_1. Expansion by the binomial theorem gives

$$y' = \pm Y_1 \left[1 + \frac{1}{2} Y_1^2 + \frac{3}{8} Y_1^4 + \frac{5}{16} Y_1^6 + \dots \right]$$

The first three terms agree with the authors' results. The convergence for y is $|Y_1| \leq 1$ and for its derivatives $|Y_1| < 1$.

Stress-Concentration Factors in Shafts With Transverse Holes as Found by Electroplating Method[1]

T. J. Higgins.[2] The writer finds this paper a very well-written one. It evidences that the authors have performed their experimental work with care and have exercised judiciousness in drawing their conclusions therefrom.

M. M. Leven.[3] The authors are to be congratulated for developing an ingenious method of experimental stress analysis. The method proposed may prove to be quite useful for measuring fatigue strength of machine parts and structures, although for the same amount of testing, a complete S-N curve could probably be obtained. However, the writer is not willing to accept the change in the color of an electroplated copper coating on a steel specimen which has been subjected to 5×10^6 cyclic reversals of stress, as an indication of the true static, elastic stress distribution. This is especially true when none of the factors of stress concentration reported by the authors agrees with other accepted theoretical and experimental results.

The authors first used their experimental method for the case of a shaft with a circumferential groove subjected to pure torsion.[4] The experimental results obtained, corroborated precisely Ōkubo's approximate analytical solution for this case.[5] Ōkubo's factors of stress concentration for this case are shown by the dashed curves in Fig. 1 of this discussion, where they are compared with the results of Neuber[6] and the photoelastic results of the writer.[7] It is of interest to note that the factors of stress concentration of Ōkubo for $h/r = 4$ are higher than those of Neuber for the infinitely deep hyperbolic groove. Moreover, the curves of Ōkubo for $h/r = 1$ and 4 actually intersect.

Still more striking is the difference in results obtained in this

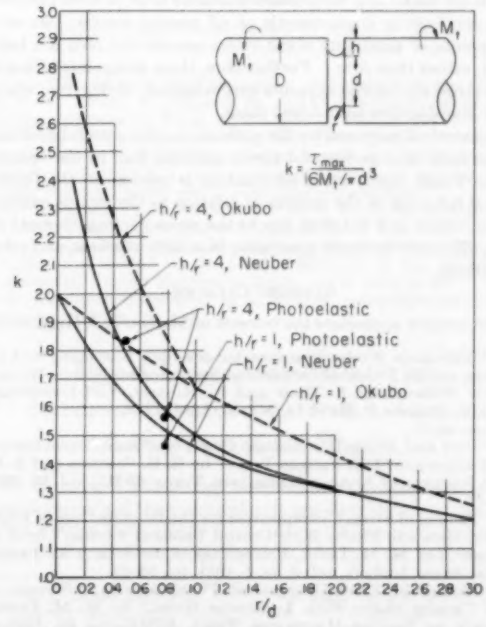

Fig. 1 Factors of Stress Concentration for a Grooved Shaft in Torsion

[7] Department of Mathematics, University of Utah, Salt Lake City, Utah.

[1] By H. Ōkubo and S. Sato, published in the June, 1955, issue of the Journal of Applied Mechanics, Trans. ASME, vol. 77, pp. 193–196.

[2] Professor of Electrical Engineering, University of Wisconsin, Madison, Wis.

[3] Research Engineer, Westinghouse Electric Corporation, East Pittsburgh, Pa.

[4] "Determination of the Surface Stress by Means of Electroplating," by H. Ōkubo, *Journal of Applied Physics*, vol. 24, 1953, p. 1130.

[5] "Approximate Approach for Torsion Problem of a Shaft With a Circumferential Notch," by H. Ōkubo, Journal of Applied Mechanics, Trans. ASME, vol. 74, 1952, p. 16.

[6] "Theory of Notch Stresses," by H. Neuber, J. W. Edwards, Ann Arbor, Mich., 1946. Neuber values obtained from Fig. 46 of "Stress Concentration Design Factors," by R. E. Peterson, J. Wiley & Sons, Inc., New York, N. Y., 1953.

[7] "Quantitative Three-Dimensional Photoelasticity," by M. M. Leven, Proceedings of the Society for Experimental Stress Analysis, vol. 12, no. 2, pp. 157–171.

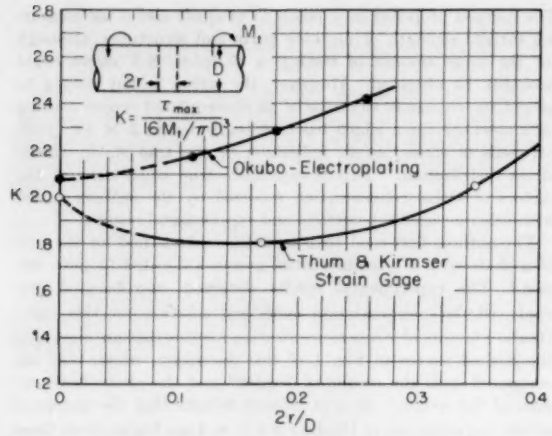

FIG. 2 FACTORS OF STRESS CONCENTRATION FOR A SHAFT WITH TRANSVERSE CIRCULAR HOLE IN TORSION

paper compared with those of Thum and Kirmser[8] for the case of a shaft with a transverse hole subjected to torsion as shown in Fig. 2, herewith. The work of Thum and Kirmser has been checked photoelastically for the case of a hole in a shaft subjected to tension[9] and there is every reason to believe that their results are accurate. Likewise, the extensometer results of Peterson and Wahl[10] for the case of shafts with fillets and holes subjected to bending have been checked photoelastically.[11, 12] All of these results indicate that for holes in shafts subjected to bending or torsion, there is an optimum ratio of hole-to-shaft diameter for which the maximum stress is a minimum (see Fig. 2).

The location of the regions of maximum shear stress on the surface of the shaft as shown by Fig. 5 of the paper is quite unusual and contrary to the results of other investigators.[13] Not only is the maximum shear stress indicated to be at some distance from the hole (a characteristic of all coating results) but only two points of maximum shear stress around the hole are indicated, rather than four. Furthermore, these two points of maximum stress are located at points approximately 45 deg from where other investigators have found them.

The method proposed by the authors may be a useful addition to the tools of experimental stress analysis, but, in the opinion of the writer, much more information is needed on the fundamental behavior of the coating in relation to the strains existing in the copper and the steel due to the stress cycling, thermal effects, difference in elastic constants, biaxiality of stress, and other conditions.

AUTHORS' CLOSURE

The authors appreciate the interest of Messrs. T. J. Higgins and M. M. Leven and their valuable discussions on the electroplating method of stress analysis. With regard to Mr. Leven's opinion, however, the authors make the following statement.

1 In accurate quantitative discussions, the validity of Neuber's formula, though most suitable for quick reference and great practical significance, must be confirmed by separate justification made prior to its use, because his formula is an approximate one based on the theoretical value for an infinitely deep hyperbolic groove.

Experimental data presented in the papers by the authors and Leven are, however, those for parallel-sided U-grooves and not for hyperbolic grooves. It is agreed that the stress-concentration factor for a twisted shaft with a circumferential semicircular groove has been evaluated accurately by Willers. Hence we must make a comparison of the results of Neuber and Willers.

As an example, consider the case for a semicircular groove of $d = 8r$. The accurate value by Willers is $K = 1.57$, while Neuber's formula gives the much smaller value of $K = 1.40$. Moreover, the latter's solution gives a small value of K which almost agrees with that for a fillet obtained by Jacobsen by means of electrical analogy(1),[14] e.g., his solution gives $K = 1.58$ for $r/d = 0.078$ and $h/r = 4$, while the corresponding value for a shaft containing a fillet is 1.53. There is every reason, however, to expect that the stress-concentration factor for the circumferential groove is much higher than that for the fillet. These theoretical and experimental results of other investigators all indicate that Neuber's solution gives much smaller value than the actual one.

The experimental value given by one of the authors in a previous paper is $K = 1.59$, which precisely agrees with the corresponding value by Willers. This excellent agreement between the theoretical and the experimental results shows that the electroplating method of stress analysis can be applied to cognate cases with sufficient accuracy.

It is true that the stress-concentration factors for U-grooves obtained by the electroplating method are, in some instances, higher than those of Neuber for infinitely deep hyperbolic groves. But one must bear in mind that the experimental results by the author and Leven are those for U-grooves and Neuber's formula for V-grooves. The essential point ignored in Leven's discussion is the effect arising from the difference between the U and V-shape, depth and radius of the grooves being identical. Quantitative comparison of the stress-concentration factors for U and V-grooves is not available for this example, owing to the absence of exact relevant data. But Neuber's solution for a flat tension bar with infinitely deep hyperbolic notches, in some instances, gives slightly smaller values of K even when compared to those for semicircular notches measured by photoelasticity (2), and his solution for semicircular notches always gives a lower value than the experimental value, as is shown by a dashed line in Fig. 3, herewith. However, the experimental value of K's is always lower than the accurate value shown in the same figure (3). This result may also be expected from the known data for shallow V-notches (4).

Such results for a flat tension bar obviously indicate that the stress-concentration factor for an infinitely deep hyperbolic groove is not always higher than that for a semicircular or parallel-sided U-groove.

With regard to the authors' approximate formula for a circumferential U-groove, another supplementary formula extending the useful range was developed in a previous paper (5), and the conflict pointed out by Leven and that occurring in the limiting case of very large r/d have been reasonably eliminated.

2 Little theoretical information is available on the stress-

[8] "Überlagerte Wechselbeanspruchungen, ihre Erzeugung und ihr Einfluss auf die Dauerhaltbarkeit und Spannungsausbildung Quergebohrter Wellen," by A. Thum and W. Kirmser, VDI-Forschungsheft 419, Ausgabe B, Band 14, March–April, 1943.

[9] Loc. cit. 7.

[10] "Two and Three-Dimensional Cases of Stress Concentration, and Comparison With Fatigue Tests," by R. E. Peterson and A. M. Wahl, JOURNAL OF APPLIED MECHANICS, Trans. ASME, vol. 58, 1936, p. A-15.

[11] "Factors of Stress Concentration for the Bending Case of Fillets in Flat Bars and Shafts With Central Enlarged Section," by J. B. Hartman and M. M. Leven, Proceedings of the Society for Experimental Stress Analysis, vol. 9, no. 1, 1951, pp. 53–62.

[12] "Studies in Three-Dimensional Photoelasticity: Stresses in Bent Circular Shafts With Transverse Holes," by M. M. Frocht, JOURNAL OF APPLIED MECHANICS, Trans. ASME, vol. 66, 1944, p. A-10.

[13] Loc. cit. 8.

[14] Numbers in parentheses refer to the Bibliography at the end of the closure.

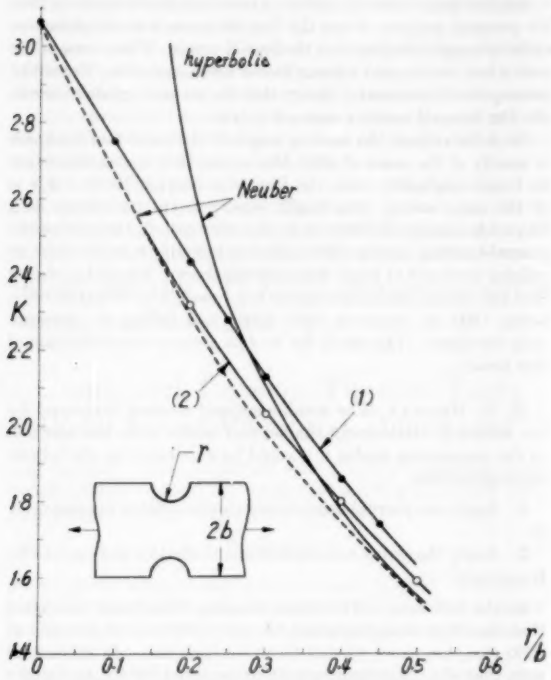

FIG. 3 STRESS-CONCENTRATION FACTORS FOR FLAT TENSION BARS WITH SEMICIRCULAR NOTCHES
[(1) Exact values by Isida; (2) Measured values by Frocht]

concentration factor for a transverse hole in a cylindrical torsion member, one notable exception being the solution based on Föppl (6) for an infinitely small hole. The accuracy of the experimental data cannot be estimated in such a case; therefore we must rely on an indirect method by which the accuracy of data can usually be estimated if the curve connecting the measured points can be "naturally" extended to a theoretically known point at the limit of an infinitely small hole. There appear to be no definite data showing that the curve of Thum and Kirmser can be extended to the theoretical value 2 when $2r/D$ approaches zero. The data actually obtained by them and also by other previous investigators for similar problems, are limited to those on comparatively large holes and within the range of their experiments K always decreases with the decrease of $2r/D$. No definite evidence has yet been presented that K increases with the decrease of $2r/D$ in the vicinity of $2r/D = 0$. Until such experimental evidence is forthcoming, the conclusion that there is an optimum ratio of hole-to-shaft diameter for which the maximum stress is a minimum must be viewed with great caution, because such a conclusion is quite contrary to usual practice.

Not only the location of the regions of maximum shear stress on the surface of the shaft (Fig. 5 of the paper) but also the magnitude of the stress are in good agreement with those expected by the theoretical results for an infinitely small hole (6), Fig. 8. The thickness of the coating metal is 0.01 mm and that of flecks produced by cylic stress is below 0.001 mm, namely, below one one-hundredth of the depth of cracks in brittle coatings usually employed. Hence the location of maximum shear stress described is not attributed to the coating characteristics. If a shaft be submitted to cyclic bending instead of to torsion, however, the shear stress on the surface of the shaft is largest at the hole edge as is shown in Fig. 4, herewith (cf. Fig. 5 of paper for torsion), but the shear stress occurring there is not a peak stress either in torsion or bending.

The shear stress at the hole edge (not on the surface of the shaft but within the bore) nearest to the peak point n may be larger, in some instances, than that at the peak point m. But the shear stress occurring at the hole edge is not essential because it is located in the same region of the peak stress at n, as is shown in Fig. 7 of the paper.

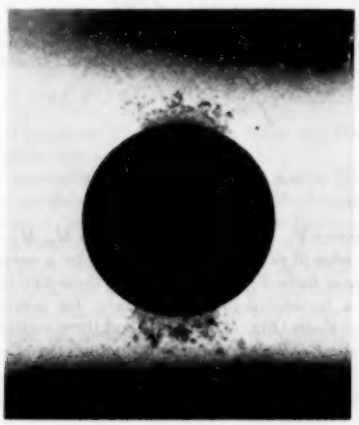

FIG. 4 CHANGE IN COLOR AT THE HOLE EDGE, BENDING

Nevertheless, the authors are glad to accept the kind suggestions of Mr. Leven and his further suggestions on any improvement of the electroplating method would be appreciated.

BIBLIOGRAPHY

1 "Torsional Stress Concentrations in Shafts of Circular Cross-Section and Variable Diameter," by L. S. Jacobsen, Trans. ASME, vol. 47, 1925, p. 619.

2 "A Photoelastic Re-Examination of Notched Tension Bars," by M. M. Frocht, R. Guernsey, Jr., and D. Landsberg, JOURNAL OF APPLIED MECHANICS, Trans. ASME, vol. 74, 1952, p. 124.

3 "On the Tension of the Strip With Semi-Circular Notches (in Japanese)," by M. Isida, Trans. Japan Society of Mechanical Engineers, vol. 19, 1953, p. 5. His analysis is based on C. B. Ling but is greatly improved in the way of numerical computations.

4 "Designing by Photoelasticity," by R. B. Heywood, Chapman and Hall, Ltd., London, England, 1952, p. 187.

5 "Stress Concentration Factors for a Circumferential Notch in a Cylindrical Shaft," by H. Okubo, Memoirs of the Faculty of Engineering, Nagoya University, Japan, vol. 6, 1954, p. 23.

6 "Kerbspannungslehre," by H. Neuber, Julius Springer, Berlin, Germany, 1937, pp. 54, 135.

Load Distribution at the Intersection of Several Coaxia Axisymmetric Shells[1]

H. MARCUS.[2] The author deserves to be commended for his careful analysis of the shear and moment-distribution cycles.

His method of distribution is based on the assumption that the edges of the interconnected shells S_1, S_2, S_3...are subjected to

[1] By H. Becker, published in the June, 1955, issue of the JOURNAL OF APPLIED MECHANICS, Trans. ASME, vol. 77, pp. 232–234.

[2] Consultant, Mechanics Division, Code 6205, Naval Research Laboratory, Washington, D. C.

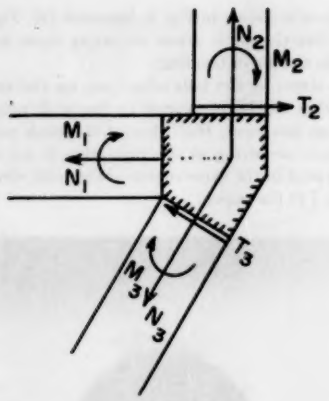

FIG. 1

horizontal forces V_1, V_2, V_3...and to couples M_1, M_2, M_3.... In reality, the edge of each shell is acted upon by a normal force N and by a shear force T; the resultant of these two forces is not necessarily a horizontal force. We have, for instance, at the joint of three shells (Fig. 1) six forces and three couples. Taking only the horizontal forces into account implies that T_1 and N_2 can be disregarded and that $N_3 \sin \phi + T_3 \cos \phi = 0$.

A justification for the validity of these assumptions is very desirable.

AUTHOR'S CLOSURE

For simplicity it was assumed that no forces are applied to the system parallel to the common axis of the shells, nor was any shell restrained in such a manner as to develop such a force. Consequently, although Dr. Marcus is correct in his contention that the resultant force on each shell is not necessarily horizontal, it will be so in view of the above assumption. This situation pertains principally to the example discussed in the paper.

Inertia Forces in Lubricating Films[1]

J. A. COLE.[2] The examination of the Navier-Stokes equations for the steady flow of an incompressible fluid on the basis that the inertia terms are of the same order of magnitude as the viscous terms is the starting point of boundary-layer theory, and the author's elegant analysis virtually duplicates the standard approach.[3,4] It is not essential to work in cylindrical co-ordinates, and the same result can be simply achieved by examination of the orders of magnitude of the terms of the Navier-Stokes equations in their Cartesian form. If L is the representative bearing length, h the representative film thickness, and U the bearing-surface velocity, the inertia terms $\rho u(\partial u/\partial x)$, etc., can be shown to be of order $\rho U^2/L$, and the significant viscous term $\mu(\partial^2 u/\partial z^2)$ to be of order $\mu U/h^2$. Thus for the inertia terms to be of the same order as the viscous terms, $Uh/\nu \backsimeq L/h$, equivalent to the author's result.

Another important conclusion in boundary-layer theory is that the pressure gradient across the film thickness is small, being one order of magnitude less than the inertia terms. Thus, even in the case when inertia and viscous forces are comparable, Reynolds' assumption in lubrication theory that the pressure gradient across the film is small remains reasonably true.

Since the ratio of the bearing length to the mean film thickness is usually of the order of 1000, this means that inertia effects are no longer negligible when the Reynolds number $\mathrm{Re} \equiv Uh/\nu$ is of the same order. One might expect actual turbulence at a Reynolds number of 2000, as in pipe flow but, in the case of the journal-bearing, inertia effects lead to instability in the form of cellular vortexes[5] at lower Reynolds numbers. Taylor has shown that the critical Reynolds number is a function of clearance ratio, being 1300 at clearance ratio 0.001 and falling as clearance ratio increases. The result $\mathrm{Re} \backsimeq L/h$ gives a clear indication of this trend.

M. D. HERSEY.[6] The nondimensional method developed by the author is attractively simple, and might seem less abstract to the engineering reader if it could be illustrated by the following applications:

1 Apply the journal-bearing criterion to a fitted bearing ($c = 0$).

2 Apply the thrust-bearing formula to the two cases solved by Kingsbury.[7]

In the first case, a 37-in-diam bearing, Kingsbury concluded that the effect of inertia would be only 1/800 that of viscosity at 1000 rpm, ten times normal speed for that size. In the second case, that of a thrust bearing with linear speed 200 fps, he found a momentum pressure of 242 psi at inlet—nearly half the mean bearing pressure.

3 Compare present method with formulas and charts for inertia effects published by G. Kahlert.[8]

AUTHOR'S CLOSURE

Cylindrical co-ordinates were used in the paper only because centrifugal terms appear explicitly in this form of the Navier-Stokes equations, and one has the feeling that if any inertia terms are to be included certainly the effect of the centrifugal field should be.

To apply the criterion to a fitted bearing, the following procedure is suggested:

(a) Analyze the bearing according to conventional methods, i.e., neglecting inertia terms.

(b) Compute a mean film thickness h and a Reynolds number $\rho R\omega h/\mu$ based on this analysis.

(c) If $\rho R\omega h/\mu << R/h$, the inertia terms are indeed negligible. If the Reynolds number is of the same order as R/h, inertia forces are not negligible and the solution (a) is not to be relied upon.

In the first of Kingsbury's examples, the Reynolds number based on the mean radius and the mean film thickness is approxi-

---

[1] By R. S. Brand, published in the September, 1955, issue of the JOURNAL OF APPLIED MECHANICS, Trans. ASME, vol. 77, pp. 363–364.

[2] Department of Scientific and Industrial Research, Mechanical Engineering Research Laboratory, Lubrication and Wear Division, Thorntonhall, Glasgow, Scotland.

[3] "Modern Developments in Fluid Mechanics," edited by S. Goldstein, Oxford University Press, London, England, vol. 1, 1938, chapter 4.

[4] "Applied Aerodynamics," by L. Bairstow, Longmans, Green and Company, New York, N. Y., 1939, second edition, chapter 9.

[5] "Stability of a Viscous Fluid Contained Between Two Rotating Co-Axial Cylinders," by G. I. Taylor, Philosophical Trans. of the Royal Society of London, series A, vol. 223, 1923, pp. 289–343.

[6] Technical Consultant, U. S. Naval Engineering Experiment Station, Annapolis, Md. Fellow ASME. All statements offered are personal opinions of the discusser, not to be construed as official or reflecting the views of the Navy Department.

[7] "On Problems in the Theory of Fluid Film Lubrication, With an Experimental Method of Solution," by Albert Kingsbury, Trans. ASME, vol. 53, 1931, pp. 66–67, sections 9 and 10.

[8] "Der Einfluss der Trägheitskräfte bei der hydrodynamischen Schmiermitteltheorie" (Influence of Inertia in the Hydrodynamic Theory of Lubrication), by G. Kahlert, *Ingenieur-Archiv*, vol. 16, 1948, pp. 321–342.

mately 35, while R/h is about 13000. That is, the inertia forces are negligible even at 1000 rpm.

In the second problem Kingsbury is considering the conditions at the entrance to a lubricant film rather than the flow within the film itself. Here the significant length to be used in computing a Reynolds number is probably the depth of the oil supply groove. In the transition from the groove to a film hundreds of times smaller, inertia forces are probably significant.

The author regrets that he was not aware of the extensive work of Kahlert. The paper cited by Dr. Hersey presents an iteration procedure for taking account of the inertia forces in bearings with no side leakage. The correction due to the inertia terms is negligibly small when $\frac{Ul}{\nu}\left(\frac{h}{l}\right)^2 << 1$, which is equivalent to the conclusion of the present paper.

Combined Tension-Torsion Tests With Fixed Principal Directions[1]

C. Torre.[2] These important tests give one qualitative functional relation between the octahedral shearing stress and octahedral shearing strain (Fig. 6 of the paper)

$$\bar{\tau}_{\text{oct}} = f(\gamma_{\text{oct}}) \quad \ldots\ldots [1]$$

similar to the author's earlier tests without torsion. It is sound procedure that the stresses and strains are related to the deformed bodies, as in this fashion $\bar{\tau}$ becomes the true shearing stress and $\bar{\gamma}$ the natural shearing strain.

A quantitative mathematical investigation to this and other papers from Davis would be important. The limit condition of ductile metals can be given by a surface of second degree, for example a paraboloid with a circular section[3] of the form

$$\left.\begin{aligned}(\sigma_1 - \sigma_2)^2 + (\sigma_2 - \sigma_3)^2 + (\sigma_3 - \sigma_1)^2 \\ + 2(c-1)\sigma_T(\sigma_1 + \sigma_2 + \sigma_3) = 2c\sigma_T{}^2\end{aligned}\right\} \ldots [2]$$

with

$$c = \sigma_C/\sigma_T$$

We also must know here, in addition to the author's results, the compression strength σ_C and the tension strength σ_T of the same test materials.

For the anisotropic metals, for example, a limit function can be given as an elliptic paraboloid

$$\left.\begin{aligned}(\sigma_1 - \sigma_3)^2\left(1 - 2\frac{3c_1{}^2 - 1}{4c_1{}^2 - 1}\right) + (\sigma_1 - \sigma_2)^2 + (\sigma_2 - \sigma_3)^2 \\ + 2\left(1 - \frac{3c_1{}^2 - 1}{4c_1{}^2 - 1}\right)(c-1)\sigma_T(\sigma_1 + \sigma_2 + \sigma_3) \\ = 2\left(1 - \frac{3c_1{}^2 - 1}{4c_1{}^2 - 1}\right)c\sigma_T{}^2\end{aligned}\right\} \ldots [3]$$

with

$$c = \sigma_C/\sigma_T \quad \text{and} \quad c_1 = \tau_V/\sigma_C$$

where τ_V is here the torsion strength.

With $c = 1$ or $\sigma_T = \sigma_C$ Equation [2] becomes the Mises-Hencky limit condition. For $\tau_T = \pm\sigma_C/\sqrt{3}$ Equation [3] reduces to Equation [2]. The terms $c > 1$ and $c_1 > 1/\sqrt{3}$ then indicate here the anisotropic effect of the metals.

We can make Equation [3] more useful for computing the anisotropic effect of metals, if we make a rotation about the axis ϑ_1 of the elliptic paraboloid in the co-ordinate system $(\vartheta_3, \vartheta_2, \vartheta_1)$ with the following transformations

$$\left.\begin{aligned}\vartheta_3 = -\frac{1}{\sqrt{2}}(\sigma_1 - \sigma_3), \quad \vartheta_1 = \frac{1}{\sqrt{3}}(\sigma_1 + \sigma_2 + \sigma_3) \\ \vartheta_2 = -\frac{1}{\sqrt{2}}[(\sigma_2 - \sigma_3) - (\sigma_1 - \sigma_3)]\end{aligned}\right\} \ldots [4]$$

The equation of the elliptic paraboloid is

$$\vartheta_3{}^2 + A\vartheta_2{}^2 + B\vartheta_2\vartheta_3 + C\vartheta_1 = D \quad \ldots\ldots [5]$$

With $C = 0$ Equation [5] becomes the Mises and Hill limit condition for anisotropic ideal plastic bodies.[4]

The four constants A, B, C, and D in Equation [5] can be determined by most simple tests; namely, by the tension, compression, and torsion tests and one more for the fourth constant, for which any limit Mohr's circle can be chosen.

It will be worth while and most interesting to carry out these tests in order to determine the constants in Equations [2], [3], and [5]. These tests will then make it possible to compute the stress distributions in the test specimens used by the author. For the strain-rate computation it is recommended that one use Prof. H. Geiringer's[5] theory of the plastic strain rate, in addition to the conditions suggested by other writers cited by the author.

Author's Closure

The remarks of Dr. Torre are very interesting and encouraging. The author is hopeful that the time will soon come when sufficient test data on one material will be available for the determination of a complete limit condition. Unfortunately the required experimental program would be quite costly. The chief obstacle is an economic one.

Fracture of Inoculated Iron Under Biaxial Stresses[1]

D. Fitzgeorge.[2] The writer would like to thank the authors for producing a very interesting paper bearing on a problem which occupied him for some time at the University of Nottingham, England. The results obtained from the tests should be directly applicable in design work, and for that reason are a valuable addition to knowledge. It is surprising that the "scatter" of experimental points in Fig. 3 of the paper is so small, bearing in mind that rigid clamps were used for holding the specimen and the wall of the tube was so thin. The writer would have been rather reluctant to test a hollow specimen with a wall as thin as that used. Its thickness is only twice the average graphite flake length; probably creating conditions different from those in a thicker piece of cast iron as normally used. It would appear, however, from the consistency of the results that this did not

---

[1] By E. A. Davis, published in the September, 1955, issue of the Journal of Applied Mechanics, Trans. ASME, vol. 77, pp. 411–415.

[2] Staff Scientist, Reed Research Inc., Washington, D. C.

[3] "Influence of the Middle Principal Stress on the Condition of Flow and Failure," by C. Torre, *Osterr. Ingenieur-Archiv*, vol. 1, 1946, pp. 316–342.

[4] "Mechanik der plastischen Formänderung von Kristallen," by R. von Mises, *Zeitschrift für angewandte Mathematik und Mechanik*, vol. 8, 1928, pp. 161–185; "The Mathematical Theory of Plasticity," by R. Hill, Clarendon Press, Oxford, England, 1950.

[5] "Some Recent Results in Theory of an Ideal Plastic Body," by Hilda Geiringer, *Advances in Applied Mechanics*, vol. III, 1953, pp. 197–294.

[1] By I. Cornet and R. C. Grassi, published in the June, 1955, issue of the Journal of Applied Mechanics, Trans. ASME, vol. 77, pp. 172–174.

[2] Senior Research Engineer, B. S. A. Tools, Limited, B. S. A. Group Machinability Laboratory, Birmingham, England.

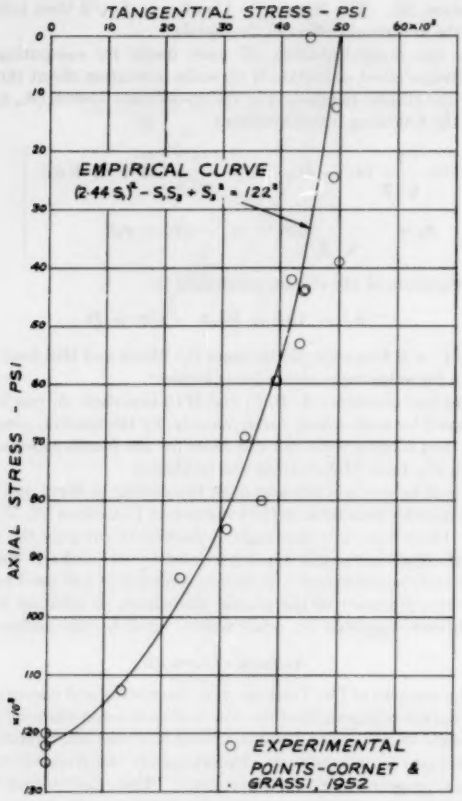

FIG. 1

affect seriously the comparative strengths of the tubular specimens used in the tests, but probably accounts to some extent for the (reasonable) discrepancy recorded by the authors between the strengths of solid and tubular specimens.

The concept of a stress-concentration factor K is useful in conjunction with the distortion-energy plasticity criterion to derive Equations [2] and [3], although deformation of cast iron actually takes place rather differently from the way which is inferred in the paper. The failure of a test piece is assumed to occur when the combined stresses at a vital point at the edge of an idealized graphite flake become equivalent to the yield strength of the matrix in simple tension (S_0). If this were so, the stress-strain curve for cast iron would be a straight line terminating at fracture. The curve is, however, not straight even at very small loads. This curvature is evidence of localized plastic flow in the vicinity of graphite flakes, which can be verified by removal of the load and the observation of permanent set.

Using the well-known expression

$$\left(1 + \frac{2a}{b}\right)$$

for the stress-concentration factor at the edge of an elliptical hole in a plate, we have that when the major axes are in the ratio 16 to 1 (which might be taken as the approximate ratio of length to width of a graphite flake) the factor has the value 33. Furthermore, since the expansion coefficient of graphite is much lower than that of the matrix material, the graphite will be in a state of hydrostatic compression due to solidification and subsequent cooling. The normal stresses between the graphite and the matrix metal will be compressive, but the tangential stresses at the edges will be tensile and probably at or near the yield stress. Thus at any time—initially, under load or after unloading—a piece of cast iron will be in a heterogeneous state of stress which may only be understood in a qualitative way. Any attempt to acquire a quantitative understanding must take the form of the analysis of simplified concepts or the determination of statistical averages from actual tests. The present paper falls under the latter classification. The quantity K may be considered as an average stress-concentration factor just prior to fracture when the stresses throughout have reached a maximum state of redistribution suitable for brittle crack propagation.

The writer is not happy about the theoretical curves in the tension/compression quadrant, which show a consistent discrepancy with the experimental points. It is assumed in the derivation of Equation [3] that there is no stress concentration due to a compressive load. This would only be true if the matrix material and graphite had the same elastic moduli (Young's modulus for graphite is about 1.2×10^6 psi). In the absence of a more precise basis for Equation [3], the equation as it stands might be modified to give a better fit for design purposes. A few quick "trials" have shown that the equation

$$(2.44S_1)^2 - S_1S_2 + S_2^2 = 122^2$$

gives quite a good fit for the inoculated iron results (see Fig. 1.)

AUTHORS' CLOSURE

The authors wish to thank Mr. Fitzgeorge for his comments. As he has pointed out, these studies on fracture under biaxial stresses have produced results which are directly applicable in design work. Investigations now in progress at the University of California are furnishing evidence that fracture of brittle materials is governed essentially by a flow criterion. The use of a distortion-energy criterion modified by a stress-concentration factor[3] permits generalizing a great deal of data on failure of materials under biaxial stresses. It may be shown that octahedral shear stress and effective stress relationships are related to the distortion-energy criterion and that all these relationships apply equally well.[4]

The inoculated iron investigated had graphite flakes of length approximately one third the thickness of the tube wall. The gray cast iron previously investigated did, however, have flakes half as long as the thickness of the tube wall. As Mr. Fitzgeorge has noted, the use of thin sections of such a heterogeneous structure would give rise to marked size effects.

Stress-strain curves for gray cast iron show marked curvature, even at low stresses. Analysis is further complicated because the modulus of elasticity depends on the state of stress, and because cast iron departs appreciably from the law of constancy of volume.[5]

It would be most desirable to be able to correlate the stress-concentration factor K with microstructural features, but so far the authors have been able to do this only qualitatively. Length-to-thickness ratios obtained for graphite flakes in gray cast iron were about 18:1, and in inoculated iron these ratios were about 12:1. For a given notch size and shape, there is still a difference

[3] "A Criterion for the Failure of Cast Iron," by John C. Fisher, ASTM Bulletin No. 181, April, 1952.

[4] "The Physical Meaning of the Stress Invariants of the Theory of Plasticity," by V. V. Novoshilov, Applied Math. and Mechanics, Academy of Science of USSR Publ., vol. 16, pp. 617–619, 1952.

[5] "The Flow and Fracture of a Brittle Material", by L. F. Coffin, Jr., JOURNAL OF APPLIED MECHANICS, Trans. ASME, vol. 72, 1950, pp. 233–248.

between the stress-concentration effect due to a single notch as compared to the effect of many notches in a structure.[6]

The authors concur with Mr. Fitzgeorge that the use of an average value of 122,000 psi rather than the value of 125,000 psi for compressive strength in the stress-concentration modified-distortion-energy theory gives a better fit for the data. However, the modified-distortion-energy theory used by the authors is based on a phenomenological approach in that the limits of biaxial stress can be determined by a tension test and a compression test.

Mr. Fitzgeorge has observed that the stresses between the graphite and the ferrite in the cast iron will make it difficult to analyze quantitatively the state of stress at a graphite flake. The notch concentration factor K should therefore be considered an averaging factor, useful for engineering purposes in flow and in fracture criteria. The notch concentration factor K integrates mechanical and metallurgical effects; it can serve to give useful information in the same way that compressibility factors or fugacities are used by engineers.

A Kinematic Notation for Lower-Pair Mechanisms Based on Matrices[1]

A. E. Richard de Jonge.[2] When about 13 years ago the writer drew attention before this Society to the then very neglected state of the sciences of mechanisms and kinematics in the United States, he had in mind to start a revival of these sciences in this country. He is very happy to state that his efforts have not been in vain. Among the papers that have appeared during this period up to the present time, one of fundamental interest is that by the authors who have been kind enough to send the writer a copy of it with the request to present his comments to it. Inasmuch as some of the references given in it were not available, they also sent the writer, upon inquiry, a reprint of a paper they published recently.[3] It is on these two communications that the remarks of the writer are based.

As has occurred on previous occasions, the request by the authors puts the writer in the embarrassing position of having to state his views which, unfortunately, differ somewhat from those of the authors.

It is true that the introduction by the authors of the matrix method into the field of kinematics and mechanisms is new; at least the writer has not seen it used previously. For this step forward the authors deserve certainly full credit, for it is only by exploiting all possible approaches that we can arrive, ultimately, at a clear insight into the problems that we have to face in kinematics, and at the simplest and most effective methods of dealing with them.

It is also true that Reuleaux's attempt to set up a symbolic notation useful not only for the analysis, but also for the synthesis of mechanisms composed of rigid bodies was only partly successful. He had in mind the creation of a symbolic notation somewhat like that in chemistry. His notation, admittedly, was cumbersome and has never been widely applied to the synthesis of mechanisms either by himself or his followers. Inasmuch as the writer studied kinematics under Reuleaux's direct successor, W. Hartmann, he is very well acquainted with the advantages and shortcomings of Reuleaux's symbolic notation.

The authors have attempted to create a new symbolic representation of mechanisms made of rigid materials, by using all parameters that enter into the description of such mechanisms and of their motions. For this purpose they took the fundamental concept of the element pair, created by Reuleaux, and used it in their representation without, however, inquiring first how this concept is arrived at or what it entails. Therein lies one serious weakness of their method, for by adopting this concept a priori, they have been able to apply their method only to the so-called "lower," but not to the "higher" element pairs, as Reuleaux has called them. In the absence of any better and readily acceptable terms, these shall still be used here wherever required.

The method of notation adopted by the authors uses both the links and the parameters of the element pairs of the mechanisms. These are assembled in matrices which, while apparently satisfying all needs for describing the configuration of mechanisms and their motions, deal only with mechanisms having binary links and lower element pairs. In their article,[3] they have considered mechanisms up to five lower element pairs, but have actually dealt completely only with those which have four binary links and four lower pairs. Therein lies the second weakness limiting the use of the matrix method.

There is, further, the difficulty of setting up and evaluating correctly the matrices, particularly for mechanisms in space. One has to be very familiar with matrix algebra and be very careful in the evaluation to avoid mistakes. Inasmuch as the method is intended by the authors as a design method, it is necessary to realize that the use of matrix algebra is, as yet, beyond the realm of mechanical-design engineers and draftsmen. Besides, it is very easy for the authors to make the matrix method appear very simple by presenting only the results of the matrix evaluations, thus concealing the great amount of careful work necessary for such evaluations. It may be seen from the paper how complex and unwieldy the matrix multiplications get, and what steps have to be taken to reduce the amount of tedious work. The final equations given are only the results of the matrix multiplications.

To the writer, it appears unlikely that the matrix method will be used widely by design engineers in the foreseeable future. It is, most certainly, useful to the academic man, that is, to the kinematician, but is, as yet, beyond the reach of the average designer and draftsman who would have to use it. For them, a symbolic method must be simple and require only ordinary mathematical methods well known to them.

Now, let us see why the new method, established by the authors, is so complex. In the first place, it attempts to describe mechanism types, and this was the purpose for which Reuleaux had created his notation method; in the second place, it is supposed to describe the movability of mechanisms; and in the third place, it attempts to set up the functional equations for their behavior in motion. These are three different and distinct purposes. In modern kinematics, they have been termed, respectively, type, number, and size analysis or synthesis as the case may be.

The first of these considers the mechanism type which depends solely on the combination of certain elements. The second considers the movability of the mechanism after it has been formed, and it depends solely on certain numerical relations involving the number of element pairs and links. The third deals with the functional relationship of the motions of the various elements, and it depends on the mechanism type, its movability, and, in particular, on the sizes of the various links or members.

To the writer, it seems simpler to consider these three different properties separately, as has been done in the past. That does not mean, however, that he is satisfied with the progress made so far.

---

[6] "Theory of Notch Stresses," by Heinz Neuber, J. W. Edwards, Ann Arbor, Mich., 1946.

[1] By J. Denavit and R. S. Hartenberg, published in the June, 1955, issue of the Journal of Applied Mechanics, Trans. ASME, vol. 77, pp. 215–221.

[2] Mechanical Engineer and Consultant, Reeves Instrument Corporation, New York, N. Y. Mem. ASME.

[3] "Systematic Mechanism Design," by J. Denavit and R. S. Hartenberg, *Machine Design*, vol. 26, September, 1954, pp. 167–175; vol. 26, October, 1954, pp. 257–265.

In fact, he has developed an entirely different approach which is quite general as far as type synthesis is concerned and which embraces the use of both lower and higher element pairs as well as multielement links. This method is simple, straightforward, and allows the determination of all mechanisms of a certain type systematically. It will be published in due course.

The methods of number synthesis to determine the movability of rigid-body mechanisms are well known and scarcely require any extensions.

The third type, the so-called size synthesis, determines the sizes of the various members in order to obtain a prescribed motion, or the determination of the motion when the sizes of the members and their types and movability are known. This, of course, is of great importance in actual applications.

The authors have shown the application of the matrix method to the simplest form of mechanism only, namely, to four-link mechanisms with their derivatives and degenerations. A different method was published recently by Freudenstein who used a simple geometrical method based, however, on highly theoretical work. Whether or not his method, which also applies only to four-link mechanisms and their derivatives, can be extended to more complex mechanisms has still to be investigated. The authors, too, have yet to show how their matrix method can be used for more complex mechanisms. Theoretically, it seems that it can be done, but the results and the calculations will be very complex.

From these remarks, it will be clear that the mixing up of these three different functions in one process cannot but make the matrix method complex. It was the cumbersomeness of Reuleaux's extended notation formulas that prevented their extensive use, while his contracted type symbols were much used by him and his followers and successors. The matrix method, too, is a cumbersome notation method and, besides, it will always require a picture, or diagram, of the mechanism, to be understood correctly. Since it does not do away with such diagrams, one may ask the question: what does it really accomplish that could not be done by the simpler methods in existence?

Let us look at the two examples given by the authors to illustrate their method. The equations for the coaxial triple-screw mechanism and its derivatives were given by Reuleaux,[4] by means of the simplest kind of mathematics. The equations of motion for the Hooke's or universal joint were also given, even before Reuleaux, by simple elementary mathematics in England. The examples discussed show the relative complexity of the matrix method as compared with the simple methods which have just been cited.

What, however, will the authors do if they have to deal with more complex mechanisms of six, eight, or more links? While it appears possible that the matrix method could be used by applying it in much the same way as in the mesh method of electric circuits, yet it seems that it will become still more complex, or even prohibitive, on account of the evaluation of the products of six or more matrices.

It may not be permissible here to comment on the paper published by the authors in *Machine Design*.[3] Yet, it completes the picture and also the correct evaluation of the matrix method. For this reason, a few words may be said about it. In it, the authors have given a catalog of "all" the mechanisms possible with binary links and up to five lower pairs. It appears doubtful, however, that all possibilities have been exhausted. At any rate, it does not present a clear grouping of the movable mechanisms, nor does it give their simplest forms. Their application to the design of a specific mechanism proves only that it also can be done by the matrix method. However, it can just as well be done by the elementary methods known.

Being mindful of Lord Kelvin's statement that "a problem is never solved until it is reduced to its simplest terms," it seems to the writer that the matrix method, though being new in kinematics, accomplishes no more that the known methods do, and has the disadvantage of requiring the acquisition of matrix algebra which cannot be learned overnight. It is, therefore, questionable whether the time necessary to acquire it will be worth the advantages claimed for this new notation method which is even more cumbersome than Reuleaux's notation.

However, the writer would like to thank the authors again for the great amount of work which they must have put into evolving this new method of notation, and he repeats that it is only by investigating all avenues of approach that we can arrive at the simplest and most effective methods for the study of mechanisms and their kinematics. For having so richly contributed to this aim, the authors deserve the highest praise.

A. W. Wundheiler.[5] The unfortunate absence of a general linkage theory arises from a profound and permanent reason: All linkage problems lead to a set of simultaneous second-degree equations, and the mobility of a linkage depends on the existence of real solutions of such a set. The celebrated theorem of Abel-Ruffini expresses, in part, the formidable difficulty of this problem; there is no general solution of an equation of degree exceeding four, in terms of radicals. As a result, the only existing wisp of a theory is highly limited to the simple case of a four-bar linkage with all the pairs axial (that is, sliding, turning, or cylindrical). This theory was developed by Dimentberg in 1948, as quoted in the paper. The difficulty of the problem is also reflected in the failure of a 50-year earnest effort of the Russian school (Assur, Artobolevskij, Dobrovolskij, etc.) to find a formula for the actual mobility of a linkage, in contrast to the minimum mobility given by Grübler's familiar expression.

The paper under discussion uses the phrase "all lower pair linkages" in the sense "all simple-chain axial-pair linkages." The paper's assertion that all other pairs (i.e., plane and spherical) are reducible to a combination of axial pairs is technologically invalid because such a reduction changes the production, tolerances, and the dynamics of the linkage (self-locking is a most important consideration in spatial mechanisms). All ramified mechanisms (common engine gearing, linkage computers) are excluded. This eliminates another formidable problem, that of the topological equivalence of linkages which stymied the prodigious work of V. F. Assur 50 years ago.

For an all-axial closed chain of pairs, the paper proposes a certain graphical arrangement of symbols for the kind of pair and symbols for the relative positions of the pair axes. The resulting *schema* symbolizes a "configuration of axial pairs" of a stated kind. The symbols for relative positions consist of four symbols for angles and distances used previously by Dimentberg as component of Clifford-Study numbers ($a + ob$, a, b real, $o^2 = 0$; also called "dual") in his theory of axial four-bar linkages. Whether the configuration symbol determines a mechanism cannot be decided until the corresponding set of algebraic equations is sufficiently investigated for existence of real solutions; that is, until the fundamental problem is solved for the tentative linkage. Whether two configuration *schemata* represent the same mechanism cannot be told until the algebraic equations are solved for the performance of each pair within the mechanism. The difficulty of this last problem is illustrated by the celebrated Bennett mechanism.

The configuration *schema* proposed is not "manipulative" (in

[4] "Theoretische Kinematik II—Die praktischen Beziehungen der Kinematik zu Geometrie und Mechanik," by F. Reuleaux, Braunschweig, Germany, 1900, pp. 391–395.

[5] Illinois Institute of Technology, Chicago, Ill.

the sense of the paper) because there does not exist a formal algebra in terms of pair-kind symbols and position symbols. It becomes "manipulative" if the symbols for position (of one pair-axis relative to the preceding one) are replaced by 4×4 matrices introduced by Euler in 1776. This matrix algebra failed, so far, to produce any significant results in spatial finite-displacement theory, a condition which led to the invention of many ingenious devices (Clifford numbers, Hamilton's quaternions, Ball-Study-von Mises motors, Clifford quaternions) for eliminating matrices. In linkage theory, the only fragmentary success known to this writer has been by Dimentberg's use of Clifford-Study numbers.

The applications given in the paper are confined to three well-known degenerate mechanisms, two of them plane (the slider crank and a coaxial-screw chain), and one spatial (the universal joint). The excessive labor arising here from the use of the matrix method should not be confused with the real reason of its impotence.

Authors' Closure

The purposes of the paper (as stated in the abstract) are (1) to formulate a symbolic notation, and (2) to exploit the symbolic notation by means of a matrix interpretation permitting displacement analysis. For the study of single-loop plane mechanisms of certain lower pairs, the subject of the *Machine Design* paper mentioned by Mr. de Jonge,[5] matrices are not needed and were not invoked. Matrices were not used for the "design of a specific mechanism." With plane mechanisms, geometric constructions and procedures may be followed readily; with space mechanisms of any complication a formalized approach, independent of geometrical aids, is desirable for the study of displacements. The symbolic notation and matrix method furnish such an approach, for once the symbolic equation is known, the pertinent matrices may be set up to deliver the displacement relations.

For space mechanisms the matrix method is a reliable analytical tool that, while laborious, is nevertheless straightforward. The working knowledge of matrices necessary for the use of this method may be learned within a short time; it is comparable in difficulty to ordinary algebra.

The separation of the theory of mechanisms into "type, number, and size analysis and synthesis" is not as clear as Mr. de Jonge indicates. While these three areas may be seen, they are not completely independent of each other. An early simultaneous consideration of all factors may have certain advantages.

The catalog given in *Machine Design* is restricted to single-loop plane mechanisms of lower pairs R and P. Within this framework the catalog is complete, for it lists all possible combinations of revolute and prism pairs together with their parameters.

The examples were not of complex mechanisms; they were deliberately chosen from the familiar and simple to demonstrate the method. Professor Wundheiler is in error in designating the coaxial screw-chain as a plane mechanism; it, like any mechanism containing a screw, is a space mechanism.

A general theory of mechanisms might include at least three distinct problems: (1) The establishment of the pertinent parameters—as is done by the symbolic notation; (2) the determination of the functional relations of the displacements—as is done by the matrix method; and (3) a general solution of the displacement equations. This third problem, as Professor Wundheiler points out, has not been solved, and it should be noted here that it is beyond the scope of the paper. However, solutions of particular cases can be obtained with numerical methods.

The symbolic notation does apply to cylindrical, spherical, and plane pairs, for the objections raised by Professor Wundheiler in terms of production tolerances and dynamics of the linkage are not pertinent to the problem at hand. Mathematically true lower pairs and rigid parts have been assumed.

The most general mechanism of four revolutes is described by the symbolic notation as

$$R_1 \begin{vmatrix} a_1 \\ \alpha_1 \\ \theta_1 \\ s_1 \end{vmatrix} \quad R_2 \begin{vmatrix} a_2 \\ \alpha_2 \\ \theta_2 \\ s_2 \end{vmatrix} \quad R_3 \begin{vmatrix} a_3 \\ \alpha_3 \\ \theta_3 \\ s_3 \end{vmatrix} \quad R_4 \begin{vmatrix} a_4 \\ \alpha_4 \\ \theta_4 \\ s_4 \end{vmatrix} = I$$

Such a mechanism may be closed and possess mobility for only certain values of the parameters. Thus, if every α is zero, the plane four-bar linkage results. If all parameters a and s are zero, the spherical four-bar linkage results. If all parameters s are zero, and $a_1 = a_3$, $a_2 = a_4$, $\alpha_1 = \alpha_3$, $\alpha_2 = \alpha_4$ with $a_1/\sin \alpha_1 = a_2/\sin \alpha_2$, the movable Bennett mechanism results.

From the very beginning the geometric analyses of the Bennett mechanism "have been beset by pitfalls and unfortunate mistakes since it was conceived by Bennett."[6] These difficulties seem to have been due to loose definitions of the parameters involved; the precise information of the symbolic notation eliminates these troubles.

The question of movable four-revolute mechanisms was considered by Dimentberg.[7] He concluded that they number three—the plane four-bar, the spherical four-bar, and one he recognizes as the Bennett. It is important to note that he started with the unspecified assumption that all the parameters we call s are zero; his proof is not rigorous in that it doesn't show that they must be zero to allow movability.

Since the publication of the paper, the authors have generalized the method[8] to mechanisms with several closed kinematic chains (mechanisms having ternary, quaternary links, etc., or "ramified" mechanisms). This is simply done by writing several symbolic equations for as many closed kinematic chains as are necessary to include all pairs. Higher pairs have been included in the theory, and the method of displacement analysis using (4 × 4) real matrices, which is admittedly cumbersome, has been simplified by using (2 × 2) dual-number matrices.[9] Many examples of space mechanisms have also been studied.

The Extended Theory of the Viscous Vibration Damper[1]

R. Plunkett.[2] The author has again made a very interesting and important practical contribution to the theory of torsional vibrations of complex systems. It is interesting and perhaps informative to approach the same problem from the standpoint of impedance theory. If we split the system at the point of application of the force (torque) into two halves, the displacement impedance of the left-hand half Z_L is pure real, that of the right-hand half Z_R, which contains the damper, is complex of the form

$$Z_R = \frac{c_a + jb\omega c_b}{c_a + jb\omega c_d}$$

---

[5] "New Five-Bar and Six-Bar Linkages in Three Dimensions," by M. Goldberg, Trans. ASME, vol. 65, 1943, p. 661.

[6] Reference (6) of the paper.

[7] "Die Darstellung und Handhabung der niederen Elementenpaare in einer auf Matrizenrechnung gegruendeten Zeichensprache," by R. S. Hartenberg, VDI-Berichte, Band 12 (to be published about January, 1956).

[8] "Description and Displacement Analysis of Mechanisms Based on (2 × 2) Dual Matrices," by J. Denavit, PhD Dissertation, Northwestern University, Evanston, Ill. (completed October, 1955, but carrying the University's date of June, 1956).

[1] By F. M. Lewis, published in the September, 1955, issue of the Journal of Applied Mechanics, Trans. ASME, vol. 77, pp. 377–382.

[2] Vibration Engineer, General Engineering Laboratory, General Electric Company, Schenectady, N. Y. Assoc. Mem. ASME.

as is pointed out by the author, or can be established by network theory for the case of a single damper b. The total impedance then is the sum of Z_L and Z_R. Since this is a linear system, if the critical section (A in the paper) is in the left-hand section, its amplitude is proportional to the amplitude and thus the impedance of the point of application of the load.

The total impedance, $Z_0 = Z_R + Z_L$, then may be reduced to the form

$$Z_0 = \frac{c_1 + jb\omega c_2}{c_3 + jb\omega c_4}$$

or

$$\frac{x}{F} = \frac{c_3 + jb\omega c_4}{c_1 + jb\omega c_2}$$

It can be shown that this same form will be valid for any displacement x_i with different frequency-dependent constants c. Thus

$$\left|\frac{x}{F}\right|^2 = \frac{c_3^2 + b^2\omega^2 c_4^2}{c_1^2 + b^2\omega^2 c_2^2}$$

which is independent of b if

$$\frac{c_1}{c_2} = \pm\frac{c_3}{c_4}$$

(It may be noted in passing that the $\pm$ sign in Equation [21] of the paper is incorrect since these constants are already squared in his derivation. This does not invalidate the subsequent work.) If we use the positive sign we have the case of no motion across the dashpot; i.e., antiresonance across the dashpot for this position of force and this frequency. If we use the negative sign we have the case where the impedance vector is of constant amplitude and variable phase and describes a semicircle, with center at the origin in the impedance-phase plane, as b varies from 0 to ∞.

The impedance approach also offers some interesting possibilities as far as plotting the curves is concerned. For example, in Fig. 1 of the paper, the $b = 0$ curve is independent of the damper mass; the $b = \infty$ curve is found from it by adding $-\omega^2 m$ to the input impedance curve with due regard to sign. The transfer impedance, which is plotted in Fig. 1, is then found by multiplying the input impedance by a frequency-dependent transfer coefficient which is independent of b.

This same approach will also serve for the more general case of the determination of optimum damping of continuous systems of any type and will be the basis for a paper now in preparation.

The Accuracy of Donnell's Equations[1]

F. V. Pohle[2] and N. Perrone.[3] The value of this paper is that results obtained from Donnell's characteristic equation are compared with similar results from Flügge's equation and limits are set which state when the latter are suitably approximated by the former.

It is important to note that the full equations were used in each case and that no intermediate approximations were made; in all too many papers various terms are simply discarded from a differential equation and little attempt is made at a more rigorous treatment. Even though only solutions to the characteristic equation have been compared, the conclusions are of importance. The boundary conditions must influence the results but it is difficult to see how more useful information can be obtained without excessive labor.

In the first method of solution to the homogeneous Donnell equation, w is given by the author's Equation [4]. The results listed in Table 1 of the paper depend upon the two parameters (a/h) and (a/L). It is unfortunate that when w is assumed in the form given by the author's Equation [20], the results, Table 2, depend only upon (a/h); thus no dependence upon the length is reflected in Table 2. The effect due to the length can be important and it is known to be most pronounced for an infinitely long shell.

To show this effect, the following problem was solved using both the Donnell equation and the Flügge equation: Assume a self-equilibrating radial line load at $x = 0$, corresponding to $n = 2$, and determine the deflections w_D (0, 0) and w_F (0, 0) for an infinitely long shell; $(a/h) = 100$, $K = 12.854$, and $\nu = 0.3$. Quantities with subscript D refer to the Donnell equation and similarly F refers to the Flügge equation. The entire calculation can be carried out explicitly for the Donnell equation, but the Flügge characteristic equation and the four simultaneous linear equations which arise from the boundary conditions at $x = 0$ must be solved numerically. The final result is

$$w_F/w_D = 1.512 \qquad \text{at (0, 0)}$$

Thus the error is +51.2 per cent, based upon the Donnell value as a standard. This is a large error and it is instructive to discuss it in more detail.

For the values stated previously, the Flügge characteristic equation can be obtained from the author's Equation [25]

$$p_F^8 - 15.4p_F^6 + 109{,}272p_F^4 - 151.2p_F^2 + 144 = 0 \quad [1]$$

The corresponding Donnell characteristic equation is

$$p_D^8 - 16p_D^6 + 109{,}296p_D^4 - 256p_D^2 + 256 = 0 \quad [2]$$

Equations [1] and [2] show that the coefficients of p^6 and p^4 are in good agreement, but that the coefficients of p^2 and the constant term are quite different. The values of p^2 are

$$\left.\begin{aligned} p_{1D}^2 &= 0.01170961 + i0.0483828; \quad p_{2D}^2 \\ &= 7.998829 - i330.474215 \\ p_{1F}^2 &= 0.00691759 + i0.0362950; \quad p_{2F}^2 \\ &= 7.699308 - i330.473292 \end{aligned}\right\} \quad [3]$$

In the notation used by the author

$$\alpha = -0.41 \quad \beta = -0.25 \quad \gamma = -0.0372$$
$$\delta = -2.8 \times 10^{-4} \quad [4]$$

Since $K = 12.854$ and the results in Table 2 of the paper show only a slight variation with K, the results of $K = 10$ are in very good agreement with Equations [4], herewith. This confirms the validity of the approach used by the author to determine $\alpha, \beta, \gamma, \delta$.

The numerical results in Equations [3] of this discussion show clearly that large values of α and γ are not as decisive as large values of β, δ for the imaginary components are much larger than the real components. Since the complex numbers will be nearly vertical in the complex plane, a large error in the real part will

---

[1] By N. J. Hoff, published in the September, 1955, issue of the Journal of Applied Mechanics, Trans. ASME, vol. 77, 1955, pp. 329–334.

[2] Assistant Professor of Applied Mechanics, Department of Aeronautical Engineering and Applied Mechanics, Polytechnic Institute of Brooklyn, Brooklyn, N. Y.

[3] Research Assistant, Department of Aeronautical Engineering and Applied Mechanics, Polytechnic Institute of Brooklyn, Brooklyn, N. Y.

have little effect. Hence α, γ are not reliable guides to be used in judging the accuracy of the p^2-values.

Instead, it would have been more useful to have tabulated similar results for the p-values. In the present case

$$\left.\begin{aligned} p_{1D} &= 0.157429 + i0.153665; \quad p_{2D} \\ &= 13.0115 + i12.7004 \\ p_{1F} &= 0.136003 + i0.133435; \quad p_{2F} \\ &= 13.0050 + i12.7056 \end{aligned}\right\} \quad \ldots [5]$$

$$\alpha = -0.136 \quad \beta = -0.138 \quad \gamma = -0.00050 \quad \delta = +0.0041. [6]$$

Hence α, for example, is the error in the imaginary part of p_{1D}.

The larger roots in Equations [5] are in good agreement, but the smaller roots, which now have components of nearly equal magnitude, differ by a large amount. In comparing p_F^2 with p_D^2 it would be best to base the comparison upon the two amplitudes and the two arguments and to find the errors in these quantities. This is of more direct significance than information about the errors in the real and imaginary components separately. If it is assumed that

$$p_F^2 = p_D^2 (1 + q) \text{ where } (p_D^2 - n^2)^4 + 4K^4 p_D^4 = 0$$

then $[|1 + q| - 1]$ is the error in the amplitude, and the argument of $(1 + q)$ is the angular error. In this form the influence of the higher powers of q can be more accurately estimated; if only linear powers of q are retained, then substitution into the author's Equation [25] yields

$$q = -\frac{2p_D^6 - 6n^2 p_D^4 + 2n^2 p_D^2 [(4 - \nu)n^2 - 2 + \nu] + n^4(1 - 2n^2)}{4p_D^2 (p_D^2 - n^2)^2 + 8K^4 p_D^4 + 6\nu p_D^6 - 12n^2 p_D^4 + 2n^2[(4 - \nu)n^2 - 2 + \nu] p_D^2}$$

This expression can be reduced to simple form; in the important case $p_D^2 = p_{1D}^2$ a quick estimate can be made of the error in amplitude alone if the dominant terms only are considered. Clearly the term $n^4(1 - 2n^2)$ is the dominant one in the numerator and $8K^4 p_D^4$ is the dominant term in the denominator. Since

$$8K^4 p_{1D}^4 = -2 (p_{1D}^2 - n^2)^4 \text{ and } p_{1D}^2$$

is small compared with n^2, this quantity can be approximated by $(-2n^2)$. Then q is given by $(1 - 2n^2)/(2n^4) = -7/32 = 0.219$ and the error in the amplitude is also -0.219, which is in good agreement with the β-value of Table 2 ($K = 10$, $n = 2$). Naturally, this approximation will not yield the small difference which measures the error in the argument. An accurate calculation shows that the error in the argument is about 2 deg, or 0.035 radian, which is in agreement with the results of Equations [3]. The present approach not only provides the necessary information about the errors in amplitude and argument for p_{1D}^2 but since

$$p_{1F} = p_{1D} (1 + q)^{1/2} \cong p_{1D} (1 + q/2)$$

the necessary information about the p_1-values is also given rather directly.

In the Flügge solution, one of the boundary conditions is a shear condition which involves $w_{,zzz}$ and hence p^3. The value of p_{1D}^3 will differ considerably from that of p_{1F}^3 and the actual numerical work shows that this root dominates the calculation. Since $(1.137)^3 = 1.466$, the coefficients which depend upon p^3 will be in error by about 47 per cent; the final computed error in w is 51.2 per cent which is very nearly of the correct magnitude and it can be stated that, in general, the error in w will be about (-1.5) times the β-value of Table 2. This is not simply an observation based upon numbers alone but can be seen from the integral form of the solution which is based upon a representation of the load in the form of a Fourier integral. This form also shows that w depends essentially upon $(1/p^3)$ and therefore the error in w will be positive if β in Table 2 is negative.

The calculation of the p^2-values from Equation [1] of this discussion can be carried out easily if it is noted that

$$p_{1D} p_{2D} = n^2 = 4 \ldots\ldots\ldots\ldots\ldots\ldots [7]$$

is rigorously true and that $|p_{1D}| \cong 0.2$, $|p_{2D}| \cong 20$. Thus we can expect $|p_{1F}|$ to be small compared with $|p_{2F}|$, and we can neglect p_{1F}^8, p_{1F}^6 in Equation [1] to obtain as a first approximation

$$109{,}272 p_{1F}^4 - 151.2 p_{1F}^2 + 144 = 0 \ldots\ldots\ldots [8]$$

which can be refined quite easily to obtain an improved value. Similarly, when the root p_{2F}^2 is considered the approximate equation is

$$p_{2F}^4 - 15.4 p_{2F}^2 + 109{,}272 = 0 \ldots\ldots\ldots\ldots [9]$$

This approach brings out clearly the role of the quantity 109,272 (substantially $4K^4$) which causes one root to be large and the other to be small in absolute magnitude. This approximation is well known.[4] Comparison with the equivalent equations obtained from the Donnell characteristic equation shows that the smaller root will be more in error than the larger, since the two characteristic equations differ most in the last two coefficients. Thus large errors must be expected in the p_{1D}^2-quantities for low n-values.

Finally it should be mentioned that in the author's Equation [29] the symbols α, β, γ, δ are used in senses different from that used in Equation [21]. The two sets of values are related by the factors $n^2/(n^2 \pm K\Omega)$. It is not necessary to use the approach of Equation [29] since if $n^2 - K\Omega$ is a small difference of nearly equal numbers, Equation [24a] can be used to write

$$n^2 - K\Omega = \Omega^4/(n^2 + K\Omega)$$

which is accurately known if Ω is accurately known. Since Ω^2 is also a small difference of nearly equal numbers, it is useful to rewrite Equation [22] as

$$\Omega^2 = n^4/\{(K^2/2) + [(K^2/2)^2 + n^4]^{1/2}\}$$

which does not have this behavior.

Limits of Economy of Material in Plates[1]

P. G. Hodge, Jr.[2] The authors have presented an interesting paper on the optimum dimensions for stepped plates and on the theoretical weight limit for a plate of continuously varying thickness. As they point out, actual design procedure must account for the effect of shear near the edge. The present discussion proposes a rough way to do this.

Near the center of the plate, bending moments are certainly most important and the analysis of the paper will be used for

[4] Author's reference (3), p. 126.

[1] By H. G. Hopkins and W. Prager, published in the September, 1955, issue of the Journal of Applied Mechanics, Trans. ASME, vol. 77, 1955, pp. 372–374.

[2] Associate Professor of Applied Mechanics, Department of Aeronautical Engineering, Polytechnic Institute of Brooklyn, Brooklyn, N. Y. Mem. ASME.

$0 < r < uR$ where u is to be determined. For $uR < r < R$, the plate will be of constant thickness $2h_0$. Since the shear force is greatest at the edge, h_0 will be determined so that the plate will just fail in shear at $r = R$. Thus, if the maximum shear-stress yield criterion is assumed, the shear stress at $r = R$ is

$$\tau = \frac{p\pi R^2}{2\pi R(2h_0)} = \frac{1}{2}\,\sigma_0$$

where σ_0 is the tensile yield stress. Therefore the edge thickness is

$$h_0 = pR/2\sigma_0 \ldots\ldots\ldots\ldots\ldots\ldots [1]$$

For $0 < r/R < u$, the authors' analysis leading to Equations [17] and [18] is valid except that the boundary condition $M(R) = 0$ must be replaced by the condition $h(uR) = h_0$. Thus Equation [18] is to be replaced by

$$\left[\frac{h(r)}{R}\right]^2 = \frac{1}{4}\left(\frac{p}{\sigma_0}\right)^2 + \frac{1}{4}\left(\frac{p}{\sigma_0}\right)\left[u^2 - \left(\frac{r}{R}\right)^2\right] \ldots [2]$$

For $u < r/R < 1$, the equilibrium equation is to be solved with $N = M_0 = \sigma_0 h_0^2$ and the boundary condition $M(R) = 0$, the result being

$$M = (pR^2/6)[(R/r) - (r/R)^2] - \sigma_0 h_0^2(R/r - 1) \ldots [3]$$

Finally, u is determined by the condition that $M(r)$ be continuous at $r = uR$. Thus

$$M(uR) = (pR^2/6)(1/u - u^2) - \sigma_0 h_0^2(1/u - 1) = \sigma_0 h_0^2 \ldots [4]$$

If h_0 is replaced by its value from Equation [1], Equation [4] of this discussion may be solved to yield

$$u = [1 - (3/2)(p/\sigma_0)]^{1/3} \ldots\ldots\ldots\ldots [5]$$

For a given value of the load ratio p/σ_0, Equations [5], [2], and [1], herewith, completely determine the design of the plate. Fig. 1 of this discussion shows the resulting shape for some specific values of p/σ_0. Also shown are the authors' design shapes taken from Equation [18].

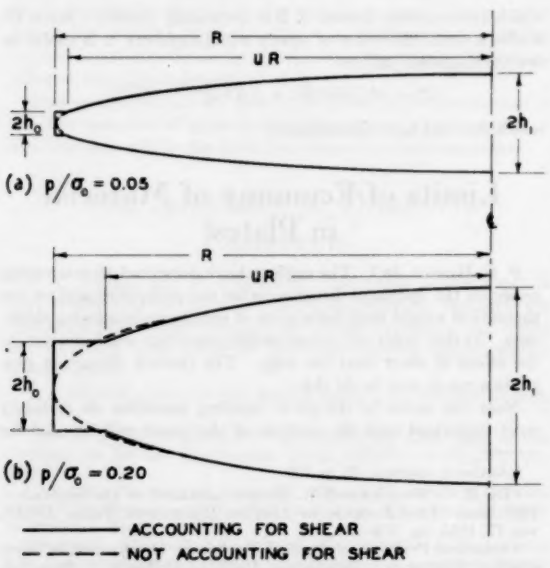

FIG. 1 DESIGN OF MINIMUM WEIGHT PLATES

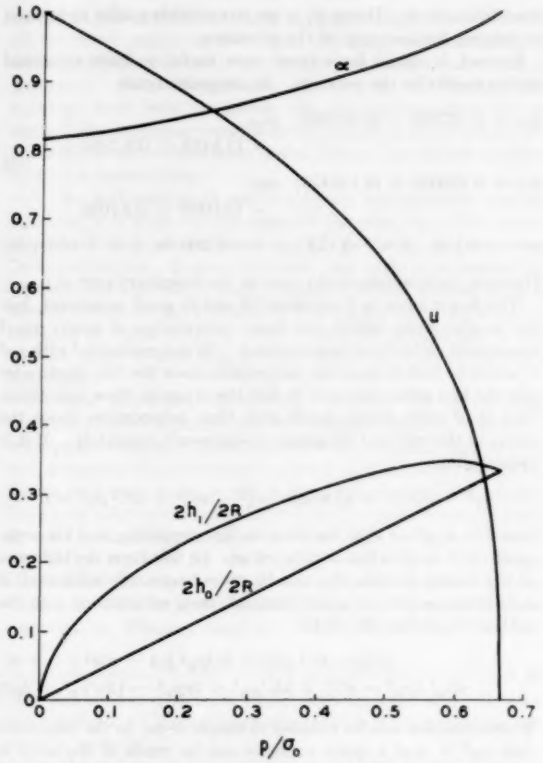

FIG. 2 WEIGHT FACTOR α AND VARIOUS DIMENSIONS AS FUNCTIONS OF p/σ_0
(Dimensions are defined in Fig. 4 of the paper.)

The weight factor α is defined by the authors as the ratio of the weight of the proposed plate to that of a plate of constant thickness capable of carrying the same load. In the present case it follows from Equation [14] of the paper that

$$\alpha = G(3\sigma_0/2p)^{1/3}/(\gamma\pi R^2)$$
$$= \left(\frac{2p}{3\sigma_0}\right)^{1/3}\left\{\frac{p}{\sigma_0}\left[\left(1 + \frac{\sigma_0 u^2}{p}\right)^{4/3} - 1\right] + \frac{3}{2}(1 - u^2)\right\} \ldots [6]$$

Here G is the total weight of the plate, γ the specific weight, and u is given by Equation [5] of this discussion. Fig. 2 shows the weight factor α, the radius u, and the edge and center thickness to diameter ratios $2h_0/2R$ and $2h_1/2R$, respectively, all as functions of the load ratio p/σ_0. If $2h_1/2R = 1/5$, which is probably about as thick a structure as can reasonably be called a plate, it is seen that the weight factor is about 0.838 as compared with the authors' limiting value of 0.816.

The preceding analysis is admittedly still only an approximation, since it accounts for shear only at the edge of the plate whereas an exact analysis would have to consider the interaction between shear and bending moment at least in some region near the edge. However, it does provide a more realistic design shape than the authors' analysis, while at the same time it indicates that their limiting weight factor of 0.816 is probably close to the true value for h/R reasonably small.

AUTHORS' CLOSURE

The authors would like to thank Professor Hodge for his valuable contribution to this subject.

The Statistical Theory of Size and Shape Effects in Fatigue[1]

G. W. Housner.[2] The author shows that a simplified model in which the strength of the specimen is reduced by a random distribution of equal flaws will not explain the observed distributions of fatigue life. To explain experimental results, therefore, requires consideration of a specimen which has a random distribution of flaws which themselves have some frequency distribution of negative strengths. The author evades the question of how to establish this frequency distribution by developing the fd of life of a specimen when the fd of the life of a small segment of the specimen is known. This leaves open the question of what fd to use for the life of a segment. The author arbitrarily selected his Equation [11] for the fd and points out that this does not provide an upper limit to the strength and leads to difficulty in determining experimentally the parameter k.

Can these difficulties be avoided by taking the following viewpoint? What is desired is to achieve an fd for the life of the specimen that has a single mode and pinches off to zero at an upper and a lower limit. The three regions of particular interest are those in the vicinity of the lower limit, in the vicinity of the upper limit, and in the vicinity of the mode. In view of the little information available on the behavior of the correct fd in the vicinity of the limits, it does not seem desirable to guess at truncated fd but a function of infinite range such as Equation [11] would seem to be adequate for the purpose so long as the specimen-life fd approaches zero on both sides of the mean at appropriate rates. This means that the two tails of the distribution should not be given much weight in any calculations, and it would thus seem that the parameters p_2, ω, k should be determined to give the best fit to the sample mean, median, and range. This procedure would give as little weight as possible to the tails of the distribution which, it seems, should really be considered separately, for it is they that cause the difficulty in estimating skewness, lower limit, etc. Of course, this procedure would not necessarily give the best prediction of the size effect since Equation [11] is only approximate. For the best estimate of k, as regards size effect, it would appear that a statistic involving tests on specimens of different sizes would be required, as for example, $\sigma_{\log N_2}/\sigma_{\log N_1}$.

Has the author made any attempt to investigate an appropriate Equation [11] by starting with some fd of flaws, that is, extending the method he used for flaws of uniform strength? In particular, it would be of interest to learn what information on the tails of the fd could be deduced by this approach and what light this might throw on the size effect.

Author's Closure

To start with the last of Professor Housner's questions, the author at first thought in terms of distributions of flaws superimposed on a constant inherent strength. As the number of flaws increases, however, the material can be described equally well by a distribution of the strengths after the flaws have been taken into account, and this latter point of view seemed easier to work with in the subsequent development. The right-hand tail of the distribution of strengths has almost no effect, since the complete specimen will almost certainly fail sooner at an element having average or lower strength.

The author believes, without proof, that the large variance of a sample range would prevent any reasonably accurate estimate of the parameters from that statistic.

The author agrees on the desirability of tests on two sizes with enough specimens at one stress level to obtain an estimate of $\sigma_{\log N_2}/\sigma_{\log N_1}$.

[1] By F. A. McClintock, published in the September, 1955, issue of the Journal of Applied Mechanics, Trans. ASME, vol. 77, pp. 421–426.

[2] California Institute of Technology, Pasadena, Calif.

Buckling of Sandwich Cylinders Under Combined Compression, Torsion, and Bending Loads[1]

P. P. Bijlaard.[2] The writer appreciates the ingenious derivation presented by the authors for obtaining Equation [31] for sandwich cylinders with a weak core.

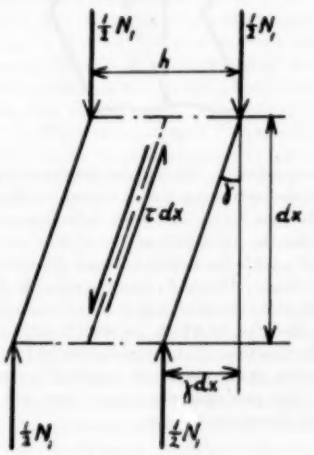

Fig. 1

This equation may also be understood from a simple reasoning. If the shell buckles under axial membrane forces N_1, assuming shear deformation of the weak core only, from Fig. 1 the equilibrium of the left or right half of the shell wall requires that (compare Equation [33])[3]

$$\frac{1}{2}N_1\gamma dx = \tau dx\left(\frac{1}{2}h\right) = \frac{1}{2}hG\gamma dx$$

or

$$N_1 = hG = C \quad \ldots\ldots\ldots\ldots\ldots\ldots [37]$$

Actually, also deformation from bending (extensional deformation of the faces) occurs, but if the core is weak this would make N_1 only slightly smaller than C. On the other hand, due to the curvature of the shell in a direction perpendicularly to N_1, other restraints would act which would increase N_1 considerably above C. Therefore the smallest value of N_1 occurs if the half-wave length of buckles becomes infinitely small, say, da (Fig. 2). This makes the deformation by bending negligible. On the other hand, however, with an infinitely small deflection w_0 (Fig. 2), $\tan\gamma =$

[1] By C. T. Wang, R. J. Vaccaro, and D. F. De Santo, published in the September, 1955, issue of the Journal of Applied Mechanics, Trans. ASME, vol. 77, pp. 324–328.

[2] Professor, Cornell University, Ithaca, N. Y.

[3] "On the Elastic Stability of Thin Plates, Supported by a Continuous Medium," by P. P. Bijlaard, Proceedings of the Royal Netherlands Academy of Sciences, Amsterdam, The Netherlands, vol. 49, no. 10, 1946, pp. 1189–1199.

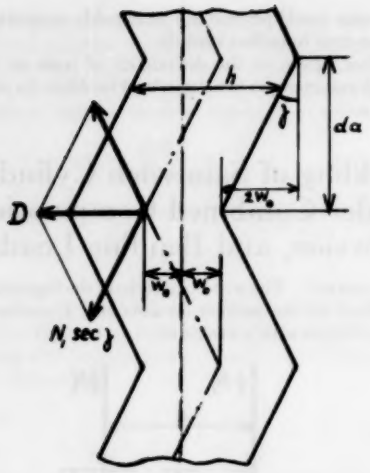

FIG. 2

$2w_0/da$ will become finite. Hence also the deflecting forces $D = 2N_1 \tan \gamma$ and the restraining forces caused by the shear strains γ in the core become finite. All other deflecting and restraining forces, caused by the curvature of the shell in a direction perpendicular to N_1, with the infinitely small deflection w_0, will remain infinitely small. Hence N_1 remains equal to C.

The same reasoning remains valid if the compressive membrane force acts in a direction in which the shell is curved. In general, the largest deflecting force D occurs if the waves form perpendicular to the direction of the maximum principal compressive membrane force. This principal membrane force will therefore be equal to C from Equation [37], or

$$N_{\text{principal}} = C \quad \ldots\ldots\ldots\ldots\ldots\ldots [38]$$

This leads to Equation [31] as shown in the paper below Equation [31], considering compression as negative.

AUTHORS' CLOSURE

The authors would like to thank Professor Bijlaard for his interest in their paper, and for his illuminating analysis. He is to be complimented for his derivation which, although simple and straightforward, retains all the features of the problem. His result is appreciated as an independent substantiation of the work of the authors.

The Elastic-Plastic Stress Distribution Within a Wide Curved Bar Subjected to Pure Bending[1]

J. C. WILHOIT, JR.[2] This is an interesting paper. However, reference should be made to W. Swida[3] who has treated the same problem as a case of plane stress rather than plane strain. The difference in the two solutions rests only with the yield condition in the inner plastic range. In Swida's paper (changing his notation to agree with the present paper) the yield condition for the inner plastic range is given by Equation [3]

$$\sigma_\theta = 2k$$

while in the present paper the condition is given by Equation [3a]

$$\sigma_\theta - \sigma_r = 2k$$

In the outer plastic range the yield condition of Swida, Equation [18], agrees with that of the present paper, Equation [3b] and is

$$\sigma_r - \sigma_\theta = 2k$$

Considering the very pronounced similarity of the two problems, it is felt that Swida should be mentioned in the present paper.

AUTHORS' CLOSURE

The authors wish to thank Professor Wilhoit for his comments. While it is true that Swida analyzed the stress distribution of a curved bar within the plastic range, no reference was made to his work because he did not treat the plane-strain problem. Instead, reference was made to the work of Hill, Lubahn, and Sachs who not only studied the plane-strain problem but did it by using Equations [3a] and [3b] for their yield conditions.

If one wishes to extend the bibliography to plane-stress problems, then reference should also be made to the work done for the Office of Naval Research at Stanford University under the direction of A. Phillips.

Incidentally, it may be noted that even though Swida started his paper by considering both σ_r and σ_θ in his solution to the plane-stress problem, the major portion of his treatise was based on the assumption that σ_r is equal to zero. The authors, on the other hand, retained the effect of σ_r in both the current and a subsequent paper in which they solved the corresponding displacement problem.[4] In view of both contributions, they are able to present the entire solution to the plane-strain problem without requiring the assumption that σ_r is equal to zero.

Nutation of a Free Gyro Subjected to an Impulse[1]

A. S. GUTMAN.[2] The paper shows that a free gyro with zero friction about its three axes of rotation will precess about the outer gimbal axis if exposed to a vibration and if the inertia of the gimbal axis is taken into account and the two gimbals are not at right angles to each other. Mathematically, the paper is correct except for a printing error in Equation [2] in which the C should be replaced by A.

Physically, however, the analysis presented in the paper does not apply to an electrically driven gyro. In such a gyro, Equation [3] does not apply. The equations of an electrically driven gyro, neglecting gimbal inertia, are

$$[A \cos^2\theta + B \sin^2\theta]\ddot{\phi} + (B - A)\dot{\phi} \sin 2\theta - A\dot{\psi}\dot{\theta} \sin\theta + A\ddot{\psi} \cos\theta = Q_1 \ldots [1]$$

[1] By B. W. Shaffer and R. N. House, Jr., published in the September, 1955, issue of the JOURNAL OF APPLIED MECHANICS, Trans. ASME, vol. 77, pp. 305–310.

[2] Assistant Professor, Mechanical Engineering Department, The Rice Institute, Houston, Texas. Assoc. Mem. ASME.

[3] "Die elastisch-plastische Biegung des krummen Stabes," by W. Swida, *Ingenieur-Archiv*. XVI Band, 1948, pp. 357–372.

[4] "Displacements in a Wide Curved Bar Subjected to Pure Elastic-Plastic Bending," by Bernard W. Shaffer and Raymond N. House, Jr. An N.Y.U. Technical Report prepared for the Office of Ordnance Research, Dept. of the Army, under Contract No. DA-30-069-ORD-1398, September, 1955.

[1] By B. T. Plymale and R. Goodstein, published in the September, 1955, issue of the JOURNAL OF APPLIED MECHANICS, Trans. ASME, vol. 77, pp. 365–366.

[2] Engineering Specialist, Waltham Laboratories, Sylvania Electric Products Inc., Waltham, Mass.

$$B\ddot{\theta} - (B - A)\dot{\phi}^2 \sin 2\theta + A\dot{\phi}\dot{\psi} \sin \theta = Q_2 \ldots\ldots [2]$$

$$A[\ddot{\psi} + \ddot{\phi} \cos \theta - \dot{\phi}\dot{\theta} \sin \theta] = Q_3 \ldots\ldots [3]$$

where Q are the generalized forces.

In our case, Q_2 is the friction torque R_2, on the inner gimbal axis; Q_3 is the friction torque R_3, on the outer gimbal axis; Q_1 is the electric motor torque M, on the spin axis minus the friction torque R_1, on the spin axis.

If an alternating current 3-phase induction motor[3] is used, the motor torque is proportional to the so-called slip frequency. The slip frequency is the difference between the electrical frequency ω and the gyro spin rate $\dot{\psi}$.

We obtain

$$M = \lambda(\omega - \dot{\psi})$$

where λ is the characteristic torque factor of the chosen motor and

$$\left.\begin{aligned} Q_1 &= \lambda(\omega - \dot{\psi}) - R_1 \\ Q_2 &= R_2 \\ Q_3 &= R_3 \end{aligned}\right\}$$

Neglecting friction about the gimbal axis

$$R_2 = 0$$

$$R_3 = 0$$

and setting

$$R_1 = \lambda\omega$$

(a condition realized in normal gyro operation) one gets for the equation of motion

$$[A \cos^2 \theta + B \sin^2 \theta]\ddot{\phi} + (B - A)\dot{\phi} \sin 2\theta - A\dot{\psi}\dot{\theta} \sin \theta + A\ddot{\psi} \cos \theta = 0 \ldots [4]$$

$$B\ddot{\theta} - (B - A)\dot{\phi}^2 \sin 2\theta + A\dot{\phi}\dot{\psi} \sin \theta = 0 \ldots\ldots [5]$$

$$A[\ddot{\psi} + \ddot{\phi} \cos \theta - \dot{\phi}\dot{\theta} \sin \theta] = \lambda\dot{\psi} \ldots\ldots [6]$$

Equation [4] corresponds to Equation [1] of the paper. Equation [5] corresponds to Equation [2] of the paper (with the exception of the printing error mentioned). Equation [6], however, does not correspond to Equation [3] of the paper.

It can be shown from Equations [4], [5], and [6] that the gyro precesses in the manner described in the paper. It is believed that this effect is much larger in a well-designed gyro than the effect of gimbal inertia which can be neglected in a first approximation.

KURT MAGNUS.[4] Having read the paper with great interest, the discusser wishes to call the authors' attention to a paper published at the beginning of this year which deals with the same phenomenon and contains the same results.[5] Naturally this publication was unknown to the authors at the time they were writing their paper, but for this very reason the discusser is pleased to see that the fin..l results are in complete agreement, a fact that is not always a matter of course in the case of approximation equations.

The authors' Equations [1] and [2] are exactly identical with the discusser's system (13), and their final Equation [6] fully agrees with Equation (29).

In addition to the approximate calculation given in Section 3*b*,[5] Section 3*a* also refers to the rigorous solution of the problem which was discovered by Seebach in 1944, but which has not been made generally available.

AUTHORS' CLOSURE

The authors wish to thank Mr. Gutman and Mr. Magnus for their interest in the paper.

We were pleased to hear that Mr. Magnus had previously written a paper on the same phenomena in which identical results were obtained.

Mr. Gutman points out that a gyroscope with an electrically driven wheel will experience additional torque due to the motor and claims that the effectiveness of the motor torque in producing gyro procession about the outer gimbal axis is much larger than that due to the gimbal inertia discussed in the paper. The authors agree that there exists additional torque attributable to the motor but point out and will verify that its effect on a practical gyro is negligible in comparison to the effect described in the paper. In the past, several gyros have been tested in our laboratories under conditions described in the paper. The phenomenon was examined with wheel power on and off (wheel coasting) and no measurable difference in the phenomenon was observed.

Physically, the motor produces a torque on the gyro wheel about its spin axis and a reaction torque which, in general, has a component along the outer gimbal axis whenever the relative angular velocity between the inner gimbal and the wheel differs from its initial value at the time the impulse was applied. First, consider the effect of the motor torque on the gyro wheel. The torque will increase or decrease (depending on the direction of the impulse) the angular momentum of the gyro. Since the change in the relative angular velocity of the wheel is caused by an angular velocity of the outer gimbal and since the inertia of the wheel prevents the motor from nulling this change in the relative angular velocity of the wheel, the change in angular momentum of the gyro has two components. One component is proportional to outer gimbal angular velocity and the other is proportional to outer gimbal angular acceleration. The component of the change in angular momentum which is proportional to outer gimbal angular velocity is in phase with inner gimbal angular acceleration and thus produces a net torque on the inner gimbal resulting in a small additional average angular rate of the outer gimbal. The component of the change in angular momentum which is proportional to outer gimbal angular acceleration is in phase with outer gimbal angular acceleration and thus produces a net torque on the outer gimbal resulting in a small average angular rate of the inner gimbal.

Similarly, the motor-reaction torque will also have two components; one component is proportional to outer gimbal angular velocity and the other component is proportional to outer gimbal angular acceleration. Since the motor-reaction torque has a component along the outer gimbal axis, torques proportional to outer gimbal angular velocity and angular acceleration act upon the outer gimbal. The torque proportional to angular velocity is in the proper phase to damp the oscillations and the torque proportional to angular acceleration results in an effective increase in outer gimbal inertia.

With the effect of the motor torque included, the equations of motion of the gyro are

$$[F + C \cos^2 \theta + (B + E) \sin^2 \theta]\ddot{\phi} + 2(B + E - C)\dot{\theta}\dot{\phi} \sin \theta \cos \theta - A(\dot{\psi} + \dot{\phi} \cos \theta)\dot{\theta} \sin \theta - \lambda(\dot{\psi} - \dot{\psi}_0) \cos \theta = 0 \ldots [7]$$

$$(B + D)\ddot{\theta} - (B + E - C)\dot{\phi}^2 \sin \theta \cos \theta + A(\dot{\psi} + \dot{\phi} \cos \theta)\dot{\phi} \sin \theta = 0 \ldots [8]$$

$$A\ddot{\psi} + A\ddot{\phi} \cos \theta - A\dot{\phi}\dot{\theta} \sin \theta = \lambda(\dot{\psi}_0 - \dot{\psi}) \ldots\ldots [9]$$

[3] If an electric motor, other than an induction motor, is used, a similar effect will be caused by the motor torque.

[4] Freiburg, Breisgau, Germany.

[5] "Beiträge zur Dynamik des kräftefreien, kardanisch gelagerten Kreisels" by Kurt Magnus, *Zeitschrift für angewandte Mathematik und Mechanik*, vol. 35, 1955.

where λ is the characteristic torque factor defined by Mr. Gutman and $\dot{\psi}_0$ is the initial angular velocity of the wheel. Equation [9] can be solved approximately by using the fundamental sinusoidal solution for $\dot{\phi}$. An approximate solution for $\dot{\psi}$ is thus obtained which can be used to simplify Equations [7] and [8] as follows

$$[F + C' \cos^2\theta + (B + E)\sin^2\theta]\ddot{\phi} + 2(B + E - C')\dot{\theta}\dot{\phi} \sin\theta\cos\theta - H\dot{\theta}\sin\theta + \frac{\lambda\dot{\phi}\cos^2\theta}{1 + k^2} + 2\left(\frac{A}{\lambda}\right)\frac{k^2}{1 + k^2} A\ddot{\phi}\dot{\theta}\sin\theta\cos\theta = 0 \quad [10]$$

$$(B + D)\ddot{\theta} - (B + E - C')\dot{\phi}^2\sin\theta\cos\theta + H\dot{\phi}\sin\theta - \left(\frac{A}{\lambda}\right)\frac{k^2}{1 + k^2} A\ddot{\phi}\dot{\phi}\sin\theta\cos\theta = 0 \quad [11]$$

where

$$C' = C + \frac{Ak^2}{1 + k^2} \quad [12]$$

$$H = A\dot{\psi}_0 \quad [13]$$

$$k = \frac{\lambda}{A\omega_n} \quad [14]$$

The last torque in Equation [10] is the net torque which produces an average angular rate of the inner gimbal of amount

$$\bar{\dot{\theta}} = \frac{\lambda\rho_0^2\sin\theta_0\cos\theta_0}{I_0(1 + k^2)} \quad [15]$$

The next to last torque in Equation [10] is the damping torque and results in a damping ratio of

$$\xi = \frac{k}{1 + k^2}\frac{A\cos^2\theta_0}{2I_0} \quad [16]$$

The last torque in Equation [11] is small in magnitude and has no net value over a cycle of the motion. This torque may be neglected in an approximate solution of the motion.

Aside from the foregoing three torques, Equations [10] and [11] are of the same form as Equations [7] and [8] of the paper. Thus the solutions given in the paper may be used with due considerations of the change in constants and damping. Parameters of a typical gyro can be used to examine the magnitude of the damping, the magnitude of the average rate of the inner gimbal, and the change in the constants. The following parameters will be used:

$\theta_0 = 30$ deg
$\omega_n = 300$ rad/sec
$\lambda = 10^4$ g cm^2/sec
$I_0 = 6000$ g cm^2
$H = 2.4 \times 10^6$ g cm^2/sec
$A = 2000$ g cm^2
$C = 1000$ g cm^2

Using these values, one obtains

$$\xi = \frac{1}{480}\quad \frac{C'}{C} = 1 + \frac{1}{1800}\quad \frac{\bar{\dot{\theta}}}{\dot{\phi}} = \frac{1}{240}$$

The damping will produce no appreciable decay in the oscillations and the change in C is negligible. The inner gimbal average angular rate is small compared to the outer gimbal average angular rate. Thus, for all practical purposes, the motor torque produces no change in the phenomena as described in the paper.

The authors also wish to state that there was no typographical error in Equation [2] of the paper.

Vibrations of a Helicopter Rotor-Fuselage System Induced by the Main Rotor Blades in Flight[1]

G. W. Brooks.[2] Helicopter vibration is a subject of much current interest, and I would like to congratulate the authors on the timely presentation of an excellent paper.

It has been said on many occasions that not a single helicopter type has been manufactured to date which did not encounter vibration problems of some sort. Unfortunately, in numerous cases, vibration problems have imposed serious limitations on the development of helicopters, resulting in large production delays and high research and production costs. The vibration level on many of the machines currently flying is much greater, it is believed, than either the manufacturer or the operator would like.

Being engineers, we ask ourselves why the big problem? The answer is thought to lie in the fact that the helicopter is a complicated piece of machinery which has many degrees of freedom. In operation, many of these degrees of freedom couple with one another to yield various natural structural mode shapes and associated natural frequencies which are difficult to predict. When we consider that a forcing function of some magnitude exists for most of the lower harmonics of the rotor speed, engine speed, tail rotor speed, and in some cases, the transmission, it becomes increasingly difficult to find a range of operation where some natural frequency of the structure is not in, or nearly in, resonance with some input force.

The authors very ably demonstrated that one of the things which we can do to understand the problems better is to derive answers for physical models which simulate helicopter structure. Whether the solution to any particular problem will be provided by such studies will depend upon the extent to which the model and analysis duplicate an actual helicopter. This necessitates the addition of more degrees of freedom in the structure, the inclusion of damping, and the addition of forces and moments having frequencies equal to all the rotor harmonics and not just those having frequencies equal to the multiples of the number of blades. It is believed the authors are anticipating studies including some of these items and I feel that their work will be of significant value to the helicopter industry.

[1] By M. Morduchow, S. W. Yuan, and H. Reissner, published in the September, 1955, issue of the Journal of Applied Mechanics, Trans. ASME, vol. 77, pp. 355–360.

[2] NACA, Langley Aeronautical Laboratory, Langley Field, Va.

Book Reviews

Mechanics

INTRODUCTION TO THEORETICAL MECHANICS. By Robert A. Becker, McGraw-Hill Book Co. Inc., New York, N. Y., 1954. Cloth, 6 × 9 in., xiii and 420 pp., illus., $8.

REVIEWED BY P. S. SYMONDS[1]

THIS is a textbook on a level appropriate for junior or senior-year courses. It is based on a course for students in engineering physics, and the choice of topics, examples, and problems has a flavor of physics rather than of engineering. Some 80 worked and 400 unworked problems are given. Vectors are used throughout, but tensor or matrix concepts are not mentioned.

After a chapter on "basic principles" which contains an introduction to vector analysis, there are four chapters on statics, including one on suspended cables. The succeeding chapters are on dynamics of a particle in a uniform field, oscillations of a particle with one degree of freedom, dynamics of a system of particles, motion of a rigid body in a plane, motion of a particle in a central force field, accelerated reference systems, general motion of a rigid body, generalized co-ordinates, and Lagrange's equations, small vibrations of systems with a finite number of degrees of freedom, and finally, on vibrations of stretched strings. There are five appendixes in which various mathematical topics are treated.

Some minor criticisms can be made. This reviewer was surprised to find no mention of d'Alembert's principle. The treatment of virtual work as an alternative method in statics seemed inadequate; the student would perhaps not realize that this is a basic analytical tool in both statics and dynamics. The chapter on vibrating systems seems too short to be satisfactory, since it is devoted mainly to statements and illustrations of properties of normal co-ordinates. It would seem essential to introduce the ideas of representing general motions by combinations of normal modes, since in practice one does not usually solve problems by transforming to normal co-ordinates. Material such as this can always be added by the instructor, however. The reviewer was favorably impressed by this as a carefully written and trustworthy textbook of basic mechanics.

Gas Turbines

GAS TURBINE PRINCIPLES AND PRACTICE. Written by 24 specialist contributors. Consulting editor: Sir Harold Roxbee Cox. D. Van Nostrand Company, Inc., New York, N. Y., 1955. Leatherette. 5 1/2 × 8 1/2 in., xii and 960 pp., plates, figs., and tables, $17.50.

REVIEWED BY T. F. STIRGWOLT[2]

THIS book has been organized into 30 sections of gas-turbine technology by Sir Harold Roxbee Cox, the consulting editor. Each section was written by a British expert in the field.

Each section of the book is devoted to a major component or field of gas-turbine work such as axial-flow compressors, axial-flow turbines, combustion systems, and so on. There are sections on thermodynamics, cycles, materials of construction, fuels, stresses, and vibration. And finally, much of the book is devoted to types of installation of the gas turbine in present-day application.

The level of treatment of the subject material in each section has been aimed at people with a technical background and an understanding of the fundamental relationships. These fundamentals are applied to the physical flows and heat balances in the gas-turbine components in a straightforward way. Of course, in any one of the fields covered it would have been possible to delve into the many complexities and barrier problems but such was not the intent of this volume. It can be concluded therefore that the authors intended to make the gas-turbine principles understandable to those engineers interested in the broad aspects of this type of power plant.

The wealth of experience of the individual authors becomes apparent in many of the sections. The applications sections describe many diverse uses of present-day operating gas turbines. Many problems which have confronted the designers in designing and operating units are discussed. On the basis of design experience, many of the sections include empirical limits and loss data. Also included are some forms of component off-design considerations. Altogether, the book forms a means of gaining a good insight into the field of gas turbines.

Turboblowers

TURBOBLOWERS—Theory, Design, and Application of Centrifugal and Axial Flow Compressors and Fans. By A. J. Stepanoff. John Wiley & Sons, Inc., New York, N. Y.; 1955. Cloth, 6 × 9 in., ix and 375 pp., illus., $8.

REVIEWED BY C. W. SMITH[3]

THIS book, supplementing the author's previous book "Centrifugal and Axial Flow Pumps" (Wiley, 1948), treats of turbomachinery as applied to the compression of gases and vapors. It is concerned primarily with the thermodynamics and aerodynamics of the processes rather than with mechanical features, although some aspects of the mechanical design are considered.

Scarcely any class of machines is capable of more different methods of analysis than turbomachinery. Sometimes these methods may be so different as to appear inconsistent. However, a little study usually reveals that they are based on different viewpoints, different concepts of "efficiency," or perhaps different objectives, so that some reasonable justification can be offered for most of them. Although the numerical values of the various measures of performance and other such quantities may vary in accordance with preferred definitions, successful designs can be made in accordance with any one of a large number of different theories.

In this book the author introduces a number of unconventional methods of analysis, some of which are new as applied to turbomachinery; others of which, though not new, are uncommon. Among these are the emphasis on energy gradient as determining the direction of flow (though "total energy" as here

[1] Professor of Engineering, Brown University, Providence, R. I. Mem. ASME.

[2] Engine Performance Analysis, AGT Development Department, Aircraft Gas Turbine Division, General Electric Company, Cincinnati, Ohio.

[3] Small Aircraft Engine Dept., General Electric Company, West Lynn, Mass.

used is not clearly defined, in spite of the author's later emphasis on "available energy"); the concept of useful output as the raising of the working medium to a certain height (head), with some consequent advantages in analysis; the expression of Euler's equation as the difference between zero flow head and a head proportional to the flow; and the introduction of Gibbs' zeta (availability of energy) function to supplement the concept of enthalpy, with consequent rigorous demonstration of some relations which are ordinarily taken for granted, or which may otherwise be misunderstood.

There will probably be little disagreement with the author's conclusion that conventional airfoil theory is no longer adequate for treatment of the axial-flow compressor. His recommended treatment, based on actual fluid deflection (i.e., essentially Euler's equation) with experimentally determined correction factors, is consistent with the modern tendency toward a more empirical design of these compressors, in spite of the viewpoint once widely held, and to some extent justified, that axial-flow compressors are more amenable to a theoretical treatment than centrifugal compressors.

Although some of the methods of analysis given in this book cannot be expected to appeal to all engineers, especially for certain practical design problems, they will certainly help to broaden and illuminate the theoretical background which most successful designers must possess. The author has had a great deal of experience with turbomachinery, and the book contains many useful design data. All persons interested in centrifugal or axial-flow compressors should have a copy of it.

Aeroelasticity

AN INTRODUCTION TO THE THEORY OF AEROELASTICITY. By Y. C. Fung. GALCIT Aeronautical Series. John Wiley and Sons, Inc., New York, N. Y., 1955. Cloth, 6 × 9¼ in., ix and 490 pp., figs., bibliographies, appendixes. $10.50.

REVIEWED BY MORRIS MORDUCHOW[4]

THE theory of aeroelasticity, which is essentially the study of the response of a structure to elastic, inertia, and aerodynamic forces and moments, is a broad field of aeronautical engineering which has developed rapidly in only the past 20 years. Despite the wealth of research articles which have been written during this period on the various general, as well as detailed, aspects of this subject, there are few textbooks in the field.

The book under review arose from a course given at C.I.T. since 1948 and is intended primarily as a textbook. Consequently, the author has chosen to present the subject from a comparatively broad point of view by treating a variety of the chief aspects of the field, emphasizing the principles of each aspect, and treating in detail relatively simple examples. Moreover, only one or two specific methods of analyzing each type of problem are given in detail. (The reviewer was nevertheless surprised to find no mention of the Rayleigh or Rayleigh-Ritz method.) The more detailed and complicated problems, as well as additional methods of analysis, are also discussed, but usually only briefly. An appreciable bibliography, however, referring to these various detailed problems is given at the end of each chapter.

Although, strictly speaking, the book might in a sense be regarded as self-contained, it would nevertheless be recommended to a beginning student in aeroelasticity that he first have a background in vibration analysis and in the elements of theoretical and applied aerodynamics before studying this book.

The book consists of 15 chapters. After a preliminary chapter on certain necessary elements of structures, practical aerodynamics, and dynamics (including influence coefficients, Lagrange equations, and coupled torsion-flexure oscillations of a beam), certain aeroelastic problems in mechanical and civil engineering (including a discussion of Karman's vortex street behind a cylinder) are discussed. Chapter 3 then treats the divergence of a lifting surface, while chapter 4 includes an analysis of aileron loss and reversal. Chapters 5–7 treat classical two and three-dimensional flutter, such as wing bending-torsion-aileron flutter. Forced oscillations due to a periodic excitation are also included here. The treatment of three-dimensional flutter is perhaps somewhat brief, and a numerical example might have been pertinent here. Chapter 8 deals with transient loads and gusts, including statistical aspects of dynamic-stress problems. The response of an airplane to a gust and to atmospheric turbulence is briefly analyzed here. In chapter 9 buffeting and stall flutter are discussed physically. Chapter 10 gives applications of Laplace transforms to response and flutter problems. The concepts of indicial admittance and of transfer functions are developed and applied in chapters 8 and 10. Chapter 11, finally, indicates the use of operators in the general formulation of aeroelastic problems. Chapters 12–14 give a mathematical analysis of (nonstationary) aerodynamic forces on oscillating airfoils, with emphasis on linearized thin airfoil theory. Both subsonic and supersonic flow are analyzed. Experimental results are included in chapter 15.

The book is on the whole well written, and despite the mathematical character of certain portions of the book (particularly in the latter half), the author gives quite adequate physical explanations of the various phenomena he treats. The reviewer noted several minor misprints and oversights which, however, could be corrected by a reader himself.

This book is a valuable contribution to the textbook literature in the field, containing much of interest previously found mostly in research papers. The book should be of value particularly to students and practicing engineers who desire a basic over-all view of aeroelasticity.

[4] Associate Professor of Applied Mathematics, Polytechnic Institute of Brooklyn, Brooklyn, N. Y.

Boundary-Layer Theory

BOUNDARY LAYER THEORY. By Hermann Schlichting. Translated by J. Kestin. (McGraw-Hill Series in Mechanical Engineering.) McGraw-Hill Book Co., Inc., New York, N. Y.; Pergamon Press, Ltd., London, England; 1955. Cloth, 6½ × 9½ in., figs., xx and 535 pp., $15.

REVIEWED BY ASCHER H. SHAPIRO[5]

WHEN the German edition of this book first appeared, this reviewer expressed the hope that it would be published in an English text (see review in the JOURNAL OF APPLIED MECHANICS, June, 1952, p. 248). Now this event has happily come to pass with the additional good fortune that the translation has been skillfully done by a scientist himself familiar with the subject.

Little need be added to the praise which the reviewer gave in 1952. Seeing the text now in his own tongue, the reviewer is more than ever impressed with its comprehensiveness, its choice of subject matter, its balance between physical description, theory and experiment, and its clear exposition. Minor criticisms might be made, but they would be trivial in relation to the work as a whole.

The English edition is not a literal translation of the German, many small additions having been made in accord with the

[5] Professor of Mechanical Engineering, Massachusetts Institute of Technology, Cambridge, Mass., U. S. A.; currently on leave of absence, as Visiting Professor of Applied Thermodynamics, Cambridge University, Cambridge, England. Mem. ASME.

progress of the four intervening years. In addition, two chapters, those on compressible boundary layers and on turbulent boundary layers with pressure gradients, have been completely rewritten.

The production of the book, its type, figures, paper, binding, and, most important, its general appearance, are all first-class. For some reason American technical books have not even approached the artistic level of appearance typified by this volume.

There is no question but that Dr. Schlichting's book far surpasses any other book on boundary-layer theory and will be a well-used reference source for several decades. It is the authoritative work on this highly important aspect of fluid motion.

Higher Transcendental Functions

HIGHER TRANSCENDENTAL FUNCTIONS. Volume 3. By the Staff of the Bateman Manuscript Project. McGraw-Hill Book Company, Inc., New York, N. Y.; Toronto, Ont.; London, England, 1955. Cloth, 6 × 9 in., xviii and 292 pp., $6.50.

REVIEWED BY ERIC REISSNER[6]

IN this final of three volumes (for a review of the preceding two, see JOURNAL OF APPLIED MECHANICS, vol. 22, p. 160) the portions of interest to the applied worker are concerned with Lamé functions (which are suitable solutions of certain ordinary differential equations arising through application of the separation of variables method to the three-dimensional Laplace equation in confocal quadric co-ordinates) and to Mathieu functions, spheroidal, and ellipsoidal wave functions (which occur in the application of the separation of variables method to the so-called wave equation written in elliptical cylinder co-ordinates, spheroidal co-ordinates, and confocal quadric co-ordinates respectively). Of these topics, the most is known on Mathieu functions and spheroidal wave functions and many of these results are the product of labor of the past 15 years which have seen much interest in the theoretical treatment of problems of acoustic and electromagnetic radiation.

The present third volume which is a worthy companion to the earlier ones should certainly be in the hands of everyone who possesses volumes 1 and 2.

Aerodynamics

AERODYNAMICS—Selected Topics in the Light of their Historical Development. By Theodore von Karman. Cornell University Press, Ithaca, N. Y., 1954. Cloth, 6 × 9 in., figs., ix and 203 pp., $4.75.

REVIEWED BY ANTONIO FERRI[7]

THIS book presents both the history of progress in aerodynamic science from its beginning to the present day and the basic theories of aerodynamics. The author is one of the few scientists who can write with authority on these topics. He presents both the historical and technical aspects of aerodynamics in a style which makes the book interesting to a wide variety of readers. The historical parts are presented in a personal and human way which gives life and personality to the scientists who contributed to the development of aerodynamic science. The theoretical parts are a synthesis of aerodynamics and of the engineering aspects of flight; they are clearly and at the same time originally presented and therefore of interest to the beginner who can obtain a panoramic and clear view of the entire field. The specialist on the other hand can find in the words of the author "how much mental effort was necessary to arrive at an understanding of the fundamental phenomena" and will enjoy the presentation. The list of references which follow each chapter is carefully chosen and is therefore valuable to all interested in aerodynamics.

The list of chapters indicates the range of topics covered; it is as follows:

I Aerodynamic Research before the Era of Flight
II The Theory of Lift
III Theories of Drag and Skin Friction
IV Supersonic Aerodynamics
V Stability and Aeroelasticity
VI From the Propeller to the Space Rocket

[6] Professor of Mathematics, Massachusetts Institute of Technology, Cambridge, Mass.

[7] Professor of Aerodynamics, Polytechnic Institute of Brooklyn, Brooklyn, N. Y.

Viscoelasticity

MATHEMATICAL STRUCTURE OF THE THEORIES OF VISCOELASTICITY. By Bernhard Gross (Actualités Scientifiques et Industrielles 1190). Hermann & C^{ie}, Paris, France, 1953. Paper, 9¼ × 6½ in. 12 figs., 74 pp., $2.25.

REVIEWED BY P. M. NAGHDI[8]

THIS is an exposition of the mathematical methods of the linear theory (phenomenological) of viscoelasticity which deal with distribution functions, Fourier transforms and their inversions, as well as the mathematical analogy between dielectric phenomena (electrical-network theory) and viscoelastic effects. Much of the contents of this booklet are recent developments to which the author himself has made numerous contributions. Even though this monograph, containing some 80 references, is short and limited in scope, it should prove very useful to those interested in the subject.

Following the introduction of creep and relaxation functions (as integral transforms), and complex compliance and complex modulus (analogous to complex impedance function in electrical-network theory), the general mathematical relations between these functions are presented for both continuous and discontinuous spectra. Next, the role played by Volterra integral equation between creep and relaxation functions is pointed out and the mathematical structure of the theory is presented in an informative diagram. The last 15 pages are concerned with applications to continuous and discontinuous spectra with reference to mechanical (general Voigt and Maxwell) models. Occasionally the presentation is vague and contains a number of misprints and grammatical errors.

Elasticity

RÉSISTANCE DES MATÉRIAUX: THÉORIQUE ET EXPÉRIMENTALE. By Robert L'Hermite. Vol. I—Théorie de l'Élasticité et des Structures élastiques. (Collection de l'Institut Technique du Batiment et des Travaux Publics.) Dunod, Paris, France, 1954. Cloth, 6¼ × 9¼ in., xv and 860 pp., 8400 fr.

REVIEWED BY A. ALI KHEIRALLA[9]

THE first volume of this encyclopedic set is devoted to the classical theory of elasticity and problems of structural design. The three volumes to follow will cover modern theories of stability and buckling, methods of approximation, analogies,

[8] Professor of Engineering Mechanics, University of Michigan, Ann Arbor, Mich. Assoc. Mem. ASME.

[9] Mathematician-Physicist, Lessells and Associates, Inc., Boston, Mass.

modeling, and strain measurements; mechanical properties of materials; modern theories of plasticity, dynamic phenomena, shocks, statistical testing, and safety factors.

The work is especially characterized by its comprehensiveness and conciseness. The author has succeeded in collecting in this volume most of the classical and modern results of elasticity theory which are applicable in engineering practice. While it has been necessary to avoid lengthy derivations in a book of this scope a pertinent exposition of the fundamentals of each general subject is given. Solutions of specific problems are supplemented by references to original papers and an extensive modern bibliography is given at the end of each chapter. Because of the thorough organization and clear presentation of the material and also because of the inclusion of a great deal of subject matter formerly available only in original papers it is certainly destined to become a sine qua non of stress analysts everywhere.

Since to cover the contents of this volume section by section would require an encyclopedic review, only a general description of the individual chapters will be given below.

There are ten chapters of which the last is a general critique. The first chapter develops the general theory of elasticity including brief discussions of finite and nonlinear deformations and three-dimensional problems of elasticity theory. Among these are Boussinesq's problem of the elastic half space, the Hertz contact problem, and thermal stresses.

The second chapter treats two-dimensional elasticity, introduces the Airy function, and presents methods of solution in curvilinear co-ordinates. Internal and boundary singularities are discussed and stresses for various objects with holes or notches are given.

Chapter 3 treats the tension and bending of rods and beams. Rectangular, circular, and variable cross sections are considered as well as I-beams, U-beams, and tubes. Notches, fillets, and finite deformations are also mentioned.

The next chapter presents torsion of beams, rods, and tube- including notches and fillets. There is also a section on approxis mation methods including difference equations and relaxation methods.

Chapter five deals with the theory of isostatic structures, cables, springs, and statically determinate frameworks. The sixth and seventh chapters treat statically indeterminate structures. Supported cantilever beams, grillage beams, and beams on elastic foundations are included as well as a discussion of suspension bridges. Curved beams, arches, rings, and frames are presented.

The eighth chapter considers plates and curved slabs including cases of variable thickness, finite deformations of circular plates as well as eccentric loading, and effect of eccentric hole on same, sectorial plates, rectangular forms with internal-point supports, built-in rectangular plates, effect of temperature, Cartesian grid supports, and triangular and elliptical plates. Lines of influence, holes of various shapes, action of a concentrated load, elastic bases and elastic supports, combined bending and tension, large deformations, and a section on difference net approximation methods are presented.

Chapter 9 treats the problems of shells. Spherical, conical, hemiellipsoidal, hyperboloidal shells, unsymmetrical flexure of spherical shells, cupolae on discontinuous supports and with concentrated load, flexure of conical shells, bending of cylindrical tubes, tubes of variable thickness, thermal tension, and thin circular cylindrical shells are among the topics discussed. Again there is a section on approximation methods. Relaxation and analog methods, thick cylinders, arch dams, conoids, helicoids, hyperbolic paraboloids, pyramidal forms, and corrugations are also dealt with.

The book will certainly become a standard reference work and is especially recommended to practicing stress analysts as well as engineering research organizations.

Conference on Fatigue of Metals, London, September, 1956

The London Section of the Institution of Mechanical Engineers, London, is organizing an International Conference on Fatigue of Metals to be held at the Institution of Mechanical Engineers, London, from Monday, September 10, to Friday, September 14, 1956.

The program already approved by a Committee of the Institution will comprise [illegible] London in September 1956 by co-operation with the Research Publication Division of The American Society of Mechanical Engineers will again be presented [illegible] a series of meetings to [illegible] the Annual Meeting of the Society, New York, December, 1956.

The program will cover the following subjects: Stress Effects, Metallurgical Aspects and Improvement, Metallurgical Aspects, Basic Studies, Practical and Engineering Significance of Failure.

Abstracts and copies of the papers, when available, may be obtained from the Secretary, The American Society of Mechanical Engineers, 29 W. 39th Street, New York 18, N. Y., U. S. A., or the Secretary, Institution of Mechanical Engineers, 1 Birdcage Walk, London, S.W. 1, England.

International Congress for Applied Mechanics, Brussels, September, 1956

The Ninth International Congress for Applied Mechanics will be held at the University of Brussels, Brussels, Belgium, from Wednesday, September 5, to Thursday, September 13, 1956.

The technical sessions will comprise a section on Fluid Dynamics and Aerodynamics and one on Mechanics of Solids (rigid dynamics, elasticity, plasticity) besides several general lectures.

Abstracts of papers (three copies) should be submitted to the General Secretary before April 5, 1956, so that these may be collected and printed for the Congress. These abstracts, either in French or English, should not exceed two typewritten pages and, if possible, authors are requested to give a translation in the second language of the Congress so as to facilitate translations of highly specialized terms.

Copies of this Congress may be obtained from the Secretary, The American Society of Mechanical Engineers, 29 W. 39th Street, New York 18, N. Y., U. S. A., or from Dr. Jean Kampé de Fériet, Cité Universitaire, Bruxelles, Belgium.